Engine Cylinder Pressure Reconstruction Using Crank Kinematics, Block Vibrations, and Time-Delay Neural Networks

by

Stuart Trimby

Submitted for the Degree of
Doctor of Philosophy

University of Sussex
School of Engineering and Informatics
Department of Engineering and Design

September 2015

Abstract

Time-delay feed-forward Artificial Neural Networks are examined for gasoline engine cylinder pressure reconstruction using both measured crank kinematics obtained from a shaft encoder, and measured engine cylinder block vibrations obtained from a production knock sensor. Initially, the study focuses on the information content associated with measured data, which is considered to be of equal importance to the particular network architecture and the training methodology. Several hypotheses are constructed, which when tested, reveal the influence of the data information content on the reconstruction potential and limitations. These hypotheses are tested on real data from a 3-cylinder (DISI) engine. Three distinct ideas emerge through this testing process, which are combined to produce a single pressure reconstruction methodology. Reconstruction results obtained via this methodology, applied to crank kinematics associated with steady-state engine operation, show a marked improvement over previously published reconstruction accuracy. Moreover, in steady-state engine operation, the application of this methodology to acceleration measurements of cylinder block vibration, obtained from a knock sensor, show very significant improvements over previous attempts. But the direct application of this same reconstruction methodology to transient engine operation, proves to be problematic. However, a novel generalisation of the approach in the form of a time-dependent feed-forward neural network is proposed and the required adaptation made to the use of the Levenberg-Marquardt training algorithm. This time-dependent approach has been tested under limited transient conditions and shown in the thesis to give good results, therefore offering considerable potential for use with real engine operation. Overall, the thesis shows that by careful processing of measured engine data, standard neural network architectures and standard training algorithms can be used to reconstruct engine cylinder pressure.

Declaration

I hereby declare that this thesis has not been and will not be, submitted in whole or in part to another University for the award of any other degree.

Stuart Trimby
September 2015

Acknowledgements

First and foremost I offer my sincerest gratitude to my supervisor, Dr J. F. Dunne, who has supported me throughout my thesis, with his patience and knowledge, whilst allowing me the room to work in my own way. I would also like to thank him for helping to secure the funding needed for me to complete the research.

I am very grateful to Dr C. Bennett for his guidance through the early stages of the thesis and alongside Mr. Ian Wallis, for assisting with the engine testing and data acquisition system.

I would also like to thank Mr Dave Richardson and colleagues at Jaguar Land Rover Ltd for their enthusiasm, advice and technical support. I am also very grateful for the financial support provided throughout the research.

Finally, I would like to thank my mother Romaine and my brother Sean for their love and continuous unwavering support and without them I would never have been able to come this far. I would also like to thank my whole family, some who are still with us and some not, for the encouragement I received from a young age and which continues today. Special thanks go to Murphy for the sometimes wanted, as well as often unwanted, distractions.

Nomenclature

Abbreviations

AI	Artificial Intelligence
ANN	Artificial Neural Network
BDC	Bottom Dead Centre
BP	Back-Propagation
BPTT	Back-Propagation-Through-Time
CA	Crank Angle
CI	Compression Ignition
CO	Carbon Monoxide
DISI	Direct Injection Spark Ignition
DOF	Degree of Freedom
ECU	Engine Control Unit
EGR	Exhaust Gas Recirculation
EKF	Extended Kalman Filter
ELM	Extreme Learning Machines
EM	Expectation–Maximization
FEM	Finite Element Methods
FFPI	Fibre-Optic Fadry-Perot Interferometer
GA	Genetic Algorithms
GD	Gradient Descent
LMA	Levenberg-Marquadt Algorithm
HC	Hydrocarbons
IC	Internal Combustion
IMEP	Indicated Mean Effective Pressure
MAP	Manifold Air Pressure
MLP	Multi-Layer-Perceptron
NANN	Non-Autonomous Neural Network
NARX	Nonlinear Autoregressive Exogenous
NOx	Nitrogen Oxides
NVH	Noise, Vibration and Harshness
PFI	Port Fuel Injected
PM	Particulate Matter
PSO	Particle Swarm Optimisation
RAGD	Robust Adaptive Gradient Descent

RBF	Radial Basis Function
RIFE	Reciprocating Inertia Force Excitation
RMSE	Root Mean Squared Error
RNN	Recurrent Neural Network
SI	Spark Ignition
TDC	Top Dead Centre

Engine Modelling Notation

a	Acceleration
A_C	Cylinder Area
b	Cylinder Bore
CG	Centre of Gravity
d	Displacement
$\dot{d}$	Velocity
$\ddot{d}$	Acceleration
F	Force
f_n	Natural Frequency
g	Gravitational Constant
J, I	Mass Moment of Inertia
k	Stiffness
l	Connecting Rod Length
m	Mass
OS	Piston Offset
P	Cylinder Pressure
r	Crank Radius
r_{eff}	Crank Effective Radius
T	Torque
x	Crank Axis to Connecting Rod CG Length
$\alpha, \ddot{\theta}$	Crankshaft Angular Acceleration
$\omega, \dot{\theta}$	Crankshaft Angular Velocity
θ	Crankshaft Angular Position
Φ	Connecting Rod Angular Position

Subscripts

T	Tangential	r	Reciprocating
C	Crank	f	Friction
G	Gas	l	Applied Load
e	Total	o	Other Effects
i	Indicated		

Artificial Neural Networks Notation

w	Synaptic Weights
b	Bias
v	Induced Local Field
φ	Activation Function
y	Output
n	Number of Neurons
k	Number of Outputs
c	Centre
H	Hessian Matrix
J	Jacobian Matrix
I	Identity Matrix
g	Gradient Vector
μ	Regularising Parameter
ε_{av}	Cost Function
d	Desired Output
t	Time

Subscripts

i	Input Number	h	Hidden Layer Number
j	Neuron Number	o	Output Layer Number
k	Output Number		

Table of Contents

Chapter 1

Introduction

1.1 Summary

Since the development of the Internal Combustion (IC) engine in the 19th century, IC engines have become essential in nearly every facet of modern life. Their uses range from stationery power production to light aircraft, from heavy duty machinery and to large marine applications. But the most significant use of IC engines is within automotive applications, with over 12.5 million automobiles being sold within Europe in 2014 and increasing yearly. Owing to the growth in the number of IC engines over the last 40 years, and to the greater understanding of their impact on the environment, there has been a drive to reduce overall emissions through legislation and emission standards, especially within the automotive industry. These standards have been formulated primarily by the European Union and the United States Environmental Protection Agency. This legislation aims to reduce carbon dioxide and harmful exhaust emissions including, unburned hydrocarbons, NOx, and particulate matter, alongside improving overall vehicle efficiency.

Most of the recent developments in reducing emissions within the automotive industry have been through improvements in exhaust after-treatment and within the combustion process, namely fuel injection. After-treatment developments within the 10 years has been significant; however it has led to adopting of large, heavy and expensive equipment, motivating researchers to focus more on reducing harmful emissions during combustion. The improvements in the combustion process have been promising, within research environments, with regard to increased understanding and decreasing emissions. However, these improvements are limited with the current technology level and only small improvements can be seen for IC engine's operation in real world scenarios. To enable these advancements to be applied and maximised, it is necessary to gain greater control over the combustion

process and to create closed-loop combustion control, which is only possible when cylinder pressure is known in or near real time.

The most common solution to measuring cylinder pressure is through the cylinder pressure transducer, whether it is a standalone transducer or a spark plug mounted transducer. However, there are significant questions over the use of these transducers within a production IC engine. The questions mainly surround the price and durability of the transducers. Even though there has been considerable work done on trying to reduce the cost and improve durability, by both spark plug and pressure transducer manufacturers, these questions are still present. The actual price of in-cylinder pressure transducers can vary depending upon different specifications, but they can cost up to £1,500 each. These are especially expensive for cars within B and C segments, but also, if transducer durability is not sufficient to last the life of the vehicle, then these transducers would become a serviceable part. This would then significantly increase the maintenance cost of the vehicles and potentially impact on sales and long term profitability. Alternatives to using cylinder pressure transducers are being researched. This thesis aims to put forward just such a robust alternative methodology to reconstruct cylinder pressure.

This thesis will demonstrate the reconstruction of cylinder pressure through the use of Artificial Neural Networks (ANN) and existing sensors that are currently fitted to production engines. Artificial Neural Networks are a form of mathematical model that can be trained to recreate a complex physical model. When trained, an ANN can be treated simply as a black box model. This modelling technique has been used for reconstructing cylinder pressure from both crank kinematics, via a crank shaft encoder, and cylinder block vibration, via the knock sensor. This thesis will also demonstrate how to optimise Artificial Neural Network capabilities and signal processing techniques required, as well as investigating the complexities involved when going from training in steady state conditions to training with transient data.

1.2 Cylinder Pressure and Cylinder Pressure Measurement

1.2.1 Cylinder Pressure

The class of automotive engines where cylinder pressure reconstruction would be most advantageous, and indeed the engine type examined within the project, are

naturally aspirated four stroke gasoline engines. These engines follow the Otto cycle developed by Nikolaus Otto in the 19th century, i.e. depending upon the engine's configuration, a simple set of processes shown in Figure 1.1, as follows: first, an air and fuel mixture is drawn into the cylinder; this mixture is compressed adiabatically by the vertical movement of the piston. When the piston reaches top dead centre (TDC), a sparkplug ignites the air/fuel mixture which rapidly burns, increasing cylinder pressure. This increased pressure accelerates the piston downward, to bottom dead centre (BDC), adiabatically expanding the combustion gases, producing a significant amount of energy. The final stage involves heat rejection from the combustion gases and their expulsion from the cylinder as the piston returns to TDC.

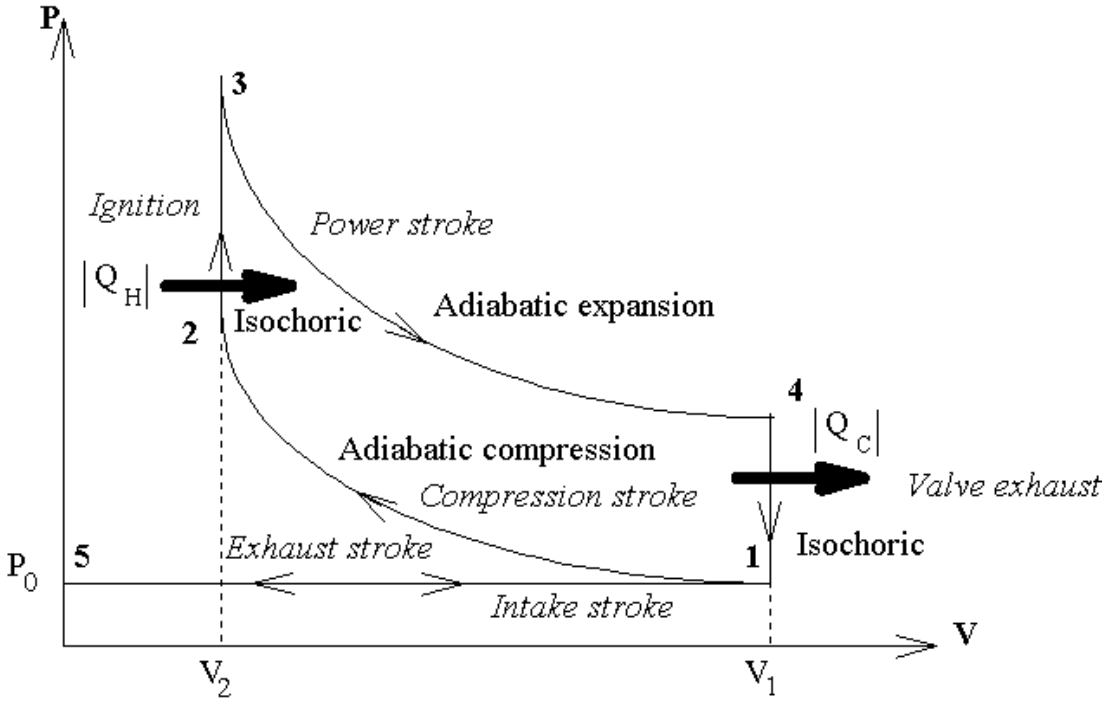

Figure 1.1: Ideal Otto Cycle (Ideal Otto Cycle, n.d)

This simple thermodynamic model of internal combustion engines is very effective in understanding the basic principles and is used extensively within idealised calculations. However, neither this model nor more contemporary models, have the ability to accurately or repeatedly determine cylinder pressure within real engines. In reality, cylinder pressure varies with crank angle as a result of cylinder volume change, combustion, heat transfer to the chamber walls, flow into and out of crevice regions and leakage (Heywood, 1988). However, these variables also depend upon numerous other factors. For example, combustion depends on air volume, density

and mass, fuel mass and dispersion, and turbulent in-cylinder air motion which is determined by the dynamics of the inlet and exhaust air.

Even though there are large numbers of variables, knowing cylinder pressure is a great advantage in terms of overall performance, increasing efficiency by ensuring complete combustion and reducing engine noise, vibration and harshness (NVH). Typical information that can be obtained through knowledge of the cylinder pressure includes maximum combustion pressure, indicated mean effective pressure (IMEP), and ignition timing. These three are the most useful when optimising engine performance, and achieving efficiency and emission goals. The remaining information can be used for various activities, such as calculating the rate-of-change of pressure, knock and misfire detection, cylinder balancing and reduction of cycle-to-cycle variation to improve NVH characteristics. This information, in addition to heat release, can be used to control multiple systems; exhaust gas recirculation (EGR) and after treatment processes, for example.

Some of the above mentioned activities, namely knock and misfire detection and EGR control, as well as some more general combustion control, is achieved using straightforward feedback from external sources, such as knock and lambda sensors. However, to successfully control all of the above parameters, and maybe more, it is necessary to have a methodology to determine the pressure inside the cylinder robustly for use in a closed-loop combustion control strategy. These closed-loop combustion control strategies have been researched in great detail and have demonstrated that a significant improvement can be obtained in all of the pre-established areas, especially within emissions and NVH (Kolbeck, 2011). This type of control strategy has also improved the engine performance across a wide range of operating conditions when running in less than standard operating conditions such as following cold starts (Rackmil and McKay, 2010).

1.2.2 Direct Cylinder Pressure Measurement

The direct measurement of cylinder pressure is the most common method within the research environment, owing to the accuracy and reliability of the measurement signal. Ideally, the methodologies and techniques used would be transferred into production engines for use in the market. However, most of the direct measurement techniques have serious limitations with regards to durability and cost. There are however, numerous direct cylinder pressure measurement techniques available. Three of the most significant and heavily researched methods include: use of

piezoelectric crystals, fibre optics strain and ion sensing. The first two both rely on material deformation, where ion sensing relies on the properties of the cylinder gases.

Use of piezoelectric crystals is the most common method for directly measuring cylinder pressure. These piezoelectric crystals are electromechanical materials that react to mechanical compression. Owing to their physical properties, they tend to be fairly robust and stable at high temperatures. They have an amplitude range which allows them to sense both small and large pressure fluctuations. They also have the ability to operate in extreme conditions making them ideal for use within the internal combustion engine.

There are two separate methods in which piezoelectric crystals can be utilised. The first is in a dedicated cylinder pressure transducer. This type of transducer is located independently within the cylinder head and is flush-mounted to the interior of the cylinder. These have proven to be more accurate and durable, but they do increase the complexity of the cylinder head and may restrict the use of other technologies to improve efficiency and performance. The second type is spark plug or glow plug mounted pressure transducers. The piezoelectric crystals are contained within the plug and are easier to integrate within an engine. However, this ease of integration is played off against the accuracy and durability of the integrated pressure transducer.

There are however, significant limitations to the use of piezoelectric pressure transducers in production engines: namely the cost and the durability. Regarding durability, piezoelectric pressure transducers have been proven to work efficiently and reliably under engine test conditions. However, they have not been proven to work for extended periods of time on production gasoline engines in real world conditions. The question about their actual lifetime has yet to be answered for spark ignition engines (SI) however, glow plug mounted pressure transducers are currently being used on mid-range and high-end compression ignition engines (CI). The application of glow plug mounted pressure transducers will be discussed in section 1.3.2 including examples of current automotive manufacturers using pressure transducers on compression ignition engines. The questionable durability within spark ignition engines also ties in closely with the concerns over cost. The cost of piezoelectric pressure transducers pastly has been high where each transducer

could typically cost in excess of £1000 and the associated electronics, such as charge amplifiers, could also be of a similar price. This would result in the price of four piezoelectric pressure transducers and its electronics being many times more expensive than the overall cost of the engine, in a small vehicle. In recent years the price has started to decrease to the point where the mass production cost could be reduced to £100 to £200 each, but would still cost in the region of £1000 for the system and would be a significant portion of the overall engine cost. These costs on their own may be justified if there is a significant improvement in efficiency and the reduction of overall emissions but if the durability is in question, these transducers may result in being a serviceable part and be a significant cost to the consumer, which would become a concern for engine manufacturers. Some additional limitations include the integration into existing designs or adaption to new designs when additional cooling is required and the required frequency of calibration. This calibration is essential to overcome phenomena such as thermal sensitivity and zero shift. These are shifts in the pressure transducer's responses due to either the prolonged or significantly high temperatures and could result in erroneous results (Nysæther et al., 1998).

The two technologies that are currently being extensively researched for measuring cylinder pressure include ion current sensing and fibre optic based sensors. Out of these two new cylinder pressure technologies ion current sensing, is in principle, the simplest and most cost effective method of measuring cylinder pressure. Ion current sensing utilises the existing components, namely spark plugs, within spark ignition engines and the electrical properties of the combustion gas to achieve the cylinder pressure measurement. Within this technique, an electric potential is applied across the spark plug producing an electric field during the period of non-sparking. Owing to the ion species that are created during the combustion process, current is generated as they move between the two electrodes of the spark plug. Using a simple electric circuit the voltage across a resistor can be measured and this voltage is proven to be useful in determining combustion characteristics (Rivara et al., 2009) (Grasso et al, 2013).

The second method, fibre optic based sensors, has been in existence for over two decades within the research environment because of the accuracy and ease of integrating them into internal combustion engines. However, owing to the relatively high cost and durability questions, it has not progressed into the production

environment. Most fibre optic based pressure sensors of this type are based on the fibre-optic Fadry-Perot interferometer (FFPI). Simplistically, these sensors contain a set of mirrors, which at rest, are a fixed length apart. Light from a semiconductor laser is transmitted down the length of the fibre-optic, and a portion is reflected by the mirrors and captured by a photodetector. When the pressure increases, even by a small amount, the distance between the mirrors will vary and will result in a variation in the signal from the photodetector. The advantages of using fibre optic based sensors for cylinder pressure measurement are numerous. They include extremely high sensitivity, capabilities of operating at elevated temperatures for extended periods of time, and being mechanically flexible and rugged (Lee and Taylor,1998).

1.2.3 Indirect Cylinder Pressure Reconstruction

As discussed in the previous section, there are a number of direct cylinder pressure measurement methods that can produce accurate results. However, the limitations of these methods predominantly relate to the cost and durability implications. Therefore there has been a drive to discover and develop a methodology to measure cylinder pressure accurately, cheaply, and be durable for the lifetime of the engine. Taking these three criteria into account, it is possible to determine which regions and characteristics are the most likely to produce results. With respect to durability and accuracy, it would be necessary to find an engine characteristic that is related to the cylinder pressure but in not such close proximity that the higher temperatures and pressures would impact on a sensor's durability. With respect to cost, it would be best to either use existing sensors or sensors that are economically priced. It has been established that the two most significant and those of most interest is crankshaft kinematics and engine block acceleration. The physics of each of these, as well as the measurement methodologies, will be discussed in detail in later chapters. However, a brief overview will now be given.

Using crankshaft kinematics to reconstruct cylinder pressure has been the approach that many have undertaken in the previous two decades. It is based on inverting a parametric engine model, which models engine acceleration from cylinder pressure, and then using this inverted model with measured crankshaft kinematics (obtained via a standard or upgraded shaft encoder) to reconstruct cylinder pressure. However, this type of analytical approach encounters numerous complications, namely in modelling engine friction and modelling manufacturing defects. The most significant complication is in the sine component of the acceleration equation, given

later in Chapter 2, which these engine models are based upon. The complication arises at top dead centre (TDC) and bottom dead centre (BDC), where the acceleration reduces to zero. This issue creates a singularity within the data at these points when inverting and results in significant difficulties during the reconstruction.

With respect to the engine block acceleration, parametric models are much more complex owing to the configuration of modern production engines and the complex geometries. Engine block acceleration reconstruction is based on structural vibrations measurements which have been generated by cylinder pressure fluctuations and transmitted throughout the engine block. These vibrations would either be measured using one or more accelerometers, or by using pre-existing knock sensors. There are numerous methods and approaches to reconstructing the cylinder pressure from engine-block acceleration, which will be discussed later. The main starting point for most approaches is using finite element methods (FEM) and identifying structure characteristics as a result of cylinder pressure. Then, differing methods are applied to invert and reconstruct. This approach has the benefit of not needing to model engine friction and does not rely on torque variations. However, the complex nature of production engine block geometries and the number of other vibration sources, both within and external to the engine, cause great difficulty in filtering and reconstruction.

Both of the approaches covered show great possibilities for indirect cylinder pressure reconstruction but there are considerable restrictions when using parametric models (Potenza et al., 2007) (Vulli, 2006). Alternative modelling approaches have also been examined, including machine learning, specifically artificial neural networks (ANN). Artificial neural networks have been used across a broad range of industries and applications and will be discussed in greater detail later. Artificial neural networks have been used on both crankshaft kinematic and engine block acceleration based reconstructions, with some success. Artificial neural networks have the benefit of, in principle, being able to map and model the behaviour between two or more related data sets with no need to model individual characteristics and do not need to understand the physics at work. With a correct methodology and the theoretical power of artificial neural networks, the prospect of indirect cylinder pressure reconstruction being successful is high.

1.3 Legislation and Applications of Cylinder Pressure Transducers

Legislation surrounding exhaust emission standards over the previous two decades have become increasingly severe, with the aim of reducing the production of pollutants and improving air quality. Owing to the globally increasing concern over automotive emissions, many of the regulators such as the EU, American, Australian and Japanese standards are converging to improve global environmental issues. The latest set of regulations within the EU, called Euro 6, took effect in September 2014 and is the most recent in a series of emission standards starting with Euro 1 in 1993. Over the years, as a result of these standards, exhaust emissions of production vehicles sold in Europe have reduced significantly. Table 1.1 outlines the basic Euro 6 standards for both gasoline and diesel passenger vehicles. These are stringent standards, but those being currently constructed and put forward for Euro 7, are expected to be much stricter on carbon emissions and will take effect between 2020 and 2025.

Table 1.1: Euro 6 Emissions Standards

	Gasoline Emission Limits	Diesel Emission Limits
CO	1.0 g/km	0.5 g/km
HC	0.10 g/km	0.17 g/km (inc. NOx)
NOx	0.06 g/km	0.06 g/km
PM	0.005 g/km 6.0x10^11/km	0.005 g/km 6.0x10^11/km

The most significant recent transformation in the emission standards was achieved with the launch of Euro 5 in January 2013. The recent push for stricter regulations, with regards to particulate matter (PM) size and number, was within diesel engines and led to manufacturers investing significantly in research to minimise it. As a result, certain new Euro 5 and Euro 6 approved diesel vehicles were fitted with glow plug mounted pressure transducers. These include the larger diesel engines, of the order of 2.0L, within VW Jetta, Audi A8 and Vauxhall Zafira. It is believed that their implementation was purely a result of the need to reduce particulate matter, not as a

method to enable closed-loop combustion control. These glow plug mounted cylinder pressure transducers can be used in a similar fashion to knock sensors. They can used in conjunction with the engine management system to prevent the engine cylinder pressure from entering regions where particulate matter production is extensive, in a similar way that knock sensors restrain the combustion parameters from causing knock. Current use of the glow plug mounted cylinder pressure transducers has little additional impact on performance or emission owing to fidelity issues.

1.4 A Literature Survey of Indirect Cylinder Pressure Reconstruction Methods

A review of the literature surrounding the theme of indirect cylinder pressure reconstruction, is essential to properly understand the topic and where the current research sits within this field. Owing to the limited number of publications that deal specifically with cylinder pressure reconstruction that use artificial neural networks, a range of similar publications will be discussed. These include articles that discuss the differing cylinder pressure reconstruction techniques and publications that discuss artificial neural network applications for estimating engine metrics. This literature review is divided into two sections: the first section will discuss in detail the most relevant research undertaken using crankshaft kinematic based reconstruction. The selection of articles reviewed will contain publications covering an analytical approach, publications that use artificial neural networks, and additional articles deemed relevant to reconstruction using other machine learning techniques. Block acceleration based reconstruction publications are then reviewed in the same manner as the first section. In addition to reviewing the approaches and achievements of each publication, the review will attempt to identify the manner in which the data is applied to the various models.

1.4.1 Crankshaft Kinematic based Reconstruction

One of the first publications to examine crankshaft speed fluctuations and relate them to engine characteristics from a modelling approach, was reported by (Rizzoni, 1989). Rizzoni's objective was to develop a deterministic model for the dynamics of an SI engine by identifying the applied torques that act on the crankshaft inducing the speed fluctuations. Rizzoni constructed mathematical approximations for the applied torques and mechanical quantities. These approximations have been

deemed to be analogous, by the author, to electrical components and circuits. This electrical circuit analogy was then tested experimentally. The experimental set up used in the model verification was a 4 cylinder in-line SI fuel injected 1.5L FIAT engine driven by an electric dynamometer. The crank kinematics or engine angular position was measured using both an optical shaft encoder and an inexpensive magnetic based encoder. Alongside engine torque measurements, the cylinder pressure was also obtained using a flush mounted piezoelectric sensor. With respect to the treatment of the input data, there is no detailed quantitative description other than stating that the low-pass filtering and analogue differentiation of the signal was undertaken. The experimental results were across a range of different steady-state engine speeds, from 1500 rpm to 3500 rpm, and at five different load points. The majority of the results were graphically presented. Therefore, determining the effectiveness of the system is difficult, however the correlation coefficient of a regression line (which was generated for comparison between measured and reconstructed torque at 25 steady-state conditions) was found to be 0.998. A test of the electrical analogy for transient conditions however, produced no quantitative error. The qualitative results provided for this method appeared good for reconstructing crankshaft torque however, the reconstruction of cylinder pressure using the electronic analogy has greater complexity.

Both (Shiao and Moskwa, 1994) and (Lim et al., 1994) continued to research deterministic models. Although each of these publications has a slightly different approach to reconstructing cylinder pressure, they both rely on the same fundamental parameters, and produce similar levels of error during reconstruction. For example, they both rely on parametric methods for reconstructing cylinder pressure. Shiao and Moskwa 1994 also attempted to use the analytical approach for misfire detection. Lim et al 1994 uses crankshaft dynamics associated with the first principles of a single-degree-of-freedom model, for system energy including energy in the crankshaft assembly, in the camshaft, the engine load, friction and vibration, and the pressure in the cylinder. The dynamic model was created for a four stroke four cylinder multipoint injection engine which has a capacity of 1.495L. The engine is installed with flush mounted piezoelectric pressure transducers in each cylinder. Conversely, Shiao and Moskwa 1994 uses a Sliding Observer methodology to reconstruct cylinder pressure. The details of how the sliding observer works are not discussed here, but these methods are created from a parametric engine model and therefore can be comparable to Lim et al 1994. Shiao and Moskwa 1994 model is

for a considerably larger engine, i.e. a 4.6L V8 engine. Other information regarding the engine, the sensing data acquisition, or data handling methodology was not given in either article. Both methods produce significant errors at TDC. The limited results in Shiao and Moskwa 1994 paper show instantaneous errors as high as 30% of the peak pressure over a range of different speeds from 2000 rpm to 4500 rpm. When using the standard single dimension engine model, similar results were produced however Lim et al 1994 did further work on friction. They measured engine friction at idle over 100 cycles, computed the average torque, and included this within the model. This produced slightly lower error values for peak pressure, averaging around 15%, however, there is a large distribution, some errors as high as 30%, with the large amount of data presented. Both methods are limited by the same factors identified by Lim et al 1994, namely friction. Friction is an integral part of dynamic engine models and estimations of this, using a singular theoretical value (as in Shiao and Moskwa 1994 model and the Lim et al 1994 first model), has grave consequences on cylinder pressure reconstruction. Even though the Lim et al 1994 approach of measuring friction levels is adequate for significantly improving the cylinder pressure reconstruction, the friction levels at idle are significantly different from high-speed friction levels and much more complex than can be described in a single value. Also these methods rely on measuring engine parameters and feeding them back into the model, and therefore have considerable limitations: namely, they do not take into account friction changes associated with engine wear or the model's transferability due to friction differences between the same class of engine.

(Gu et al., 1996) was one of the first publications that successfully used machine learning techniques to model engine dynamics. It used a radial basis function (RBF) neural network model to reconstruct the cylinder pressure of an internal combustion engine. Instead of using either pre-existing engine parametric model-based approaches, or pure pattern recognition techniques, a neural network was used. These neural networks combined both the pattern recognition features as well as the interpretation, and can be considered a non-parametric model of the engine process. This paper covers efforts on both parametric model description and radial basis function neural network structure in general. Other than stating that this RBF neural network was trained on and validated with a four cylinder direct injection diesel engine, it had a high performance pressure transducer fitted to cylinder one, and the instantaneous speed was obtained at the flywheel, no other information was given regarding to how the data had been handled. There was little information

regarding the exact size of the RBF neural network, other than stating that it was large. The network trained on a reasonably sized data set including 39 different test points with 100 rpm and 20 Nm divisions, which included data that was divided for the purpose of testing the neural network on generalised data. However, it was not stated whether the results given were the training results or generalised results, but it was reported that the difference in peak pressure was ±0.3 MPa with a standard deviation of 9.29%. It was reported that the indicated mean effective pressure (IMEP) average error, generated by RBF neural networks reconstruction, was just above 10% at ± 0.046 MPa. It was also noted that this type of approach worked well for fault diagnosis, as evidence of misfiring was seen in the reconstructed data. This approach shows good results, but owing to the large neural network size, the practicality is questionable in both training with the required large data sets and the computational effort for real time reconstruction.

(Jacob et al., 1999) and (Gu et al., 1999) form a two-part series on non-parametric models for reconstructing cylinder pressure and other combustion parameters. Part one (Jacob, 1999), discusses the theoretical approach and sets out the model architecture in great detail. The work proposed used a radial basis function neural network to model nonlinear engine processes. It considers the differences between parametric and non-parametric models for this application, including the creation of a conventional parametric model and discusses its limitations. The paper then discusses the architecture and creation of a radial basis function neural network for this application. Part two (Gu, 1999), takes the theoretical approach examined in part one, and applies the model to an internal combustion engine. The engine used within this application was a production four cylinder Ford diesel engine with a capacity of 2.5 L, and direct injection. A flywheel mounted magnetic pickup had been installed to record the crankshaft angular velocity and flush-mounted pressure transducer installed on cylinder 1. The same method was used for acquiring data, and for training the neural network as in (Gu, 1996). A total of 390 data items were collected at 39 different test points between 1000 rpm and 2600 rpm, with intervals of 100 rpm, and 20 Nm. Each pressure and crank velocity data pair was measured simultaneously but with different sampling rates and with 216 samples windowed over 160°CA around TDC, and 54 samples windowed over 180°CA around TDC. With respect to the accuracy of the cylinder pressure reconstruction, the results were reasonable, with the average error at peak pressure being 5%, with similar results of the other combustion parameters, namely IMEP, and a location of peak

pressure being ± 2°CA. Similar conclusions have also been made to the findings in (Gu, 1996).

An alternative approach to cylinder pressure reconstruction was undertaken by (Hamedović et al., 2005), alongside an estimation of indicated-mean-effective-pressure (IMEP) using engine speed fluctuations and a single cylinder pressure sensor. This method of using a single cylinder pressure sensor has the advantage of reducing the overall cost along with improving accuracy and having the possible means of adapting to changing conditions. The cylinder pressure was reconstructed via a model based approach with a combination of torque approximation and parametric pressure model. No information was provided with regards to the experimental setup or sensors used on the four cylinder SI engine. The results presented show a good reconstruction capability of a model based approach, when compared with others that do not use a single cylinder pressure sensor. Most of the error results are presented in the form of histograms with average peak pressure error in the range of 6% and position of peak pressure which had an average error of 3°CA.

(Potenza et al., 2007) describes an approach for reconstructing the cylinder pressure trace for multi-cylinder engines. This approach is based on the use of NARX neural network architectures in addition to examining two different fully-recurrent training algorithms and validating on a real engine. The experimental data was collected from a production 1.12 L three-cylinder direct injected gasoline engine, fitted with a spark plug mounted pressure transducer on all cylinders. Crank kinematics was measured with a digital incremental encoder. The first training methodology used was a back-propagation-through-time algorithm (BPTT) and the second was training via the extended Kalman filter (EKF). Each method has disadvantages but both aim to reduce the training time for NARX neural network architectures, which can be significant. This paper is also one of only a few that mentions how they apply the data to the neural network. The networks have numerous inputs including crankshaft position, crankshaft acceleration, delayed crankshaft acceleration, and a feedback loop containing previous reconstructed cylinder pressure. The output is cylinder pressure, but what makes this different from most other attempts where multiple cylinders are reconstructed, is that a separate neural network is created for each cylinder. Owing to the complexity and long training times of NARX neural networks, a single steady-state engine operating

condition was selected; at 1500 rpm and 25.5 Nm. As a consequence of this issue, a relatively small network was created and only 6 cycles of data was used throughout. It contained 8 neurons in the hidden-layer and 49 weights/biases in total. The training and generalisation results for both approaches are fairly promising where, for most cases, the root mean squared error was below 2%. However, in some localised regions, the error increased to a level as high as 25% and the results became unstable. The most significant result from this use of NARX neural network architectures is that even with training algorithms that are efficient, the training time is significant. It is reported that the training time (with a representative computer at the time i.e. a Pentium 4 PC), was measured in tens of hours. For example, the NARX model trained using the back-propagation-through-time algorithm was reported to take 42 hours.

Work using recurrent neural networks was continued by (Saraswati and Chand, 2010) to attempt to reconstruct cylinder pressure for an SI engine. This uses the same basic approach which has previously been discussed with one significant step. Where most previous studies train the model or neural network on large sets of experimental results, gathered on an engine test bed, the approach outlined aimed to use a different modelling philosophy to minimise the size of the experimental results. This new philosophy uses a combination of engine test data with a phenomenological two zone model to generate more data for training and validating black box models i.e. artificial neural networks. This two zone model for generating additional data sets was optimised using Levenberg-Marquardt method which is an iterative technique used for locating minima of functions with multiple variables (Haykin, 2008). The Levenberg-Marquardt method is a combination of the gradient decent and Newton method and approximates the Hessian matrix using the Jacobian matrix. This is described in detail in section 3.5.2. This method can be seen to be successful for the small amount of data presented. This data along with actual experimental data is used to train a recurrent neural network. The details surrounding the training are however inconsistent. The Levenberg-Marquardt method is again mentioned and consequently it will have to be assumed that a 'teacher forcing' methodology has been used. The small number of results presented seems fairly consistent, with a relatively good accuracy, i.e. within 10%, however there is no indication as to the number of cycles trained or whether the data is generalised or not. The paper does not address the proportion of results that are produced from training using experimental results or training from the two zone

model. This ratio is important in determining whether or not the network has over-trained to the two zone model and the overall effectiveness of this approach.

In this more recent work by (Mocanu and Taraza, 2013), several different combustion parameters were estimated using crank shaft speed fluctuations. This article aimed to estimate the cylinder pressure trace, including peak pressure, position of peak pressure and ignition delay. The work used two model based approaches. The first approach was a complex fully-dynamic model that included flexibility of the crankshaft. This approach was first applied to a single cylinder test engine, which had a capacity of 0.7L, and was fitted with both a pressure transducer and shaft encoder. The estimated cylinder pressure traces shown in the paper are somewhat limited, and are also only at a single steady-state condition with no quantitative error values given. Given the limited results however, the fully dynamic engine model seems promising. A simpler model, called the 'direct approach', was also examined which only takes account of the inertial torque and omits several variables namely, crankshaft flexibility and friction. As a result, the capability of estimating cylinder pressure is diminished and results have significant errors. The use of both of these methods was also attempted on a larger 4 cylinder VM Motori 2.5L engine, again fitted with both a pressure transducer and shaft encoder. The general results using the more complex model were poor and owing to the complexity of the model, it was deemed not possible to run in real time. With regards to the comparison between the two models, a further reduction in quality of the reconstruction was observed when using to the simpler model. This is consistent with the observations for the single cylinder tests. This paper highlights several important limitations for model-based reconstruction, specifically the intricacies of crank shaft flexibility and friction levels and the complexity of going from a single cylinder test engine up to a four cylinder production engine. The most significant limitation is the larger and more complex the model, the greater computational efforts required, and the more difficult it is to reconstruct cylinder pressure in real-time.

(Taglialatela et al., 2013) took a distinctly different approach in determining combustion parameters than those discussed in the other papers presented. Where previously, crank kinematics have been used to reconstruct entire cylinder pressure traces, this paper uses the crank kinematics only to reconstruct the magnitude of peak pressure and the angular location of peak pressure. The validation of the

neural network models was produced using a single cylinder research engine; it was a port fuel injected (PFI) turbocharged gasoline engine with a flush mounted piezoelectric pressure transducer fitted. It was also fitted with a high precision crank angle optical encoder that was used for instantaneous crank kinematic measurements with the precision of 0.1°CA crank angle. Data was acquired over a range of engine speeds from 1000 to 2000 rpm with 200 rpm increments and at each of the operating conditions 400 consecutive cycles were gathered. The neural network selected for this application was a Multi-Layer-Perceptron (MLP) network with two inputs; crankshaft speed and crankshaft acceleration, and two outputs; peak pressure and location of peak pressure. Each MLP neural network trained was restricted to a hidden layer containing 30 neurons and the activation function was selected to be arctan. The training of the neural network was undertaken within, and taking advantage of, the Matlab neural network library. The training algorithm used was a Bayesian regularisation owing to its proposed guarantee of satisfactory generalisation capabilities, avoiding over-fitting issues. With the significantly reduced model, only extracting two combustion parameters, it would be expected that gains would be made with regards to the reconstruction performance. This however, has not been seen in the results, with the lowest relative error for the magnitude of peak pressure being greater than 4% and reaching as high as 20%. The angular location of peak pressure had similar results with the relative error and varying between 1.66° and 5.20°. As defined later in the objectives, the average target error for the overall reconstruction is below 4% with the angular position of peak pressure averaging below 2°. From these results it can be seen that there are no significant advantages of using neural networks to reconstruct combustion parameters directly instead of reconstructing the entire pressure trace.

1.4.2 Block Acceleration based Reconstruction

A novel approach to reconstructing cylinder pressure was taken by (Villarino and Böhme, 2003) using engine block vibrations. The method takes block vibrations and uses the expectation–maximization algorithm to estimate cylinder pressure. The expectation–maximization algorithm (most commonly known as the EM algorithm) is a statistical model which uses an iterative process to estimate its parameters using maximum likelihood. This research creates a statistical model for cylinder pressure estimation using engine block vibrations. The paper extensively covers an analytical method for the decomposition of the engine block acceleration as well as the application of the EM algorithm. The experimental data was collected from a four cylinder, 1.8 L, turbocharged spark ignition engine on a test bed. Spark plug

mounted pressure sensors were used in all cylinders, as well as four accelerometers mounted just below the cylinder head, each one aligned with the axis of one of the cylinders. Only one condition for the estimated results was presented at relatively high engine speed, i.e. 4000 rpm. This method heuristically combined 100 misfires and 500 normal combustions to produce three curves relating to a parametric pressure model. The reconstructed cylinder pressure was then formed from these three profiles. The results show relatively good reconstruction of the correlation coefficient of 0.9. However, when expanding to over 1000 cycles, generalised results drop significantly with a correlation coefficient of 0.68. Combustion misfires can however be seen to cluster, within the model results, making this method a possible candidate for misfire detection. The advantage of this method is that it is not required to understand the physics in detail since it relies on extracting statistical patterns. However, the inability of the method to expand to larger data sets and to produce sufficient accuracy may be a serious limitation.

(Johnsson, 2006) has taken, modified and combined several different techniques for cylinder pressure reconstruction. The reconstruction is based on a combination of both engine block vibration and crankshaft speed fluctuations. Both were used with the hypothesis that both the high frequency and low frequency information content would be available respectively. These are applied to a complex radial basis function network model. This publication is different from the other papers discussed in that not only is there a combination of inputs, but these inputs are presented to the neural network in a different form, i.e. the output from a Fourier transform. It was reported that the primary reason for using the Fourier transform is that different frequency regions of the signals are used for the reconstruction process, also that it is an easy method of reducing the amount of information used as an input to the RBF Network. The experimental measurements were carried out on a 9 L, 6-cylinder, inline, four stroke, turbocharged, ethanol powered diesel engine. The cylinder pressure was measured using a transducer mounted on cylinder one, with the accelerometer mounted to a head bolt on cylinder one, and crankshaft speed measured using an angle sensor with 1800 pulses per revolution. Measurements were taken at 39 different conditions with speeds between 800 rpm and 2000 rpm, from 10% to 90% load. During training the optimum neural number was found to be 39. The results presented were rather extensive and comparable with the error in maximum cylinder pressure being within ± 6 bar for 100 bar cylinder

pressure, i.e. an average error of 3.5%. The location of peak pressure had an average error of 1.5°CA under generalisation conditions.

Engine vibration signals was the focus for (Yong et al., 2010) and approaching the problem of reconstructing cylinder pressure using artificial neural networks. This work attempts to use the vibration signals produced at the cylinder head in the belief that excitations consist of a series of instantaneous responses with frequencies and amplitudes at different levels. Furthermore, it was reported that by analysing combustion signals of multiple periods, there is an obvious impacting response near to the combustion dead point, which results from cylinder pressure. There is little detail on the system used to acquire the data other than stating it was collected on a 6 cylinder 4 stroke diesel engine fitted with a vibration and pressure sensor on cylinder No.6. There is no mention of the speed at which the data or the exact torque values are gathered but it does state the load as a percentage. Again, little information was provided regarding the size of the artificial neural network architecture or training results. It states that a back propagation model has been utilised for a Multi-Layer-Perceptron architecture. This paper reveals that instead of applying data to the neural network in a time series approach (i.e. reconstructing a single cylinder pressure value at a time), this approach uses 140°CA around TDC for the cylinder head vibration inputs and reconstructs 140°CA around TDC for the cylinder pressure. The quantitative results for reconstruction of cylinder pressure appear to be very good, but with rather limited results presented at a single condition, producing a peak pressure error of 1.8% and a position error of up to 5˚CA. Again, this paper does not state whether these results were obtained for training or generalised data and gives no indication on the average or maximum errors produced using this neural network.

(Bizon et al., 2011) attempts to construct an effective and robust method of determining cylinder pressure, from vibration signals, using artificial neural networks. This work also aimed to create a model that would be robust with changing engine parameters as well as with respect to changes in the nature of fuel. For this application a radial basis function (RBF) artificial neural network was selected. The experimental data was collected from a single cylinder four stroke diesel research engine. This engine was fitted with the piezoelectric pressure transducer as well as a low cost capacitive accelerometer glued directly to the cylinder, just below the cylinder head. The data for six test conditions, ranging from 1000 rpm to 2000 rpm using a variety of fuels, was acquired with a number of consecutive combustion

cycles varying from 209 to 600 cycles depending on the operating condition. In this research, RBF feed-forward neural networks were trained using pre-existing MatLab functions, using 100 cycles of data. Comparisons were made between differing architectures. It was found that during generalisation there is little difference in the network's performance, between an architecture with 5 neurons and one with 50 neurons. However, even though there is no mention of how the vibration data is applied to the network, the manner in which the data is collected and the neural network architecture is discussed. It could be interpreted that all 60° of vibration data is applied producing an output of 60° for the reconstructed cylinder pressure. The models produced were very accurate, producing a peak pressure error less than 2.7%, and location of peak pressure, root-mean-squared error, less than 1.45°. The results discussed in this paper appear to be the best examples of neural network based cylinder pressure reconstruction. However, the position of the accelerometer is unrealistic for production applications and it is unlikely that this method would produce similar results if directly applied to a production multi cylinder engine.

A method of pattern recognition was demonstrated by (Zhao, Cheng and Wang, 2014) using measured vibration signals to extract cylinder pressure responses. This method essentially uses a pattern recognition model to describe the reciprocating inertia force excitation (RIFE). As the cylinder block vibration consists of the RIFE and cylinder pressure information, the subtraction of the RIFE from cylinder block vibration produces content that closely resembles the rate of cylinder pressure rise. The data in this paper was acquired from a single cylinder diesel engine with the piezoelectric cylinder pressure sensor and piezoelectric vibration velocity sensor mounted directly to the surface of the cylinder. Numerous conditions were tested with speeds ranging from 800 rpm to 1400 rpm, and loads from 0 to 50 Nm. It was also noted that the signals were converted from the time domain to the crank domain in order to overcome difficulties in pressure estimations at different speeds. The paper presents comparisons between the vibration velocity, and the vibration velocity with the RIFE removed, shown against rate of cylinder pressure rise. The metric used to compare the two methods was a correlation coefficient between the rate of cylinder pressure rise and the vibration velocities. It shows at low speed, i.e. 800 rpm, and zero torque that raw vibration velocity produces a correlation coefficient of 0.77 compared to processed results which produce a value of 0.86. However, the most noteworthy results from this paper come at a higher speed of

1200 rpm and load of 10 Nm. The role vibration velocity produces a correlation coefficient of 0.01 compared to processed results of 0.93.

1.5 The Objectives of the Thesis

From the literature review, it can be seen that the use of non-parametric models, such as artificial neural networks, appear to be the most promising methods for reconstructing cylinder pressure. However, there are several key areas which are either only partially resolved or not resolved at all. These include a clear determination of the best performing network architecture and the corresponding training algorithm to use. Moreover, one of the most challenging aspects of cylinder pressure reconstruction is the reconstruction of transient engine operation. The aim of this project is to not only attempt to resolve these areas but also to break through an apparent limit on the reconstruction capability, as seen in the literature. It has been demonstrated that, with the methodologies undertaken, there has not been a single case where the error for the generalised reconstruction of peak cylinder pressure has been consistently below 4%, and the position of peak cylinder pressure within ± 2°CA. This improvement maybe found either within the network architecture, or within the training algorithm, or it may be established that the above results are actually at the limit of the ability of the reconstruction. However, there is one aspect which should not be overlooked and that is the role the data plays in the application of machine learning methodologies (such as artificial neural networks). From the research in the broad field of machine learning (Haykin, 2008), one key idea is reiterated many times: that the successful application is not solely or significantly dependent on the algorithm used, but rather is equally shared in importance between the use of effective algorithms and the correct use of the data. It is believed that disproportionate weighting has been given to the algorithmic approach over the data and its use. The underlying theme within this thesis will be keeping faithful to the idea that both algorithms and data are equally important for machine learning applications. With this philosophy foremost in the drive to improve cylinder pressure reconstruction for production engines, the following objectives of the work can be stated:

1. To find the most promising artificial neural network architecture and training algorithm for cylinder pressure reconstruction.

2. To improve the understanding of the relationship between cylinder pressure, crankshaft kinematics and engine block vibration.
3. To develop a methodology aimed at improving cylinder pressure reconstruction under steady state conditions by extracting maximum information content from the data.
4. To optimise an artificial neural network architecture and to reconstruct cylinder pressure using crankshaft kinematics and engine block acceleration, with the aim of producing generalised results with an error of less than 4% for peak pressure error and a position of peak pressure within 2°.
5. To further develop the methodology that allows successful cylinder pressure reconstruction for fully transient engine operation.

1.6 Overview of Thesis Structure

A breakdown of the thesis structure is given below:

Chapter 1 gives an overview of the current state of the art with regards to direct and indirect cylinder pressure measurement. It also provides a concise evaluation of recent literature followed by the thesis objectives.

Chapter 2 is dedicated to examining the physics of cylinder pressure reconstruction and engine dynamics. The initial portion of this chapter examines both the crank kinematics from first principles, including a single cylinder model to demonstrate the relationship between cylinder pressure and both crank kinematics. The chapter also describes the process (and difficulties) of inverting the model to reconstruct cylinder pressure, which is key to this application. The chapter concludes by discussing the basic modelling techniques used when reconstruction via engine block vibrations.

Chapter 3 provides a concise overview of artificial neural networks and their associated training algorithms. It includes the origins and basic structure of simple neural networks alongside more relevant architectures, such as multilayer perceptrons and recurrent structures. It also goes into detail about the training algorithms for each architecture, as well as investigating the suitability of different training algorithms for differing applications.

Chapter 4 gives an overview of the engine testing and data acquisition. A description of the facilities is also given, including the engine, the dynamometer and test cell. The details of the data acquisition system are outlined including the required post processing of the data. It then describes some issues that had been found by other researchers and the solutions that have been put in place to enable reliable data acquisition. The last part of the chapter outlines tests undertaken by other researchers and the tests which formed part of the current research.

Chapter 5 is dedicated to examining the optimisation of the artificial neural network architecture, training algorithm and signal processing, with the main focus on using crank kinematic based reconstruction. Initially this involves comparing and establishing the best artificial neural network architecture and training algorithm. The remainder of the chapter is dedicated to understanding (from the point of view of the reconstructed data) the dynamics of the system. Three significant ideas of how the signal processing of the input can achieve substantial improvements in the reconstruction are examined.

Chapter 6 details the neural network results for crank kinematic based cylinder pressure reconstruction. The results for the time-delay network architecture and Levenberg-Marquardt algorithm using the three signal processing methodologies, is presented. It shows the results at a number of significant steady state test points precisely across the operating range this project is designed for.

Chapter 7 draws on the findings of Chapter 5 and Chapter 6 and applies these to block vibration based cylinder pressure reconstruction. Additional work is then demonstrated to optimise for block vibration, including alterations to the time-delay network internal architecture, and the signal processing methods. The remainder of the chapter then presents the results for block vibration reconstruction at the same steady state test points as described in Chapter 6.

Chapter 8 pursues the aim of reconstructing cylinder pressure for transient conditions. Initial work within this chapter attempts to construct a single neural network to achieve this. Additional methods of reconstruction are then examined including the use of multiple neural networks. The final attempt at reconstructing cylinder pressure for transient conditions uses a non-autonomous neural network.

This has been developed from the knowledge gathered within this project. Results of all the methods are presented.

Chapter 9 draws appropriate conclusions found within the preceding chapters. It also offers suggestions of where the project and application can make progress in the future.

Chapter 2

IC Engine Physics Including Forward and Inverse Modelling

2.1 Motivations and Background

This chapter is dedicated to examining the relationship between cylinder pressure reconstruction and engine dynamics. It is undertaken mainly with respect to crank kinematics but also briefly considers the dynamics of engine block acceleration. The most effective approach to understanding the problem of cylinder pressure reconstruction is to analyse engine dynamics and to construct a physical model using established methods. As well as aiding understanding, a model will enable the testing of different artificial neural network architectures and training algorithms on controlled data. Furthermore, this approach is used to highlight the fundamental differences between the forward and inverse models. It will also, more importantly, enable the resolution of intrinsic issues highlighted later in the thesis. The approaches outlined are not the entire extent of the use of these physical models because they can also be useful in understanding operational and time-varying issues, as well as engine parameter optimisation.

Most established methods of mathematically modelling engine dynamics and analytical approaches to cylinder pressure reconstruction, are based on the same concept. They construct parametric models using torque balancing equations. By equating pressure, inertia, and friction induced torques, a model can be constructed that can be effective. Numerous papers have been published using this basic concept to model for multi-cylinder engines namely (Shiao and Moskwa, 1994), (Lim et al., 1994) and (Larson and Schagetberg, 2004) as well as single cylinder engine models (Mocanu and Taraza, 2013) and (Shadloo et al.,2015). However, these physical models have significant limitations with respect to the inversion of the model as well as inherent problems with calibration. These issues will be examined and discussed in detail as this chapter progresses.

The initial portion of this chapter will examine engine crank kinematics from first principles for the forward model. This section will cover the basic principles of parametric engine models using torque balancing equations and describe both the principles and limitations in induced torque estimations for pressure, inertia, and friction. It will then develop a simplified single cylinder model to demonstrate the relationship between cylinder pressure and crank kinematics. This model will then be translated into a multi-cylinder (3 cylinder) model, using the test engine geometry and data, to develop additional understanding of the complexity of multi-cylinder pressure reconstruction. The chapter will then describe the process of, and difficulties in inverting a physical model to reconstruct cylinder pressure, which is fundamental to this application. The chapter will end by examining engine block acceleration for the forward model and discussing inversion difficulties.

2.2 Theory and Description of Crank Kinematic Forward Models

2.2.1 Principles of Parametric IC Engine Modelling and Torque Balancing Equations

There are two primary modelling approaches to explicitly describe the behaviour of crank kinematics for IC engines. These include the use of the Lagrange approach (Ranjbarkohan et al, 2011) (Weißenborn et al, 2011), and most frequently used, torque balancing (Rizzoni, 1989) (Mocanu and Taraza 2013). The Lagrange approach is based on principles of work and energy. This has advantages and is considered a simpler methodology conceptually, owing to not needing a unified coordinate system in complex assemblies, and it can be applied to wide ranging problems. However, even though the use of the Lagrange equations to model IC engine crank kinematics can be shown to be an equal to the torque balancing approach, the latter is preferred by most researchers. This preference stems from errors otherwise generated through the lumped-mass approximation and the possibility of the final model having inaccuracies. The abstract nature of the final parametric equation has a considerable impact on the understanding of the model, and the significance of key variables. From the torque balancing methods (Rizzoni, 1989), the more basic approach, using Newtonian laws and a common coordinate system, creates a model which clearly makes the model dependencies explicit and gives a better insight into modelling IC engine dynamics.

As stated, torque balancing methods are based on Newton's laws of motion, namely Newton's second and third laws. Newton's second law can be simplified to the sum of all external forces applied to a body equating to the product of the body's mass and its acceleration, shown in equation 2.1.

$$F = ma \tag{2.1}$$

and

$$T = I\alpha = J\ddot{\theta} \tag{2.2}$$

Equation 2.1 is the standard form of Newton's second law for linear motion where F is the force applied to the body, m is mass of the body and a is the acceleration of the body. Equation 2.2 is the application of Newton's second law for rotary motion and is used in constructing the parametric model; where T is the torque applied to the body, J (or I depending on convention) is the mass moment of inertia of the body and α is the angular acceleration of the body ($\ddot{\theta}$ is the second derivative of angular position).

Equation 2.2 is used in conjunction with the Newtonian third law of motion, which states that for every action, there is an equal and opposite reaction to construct the torque balancing equation. The net torque applied to the crankshaft, T_e, is equal to the sum of all the independent torques which are applied to the crankshaft, i.e.:

$$\sum T = J\ddot{\theta} \tag{2.3}$$

where

$$\sum T = \quad T_e \; = T_i + T_r + T_f + T_L + T_o \tag{2.4}$$

Each torque term on the left-hand-side of equation 2.4 represents a parameter that directly impacts on the dynamic behaviour of the engine crankshaft. The definition of each torque is as follows: T_i is the indicated torque or gas pressure torque, T_r is the reciprocating torque, T_f is the torque generated by friction and losses, T_L is the load torque. T_o is the torque generated by other effects, discussed in greater detail in Section 2.2.4. This includes valvetrain and auxiliary components, dependent on engine age and configuration, plus the oil, water, and air conditioning pumps, alternators, superchargers and other hydraulic systems. When considering these

applied torques with respect to the general form of the torque balancing equation, equation 2.3, it can be seen that the net torque applied is equal to the product of the moment of inertia of the engine J, and the angular acceleration $\ddot{\theta}$. The final forward model for determining crankshaft behaviour and the inverse model for reconstructing cylinder pressure, will be discussed later in the chapter. It is useful to briefly show the general form of each of these models alongside the description of the torque balancing equation.

$$\ddot{\theta} = \frac{T_e}{J} \tag{2.5}$$

$$T_i = J\ddot{\theta} - \left(T_r + T_f + T_L + T_o\right) \tag{2.6}$$

Equation 2.5 is the general form for the forward model using the net torques and engine inertia to generate the kinematic behaviour, whereas equation 2.6 presents the required structure for inverting the crankshaft kinematics and gives an indication of the key parameters required to reconstruct cylinder pressure.

One key aspect to make clear at this point, is that all modelling undertaken with respect to crankshaft kinematics will only be considering vertical loading on the piston crown, assuming negligible side thrust. This was considered appropriate owing to the engine geometry, to be discussed in chapter 4, and also because the impact of this on the crankshaft kinematics is more closely related to friction, than gas pressure, or reciprocating torque, and can therefore be considered together.

2.2.2 Gas Pressure Induced Torque

The torque generated by in-cylinder gas pressure variations is conceptually quite simple, i.e. based on the use of a crank-slider mechanism. The gas within the cylinder exerts a force onto the piston crown and rings, in proportion to the in-cylinder pressure, either a result from compression or the combustion. This force is transmitted through the connecting rod and to the crankshaft generating a torque relative to the gas pressure. However, as mentioned in the introduction, reconstructing gas pressure is a highly complex process with numerous variables. As a result, there are several key principles and effects that need to be mentioned which relate to this crank-slider mechanism and the gas pressure. These relate to, and are better described alongside, the theory.

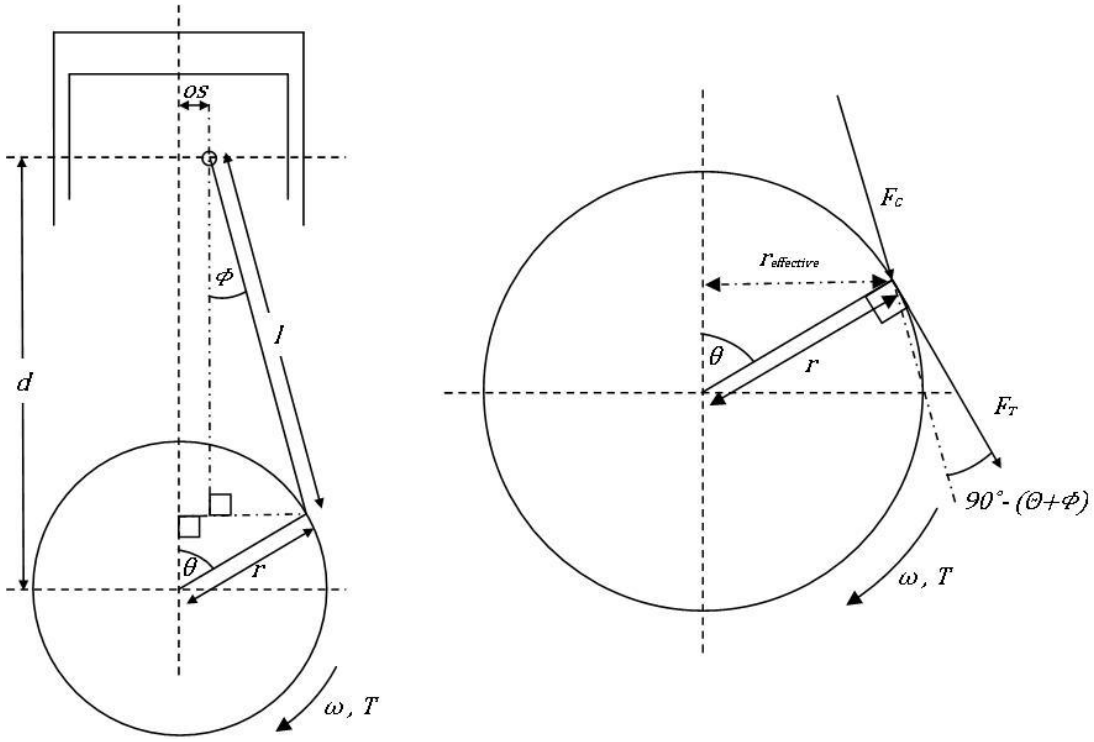

Figure 2.1: Diagram of Crank-Slider Mechanism for Gas Pressure Torque Calculations (left) and Effective Crank Radius and Resolution (right)

The most straightforward of these is the geometry of the crank-slider mechanism, shown in Figure 2.1. Although the geometry is simple, piston offset has a significant effect on the gas pressure induced torque. The primary motivation for using a significant amount of piston offset is in respect to NVH; however, piston offset plays a significant role when understanding the relationship between cylinder pressure and crank kinematics. The offset of the small end bearing, relative to the centreline of the cylinder, has a considerable effect on the torque, effectively shifting its phase. This is also closely related to another key principle, namely resolution, which will be described alongside offset. Resolution relates to the effect of the gas pressure torque on the crankshaft as the shaft rotates. The term effective radius, which will be used throughout the thesis, is defined as the horizontal component of the crank pin motion, shown in Figure 2.1. As the crankshaft rotates, the effective radius of the crank varies, varying the gas pressure torque with respect to the crank angle, θ, also shown in Figure 2.1. This torque variation has a considerable impact on the transmission of the gas pressure force when the piston moves through TDC and BDC. This effect can be clearly demonstrated in equation (2.16) which describes resolved crank force F_T. In the regions that crank angle approaches 0/180/360 degrees, the gas pressure induced force reduces to zero. Understanding the

principle of how the gas pressure induced force and as a result torque is crank angle dependent is important in the modelling of the crank kinematics. It is especially important later in the thesis when considering the inverse kinematics.

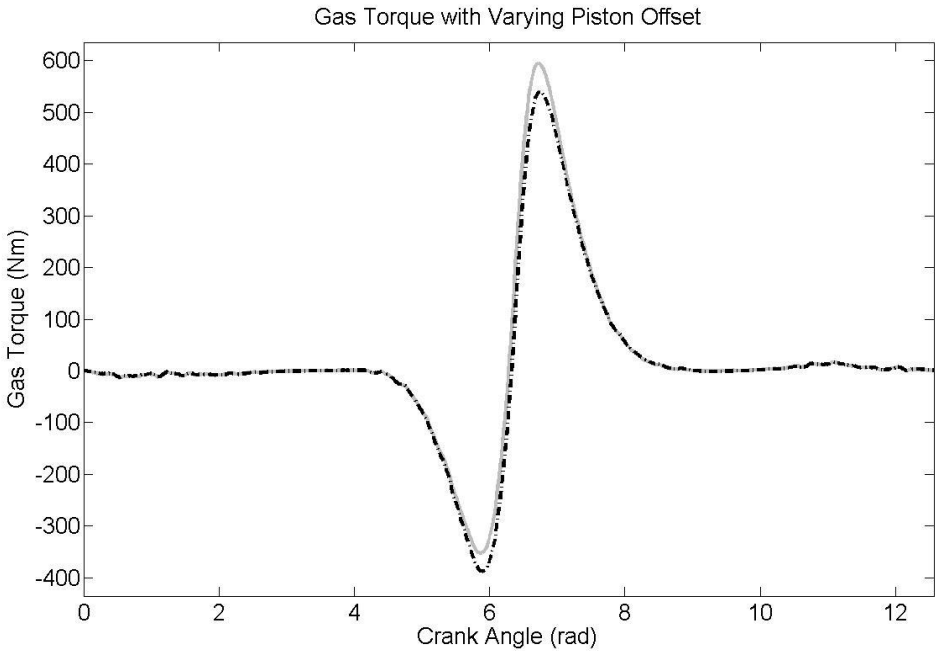

Figure 2.2: Piston Offset Comparison at Top Dead Centre. (Solid grey line - zero piston offset. Dashed black line - 0.01 m piston offset.)

To further explain the relationship between the piston offset and resolution, it is necessary to consider two situations: one with zero piston offset, and one with substantial piston offset. If an engine has zero piston offset, assuming the peak pressure within the cylinder occurs at or near TDC, the resultant torque is massively compromised. This would be caused by the effective crank radius reducing to zero, resulting in a negligible transfer of energy from the combustion gases to the crankshaft and a loss of information relating to the maximum pressure. However, this effect is not limited to TDC, it also has a significant impact for a period immediately before and after TDC owing to the relationship to the crank angle, Figure 2.1. In contrast, if an engine has a considerable piston offset, again assuming the peak pressure within the cylinder occurs at or near TDC, the resultant torque is less compromised in comparison. This is a result of the effective radius at TDC, shown in Figure 2.2. It can be seen that with significant piston offset, TDC occurs later in the cycle, effectively shifting its phase, resulting in the crank angle being larger than zero at TDC. This delayed TDC, relative to having zero piston offset, also delays the occurrence of the ignition and as a result peak pressure within the

cycle. This delay produces a small effective crank radius, generating gas pressure related torque and imparting information relating to the maximum pressure to the cranktrain.

Another important principle to identify is the domain used to describe the gas pressure torque i.e. whether time, or crank angle domain. The gas pressure torque, T_i, and the crank angle, θ will shortly be demonstrated. However, the gas pressure described in the introduction, is also obviously related to the gas pressure torque, and is predominantly best described within the time domain. Examples of this include the in-cylinder air motion, the fuel injection durations, the fuel burn rate and combustion related pressure rise. Consequently, the gas pressure torque is in a combination of both time and crank angle domain. Again, the importance of this is not evident at this stage but the effects of this will be examined fully.

With respect to modelling the gas pressure induced torque, the starting point is at the interaction between the cylinder gases and the piston ring pack (piston and piston rings). This interaction is central to the function and effectiveness of the IC engine. This can be described using a simple relationship of force on the piston ring pack (gas pressure force, F_G) with the gas pressure, P_G, and cylinder area, A_C, are given by:

$$F_G = P_G A_C \tag{2.7}$$

and

$$F_G = P_G \pi \frac{b^2}{4} \tag{2.8}$$

Where the cylinder area can be expressed in terms of the cylinder bore, b.

This section concentrates on examining the transfer of the piston force to the crankshaft via the connecting rod. Figure 2.1 is the representation of the crank-slider mechanism that is used in the construction of the model and defines the most important variables. These variables include: θ, the angle between the crankshaft and vertical plane, φ the angle between the connecting rod and vertical plane, r the radius of the crank, l the length of the connecting rod, and os the piston offset. Other important definitions also include F_C and F_T which are the forces acting on the crank and the tangential force acting on the crankshaft. These use trigonometric identities

to expand and simplify a relationship between the motion of the crankshaft and the connecting rod. Using Figure 2.1, the kinematic equation associated with crank pin is:

$$\mathrm{r}\sin\theta = l\sin\varphi + os \tag{2.9}$$

and

$$\sin\varphi = \frac{\mathrm{r}\sin\theta}{l} - \frac{os}{l} \tag{2.10}$$

then

$$\cos\varphi = \sqrt{1 - \left(\frac{\mathrm{r}\sin\theta}{l} - \frac{os}{l}\right)^2} \tag{2.11}$$

and

$$\cos\varphi = \sqrt{1 - \frac{\mathrm{r}^2}{l^2}\sin^2\theta + 2\frac{\mathrm{r}}{l}os\sin\theta + \frac{os^2}{l^2}} \tag{2.12}$$

This trigonometric relationship can be used to find the vertical force acting on the crank. The crank pin force is given by:

$$F_C = \frac{F_G}{\cos\Phi} \tag{2.13}$$

and using equation (2..12) is:

$$F_C = \frac{P_G\pi\frac{b^2}{4}}{\sqrt{1 - \frac{\mathrm{r}^2}{l^2}\sin^2\theta + 2\frac{\mathrm{r}}{l}os\sin\theta + \frac{os^2}{l^2}}} \tag{2.14}$$

This resolved crank force F_T is given by:

$$F_T = F_C\cos\big(90 - (\theta + \varphi)\big) \tag{2.15}$$

or

$$F_T = F_C\sin(\theta + \varphi) \tag{2.16}$$

or

$$F_T = \frac{F_G}{\cos\Phi}(\sin\varphi\cos\theta + \sin\theta\cos\varphi) \tag{2.17}$$

which expands to :

$$= \frac{P_G \pi \frac{b^2}{4}\left(\cos\theta\left(\frac{\mathrm{r}\sin\theta}{l} - \frac{os}{l}\right) + \sin\theta\left(\sqrt{1 - \frac{\mathrm{r}^2}{l^2}\sin^2\theta + 2\frac{\mathrm{r}}{l}os\sin\theta + \frac{os^2}{l^2}}\right)\right)}{\sqrt{1 - \frac{\mathrm{r}^2}{l^2}\sin^2\theta + 2\frac{\mathrm{r}}{l}os\sin\theta + \frac{os^2}{l^2}}} \tag{2.18}$$

or

$$= P_G \pi \frac{b^2}{4}\left(\frac{\cos\theta\left(\frac{\mathrm{r}\sin\theta}{l} - \frac{os}{l}\right)}{\sqrt{1 - \frac{\mathrm{r}^2}{l^2}\sin^2\theta + 2\frac{\mathrm{r}}{l}os\sin\theta + \frac{os^2}{l^2}}} + \sin\theta\right) \tag{2.19}$$

The resolution of the tangential crankshaft force F_T, from the crank force, equation (2.15), can be produced using the illustration in Figure 2.1. Equations (2.17) to (2.19) show the expansion and simplification of equation (2.16) to produce an equation which relates the tangential force to cylinder pressure, engine geometry and crank angle.

The final solution of the gas pressure induced torque is:

$$T_i = r\, P_G \pi \frac{b^2}{4}\left(\frac{\cos\theta\left(\frac{\mathrm{r}\sin\theta}{l} - \frac{os}{l}\right)}{\sqrt{1 - \frac{\mathrm{r}^2}{l^2}\sin^2\theta + 2\frac{\mathrm{r}}{l}os\sin\theta + \frac{os^2}{l^2}}} + \sin\theta\right) \tag{2.20}$$

This is formed by the multiplication of the tangential crankshaft force and the crank radius. This solution is more complex than others (Bennett, 2014) as it includes the piston offset which has been shown to have a significant impact on the gas pressure torque.

Figure 2.3 is a worked example of the gas pressure induced torque calculation. This was undertaken using the engine geometry and data used in this thesis, a 4-stock I3 gasoline engine (see Chapter 4). This was calculated from a test condition at 1000 rpm and 10 Nm. The figure shows both the gas pressure torque for Cylinder-1 and the combined gas pressure torque from all three cylinders.

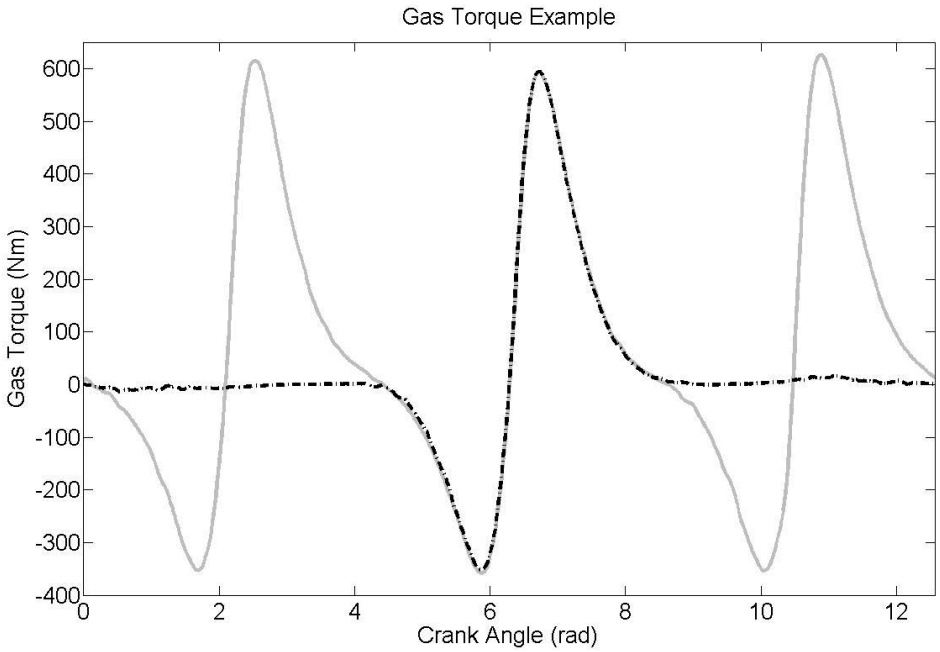

Figure 2.3: Gas Pressure Torque for Cylinder 1 (black dashed line) and Combined Gas Pressure Torque for Three Cylinders (grey solid line).

2.2.3 Reciprocating Inertia Forces and Torque

The reciprocating inertia forces and torque generated by the piston ring pack and the connecting rod, behave in a similar way to the gas pressure torque in that they are periodic, with primary variables including crank angle and engine geometry. The key difference is the increased frequency. Owing to the relationship between the frequency of the combustion and engine speed, the frequency of the reciprocating inertial forces are double that of the combustion frequency. These forces are generated through the cyclic vertical motion of the piston ring pack and the connecting rods, which results in reciprocating inertia torques. This acceleration is produced by the sinusoidal motion of the piston assembly, where the vertical component of the speed at TDC and BDC reduces to zero and at its maximum mid-stroke. Another significant variable, which ties in closely with the acceleration, is the engine speed. Higher engine speeds generate greater acceleration of the piston assembly at TDC and BDC.

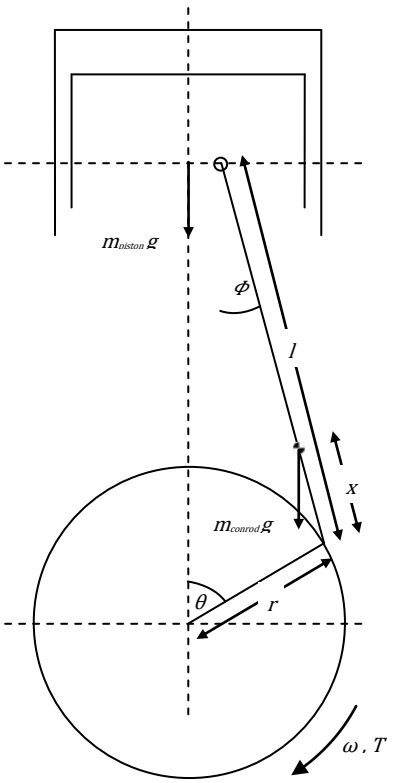

Figure 2.4: Diagram of Crank-Slider Mechanism for Reciprocating Inertia Forces and Torque Calculations

The approach to the reciprocating inertia calculations is initially similar to the gas pressure torque calculations. The basic equations are formed using Figure 2.4 and straightforward trigonometric relationships. These equations are then differentiated twice with respect to the crank angle to generate the acceleration. This is then used in combination with Newton's second law and resolved for the tangential force. The reciprocating inertia torque can then be found. This approach will be demonstrated separately for both the piston ring pack and the connecting rod.

Piston Ring Pack Inertial Torque

The vertical displacement of the piston ring pack is given by:

$$d = \mathrm{r}\cos\theta + l\cos\Phi \tag{2.21}$$

and using equations (2.10) and (2.11):

$$d_{Piston} = \mathrm{r}\cos\theta + l\sqrt{1 - \left(\frac{r\sin\theta}{l} - \frac{\mathrm{os}}{l}\right)^2} \tag{2.22}$$

Equations (2.21) and (2.22) are the equations found through resolving the vertical displacement, d_{Piston} , of the piston relative to the crank axis. The vertical displacement of the piston was then differentiated twice. The first derivative was found through standard techniques. However, owing to the complexity of the second differential, this derivative was computed using the MatLab symbolic calculator MuPAD:

$$\dot{d}_{\,Piston} = \quad \omega \left(\frac{\mathrm{r}\cos\theta\left(\frac{\mathrm{os}}{l} - \frac{r\sin\theta}{l}\right)}{\sqrt{1 - \left(\frac{\mathrm{os}}{l} - \frac{r\sin\theta}{l}\right)^2}} - \mathrm{r}\ \sin\theta \right) \tag{2.23}$$

$$\ddot{d}_{Piston} = -r\omega^2 \left(\cos\theta + \frac{\mathrm{r}\cos^2\theta\left(\frac{\mathrm{os}}{l} - \frac{r\sin\theta}{l}\right)^2}{l\left(1 - \left(\frac{\mathrm{os}}{l} - \frac{r\sin\theta}{l}\right)^2\right)^{3/2}} + \frac{\sin\theta(\mathrm{os} - r\sin\theta) - \mathrm{r}\cos^2\theta}{l\left(1 - \left(\frac{\mathrm{os}}{l} - \frac{r\sin\theta}{l}\right)^2\right)^{1/2}} \right) \tag{2.24}$$

Equation (2.23) is the first differential of piston displacement, piston velocity $\dot{d}_{\,Piston}$, and equation (2.24) is the second differential of piston displacement, piston acceleration, $\ddot{d}_{Piston}$.

Using Newton's second law and including the gravitational force of the piston ring pack, the force exerted through the crankshaft, F_c, can be found. This force can be resolved for the tangential crankshaft, F_T, force using Figure 2.1.

$$F_c = m_{Piston} \cdot \ddot{d}_{Piston} \ - \ m_{Piston} \cdot g \tag{2.25}$$

and

$$F_T = F_C \sin(\theta + \varphi) \tag{2.26}$$

where

$$T_{r-p} = r\left(\frac{\cos\theta\left(\frac{\mathrm{r}\sin\theta}{l} - \frac{os}{l}\right)}{\sqrt{1-\left(\frac{\mathrm{os}}{l} - \frac{r\sin\theta}{l}\right)^2}} + \sin\theta\right) \cdot \left[m_{Piston} r\omega^2 \left(-\cos\theta - \frac{\mathrm{r}\cos^2\theta\left(\frac{\mathrm{os}}{l} - \frac{r\sin\theta}{l}\right)^2}{l\left(1-\left(\frac{\mathrm{os}}{l} - \frac{r\sin\theta}{l}\right)^2\right)^{3/2}} - \frac{\sin\theta(\mathrm{os} - r\sin\theta) - \mathrm{r}\cos^2\theta}{l\left(1-\left(\frac{\mathrm{os}}{l} - \frac{r\sin\theta}{l}\right)^2\right)^{1/2}}\right) + m_{Piston}\cdot g\right] \quad (2.27)$$

Equations (2.25) to (2.27) show the development of the final solution for the reciprocating inertial torque generated by the piston ring pack, T_{r-p}.

Connecting Rod Inertial Torque

The vertical displacement of the connecting rod centre of gravity is given by:

$$d_{Conrod} = \mathrm{r}\cos\theta + x\cos\Phi \quad (2.28)$$

The connecting rod reciprocating inertial torque is found using the same approach as the piston ring pack inertia. Again, the basic equations are formed using Figure 2.4 and straightforward trigonometric relationships, equation (2.28). The structure of equation (2.28) closely resembles that of equation (2.21), apart from the use of x in place of l, where x is the distance between the crank axis and the connecting rod's centre of gravity. The detailed development of the connecting rod reciprocating inertial torque will not be provided in this section, see appendix A. This is owing to the similarities between the initial equation and the use of the same approach: finding the second differential of the connecting rod's centre of gravity vertical displacement, using Newton's second law, resolving for the tangential force and then the reciprocating inertial torque, T_{r-c}.

$$T_{r-c} = r\left(\frac{\cos\theta\left(\frac{\mathrm{r}\sin\theta}{l} - \frac{os}{l}\right)}{\sqrt{1-\left(\frac{\mathrm{os}}{l} - \frac{r\sin\theta}{l}\right)^2}} + \sin\theta\right) \cdot \left[m_{Conrod} r\omega^2 \left(-\cos\theta - \frac{\mathrm{x\,r}\cos^2\theta\left(\frac{\mathrm{os}}{l} - \frac{r\sin\theta}{l}\right)^2}{l^2\left(1-\left(\frac{\mathrm{os}}{l} - \frac{r\sin\theta}{l}\right)^2\right)^{3/2}} - \frac{x\sin\theta(\mathrm{os} - r\sin\theta) - \mathrm{r}\cos^2\theta}{l^2\left(1-\left(\frac{\mathrm{os}}{l} - \frac{r\sin\theta}{l}\right)^2\right)^{1/2}}\right) + m_{Conrod}\cdot g\right] \quad (2.29)$$

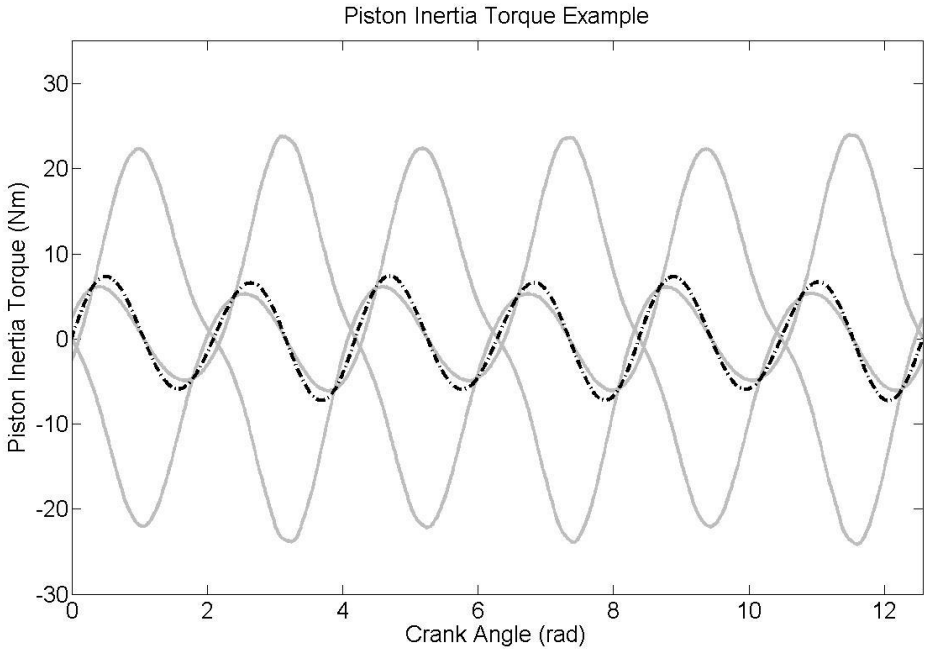

Figure 2.5: Combined Piston Inertia Torque (black dashed line) and Piston Inertia Torque for Three Cylinders (grey solid lines).

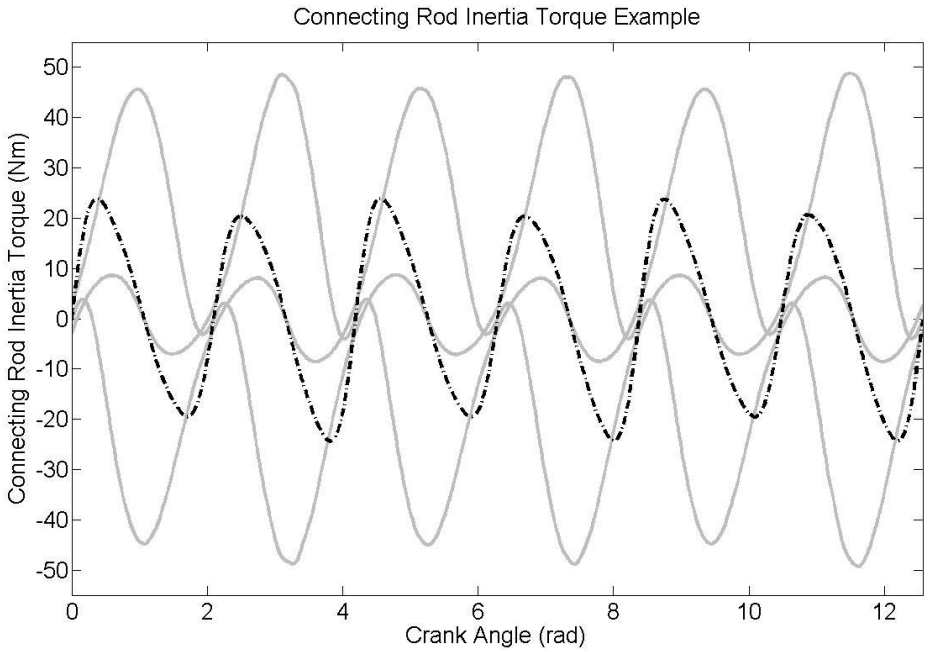

Figure 2.6: Combined Connecting Rod Inertia Torque (black dashed line) and Connecting Rod Inertia Torque for Three Cylinders (grey solid lines).

Figure 2.5 and 2.6, are worked examples of both the piston ring pack and connecting rod reciprocating inertial torque calculation. This was undertaken using the same engine geometry and data used within section 2.2.2. Figure 2.5 shows the combined piston inertia as well as the individual piston inertias. Figure 2.6 shows the combined connecting rod inertia as well as the connecting rod inertia for all three cylinders individually.

Giving the equations in this form brings forward one important characteristic of the particular engine: the connecting rod inertial torque is significantly larger than the piston inertia. This was not anticipated, but an explanation for this can be described with respect to equation (2.29) and the description of the engine in Chapter 4. Firstly, the mass of the connecting rod is significantly larger than the piston, ≈1.5 times greater. The second reason is the ratio of the crank radius to the length of the connecting rod, r/l. However, in equation (2.27), the connecting rod length, l, term is replaced by the connecting rod centre of gravity position x. As a result of x being a fraction of l, the r/x ratio causes the connecting rod inertia torque to be greater than the piston inertia torque.

2.2.4 Friction Torque and Other Losses

This section is divided into two distinct areas. The first is concerned with the engine friction, and the second focuses on the issue of additional mechanical losses that would impact on the modelling of the crank kinematics. The following will be used as reference, but will not be used in the single or multi-cylinder models owing to the complexity and because it relates to specific engine units.

Engine friction is one of the most complex areas in IC engine development especially within the field of engine modelling. IC engine friction losses also account for up to 5% of total engine power. Figure 2.7, shows a breakdown of the losses in a typical engine. This section will cover the fundamentals and basic calculation methods for the key sources of friction.

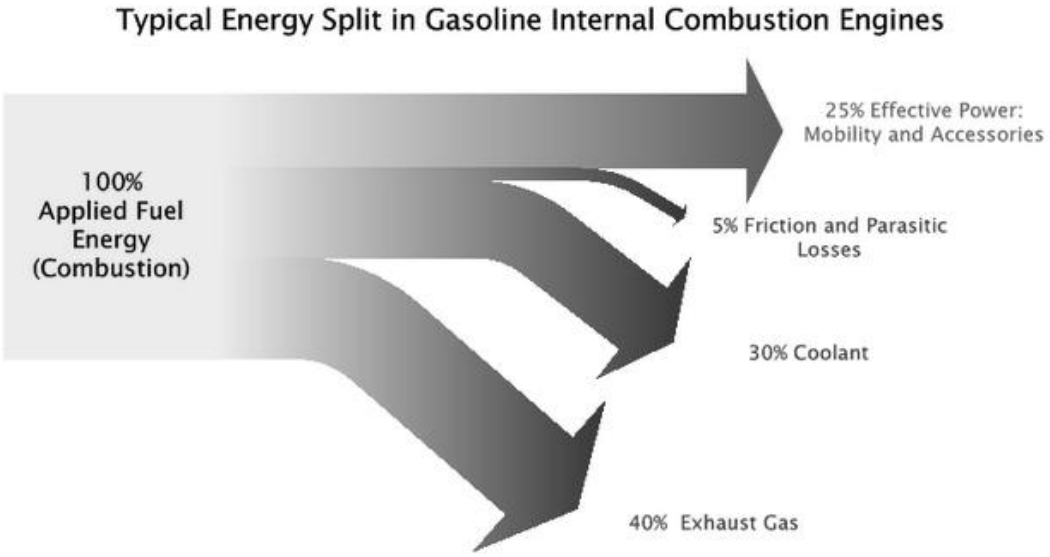

Figure 2.7: Energy Dispersion within a Typical IC Engine (IC Engine Energy, 2005)

There are numerous sources of friction in an IC engine. The largest of these include the piston rings and skirt, the big end bearing and main journal bearings. Other less important examples include the small end bearing, the camshaft and auxiliaries. A list of auxiliaries is contained later in the section. Each of these sources of friction will be described in turn.

With respect to the friction, the piston rings and skirt are the most complex components to model. There are many variables that impact on the piston rings,

skirt operation, and friction. These can include engine speed and load, magnitude of piston slap, tolerances, oil type and condition, engine wear and temperature.

The simplest approach to friction prediction is through a thermodynamic approach, using Newton's law of viscosity. An example of this approach is given in (Abu-Nada et al.,2008). Where Abu-Nada *et al* state that piston friction work, in the combustion chamber, consists of two major parts, i.e. the skirt friction and pressure ring friction. The irreversible friction work can be expressed in terms of piston speed, the skirt clearance, the clearance between the liner and the pressure ring, the oil dynamic viscosity, and the distance from top dead centre.

Examples of friction modelling methods with increased complexity include (Sutaria et al. 2009) and (Bedajangam et al., 2013). Figure 2.8 gives the friction force variation of the piston rings and piston skirt though one cycle for a single cylinder.

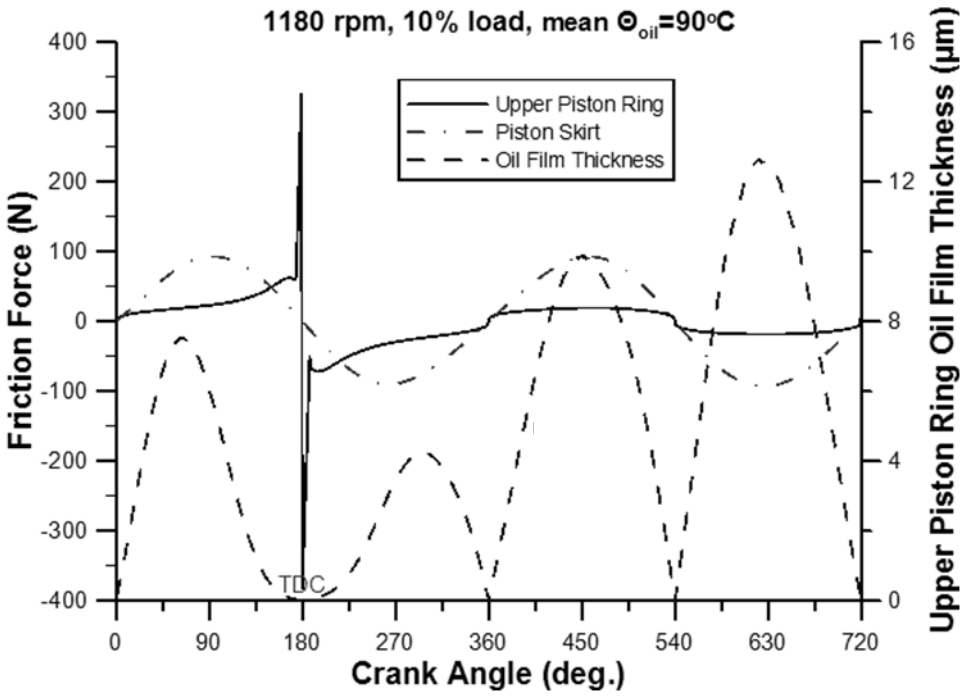

Figure 2.8: Variation of Upper Piston Ring Friction Force and Oil Film Thickness during an Engine Cycle (Rakopoulos et al, 2007)

The next four main sources of dampling all behave similarly as they are located in the journal bearing; the main journal bearings, the camshaft bearing and the big and small end bearings. Journal bearings (or plain bearings) consist of a shaft or journal which rotates in a supporting metal sleeve or shell. These are used over other

bearing types in IC engines owing to the distribution of the applied load over a relatively wide area, where the load is cyclical as a result of varying gas pressure. The bearings liable to be under the greatest loads are the main journal bearings, the big and small end bearings, as they directly transfer the varying gas pressure load. However, the load on the camshaft bearings still varies cyclically but is more predictable with respect to engine speed.

Journal bearings may produce better distributed load than other types but friction in the bearing is significantly dependent on the surface roughness. Therefore, lubricants are used to substantially reduce the friction. Hydrodynamic lubrication, shown in Figure 2.9 and 2.10, results from high rotation speed and relatively low load, generating a thin film of lubricant *h*, greater than the surface roughness *Ra*. However, the variation in the loads on the bearings involved, can result in various regimes of lubrication occurring, including boundary (*h*>*Ra*), mixed (*h*≈*Ra*) and hydrodynamic lubrication (h<Ra). Varying lubrication regimes, not only cycle-to-cycle but also varying within a cycle, is a source of complication for modelling journal friction in IC engines.

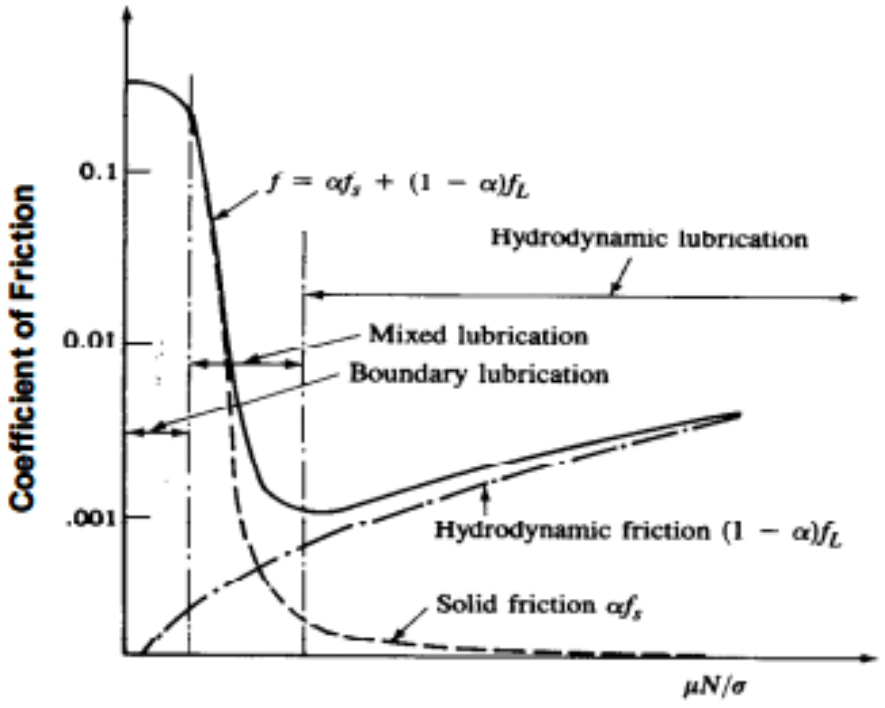

Figure 2.9: Stribeck Diagram for Journal Bearing (Haywood, 2010)

The Stribeck diagram, Figure 2.9, shows the lubrication regimes where the coefficient of friction f, for a journal bearing is plotted against a dimensionless duty parameter $\mu N/\sigma$, where μ is the dynamic velocity of the lubricant, N is the rotational

speed, and σ is the loading force per unit area (Haywood, 2010). The coefficient of friction can be expressed as:

$$f = \alpha f_s + (1 - \alpha) f_L \tag{2.30}$$

where f_s is the metal-to-metal coefficient of dry friction, f_L is the hydrodynamic coefficient of friction and α is the metal-to-metal contact constant, varying between 0 and 1.

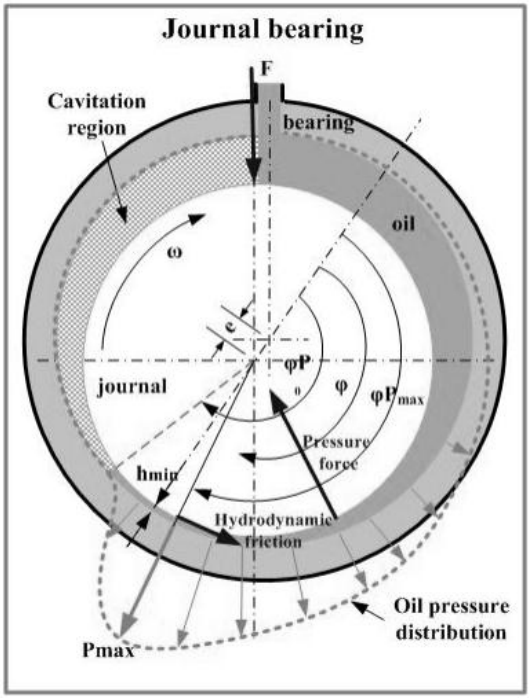

Figure 2.10: Hydrodynamic Journal Bearing (Kopeliovich, [no date])

Below is a summary of the variables that may cause a reduction in the oil film thickness causing direct contact between the bearing and journal surfaces (Kopeliovich, n.d.) and need to be considered when modelling.

- oil starvation, high loads;
- low rotation speed;
- low viscosity oil;
- elevated temperature additionally decreasing the oil viscosity;
- roughness of the bearing and shaft surfaces;
- oil contaminants;
- geometrical distortions and misalignments.

Another consideration needed when modelling the friction of journal bearings within IC engines is its variation with respect to time. All journal bearings are at risk of wear, which could either increase or decrease relative friction levels, and the formation of cavities through cavitation, which would impact surface roughness negatively.

To demonstrate the complexity of fiction models, a series of equations (Kamil *et al*.,2013) are explained fully in Appendix A. These are equations for the calculating the friction mean effective pressure (FMEP) for the crankshaft, the reciprocating and the valvetrain friction.

The large numbers of variables that affect both the piston ring pack and journal bearing friction levels, alongside the friction generated by the numerous auxiliary components attached, leads to the modelling becoming extremely complex. Within this thesis, the task of accurately modelling the I3 would be large, unnecessary and will not be undertaken. However, use of parametric equations to model either engine kinematics or inverse torque models to reconstruct cylinder pressure; the friction plays a considerable part. Therefore, it would be necessary to generate a comprehensive model for T_f containing as many of the variables, outlined above, containing the ability to adapt to wear and manufacturing tolerances.

In addition to friction losses in IC engines, there are noteworthy energy losses from internal operations such as pump and camshaft load, and from auxiliary devices necessary for engine operation, such as hydraulic, electricity harvesting and air conditioning. Pumping losses are generated by the piston drawing in and expelling gases within the cylinder during the inlet and exhaust strokes. Camshaft torque comes from the force required to open valves, from inertia and from transmission of power (belt or chain). There are numerous hydraulic systems in an automobile that draw energy. These include the oil and water pump, steering, and braking systems.

2.2.5 Engine Inertia Calculations Including Consideration of the Dynamometer and Engine Couple

The previous three sections have focused on the different torques generated and lost through the engine, with respect to equation (2.3) and (2.4). These torques have been shown to be straight forward to calculate of an ideal engine, as are the mass moment of inertia of an ideal engine even with complex geometries i.e. the

crankshaft. However, difficulties arise when calculating the torque and the inertias for real engines with production defects, tolerance issues and wear. These would only be able to be determined accurately through experimentation which is not possible with the final application; production vehicles.

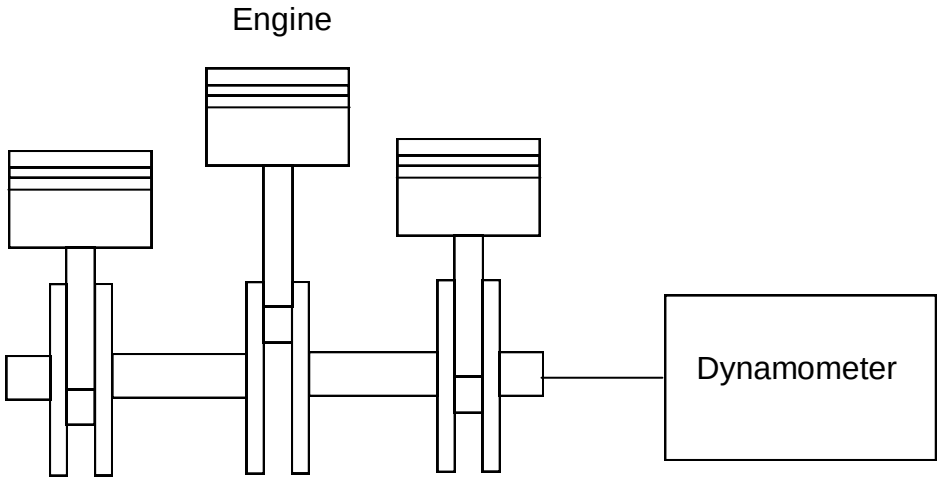

Figure 2.11: Illustration of I3 Engine Including Dynamometer

Fortunately, the exact values for the crankshaft, flywheel and dynamometer inertia are known for the I3 DISI engine used in this research. The known values for the crankshaft and flywheel are 0.02579 kgm^2 and 0.12021 kgm^2. However, to be thorough and to demonstrate the effort required to find the inertia of a crankshaft for the single cylinder model, the basic equations are set out in appendix A. The work into determining moments of inertia with complex shapes was undertaken by Hajderi and Hajdari and is the basis for the following equations (Hajderi and Hajdari, 2012).

So far this chapter has only considered 1 degree of freedom models. The extension to a 2 degree of freedom model is conceptually simple as can be seen in equation (2.31) and (2.32). It is the same basic form used in equation (2.3) and (2.4). However, it also contains two additional terms, T_K for the torque losses from the couple stiffness and T_D for the torque losses from the couple damping.

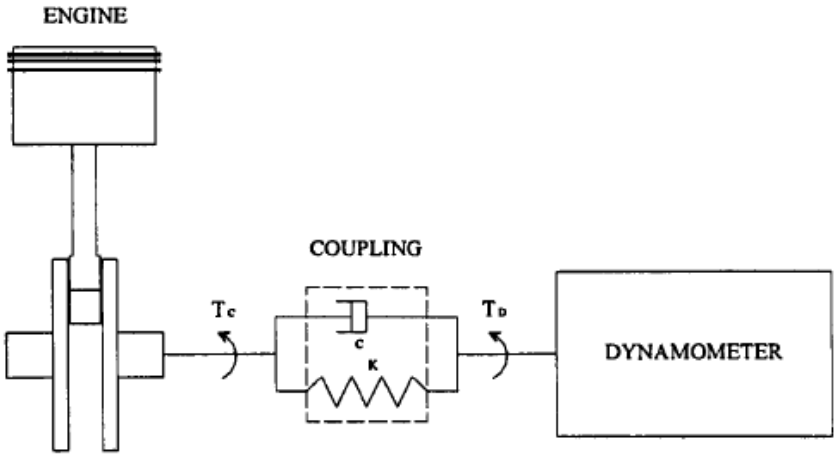

Figure 2.13: Illustration of a 1-Cylinder engine coupled to a dynamometer 2-DOF model (Potenza, 2006)

Simple 2 degree of freedom single cylinder engine model:

$$J_{Engine}\ddot{\theta}_{Engine} = T_i + T_r + T_f + T_L + T_o + T_K + T_D \qquad (2.31)$$

$$J_{Dyno}\ddot{\theta}_{Dyno} = T_f + T_L - T_K - T_D \qquad (2.32)$$

Where the T subscript i represents is the indicated torque, r the reciprocating torque, f the friction, l the dynamometer load, o other losses, K the stiffness of the coupling and D the damping of the coupling. As a result of the difficult in isolate all of these values for the I3 engine, they will not be included in the single cylinder or multi-cylinder models.

2.3 Single Cylinder and Multi-Cylinder Model

The construction of the single cylinder equations was undertaken for a 1- degree-of-freedom (DOF) model, assuming no torque losses as a result of friction or auxiliary components and a solid coupling between the engine and the dynamometer.

$$\alpha = \ddot{\theta} = \frac{T_i + T_r + T_L}{J} \qquad (2.33)$$

The model takes the general form of equation (2. 33). The complete 1 DOF frictionless model is presented in appendix A. Figure 2.14 shows the theoretical acceleration for the single cylinder engine model. The cylinder pressure and

dimensions used in this example were taken from the I3 engine geometry. Where necessary, the values were adjusted to match the single cylinder example, namely crankshaft inertia. This model was not created for accurately modelling crankshaft acceleration or to reconstruct cylinder pressure, using parametric models. Its primary use was to formulate a sound understanding of engine dynamics. This included understanding the factors that influence the cylinder pressure / crankshaft kinematic relationship, as well as highlighting fundamental characteristics of IC engines that may limit the cylinder pressure reconstruction potential.

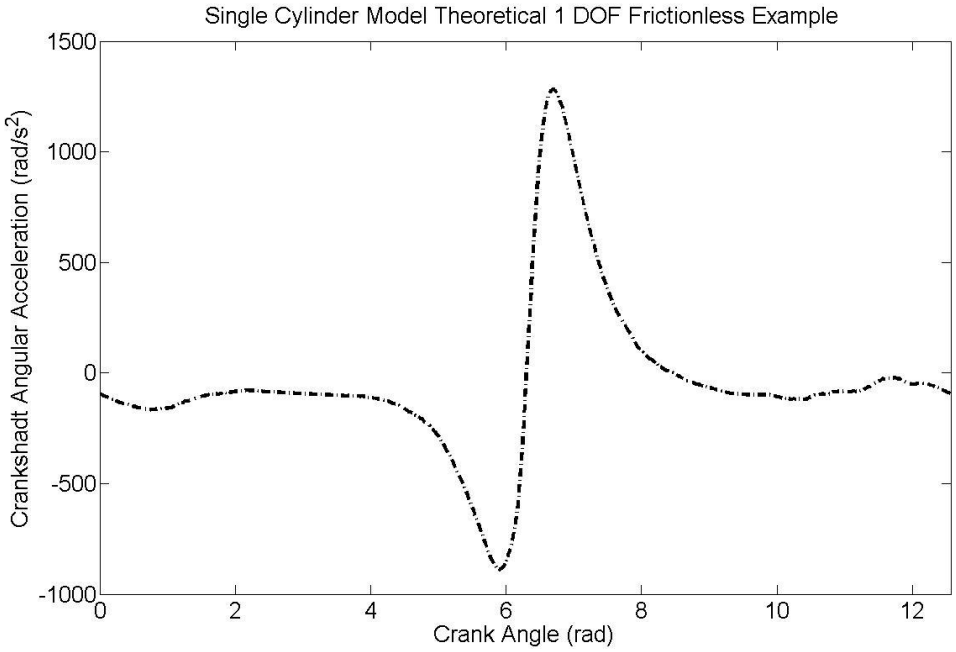

Figure 2.14: Single Cylinder Model Theoretical 1 DOF Frictionless Example

The development of the multi-cylinder equations, 3 cylinders in this example, was undertaken again for a 1 degree of freedom (DOF) model, with the same assumptions: no friction or auxiliary components and a solid coupling. Similar to the single cylinder model, this three cylinder model also helped formulate a sound understanding of the engine dynamics. However, the three cylinder model had additional benefits. The three cylinder model helped realise the connection between the cylinders and the cross over points with regards to individual cylinder dominance. The three cylinder model also helped in formulating key strategies and will be used throughout this thesis, including the concatenation of the pressure data (Section 2.5) and the training approaches (Chapter 5).

The single cylinder model used the gas pressure torque, reciprocating piston and connecting rod torques and moment of inertia, in phase with a single crankshaft angle. With the three cylinder model, these torques will be considered for each cylinder with independent gas pressures and phased correctly. The three cylinder model takes the general form;

$$\alpha = \ddot{\theta} = \frac{\sum_{n=1}^{3}(T_{in} + T_{rn}) + T_L}{J} \tag{2.34}$$

where torques for each cylinder is incorporated. The complete three cylinder 1 DOF frictionless model is also presented in appendix A.

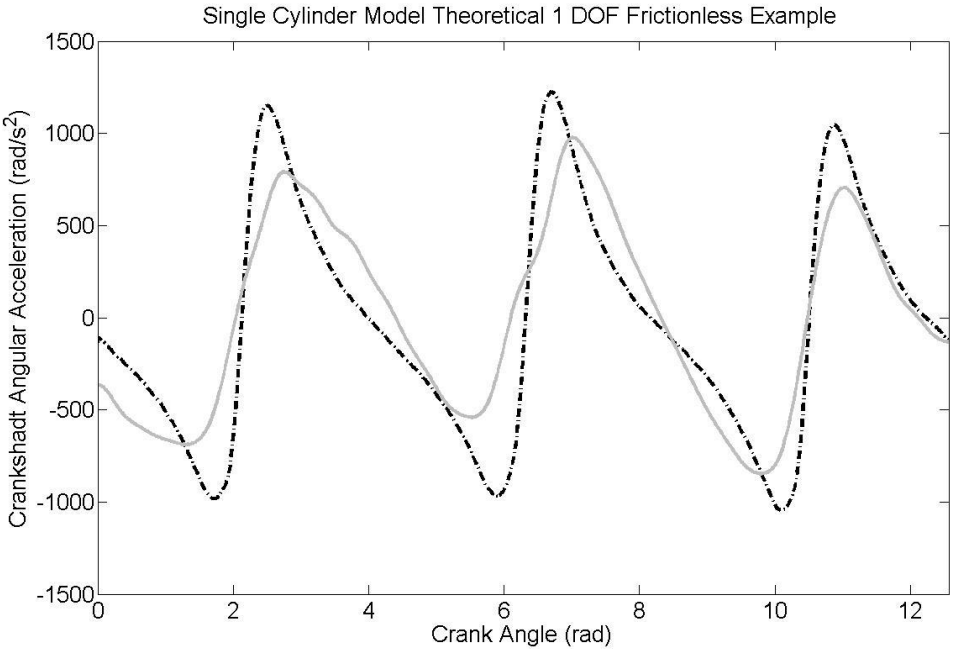

Figure 2.15: Three Cylinder Model Theoretical 1 DOF Frictionless Example (Dashed black) and Measured Three Cylinder Acceleration (Solid grey)

Figure 2.15 shows a theoretical prediction of the acceleration from the three cylinder engine model alongside the I3 engine measured results previously obtained by Bennett (Bennett, 2014) . Even though there is some agreement with regards to the phasing and the relative position of the three peaks in each, the differences are notable. These differences include reduced maximum and minimum values, more irregular profiles and the accelerations are more distributed in the measured data compared to the larger localised accelerations in the model. This was expected owing to the assumptions of no friction or auxiliary components and a solid coupling,

but as stated, the aim of this thesis was not to accurately model crankshaft acceleration parametrically. The modelling of the friction and other complex non-linear aspects will be undertaken within the non-parametric models selected later in the thesis.

2.4 Theoretical Inverse Kinematic Modelling and Inherent Complexities

The primary aim of this thesis is to reconstruct cylinder pressure through the inverse torque modelling of the crankshaft kinematics and engine block acceleration. The forward models presented in this chapter are useful to demonstrate the difficulty and complexity in producing accurate parametric models for crankshaft kinematics. However, there are additional complications in inverting these models.

To demonstrate the most important complication in the inversion of the parametric engine model, a simpler gas pressure related crankshaft kinematics equation was used (2.30), ignoring piston offset and reducing the smaller terms to zero (Bennett, 2014).

$$T_i \approx r\, P_G \pi \frac{b^2}{4} \sin\theta \left(1 + \frac{\mathrm{r}\cos\theta}{l}\right) \tag{2.35}$$

$$P_G \approx \frac{J\ddot{\theta}}{r\pi \frac{b^2}{4} \sin\theta \left(1 + \frac{\mathrm{r}\cos\theta}{l}\right)} \tag{2.36}$$

Equation (2.36) is the inverse of the simplified gas pressure related crankshaft kinematics equation. Both examples of the forward and inverse models are presented in Figure (2.16).

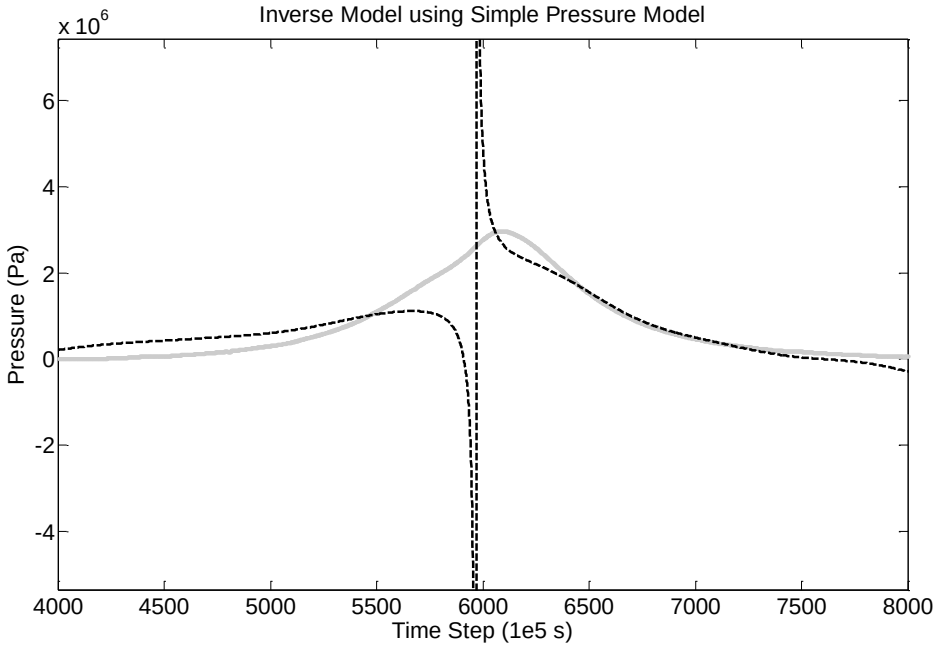

Figure 2.16: Inverse Model using Simple Pressure Torque Model (black dashed line) and Measured Cylinder Pressure (grey solid line).

The reconstructed gas pressure in Figure (2.16) shows an event that is not present in the gas pressure data. Surrounding TDC, the reconstructed gas pressure spikes producing a large error. This spike results from the $1/\sin\theta$ term in the inverse model, equation (2.36). Inverting $\sin\theta$ forms a significant issue for the reconstruction at both TDC and BDC, where crank angle θ is 0˚ and 180˚, the inverse of $\sin\theta$ becomes infinite. This causes problems when reconstructing as these large errors are present four times per cycle for each cylinder. Methods have been created to overcome this problem at TDC for parametric models, e.g. (Chen and Moskwa, 1997) and (Gao and Randall, 1999). These methods show improved capabilities in inverting the model at TDC but still do not adequately correct the reconstructed gas pressure. This is linked to the effective crank radius reducing to zero and a lack of information surrounding TDC. Even though the effective crank radius and the $1/\sin\theta$ term have the greatest impact at TDC, they both have an effect before and after TDC. The magnitude of this impact plays a significant role in the reconstruction performance and will be an important focus of the thesis.

In addition to the inverse of the sine in the gas pressure component of the model, the same issue will arise in other areas which vary sinusoidally. One area where the inverse of the sine term could impact significantly, is within friction modelling. There are other broader areas not taken into consideration in the models presented which

could impact on the inversion. These may include the inversion of the hydraulic systems, inversion of superchargers and other auxiliaries.

The final consideration with regards to parametric models and their inversion is the practical role of noise in the reconstructed pressure. As in all automotive systems, noise can play a considerable role. However, the noise within the context of crankshaft angular acceleration is more critical. As the measurement will be taken with respect to angular position, any noise within the measurements will be magnified when differentiated twice. This increased noise could result in additional high frequencies and unrealistic results within the reconstructed gas pressure, using the parametric models.

Apart from the limitations of inverting the parametric models, one key aspect needing consideration is the application of the inverted model with respect to the gas pressure. The strategy used for the gas pressure is important as it dictates the accuracy of the final model. Within the forward multi-cylinder model, the pressure from each cylinder is used independently to produce a single output, crankshaft angular acceleration. When inverting the model, there is only one key input, the crankshaft angular acceleration, which in principle holds information on the gas pressure in every cylinder. However, there is no way of determining how the pressure from each cylinder impacts the total acceleration when considering the inverse model. As a consequence of this, the pressures from all cylinders can only be considered as one, the total pressure required to drive the engine. Therefore, the pressure from all cylinders can either be summed or concatenated to form the target pressures when testing both parametric and non-parametric models.

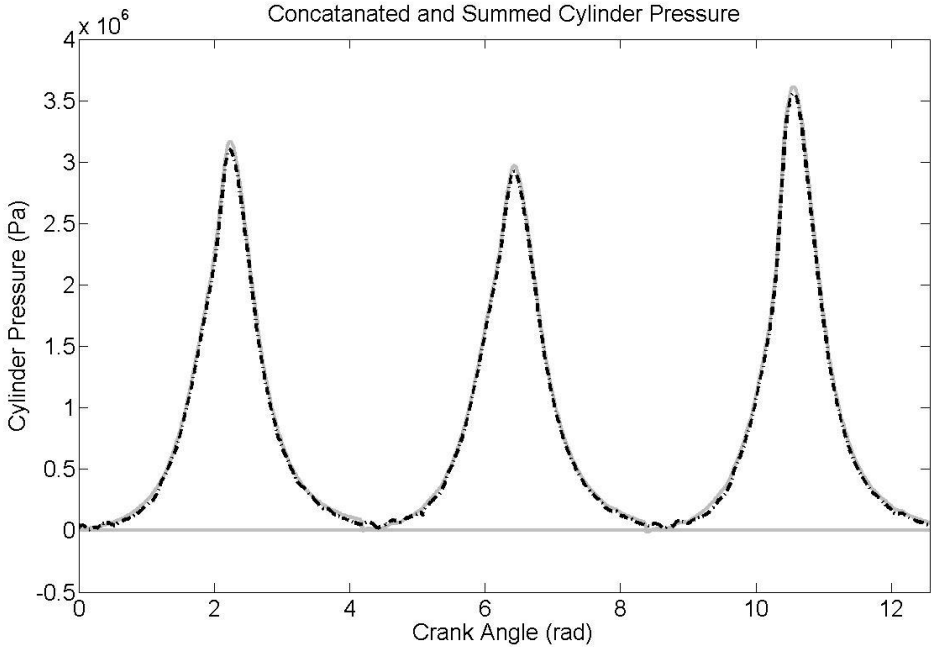

Figure 2.17: Cylinder Pressures for I3 Engine Summed (Black dashed line) and Concatenated (Grey solid line)

2.5 Theory of Engine Block Acceleration Forward Models

The focus so far in this chapter has been on crankshaft kinematic based parametric modelling. This stems from the relative ease of creating a simplified kinematic models as well as aiding in the explanation of key ideas. The main difficulty in developing parametric model for engine block acceleration is the complexity of engine block geometry. Engine block acceleration models do not rely on the displacement or rotation of components; it is purely the transmission of pressure waves from the cylinder through the engine block. Therefore, with the complex profile of modern engine blocks with numerous cavities, a generic parametric model (similar to equation (2.20)) cannot be constructed.

There is an approach undertaken by many researchers, as detailed in the literature review, which has had some success in parametric modelling of engine block acceleration; i.e.: finite element modelling. These models are used to examine high frequency vibration transmitted through the engine block. With finite element models it is also possible to model different dynamic events such as injector-pulse-forces, valve-impact forces, and piston-slap induced forces (Vulli, 2006).

However, there are significant limitations to using finite element models with respect to both the size of the model, and inverting the model. The size issue is a result of the high frequencies in the block acceleration. To accurately model these high-frequency, low-wavelength accelerations, particularly small elements are required. The requirement of small element size and the complex geometry, drives the need for an extremely large model.

When inverting a finite element model of engine block acceleration, there are two key interconnecting factors; the size and the nature of what is being asked. The size plays a significant role in the inability to accurately invert the model. These models are set up in such a way that the cylinder pressure is applied to a large area containing several hundred nodes. However, most often, only one node is used to measure block acceleration. The idea, that a single input to a model can contain sufficient information to suggest the pressure being applied to several hundred nodes, is difficult. This idea is comparable to the discussion on concatenating the pressure data; generally within parametric models, a single input cannot distinguish between several outputs. For this very reason the techniques predominantly used in reconstructing cylinder pressure from engine block acceleration are not parametric or statistical models such as using the EM algorithm by (Villarino and Böhme, 2003).

All the limitations of inverting physical parametric-based models discussed have caused researchers to investigate non-parametric methods of modelling the reconstruction of cylinder pressure. One type of non-parametric model is discussed in detail in Chapter 3, i.e. Artificial Neural Networks.

Chapter 3

Artificial Neural Networks and their Application

3.1 Motivations and Background

The complexity and limitations of using parametric models to create and fit an inverse model for the purpose of reconstructing cylinder pressure has been proven. Therefore, it is necessary to use other types of models and modelling techniques to achieve the desired accuracy. A model would need to be non-parametric with the capability of describing highly complex non-linear behaviour. Consideration has to be given to the operation of the model in the final system. It has been suggested that the models most likely to meet all these criteria are Artificial Neural Networks (ANNs). The use of these models has been shown with some success in similar applications, in (Gu et al., 1999) and (Potenza et al., 2007). But the overall accuracy and efficiency needs to be significantly improved.

This chapter will introduce ANNs from their conception through to the challenges in their applications. The chapter will start by discussing the general area of machine learning and the origins of ANNs. This is followed by introducing the most basic form of ANN, the perceptron. The chapter then describes four of the most commonly used ANNs classified with respect to architecture: (i) the single layer feed-forward network, (ii) the multilayer perceptron, (iii) the radial basis network, (iv) recurrent neural networks. The most popular training methodologies will then be described briefly, followed by a detailed examination of the Levenberg-Marquardt algorithm, used extensively in training the feed-forward neural networks used in this thesis. The penultimate section of this chapter will discuss key considerations in training, as well as the approach required for the optimisation of ANNs. The final part of the chapter will review automotive applications of ANNs.

3.2 Machine Leaning and Artificial Neural Networks

Machine learning is an extremely broad area of computer science. It involves the development of programs that learn and act without being explicitly programmed. Machine learning applications include internet search engines, spam filters, recommender systems, advertisement placement, credit scoring, fraud detection, stock trading and drug design. More recently has covered self-driving cars, practical speech recognition, and as a tool to greatly improve the understanding of the human genome. Machine learning is also widely considered to be the most likely route to produce human-level Artificial Intelligence (AI). Machine learning has become increasingly attractive, avoiding the need to manually construct programmes to undertake these complex tasks, and has grown in popularity in computer science, engineering and in the physical and life sciences.

The extremely broad area of machine learning comprises a number of different approaches depending upon the application. These approaches include decision trees, inductive logic programming, support vector machines, clustering, Bayesian networks, and genetic algorithms (GA). Machine learning and the approaches mentioned can also be classed in three additional ways namely: supervised, unsupervised, and reinforcement learning. Supervised learning is the learning of a function from labelled data where the input and output data is defined. Unsupervised learning is the learning of an unknown function from unlabelled data, where the input data is defined but output is not, and reinforcement learning is the learning of behaviour from labelled sequential data. However, one of the most researched machine learning approaches, and the approach used in this thesis, is the supervised learning of Artificial Neural Networks, which more recently has been rebranded as 'Deep Learning'.

As described in (Haykin, 2008), artificial neural networks have been motivated by the design of the human brain. The human brain can be described as a highly complex, nonlinear, and parallel computer with the capability of organising its structural constituents, i.e. neurons, to perform computations many times faster than the fastest digital computers in existence today. These computations can include pattern recognition, perception, and motor control. One of the most remarkable characteristics of the human brain is its ability to learn. At birth, the human brain has an adequate amount of structure to preserve life, but also has the potential to learn extremely complex relationships, through "experiences", at a remarkable rate.

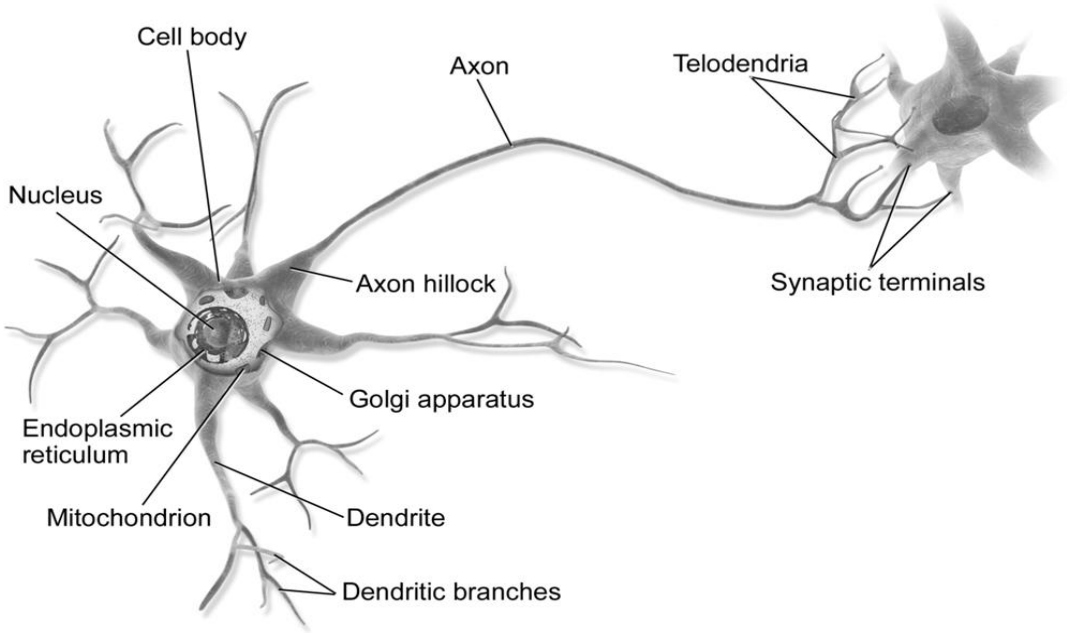

Figure 3.1: the Human Neuron

Figure 3.1 illustrates a human neuron. A neuron is an electrically excitable cell that processes and transmits information by electro-chemical signalling. The average human brain has about 100 billion neurons and each neuron may be connected to up to 10,000 other neurons, passing signals to each other via as many as 1,000 trillion synaptic connections. Estimates of the human brain's memory capacity vary wildly from 1 to 1,000 terabytes of data (by comparison, the 19 million volumes in the US Library of Congress represents about 10 terabytes of data).

Artificial neural networks attempt to mimic this ability through a computational model, which contains a series of interconnected neurons that are trained to undertake tasks. The aim is to take advantage of this potentially large processing power and maximise its capabilities. These include the ability to be either linear or non-linear, depending on the structure, and the ability to undertake input-output mapping through supervised learning and to adapt to environmental changes.

The history of artificial neural networks is relativity long compared to other types of machine learning approaches. The first concept of an artificial neural network was proposed in order to describe how neurons in the brain might work and modelled using electrical circuits by neurophysiologist Warren McCulloch and mathematician Walter Pitts in 1943. A neural network was first applied to a real world problem in 1959 by Bernard Widrow and Marcian Hoff. They developed two models, that are

comparable to current models, which they called "ADALINE" and "MADALINE." ADALINE was developed to recognise binary patterns so that if it was capable of reading streaming bits from a phone line, it could predict the next bit, and MADALINE was developed to eliminate echoes on phone lines using an adaptive filter (which is still in commercial use). Artificial neural networks have grown enormously since their development in the 1980's, particularly as computational power has increased.

3.3 The Perceptron

The human brain organises its structural constituents called neurons, to undertake certain tasks. Similarly, ANNs are constructed with smaller components, namely the artificial neuron, commonly referred to as just a neuron. The best method of describing how neurons (and ANNs in general) work is first to describe a basic ANN. The simplest ANN structure consists of a single neuron called the perceptron.

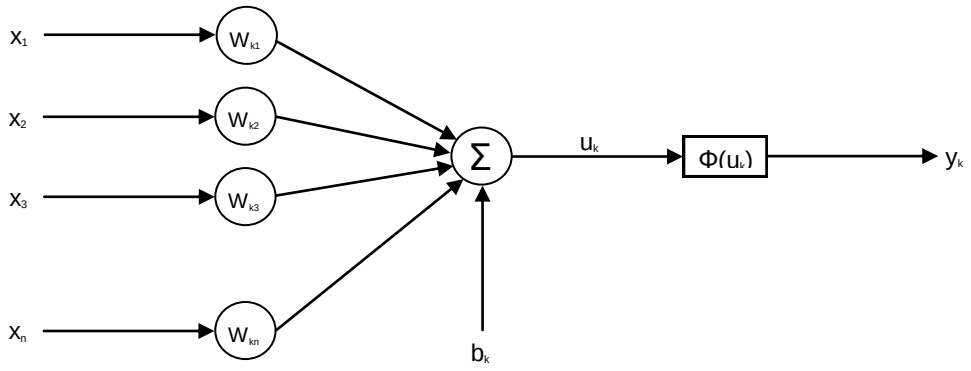

Figure 3.2: The Perceptron

Figure 3.2 shows a perceptron, where it can be seen that there are several key elements, some of which are analogous to human neurons. The network has multiple inputs which are connected to the neuron through synaptic connections. These synaptic connections are individually weighted similar to the synapse of the human brain. These weighted inputs are then added, along with an additional weighted input, called the bias. The value of the bias is nominally 1 which applies an affine transformation to the inputs, which produces a translation of the summed inputs. This value is referred to as the induced local field and is analogous to the axon's signal (in Figure 3.1). This then passes through an activation function which is used to transform the activation level of a neuron into an output signal, also

referred to as a squashing function. The most common activation functions are shown in (Figure 3.3). The resultant signal is the output of the ANN, and is analogous to the synaptic terminals in the human neuron.

Mathematically the processing of the information passing into a neuron is given as:

$$v = \sum_{i=1}^{n} (w_i x_i) + b_i \tag{3.1}$$

and

$$y = \varphi(v) \tag{3.2}$$

Equation (3.1) and (3.2) are basic equations of a perceptron ANN. The network inputs are represented by variable x_i and the input synaptic weights are represented by w_i, b_i is the neuron bias with v being the induced local field, φ is the activation function, and y the network output.

The activation function of a neuron, equation (3.2), uses the induced local field value to determine the output of the neuron. These transfer functions can take several forms depending upon network structure and requirements of the model, and can be linear or non-linear. Examples of the most common activation functions include the; threshold function (Heaviside function), the sigmoid function, the piecewise linear function and the Gaussian function. Figure 3.3 shows the graphical representation for some common linear and sigmoid activation functions. Figure 3.6, in section 3.4.3, presents a graphical representation of a Gaussian activation function.

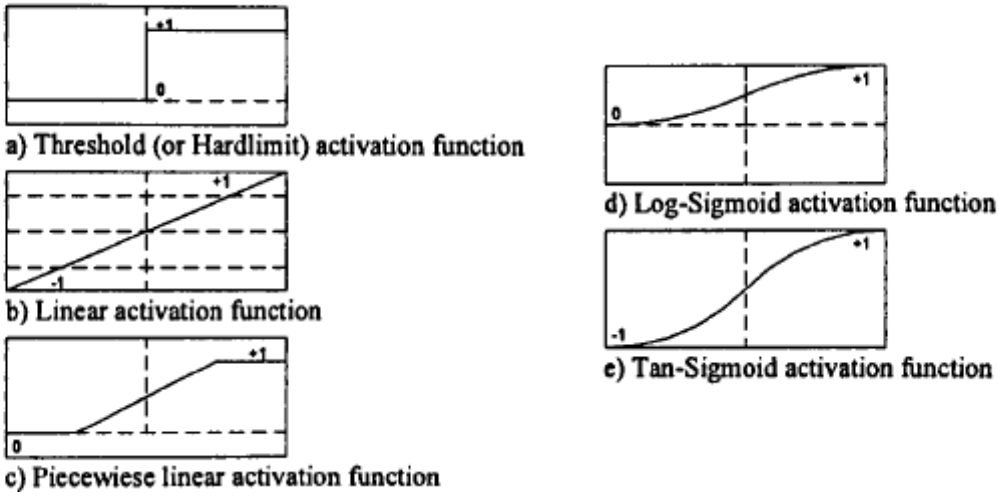

Figure 3.3: Transfer Functions

Since the basic structure of the perceptron has been described, it is now possible to describe, in simple terms, the method in which these perceptron structures can adapt and learn to undertake tasks. Equation (3.1) and (3.2) show the mapping of inputs x_i to output y. The ability of the mapping to be accurate for a given activation function is dependent upon the values of the input weights and the bias. Varying these values will change the outputs from the perceptron. This dependence on the weights and the bias is key to producing an accurate model using an ANN. The objective is to find a combination of the weights and bias that will produce the required mapping capability. This is generally undertaken using an optimisation algorithm as described in Section 3.5.

The examination of the perceptron is important to describe both the basics of the artificial neuron, and ANNs in general. However, apart from very few examples, the use of the perceptron is limited, since it does not have the capability to be used practically for mapping, pattern recognition or prediction. Therefore, in order to increase the capability of an ANN, neurons are grouped together to form a network. The greater the complexity of these interconnected neurons the greater the capability to be able to model highly complicated non-linear systems. But an increase in the number of neurons is not the only method of improving an ANN's capability. The arrangement of these neurons, as well as the types of connections between them, can have a significant on training efforts. A description of four ANN architectures is now given.

3.4 Artificial Neural Network Architectures

The development of the ANN has been rapid and, as a result, there are a large number of network architectures, for a variety of applications. However, only four different ANN architectures have been proven to work successfully on a wide range of applications, including some success on reconstructing cylinder pressure. These architectures include the single-layer feed-forward, the multilayer perceptron, the radial basis, and recurrent neural networks. Time-delay neural networks will also be discussed within the multilayer perceptron sub-section, owing to their similarity. This section will describe each network, including the approach required, highlighting the network's limitations, ultimately to assist in the selection of an appropriate neural network.

3.4.1 Single Layer Feed-Forward Network

The single-layer feed-forward neural network is the simplest structure out of the four that will be discussed. As the name suggests, the network consists of a single layer of neurons with *n* inputs and equal number of neurons and *k* outputs. The connectivity of the network is relatively simple since each input is connected to all neurons, producing *n* x *k* connections, and the output is directly obtained from each neuron. The network is 'feed-forward' because the information is considered to flow in the forward direction. There is no specific rule in the choice of activation function for a single-layer feed-forward neural network. However, for most applications, threshold functions are used. In general the output of a single-layer feed-forward network is given as:

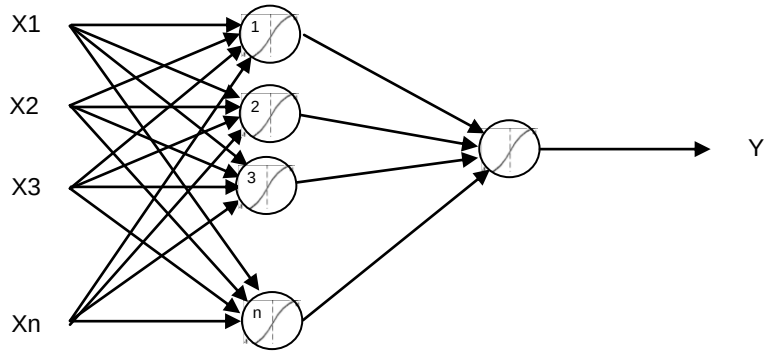

Figure 3.4: Single Layer Perceptron Network Architecture

$$y = \varphi\left(\sum_{i=1}^{n}(w_{ki}x_i) + b_k\right) \tag{3.3}$$

Where the network inputs are represented by x_i and the input synaptic weights are represented by w_{ki}. b_k is the neuron bias with φ being the activation function, y_k the network output, and k is the neuron number.

The training time of any neural network can vary significantly depending upon the number of neurons. However, its relatively small size and few connections has the benefit of quick and reliable training. But the architecture's small size, prevents the network from representing complex relationships. For example, this network does not generally lend itself to the solution of time series problems. In principle, the ability to undertake exceptionally simple time series tasks can be improved by using the time-delay approach as now discussed.

3.4.2 Multilayer Perceptron and Time-Delay Networks

The multilayer perceptron and time-delay networks will be discussed together as the time-delay network is a variant of the multilayer perceptron network. They share the same basic structure and equations, with only the different being the inputs designation. The more general multilayer perceptron network will be discussed first. The multilayer feed-forward neural network, or more commonly known as the multilayer perceptron (MLP) neural network, is the frequently used network which forms the fundamental structure of many architectures. The basic form of an MLP is shown in Figure 3.5, comprising multiple layers of neurons, with n inputs with k neurons in multiple layers and outputs.

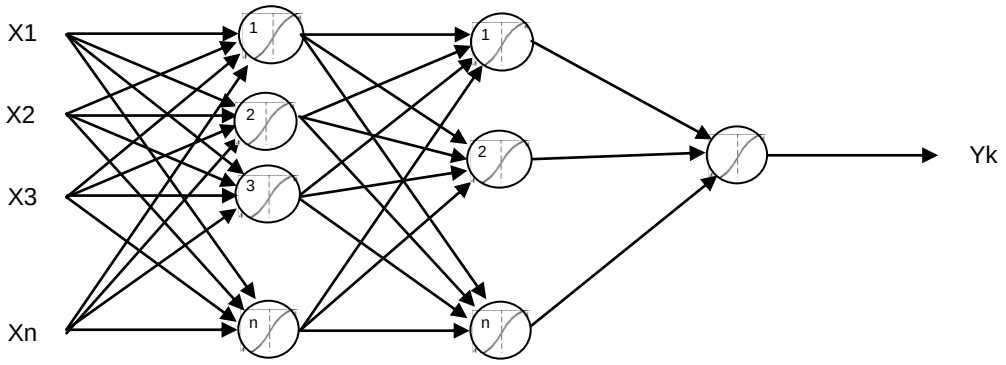

Figure 3.5: Multilayer Perceptron Network Architecture (2 hidden layers and n neurons)

There is no restriction on the number of layers or outputs in a MLP network. The final layer of an MLP network is called the output layer. Conventionally, the preceding layers are referred to as 'hidden' layers, labelled 1 to l. The example in Figure 3.5 has 2 hidden and 1 output layer with a single output. The connectivity of the network is the same as the single layer feed-forward network architecture, with the additional connections between each layer in the forward direction. Similarly, there is no specific rule in the choice of activation functions for MPLs. However, for most applications, linear activation functions are used for the output layer and a sigmoid function is generally used for the neurons in the hidden layers. The selection of different activation functions produce networks with differing characteristics and can require fundamentally different approaches, namely training.

The mathematical description of a multilayer perceptron network with a single hidden layer is given by:

$$y_k = \varphi_o\left(\sum_{j=1}^{n_l}\left(w_{lj}\cdot\varphi_h\left(\sum_{i=1}^{n_l}(w_{li}x_i) + b_{lk}\right)\right) + b_{lk}\right) \tag{3.4}$$

The network inputs are represented by x, the synaptic weights are represented by w. b is the neuron bias with φ_h being the activation function of the hidden layer, φ_o is the activation function of the output layer, and y is the network output, where *k* is the neuron number. l is the layer number.

This network architecture is suitable for a wide range of complex problems, such as mapping, pattern recognition, or prediction. This ability to handle complex problems is highly dependent upon the number of neurons and the number of hidden layers. Increasing both should expand the potential. However, the increased size and number of connections impacts the speed and reliability of training. Therefore, this network does not generally lend itself to the solution of time series problems as it does not have the capacity for internal memory, thus has no perception of time variations. This network architecture does, however, have the ability to do some fairly complex time series tasks by using time-delays, as now explained.

Time-Delay Neural Networks

Fundamentally, time-delay neural networks are structured the same as the multilayer perceptron. The difference lies in the approach to using the network. In general, MLP networks use a number of different inputs which are normally not time dependent, whereas time-delay networks use a series of inputs comprising a single variable, along with previous states. This effectively produces a network with a short-term memory (depending on the number of delays) which is simulated in practice using a 'tapped delay line'. Figure 3.6 shows the structure of a time-delay neural network. It is identical to the structure of the MLP in Figure 3.5 with the exception of the different input designations.

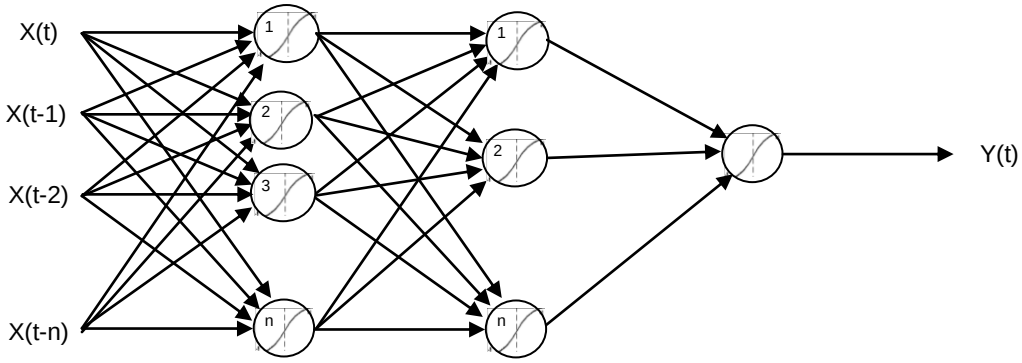

Figure 3.6: Time-Delay Network Architecture

The use of a time-delay network approach has significant advantages over the MLP network as it is much more suited to solving time series problems, without significantly increasing the network size or training effort. However, even with the short-term memory gains, there may be, in some instances, difficulties in training complex problems with longer-term memory. Chapter 5 addresses this question in connection with reconstructing cylinder pressure.

3.4.3 Radial Basis Function Network

As stated, the multilayer perceptron network is the basis for numerous other networks; the radial basis function (RBF) network is one of them. The RBF network structure and connectivity is fundamentally the same as the MLP. The difference is the choice of activation function used, i.e. a non-linear RBF activation function of the form:

$$\varphi(R) = e^{\left(\frac{-R^2}{2\sigma_j^2}\right)} \qquad \text{where} \qquad R = \left\|x - c_j\right\| \tag{3.5}$$

This is example uses the Gaussian function where the activation function output is φ, the input to the function is x, the centre of the function c_j for jth input data point and σ_j is a measure of the width of the jth function. In the MLP and time-delay neural networks, the activation function used for the hidden layers is the sigmoid function, which is the same for all neurons. In an RBF network this is not the case because the RBF 'centres' (c in equation (3.5)). The RBF takes the form of a Gaussian function centred at a predetermined point. Figure 3.7 shows two RBF functions with different centres.

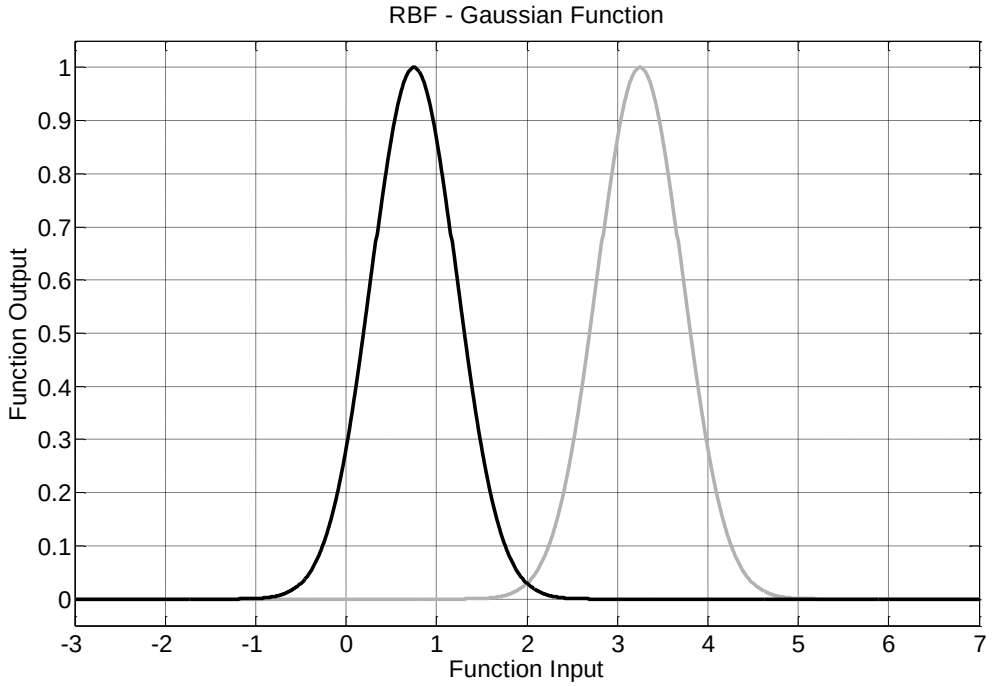

Figure 3.7: Radial Basis Function for 2 Centres, *c*. (Black line *c* = 0.75, grey line *c* = 3.25)

RBF networks take advantage of these variable activation functions to model high level problems. With the previous architectures, the training is carried out in a single step; involving optimisation of the weights and biases. RBF networks also require optimisation of the weights and biases but prior to this, the centres for each neuron require defining. The two most accepted methods of defining the centres is either by setting them to a random subset of the input vectors or by using 'k-means clustering'. k-means clustering is an unsupervised method for clustering n inputs into k clusters, and is used extensively in machine learning and signal processing applications.

The added layer of complexity through the use of the radial basis function and the centre selection is beneficial in the modelling of numerous problems, including time series approximations, clustering, and control. With respect to the computational effort, the training time for the weights and biases is comparable to MLP networks of similar size and the additional level of optimisation using k-means clustering is related to the training data size.

3.4.4 Recurrent Neural Network

Recurrent neural networks (RNNs) are commonly adopted network structures for time series approximations with numerous variations where the fundamental

structure is similar to the MLP network. Again, as can be seen in Figure 3.8, the network consists of multiple layers of neurons with *n* number of inputs and with *k* neurons in numerous layers and outputs. The final layer of an RNN is the output layer, conventionally the preceding layers are the hidden layers, labelled 1 to *l*.

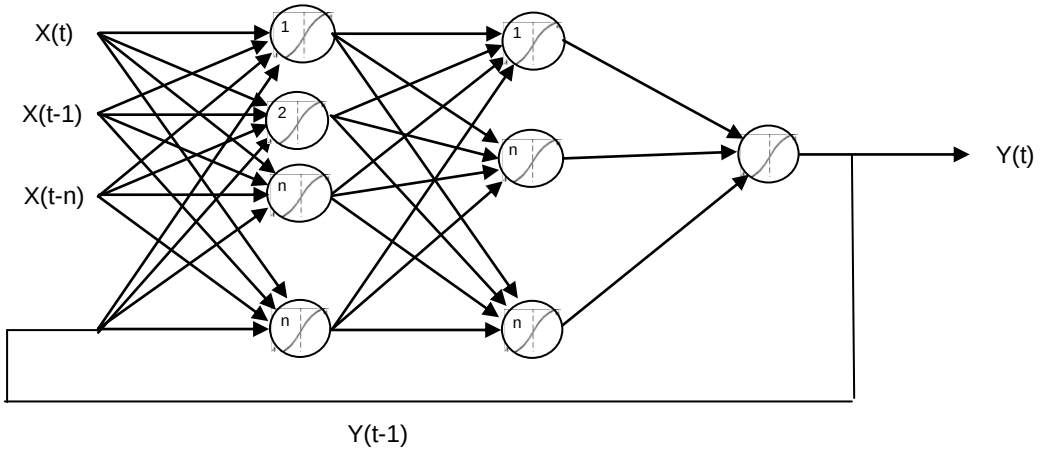

Figure 3.8: Recurrent Neural Network Architecture (with single feedback)

The connectivity is usually the same as the MLP network architecture with the connections between each layer in the forward direction, but with additional connections. These additional connections come in the form of delayed feed-backs; from the output to the input, see Figure 3.8. These additional connections create neural networks with the ability to have an extended memory, critical in certain time series applications. The feed-back connections are weighted and optimised in the same manner as the neuron connections. Similarly, there is no strict rule in the choice of activation function for multilayer perceptron neural networks. However, for most applications, linear activation functions are used for the output layer, and sigmoid functions are generally used for the neurons of the hidden layers.

The RNN architecture is suitable for a wide range of complex time series problems owing to its internal memory. A recurrent neural network architecture that is particularly suited to time series approximations is the nonlinear autoregressive exogenous (NARX) model. The 'autoregressive' portion refers to the output variable which depends linearly on its own previous values (i.e. feed-back connections) and the 'exogenous portion refers to a change that comes from outside the model (i.e. input connections). This is the particular recurrent architecture depicted in Figure 3.8. However, the addition of the feed-back connections creates significant issues in the training. The increased complexity of the training impacts on the speed and

reliability of the training owing to stability difficulties. More of the difficulties regarding the training are discussed now in section 3.5. Chapter 5 discusses the limitations of this approach in reconstructing cylinder pressure.

3.5 Artificial Neural Network Training Methodologies

3.5.1 Fundamentals of Artificial Neural Network Training

As described in the previous sections, there are numerous ANN architectures, each with different training requirements. Examples of these include; the different approaches for supervised and unsupervised learning and the different approaches in training feed-forward and recurrent ANNs. For this application, supervised learning is required, and regardless of the specific ANN architecture selected, the basic approach is the same. Supervised learning is a method of training where, for every input (training vector) used, there is a corresponding desired response. The desired response represents the ideal action to be performed by an ANN. The process of weight and bias optimisation is achieved through an examination of the difference between the desired and actual response; namely the network error. Adjustments are iteratively made with the aim of eventually making the ANN emulate the desired responses (Haykin, 2008).

This section briefly covers the most common methodologies for training both feed-forward and recurrent ANNs, and includes the methodology used extensively throughout this thesis, namely the Levenberg-Marquadt algorithm (LMA). The Levenberg-Marquadt algorithm will be explained in full including the governing equations, uses, and limitations. Although the LMA is used extensively, the other methods covered in this section have also been examined and tested. However, as the focus of this thesis is on the application of the data with more simplified structures and algorithms, they have not been detailed in the results. The additional training methodology covered is Back Propagation (BP) with Gradient Descent (GD) as well as two less common approaches; particle swarm optimisation (PSO), and extreme learning machines (ELM). For these, as well as the remaining algorithms and optimisation approaches, a brief description will be given along with their general limitations and the reason why they have not been used in this work. Three different recurrent training methodologies will be mentioned including Back-Propagation-Through-Time (BPTT), "teacher forcing" and RAGD methods.

3.5.2 Levenberg-Marquadt Training Algorithm

The Levenberg-Marquadt algorithm (LMA) is second-order method which means that it works with only function evaluations and gradient information. Even though this method is commonly used for non-linear least-square problems, it also has a wide range of applications and works extremely well in training ANNs. It is an iterative technique used for locating minima of functions with multiple variables (Haykin, 2008).

The LMA can be considered as a compromise between two other well established optimisation methods; the Newton method and the gradient descent method. The Newton method converges rapidly during the optimisation when near a local minimum however there is potential for it to diverge. The gradient descent does not have a significant divergence risk and is almost guaranteed to converge but as a result, is significantly slower (Haykin, 2008). Equation 3.6 is the general form of the LMA and the optimum adjustment, Δw between iterations, is given by:

$$\Delta w = [H + \mu I]^{-1} g \tag{3.6}$$

where H is the Hessian matrix, g is the gradient vector, I is the identity matrix and μ is a regularising parameter. The following set of equations define the gradient vector and Hessian matrix in relation to ANN training (Haykin, 2008). For example the gradient vector is the derivative of the cost function $\varepsilon_{av(w)}$ with respect to the weight vector w i.e.:

$$g(w) = \frac{\partial \varepsilon_{av}(w)}{\partial w} = -\frac{1}{N}\sum_{i=1}^{N}[d(i) + \boldsymbol{F}(x(i), w)] \frac{\partial \boldsymbol{F}(x(i), w)}{\partial w} \tag{3.7}$$

where the cost function is:

$$\varepsilon_{av}(w) = \frac{1}{2N}\sum_{i=1}^{N}[d(i) + \boldsymbol{F}(x(i), w)]^2 \tag{3.8}$$

and where N is the length of the training sample, d is the desired output, and $F(x; w)$ is the approximating function realised by the network with x being the input vector. A Hessian matrix associated with the cost function (equation (3.8)) can be defined as:

$$H(w) = \frac{\partial^2 \varepsilon_{av}(w)}{\partial w^2} = \frac{1}{N}\sum_{i=1}^{N}\left[\frac{\partial \boldsymbol{F}(x(i),w)}{\partial w}\right]\left[\frac{\partial \boldsymbol{F}(\boldsymbol{x}(\boldsymbol{i}),\boldsymbol{w})}{\partial \boldsymbol{w}}\right]^T - \frac{1}{N}\sum_{i=1}^{N}[d(i) + \boldsymbol{F}(x(i),w)]\ \frac{\partial^2 \boldsymbol{F}(x(i),w)}{\partial w^2} \quad (3.9)$$

The Hessian is used to describe the local curvature of a multi-variable function necessary for ANN training. Equation (3.9) shows the complexity of the Hessian which, in practice, is extremely difficult to compute. As a result, approximations have been developed to obtain an estimate of the Hessian matrix. One such approximation uses the Jacobian matrix J:

$$J = \frac{\partial \boldsymbol{F}(x(i),w)}{\partial w} \quad (3.10)$$

Equation (3.10) appears frequently within the Hessian equation, equation (3.9). As a result of the practical difficulty of constructing the Hessian matrix, the second term in equation (3.9) is ignored, and the Jacobian is inserted to approximate the Hessian matrix, namely:

$$H \approx JJ^T \quad (3.11)$$

producing an approximate optimum adjustment *w* as follows:

$$\Delta w \approx [JJ^T + \mu I]^{-1}\varepsilon_{av}J \quad (3.12)$$

The LMA has been selected for the training owing to the relatively easy way of implementation producing highly accurate training, and good generalisation capability. However, it has been noted that the LMA may only find a local minimum. As a result, several networks with different initial conditions, may need to be trained to find the global minimum, (see section 3.6). Sample Matlab code for the LMA and a test function is given in Appendix B. The code was created for the Non-Autonomous Neural Network which will be discussed in Chapter 8.

3.5.3 Other Optimisation Approaches

Back Propagation (BP) is a specific technique used for implementing gradient descent in feed-forward ANN architectures (Haykin, 2008). BP computes the partial

derivatives of an approximation, produced by the network, which depends on both the inputs and the weights. The Gradient Descent optimization algorithm is then used to find a local minimum for the partial derivatives within the gradient vector, see equation (3.7). There are two key stages in the implementation of the BP algorithm. First, a forward pass, or computation, is undertaken to compute the local fields and function signal. Second, a backward pass, or computation, is undertaken to compute the local gradients at each neuron. The weights are then updated using the delta rule, namely:

$$\begin{pmatrix} Weight \\ correction \\ \Delta w_{ij}(n) \end{pmatrix} = \begin{pmatrix} Learning\ rate \\ parameter \\ \eta \end{pmatrix} \times \begin{pmatrix} Local \\ gradient \\ \delta_i(n) \end{pmatrix} \times \begin{pmatrix} Input\ signal \\ of\ neuron\ j \\ y_i(n) \end{pmatrix} \quad (3.13)$$

Back Propagation with gradient descent is a powerful method of training networks relatively quickly, and is ideal for simple pattern recognition and mapping tasks. However, the results are limited in the generalisation of the cylinder pressure reconstruction, a time series problem.

There are two different optimisation approaches which are notably different from the methods described so far. They are Particle Swarm Optimisation and Extreme Learning Machines. They both apply the same basic approach of supervised learning however, one uses a highly parallel approach whilst the other takes advantage of the random nature of the weight and bias initiation, and of the power of the other training methodologies already discussed.

Particle Swarm Optimization (PSO) is an evolutionary computation technique (Eberhart and Kennedy,1995). In the PSO algorithm, potential solutions, known as particles, are obtained by ‘‘flowing’’ through the problem space by following the current optimum particles (Zhang et al., 2007). The PSO optimisation is iterative, and works by examining the best value of each particle’s in the previous iterations, and the best value obtained by all the particles previously. These are then used, alongside additional parameters, to update the value for each particle to reach the global optimum. The advantage of using this methodology is that it is relatively easy to implement and guarantees an optimum will be reached. However, if the additional parameters are not appropriately set, the search will become very slow near the global optimum (Zhang *et al.*, 2007). Also, it has a disadvantage of easily getting into a local optimum and owing to the highly parallel approach of using numerous

particles computationally, it is expensive. Both of these disadvantages were experienced when training for cylinder pressure reconstruction, therefore it was not selected for this application, and was not considered further.

Extreme learning machines (ELM) are a very powerful, and yet a simple approach to training ANNs. Fundamentally, whereas all the preceding training methodologies attempt to optimise every weight and bias within a network, the ELM approach does not. The ELM approach optimises every weight and bias in the output layer, however, the hidden layer weights and biases are not optimised; they are fixed at the random initial values. The remaining weights and biases can be trained using any other optimisation approach. The fixed random weights and biases ensure the universal approximation capability and makes it very efficient in training. This approach also leads to better generalization performances and alleviates the problem of over-fitting and overtraining (Huang *et al.*, 2015). Over-fitting and overtraining are discussed in section 3.6. Practically, ELMs are implemented by using significantly more neurons in the hidden layers to ensure adequate accuracy but this does not influence the training efficiency as these are fixed. The results are extremely good when testing with cylinder pressure reconstruction during training however, the LMA performance (of section 3.5.2) was actually better in generalisation for this application.

3.5.4 Recurrent Training

Back-Propagation-Through-Time (BPTT) is a popular method of training recurrent neural networks and is an extension of the BP method. The BPTT method essentially unfolds the temporal operation of a network into a layered feed-forward network. Consider a recurrent network with a single feedback. The value of the current feedback at time t is equal to the network output at time t - 1. This recurrent network can be reorganised, duplicating and combining the network into a feed-forward network, as the output from the network is one of the inputs at the next time step. Therefore, when considering all the time steps in a training set, it is possible to consider the recurrent network as one large feed-forward network with size $n \cdot S$, where n is the number of time steps, and S is the size of the recurrent network. With the recurrent network arranged in the feed-forward configuration, the BP algorithm can be implemented. The BPTT method has the same advantages as the BP method except that the training time is significantly longer. This is because the network is significantly bigger. As a result, the training time is expected to be n (the number of time steps) times longer than a feed-forward network of equivalent size to

the recurrent. BPTT was not used for this application because the training requirement would make training impractical.

The complexity and computational effort experienced by others with BPTT training was the motivation behind developing faster methods to train recurrent networks. One such method is called "teacher forcing". This approach to training recurrent networks is simple and extremely fast in comparison to BPTT. Essentially, it recognises that in training, the optimum values for the feedbacks are already known, i.e. the target values from the previous test points. It is therefore possible to break the feedback, creating a feed-forward network, and use the knowledge of the desired feedbacks as additional inputs to the network. This feed-forward structure can then be trained using any type of feed-forward training algorithm. This method forces the network to train on the correct feedbacks. The advantages have been outlined, namely the reduced computational effort required. There is one major disadvantage in using "teacher forcing" and that is the instability of the network when the feedbacks are reconnected and the network is tested. This is owing to the small errors present in the network's output which is fed back into the network; a condition that the network has not be trained for. Consecutive errors can be compounded and destabilise the results. This was selected when comparing the difference between recurrent and time-delay networks as a result of the simplicity of the implementation. However, the stability of the network was closely examined prior to the comparison.

An alternative training methodology used to train recurrent network architectures for the reconstruction cylinder pressure, is the Robust Adaptive Gradient Descent (RAGD) algorithm (Bennett, 2014). This method is an adaptive hybrid learning method. It is employed to optimize the convergence speed and make an optimal trade-off between the real-time BP and RTRL training strategies, to maximize the learning speed (Song *et al*., 2008). Owing to the extensive work undertaken by Bennett, and the complexity of optimising the algorithm parameters, this method was not employed.

3.6 Optimising an Artificial Neural Network Structure and Training

This section explains the general approaches and practical considerations in constructing and training Artificial Neural Networks. The main aim of this section is to explain this key issue, once both the architecture and training algorithms have been selected, in optimising and training of an ANN. Some of the points described in this section form the foundation of the thesis and are expanded in Chapter 5. This section will conclude with a summary of the ANN architecture, training algorithm and general constrains which have been selected and that will be used throughout the research.

With the ANN architecture selected, one of the biggest difficulties is in the optimisation of the network structure. There are four main variables with regards to the structure: the number of inputs, the feedbacks, the neurons and the hidden layers. For optimisation, in deciding the number of neurons and hidden layers, there is, in general, no standard method. The basic rule is that the more complex the application, the more layers are needed and the more detailed or precise the ANN is required to be, the more neurons are needed. Ultimately, the exact number for these can only be found through an iterative process. However, literature on similar ANN applications can provide neuron and layer numbers, or at least a reasonable starting point for the optimisation. In the main, for the structure optimisation, the number of inputs and feedbacks can be considered the same. The number of inputs for any ANN is again application specific; literature could be a starting point but an iterative process is the only valid solution. Also, especially for time-series applications, the number of inputs or delays depends on the information content and the values of the data as well as the application limitations. The key reason behind finding the optimum structure for the ANN is time and computational effort. In principle two different ANNs with the same architecture and training algorithm, can produce the same result even though one has more inputs, feedbacks, neurons or hidden layers. The only difference is the time taken for the training. The greater any of these variables are, the longer the training time. Therefore, the goal is to produce an ANN large enough to train sufficiently but not too large to make the computational effort excessive.

Similarly, the selection of the activation function is application specific and literature can be used in the selection. However, unlike the optimisation of the inputs,

feedbacks, neurons or hidden layers, in general, their selection is not critical to the success of the network, owing to the universal approximation theorem (Cybenko, 1989). The universal approximation theorem ensures that, in principle, an ANN using the same data will train the same regardless of the activation function selected. As a result, any activation function can be selected as it has no significant effect on time series feed-forward application. However, the ability of the activation function to be differentiated is useful for certain training algorithms.

Prior to commencing training of an ANN, the weights and biases require initialisation. This is the process of defining the initial values of the weights and biases and the convention is to randomise these values using a normal distribution around 0 with a standard deviation of 1. One thing to note is that, depending on the training algorithm selected, the initial values may affect the network performance. If a training algorithm is selected which has a tendency to only find local minima and if the random initialisation results in the network being close to a local minimum, then there is little chance of a global minima being reached during training. As a result, it may be necessary to train multiple networks, with different initial values for the weights and biases, to ensure the global minimum of the network is reached (Lawrence *et al*., 1997).

As described previously, the basic principle of training a time-series ANN is to optimise weights and biases, for both the input layer and hidden layers, to model, cluster, or predict. This process is iterative. At each iteration (or epoch), the training algorithm assesses the performance of the network, evaluates how much each weight or bias impacts on the performance, then produces a new set of weights and bias. This process repeats until one or more of the targets are met, then the training is terminated. These can include the performance goal, maximum epoch number, and the gradient. It is important to note that there are additional variables within training algorithms that are also used as limits. For the Levenberg-Marquadt algorithm, the parameter μ is often given an maximum limit, defined prior to training, to control the accuracy of the training. If this limit is reached the training will also terminate.

Within all areas of machine learning, and especially ANN the ultimate goal is the successful training of the ANN, and the implementation of the model. This usually involves using the trained network on unseen or generalised data. However, the

successful training of an ANN does not determine the network's ability to generalise. Very accurate training results, can sometimes, worsen the ability of the network to generalise. This stems from the behaviour known as overtraining. As mentioned, in ANN training, data is used to optimise the weights and biases. This method essentially trains the ANN to recreate the pattern which links the inputs to the outputs. However, if the training is too long, or the goals and limits are too severe, then the network may not just learn the general pattern but will over-fit to the training data. An overtrained ANN will tend to produce very good results when using the training data but it will most likely produce poor results for anything not in the training set.

Another important factor in preventing overtraining is the selection of the training, validation, and generalisation data. The training data is the data used to train the ANN. In an ideal situation, ANNs would be trained on every possible combination of inputs and outputs to avoid overtraining. Although this is not possible in practice, because either the quantity of states is too big to be computed and trained using the technology available, or there is no way of determining all possible states within an application. Therefore, the approach is to train on a subset of all possible states, which must be used to give adequate results when generalised. An important consideration in the sourcing and handling of the training data is to make it representative of the application. It is possible to select training data which appears to be typical of the application. However, without a study of the statistical properties of the data, there is no guarantee provided. The validation data is the data used within the training methodology. This data is not used to train the network but as a check on the network's generalisation capability. The validation data tends to be a fraction of the size of the training data set. Similarly, the validation data must be representative of the application. The generalisation data is not used as part of the training. It is used after the training is complete to determine the final performance of the network. To do an accurate test of a network's performance, the generalised data must not have been seen by the network during the training. This is the ultimate test of the success of the training and of the network itself.

Similarly, there is no standard process in deciding the size of the training, validation and generalisation data sets. Ideally, for improved performance, as much training data as possible should be used. The more training data used, in general, the better the generalisation results will be. The validation size can be any proportion of the

training data but in general, 20% is a good starting point. These sizes, again can be improved iteratively, but the size of the generalisation results are also application specific.

The main task then, for constructing ANNs, is to produce a training methodology which takes into account the selection of the epoch number, the performance function, the goals and other limits, and a suitable training set that produces an ANN that performs well when generalised.

Conclusions

This chapter has discussed a number of different ANN architecture and training algorithm that are used across many applications of ANN's including several that have previously been used for reconstructing cylinder pressure. These include multilayer perceptron, radial basis function and recurrent network architectures and Levenberg-Marquadt and gradient decent training algorithms. Examining all of these architectures and training algorithms would require extensive work and as some of them have previously been researched in detail, this would not be necessary. Therefore, a single ANN architecture and training algorithm was selected for the main focus of the research; time-delay neural network and Levenberg-Marquadt training algorithm. A recurrent architecture would be used on one occasion, early in Chapter 5, but only as a means of comparison and to assess the potential of the time-delay neural network. This time-delay architecture was selected as it has not yet been examined within this line of research and was believed to have the capacity to handle complex time series modelling without the added complexity of the feedbacks, which the recurrent networks had. The Levenberg-Marquadt training algorithm was selected because of its robustness in training ANN's for many different applications including cylinder pressure reconstruction (Saraswati and Chand, 2010). This research also follows the optimisation practice for both the structure and training given in this section. The specific architecture, structure and training constraints are given with each test undertaken in the later chapters.

Chapter 4

The Engine Testing Facilities and Data Acquisition System

4.1 Introduction

The theoretical background to cylinder pressure reconstruction, and the methods used to construct and successfully train an ANN, have been described in Chapters 2 and 3. Therefore prior to developing a ANN for this application, it is necessary to discuss the data used in the training of the networks. There are several approaches to obtaining training data for cylinder pressure reconstruction, namely, using simulation model-based approaches (Potenza *et al.*, 2007), measurements from real systems (Gu *et al*., 1996) and (Potenza *et al.*, 2007), or a combination of both (Saraswati and Chand, 2010). However, when considering the limitations of the models discussed in Chapter 2, and an ANNs dependence on reliable data to train successfully, the model based approaches, even though fast, are a false economy. The only practical method of producing accurate data for training, which is capable of reconstructing cylinder pressure, is through the acquisition of real data from an engine.

The focus of this thesis is to examine the application of data to ANNs, its structure, and then to develop methodologies to successfully reconstruct cylinder pressure. Again, this relates to understanding the information content within the data which is a key limitation to successfully training an ANN. It is not just the accuracy of the data that is in question. The focus of this thesis is not to develop or improve a data acquisition system for generating engine test data, as this was undertaken by a previous researcher (Bennett, 2014). This chapter will describe the engine test facilities and summarise the robust data acquisition system developed by Bennett, and how this system overcame numerous problems in order to produce accurate data.

This chapter will start with a description of the engine, and the test facilities used to generate test data. It will also include a description of the instrumentation used. Then, the data acquisition system hardware is summarised followed by an outline of the software implementation. The chapter then describes the method used to process the data. The penultimate section discusses the most significant problems arising from both the overall acquisition process and the hardware. The chapter ends by describing the tests undertaken initially by Bennett, plus additional tests.

4.2 The Engine

The engine selected to generate test data for the cylinder pressure reconstruction ANN model training was a 4-stroke 3-cylinder inline gasoline direct injection spark ignition (DISI) engine. This was a prototype of a production engine model, designed and developed by the Ford Motor Company and Yamaha. However, it did not go into production. It was supplied to the University of Sussex by Ford. Even though the engine was supplied more than a decade ago, it is still very relevant to current engine developments. The 3-cylinder design in particular is beneficial because current thinking and developments, within the automotive industry, is that smaller engines are better. Therefore, there has been a push for smaller (downsized) highly-boosted engines with fewer cylinders which produce a similar performance to the original larger engine it will replace. The 3-cylinder engine design actually increases the likelihood of creating an ANN model that successfully reconstructs cylinder pressure. This is because the successive firing cylinders are spaced 120° crank angular displacement apart. The larger the spacing between firing events (with smaller overlaps in cylinder pressures) the easier it becomes to extract trends within the crankshaft kinematic and block vibration data. As discussed earlier, the better the data is (i.e. with the correct information content) the more effective the machine learning process becomes.

Figure 4.1 shows a photograph of the engine on a 130 kW dynamometer in the test cell. The head and block are aluminium, with 4 valves per cylinder. The valve arrangement involves 2 valves for the intake, and 2 valves for the exhaust. The valve train is belt driven. This engine also contains swirl control valves on the inlet, which aids inlet air turbulence and an exhaust gas recirculation (EGR) system to reduce the in-cylinder temperature and NO_x emissions. The numbering of the cylinders is important later in the thesis; therefore it is essential to define them:

Cylinder-1 is at the nose of the engine, Cylinder-2 is in the middle of the engine and Cylinder-3 is nearest to the flywheel.

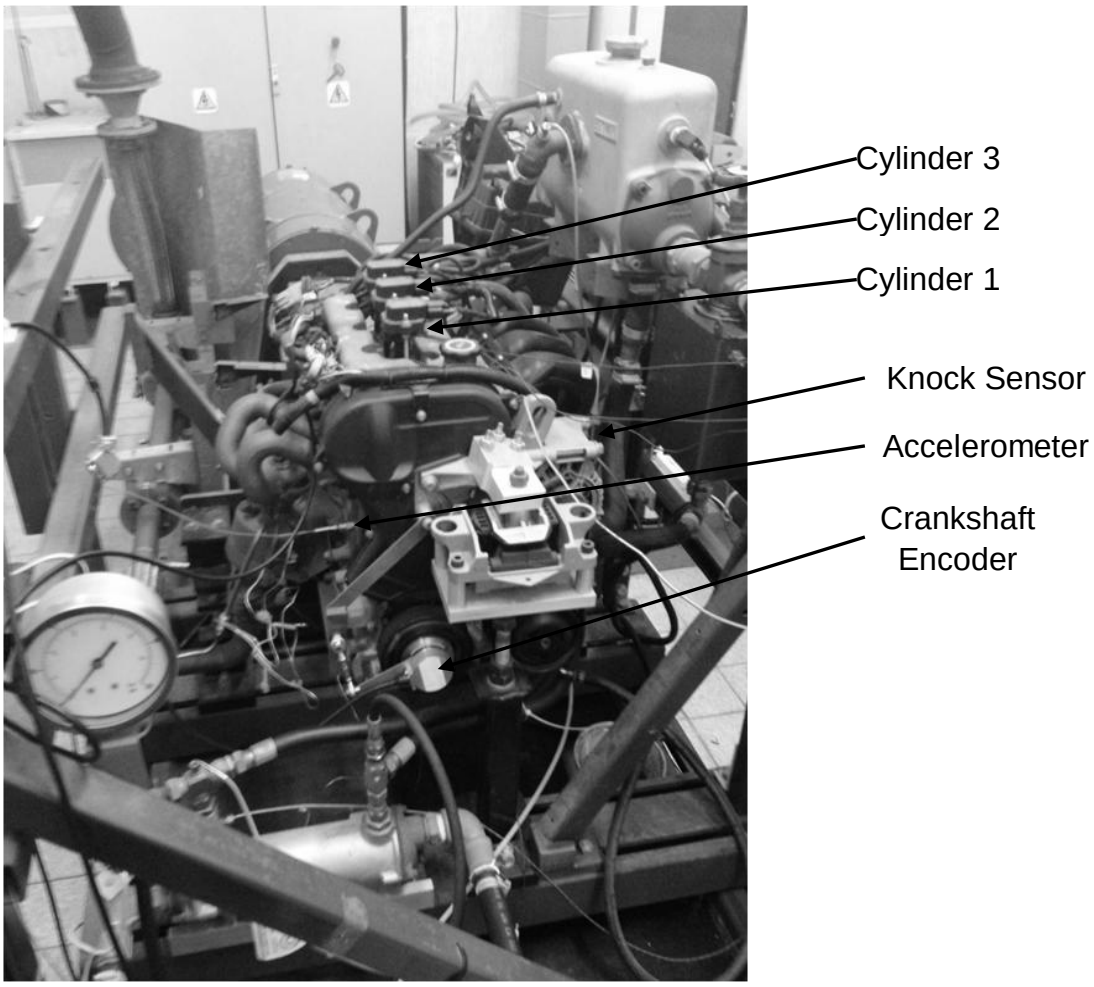

Figure 4.1: Ford 3-Cylinder 4 Stroke Direct Injection Spark Ignition (DISI) Engine in Test Cell

With respect to this application and the engine dynamics, there are three important attributes of this engine that need to be stated. First, there is a torsional vibration damper fitted to the engine, which could cause issues when modelling the finer cylinder pressure details. Second, there is no clutch fitted to the test rig, which may also cause issues with the application of this technology in a vehicle. Finally, the dynamometer is connected directly to the engine flywheel via a compliant torsional coupling. This compliant torsional coupling may generate additional excitations to the crankshaft and engine block at critical frequencies. Table 4.1 gives key parameter values for the engine.

Table 4.1: Ford 3-Cylinder Specifications

Engine Kinematic Parameters	Value
Number of Cylinders	3 Inline
Bore	79.0 mm
Stroke	76.5 mm
Swept Volume	1125 cc
Connecting Rod Length	137 mm
Piston Pin Offset	0.8 mm
Compression Ratio	11.5
Piston Mass	270 g
Connecting Rod Mass	395 g
Crankshaft Primary Inertia	0.02579 kgm^2
Flywheel Inertia	0.12021 kgm^2

The exact torsional characteristics values of this production engine, dynamometer, and coupling system are difficult to define. It is difficult to minimise the torsional effect entirely in either the crankshaft kinematics or engine block vibration, although identifying the natural frequency of the system and testing at frequencies well away from it when acquiring the data, will improve the quality of the results.
The undamped natural frequency of the engine and drive line system is given as

$$f_n = \frac{1}{2\pi}\sqrt{k\frac{I_1 + I_2}{I_1 I_2}} \tag{4.1}$$

Where I_1 and I_2 are the inertias of the engine and drive line and k is the stiffness of the compliant torsional coupling. The natural frequency of this particular test engine, dynamometer and coupling system is 16.5 Hz. When converted, this results in an engine speed of 990 rpm. This, however, does not take into account the dominant excitation of the system. As the engine has 3 cylinders and it is a reciprocating engine, the excitation of the system occurs 1.5 times every rotation. This leads to the systems critical speed being 660 rpm. It is crucial to run the engine at a

significant distance away from this speed, at least 200 to 300 rpm, to enable the accurate acquisition of the data and prevent long term reliability issues.

4.3 The Test Facilities and Instrumentation

This section discusses two key areas: the engine test facilities, and the instrumentation installed on the engine. The 3-cylinder engine is installed in the gasoline research laboratory and connected to a McClure 130kW / 7000 rev/min DC dynamometer, which is controlled by a Eurotherm control cabinet.

Table 4.2: McClure DC Dynamometer Specifications

Dynamometer Parameters	Value
Maximum Absorption Power	130 kW
Maximum Motoring Power	100 kW
Maximum Speed	7000 rpm
Armature Inertia	0.87 kgm^2
Coupling Torsional Stiffness	1260 Nm/rad

Table 4.2 gives key parameter values associated with the dynamometer shown in Figure 4.2. The dynamometer was mounted in a rotating frame and torque measurements were taken by a load cell on a moment arm. The engine can be controlled manually by either setting the speed or load first and then varying the throttle angle. For all tests undertaken, the load was set at a constant and as a result of varying the, throttle the engine speed fluctuated. Alongside the engine speed and dynamometer load, both the water and oil temperatures were monitored.

Numerous sensors were installed on the test engine including cylinder pressure transducers, a shaft encoder, a knock sensor, and an accelerometer. There were additional sensors attached which were not used in this thesis, however, they will be summarised after discussing the main sensors in detail.

Figure 4.2: McClure DC Dynamometer in Test Cell

The cylinder pressure sensors used were Kistler type 6117BCD36 spark plug integrated transducers which have the advantage of easy installation owing to there being no need to modify the cylinder head. These cylinder pressure sensors have an operational range of 0 to 150 bar and are connected to Kistler type 5044 charge amplifiers via low noise charge cables. The inputs are individually set to the transducer's charge sensitivities and the output gain set to 10 bar/volt (Bennett, 2014). The sensor serial numbers corresponding to particular cylinders are shown in Table 4.3.

Table 4.3: Kistler Spark Plug Integrated Transducer Serial Numbers

Cylinder Numbers	Serial Number
1	1282636
2	1346612
3	1346611

The crankshaft kinematics (crankshaft position) are collected through a crankshaft nose 360 pulse encoder with TDC marker. The encoder installed is a Kistler type 2614A1 optical encoder which is installed on the nose of the engine and securely fixed to the cylinder block to prevent excessive noise in the crank kinematic signal being caused by vibration and motion of the engine. The low inertia of the encoder's rotational element allows for increased sensitively in the crankshaft kinematics. The signal is passed through a Kistler type 2614A4 pulse multiplier and results in two output signals. The first is a 1 pulse for each rotation which can be used as the TDC marker when aligning the rising edge of the TTL signal equal to TDC. The second signal produces 360 or 3600 pulses for each rotation where the first pulse equates to the TDC signal. The encoder is constructed to actually produce 360 physical pulses per revolution (1° resolution) but the Kistler equipment has the capability to produce a 3600 pulse per revolution signal (0.1° resolution). Through experimentation Bennett found that the additional resolution were equally spaced, which suggests the use of linear extrapolation within the encoder's core hardware/software with no means to modify. The limitations and reliability of the 3600 pulse per revolution signal will be discussed in section 4.5. In addition, in section 4.5, the general issues using the encoder will be discussed; namely the errors in the angular displacement.

The application of a standard knock sensor to reconstruct cylinder pressure from engine block vibrations is very appealing as they are now already installed on the majority of gasoline production engines. In (Vulli, 2006) it was found that using the pre-existing knock sensor on the 3-cylinder engine was problematic, owing to the insufficient signal strength for both the ECU and the data acquisition. Therefore, an additional standard Bosch A-261-231-114 knock sensor was fitted to the intake side between Cylinder-2 and Cylinder-3. This position was selected primarily for convenience, as the optimum position for cylinder pressure reconstruction may differ. However, it might be concluded that the location and quality of the signal, optimum for the reconstruction, may not coincide with the optimum for detecting knock. In this case, an additional sensor may be required.

In addition to the engine block accelerations measurements obtained with the knock sensor, a piezo-electric accelerometer was also fitted. The standard knock sensor may also include internal filters that could restrict the desired signal. Therefore an instrument quality Sensonics PZP1 piezo-electric sensor was fitted to record

unmodified accelerations. This was fitted to the exhaust side and mounted in a bolt boss, again for convenience. The accelerometer frequency, and *g* load range are: 0-29 kHz and 0-600 g respectively.

The cylinder pressure sensors, crankshaft encoder, knock sensor and accelerometer were used extensively in this thesis. There are two additional sensors fitted which have been examined by other researchers in relation to cylinder pressure reconstruction. The lesser of the two sensors was the inlet air pressure sensor or MAP (manifold air pressure) sensor. The inlet air pressure is believed to be a valuable indicator, however has not yet been utilised. The second is an inductive probe which is targeted at the teeth of the flywheel to gain additional crank kinematic data. This sensor has two key functions. First, it was used to conclude the degree of angular twist in the crankshaft across the desired speed range, which is vital in understanding crankshaft based reconstruction. The kinematics gathered through the inductive probe were compared to the encoder data and found to include negligible twist (Bennett, 2014). Second, the successful reconstruction using the inductive probe would help the transition of this technology from the research environment to production. The crankshaft encoder, even though accurate, has several limitations when considering its use in production engines. The most significant is the cost which is many times that of existing lower resolution production crankshaft position sensors. In addition there are concerns over the robustness of the encoder and packaging issues. The inductive probe has none of these problems as it is similar to the production position sensor used by the ECU.

4.4 Data Acquisition System

The data acquisition setup has been fully described by (Bennett, 2014). This section will briefly describe the hardware used and important setup decisions that have impacted the work in this thesis. The hardware selected for the data acquisition system was made by National Instrument (NI), and the software used was LabVIEW.

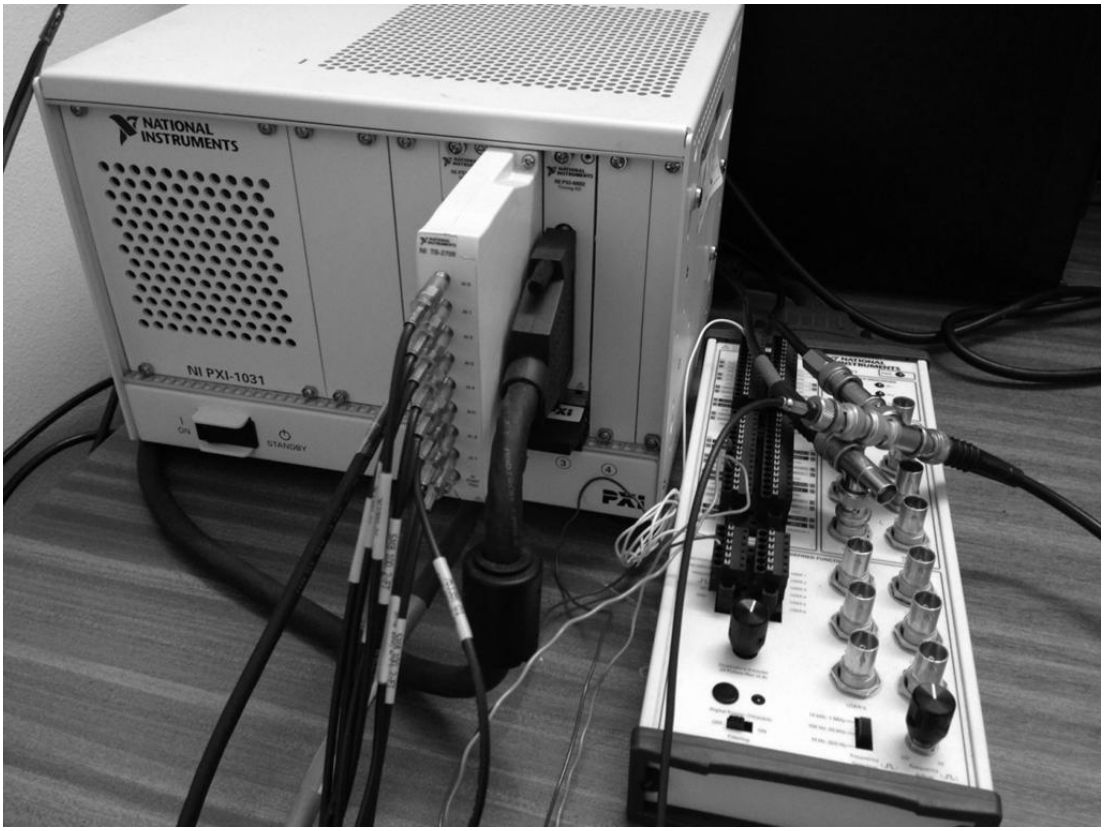

Figure 4.3: National Instruments Data Acquisition System

The hardware used for the acquisition system was a NI PXI system which consists of a NI PXI-1031 chassis and a NI PXI-8331 interface for Windows PC connectivity. This system contained two input modules; the NI PXI-6133 analogue input module and the NI PXI-6602 counter or timer module. The NI PXI-6133 analogue input module has 8 channels with 14-bit synchronous sampling. The analogue inputs were connected using low noise co-axial cables via a TB-2709 terminal block with max sampling rate of 2.5 MHz and max input amplitude of 10V. The NI PXI-6133 module's high sampling rate and dynamic range is particularly suited for this application as it is comparable with other engine combustion analysis systems. This module was used to acquire the data from all of the inputs except the crankshaft encoder owing to it using a TTL signal. The NI PXI-6602 counter or timer module is used for the crankshaft encoder signal and has a 32-bit with a maximum source frequency of 800 MHz. Again, this signal is transmitted through low noise co-axial cables and then into a BNC-2121 terminal block.

The LabVIEW program created to read the data from the hardware, to synchronise the signals and format it appropriately is shown in Appendix C. The details of this have also been comprehensively described by (Bennett, 2014), along with the data

acquisition rates, noise suppression and pegging of the cylinder pressure signals; therefore it is not necessary for further explanation.

There is however, one important subject in the setup of the data acquisition system, which is covered by Bennett, which will be shown to have an effect on the cylinder pressure reconstruction. This effect will be presented in Chapters 5 and 8, and relates to the basis of the acquisition: time or crank angle based acquisition. The NI PXI-6133 module allows for both time based and crank based acquisition depending on the application requirements. Within most combustion analysis systems, the data is commonly acquired in the crank domain; with constant crank angle. However, Bennett determined that this would not be adequate as the sampling frequencies would vary with engine speed and as there was no aliasing protection, there would be little confidence in producing uncorrupted low frequency data. Bennett also came to the conclusion that the ANNs would train more successfully using time based data rather than crank angle based data. The selection of time based data acquisition would remove the need for re-sampling. However, the main concern with using time domain sampling is the synchronisation between the analogue inputs and the TTL signal from the crankshaft encoder. Bennett (2014) overcame this by using the TDC pulse from the encoder to trigger the acquisition of all the inputs for each cycle. This method removes any drift in the acquisition data which could be compounded over many cycles. Bennett describes this method fully (Bennett, 2014).

4.5 Data Acquisition Issues for Engine Tests

The main data acquisition difficulties in both the hardware and software, along with their solutions, have been covered by Bennett (Bennett, 2014). However, it is useful to describe the two most significant issues relating to the data acquisition hardware as it may later impact the results. The biggest issue is the error associated with the crankshaft encoder and its need for calibration. The second is the non-physical 0.1° resolution of the Kistler crankshaft encoder.

Regarding the error in the encoder, this arises from significant high frequency noise on the crankshaft encoder signal which appeared to be cyclical (Bennett, 2014). The hypothesis was that the tolerance of the slits on the rotating disc was such that the actual angle between each slit was not exactly 1°. For the typical uses of this

encoder (i.e. for measuring angular position) this is acceptable. However, the effect of the variability increases significantly when it is numerically differentiated to obtain angular velocity, which increases even more when it is again numerically differentiated to obtain angular acceleration. There was a need therefore for the encoder to be calibrated. Bennett described two different techniques (Bennett, 2014): First, an electric motor was considered. However, owing to small speed fluctuations, it was decided that electric motors would not be appropriate. The second technique, and indeed the method chosen for the calibration, was to use a large inertia disc. The disc and encoder were spun up to speed and allowed to coast, only restricted by encoder bearing friction, which was considered to be uniform. This method was extremely successful and minimised a significant amount of the crankshaft kinematic noise (Bennett, 2014). However, some noise still remained owing to the inherent problem with numerically differentiating measured data.

With respect to the non-physical 0.1˚ encoder issue, there was some uncertainty as to how the optical encoder used the 360 slit disc to achieve 3600 reference points, especially as there was no information in Kistler's literature (Bennett, 2014). Tests were undertaken and it was found that the encoder did not actually have a resolution of 0.1˚. Bennett found that the additional resolution between the 1° pulses were equally spaced and suggested that the two previous positions were used and extrapolated forward assuming little had changed. As a result, there was little useful information in the additional data and therefore was not recorded.

4.6 The Acquired Test Data Sets

The engine test condition selection for acquiring the data is important first to represent real operating conditions, and second to fit within the restrictions of the applications, i.e. the ANN model. In fact, the application of the cylinder pressure reconstruction ANN model has no restrictions as it can, in principle, work across any operational range of an engine. The engine test condition selection was influenced by Jaguar Land Rover, who partly funded the project. They believed that this technology would be most useful in low speed and low load reconstruction conditions. This is motivated by the high cycle-to-cycle variability at these conditions, which makes cylinder pressures less predictable. The higher variability links with the discussion in Chapter 1 on cylinder pressure and its dependencies.

One of the factors that impact the cylinder pressure is in-cylinder air motion. This motion helps determine the quality of the air-fuel mixture. The better and more consistent the in-cylinder air motion is cycle-to-cycle, the less variability and greater the prediction accuracy. At high speed and load conditions, when the throttle is wide open, the air flow into the engine is more uniform, producing more consistent air motion and less variability. However, at lower speed and load conditions, when the throttle is partially open and the volumetric efficiency decreases, the air flow into the engine is compromised. This compromised air flow leads to inconsistent in-cylinder air motion cycle-to-cycle. Therefore, the ability to reconstruct the cylinder pressure at low speed and low load conditions would greatly benefit engine emissions through better control.

The initial tests undertaken (Bennett, 2014) were at both steady-state conditions and speed ramps to represent transient conditions. Three different speed conditions were selected (1000, 1500 and 2000 rpm) along with three different torques (10, 20 and 30 Nm). For the speed ramps, the torque was fixed at 20 Nm and the throttle position was varied to increase the speed from 1000 rpm to 1500 rpm, and 1000 rpm to 2000 rpm over a 60 second period. Each of the tests were undertaken twice to create a reasonably large set of data to train and test the ANNs.

The data produced was sufficient for the previous ANN training and testing (Bennett, 2014) and was also sufficient for the initial work on steady-state conditions within this thesis. In Chapter 8, the need for a more comprehensive set of data will be put forward. This more comprehensive set of data was still within the same operating condition restrictions; between 1000 and 2000 rpm and at 10, 20, and 30 Nm. The difference is in the number of speed conditions used. Instead of the 500 rpm difference between each test, the new data would require a much finer speed increment of only 100 rpm speed difference.

There was also a need for more speed ramps to represent additional transient conditions. These included ramp-up and down in speed over the same 60 second period as well as more complex speed variations. The increased speed variations included speed ramps-up and down, as well as down and up. This was carried out within the same 60 second period to recreate more complex engine behaviour such as overrun conditions.

Chapter 5

Creation of a Methodology for Cylinder Pressure Reconstruction

5.1 Introduction

All the previous effort put into using feed forward and recurrent networks has not, unfortunately, delivered the accuracy and robustness required (see Literature review). This chapter creates a methodology through a series of systematic examinations that overcomes the shortcomings of previous methods. The identification of a single reconstruction methodology involved the testing of NARX networks and standard Time-Delay networks. This led to a deeper understanding of how an ANN reconstructs, with the discovery of a reason for its failure. The standard Time-Delay networks were applied to the reconstruction of cylinder pressure from engine block vibrations and compared with the crankshaft kinematic reconstruction results. This knowledge laid the foundations for the creation of a methodology for the reconstruction of cylinder pressure, comprising of three main concepts; the impact of inertia on the reconstruction accuracy, the filtering of the input data and the reconstruction of individual cylinders.

The initial area to be discussed in section 5.1 will focus on the quantitative limitation of recurrent neural networks and an alternative, time-delay neural networks, using crank kinematics. In section 5.2 and 5.3 early proposals are put forward as to the possible causes for the errors using crank kinematics. In section 5.4, the focus switches to block acceleration, where a significant aspect, inertia, which appears in both crank kinematics and block acceleration is identified, causing a re-examination of crank kinematic based reconstruction in section 5.5. Sections 5.6 through to 5.8 develop and test three concepts that collectively improve the reconstruction performance. The final section, 5.9, will combine the knowledge and processes developed into a single methodology that will be shown to significantly improve the reconstruction of cylinder pressure.

5.2 Recurrent Versus Time-Delay Network Comparison

5.2.1 The Limitations of Recurrent Neural Networks

Prior to optimising different ANN architectures, training algorithms, and signal processing techniques for reconstruction, it is necessary to understand the limitations of previously examined ANNs. The dominant network architectures examined to date have been recurrent neural networks. This section will go into detail about the limitations of recurrent neural networks, as well as the previous reasons for their selection, from the point of view of ANN training and application. A modification from the current view is suggested, namely that recurrent neural networks are not the most suitable architectures for this application. Examination of a different ANN architecture is therefore undertaken.

Efforts had been made in testing more complex ANN architectures and associated training algorithms, but with no significant steps forward in the ANN generalisation performance see Table 5.1. Table 5.1 and Figure 5.1 show the typical results obtained when using recurrent neural networks in both the training and generalisation for the cylinder pressure reconstruction. Figure 5.1 shows is a trend towards good reconstruction in the lower pressure regions but there are significant errors in some high pressure regions which is typical of most of the results published in the papers highlighted. These errors in the high pressure regions will be described and investigated later in the chapter.

Table 5.1 Previous training and reconstruction results when compared with measured cylinder pressure

	Training Root-Mean-Squared Error	Generlised Root-Mean-Squared Error
Potenza et al., 2006	4.96 %	5.12 %
Vulli, 2006	6.52 %	8.19 %
Bennett, 2014	2.6 %	4.8 %

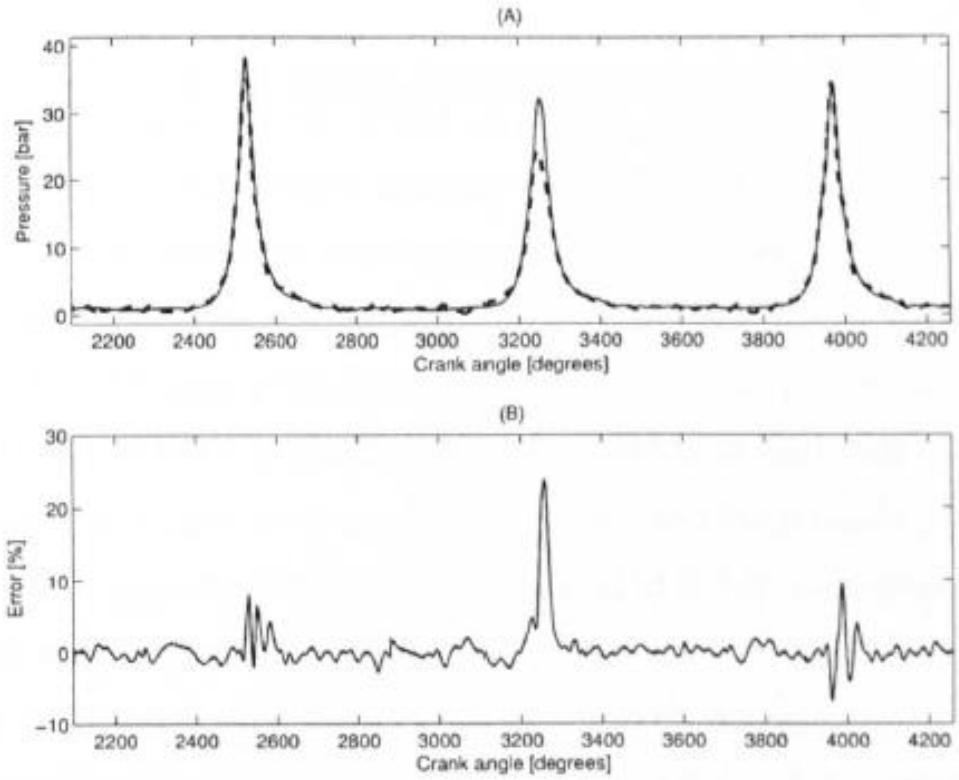

Figure 5.1: Illustration of Previous Results with RMSE = 2.6648% (Potenza, 2006)

Results obtained by other researchers also show good cylinder pressure reconstruction in some regions when using the generalised data. However, there is a tendency for the reconstruction model to become unstable with only a small chance of stability returning. These areas of poor reconstruction at high pressure, along with the stability issues using recurrent neural networks, are two of the main limitations to achieving the desired goals. It is noted that there are diminishing returns in optimising recurrent neural networks; the more time spent optimising on training data, the smaller the increase in reconstruction generalisation performance. The suggestion that simple network architectures and associated training algorithms may not be able to identify or interpret less dominant dynamics present in the data (Vulli, 2006) and therefore be the limiting factor to the ANN's reconstruction capability, was examined; yet they failed to have the desired effect.

In this thesis, a hypothesis is proposed, namely that the complexity of the ANN architecture and associated training algorithm are independent of the limitations to reconstruct, and may cause unjustified complexity. This position can be reasoned from the use of the universal approximation theorem (Cybenko, 1989), and supported by the significant number of previous attempts at optimising ANNs. The

universal approximation theorem states "that simple neural networks can represent a wide variety of interesting functions when given appropriate parameters". With the large number of recurrent network architectures trained by different researchers using complex training algorithms and large numbers of training iterations, an ANN should have been able to successfully reconstruct cylinder pressure; especially if all the "appropriate parameters" or information content is available. The failure to train an ANN to successfully generalise for this application, calls into question the need for complex recurrent architectures and associated training algorithms.

This hypothesis that the complexity of recurrent architectures and associated training algorithms is not necessarily required for this problem, is examined throughout this chapter and throughout the remainder of the thesis. This will be achieved using relatively simple network architectures with simple standard training algorithms. Moreover, not only are there concerns with the use of recurrent neural networks from a training point of view, but they have additional limitations when considering their practical application of cylinder pressure reconstruction. The initial justification for the use of recurrent neural networks is however sound.

To recap, the data requirement, in general, for recurrent neural network architectures consists of two types of inputs where each has their own task. The first type, the cylinder pressure feedback (recurrent connection), is intended to increase the reconstruction capability, as previously reconstructed pressure can give some indication as to the magnitude of subsequent cylinder pressure values. These inputs also facilitate noise reduction of the reconstructed pressure signal and provide a form of internal memory. The second type, involving delays of the crankshaft kinematics or engine block vibration, is believed to be more critical in reconstructing cylinder pressure. These delays capture significant changes in either the crankshaft or engine block behaviour, that inversely relate to the cylinder pressure. The use of the cylinder pressure feedback may certainly have a positive impact on the ANN's ability to reconstruct. But this idea can be shown to be flawed in one of the most significant regions within the combustion process; at the point of ignition. The ignition point is particularly important with regards to reconstructing cylinder pressure as from this time forward, within a combustion event, the cylinder pressure can vary significantly cycle-to-cycle.

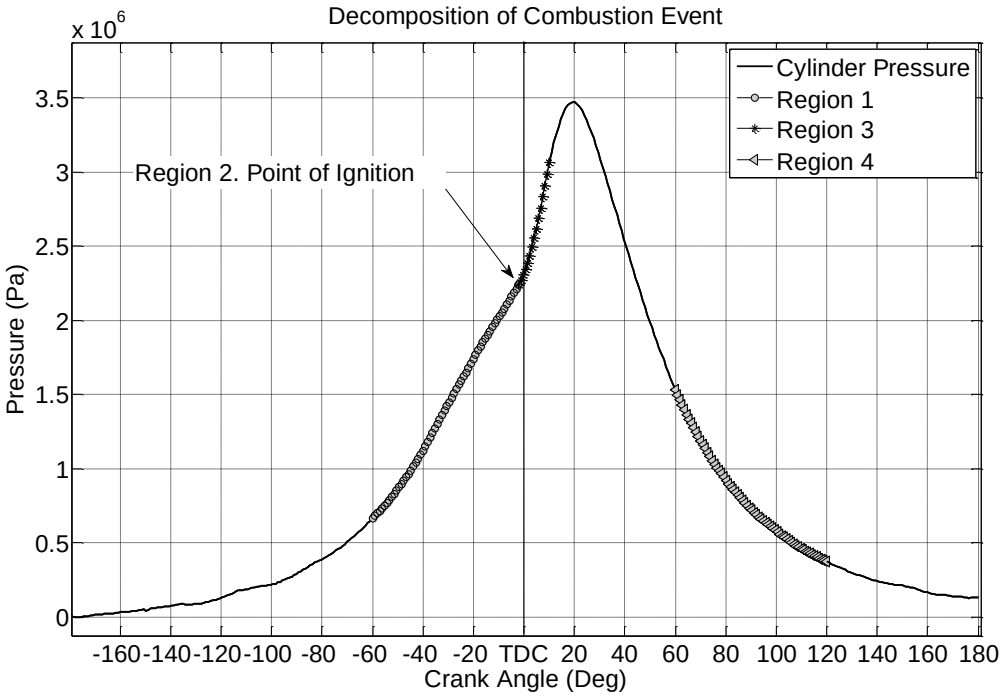

Figure 5.2: Pressure Event Diagram

The best way to explain the reason why the recurrent neural network architecture is limited within this application, is to break down the reconstruction of the cylinder pressure into different regions within the combustion event. When considering a cycle under steady state conditions, it must be examined in four parts: the reconstruction prior to the ignition, the reconstruction at the point of the ignition, the reconstruction immediately after the ignition, and reconstruction at a significant period of time after the ignition. These have been illustrated in Figure 5.2.

First, prior to ignition, the cylinder pressure is relatively consistent, cycle-to-cycle, as the compression process is nearly identical under steady-state conditions. Therefore, the pressure feedback delays would have little significance on the reconstruction in this region. Second, at the point of the ignition, the crankshaft kinematics or block vibration has not yet started to alter as the cylinder pressure rises would be extremely small in magnitude at this stage. The feedback delays would again have no relevant information related to the ignition process as it is only presenting the information pertaining to the compression process. Directly after the start of ignition, the crankshaft kinematics or engine block vibration would vary as the cylinder pressure rises. The pressure feedback delays would then have only partial ignition process information, the rest pertains to the compression process. Finally, at a significant period after ignition, both the crankshaft kinematics or block

vibration variation, should be fully developed and the cylinder pressure feedback delays should contribute to the reconstruction.

It is therefore proposed that, within certain regions of the reconstruction, the cylinder pressure feedbacks would have either little importance or be unnecessary for the reconstruction. The ANN would then essentially become a time-delay network (discussed in Chapter 3). Even though feedbacks would be useful for reconstruction in the second half of the combustion event, they may generate reconstruction errors early in the combustion event, which may induce subsequent errors and cause instabilities within the recurrent neural network. For the reasons outlined, the use of recurrent networks is considered problematic within this application. The fact that at certain points within the reconstruction these networks can be simplified to time-delay networks, suggests that pressure feedback may inadvertently be the source of some of the reconstruction problems.

5.2.2 A Test Using a Time-Delay Neural Network

This section examines the use of time-delay neural networks as an alternative to recurrent networks for reconstructing cylinder pressure. Each test will be undertaken with the same architecture size, number of neurons and delays, and the same training algorithm, and the same number of epochs and performance targets. Prior to carrying out three independent tests using the time-delay network, an optimisation will be undertaken to obtain the best number of neurons and delays to ensure the best performing network. Tests will be carried out at three different steady state conditions, as outlined in Table 5.1.

Table 5.1: Engine Test Conditions

	Engine Speed (rpm)	Engine Load (Nm)	Data name
Condition-1	1000	10	1000_10_01p_jun2010
Condition-2	1000	20	1000_20_01p_jun2010
Condition-3	1000	30	1000_30_01p_jun2010

To follow the proposal that recurrent neural networks may be too complex for the proposed application, a simpler training algorithm was selected that has a proven history of being robust with multilayer perceptron architectures and time-delay

neural networks. The standard training algorithm used is the Levenberg–Marquardt algorithm (LMA) which will take place using MATLAB, which has a pre-existing LMA training algorithm within the Neural Network Toolbox. Table 5.2 shows an example of the initial settings and goals which have been outlined.

Table 5.2: Neural Network Settings and Training Goals

Network Name	Net_TD_Test1	**Network Architecture**	Time-Delay	**Test Data**	1000_10_01p_jun2010
Network Training Algorithm	Levenberg–Marquardt	**Hidden Layers Number**	1	**Speed (rpm) / Load (Nm)**	1000/10
Cost Function	Mean Squared Error	**Neurons Number**	15	**Time/Crank Domain**	Time
Training Goal	1E8	**Delay Number**	60	**Time/Crank Step**	0.0001 s
Maximum Epoch	1000	**Transfer Function Layer 1**	Sigmoid	**Number of Iterations**	10
Weights Initialisation	Randomised	**Transfer Function Layer 2**	Linear		

The data for the three test points was selected from the database of training gathered over the past several years. These three test points were chosen to show the reconstruction for a number of steady state conditions. The output data, cylinder pressure, for the entire test, was processed using the same approach. The pressure data from each cylinder was concatenated into a single data string without the need for filtering. The input data, crank kinematics, had a minimal amount of low-pass filtering to remove the high frequency noise content. The crank kinematics were then converted into a structure required for the training of a time-delay network. This included the kinematics for the current time step as well as the delays, which is the set number of previous kinematic points.

The optimisation of the network's neuron and delay numbers are important for the following reasons. First, if there are too few delays, the information content presented to the network may not be sufficient. However, if there are too many delays, the network would be presented with too much information which may lead to difficulties in training and generalisation. Second, if there are too few neurons then the network may be too restricted, and will be prevented from successfully training. Finally, if there are more neurons or delays than necessary, the size of the network can increase significantly, leading to a considerably longer training time and increased computational requirements. The optimisation of the neuron and delay numbers was undertaken through a brute force analysis, by training and testing a range of networks with a varying number of neurons and a varying number of delays, at a single steady-state condition.

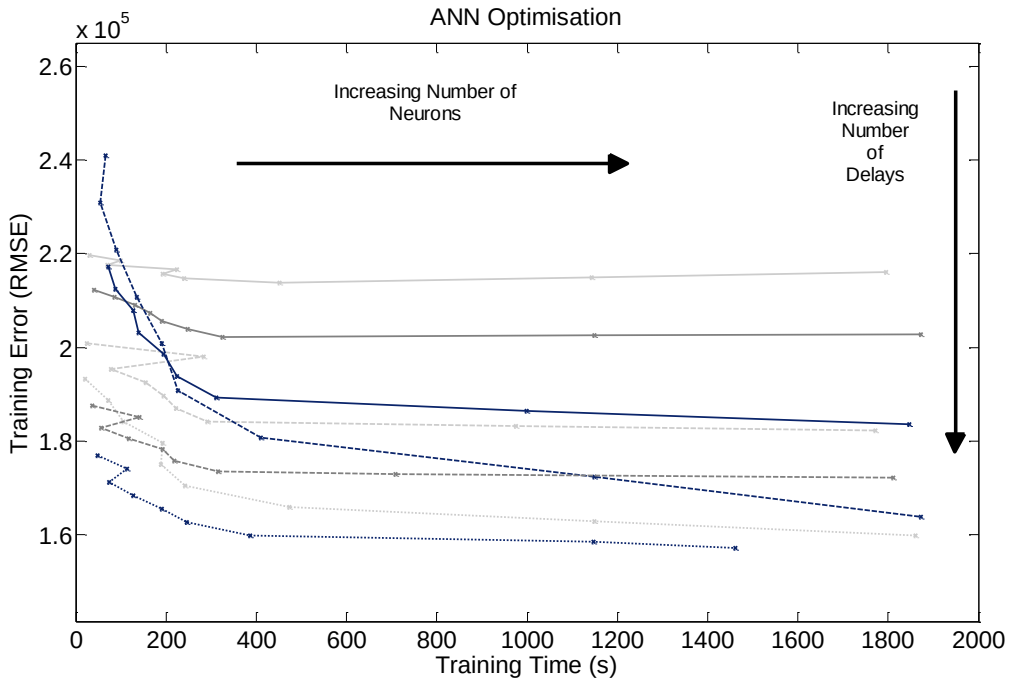

Figure 5.3: Optimisation of Neuron Number and Delay Number. Each line represents a different number of input delays and each point on the line represents a different number of neurons.

Figure 5.3 shows the generalised performance of the network against the computation time for a number of differing networks, with different numbers of neurons and delays. The optimum network is selected by weighing up the performance and computation time. The best architecture is the one with very good performance but not excessive computation time. It was seen that the best neural network architecture had between 10 to 15 neurons in the hidden layer, and around

120 delays. From the literature review, and the efforts of previous researchers, the number of neurons found to be optimum was expected, but the optimum number of delays was greater than anticipated, and previously unseen. The number of delays was actually found to be important and the significance of this will be discussed later in the thesis.

The next series of figures show both the results of training and generalisation at three engine test conditions. The networks were trained using the same architecture with 10 neurons. However, in order to find the best network possible, numerous ANNs were trained with different initial conditions, meaning that only 60 delays were selected owing to the computational requirements. There was little difference in performance from the optimum number of 120. Further examinations were undertaken to find the number of delays within time-delay neural networks. The following figures present the typical training and generalisation results for these three test conditions using a time-delay neural network. Generalisation refers to test the ANN on data which has not been used during the training to assess the performance of the ANN.

Test 1 Training Results

Figures 5.4 and 5.5 show the training results for condition-1 (1000 rpm and 10 Nm).

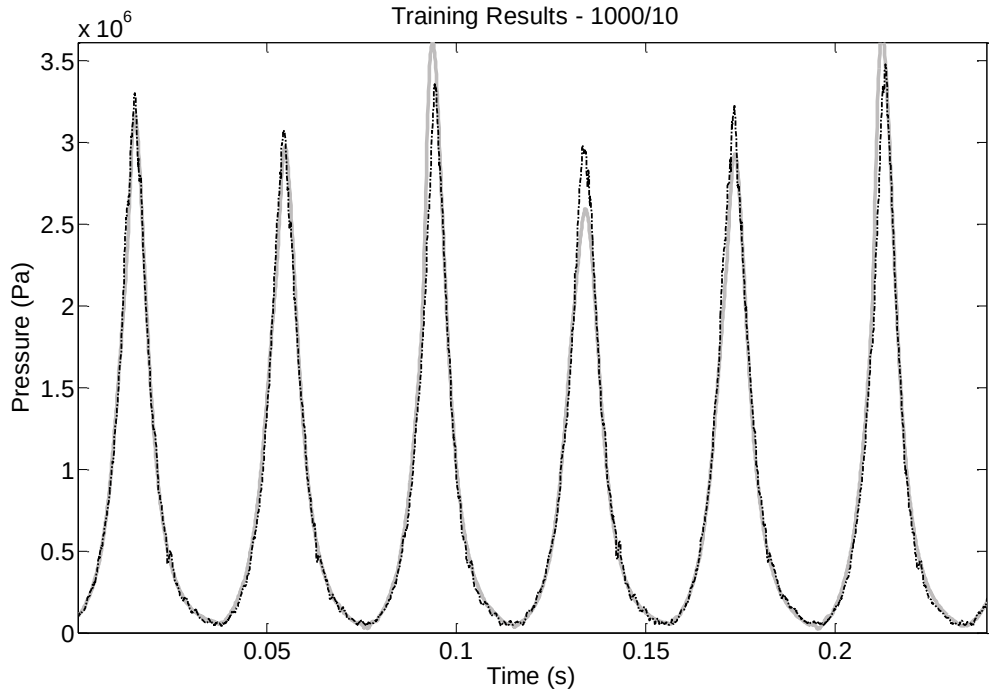

Figure 5.4: Condition-1 Training Results. Target pressure (grey continuous line) and predicted pressure (dotted line).

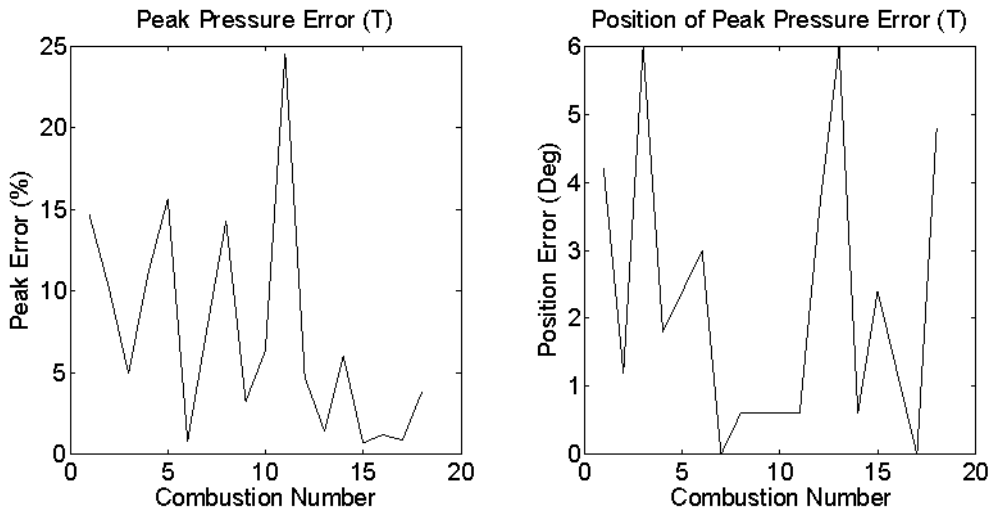

Figure 5.5: Condition-1 Training Results. Left shows training peak pressure error and right shows training position of peak pressure error.

Test 1 Generalisation Results

Figures 5.6 and 5.7 show the generalised results for condition-1 (1000 rpm and 10 Nm).

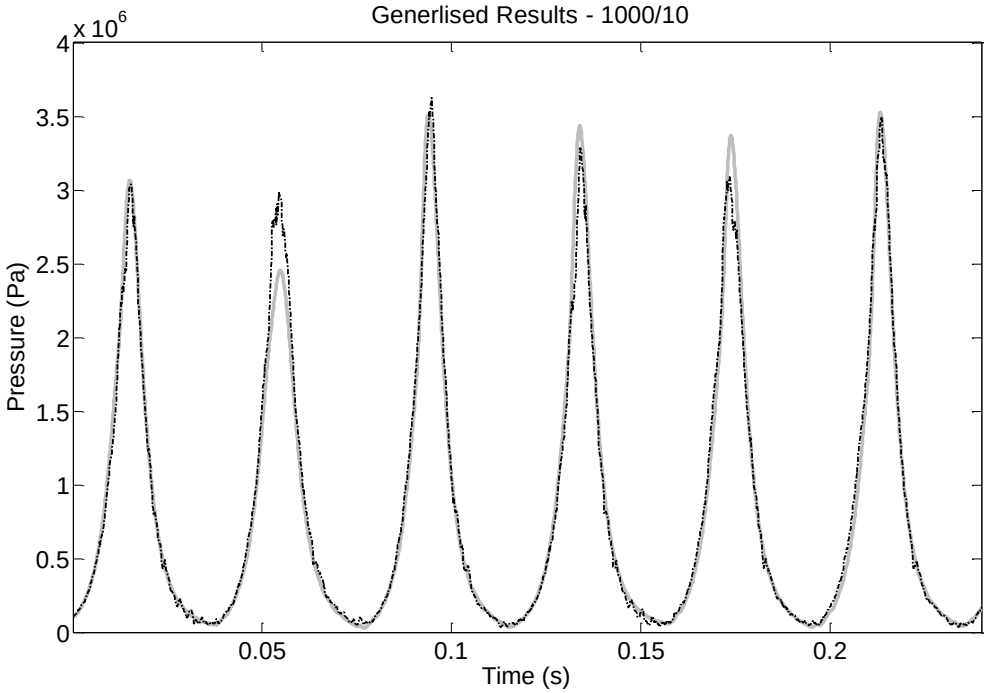

Figure 5.6: Condition-1 Generalised Results. Target pressure (grey continuous line) and predicted pressure (dotted line).

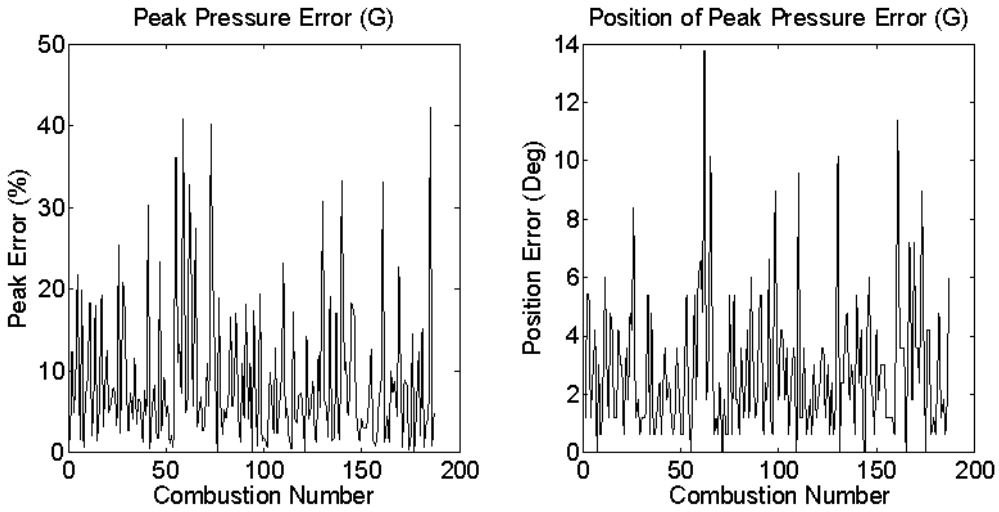

Figure 5.7: Condition-1 Generalised Results. Left shows training peak pressure error and right shows training position of peak pressure error

Test 2 Training Results

Figures 5.8 and 5.9 show the training results for condition-2 (1000 rpm and 20 Nm).

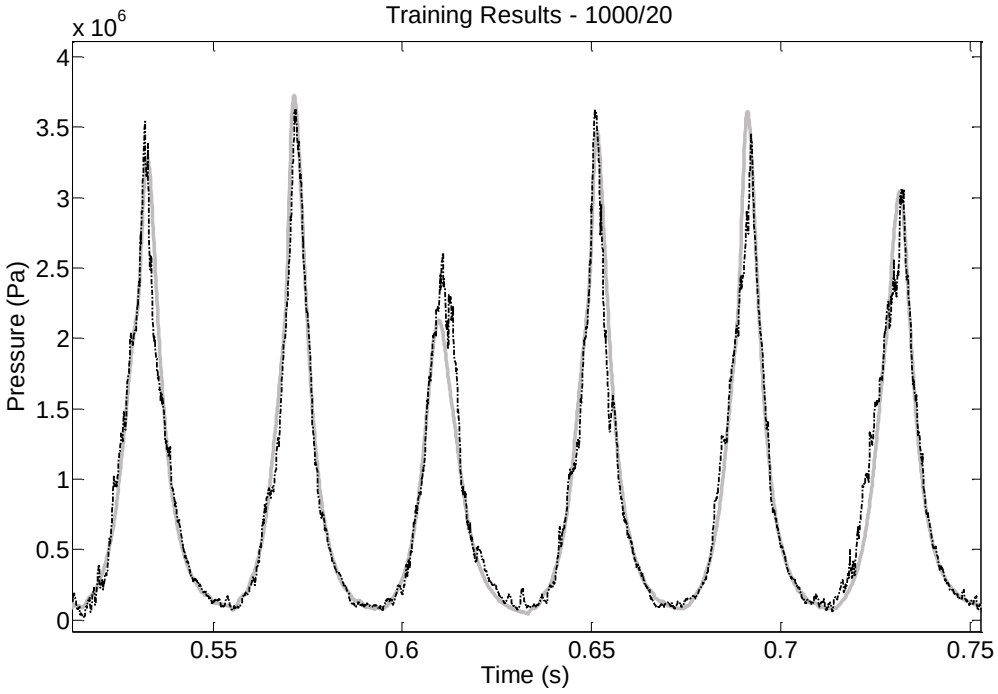

Figure 5.8: Condition-2 Training Results. Target pressure (grey continuous line) and predicted pressure (dotted line).

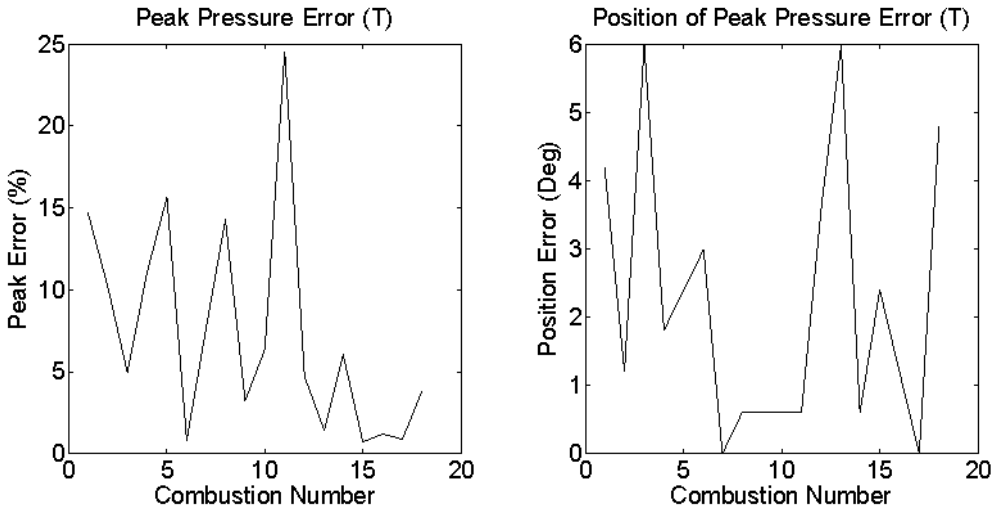

Figure 5.9: Condition-2 Training Results. Left shows training peak pressure error and right shows training position of peak pressure error

Test 2 Generalisation Results

Figures 5.10 and 5.11 show the generalised results for condition-2 (1000 rpm and 20 Nm).

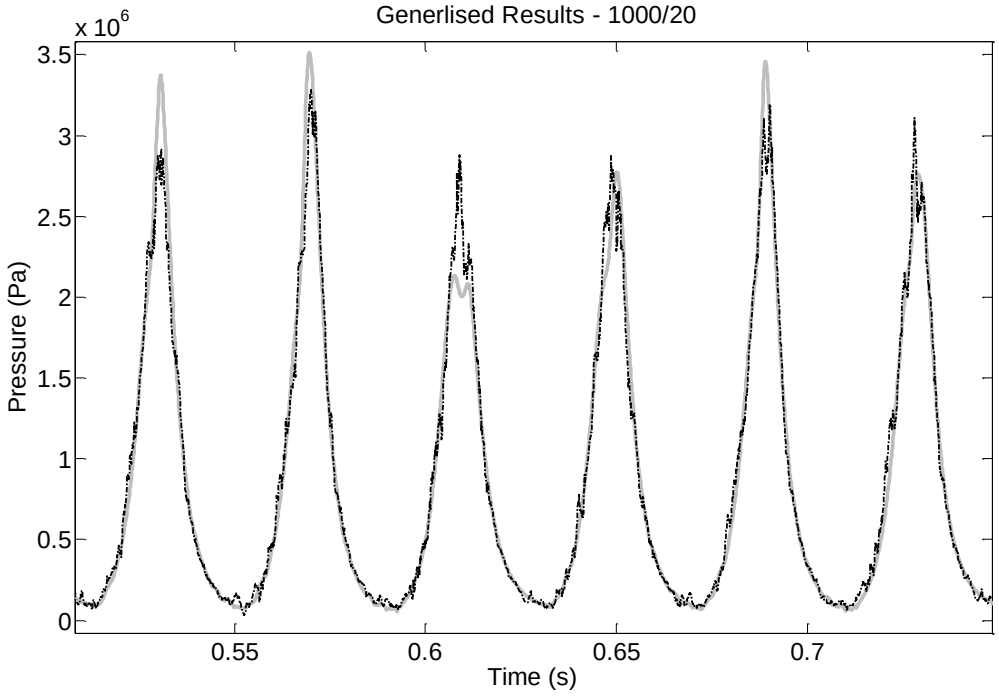

Figure 5.10: Condition-2 Generalised Results. Target pressure (grey continuous line) and predicted pressure (dotted line).

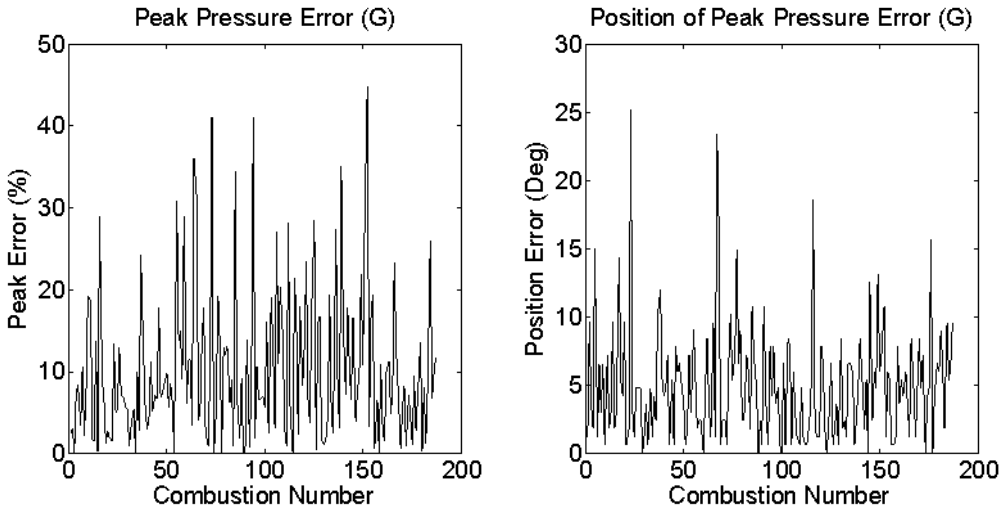

Figure 5.11: Condition-2 Generalised Results. Left shows training peak pressure error and right shows training position of peak pressure error

Test 3 Training Results

Figures 5.12 and 5.13 show the training results for condition-3 (1000 rpm and 30 Nm).

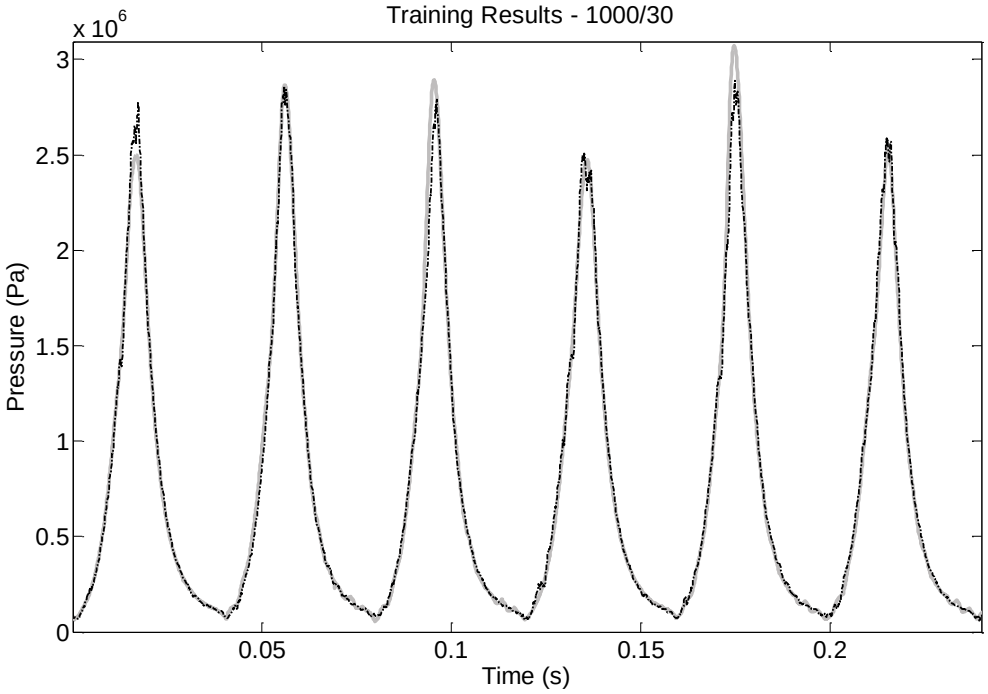

Figure 5.12: Condition-3 Training Results. Target pressure (grey continuous line) and predicted pressure (dotted line).

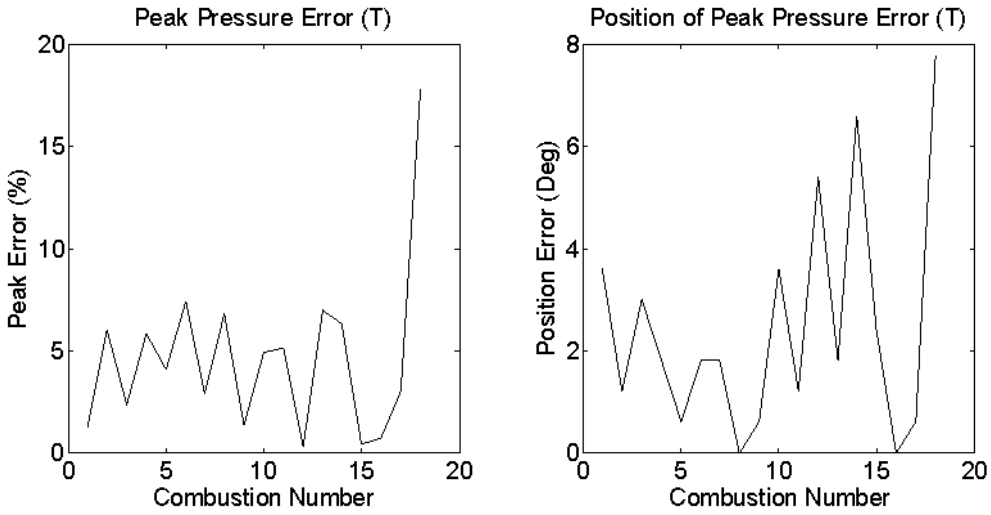

Figure 5.13: Condition-3 Training Results. Left shows training peak pressure error and right shows training position of peak pressure error

Test 3 Generalisation Results

Figures 5.14 and 5.15 show the generalised results for condition-3 (1000 rpm and 30 Nm).

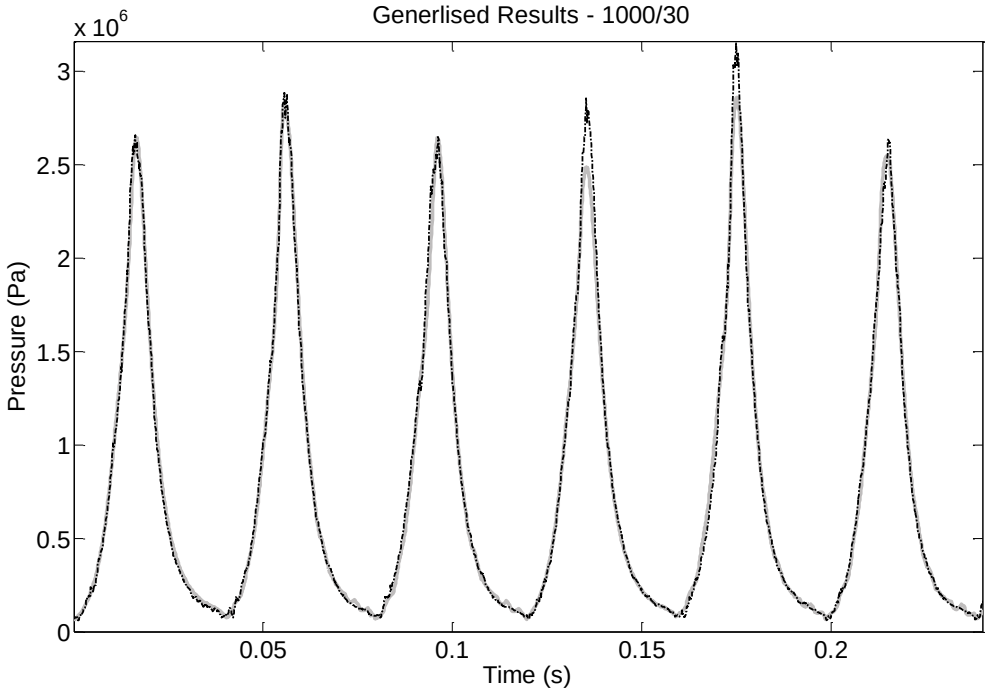

Figure 5.14: Condition-3 Generalised Results. Target pressure (grey continuous line) and predicted pressure (dotted line).

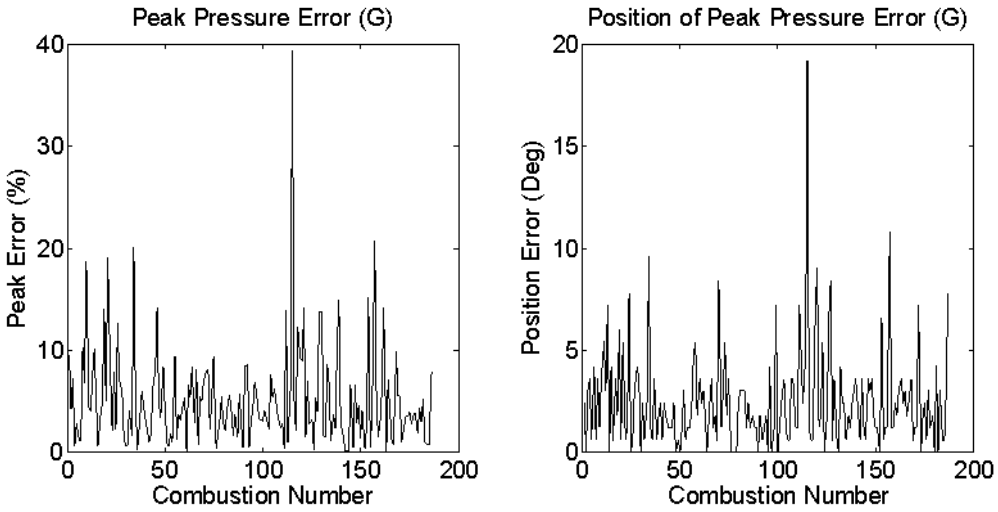

Figure 5.15: Condition-3 Generalised Results. Left shows training peak pressure error and right shows training position of peak pressure error

Table 5.3: Mean of the Training and Generalisation Results

	Mean Training Peak Pressure Error (%)	Mean Training Peak Pressure Position Error (Deg)	Mean Generlised Peak Pressure Error (%)	Mean Generlised Peak Pressure Position Error (Deg)
Condition-1	9.13	5.63	10.32	5.91
Condition-2	11.19	5.82	10.67	7.60
Condition-3	4.72	4.92	4.93	4.33

Table 5.4: Standard Deviation of the Training and Generalisation Results

	Standard Deviation of Training Peak Pressure Error (%)	Standard Deviation of Training Peak Pressure Position Error (Deg)	Standard Deviation of Generlised Peak Pressure Error (%)	Standard Deviation of Generlised Peak Pressure Position Error (Deg)
Condition-1	12.68	7.48	12.77	6.85
Condition-2	12.24	7.44	13.30	9.56
Condition-3	6.40	6.69	6.35	5.45

Discussion of the Test-1, Test-2 and Test-3 Results

The results for the three test conditions show a variety of both successful and unsuccessful generalised reconstructed cylinder pressure events. The results shown in Figures 5.4 to 5.15, as well as the tables 5.3 and 5.4, show several notable features; predominantly, the large difference between the performance of the higher load test, condition-3, and the other two tests. The exact reason for this difference is unclear. However, there is one possible explanation for this, which can be explained from either the perspective engine behaviour or the ANN training but fundamentally is concerning the variability of the dynamics and size of the training data. The dynamics of condition-1 and condition-2 are affected significantly by additional factors which are also present in condition-3 but are not as dominant. The most notable are the relative increase in friction and inertia for condition-1 and the retarded ignition by the engine management system for condition-2. These are factors which should easily be overcome by the ANN with the right data but the size of the training data used for these test was restricted through practicality. Even though the later work uses more comprehensive data, the following observations are still present. One observation is the consistency of the errors in both the training and generalisation results. This is a sign that the network is not over-training and this is particularly promising for this architecture and training algorithm, in this application. Another noteworthy feature is the poor generalised reconstruction at the extremes, i.e. at the high and low pressures. However, with more constant pressure events and less cycle-by-cycle variability, the generalised reconstruction capabilities are outstanding. This is observation is believed to be of most importance as at this stage there appears to be little understood about the cause of this or any suggestion about methods to remove or reduce this affect.

5.2.3 A Comparison between Recurrent and Time-Delay Neural Networks

To adequately test the hypothesis that a time-delay network would do a better job at reconstructing cylinder pressure than a recurrent neural network, it was necessary to produce a recurrent network for comparison. A similar approach to section 5.2.2 was undertaken but with the recurrent architecture, specifically the NARX architecture, and trained via 'teacher forcing' using the Levenberg–Marquardt algorithm. The results produced show a clear resemblance to the work previously undertaken by others (Potenza, 2006) and the characteristics of the reconstruction in both training and generalised data.

NARX Training Results

Figures 5.16 and 5.17 show the training NARX results for condition-1 (1000 rpm and 10 Nm).

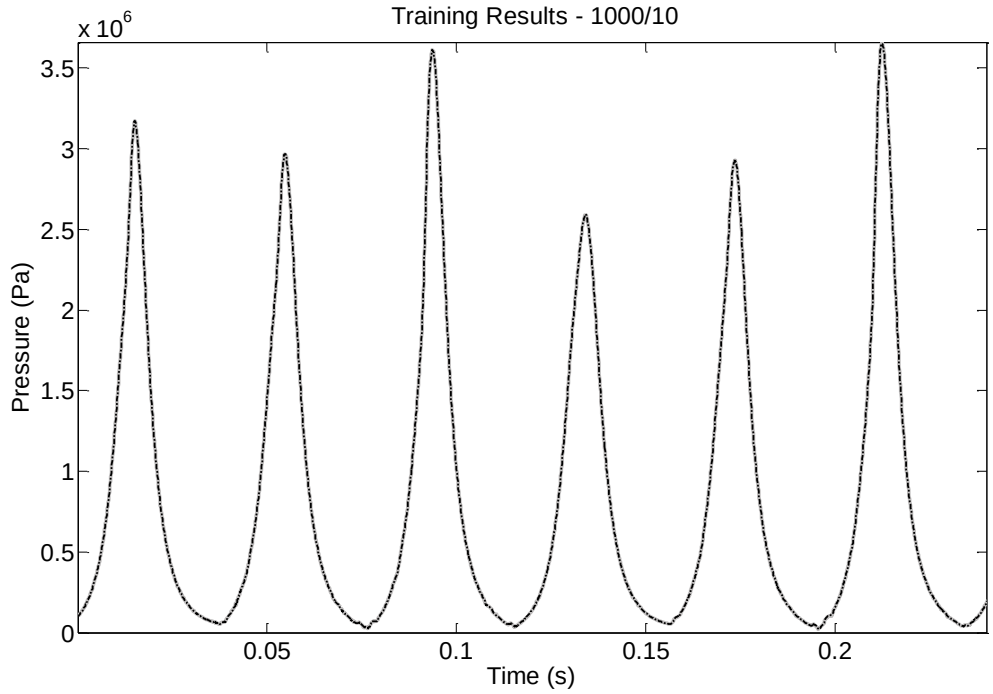

Figure 5.16: Recurrent Training Results via Teacher Forcing. Target pressure (grey continuous line) and predicted pressure (dotted line).

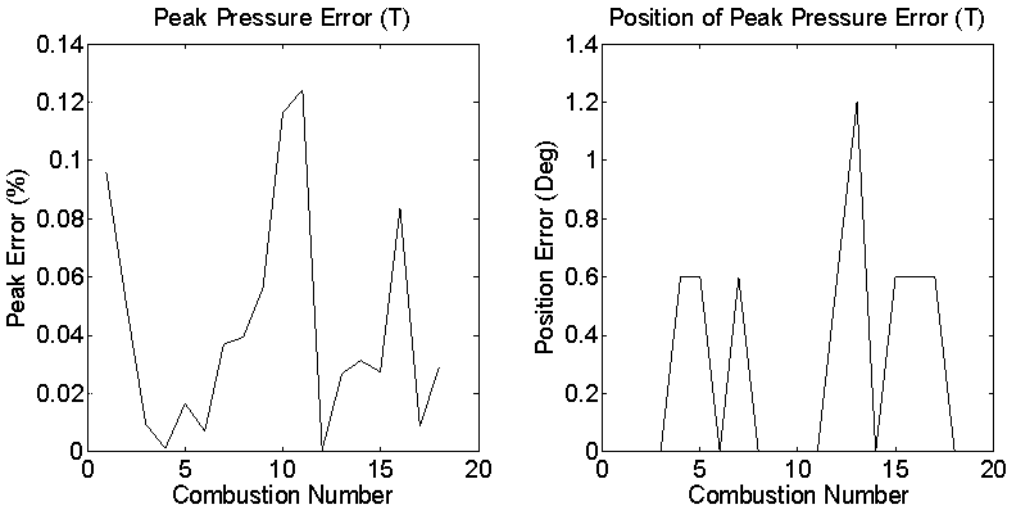

Figure 5.17: Condition-3 Training Results. Left shows training peak pressure error and right shows training position of peak pressure error

NARX Generalisation Results

Figures 5.18 and 5.19 show the generalised NARX results for condition-1 (1000 rpm and 10 Nm)

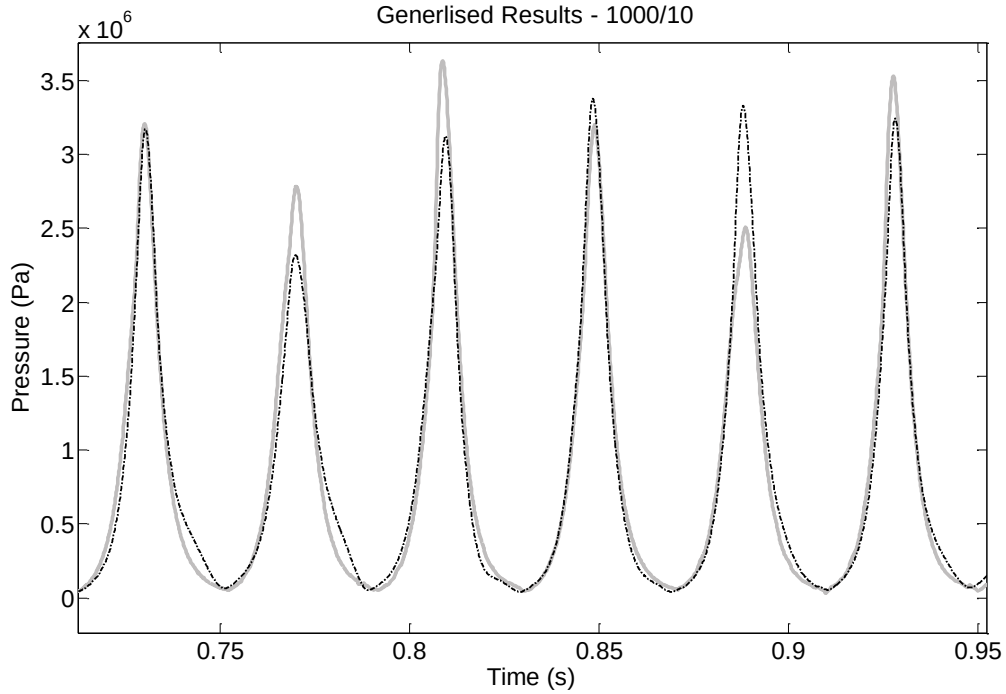

Figure 5.18: Recurrent Generalised Results. Target pressure (grey continuous line) and predicted pressure (dotted line).

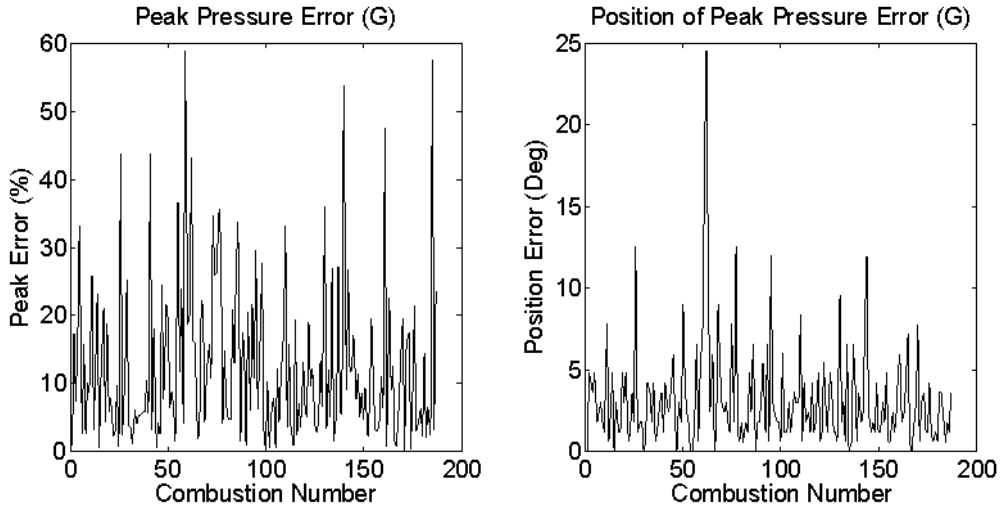

Figure 5.19: Recurrent Generalised Results. Left shows training peak pressure error and right shows training position of peak pressure error

Discussion of NARX Results

The time-delay network results can be seen to have similar characteristics to the recurrent network in the areas of good and poor cylinder pressure reconstruction in Figures 5.16 to 5.19. The similarities go even further in that the errors generated, not only occur in a similar position, but they are also of the same magnitude. A direct comparison between a recurrent neural network and a time-delay network is shown in tables 5.5.and 5.6 as well as Figure 5.20.

Table 5.5: Comparison of Mean for both Time-Delay and Recurrent Networks

	Mean Training Peak Pressure Error (%)	Mean Training Peak Pressure Position Error (Deg)	Mean Generalised Peak Pressure Error (%)	Mean Generalised Peak Pressure Position Error (Deg)
Time-Delay Network	9.13	5.63	10.32	5.91
NARX Network	0.04	0.55	12.89	6.02

Table 5.6: Comparison of Standard Deviation for both Time-Delay and Recurrent Networks

	Standard Deviation of Training Peak Pressure Error (%)	Standard Deviation of Training Peak Pressure Position Error (Deg)	Standard Deviation of Generalised Peak Pressure Error (%)	Standard Deviation of Generalised Peak Pressure Position Error (Deg)
Time-Delay Network	12.68	7.48	12.77	6.85
NARX Network	0.05	0.82	17.59	8.28

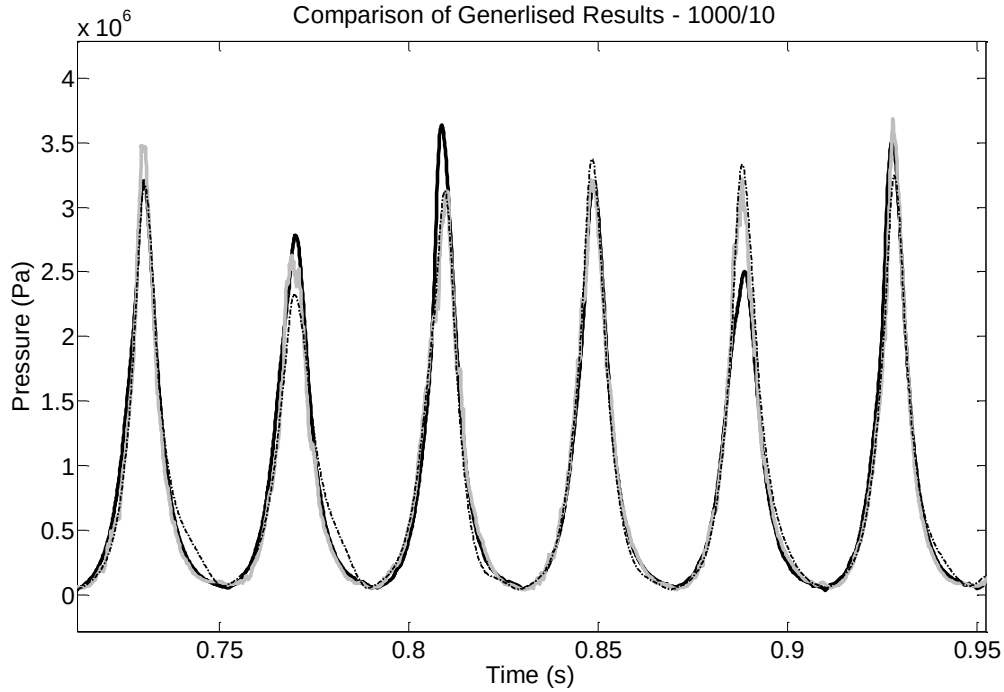

Figure 5.20: Comparisons between Time-Delay and Recurrent Network Generalised Results. Target pressure (black continuous line), predicted with time-delay network pressure (grey continuous line) and predicted with recurrent network pressure (dotted line).

The similarities between the time-delay and recurrent networks, figure 5.20, shows that highly complex ANN architectures and training algorithms are not necessarily required to reconstruct cylinder pressure to the pre-established level. What has also been evident in the training of numerous recurrent networks, is a tendency for the reconstruction in generalised conditions to become unstable. Figure 5.21 is an extreme example of the unstable nature of recurrent neural networks. This would appear to be as a result of high frequency noise within the input data; however this is not necessarily the case. The most likely reason could be that the dynamics of the engine are distinctly different to the training data in this region causing the destabilisation of the ANN feedbacks and the reconstruction.

Within that trained network, the instability occurs very quickly and does not recover. However, there are examples of recurrent networks becoming unstable, to a lesser extent than shown in Figure 5.21, and recovering. The capacity of the recurrent neural network to become unstable is evident, but also unpredictable when generalising, causing questions to be asked of the efficacy of this architecture.

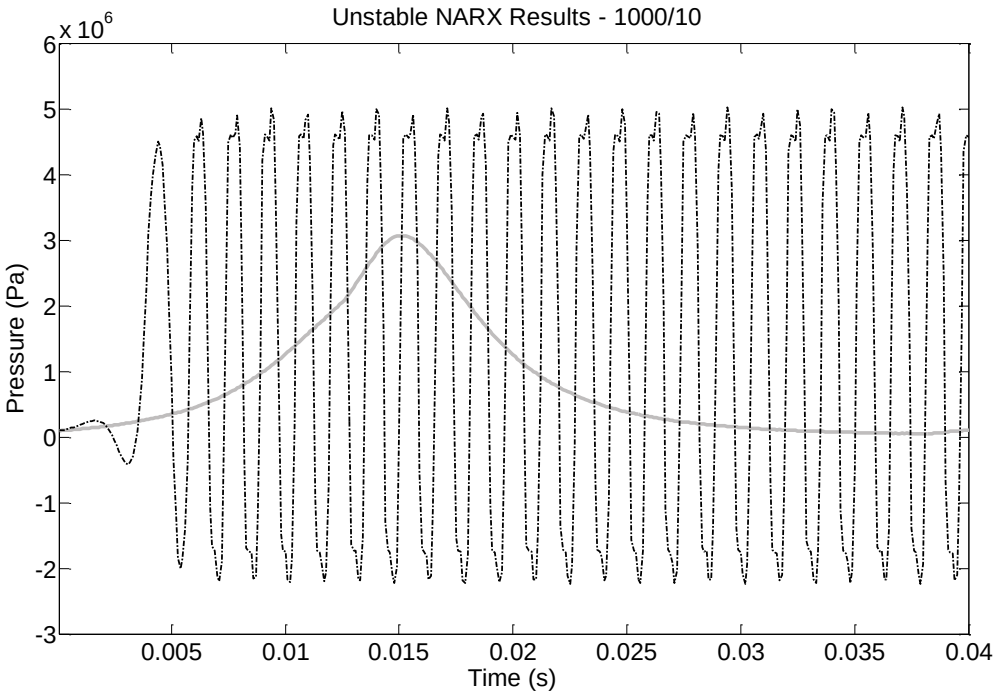

Figure 5.21: Unstable Recurrent Network Generalised Results. Target pressure (grey continuous line) and predicted pressure (dotted line).

Alongside the stability issues, the use of these complex network architectures and training algorithms may have masked the underlying problem preventing the successful reconstruction. Furthermore, the suggestions and subsequent research paths undertaken in improving the neural networks performance by mastering the architectures and training algorithms, could have underestimated other influential factors.

When comparing the limitations of recurrent neural networks and their similarities to time-delay neural networks, the comparison negates the belief that architecture is key to the reconstruction, alongside the ideas presented previously, namely the large number of iterations using recurrent neural networks and the universal approximation theorem. It is evident that there must be additional factors not yet understood affecting cylinder pressure reconstruction. This is now the focus of the

remainder of this chapter, to determine what overriding aspect has been overlooked, in the successful application of ANNs in reconstructing cylinder pressure.

5.3 Over and Under Cylinder Pressure Reconstruction

Two key principles have been demonstrated which indicate the research direction. The first is the fact that the level of complexity of both the neural network architectures and training algorithms appears to have negligible impact on the performance of the cylinder pressure reconstruction. The second is the large number of network iterations required (Lawrence,1997). These ideas, alongside the universal approximation theorem (Cybenko,1989), support the proposal that the neural networks within section 5.1 should have trained and be able to reconstruct the cylinder pressure accurately. The failure of the networks and training algorithms to do this, demonstrates that the networks must not have been “given appropriate parameters" to be able to train sufficiently. This observation then brings us to the idea that the key to improving the network's performance lies more in the data, and application of the data, rather than the network architectures or training algorithms. This direction was therefore pursued further.

The initial work undertaken in section 5.1, where the inability to successfully train both recurrent and time-delay neural networks was presented, posed considerable doubt on the viability of accurately reconstructing cylinder pressure. Subsequent work was undertaken with the aim of improving the reconstruction capabilities by focusing more on the content of the crankshaft kinematic data sets, and the way they are presented to ANNs.

One of the proposals was the manipulation of the input data to aid in the ANN's training effectiveness. The reasoning was that if some known and measurable physical characteristic of the input data could be removed, modified or presented differently, the training might be more successful. Examples of the presentation of the data differing from the crank velocity, solely used at that point, include crank position, crank acceleration and the third derivative of position: crank jerk. The methodology was put forward with the belief that the ANN could focus more of its computational effort and on the complex and unknown nonlinear aspects of the crank kinematics, when reconstructing cylinder pressure. Many tests were

undertaken with a combination of manipulations to the data. These tests produced no significant improvement with regard to the ANN's reconstruction performance and therefore are not presented in any more detail. However, improvements were established in reducing the time required for training and computational effort. It appeared that these manipulations aided in reducing the void between the input and output, similar to the work done with regression problems, but did not overcome the crucial problem. These tests prove that the missing or masked portion of the data is much more ingrained in the crank kinematics; therefore simple manipulations will have little effect on the reconstruction capability.

It has therefore been established, that the difficulty in reconstructing cylinder pressure lies more with the crankshaft kinematics and the method by which this data is presented to the ANN. The identification of this problem and the solution to this was not obvious. By reviewing the results within the later part of section 5.1, a trend became apparent. There was seemingly a pattern of reconstruction surrounding TDC, where some combustion events were significantly higher than measured: i.e. over reconstructed, and some combustion events were significantly lower than measured: i.e. under reconstructed. This pattern presented itself in the form where a higher peak pressure combustion event preceded a significantly lower peak pressure combustion event, the reconstruction appeared to over reconstruct. The reverse was also true, that where a lower peak pressure combustion event preceded a significantly higher peak pressure combustion event, the reconstruction appeared to under reconstruct. Both of these can be seen in Figure 5.22 and 5.23 respectively.

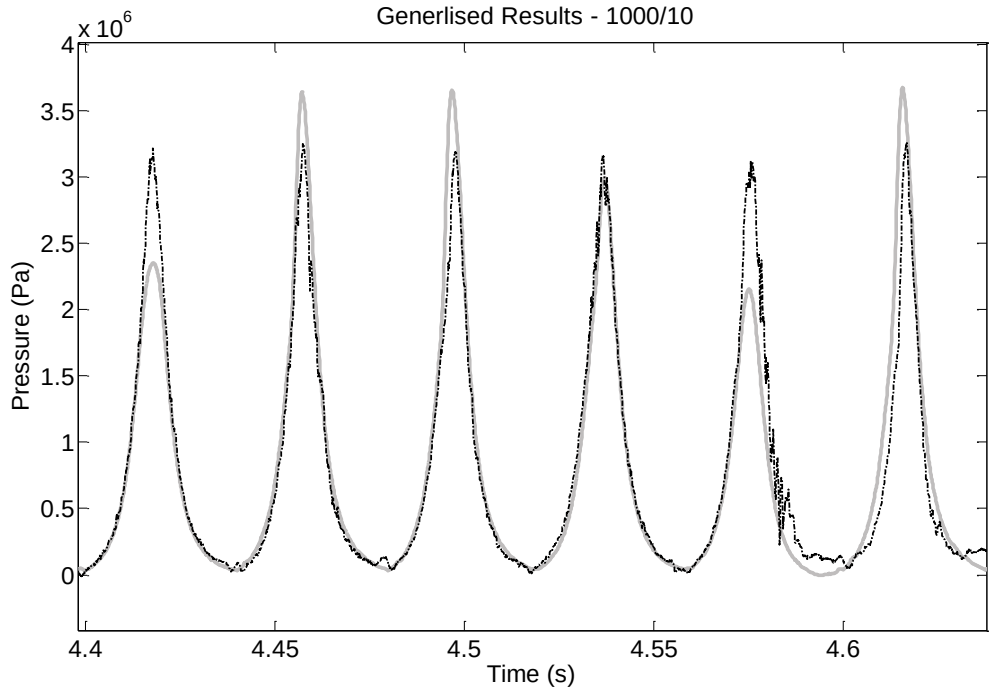

Figure 5.22: Over reconstruction. Seen at combustion event 2 and 4. Target pressure (grey continuous line) and predicted pressure (dotted line).

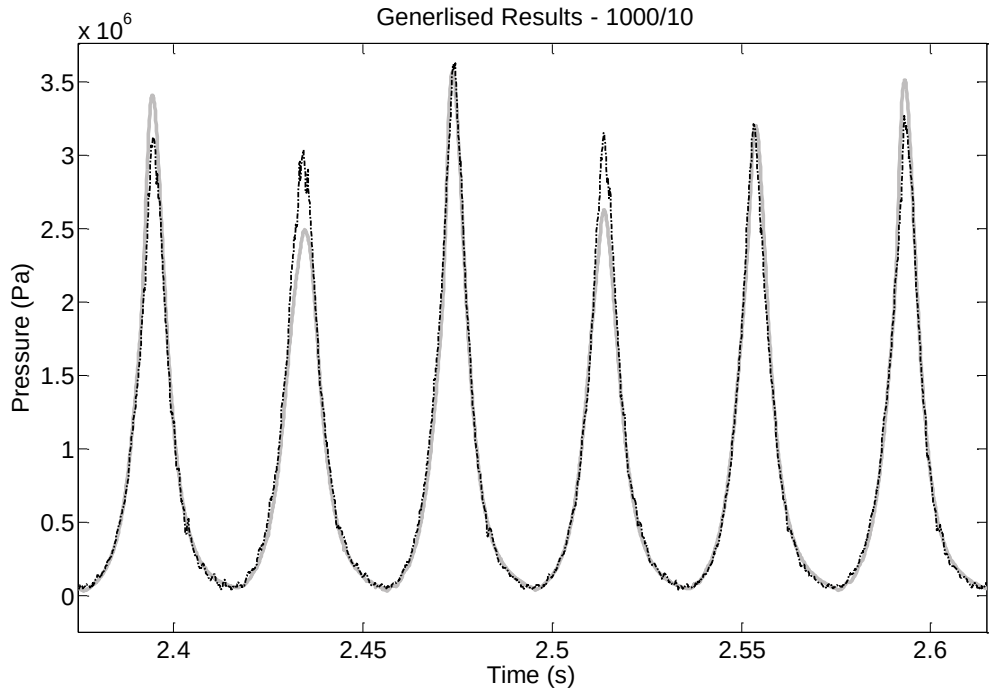

Figure 5.23: Under reconstruction. Seen at combustion event 2, 3 and 6. Target pressure (grey continuous line) and predicted pressure (dotted line).

A second proposal was constructed, namely that the possible reason behind the apparent over and under reconstruction of the cylinder pressure, could be due to the dominance of the system's inertia over the cylinder pressure related dynamics. This

idea was not unexpected owing to the nature of the application. However, it was believed that the use of ANNs and their inherent nonlinear modelling capabilities, could surmount this. It was then theorised that alongside the inertial influence, there may be some information surrounding TDC that was either missing or being masked within the crankshaft kinematics, reducing the ability to reconstruct the cylinder pressure successfully.

To test the second hypothesis, further testing was needed, involving a time-delay neural network at a number of differing engine conditions. A single engine speed was initially selected, as it was believed focusing on a single speed would allow for better evaluation. The speed of 1000 rpm, was selected, as it had the most significant cycle-by-cycle variability and it was believed that if the neural network managed to reconstruct the cylinder pressure at this condition, then the network should reconstruct under any degree of cycle-by-cycle variability. A further set of tests involved examining at varying engine speeds corresponding to: 1000 rpm, 1500 rpm, and 2000 rpm. These tests were carried out in the same manner as described in section 5.1. A separate network was created for each condition which was then optimised individually. Figures 5.24 to 5.26 show the generalised results at condition-1, 4 and 6 (1000, 1500 and 2000 rpm at 10 Nm)

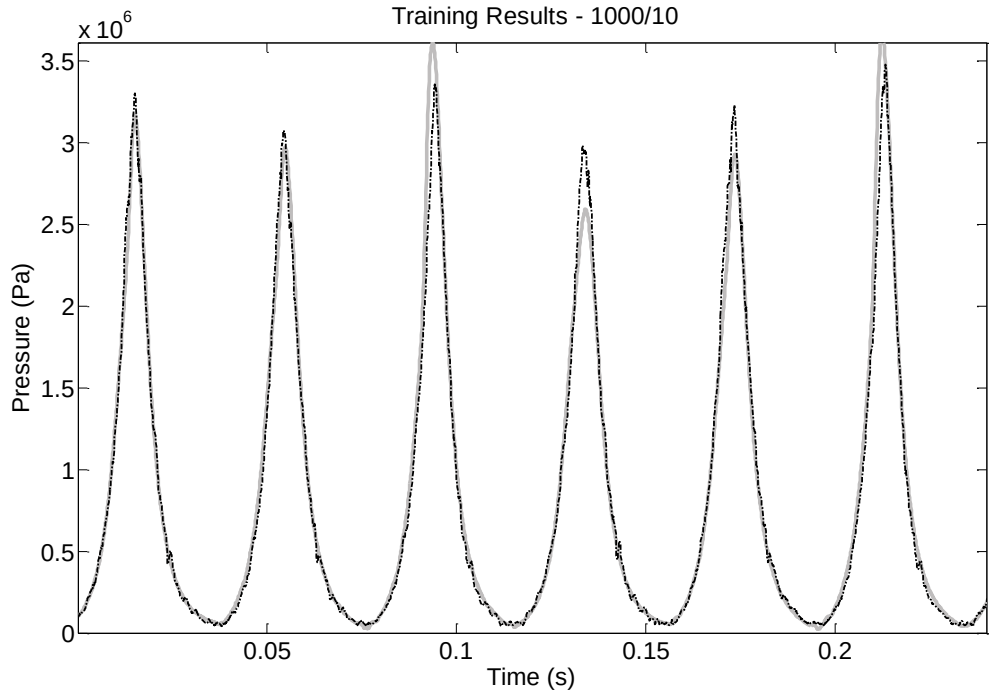

Figure 5.24: 1000 rpm reconstruction results. Target pressure (grey continuous line) and predicted pressure (dotted line).

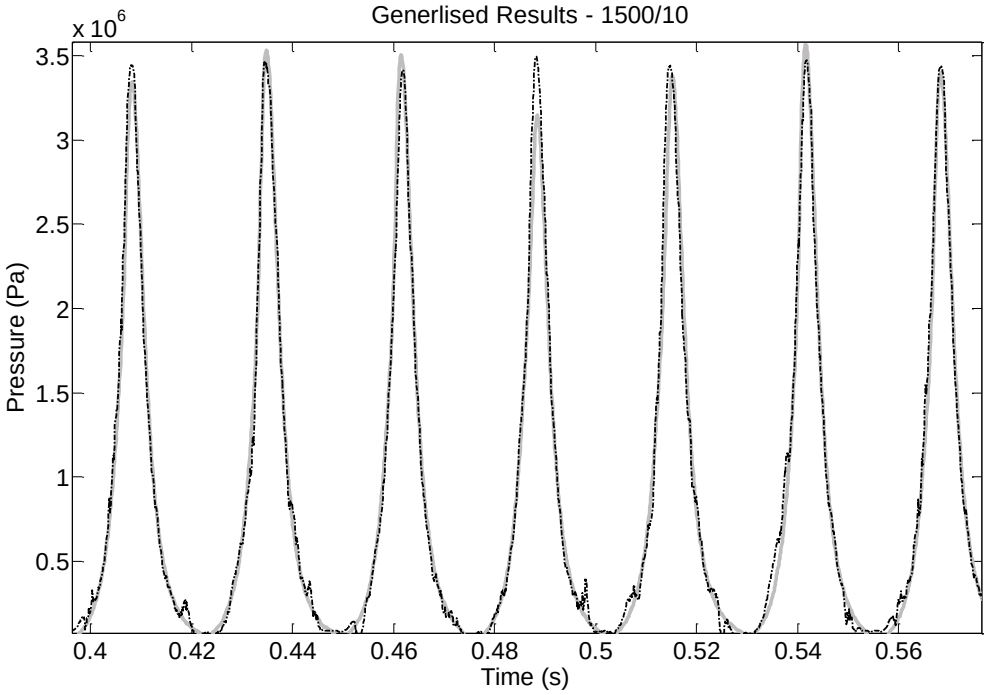

Figure 5.25: 1500 rpm reconstruction results. Target pressure (grey continuous line) and predicted pressure (dotted line).

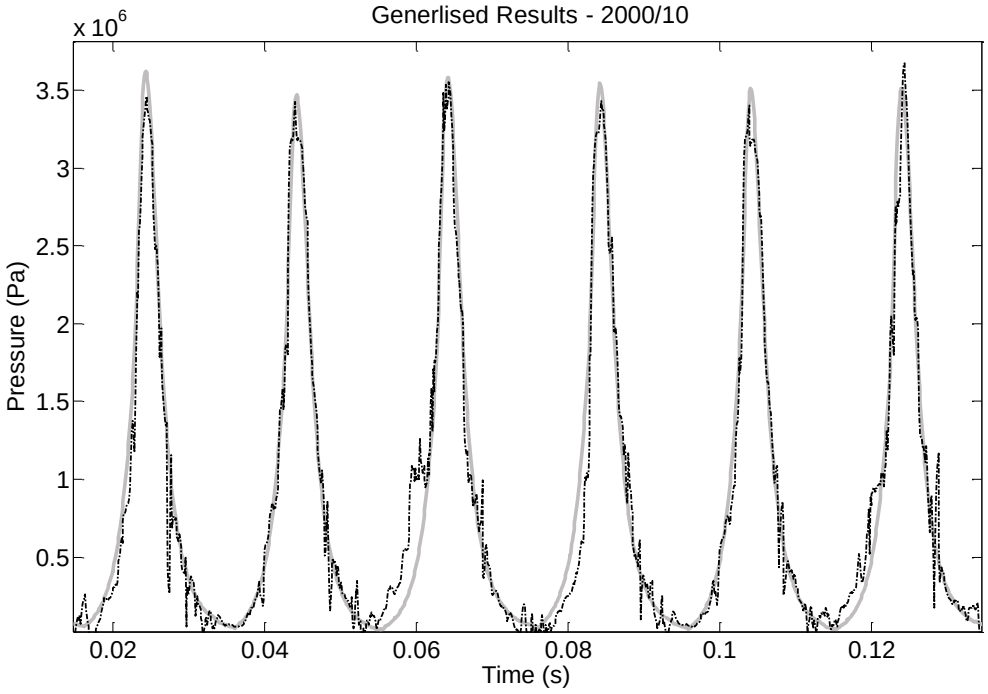

Figure 5.26: 2000 rpm reconstruction results. Target pressure (grey continuous line) and predicted pressure (dotted line).

The results shown in Figures 5.24 to 5.26 have one significant attribute that has not previously been seen. They show that at the higher power (speed) conditions, high speed and load, there is significantly better reconstruction of the cylinder pressure.

Discovering the reasons behind this failure to reconstruct the cylinder pressure successfully at lower power conditions around TDC, had the potential to lead to a greater understanding of the problem. The inability to translate the crank kinematics into cylinder pressure has previously been hypothesised, as an issue of inertia dominance and decreasing crank torque, as the piston approaches TDC. A neural network's nonlinear modelling potential was believed to have the capability to circumvent these issues. However, through extensive consideration of the test results, one attribute of the engine's kinematics had been overlooked. This was the friction, and the frictional changes that occur at TDC to the piston assembly, and its effects on the relationship between crankshaft kinematics and cylinder pressure. The frictional changes of the piston assembly, which include the piston and piston rings, are significant at TDC and BDC. Also, the decreasing crankshaft torque as the piston approaches TDC reduces the effect of cylinder pressure on varying the crank kinematics. The occurrence of these frictional changes, together with decreasing crank torque, could lead to substantial losses of information within the crankshaft kinematics. This substantial loss of information would result in difficulties in training a neural network successfully given the current approach.

To further explain the decreasing crank torque effect on the losses of information, an analogy can be put forward to illustrate this. Consider a large force (generated by pressure within this application) striking the piston crown at exactly TDC. Because the crank torque is zero at this point, the large force applied to the piston has no impact on the crank kinematics. This example illustrates that the energy imparted to and extracted from the system, at or around TDC, has little or no effect on the crankshaft kinematics. Therefore, the addition of energy, through combustion, and the subtraction, through frictional forces, forms a complex system of energy changes which ANNs struggle to model with the current information presented.

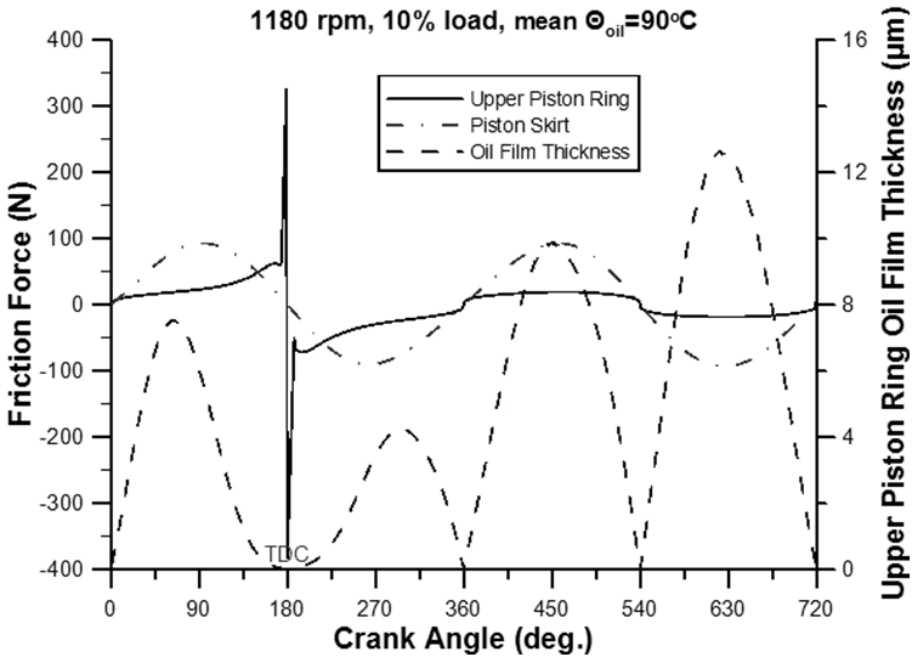

Figure 5.27: Engine friction variation with crank angle (Rakopoulos et al., 2007)

The above analysis describes why there is difficulty in reconstructing cylinder pressure but not why the higher power conditions reconstruct better than lower power conditions. Part of this difficulty maybe the result of different levels of variability but also could be the impact of additional factors. Some of these factors can be revealed through a better understanding of the friction of the piston assembly. The friction between the piston, piston rings and cylinder wall can, in simple terms, be best described at hydrostatic. This is due to the friction between the components varying with piston velocity. At higher velocities, the friction level is less than that at lower velocities, see Figure 5.27 upper piston ring friction force, and this relationship between the velocity and the friction level could explain the better reconstruction. The sinusoidal motion of the piston dictates the fiction level between it and the cylinder wall. The friction is greater at the extremes of the motion, i.e. TDC and BDC, and lesser friction mid-stroke. The higher the engine speed and the greater the mid-stroke velocity of the piston results in lower instantaneous friction. Even though the peak instantaneous friction at TDC and BDC would be similar at different operational speeds, as the piston velocity will always reduces to zero at these points, the average friction tends to decrease with increased engine speeds. The next step in proving the impact of the combined inertia and friction on the crankshaft kinematics with certainty, would involve a considerable empirical study of the engine. This would not be practical and it would be counter to the objectives of the study, which were designed to use ANNs to model and reconstruct cylinder

pressure and not use an analytical model that has significant limitations. The detailed study of the engine in terms of the inertia and friction would only result in such a model. Other than accepting the impact on the combined inertia and friction, within the crank kinematics, as highly probable, the only possible remaining direction was believed to examine other sources for the reconstruction, namely engine block acceleration.

5.4 Reconstruction Using Engine Block Vibrations

The limitations of using crankshaft kinematics outlined in section 5.2, necessitated the change in direction from crank kinematics to engine block vibration based ANN cylinder pressure reconstruction.

The approach to this new area of interest was similar to that of the previous, in that the most gains, with regards to the capability of engine block acceleration based reconstruction, would be through the training and testing of ANNs. Time-delay neural networks were still used for the same reasons highlighted in section 5.1 and the same training algorithm was selected, Levenberg–Marquardt. The only difference was in the method in which the data was formatted prior to it being presented to the ANN. Previously, there was a degree of low pass filtering to remove unrelated frequencies that had no relationship to the crankshaft kinematics and is believed to be a result of a small amount of noise within the experimental setup, that is magnified by the numerical differentiation. However, when considering the engine block acceleration, the frequency range is large and it is highly likely that there is relevant information from low frequency, near engine speed, up to higher frequencies, where content such as engine knock is measured (around 6 kHz). For this reason, it was decided that there should initially be no filtering of the acceleration until a greater understanding of the engine block acceleration was found.

The initial results produced using engine block acceleration are shown in Figure 5.28. Both the detailed setup of the ANN and results are covered within appendix D. Similar to the crank kinematics results within generalisation, there was good agreement between the measured cylinder pressure and the reconstructed cylinder pressure. However, there were also similarities with regards to the erroneous sections of cylinder pressure reconstruction and there appeared to be a greater

correspondence between engine block acceleration reconstruction and crank kinematics reconstruction than expected.

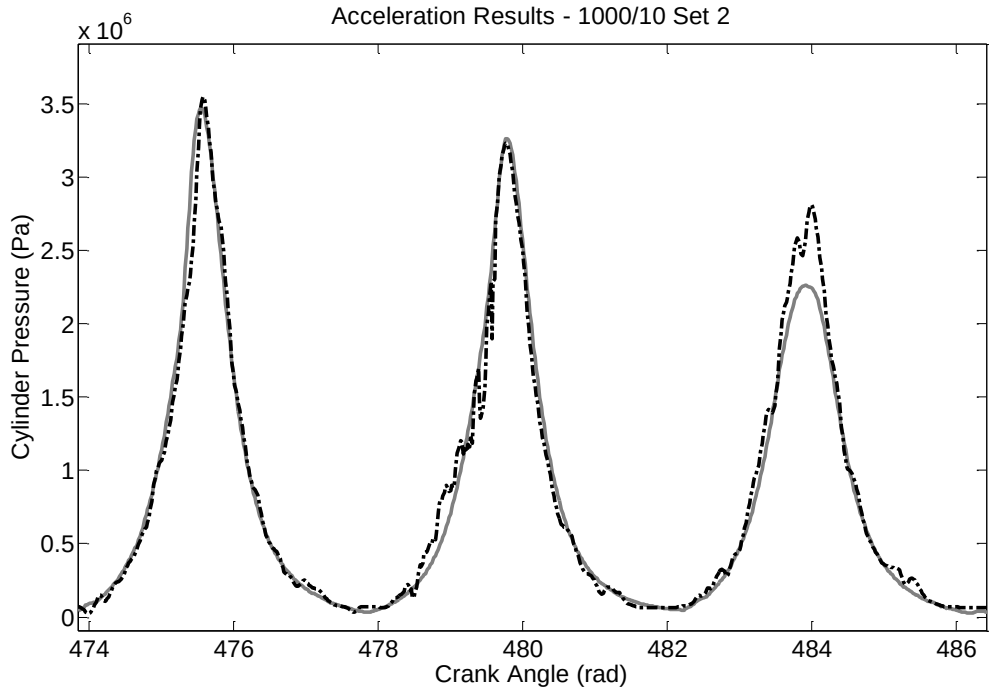

Figure 5.28: 1000 rpm 10 Nm acceleration generalisation results. Target pressure (grey continuous line) and predicted pressure (dotted line).

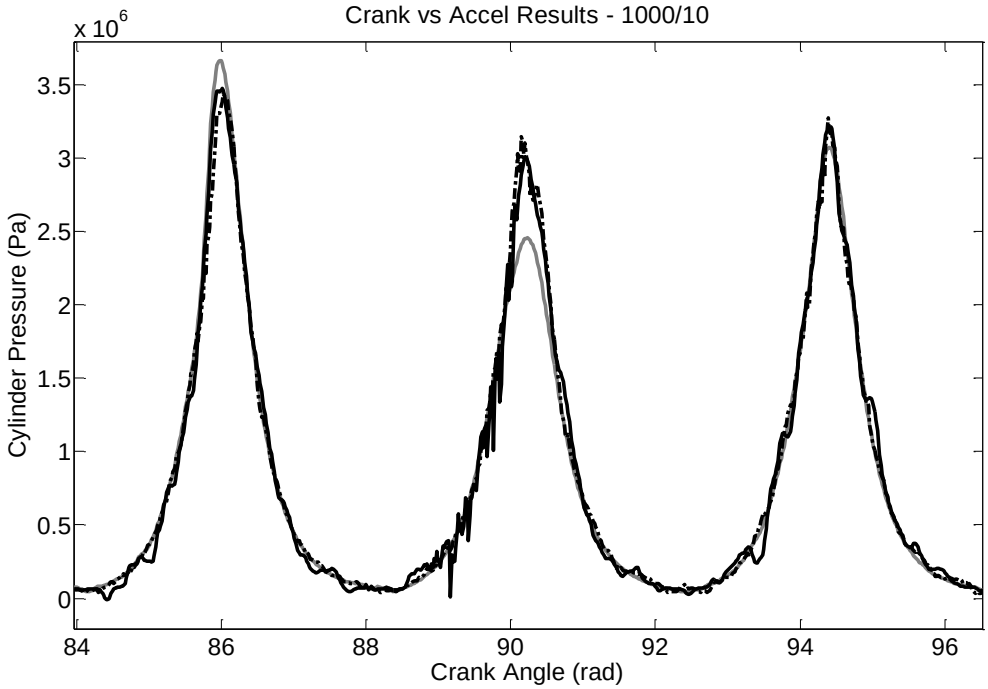

Figure 5.29: 1000 rpm 10 Nm acceleration generalisation results. Target pressure (grey continuous line), reconstructed with crankshaft kinematics (black dash dot line) and block vibration (black dotted line).

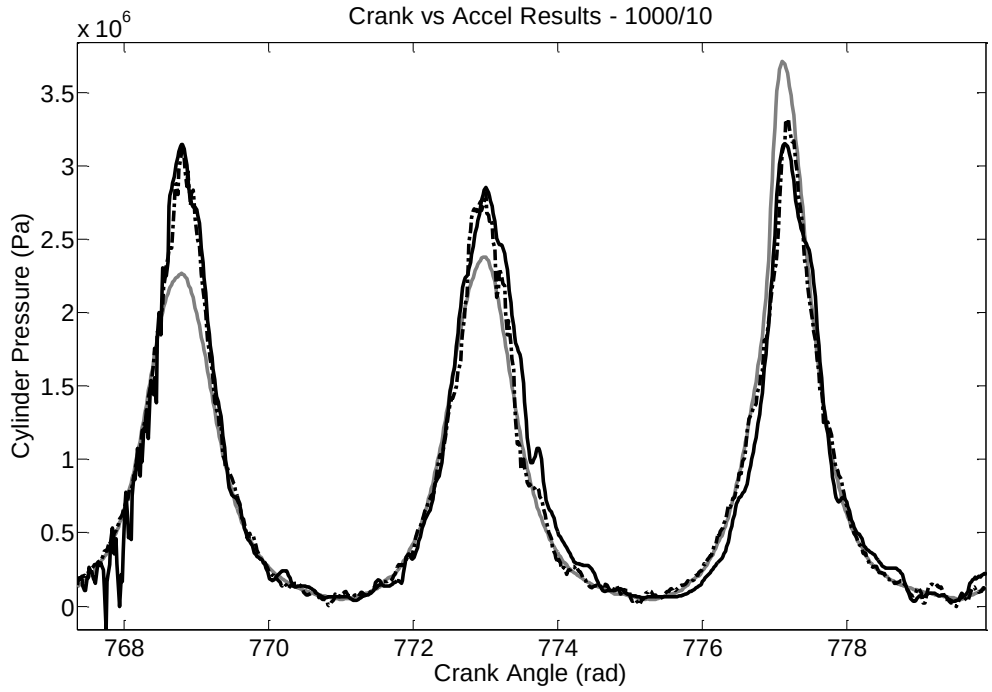

Figure 5.30: 1000 rpm 10 Nm acceleration generalisation results. Target pressure (grey continuous line), reconstructed with crankshaft kinematics (black dash dot line) and block vibration (black dotted line).

The comparison between the normally independent engine block acceleration based and the crankshaft kinematics based reconstruction, actually show significant similarities. Not only are there similarities in the position of the errors, but as can be seen in Figure 5.29 and 5.30, the magnitude of these errors are similar, which implies that there is some previously unknown commonality between these two ANNs and the data sets.

Through extensive experimentation using differing ANNs and training algorithms, alongside the previous work and Lawrence et al.,1997, it can be confidently stated that this issue is not network dependent. Therefore, the similarity between the two different results must originate from the input data, when considering the universal approximation theorem. For both engine block acceleration and the crankshaft kinematics results to be so similar, there must be some common feature of the engine's kinematics or dynamics that is affecting both reconstructions.

A study was undertaken into which features of engine dynamics affect both sets of input data. It was determined that the only possible rationale to explain the similarities was, if the engine block acceleration picked up some aspect of the crankshaft kinematics, because the mechanism required to do the reverse

operation, crank kinematics influenced by engine block acceleration, is too complex and believed to be unlikely. This led to deconstructing the differing modes of the crank kinematics to find sources which could influence the engine block acceleration and lead to the reconstruction similarities.

Through this process, the differing modes which could have caused this engine block acceleration were reduced and the most apparent source was the connecting rod inertia. The mechanism by which the connecting rod inertia impacts on the engine block acceleration is as follows: the elliptical motion of the connecting rod's centre of gravity, shown in Figure 5.30, generates a lateral force component at some distance from the crank axis, generating moment about the crank axis. To further complicate the rolling moment, the moment about the crankshaft axis varies with crank angle due to the change in distance between the crank axis and the connecting rod's centre of gravity. This variation induces a complex rolling moment within the engine block about the crank axis and in turn, this accelerates the engine block both laterally and vertically. However, as only the lateral acceleration is measured, we are only concerned with the lateral component.

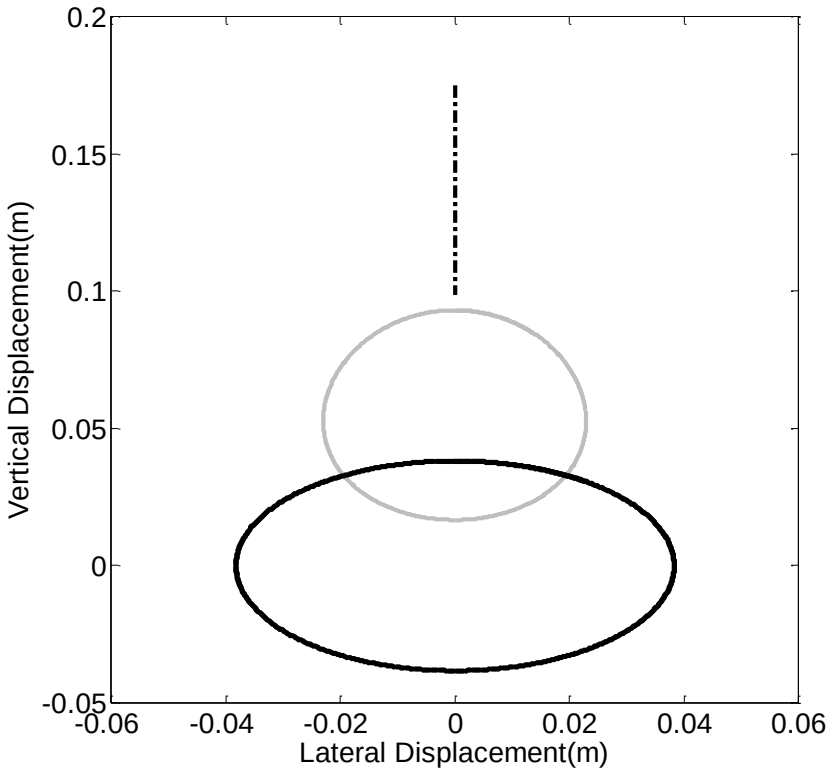

Figure 5.31: Connecting rod position with respect to crank angle. The position of the big end (black), the small end (black dot dash) and the connecting rods centre of gravity (grey).

To provide reasonable support to this, the connecting rod inertia and resulting acceleration was reconstructed theoretically using the known engine component sizes, weights and estimations of component inertias. First, a relationship between the connecting rod inertia and the crank angle was formulated. Using the geometry of the engine block, an estimation was then made of the rolling moment, as defined previously, and the resultant engine block acceleration.

$$P_{bex} = \mathrm{r}\sin\theta \qquad \text{and} \qquad P_{bey} = \mathrm{r}\cos\theta \tag{5.1}$$

The position of the small end bearing, P_{se}, is given by:

$$P_{sey} = \mathrm{r}\cos\theta + \sqrt{l^2 + (\mathrm{r}\sin\theta)^2} \tag{5.2}$$

where the x displacement for the small end bearing is zero. The position of the connecting rod's centre of gravity is:

$$CR_{cgy} = x \cdot \left(P_{sey} - P_{bey}\right) + P_{bey} \quad \text{and} \quad CR_{cgx} = x \cdot P_{bex} \tag{5.3}$$

The rolling moment, M, is found by the multiplication then summation of all three connecting rod's mass at their centre of gravity m_{CR}, their lateral acceleration and the distance between the connecting rod's centre of gravity and crank axis.

$$M = \sum m_{CR} \cdot \frac{d^2\, CR_{cgx}}{dt^2} \cdot \sqrt{{CR_{cgx}}^2 + {CR_{cgy}}^2} \tag{5.4}$$

The basic equations for calculating the rolling moment are given in equations 5.1 to 5.4 and use the same definition described in Chapter 2, when the position of the big end bearing, P_{be}, in cartesian coordinates, is given by equations 5.1. The resulting solutions show clearly a significant link between the theoretical connecting rod inertia and the engine block acceleration. The result is even more evident when examining both sets of data in the frequency domain. The magnitude for each data set is shown in Figure 5.33 after taking a Fourier transform. It can be seen that there is a significant response present in both the connecting rod inertia (50Hz), and the engine block acceleration (100Hz), which is a third order response, at three times the engine speed; 1000 rpm or 16.7 Hz.

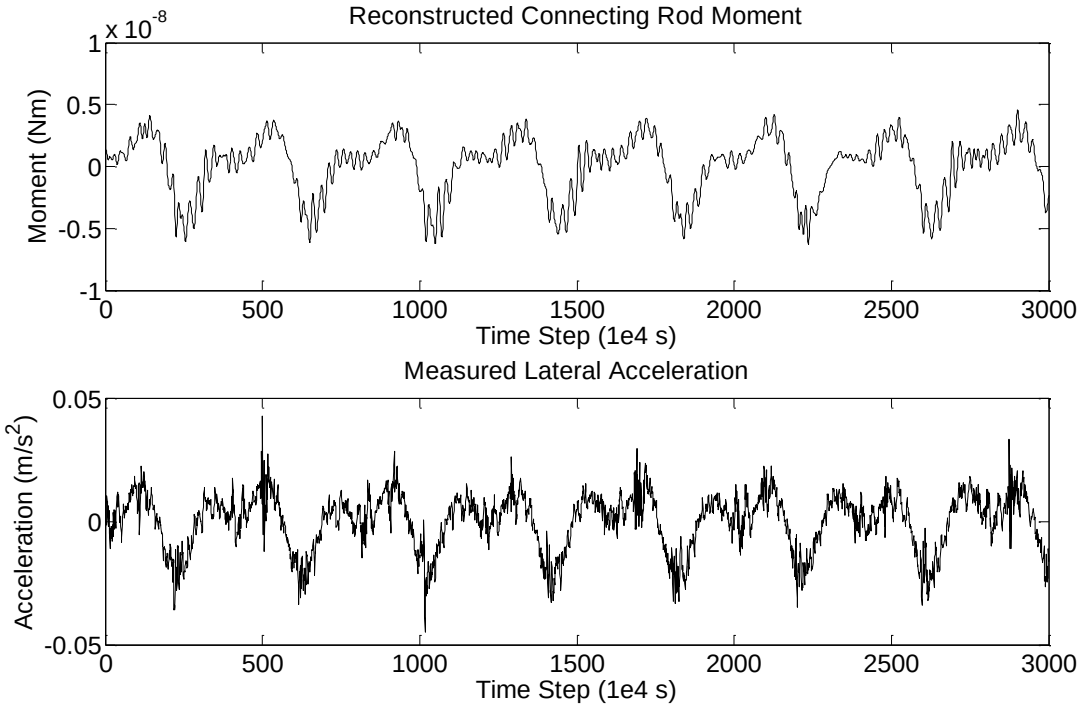

Figure 5.32: Connecting rod moment (top) and engine block acceleration (bottom)

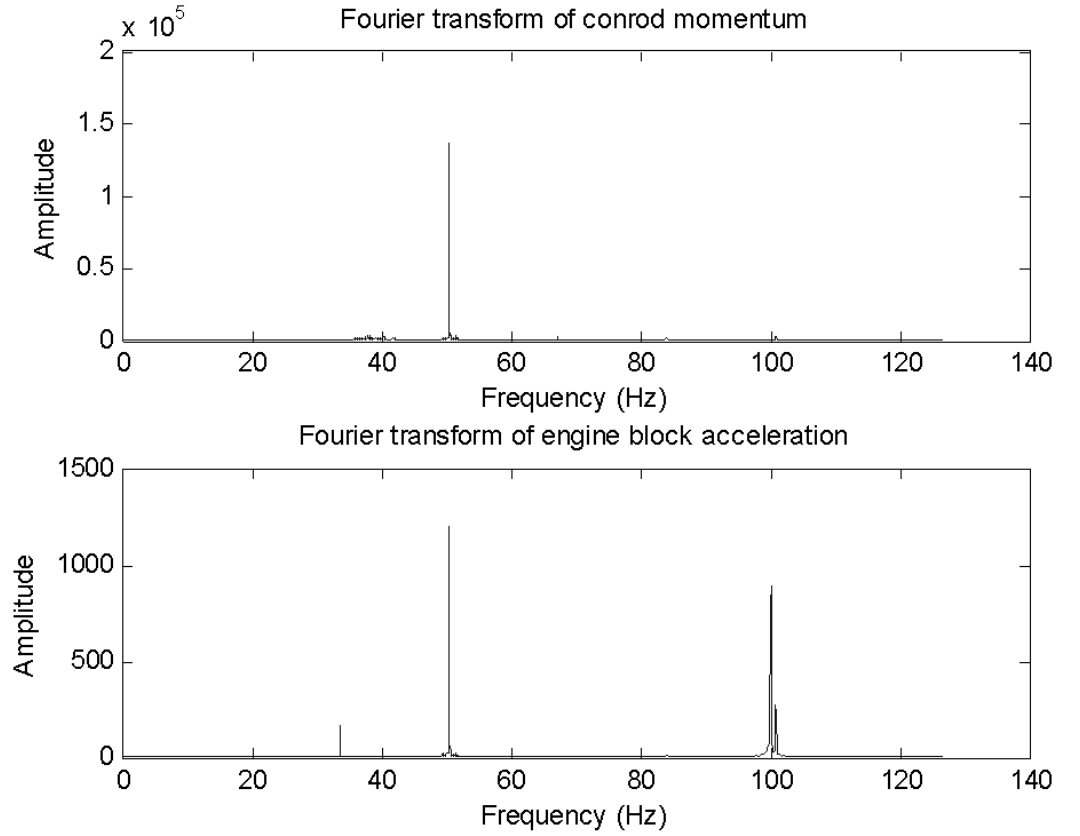

Figure 5.33: Connecting rod inertial and engine block acceleration frequency domain comparison

The similarity between the two results within the frequency domain and the dominance of one key frequency within both, can only lead to one conclusion. It shows that the apparent over and under reconstructing, previously seen in the cylinder pressure reconstruction, using engine block acceleration, must be linked to the inertia of the system and not solely to the cylinder pressure.

This confirmation of the link between the engine block acceleration and the inertia of the system and the subsequent impact on the cylinder pressure reconstruction, has serious implications on the crankshaft kinematics. Earlier, it was hypothesised that the errors in the reconstruction with crankshaft kinematics, the over and under reconstruction, was a combination of system inertia and friction fluctuations at TDC, section 5.2. This hypothesis, alongside the conclusion that there was a commonality between crankshaft kinematics and engine block acceleration and that the engine block acceleration is dominated by the crankshaft inertia, can only lead to one conclusion. The partial confirmation of the hypothesis that the crankshaft kinematics is solely dominated by the inertia of the system and therefore, the resulting cylinder pressure reconstruction would only reconstruct from crankshaft inertia.

This conclusion can now better explain the difference in the reconstruction capabilities at differing engine speeds and load conditions. At high power conditions, the fluctuations in the inertia of the system are more consistent and as such, the performance of the reconstruction is greater. However, at low power conditions the fluctuations in the inertia of the system are erratic, which leads to more over and under reconstructions, reducing the overall performance. Further implications of this finding and an additional study of the crank kinematics are now discussed in Section 5.5.

5.5 A Re-examination of Crankshaft Kinematics

Within the previous section 5.4, a significant relationship between the inertia of the system and the crankshaft kinematics was found, which had considerable implications for the effectiveness of using crankshaft kinematics for cylinder pressure reconstruction. This breakthrough meant that the reconstruction using engine block acceleration could be temporarily suspended and allowed a re-investigation of the crankshaft kinematics for reconstructing cylinder pressure.

Through this re-investigation of the crankshaft kinematics, several areas were focused on with the most effective and the most productive being by deconstructing the torque loads being applied to the cranktrain. This was not just an identification of the loads but also the time and duration.

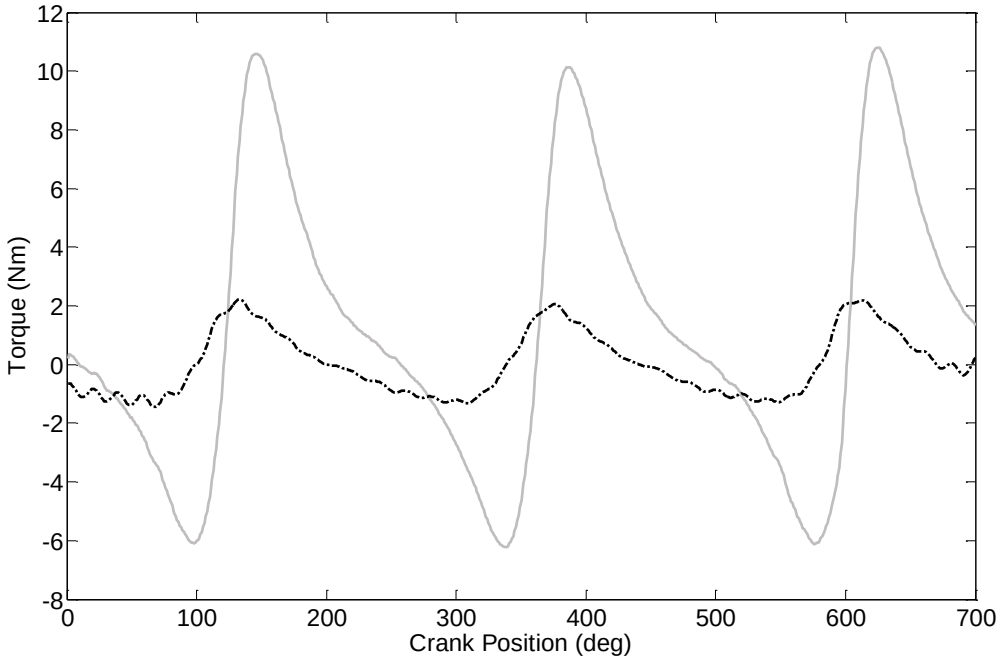

Figure 5.34: Torque loads by the 3 cylinder (Grey solid line) and system inertia (Black dot dash line).

One aspect of this re-investigation that produced a greater understanding is shown in Figure 5.34 and directly relates to the discovery in section 5.4. This figure breaks down both the torque related to cylinder pressure and associated with the overall inertia of the system. It can be seen that the load on the crankshaft from the inertia is relatively consistent throughout the cycle. However, the loading on the crankshaft from the cylinder pressure is only intermittent. Although this was already established, when presented with the cylinder pressure below, and taking into account the consistency of the inertial load, the data being applied to the neural network has little information regarding cylinder pressure changes.

The errors in reconstruction can be further explained by way of what is actually being presented to the ANN. As the cylinder pressure related torque is intermittent through the cycle, the ANN was being trained primarily on the variation of the inertia. This not only resulted in the observed failures and inadequately reconstructed

cylinder pressure, but also suggested that this method of using crankshaft kinematics may never work successfully owing to the lack of pressure related information surrounding TDC.

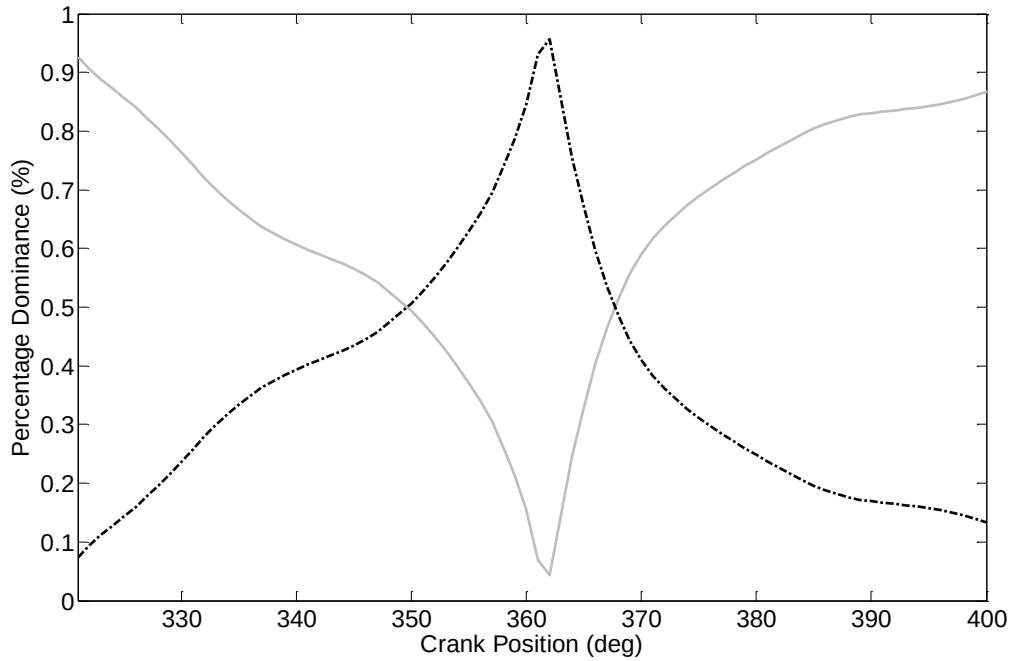

Figure 5.35: The dominance of the inertia relative to the cylinder pressure. Black dot dash line is the normalised crankshaft torque. Grey solid line is the normalised cylinder pressure torque.

This failure to train using crankshaft kinematics in its current form, does not mean that the crankshaft kinematics are not useful. In fact the above figures clearly show regions where crankshaft kinematics due to cylinder pressure is present and potentially accessible. Therefore, the next set of work will attempt to find an ANN architecture that will target the regions of useful information with the aim of getting significantly better reconstructions.

Current ANNs use delays which only cover the 60 degrees prior to the reconstructed pressure. As can be seen, the information content within the 60 degrees prior to TDC, and surrounding TDC, is primarily inertial based, resulting in the poor reconstruction of the cylinder pressure. Also, the portion of the data that contains information pertaining to the cylinder pressure is firstly, only concerned with the compression stroke which varies little in steady state conditions and secondly, this is a significant period before TDC. The only relevance this information will give to the

ANN is to state the initial conditions of the system prior to combustion, but has no information relating to the combustion process.

As the relevant information content prior to TDC has been deemed to be of little use in reconstructing the cylinder pressure, the only remaining content is after TDC. This information, 60 degrees after TDC, would still contain inertia information but would also contain information regarding the cylinder pressure changes post combustion. This information, alongside the compression information before TDC, would contain the initial and final conditions of the system and may result in improved reconstruction capabilities.

On the understanding that this approach would affect the real time nature of the application, it is believed to be the best method to reconstruct cylinder pressure. The real time nature will be discussed in greater detail in the next section but the primary focus was on the verification of this method in the short term.

5.6 Optimisation of the Delay for Crank Kinematic Based Reconstruction

The suggestion that the past information within the crankshaft kinematic data had little knowledge in aiding the cylinder pressure reconstruction and that only future crank kinematic data, which is ahead of the point of reconstruction, is significant. The use of past and future in this context refers to a certain amount of data that is either acquired before the point of reconstruction or acquired after the point of reconstruction. As a result, this application will not be able to produce real time cylinder pressure reconstruction; it would be delayed by the same number of degrees as the amount of future information required.

If proven, this hypothesis could lead to substantial improvements in the ability of an ANN to carry out cylinder pressure reconstruction. So far, this idea has been explained purely in terms of the effective radius, the system inertia and the lack of information at TDC; namely the issues surrounding the significant changes in friction. However, it can be explained in a more generalised manner for any application where the system and the transfer of energy is time dependent. It can be simply put that there is a time element to the transfer of energy from one part of the system to another; cause and effect. Within any system with time dependant

changes in energy, the cause always precedes the effect. In this application, ignoring the effective radius, there is a delay between the cylinder pressure rising, it acting on the piston crown, it overcoming the inertia and kinematic changes occurring. This idea may seem simple and obvious, but it has not be recognised or applied within this application. With the exception of researchers using the pattern recognition approach (Gu et al., 1996), the time-series approaches have predominately used only the current and past crank kinematic data with no reference to using future crankshaft kinematics.

It is important to note that just because the future kinematic data may hold more relevant information, it does not mean that the past kinematics is irrelevant. Referring back the description using energy, the past kinematics describes the initial energy of the system at the beginning of the combustion event and the future kinematics describes the resultant energy once the combustion event has finished. Using both should enable the ANN to construct a model that will take account of not only the total energy imparted to the cranktrain by the cylinder pressure, but also using multiple delays, recognise how the energy is distributed across the combustion event.

This hypothesis was tested in the same way as the previous hypotheses. The ANN architecture was a Time-Delay neural network and training was achieved using the Levenberg–Marquardt algorithm. Previously, there has been some success using delays encompassing 60 degrees of past kinematics. Therefore 60 degrees of past kinematics was again selected and to give symmetry, 60 degrees of future information was selected for the initial training attempts. Below are both the training and generalisation results for this hypothesis.

Future and past training results

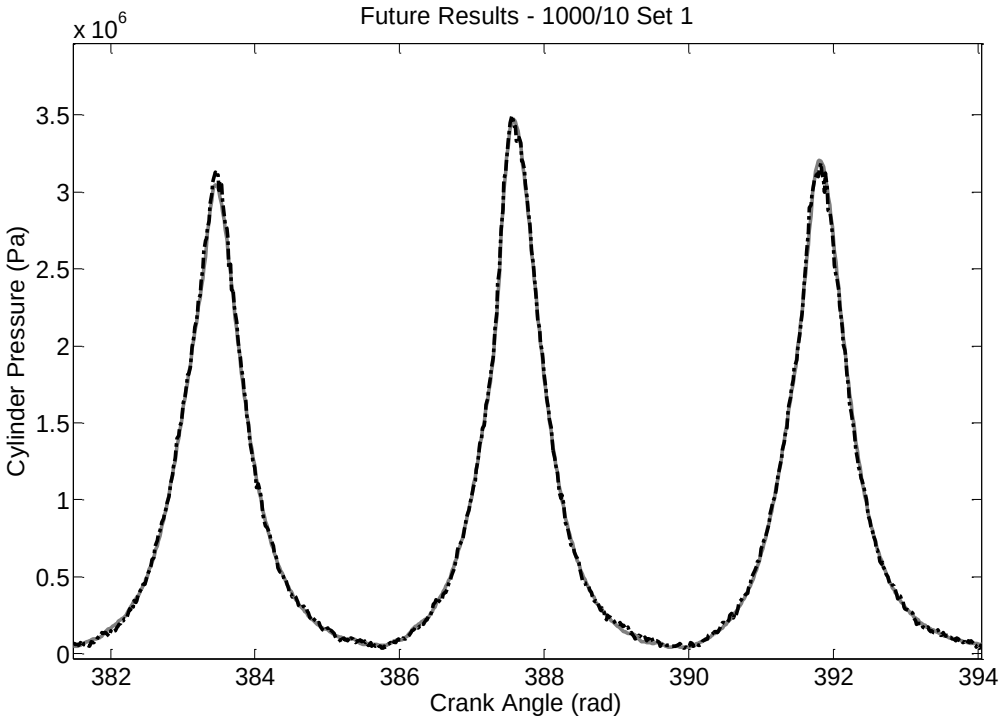

Figure 5.36: Future and Past Training Results. Target pressure (grey continuous line) and predicted pressure (dotted line).

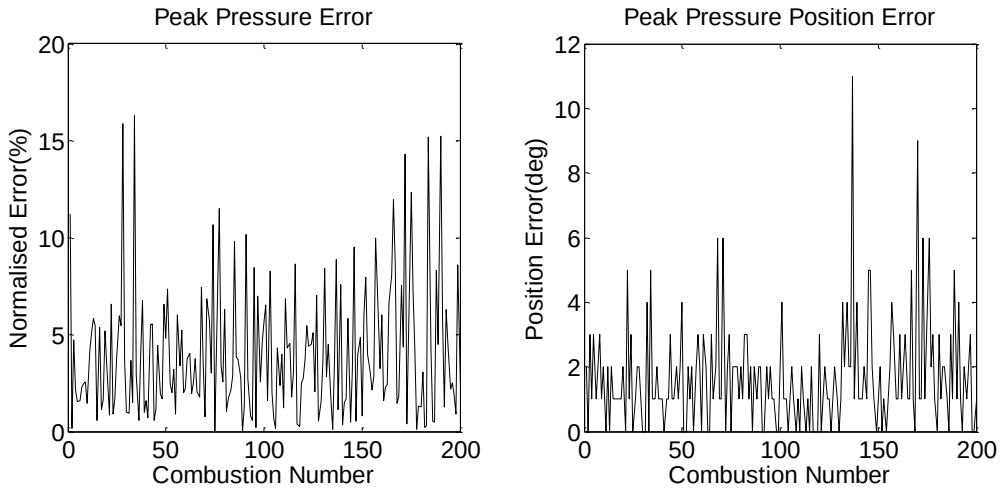

Figure 5.37: Future and Past Training Results. Left shows training peak pressure error and right shows training position of peak pressure error

Future and past generalisation results

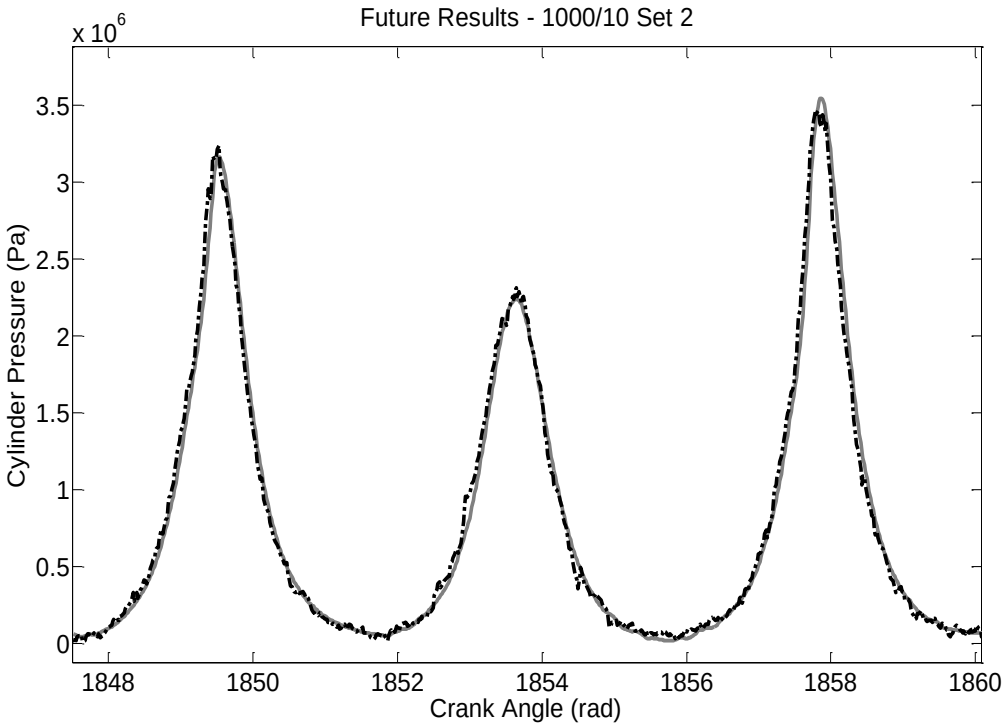

Figure 5.38: Future and Past Generalised Results. Target pressure (grey continuous line) and predicted pressure (dotted line).

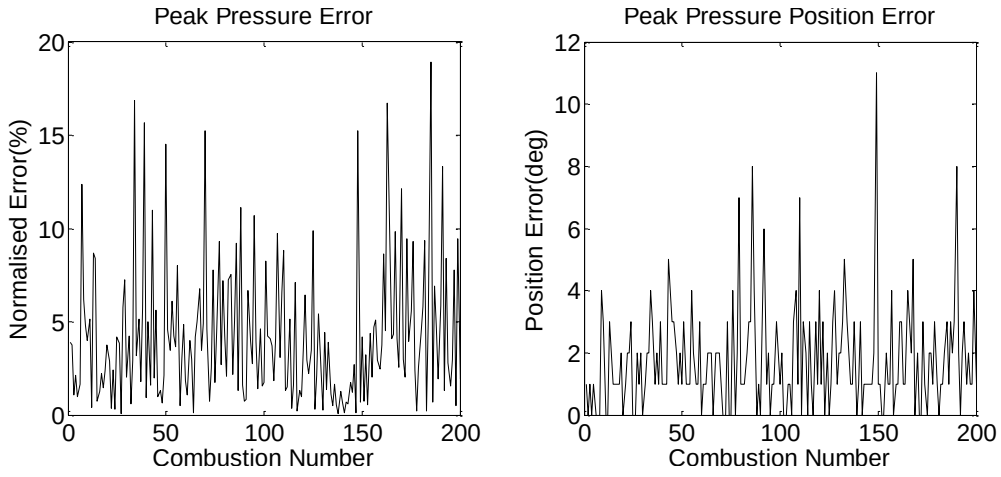

Figure 5.39: Future and Past Generalised Results. Left shows training peak pressure error and right shows training position of peak pressure error

With the apparent success of using this technique visible in the training and generalised results in Figures 5.36 to 5.39, a comparison between the future and past and the past inputs was undertaken

Table 5.7: Comparison of the Training Results for both Future and Past and Past Approaches

Training Results	Past Delays Only		Future and Past Delays	
	Root-Mean-Squared Error	Standard Deviation	Root-Mean-Squared Error	Standard Deviation
Overall Performance	3. 38 %	3.38 %	1.82 %	1.82 %
Normalised Peak Error	10.9 %	8.23 %	5.13 %	3.33 %
Peak Pressure Position Error (deg)	3.79	2.44	2.29	1.51

Table 5.8: Comparison of the Generalisation Results for both Future and Past and Past Approaches

Generalisation Results	Past Delays Only		Future and Past Delays	
	Root-Mean-Squared Error	Standard Deviation	Root-Mean-Squared Error	Standard Deviation
Overall Performance	3.49 %	3.49 %	2.15 %	2.15 %
Normalised Peak Error	12.6 %	9.27 %	5.58 %	3.74 %
Peak Pressure Position Error (deg)	3.45	2.06	2.54	1.64

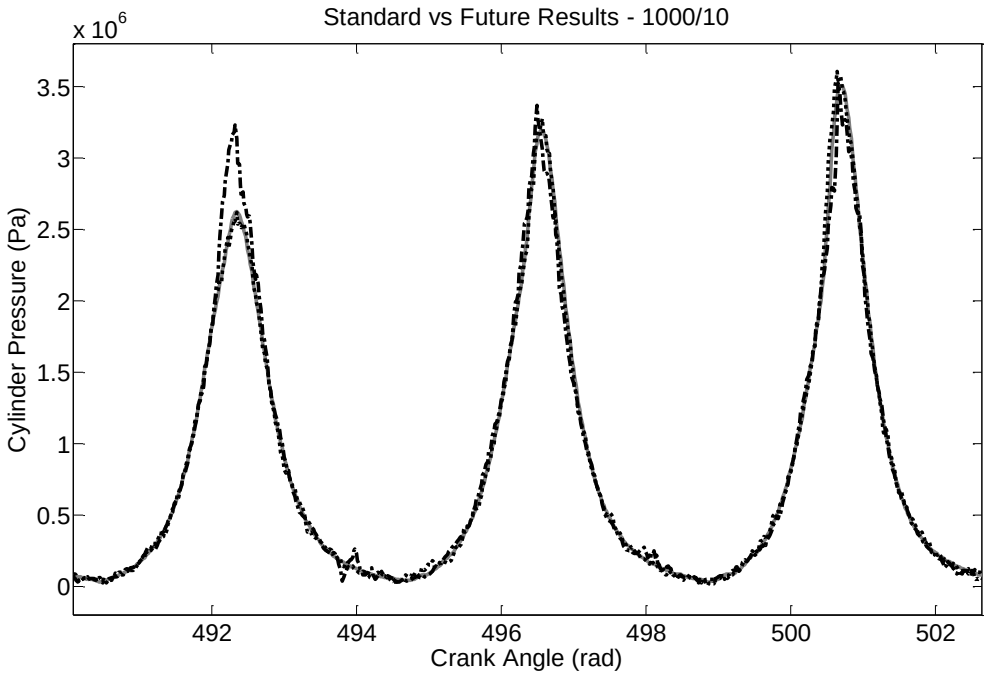

Figure 5.40: Comparisons between the Future and Past (black dotted line), the Past (black dash dot line) Generalised Results and Target pressure (grey continuous line).

The above results, using a combination of future and past inputs, and the comparison between the future and past delays and the previous, show significant gains. The overall performance improvements from 3.49 % to 2.15 % for the generalised RMSE as well as a qualitative improvement seen in Figures 5.36 to 5.40, give an indication of the potential for accurately reconstructing cylinder pressure; where the over and under reconstruction shown in the earlier test is no longer present and the generalised results accuracy is exceptional. As stated, the tests described used ± 60° for the inputs of the ANN. These values were selected based on the combination of previous optimisation for the delay number and convenience. As the methodology was developed, it was prudent to undertake a new optimisation for the number of delays, taking into account both future and past inputs.

The results from the optimisation of the delay number were similar to the previous optimisation; the best results were produced with 120° of past inputs in addition to 120°of future inputs. In the previous optimisation discussion, the significance of the 120°of inputs was stated. The fact that the optimum total number of delays: i.e. 240°, is equal to a third of a cycle and the exact length of a combustion event, is not coincidental. Generally, when modelling any time-series problem, the greater the amount of data, the better the accuracy. However, within certain systems there is a

limit to the amount of useful information available before other unrelated and potentially problematic content may have a negative impact. This result for the optimum delay number can be best explained through considering the influence cylinder pressure has on the crankshaft kinematics. Through an individual cylinder's 240° combustion event, the majority of crankshaft kinematic variations will be as a direct result of the firing cylinder. The influences by the other cylinders will be relatively small and consistent cycle-to-cycle. However, the crankshaft kinematics outside of the 240° window of the combustion event will be greatly influenced by either the compression or exhaust strokes of the other cylinders. These delay numbers will not be examined in detail in this chapter, they will be combined with the other developments made and tested in depth, using both crankshaft kinematics in chapter 6 and cylinder block vibrations in chapter 7. The exact implementation for each approach will be described in detail within each chapter.

The general evidence for using both future and past inputs has been proven, with substantial improvements in the reconstruction results both qualitatively and quantitatively. However, there are still some problems in the reconstruction which appear to be independent of the ANN architecture, training algorithm and the optimum input arrangement. The next task therefore was to examine the processing of the data prior to its application to the ANN; namely the filtering.

5.7 Filtering Crankshaft Kinematics

Up to this point, little has been discussed regarding the filtering of the data in general, with the exception that a small amount was required on the crankshaft kinematics in order to remove high frequency noise. This noise is believed to be relatively insignificant within the acquisition of the crankshaft position. However, this noise has been magnified as a result of numerically differentiating the position to get crankshaft velocity. The numerical differentiation was carried out within the same code that converted the raw data from the LabVIEW environment to the Matlab environment, implemented the corrections for the shaft encoder and collated the data. This process was previously carried out on the earlier data acquired with none of the original raw LabVIEW data retained. To maintain consistent data acquisition procedures this method was continued with the newly acquired data, discussed in Chapter 8. A Fast Fourier Transform (FFT) method has been used to remove the higher frequencies up until this point within the thesis. It was believed, with little

gains being made through additional examination of the ANN architecture, training algorithm and the optimum input arrangement, further improvement might have been found by using a less indiscriminate means of filtering the data. Using the FFT might have been filtering out more obscure data with relevant information pertaining to cylinder pressure.

A series of experiments were undertaken examining the cylinder pressure and crankshaft kinematics in both the time and frequency domain. Each experiment aimed to find important frequencies in both that in some way related one to the other. One of the most significant observations made was seen when examining the cylinder pressure in the frequency domain. The aim of this particular test was to determine when filtering out high frequency content, what was the critical frequency that the cylinder pressure signal would start to deteriorate when returned to the time domain. This was carried out using 200 engine cycles of data. Results from this test proved that extremely large number of frequencies are required to successfully reconstruct the signal in the time domain. It was also apparent that the filtering used previously to minimise the high frequency content, had the effect of degrading the signal notably in this test. A comparison between the raw measured cylinder pressure and current filtering method is shown in Figure 5.41.

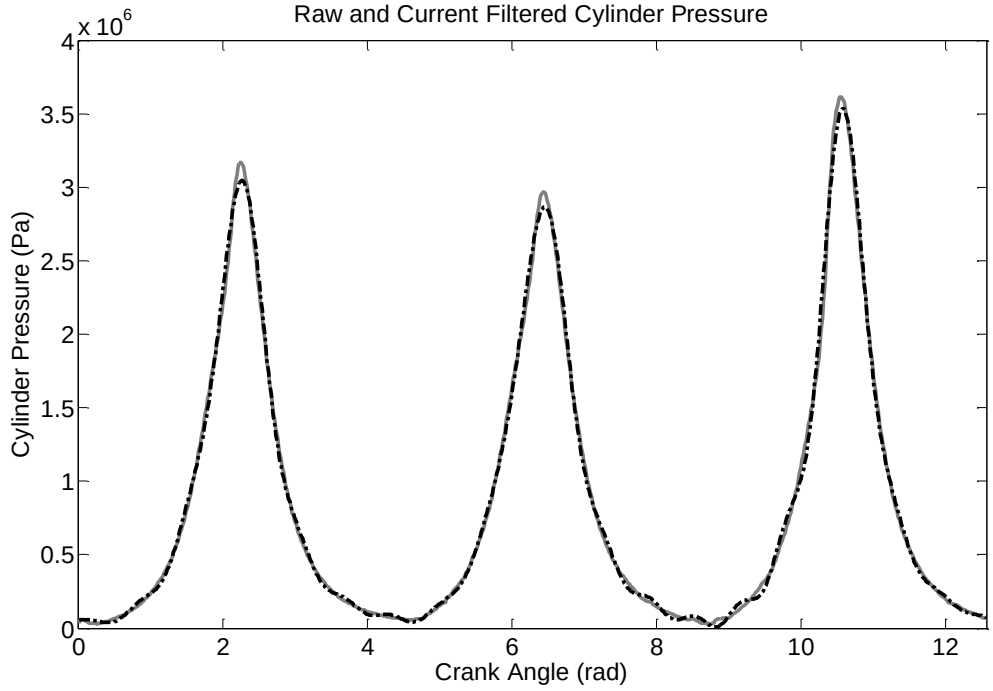

Figure 5.41: A comparison between the raw measured cylinder pressure and current filtering method. Measured pressure (grey continuous line) and filtered pressure (dotted line).

This result led to reconsidering the purpose of the filtering and the application. There are numerous nonlinear processes that occur within an IC engine. Some of these are cyclical, namely bearing fiction, but most are not. The most significant in this application is the inlet air flow dynamics and in particular the engine used for acquisition has an EGR system installed. The dynamics of systems like these are not contained and do not significantly vary within a single cycle, they vary across many. Therefore, the behaviour and control of the whole engine is dependent on the dynamics of the numerous previous cycles. This creates an issue when attempting to filter out the high frequencies in the data. As the behaviour of the engine is in some way affected by dynamics outside of the time window the data is acquired; this can be considered as a non-stationary signal. Therefore, the use of a FFT for filtering out high frequency content in its entirety would be problematic and could cause the notable errors, seen in Figure 5.41. The result is that through using the filtering techniques across a number of cycles, a portion of valuable information could be lost.

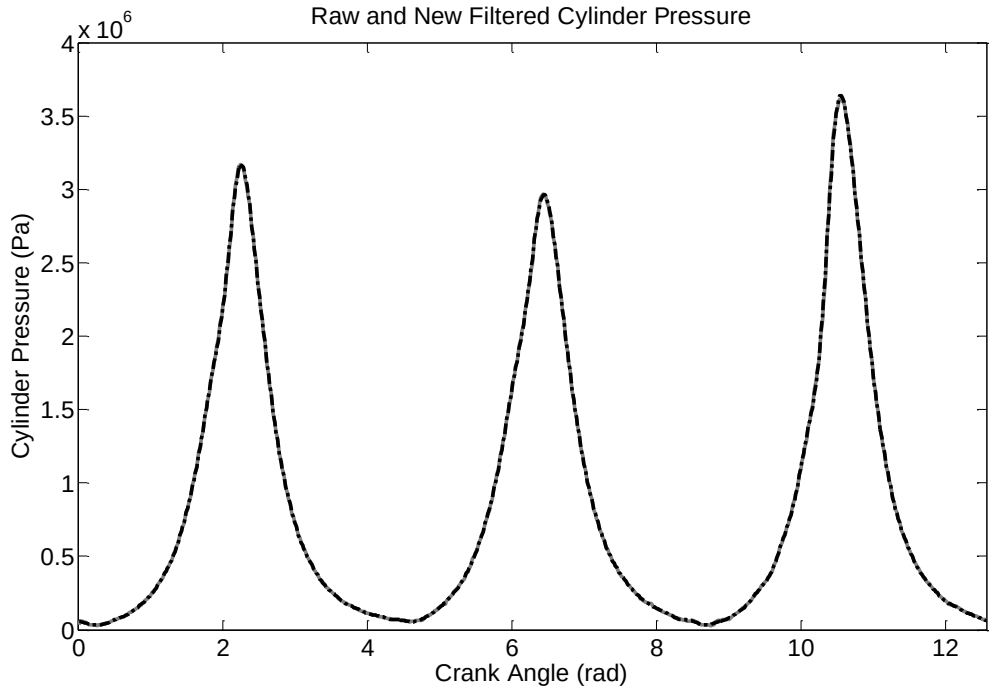

Figure 5.42: A comparison between the raw measured cylinder pressure and new filtering method. Measured pressure (grey continuous line) and filtered pressure (dotted line).

The use of different filtering techniques was considered. However, as a substantial amount of the nonlinear effects appeared to vary cycle-to-cycle, a different approach was preferred. Instead of filtering across numerous cycles, it was proposed that a piecemeal approach could be used by filtering within a single cycle, where the non-

cyclical effects were minimised and little information would be lost. This method assumes the input data is stationary and to some extent disregard some of the nonlinear aspects within the data, which seem to be more prominent when examining numerous cycles. Figure 5.42 shows a comparison between the raw measured cylinder pressure and individual cycle filtering method. This method appears, in the initial comparisons, to be successful in minimising degradation of the signals whilst still filtering a significant proportion of the higher frequency noise. The next series of figures and tables present the results from tests using this new filtering approach. Again, it was undertaken using the same ANN architecture and training algorithm used in the previous sections.

Individual Filtered Training Results

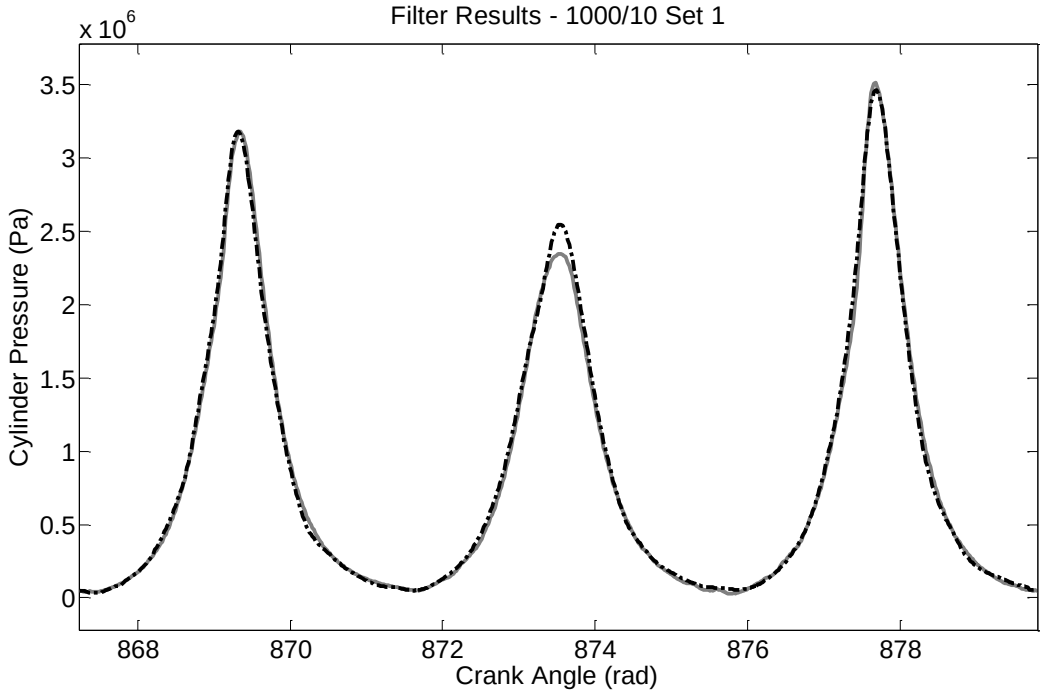

Figure 5.43: Individually Filtered Training Results. Target pressure (grey continuous line) and predicted pressure (dotted line).

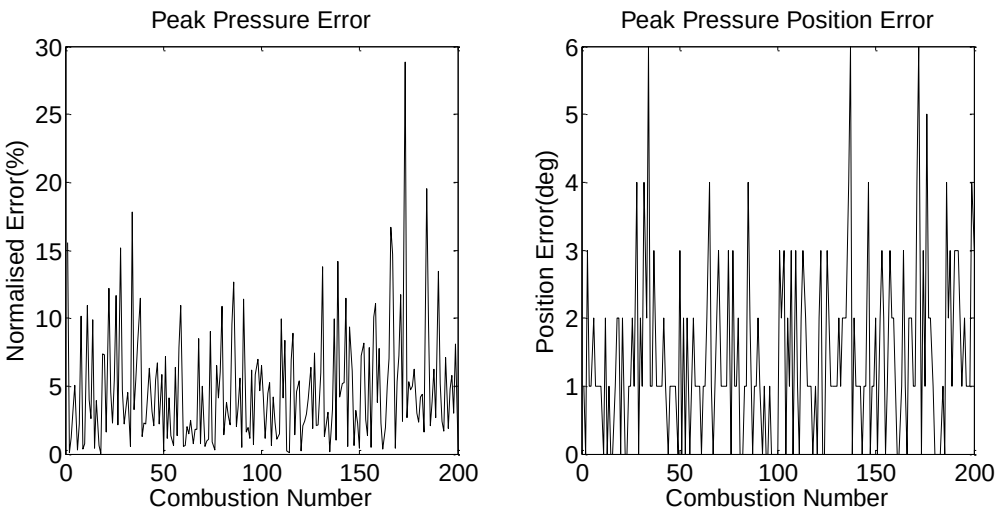

Figure 5.44: Individually Filtered Training Results. Left shows training peak pressure error and right shows training position of peak pressure error

Individual Filtered Generalisation Results

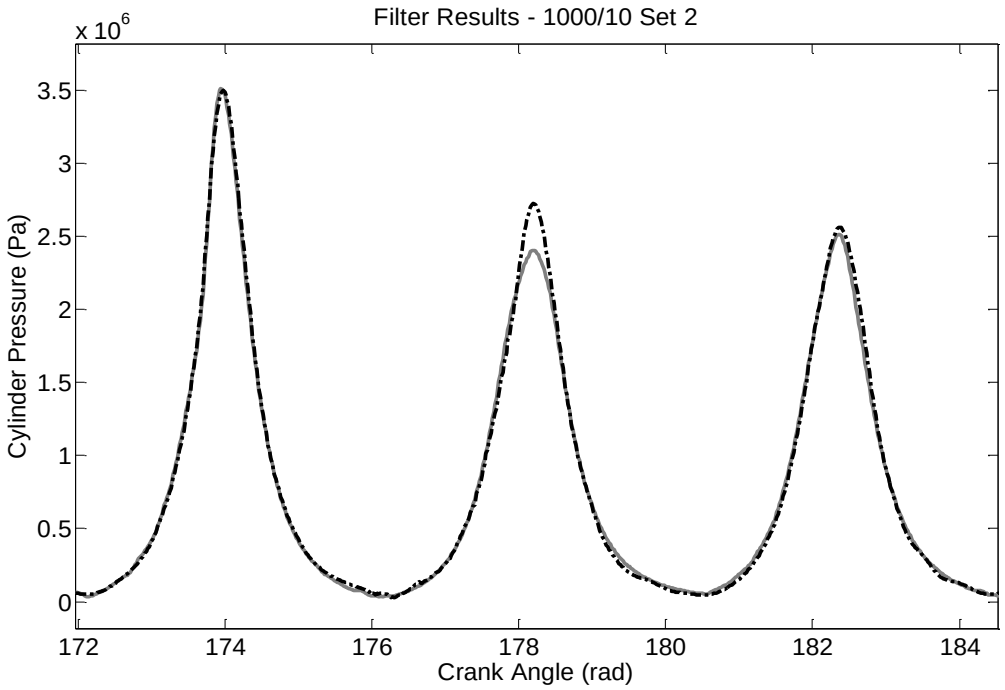

Figure 5.45: Individually Filtered Generalised Results. Target pressure (grey continuous line) and predicted pressure (dotted line).

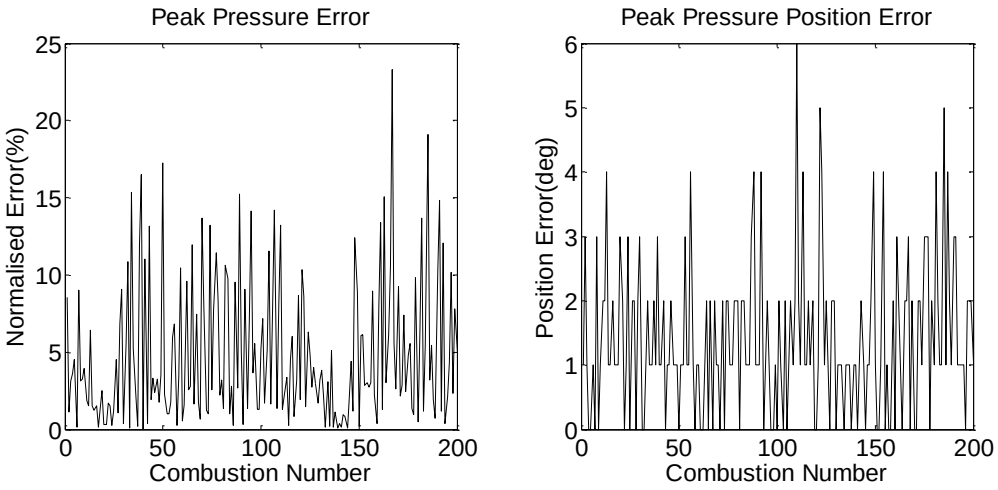

Figure 5.46: Individually Filtered Generalised Results. Left shows training peak pressure error and right shows training position of peak pressure error

With the success of using individually filtered cycles evident in the training and generalised results in Figures 5.43 to 5.46, a comparison between the filtering techniques inputs was undertaken.

Table 5.9: Comparison of the Training Results for both Individually Filtered and Group Filtered Approaches

Training Results	Group Filtered		Individually Filtered	
	Root-Mean-Squared Error	Standard Deviation	Root-Mean-Squared Error	Standard Deviation
Overall Performance	3.38 %	3.38 %	2.29 %	2.29 %
Normalised Peak Error	10.9 %	8.23 %	5.98%	4.02 %
Peak Pressure Position Error (deg)	3.79	2.44	1.95	1.32

Table 5.10: Comparison of the Generalisation Results for both Individually Filtered and Group Filtered Approaches

Generalisation Results	Group Filtered		Individually Filtered	
	Root-Mean-Squared Error	Standard Deviation	Root-Mean-Squared Error	Standard Deviation
Overall Performance	3.49 %	3.49 %	2.53 %	2.53 %
Normalised Peak Error	12.6 %	9.27 %	6.53 %	4.46 %
Peak Pressure Position Error (deg)	3.45	2.06	1.95	1.28

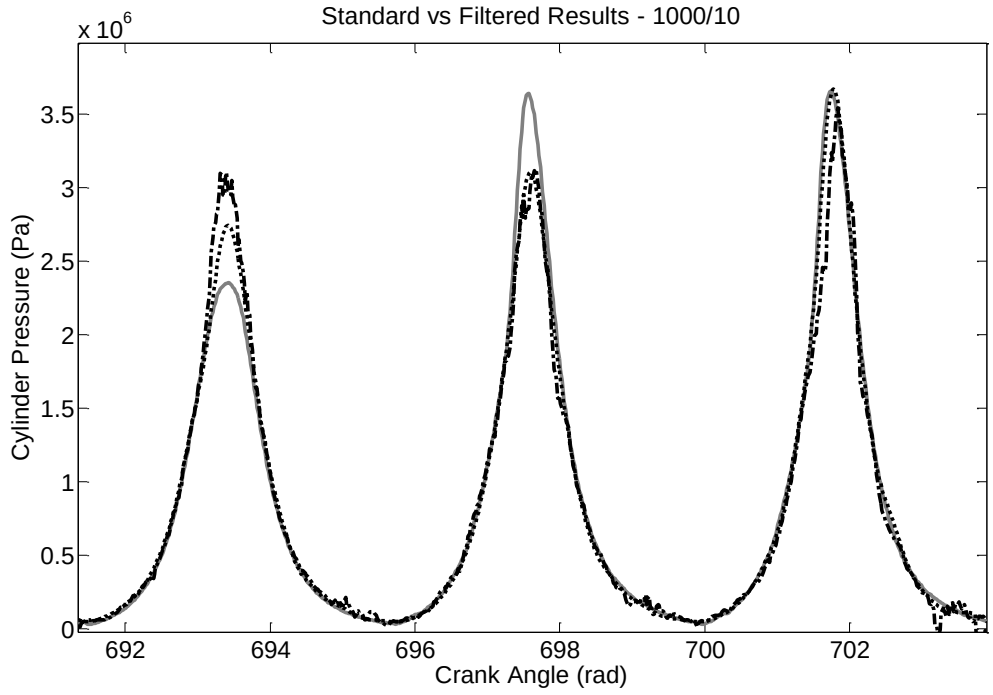

Figure 5.47: Comparisons between the Individually Filtered and Group Filtered Generalised Results. Target pressure (grey continuous line), predicted with past approach (black dash dot line) and predicted with Individually Filtered approach (black dotted line).

The results from this test clearly show an improvement on using the new approach that filters out high frequency for each cycle, rather than filtering numerous cycles at

a time. The overall performance improved from 3.49 % to 2.53 % for the generalised RMSE result. This approach appears not to filter out the nonlinear cycle-by-cycle effects but at the same time improves the quality of the signal. The over and under reconstruction is still present, as the future delays have not been used in this test. Within the above results, the approach's additional computational requirement was relatively small. However, the exact method used to filter within a cycle may have to be modified when considering the practical application of this technology. This approach will be combined and tested with the developments made in optimising the delay in Chapters 6 and 7.

5.8 Independent Cylinder Reconstruction

As described in the introduction, the ultimate goal for reconstruction is for the ANN to adapt to not only different engines, but also to changing engine dynamics as a result of excessive journal bearing wear. The subtle differences in manufacturing tolerances and increased friction from engine to engine may seem negligible however, it can lead to substantial differences. So far, what has not been considered is the difference between individual cylinders within the same engine. The differences can be caused by the different tolerances of components such as pistons, piston rings and connecting rods. They can be from different friction and wear rates, injector tolerances or the condition of the spark plug. They can even be a result of the different geometries of the inlet and exhaust manifolds for each cylinder. All of these differences cylinder to cylinder, along with different wear rates, could significantly impact the overall performance of the reconstructed cylinder pressure. Therefore, using the same premise that different engines require different ANNs with a degree of adaptively to produce accurate reconstruction, different cylinders within the same engine also require subtly different ANNs to achieve the best reconstruction possible. The following results show the tests of this hypothesis, again using the same ANN architecture and training algorithm used in the previous sections. The next series of figures show the results from the training and generalisation from an ANN trained only on crankshaft kinematics and cylinder pressure from one of the three cylinders.

Individual Cylinder Training Results

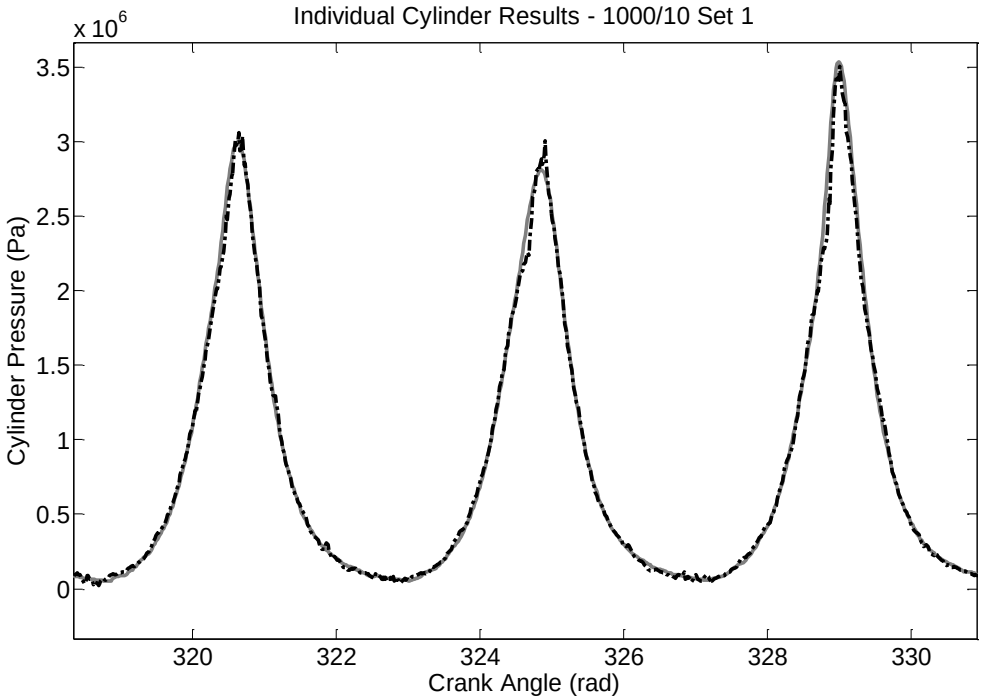

Figure 5.48: Individual Cylinder Training Results. Target pressure (grey continuous line) and predicted pressure (dotted line).

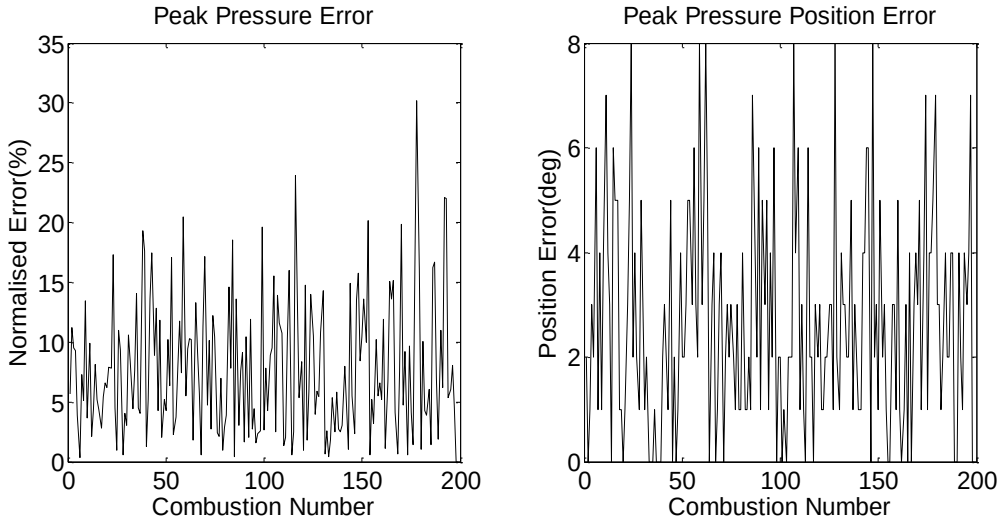

Figure 5.49: Individual Cylinder Training Results. Left shows training peak pressure error and right shows training position of peak pressure error

Individual Cylinder Generalisation Results

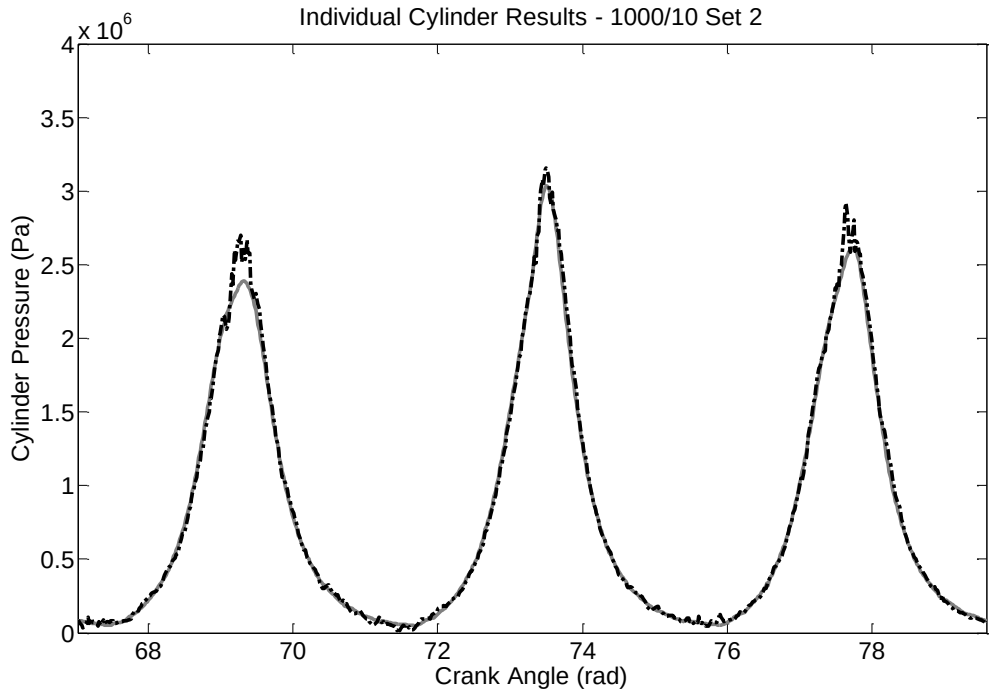

Figure 5.50: Individual Cylinder Generalised Results. Target pressure (grey continuous line) and predicted pressure (dotted line).

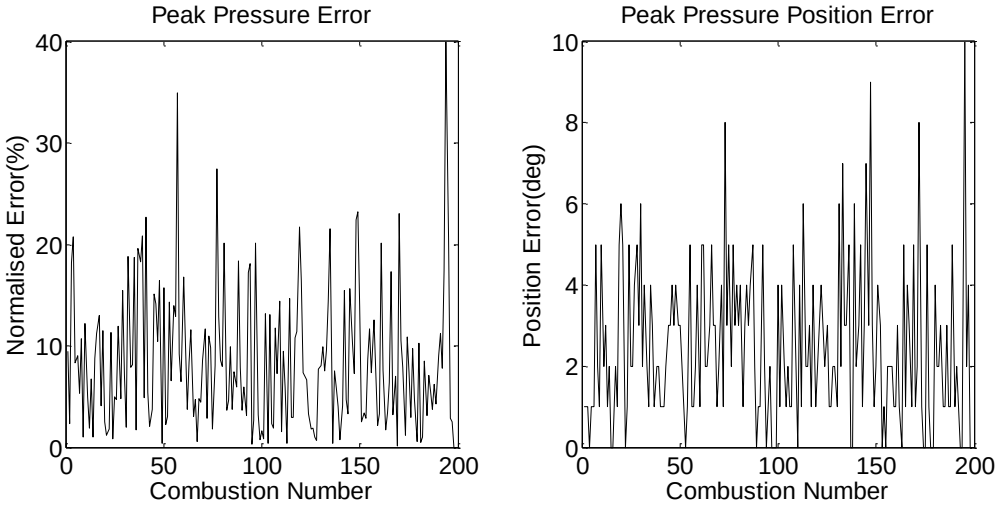

Figure 5.51: Individual Cylinder Generalised Results. Left shows training peak pressure error and right shows training position of peak pressure error

With the success of using individual cylinders for training and generalisation shown in the results in Figures 5.48 to 5.51, a comparison between using individual cylinders and multiple cylinders was undertaken.

Table 5.11: Comparison of the Training Results for both Individual Cylinder and Multiple Cylinder Approaches

Training Results	Multiple Cylinder		Individual Cylinders	
	Root-Mean-Squared Error	Standard Deviation	Root-Mean-Squared Error	Standard Deviation
Overall Performance	3.38 %	3.38 %	2.34 %	2.34 %
Normalised Peak Error	10.9 %	8.23 %	9.57%	5.66 %
Peak Pressure Position Error (deg)	3.79	2.44	3.35	2.04

Table 5.12: Comparison of the Generalisation Results for both Individual Cylinder and Multiple Cylinder Approaches

Generalisation Results	Multiple Cylinders		Individual Cylinder	
	Root-Mean-Squared Error	Standard Deviation	Root-Mean-Squared Error	Standard Deviation
Overall Performance	3.49 %	3.49 %	2.49 %	2.49 %
Normalised Peak Error	12.6 %	9.27 %	10.8 %	6.78 %
Peak Pressure Position Error (deg)	3.45	2.06	3.10	1.91

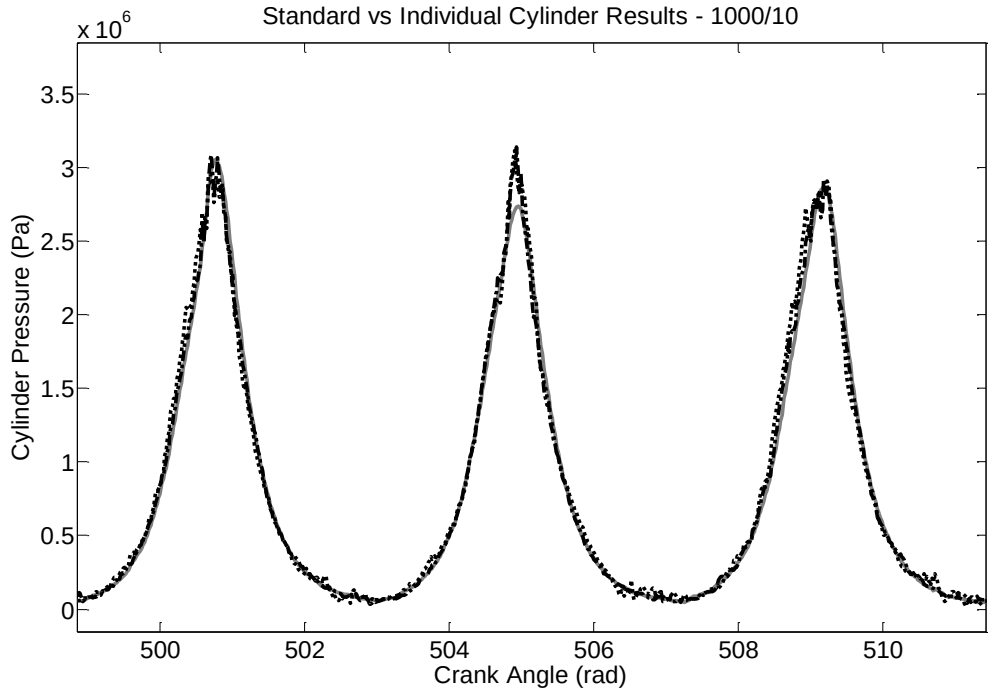

Figure 5.52: Comparison between Individual Cylinder and Multiple Cylinder Generalised Results. Target pressure (grey continuous line), predicted with past approach (black dash dot line) and predicted with Individual Cylinder approach (black dotted line).

Similar to the last two sections, this approach detailed in this section, showed a notable improvement in both the training and generalised results; although not to the extent of the other sections. The overall performance improved from 3.49% to 2.49% for the generalised RMSE result. Even though this approach requires more training, one ANN for each cylinder, practically it would require more computational effort to run and adapt. The over and under reconstruction and filtering issues are still present as the previous schemes have not been utilised in this test.

5.9 Conclusions of Chapter 5: Combined Methodology

This chapter shows that complex recurrent neural networks are not necessary for the accurate reconstruction of cylinder pressure - a more simple architecture could be used to produce the same level of accuracy. It was also found that by examining both crankshaft kinematics and engine block vibration reconstruction results, key information about the cylinder pressure was being missed through the training. This missing information was deemed to be the result of several main factors; the

variation of the effective radius, the variation in friction at TDC and more importantly, the dominance of the inertia.

One of the key solutions developed to overcome the problems identified, was a different approach to the ANN input organisation; the use of both future and past delays. This method examined the crankshaft kinematics prior to and after TDC, which successfully overcame the majority of the above mentioned issues. Two additional solutions were found to solve some additional inaccuracies in reconstructing cylinder pressure. These included a less indiscriminate method of filtering crankshaft kinematics in order not to eliminate useful information and creating an ANN for each cylinder, which will take into account the variability between the different cylinders. The combination of these three solutions into a single methodology, along with the use of a time-delay neural network and Levenberg-Marquardt algorithm, should prove to be the solution to overcoming the reconstruction difficulties.

Chapter 6 will take the conclusions from this chapter and apply them directly to crankshaft kinematic cylinder pressure reconstruction. Chapter 7 will also apply this methodology and discuss slight modifications needed in order to successfully reconstruct from engine block vibration. Once the successfulness of this methodology has been established, using the steady-state conditions, work will then focus on applying the methodology to transient conditions.

Chapter 6

Crankshaft Kinematics Based Cylinder Pressure Reconstruction Results

6.1 Introduction

Chapter 6 presents the final and most significant results using the methodology discussed in Chapter 5 with crankshaft kinematics to reconstruct cylinder pressure for the Ford 3-cylinder engine. Chapter 5 only examined each part of the methodology in isolation; this chapter examines the complete methodology. Owing to the complexity of transient engine dynamics, this chapter will only focus on steady-state reconstruction. The first objective of this chapter is to demonstrate the capability of using simple ANN architectures and training methodologies, namely Time-Delay neural networks and Levenberg-Marquardt algorithm. Second, this chapter will aim to show that the trained and generalised cylinder pressure reconstruction results are significantly improved and within the desired performance goal. The final objective is to show how the training and generalisation performance vary depending on the test condition.

Initially, the method used to process the data from its raw state to the form required for its application to the ANN, will be discussed and will summarise the methodology developed in Chapter 5. The remainder of this chapter will present the training and generalised results of a range of test conditions, compare each condition and discuss the implications. Some important observations will also be highlighted, which will have a significant impact on work undertaken in later chapters , namely the reconstructing cylinder pressure under transient conditions.

Table 6.1: Test Conditions used for Assessing the Performance of the Developed Methodology and ANNs

	Engine Speed (rpm)	Engine Load (Nm)	Training Data File Name	Generalised Data File Name
Condition-1	1000	10	1000_10_01p_jun2010	1000_10_02p_jun2010
Condition-2	1500	10	1500_10_01p_jun2010	1500_10_02p_jun2010
Condition-3	2000	10	2000_10_01p_jun2010	2000_10_02p_jun2010
Condition-4	1000	20	1000_20_01p_jun2010	1000_20_02p_jun2010
Condition-5	1500	20	1500_20_01p_jun2010	1500_20_02p_jun2010
Condition-6	2000	20	2000_20_01p_jun2010	2000_20_02p_jun2010
Condition-7	1000	30	1000_30_01p_jun2010	1000_30_02p_jun2010
Condition-8	1500	30	1500_30_01p_jun2010	1500_30_02p_jun2010
Condition-9	2000	30	2000_30_01p_jun2010	2000_30_02p_jun2010

In total, 9 separate test conditions were examined and an ANN was trained for each, shown in Table 6.1. However, this chapter will only be presenting 3 of the test conditions in full; the remaining 6 are presented in Appendix E. The 3 test conditions selected were condition-1, condition-5 and condition-9. These conditions demonstrate a broad range of variability and potentially a significant difference in the reconstruction performance. At each test condition, full details will be given regarding the network structure, training limits and training data selected. The results for both the network training and generalisation will be presented and analysed. The presented results will be classified as best, average or worst. These are classified statistically by ranking each cycle of data using three metrics; mean squared error, peak pressure error and position of peak pressure error. The best results are the reconstructions cycles with the highest rank in each metric. The worst is the lowest ranked cycle and average is the average ranked cycle. The chapter will conclude with a discussion on the overall performance of the ANN architecture, training algorithm and the methodology developed in Chapter 5.

6.2 Test Data Preparation

In this section, the preparation and processing of the data used for the training of all test conditions will be discussed and will be identical in both Chapter 6 and 7. The preparation, described below, will cover every step undertaken for reading the raw data acquired, to the form required for training and generalisation testing. All processing was undertaken within Matlab.

The first step in processing the data was to prepare the cylinder pressures. This was done by concatenating the pressure from each cylinder separately. This process truncates the 720° cylinder pressure signal to the 240° surrounding TDC and then combines into a string of pressure events. This process ensures that firstly, only the relevant and measurable pressure data is used and secondly, it guarantees that the reconstruction undertaken only takes into account the cylinder pressure and input data from the current combustion event. The remainder of the processing involved the input data, namely crankshaft kinematics. The first step in preparing the crankshaft kinematics was to isolate each cycle so that the successive steps could be undertaken more accurately and efficiently. This was carried out by using the TDC marker that was acquired from the crankshaft encoder. As described in Chapter 4, the current data acquisition system has been set up to acquire data in the time domain. However, for this work it was believed that the crank angle domain would have the most success in reconstructing cylinder pressure. The samples per cycle in the time domain vary depending on speed with ~1200 samples per cycle at 1000 rpm to with ~600 samples per cycle at 2000 rpm. The samples per cycle in the crank domain remains constant at 720 per cycle. It is there for necessary to use interpolation for the conversion from the time domain to the crank domain. At higher speeds the difference between the time and crank domain samples per cycle is relatively small resulting in negligible potential loss in information during the conversion. However, at lower speeds the difference in samples per cycle is greater leading to a significant chance of aliasing or the distortion of the signal when sampled. To attempt to negate some of this effect during the conversion cubic interpolation was selected in place of linear interpolation. Instead of assuming a linear change between each sample, cubic interpolation uses a spline to describe the difference between each sample, with a third-degree polynomial. This more accurate form of interpolation hopes to reduce some of the aliasing effect, even though it is impossible to guaranty without using anti-aliasing filter. This conversion

was applied to both the crankshaft kinematics and the cylinder pressure; this was the last process to take place regarding the cylinder pressure.

The final stage in processing the data, prior to arranging the data, was filtering the higher frequencies contained within the crankshaft kinematics. The exact frequencies and methodology used has been described in detail within Chapter 5. The practical filtering was carried out using the Matlab Fast Fourier Transform (FFT) function for each cycle of crankshaft kinematics independently. This independence reduced errors generated because of the cyclic nonlinearity and time dependent phenomena.

The remainder of the processing was concerned with the final arrangement of the data so that it could be presented to the ANN for training and assessing generalisation capabilities. The first stage was to arrange the delays for the input which relate to specific cylinder pressure, second to randomise the order and finally to select the training and validation sets.

The input was arranged in a matrix form where each column related to a different cylinder pressure and in each column there were 240 crankshaft kinematic data points, 120 prior to the particular pressure and 120 subsequent to the pressure. The cylinder pressures were simply arranged into vectors, the same length as the input matrix. To note, crankshaft kinematics were not concatenated. As a result, the crankshaft kinematics taken outside the 240° window, at the beginning and end of the combustion event, were not associated with the adjacent combustion events; they were from the kinematics associated with the combustion events from the other cylinders at that specific instance. As the adjacent combustion events in this context relates to the previous combustion in the same cylinder and not the previous firing event.

These combustion events were then randomised in order to prevent the over-training of the ANN and to eliminate any other time dependent phenomena which might be trained. Similarly, the training and validation sets were also selected randomly to prevent over-training. The data was then presented in this form to the ANN for training purposes and generalisation.

6.3 Results - Test Condition-1

6.3.1 Data and Network Configuration

The first test condition used measured data from running the engine at steady-state with a speed of 1000 rpm and a load of 10 Nm. This test condition was selected as it was the lowest power condition acquired and as a result should contain the most cylinder pressure variability cycle-to-cycle. Both the training and generalisation data sets underwent the same data process using the steps covered in section 6.2. The ANN used was a time-delay network with one hidden-layer of 15 neurons. The ANN had 200 input delays, where 100 were dedicated to the 'past' inputs and 100 were dedicated to the 'future' inputs. The Levenberg-Marquardt training algorithm was used with a mean squared error cost function and a maximum epoch number of 1000. More information regarding the setup of the training is given in Table 6.2.

Table 6.2: ANN Training Setup for Test Condition-1

Network Name	Net_TD_CK_Test1	**Network Architecture**	Time-Delay	**Test Data**	1000_10_01p_jun2010
Network Training Algorithm	Levenberg–Marquardt	**Hidden Layers Number**	1	**Speed (rpm) / Load (Nm)**	1000/10
Cost Function	Means Squared Error	**Neurons Number**	15	**Training to Validation Ratio**	60:40
Training Goal	1E8	**Delay Number**	240	**Crank Step**	1 Deg
Maximum Epoch	1000	**Transfer Function Layer 1**	Sigmoid	**Number of Iterations**	10
Weights Initialisation	Randomised	**Transfer Function Layer 2**	Linear		

6.3.2 Training Results

This subsection presents the results from training the ANN using data from condition-1 (1000 rpm and 10 Nm). In total, 10 ANNs different initial conditions were trained with the overall performance of the ANNs ranging from 0.98% to 1.91% RMSE. The best performing ANN was selected, which trained in 1719 seconds (0.4775 hours) and 121 epochs. Figures 6.1 to 6.3, present training results for best, average, and worst regions of cylinder pressure reconstruction. Each of these regions have been evaluated and compared against the mean values to rank their degree of success.

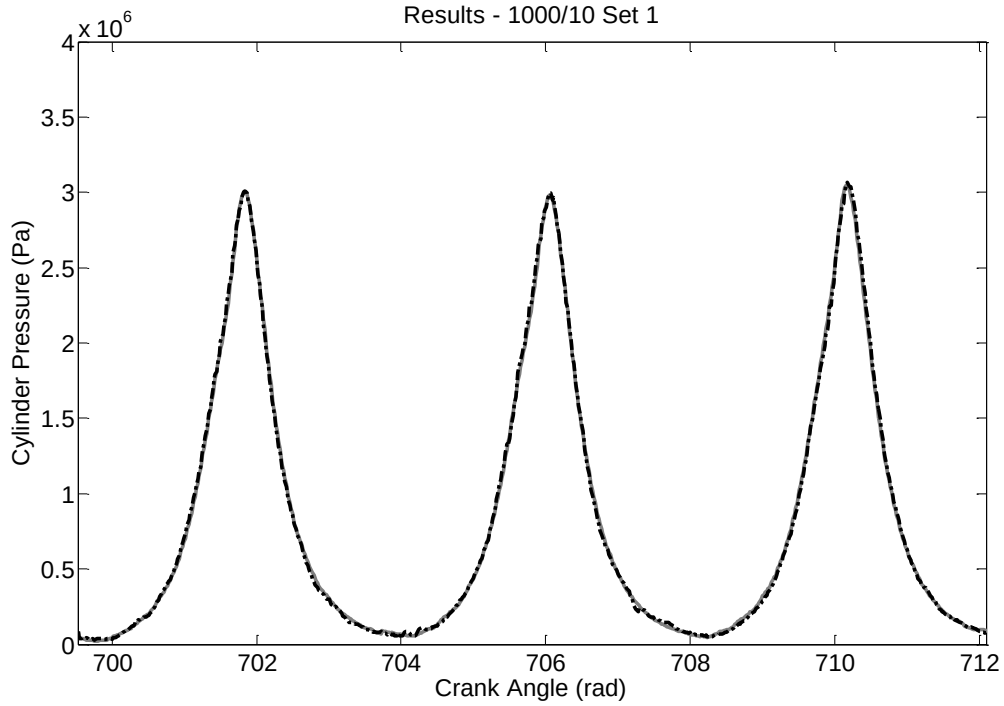

Figure 6.1: Condition-1 Training Results - Best. Measured Cylinder Pressure (Grey Solid Line). Reconstructed Cylinder Pressure (Black Dashed Line). RMSE = 0.64%.

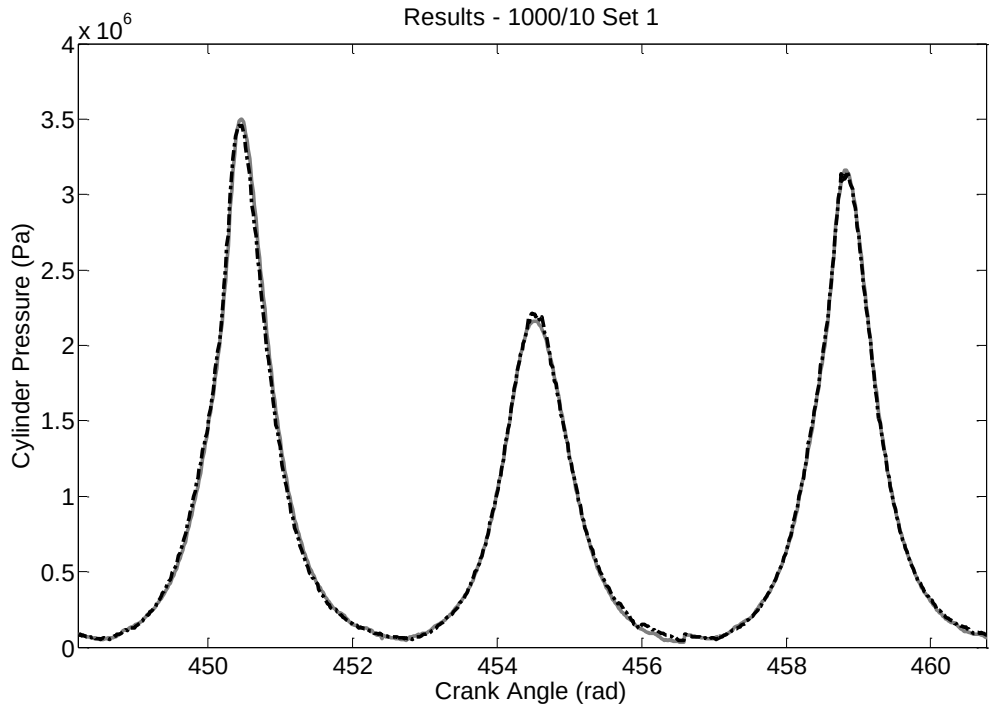

Figure 6.2: Condition-1 Training Results - Average. Measured Cylinder Pressure (Grey Solid Line). Reconstructed Cylinder Pressure (Black Dashed Line). RMSE = 0.95%.

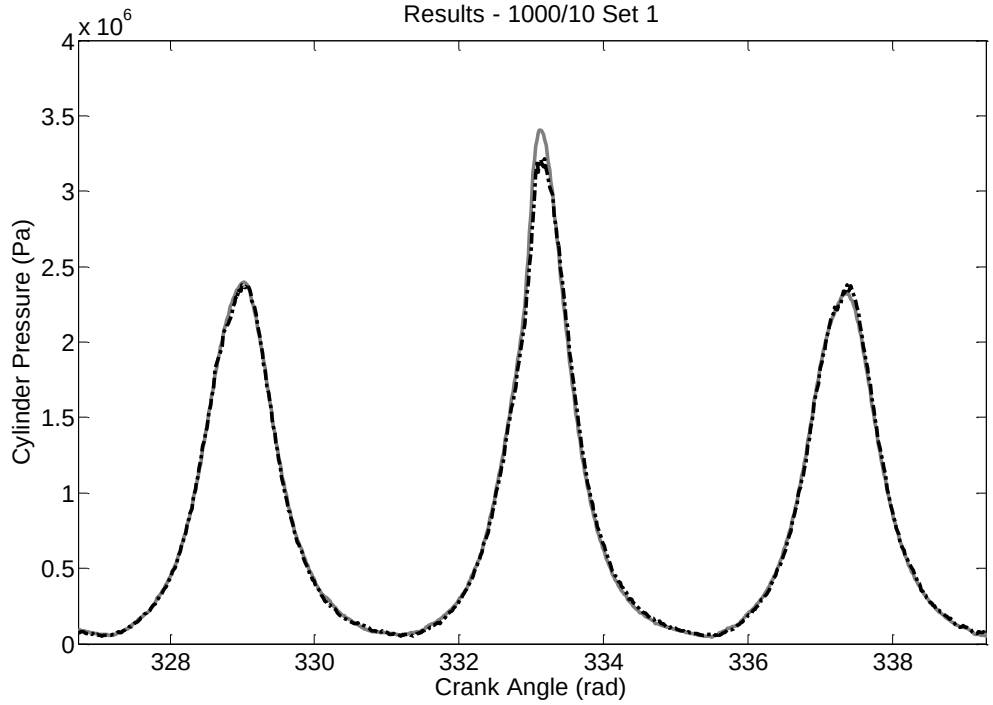

Figure 6.3: Condition-1 Training Results - Worst. Measured Cylinder Pressure (Grey Solid Line). Reconstructed Cylinder Pressure (Black Dashed Line). RMSE = 1.36%.

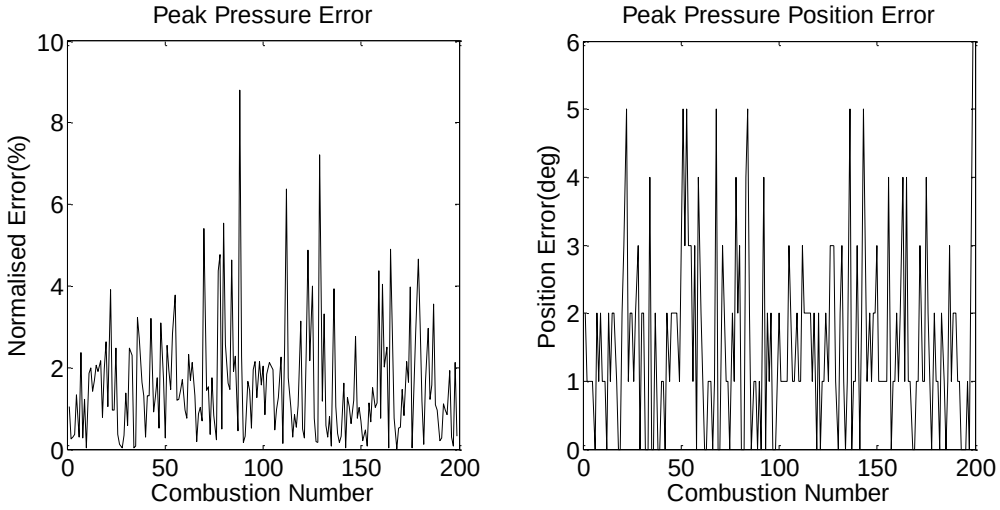

Figure 6.4: Condition-1 Normalised Peak Error Training Results (left). Condition-1 Position of Peak Error Training Results (right)

Figure 6.4 presents the normalised peak error and the peak position error between the measured cylinder pressure and training results for 180 cycles of data. The following table, Table 6.3, presents the root-mean-squared error and the standard deviation for 3 key parameters; the overall error, the normalised peak pressure error and the position of peak pressure error.

Table 6.3: Condition-1 Root-Mean-Squared Error (RMSE) and Standard Deviation for the ANN Training

	Training Root-Mean-Squared Error	Training Standard Deviation
Overall Performance	0.98 %	0.98 %
Normalised Peak Error	2.1 %	1.4 %
Peak Pressure Position Error (deg)	2.01	1.30

6.3.3 Generalisation Results

The data used for the generalisation tests was from the same condition (1000 rpm and 10 Nm). However, it was acquired separately from the training data and has not been used by the ANN for training. Figures 6.5 to 6.7, gives generalisation results for best, average, and worst regions of cylinder pressure reconstruction. Each of these regions again, have been evaluated and compared against the mean values to rank their degree of success.

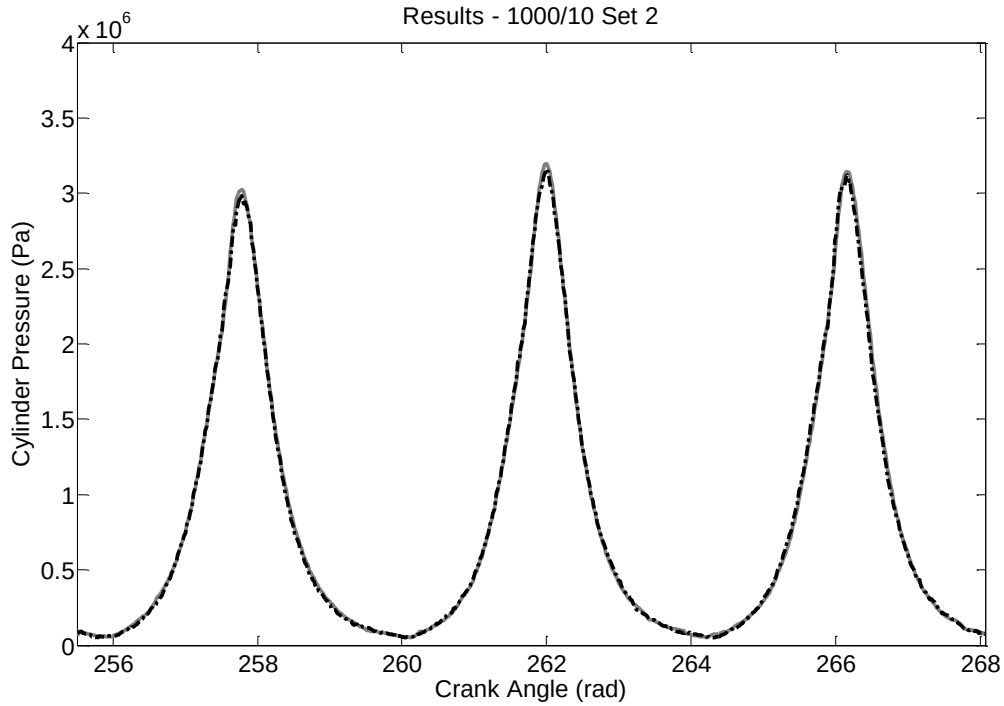

Figure 6.5: Condition-1 Generalisation Results - Best. Measured Cylinder Pressure (Grey Solid Line). Reconstructed Cylinder Pressure (Black Dashed Line). RMSE = 0.57%.

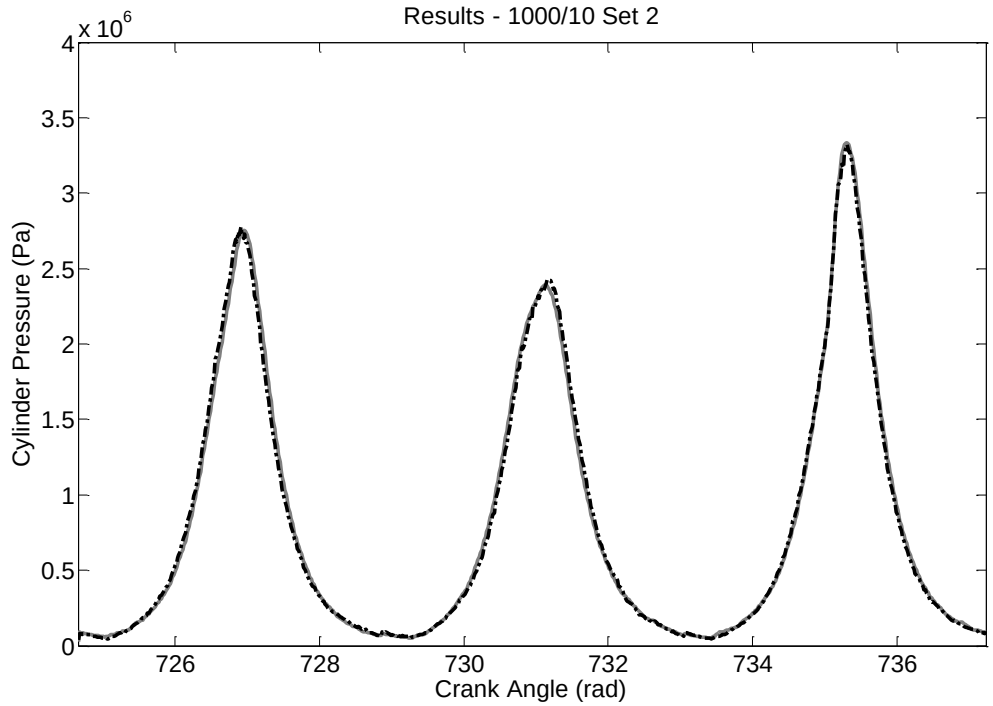

Figure 6.6: Condition-1 Generalisation Results - Average. Measured Cylinder Pressure (Grey Solid Line). Reconstructed Cylinder Pressure (Black Dashed Line). RMSE = 1.25%.

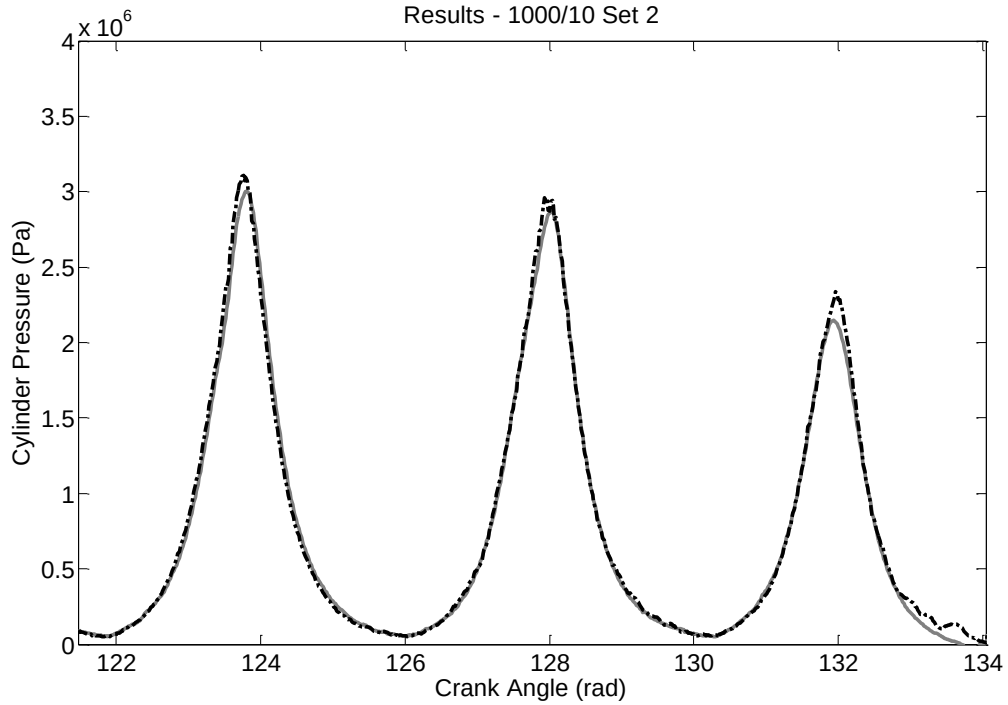

Figure 6.7: Condition-1 Generalisation Results - Worst. Measured Cylinder Pressure (Grey Solid Line). Reconstructed Cylinder Pressure (Black Dashed Line). RMSE = 1.56%.

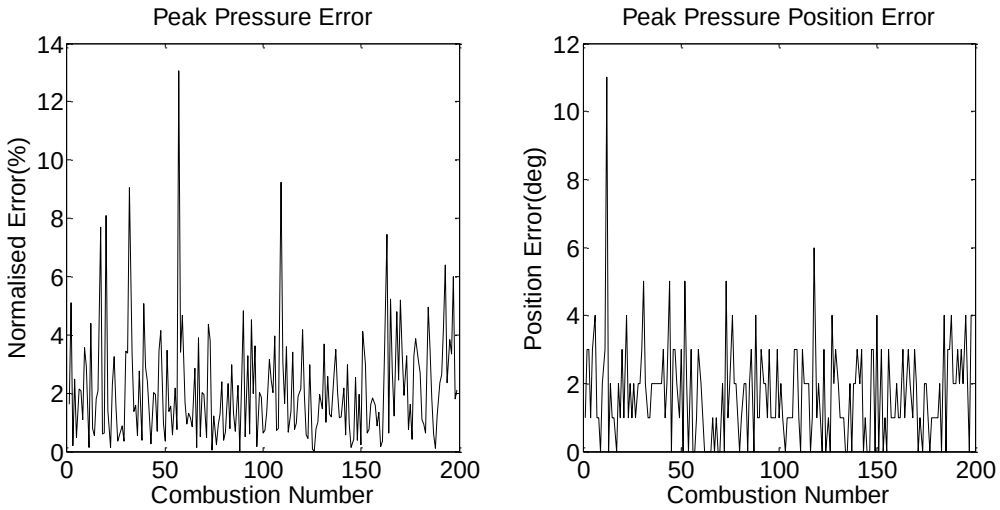

Figure 6.8: Condition-1 Normalised Peak Error Generalisation Results (left). Condition-1 Position of Peak Error Generalisation Results (right)

Figure 6.8 shows the normalised peak error and the peak position error between the measured cylinder pressure and generalised results for 180 cycles of data. Table 6.4, gives the root-mean-squared error and the standard deviation for 3 key parameters: the overall error, the normalised peak pressure error and the position of peak pressure error.

Table 6.4: Condition-1 Root-Mean-Squared Error (RMSE) and Standard Deviation for the ANN Generalisation

	Generalisation Root-Mean-Squared Error	Generalisation Standard Deviation
Overall Performance	1.14 %	1.14 %
Normalised Peak Error	2.8 %	1.8 %
Peak Pressure Position Error (deg)	2.24	1.45

6.3.4 Discussion of Test Condition-1 Results

The training results at condition-1 (1000 rpm and 10 Nm) were very promising and are significantly better than predicted. It was expected that the high cylinder pressure variability, caused by part-throttle low power conditions, would create difficulties in training. One notable observation from the training results was that the overall error is still present, i.e. an RMSE = 0.98%, and more work could be done to improve the training results by more neurons, more stringent limits, and a lower

threshold on the training goal. This approach would require more epochs and have greater effect on the computational effort, which at present, is fairly minimal. Figure 6.1 and 6.2 show examples of best, and average, cylinder pressure reconstruction. These training results are very promising and the latter shows better than expected reconstruction with a high degree of variability. Even Figure 6.3, which shows an example of worst reconstruction, is acceptable given the significant variation. The generalisation results are also considerably better than previous attempts, with an RMSE value equal to 1.14% over 200 cycles; well below the targeted error of 4%. Another positive result from the training at this condition, is that there is a relatively small difference between the training and generalisation performances which gives a reassurance that the ANN is not over-training. Figure 6.5 and 6.6 demonstrate that this ANN is good at generalisation with only relatively small errors being generated at higher variability, as shown in Figure 6.7. However, across both the training and generalisation, the position of peak pressure is fairly poor with a mean of 2.01°and 2.24°.

6.4 Results - Test Condition-5

6.4.1 Data and Network Configuration

The next test condition used measured data taken when running the engine at steady-state with a speed of 1500 rpm and a load of 20 Nm. This test condition was selected as it was in the middle of the power range of interest. Both the training and generalisation data sets underwent the same data process using the steps covered in section 6.2. The ANN used was a time-delay network with one hidden-layer of 15 neurons. The ANN had 240 input delays, where 100 were dedicated to the 'past' inputs and 100 were dedicated to the 'future' inputs. The Levenberg-Marquardt training algorithm was used with a mean squared error cost function and a maximum epoch number of 1000. More information regarding the configuration for training is given in Table 6.5.

Table 6.5: ANN Training Setup for Test Condition-5

Network Name	Net_TD_CK_Test5	**Network Architecture**	Time-Delay	**Test Data**	1500_20_01p_jun2010
Network Training Algorithm	Levenberg–Marquardt	**Hidden Layers Number**	1	**Speed (rpm) / Load (Nm)**	1500/20
Cost Function	Means Squared Error	**Neurons Number**	15	**Training to Validation Ratio**	60:40
Training Goal	1E8	**Delay Number**	240	**Crank Step**	1 Deg
Maximum Epoch	1000	**Transfer Function Layer 1**	Sigmoid	**Number of Iterations**	10
Weights Initialisation	Randomised	**Transfer Function Layer 2**	Linear		

6.4.2 Training Results

This subsection gives the results from training the ANN using data from condition-5 (1500 rpm and 20 Nm). In total, 10 ANNs different initial conditions were trained with the overall performance of the ANNs ranging from 1.31% to 1.52% RMSE. The best performing ANN was selected which trained in 1142 seconds (0.32 hours) and 65 epochs. Figures 6.9 to 6.11, gives training results for best, average, and worst regions of cylinder pressure reconstruction. Each of these regions have been evaluated and compared against the mean values to rank their degree of success.

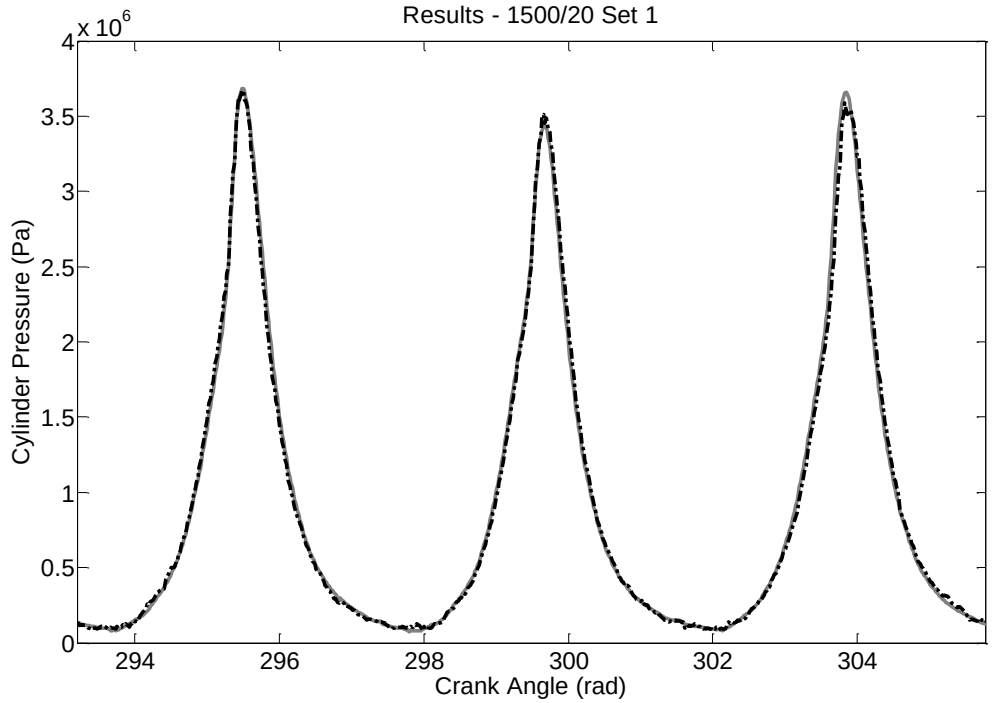

Figure 6.9: Condition-5 Training Results - Best. Measured Cylinder Pressure (Grey Solid Line). Reconstructed Cylinder Pressure (Black Dashed Line). RMSE = 0.77%.

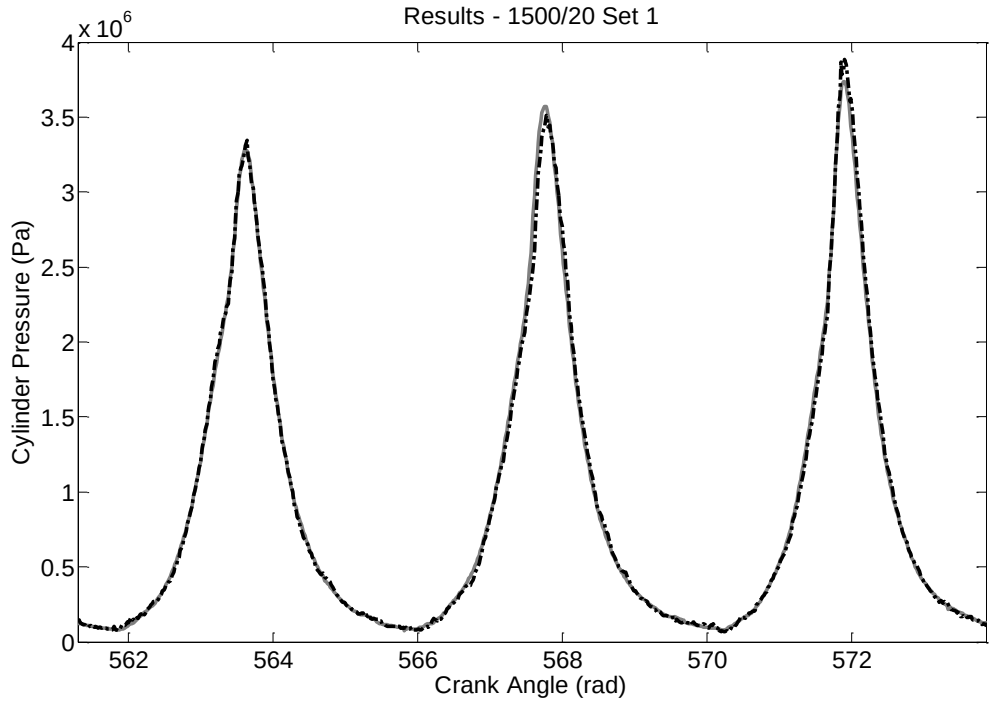

Figure 6.10: Condition-5 Training Results - Average. Measured Cylinder Pressure (Grey Solid Line). Reconstructed Cylinder Pressure (Black Dashed Line). RMSE = 1.19%.

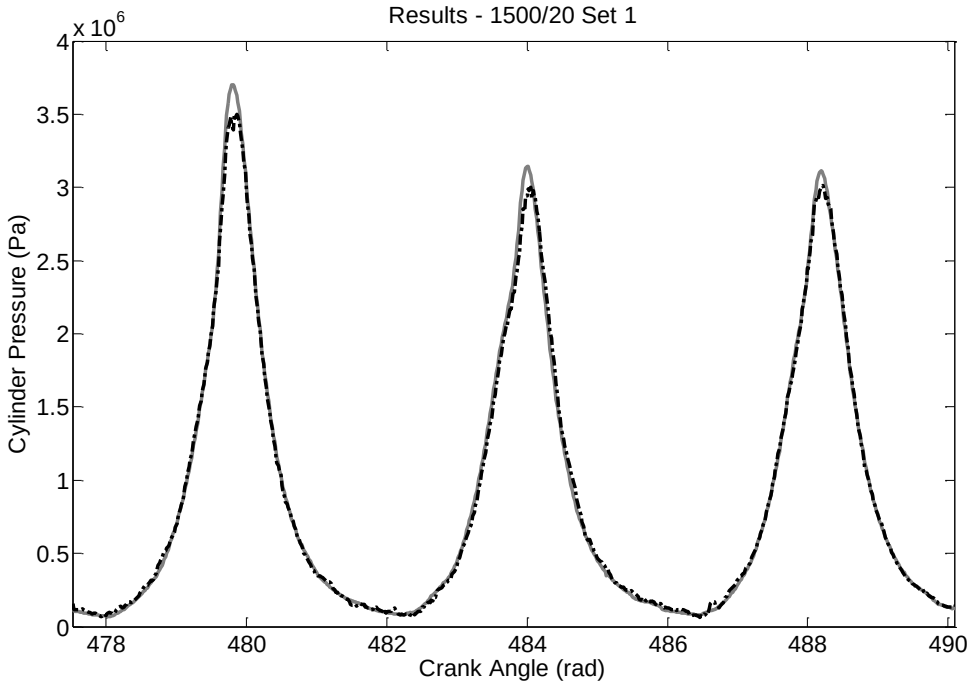

Figure 6.11: Condition-5 Training Results - Worst. Measured Cylinder Pressure (Grey Solid Line). Reconstructed Cylinder Pressure (Black Dashed Line). RMSE = 1.33%.

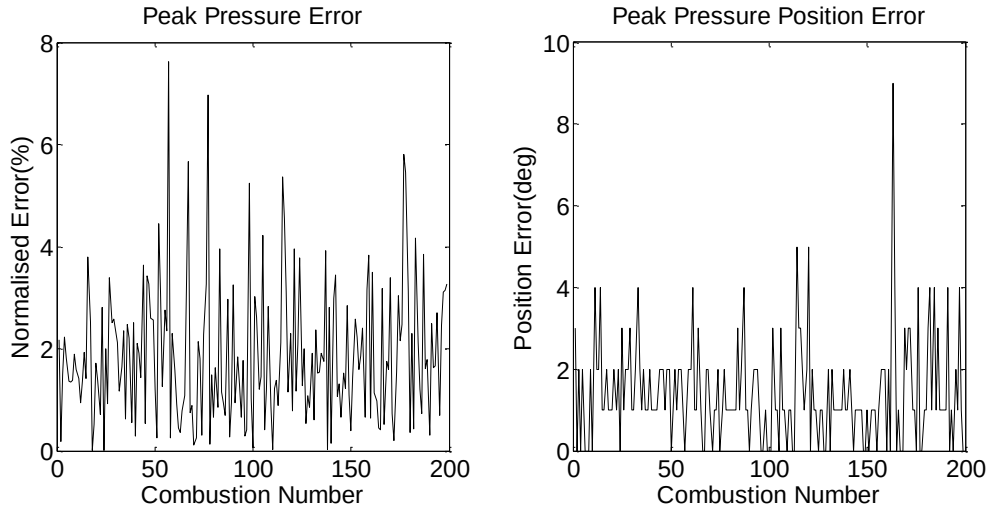

Figure 6.12: Condition-5 Normalised Peak Error Training Results (left). Condition-5 Position of Peak Error Training Results (right)

Figure 6.12 gives the normalised peak error, and the peak position error between the measured cylinder pressure, and training results for 180 cycles of data. Table 6.6, gives the root-mean-squared error and the standard deviation for 3 key parameters: the overall error, the normalised peak pressure error, and the position of peak pressure error.

Table 6.6: Condition-5 Root-Mean-Squared Error (RMSE) and Standard Deviation for the ANN Training

	Training Root-Mean-Squared Error	Training Standard Deviation
Overall Performance	1.19 %	1.19 %
Normalised Peak Error	2.3 %	1.3 %
Peak Pressure Position Error (deg)	1.87	1.25

6.4.3 Generalisation Results

The data used for the generalisation tests was from the same condition (1500 rpm and 20 Nm). However, it was acquired separately from the training data and has not been used by the ANN for training. The following series of figures, Figures 6.13 to 6.15, present generalisation results for best, average and worst regions of cylinder pressure reconstruction. Each of these regions again, have been evaluated and compared against the mean values to rank their degree of success.

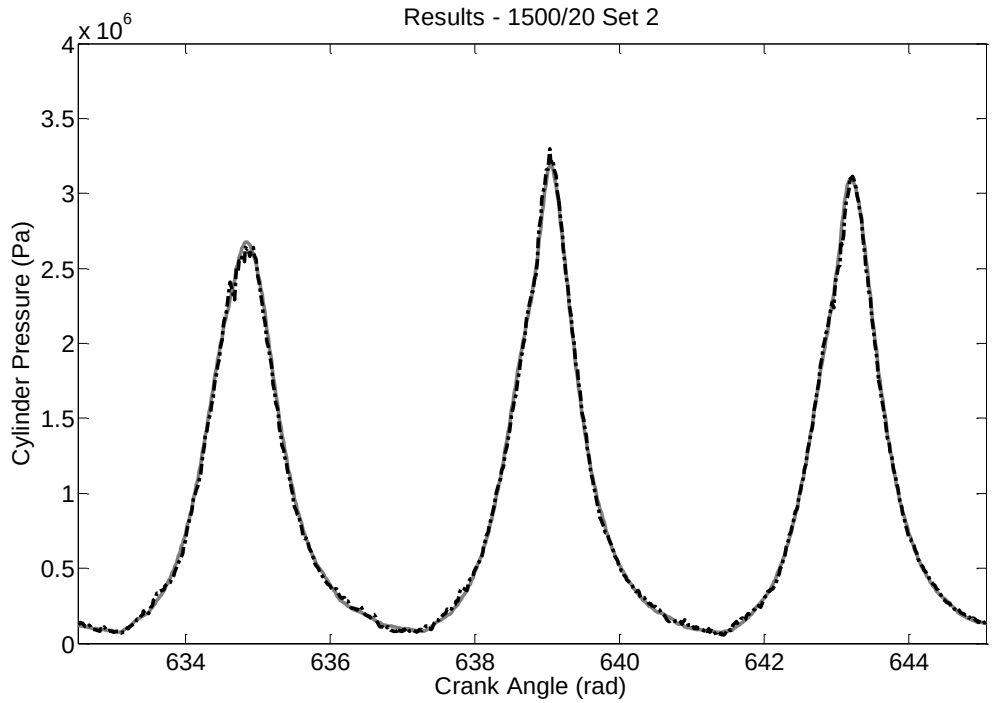

Figure 6.13: Condition-5 Generalisation Results - Best. Measured Cylinder Pressure (Grey Solid Line). Reconstructed Cylinder Pressure (Black Dashed Line). RMSE = 0.71%.

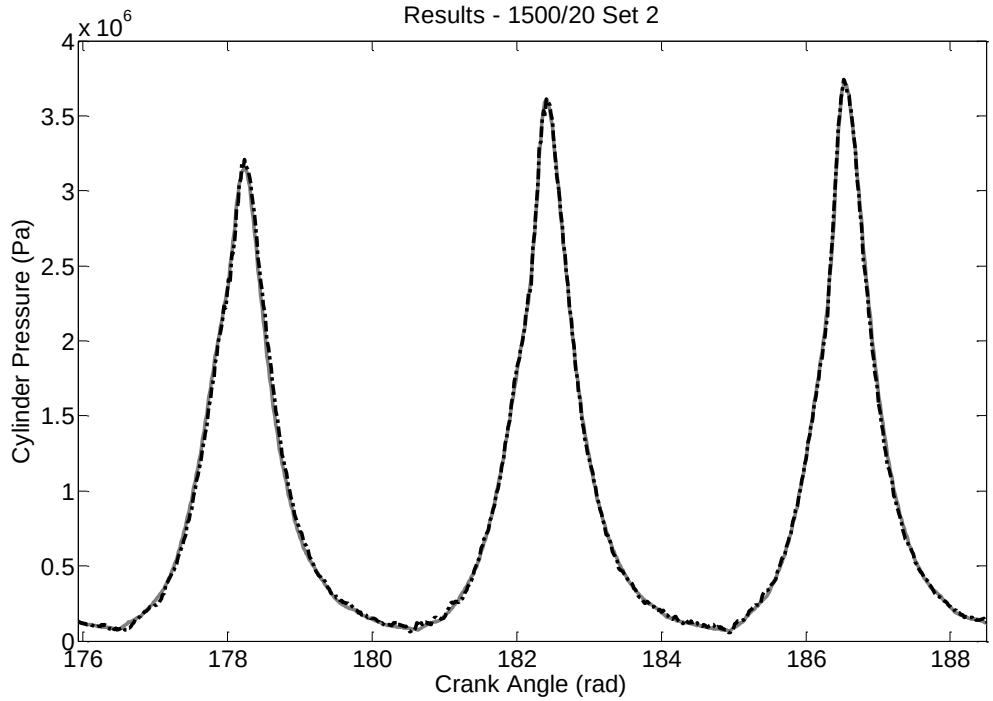

Figure 6.14: Condition-5 Generalisation Results - Average. Measured Cylinder Pressure (Grey Solid Line). Reconstructed Cylinder Pressure (Black Dashed Line). RMSE = 0.79%.

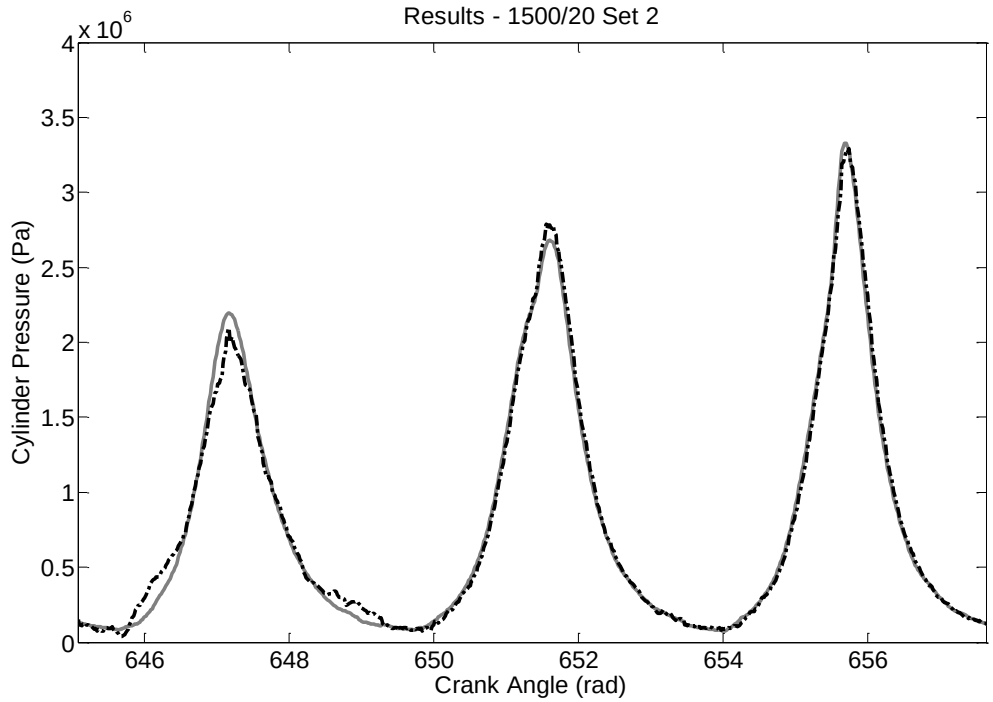

Figure 6.15: Condition-5 Generalisation Results - Worst. Measured Cylinder Pressure (Grey Solid Line). Reconstructed Cylinder Pressure (Black Dashed Line). RMSE = 1.59%.

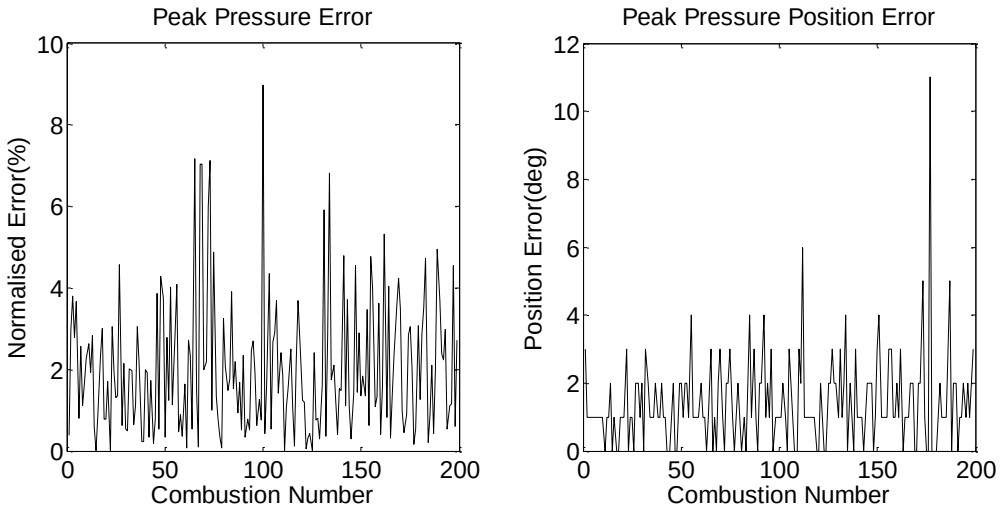

Figure 6.16: Condition-5 Normalised Peak Error Generalisation Results (left). Condition-5 Position of Peak Error Generalisation Results (right).

Figure 6.16 gives the normalised peak error and the peak position error between the measured cylinder pressure and generalised results for 180 cycles of data. Table 6.7, gives the root-mean-squared error, and the standard deviation, for 3 key parameters: the overall error, the normalised peak pressure error, and the position of peak pressure error.

Table 6.7: Condition-5 Root-Mean-Squared Error (RMSE) and Standard Deviation for the ANN Generalisation

	Generalisation Root-Mean-Squared Error	Generalisation Standard Deviation
Overall Performance	1.21 %	1.20 %
Normalised Peak Error	2.6 %	1.6 %
Peak Pressure Position Error (deg)	1.91	1.29

6.4.4 Discussion of Test Condition-5 Results

The training results at condition-5 (1500 rpm and 20 Nm) are again promising, and are significantly better than previously seen. Similarly, the training overall error was not insignificant, RMSE = 1.19%. The same methods could be used as discussed when commenting on test condition-1. However, this could impact considerably on

the ANN's chances of over-training, which the trained ANN has not shown, as can be seen by the small difference between the training and generalisation overall performances. Figure 6.9 and 6.10 show examples of best and average cylinder pressure reconstruction. These training results are very promising and the latter shows better than expected reconstruction with limited variability. However, Figure 6.11 shows more significant variation and as a result produces a slightly poorer reconstruction. The generalisation results are also considerably better than previous attempts, with an RMSE value equal to 1.21% over 200 cycles. Figure 6.13 and 6.14 demonstrate that this ANN is extremely good at generalisation. However, there is a significant unexplained error in the first combustion event of Figure 6.15, and again, the position of peak pressure error is relatively large for both the training and generalisation.

6.5 Results - Test Condition-9

6.5.1 Data and Network Configuration

The final test condition used measured data taken when running the engine at steady-state with a speed of 2000 rpm and a load of 30 Nm. This test condition was selected as it was in the highest power condition acquired and should have more consistent cylinder pressures. Both the training and generalisation data sets underwent the same data process using the steps covered in section 6.2. The ANN used was a time-delay network with one hidden-layer of 15 neurons. The ANN had 240 input delays where 100 were dedicated to the 'past' inputs, and 100 were dedicated to the 'future' inputs. The Levenberg-Marquardt training algorithm was used with a mean squared error cost function and a maximum epoch number of 1000. More information regarding the setup of the training is given in Table 6.8.

Table 6.8: ANN Training Setup for Test Condition-9

Network Name	Net_TD_CK_Test9	**Network Architecture**	Time-Delay	**Test Data**	2000_30_01p_jun2010
Network Training Algorithm	Levenberg–Marquardt	**Hidden Layers Number**	1	**Speed (rpm) / Load (Nm)**	2000/30
Cost Function	Mean Squared Error	**Neurons Number**	15	**Training to Validation Ratio**	60:40
Training Goal	1E8	**Delay Number**	240	**Crank Step**	1 Deg
Maximum Epoch	1000	**Transfer Function Layer 1**	Sigmoid	**Number of Iterations**	10
Weights Initialisation	Randomised	**Transfer Function Layer 2**	Linear		

6.5.2 Training Results

This subsection presents the results from training the ANN using data from condition-9 (2000 rpm and 30 Nm). In total, 10 ANNs different initial conditions were trained with the overall performance of the ANNs ranging from 1.17% to 1.44% RMSE. The best performing ANN was selected which trained in 523 seconds (0.15 hours) and 30 epochs. Figures 6.17 to 6.19, gives training results for best, average, and worst regions of cylinder pressure reconstruction. Each of these regions have been evaluated and compared against the mean values to rank their degree of success.

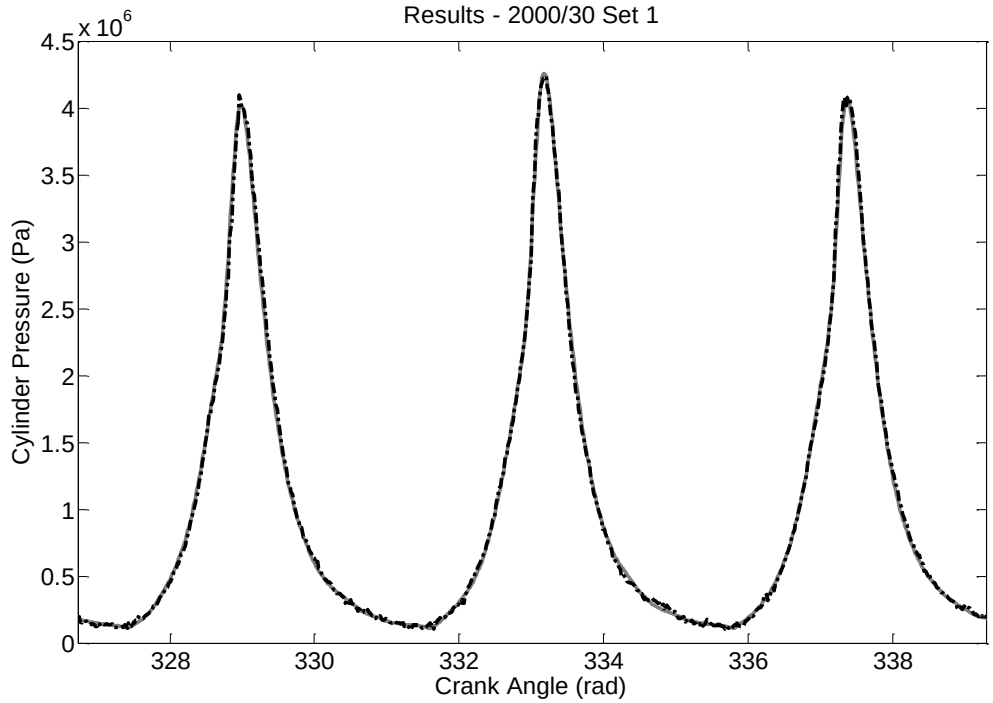

Figure 6.17: Condition-9 Training Results - Best. Measured Cylinder Pressure (Grey Solid Line). Reconstructed Cylinder Pressure (Black Dashed Line). RMSE = 0.76%.

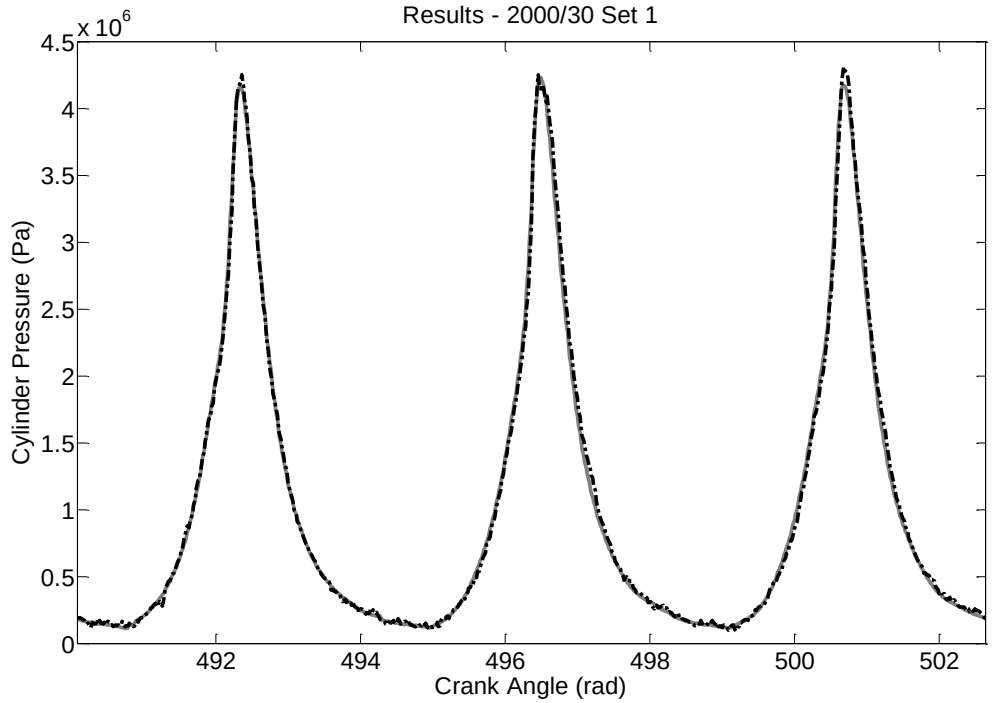

Figure 6.18: Condition-9 Training Results - Average. Measured Cylinder Pressure (Grey Solid Line). Reconstructed Cylinder Pressure (Black Dashed Line). RMSE = 1.17%.

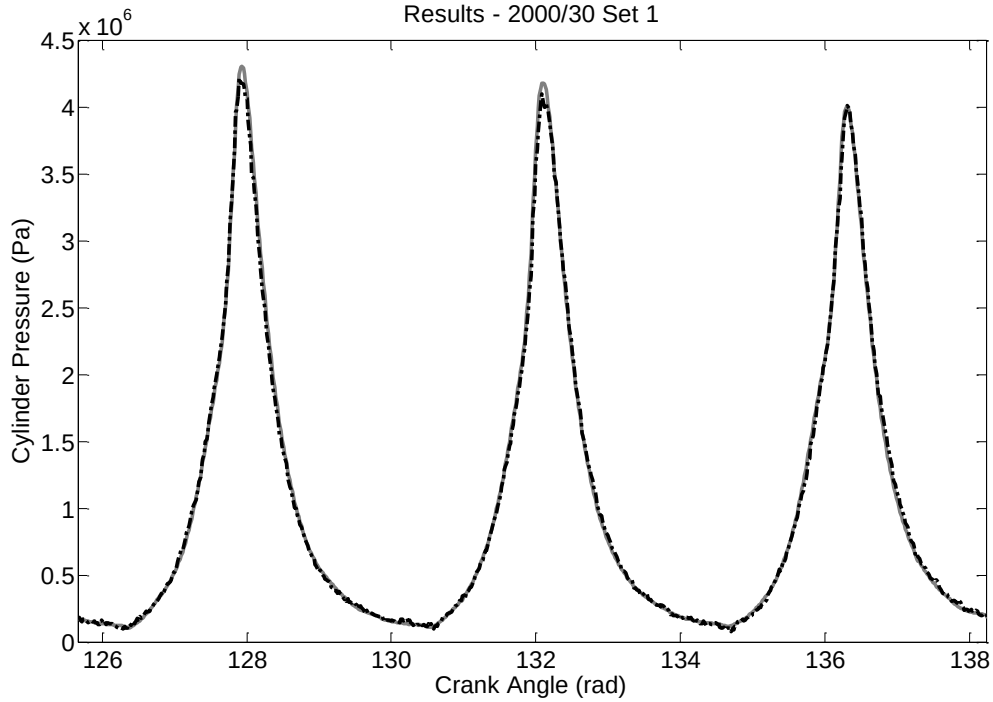

Figure 6.19: Condition-9 Training Results - Worst. Measured Cylinder Pressure (Grey Solid Line). Reconstructed Cylinder Pressure (Black Dashed Line). RMSE = 1.42%.

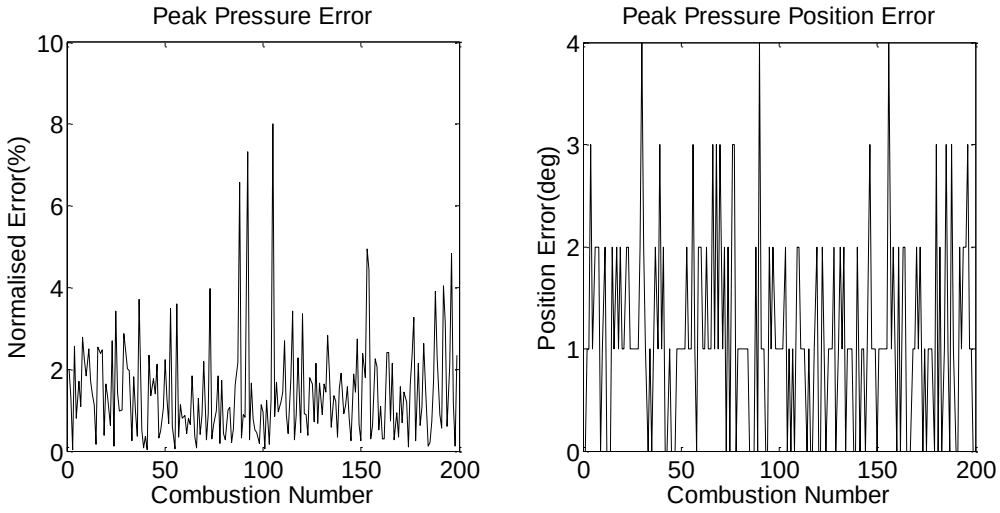

Figure 6.20: Condition-9 Normalised Peak Error Training Results (left). Condition-9 Position of Peak Error Training Results (right).

Figure 6.20 presents the normalised peak error, and the peak position error between the measured cylinder pressure and training results for 180 cycles of data. Table 6.9, gives the root-mean-squared error, and the standard deviation for 3 key parameters; the overall error, the normalised peak pressure error, and the position of peak pressure error.

Table 6.9: Condition-9 Root-Mean-Squared Error (RMSE) and Standard Deviation for the ANN Training

	Training Root-Mean-Squared Error	Training Standard Deviation
Overall Performance	1.15 %	1.15 %
Normalised Peak Error	1.91 %	1.25 %
Peak Pressure Position Error (deg)	1.45	0.92

6.5.3 Generalisation Results

The data used for the generalisation tests was from the same condition (2000 rpm and 30 Nm). However, it was acquired separately from the training data and has not been used by the ANN for training. Figures 6.21 to 6.23, gives generalisation results for best, average, and worst regions of cylinder pressure reconstruction. Each of these regions again, have been evaluated and compared against the mean values to rank their degree of success.

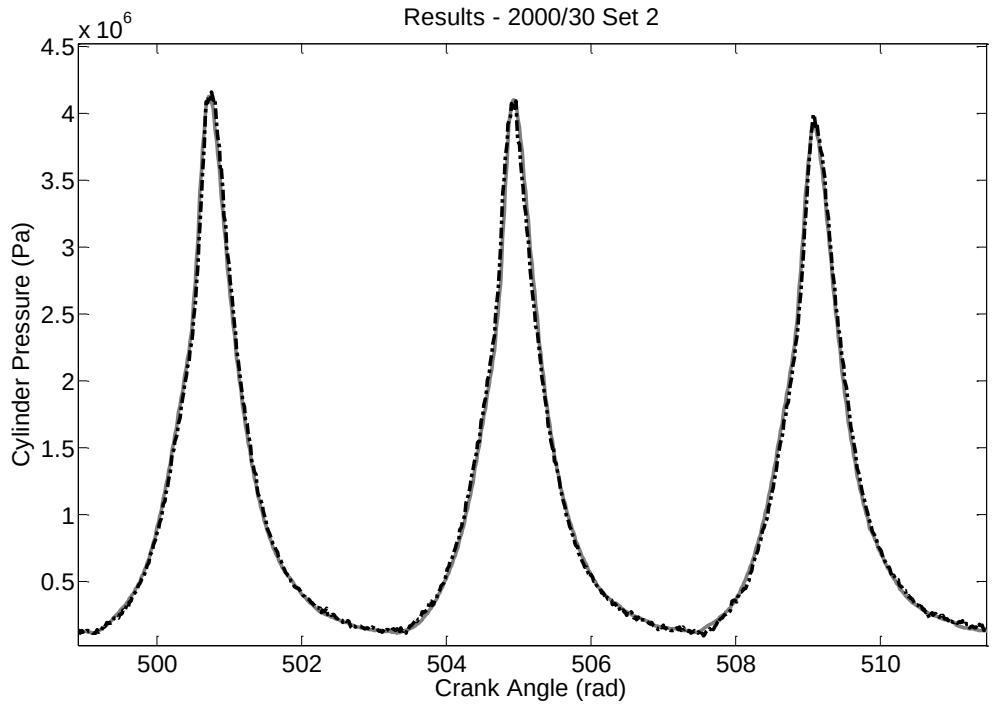

Figure 6.21: Condition-9 Generalisation Results - Best. Measured Cylinder Pressure (Grey Solid Line). Reconstructed Cylinder Pressure (Black Dashed Line). RMSE = 0.87%.

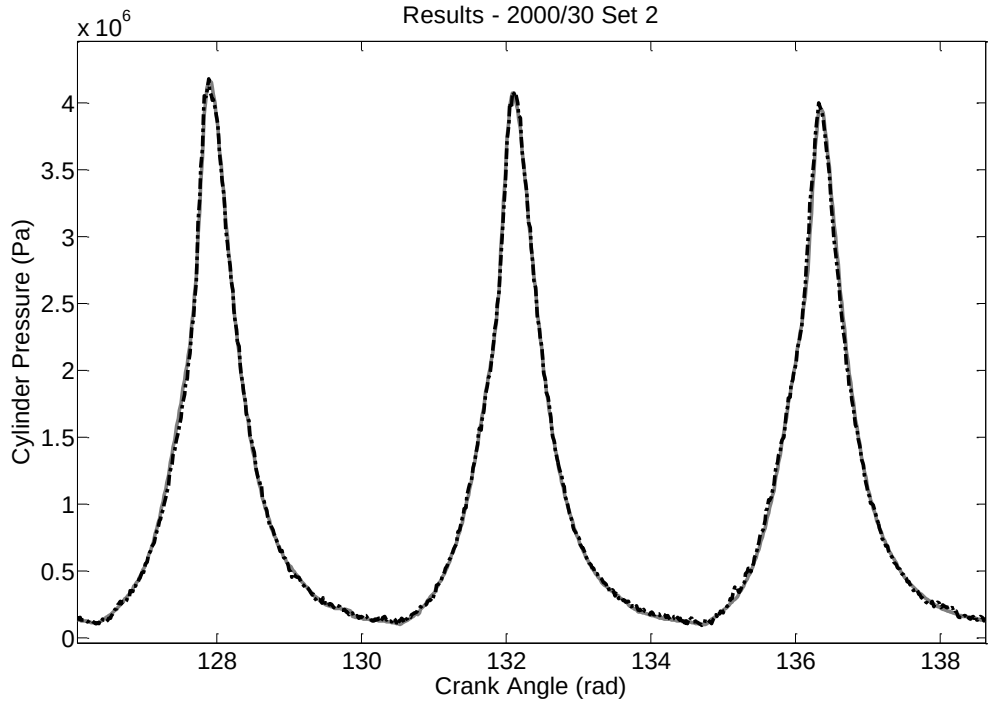

Figure 6.22: Condition-9 Generalisation Results - Average. Measured Cylinder Pressure (Grey Solid Line). Reconstructed Cylinder Pressure (Black Dashed Line). RMSE = 1.24%.

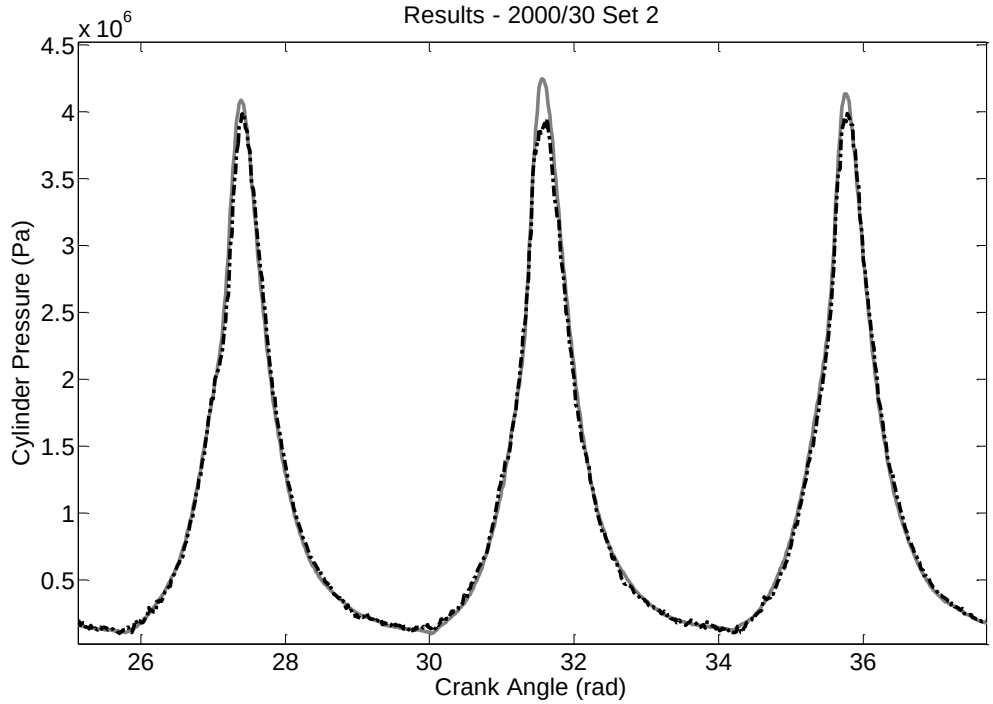

Figure 6.23: Condition-9 Generalisation Results - Worst. Measured Cylinder Pressure (Grey Solid Line). Reconstructed Cylinder Pressure (Black Dashed Line). RMSE = 1.47%.

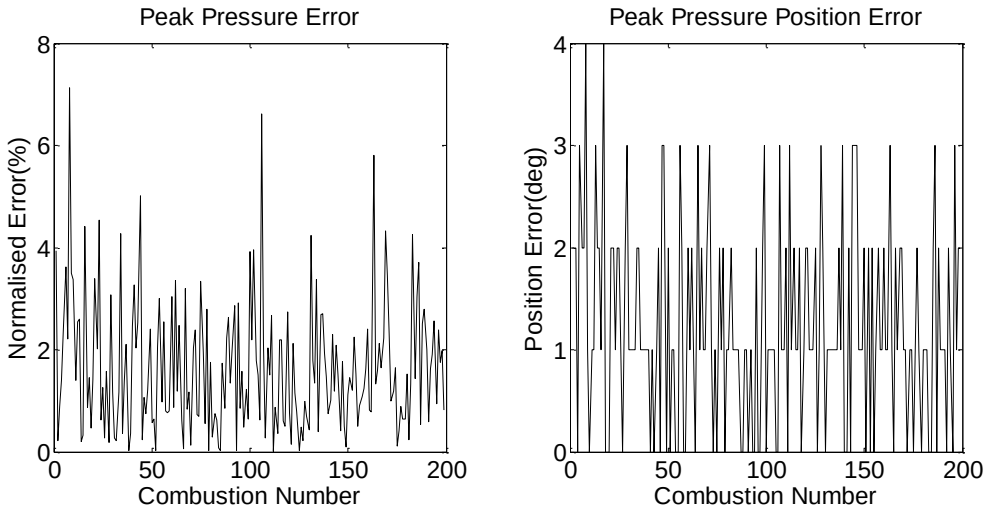

Figure 6.24: Condition-9 Normalised Peak Error Generalisation Results (left). Condition-9 Position of Peak Error Generalisation Results (right).

Figure 6.24 gives the normalised peak error and the peak position error between the measured cylinder pressure and generalised results for 180 cycles of data. Table 6.10, gives the root-mean-squared error, and the standard deviation for 3 key parameters; the overall error, the normalised peak pressure error, and the position of peak pressure error.

Table 6.10: Condition-9 Root-Mean-Squared Error (RMSE) and Standard Deviation for the ANN Generalisation

	Generalisation Root-Mean-Squared Error	Generalisation Standard Deviation
Overall Performance	1.24 %	1.23 %
Normalised Peak Error	2.08 %	1.28 %
Peak Pressure Position Error (deg)	1.55	0.95

6.5.4 Discussion of Test Condition-9 Results

The training results at condition-9 (2000 rpm and 30 Nm) are equally promising. It was believed that the high power conditions with the decreased pressure variability would create the best performing ANN. Again, improvements could be made on training but again this may have the effect of over-training the ANN, which has not been seen in any of the 9 trained test conditions using the methodology outlined.

The key difference between this test condition and the two previously covered, is that for all three different reconstruction regions (best, average and worst) the results are extremely good. These can be seen in Figure 6.17, 6.18, and 6.19. Even the statistically poorest series of reconstructions is a great deal better than previously seen. The generalisation results for both the best and average regions are as accurate as the training results; Figure 6.21 and 6.22 respectively. However, the worst results shown in Figure 6.23 do contain significant errors. Again, it can be seen in Tables 6.9 and 6.10 that the position of peak pressure error is relatively large for both the training and generalisation.

6.6 A Comparison and Overall Discussion of Results

This section will compare and discuss the generalised results from the trained ANNs for all 9 test conditions. It includes the 3 conditions discussed in detail as well as the other 6. All 9 ANNs were trained and tested using the same methodology and the additional results are provided in Appendix E. Initially, all 9 test conditions are compared with regard to the overall RMSE performance, the normalised peak pressure error and the position of peak pressure error. The range of the cylinder pressure reconstruction results will then be discussed, including notable results. Finally, this section will make some more general conclusions regarding the capability of reconstructing cylinder pressure using crankshaft kinematics, the ANN architecture, the training methodology, and most significantly, the successfulness of the methodology developed in Chapter 5.

Table 6.11: Mean Generalised Performance of 9 Test Conditions

	Test Condition Power	Overall Performance (RMSE)	Normalised Peak Error	Peak Pressure Position Error (deg)
Condition-1	1.05 kW	1.14 %	2.80 %	2.24
Condition-2	1.57 kW	1.32 %	1.76 %	1.65
Condition-3	2.09 kW	1.24 %	1.52 %	1.64
Condition-4	2.09 kW	1.15 %	2.48 %	3.08
Condition-5	3.14 kW	1.21 %	2.60 %	1.91
Condition-6	4.19 kW	1.34 %	1.84 %	1.73
Condition-7	3.14 kW	1.32 %	2.56 %	1.78
Condition-8	4.71 kW	1.30 %	2.86 %	2.24
Condition-9	6.28 kW	1.24 %	2.08 %	1.55

Prior to the development and testing of the ANNs for reconstructing cylinder pressure using crankshaft kinematics, it was believed that one of the limits to achieve optimum reconstruction was the variability of the cylinder pressure. This stems from the idea that high levels of variability, which appears to be random, may be unpredictable and may not significantly impact crankshaft kinematics. With this assumption, it was believed that at low power conditions where the variability is greatest, successful training of an ANN may be difficult. Table 6.11 shows the mean performance for all 9 test conditions including the power at each condition. It can be seen that the normalised peak pressure error appears to be fairly random and has no discernible pattern with increasing power, contrary to what was seen by examining just 3 conditions. Similarly, the results shown for the position of peak pressure error for the 3 conditions discussed in detail prove the assumption to be correct. However, when examining all 9 conditions there again is no discernible pattern with increasing power. This also applies to the overall RMSE performance.

The results shown in Table 6.11 provide strong evidence that the variability does not impact on the reconstruction capability. Each individual ANN has no knowledge of other test conditions or the degree of variability present in the training data. The ANN only has knowledge of the information presented to it, and if it contains

information pertaining to the cylinder pressure, the variability compared to other test conditions is irrelevant. The ANN and its training methodology will extract the optimum information from each condition. The results verify that the success of any given ANN, trained at a single test condition, is only limited by the optimisation and methodology used.

Figure 6.25 to 6.26 gives some of the best and worst performing generalised regions of the 9 ANNs trained, giving an overall perspective of the successfulness of using time-delay neural networks, the Levenberg Marquardt algorithm and the methodology developed in Chapter 5. They also include generalised cylinder pressure reconstruction results that are noteworthy.

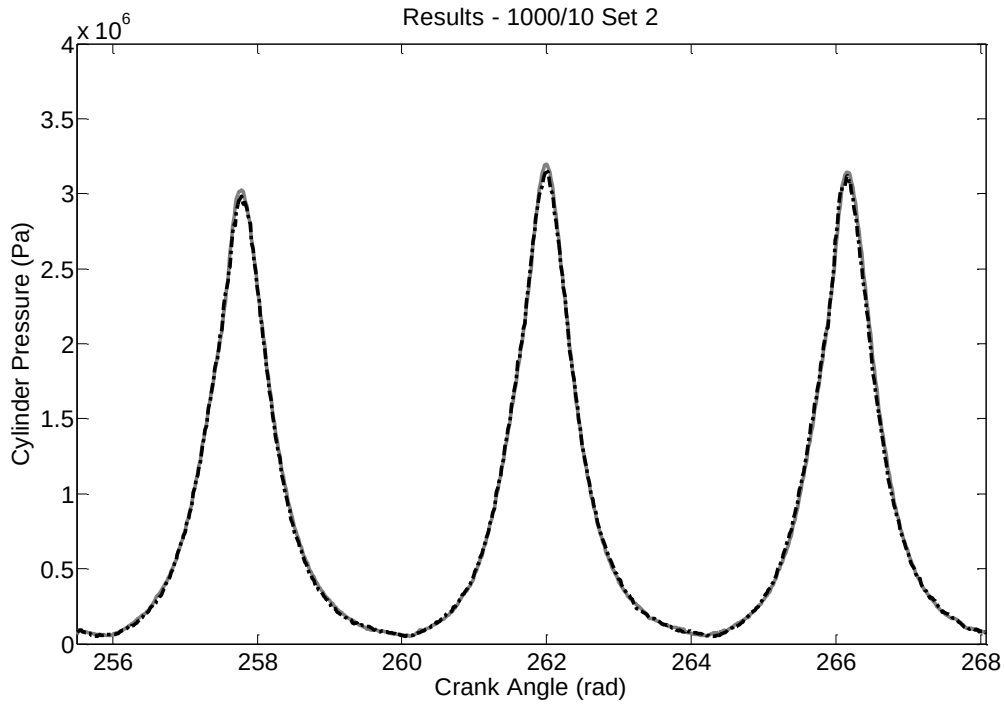

Figure 6.25: Best Performing Generalisation Results - Condition-1. Measured Cylinder Pressure (Grey Solid Line). Reconstructed Cylinder Pressure (Black Dashed Line). RMSE = 0.57%.

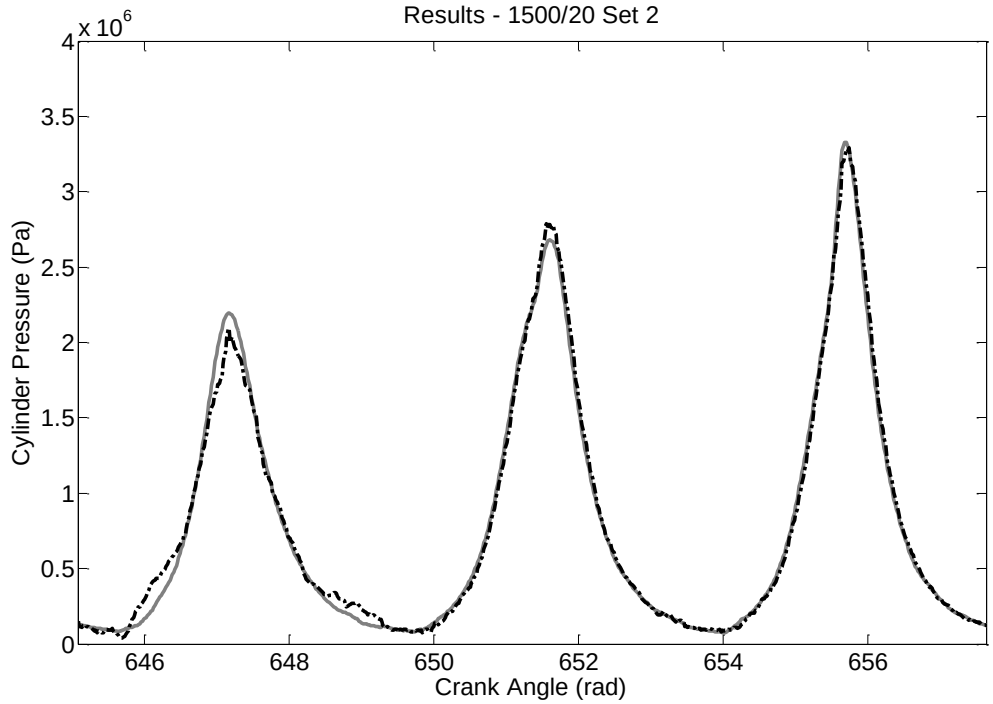

Figure 6.26: Worst Performing Generalisation Results - Condition-5. Measured Cylinder Pressure (Grey Solid Line). Reconstructed Cylinder Pressure (Black Dashed Line). RMSE = 1.59%.

Figure 6.25 and 6.26 show the best region of generalised reconstruction and the worst region of reconstruction across all 9 ANNs and test conditions. The performance of each is 0.7% and 2.1% RMSE. The errors within the results in Figure 6.25 are negligible and demonstrate that the cylinder pressure can be reconstructed to a high degree of accuracy under general conditions using crankshaft kinematics. What is also evident in Figure 6.26 is that the significant errors are not restricted to just the peaks of the cylinder pressure; the errors are distributed along the whole cylinder pressure profile. This proves that the use of 'future' and 'past' inputs, described in Chapter 5, have the desired effect in reconstructing, based on the cylinder pressure rather than system inertia.

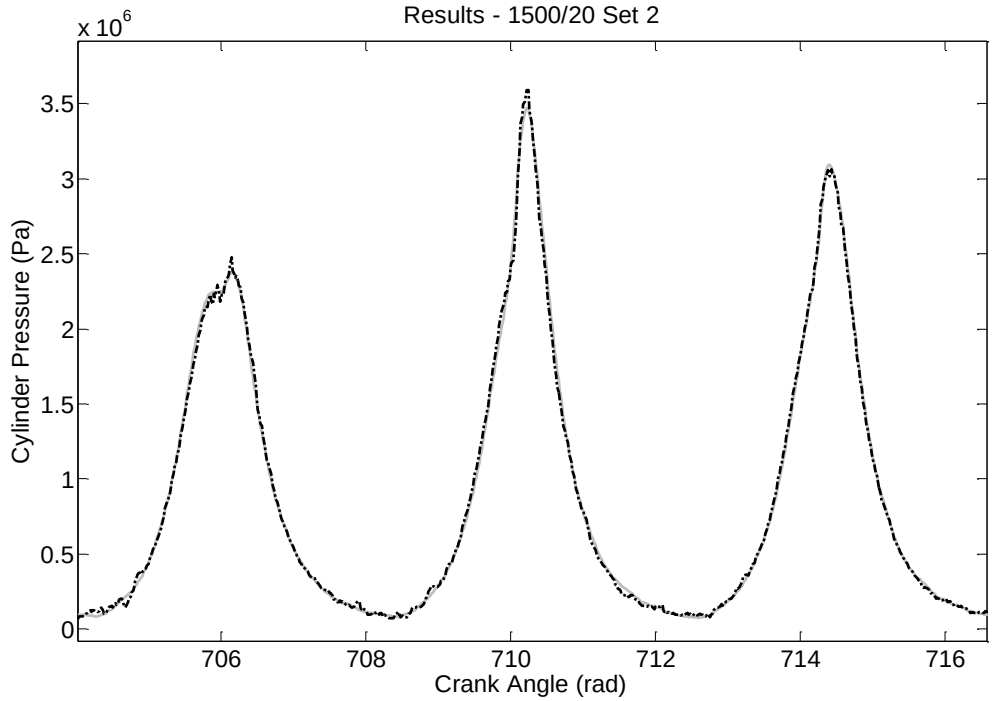

Figure 6.27: Notable Generalisation Results - Condition-8. Measured Cylinder Pressure (Grey Solid Line). Reconstructed Cylinder Pressure (Black Dashed Line). RMSE = 1.73%.

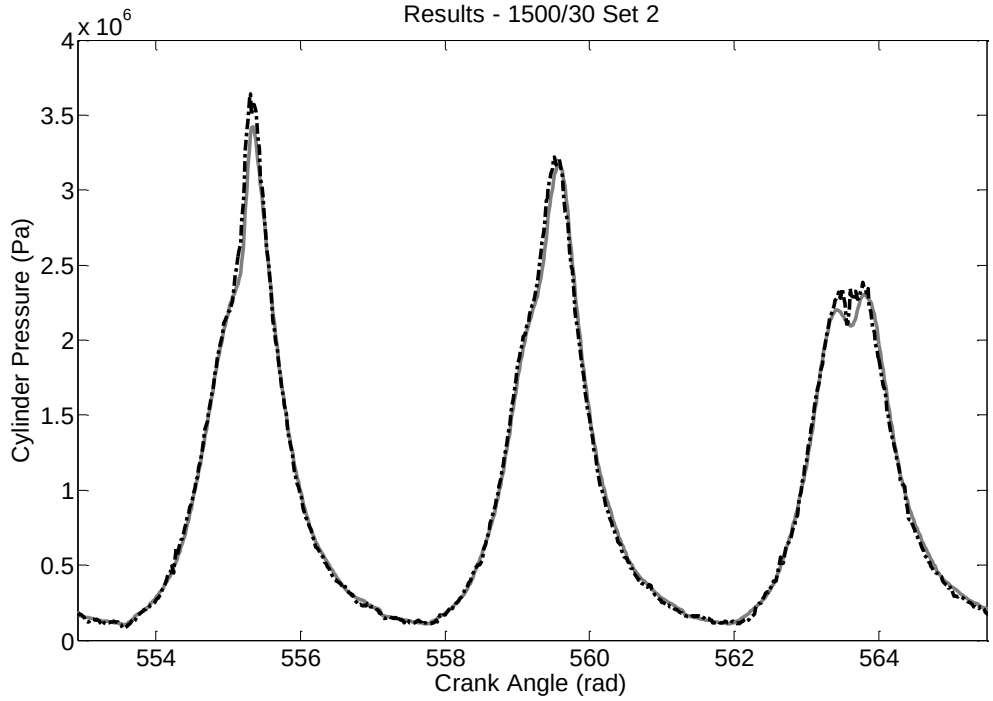

Figure 6.28: Notable Generalisation Results - Condition-5. Measured Cylinder Pressure (Grey Solid Line). Reconstructed Cylinder Pressure (Black Dashed Line). RMSE = 1.07%.

Figure 6.27 and 6.28 gives two noteworthy reconstruction results. Each figure shows the ability of the ANN to reconstruct the cylinder pressure from abnormal or uncommon combustion events. In Figure 6.27 the reconstruction of interest is the third combustion event, and in Figure 6.28, it is the first. In these cases, the ANNs do not necessarily reconstruct the most accurate cylinder pressure but they do recognise that the combustion event differs from the average and produces a reasonable reconstruction. Both Figure 6.27 and 6.28 show combustion events with an appreciably late ignition.

Considering the reconstruction of cylinder pressure using crankshaft kinematics more generally, the results are very promising. The overall results for generalised reconstruction are much improved on previous published results and present very little evidence of the instability or significant peak pressure errors. This is believed to be the result of the methodology developed in Chapter 5. These results have also demonstrated that for independent ANNs, trained at different test conditions, that cycle-by-cycle cylinder pressure variability has no effect on the accuracy of cylinder pressure reconstruction. With respect to the training time and computational effort required, this efficient performance was unexpected. The resultant training times using on average 240 inputs, 15 neurons with 3,631 weights and in excess of 30,000 data points the ANNs, on average, trained within 0.5 hours using a Pc with an Intel i7 quad core processor with 12Gb ram and solid-state drive.

Conclusions of the Findings in Chapter 6.

The results presented in Chapter 6 validate the use of crankshaft kinematics for reconstructing cylinder pressure as results are well within the target. The targeted error was consistently below 4% for the generalised reconstruction and depending on the test condition, the results ranged between 1.14% and 1.34%. There is still some room for improvement, but it is believed this is only possible if considerably more cycles of data are used to train the ANNs; from the current number of 200 cycles to several 1000 or more cycles. However, this would compromise the time and computational effort of training and require significantly more engine testing and data acquisition. This chapter demonstrates that reconstructing cylinder pressure can be achieved very successfully on steady-state data. However, the ultimate proof of the success of this technology is next to test it on engine block vibrations under steady-state conditions, and more vitally, to test it on transient engine conditions.

Chapter 7

Engine Block Vibration Based Cylinder Pressure Reconstruction Results

7.1 Introduction

The success of using the combined methodology developed in Chapter 5 using crankshaft kinematics, has meant that creating a robust and adaptive system for reconstructing cylinder pressure is one step closer. The key to producing an adaptive system is to have two independent sources of reconstruction. This chapter presents detailed results using engine block vibrations to reconstruct cylinder pressure (using data obtained from the Ford 3-cylinder engine). Again, owing to the complexity of transient engine dynamics, this chapter will only focus on steady-state reconstruction. It will use the same basic methodology developed and aim to show that the trained, and generalised, cylinder pressure reconstruction results are significantly improved. However, some modifications will be required to achieve the same level achieved using crankshaft kinematics. The chapter will also show how the training and generalisation performance can vary depending on the test condition.

Initially, the modifications required to the methodology, will be discussed following the same structure as in Chapter 6. The chapter will then present the training and generalised results for a range of test conditions, comparing each condition and discussing the implications.

Table 7.1: Test Conditions used for Assessing the Performance of the Developed Methodology and ANNs

	Engine Speed (rpm)	Engine Load (Nm)	Training Data File Name	Generalised Data File Name
Condition-1	1000	10	1000_10_01p_jun2010	1000_10_02p_jun2010
Condition-2	1500	10	1500_10_01p_jun2010	1500_10_02p_jun2010
Condition-3	2000	10	2000_10_01p_jun2010	2000_10_02p_jun2010
Condition-4	1000	20	1000_20_01p_jun2010	1000_20_02p_jun2010
Condition-5	1500	20	1500_20_01p_jun2010	1500_20_02p_jun2010
Condition-6	2000	20	2000_20_01p_jun2010	2000_20_02p_jun2010
Condition-7	1000	30	1000_30_01p_jun2010	1000_30_02p_jun2010
Condition-8	1500	30	1500_30_01p_jun2010	1500_30_02p_jun2010
Condition-9	2000	30	2000_30_01p_jun2010	2000_30_02p_jun2010

Table 7.1 shows the same 9 separate test conditions examined (as in Chapter 6) where an ANN is trained for each. However, this chapter will only present 3 of the test conditions in full; the remaining 6 are presented in Appendix F. The 3 test conditions selected are condition-1, 5, and 9. Even though the belief has been disproven that a broad range of variability would result in significant differences in the reconstruction performance using crankshaft kinematics, variability may still be a factor when using engine block vibrations. At each test condition, full details will be given regarding the ANN structure, training limits, and training data selected. The results for both the ANN training and generalisation will be presented and analysed. The presented results will be classified as best, average or worst. These are classified statistically by ranking each cycle of data using three metrics; mean squared error, peak pressure error and position of peak pressure error. The best results are the reconstructions cycles with the highest rank in each metric. The worst is the lowest ranked cycle and average is the average ranked cycle. The chapter will conclude with a discussion of the overall performance of the ANN architecture, training algorithm, and the methodology developed in Chapter 5.

7.2 Methodology and ANN Structure Modifications

The methodology developed for crank kinematics has been shown to work successfully in Chapter 6. With modifications, the same methodology and ANN structure could, in principle, also be applied to the reconstruction of cylinder pressure using engine block vibrations. The three basic ideas developed in the methodology described in Chapter 5 are: i) the use of future and past delays, ii) filtering the data within a cycle, and iii) the training of an ANN for each cylinder. The reasons behind this methodology also apply to engine block vibration. The hypothesis is that greater signal is contained in the signal subsequent to the point of reconstruction, because pressure-related vibrations will have to travel for a relatively significant period of time, prior to reaching the measurement point (e.g. via an accelerometer). There is equivalence between this idea and the use of delays within the crankshaft based reconstruction to extract information from a gap in the data. Similarly, the differences in the path travelled by each grouping of pressure related vibration waves, from each of the three cylinders to the accelerometer, is considerable. Therefore even though the filtering within the cycle is still appropriate for engine block vibration reconstruction, the frequencies to be filtered require more consideration.

Filtering Frequencies

As the relationship between the cylinder pressure and crank kinematics is relatively straightforward, the frequencies in both are fairly similar. As a result, a simpler low-pass filter is used with a cut-off frequency equivalent to the largest significant cylinder pressure frequency, to achieve a high degree of success. However, as the relationship between the cylinder pressure and engine block vibration is significantly more complex, and the frequencies related to cylinder pressure have been shown to be significantly higher (Vulli, 2006), a modification to the cut-off frequency selection is required. A considerable amount of work has been carried out on the identification of events surrounding IC engine operation within vibration signals i.e. valve opening and closing, and injector timing (Vulli, 2006). It is not unexpected for vibration frequencies within the engine to exceed 10 kHz. The amount of information held within the engines vibration frequencies is significant and without undertaking the training of an ANN with a very large number of neurons to handle high frequencies, the training using the raw vibration data is not practical. The selection of the cut-off frequency is therefore critical for successful training and reconstruction. It is chosen by considering the typical frequencies of different

combustion characteristics; i.e. the engine knock frequency. The test engine is set up to run below the critical frequencies that knock occurs, typically above 6 kHz. Engine knock frequency is dependent on the speed of sound of the combustion gases and the engine cylinder bore. Given that the knock frequency is mainly a geometric constraint varying engine speeds will have little effect on this frequency. The knock frequency is also significantly above typical engine speeds used within this research; which are between 16 Hz and 34 Hz for engine speed between 1000 and 2000 rpm. As a result of filtering above 6 kHz, there should not be any significant cylinder pressure related vibration information at or above the knock frequency and this was selected as the low-pass filter cut-off frequency. Filtering will be tested in the following sections.

A second modification was required but this time, to the ANN structure, not the developed methodology. The tests in Chapters 5 and 6 have all used the same basic structure: a single hidden layer with 15 neurons. As described in Chapter 3, the number of hidden layers and neurons are dependent on the complexity of the problem. The complexity of the crank kinematic and cylinder pressure relationship is relatively simple compared to ANNs in general. Therefore, only a relatively small ANN size is required. The relationship between engine block vibrations and cylinder pressure is significantly more complex. As a result, the size of the ANN needs to be large and will take significantly more time to train successfully. A similar brute force analysis, as demonstrated in section 5.2.2, was used. This was done by training and testing a range of networks with a varying number of neurons, layers and a varying number of delays. It was found that by increasing the number of hidden layers to two, and having 15 neurons in each, was optimum without the need to significantly increase the training time.

7.3 Results - Test Condition-1

7.3.1 Data and Network Configuration

The first test condition used measured data taken from running the engine at steady-state with a speed of 1000 rpm and a load of 10 Nm. This test condition was selected as it was the lowest power condition acquired and as a result, should contain the most cylinder pressure variability cycle-to-cycle. Both the training and generalisation data sets underwent the same data processing, using the steps covered in section 7.2. The ANN used was a time-delay network with one hidden-

layer of 15 neurons. The ANN had 240 input delays, where 120 were dedicated to the 'past' inputs, and 120 were dedicated to the 'future' inputs. The Levenberg-Marquardt training algorithm was used with a mean squared error cost function, and a maximum epoch number of 1000. More information regarding the setup of the training is given in Table 7.2.

Table 7.2: ANN Training Setup for Test Condition-1

Network Name	Net_TD_BA_Test1	**Network Architecture**	Time-Delay	**Test Data**	1000_10_01p_jun2010
Network Training Algorithm	Levenberg–Marquardt	**Hidden Layers Number**	2	**Speed (rpm) / Load (Nm)**	1000/10
Cost Function	Mean Squared Error	**Neurons Number**	15/15	**Training to Validation Ratio**	60:40
Training Goal	1E8	**Delay Number**	240	**Crank Step**	1 Deg
Maximum Epoch	1000	**Transfer Function Layer 1**	Sigmoid	**Number of Iterations**	10
Weights Initialisation	Randomised	**Transfer Function Layer 2**	Linear		

7.3.2 Training Results

This subsection presents the results from training the ANN using data from condition-1 (1000 rpm and 10 Nm). In total, 10 ANNs different initial conditions were trained, with the overall performance of the ANNs ranging from 2.18 % to 2.98 % RMSE. The best performing ANN was selected, which trained in 1891 seconds (0.53 hours) and 55 epochs. Figures 7.1 to 7.3, show training results for best, average, and worst regions of cylinder pressure reconstruction. Each of these regions have been evaluated and compared against the mean values to rank their degree of success.

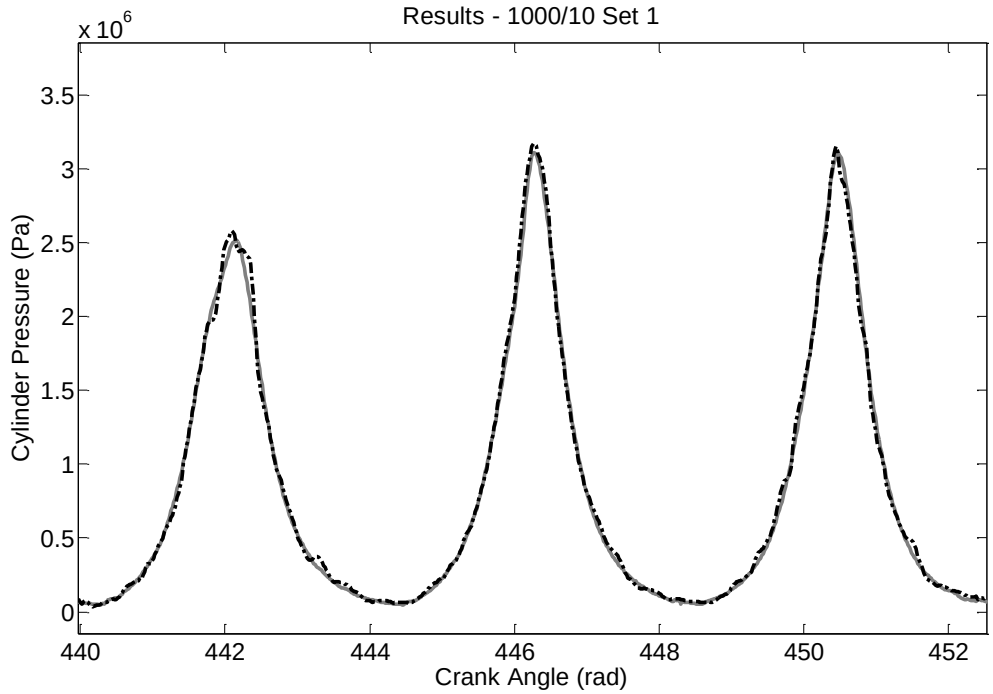

Figure 7.1: Condition-1 Training Results - Best. Measured Cylinder Pressure (Grey Solid Line). Reconstructed Cylinder Pressure (Black Dashed Line). RMSE = 1.28%.

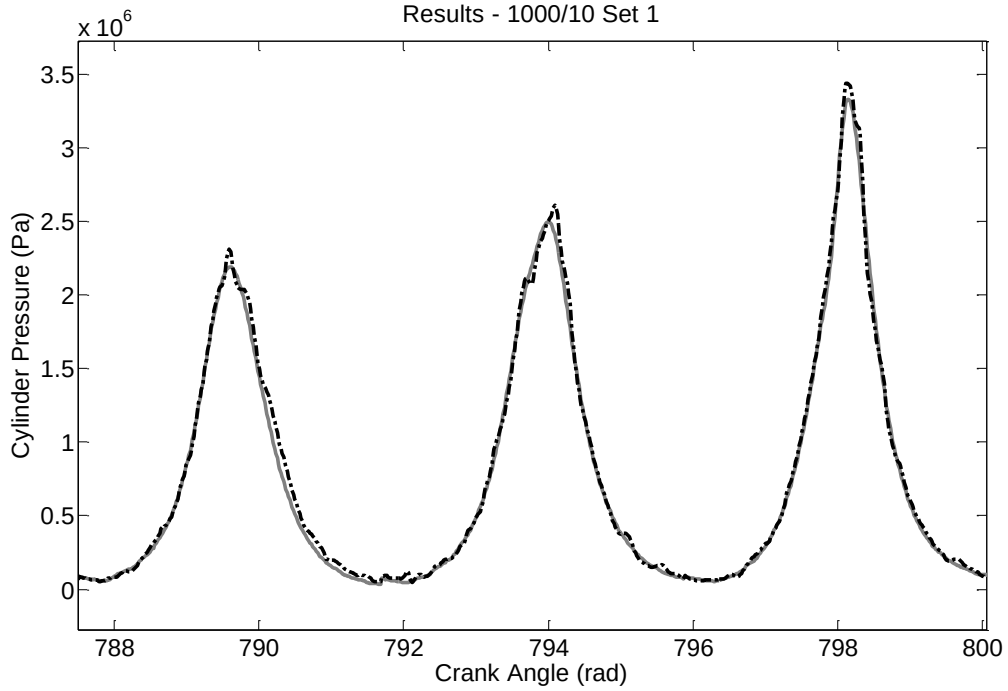

Figure 7.2: Condition-1Training Results - Average. Measured Cylinder Pressure (Grey Solid Line). Reconstructed Cylinder Pressure (Black Dashed Line). RMSE = 1.92%.

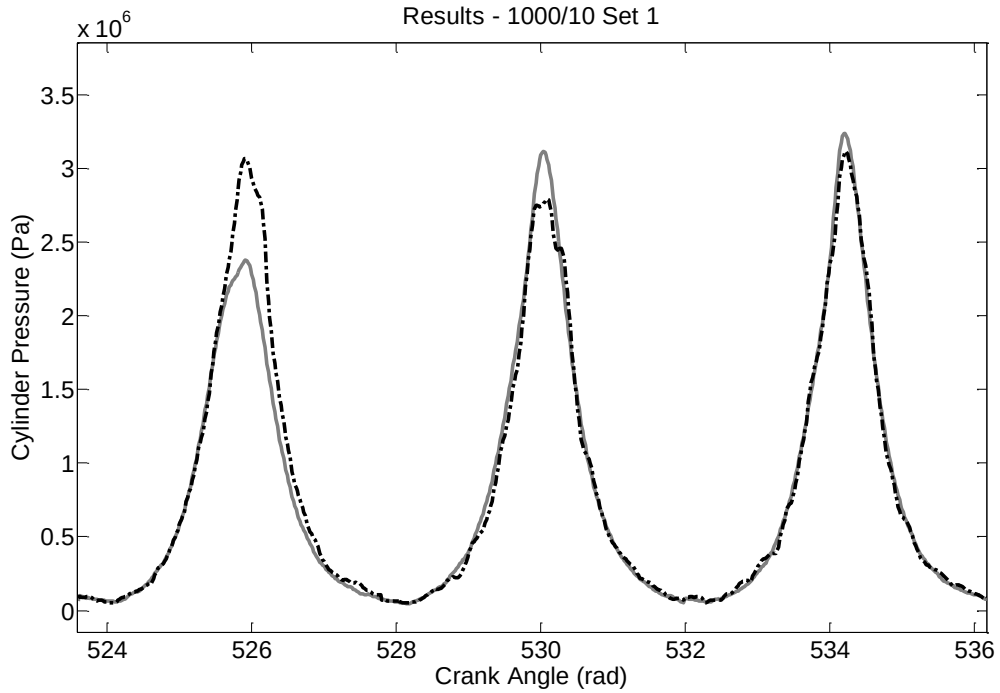

Figure 7.3: Condition-1Training Results - Worst. Measured Cylinder Pressure (Grey Solid Line). Reconstructed Cylinder Pressure (Black Dashed Line). RMSE = 4.22%.

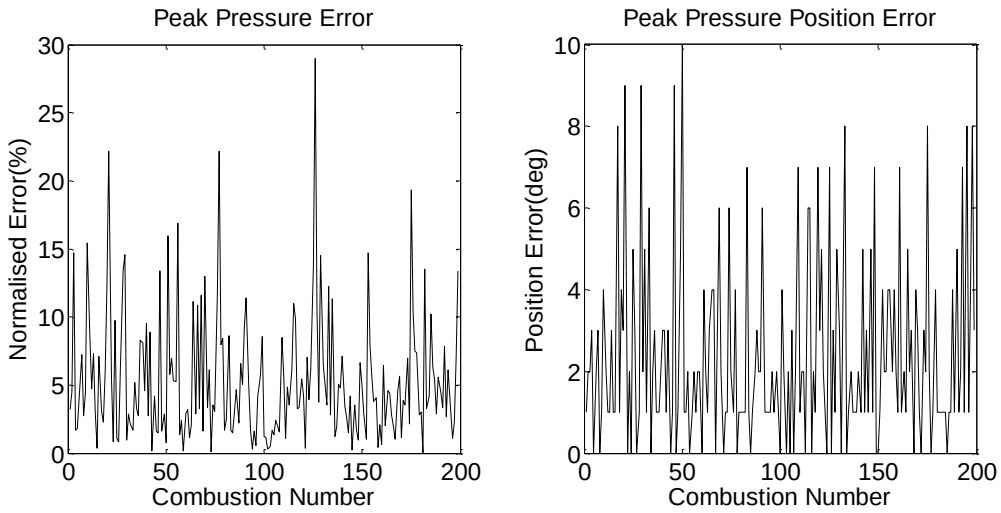

Figure 7.4: Condition-1 Normalised Peak Error Training Results (left). Condition-1Position of Peak Error Training Results (right)

Figure 7.4 shows the normalised peak error, and the peak position error, between the measured cylinder pressure and training results for 180 cycles of data. Table 7.3, gives the root-mean-squared error, and the standard deviation for 3 key parameters; the overall error, the normalised peak pressure error and the position of peak pressure error.

Table 7.3: Condition-1 Root-Mean-Squared Error (RMSE) and Standard Deviation for the ANN Training

	Training Root-Mean-Squared Error	Training Standard Deviation
Overall Performance	2.18 %	2.15 %
Normalised Peak Error	7.04 %	4.62 %
Peak Pressure Position Error (deg)	2.25	1.23

7.3.3 Generalisation Results

The data used for the generalisation tests was from the same condition (1000 rpm and 10 Nm). However, it was acquired separately from the training data and has not been used by the ANN for training. Figures 7.5 to 7.7, gives generalisation results for best, average, and worst regions of cylinder pressure reconstruction. Each of these regions again, have been evaluated and compared against the mean values to rank their degree of success.

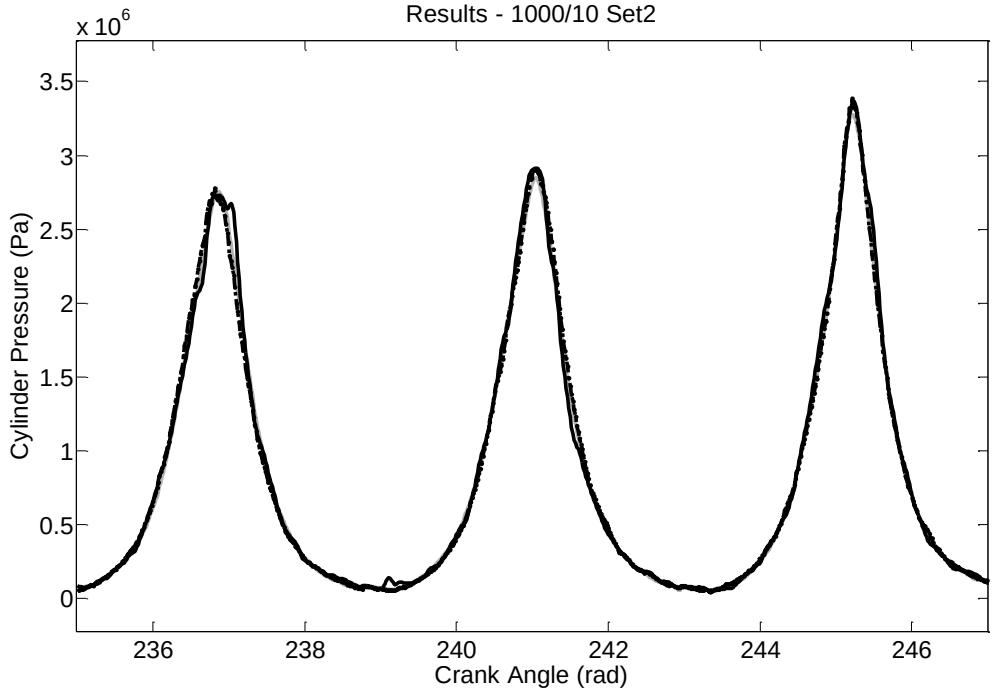

Figure 7.5: Condition-1 Generalisation Results - Best. Measured Pressure (Grey Solid Line). Acceleration Reconstructed Pressure (Black Solid Line). Crank Reconstructed Pressure (Black Dashed Line). RMSE = 1.40%.

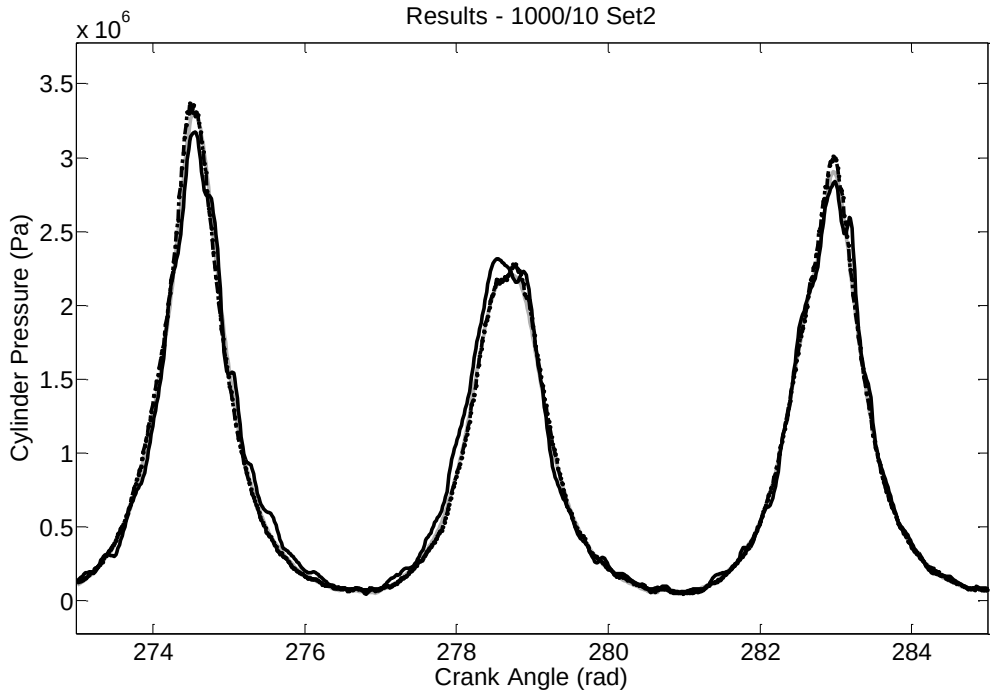

Figure 7.6: Condition-1 Generalisation Results - Average. Measured Pressure (Grey Solid Line). Acceleration Reconstructed Pressure (Black Solid Line). Crank Reconstructed Pressure (Black Dashed Line). RMSE = 2.07%.

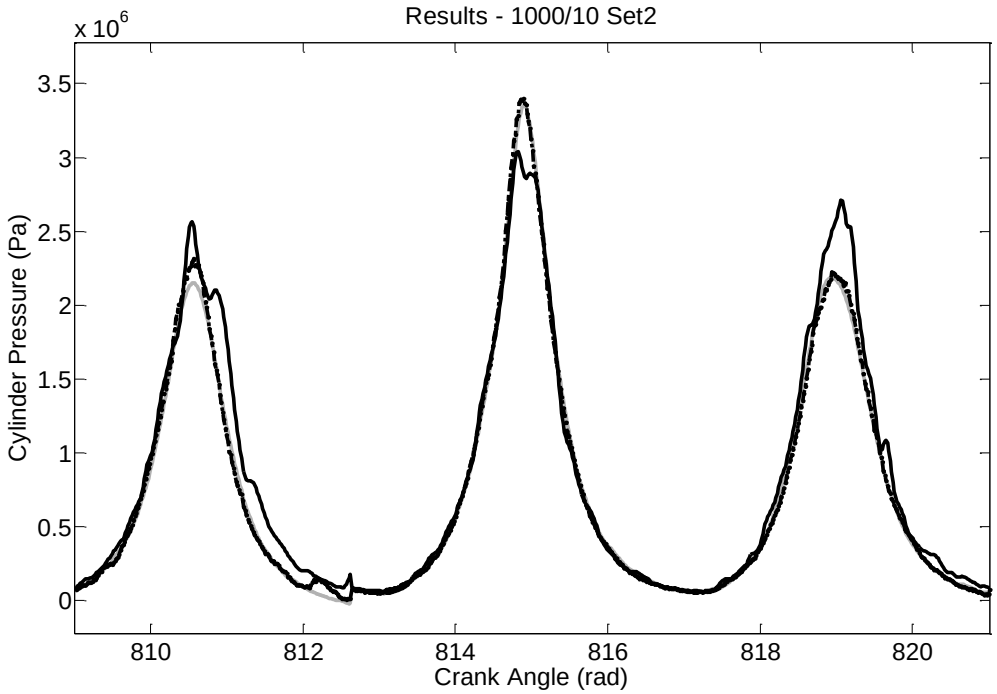

Figure 7.7: Condition-1 Generalisation Results - Worst. Measured Pressure (Grey Solid Line). Acceleration Reconstructed Pressure (Black Solid Line). Crank Reconstructed Pressure (Black Dashed Line). RMSE = 4.76%.

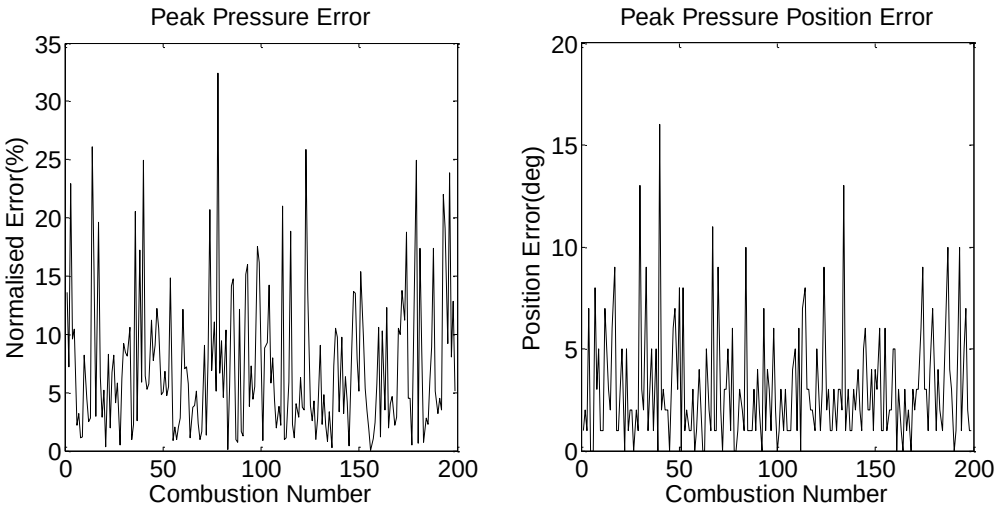

Figure 7.8: Condition-1 Normalised Peak Error Generalisation Results (left). Condition-1 Position of Peak Error Generalisation Results (right)

Figure 7.8 gives the normalised peak error, and the peak position error between the measured cylinder pressure and generalised results for 180 cycles of data. Table 7.4 shows the root-mean-squared error and the standard deviation for 3 key parameters; the overall error, the normalised peak pressure error and the position of peak pressure error.

Table 7.4: Condition-1 Root-Mean-Squared Error (RMSE) and Standard Deviation for the ANN Generalisation

	Generalisation Root-Mean-Squared Error	Generalisation Standard Deviation
Overall Performance	2.72 %	2.71 %
Normalised Peak Error	9.69 %	6.19 %
Peak Pressure Position Error (deg)	2.16	1.81

7.3.4 Discussion of Test Condition-1 Results

The training results at condition-1 (1000 rpm and 10 Nm), showed regions where the reconstruction was promising and were significantly better than previously achieved. However, even in the training results, there are some poor regions, shown in Figure 7.3. Even though the overall performance of the training is within the desired range, RMSE = 2.18%, this is large for training and the magnitude of the normalised peak error is significantly large at 7.04%. These errors were constant through the 10 training attempts and suggested that there was a more fundamental issue. Figure

7.1 and 7.2 show examples of best, and average, cylinder pressure reconstruction. These training results were very promising where the latter shows better than expected reconstruction with a high degree of variability. The generalisation results were also considerably better than previous attempts with an RMSE value equal to 2.72%, and reasonable position of peak error over 200 cycles. Again there are poorer regions, Figure 7.7, shows large errors, where the normalised peak error is 9.69%. This demonstrates an inability for this ANN to accurately reconstruct a sizable portion of the data to the same accuracy as the crankshaft kinematics for this condition. Similarly at this condition, there is a relatively small difference between the training and generalisation performances, which gives a reassurance that the ANN is not over-training. Again Figure 7.5 and 7.6 demonstrate that this ANN is good at generalisation with only relatively small errors. As the reconstruction errors are frequent, there seems to be no consistent correlation between the errors generated in the acceleration and crank kinematic based reconstructions. However, within isolated results for this condition, when there is a small error in the crank kinematic data the corresponding in the acceleration base reconstruction's error is large. This is not true in reverse; with acceleration based errors there in no significant crank based errors. The results from the following will reveal whether this is true for all conditions or just coincidental.

7.4 Results - Test Condition-5

7.4.1 Data and Network Configuration

The next test condition used measured data taken from running the engine at steady-state with a speed of 1500 rpm and a load of 20 Nm. This was selected as it was in the middle of the power range that is of interest. Both the training and generalisation data sets underwent the same data process using the steps covered in section 7.2. The ANN was a time-delay network, with one hidden-layer of 15 neurons, and 240 input delays, where 120 were dedicated to the 'past' inputs and 120 were dedicated to the 'future' inputs. The Levenberg-Marquardt training algorithm was used with a mean squared error cost function, and a maximum epoch number of 1000. More information regarding the setup of the training is given in Table 7.5.

Table 7.5: ANN Training Setup for Test Condition-5

Network Name	Net_TD_BA_Test5	**Network Architecture**	Time-Delay	**Test Data**	1500_20_01p_jun2010
Network Training Algorithm	Levenberg–Marquardt	**Hidden Layers Number**	2	**Speed (rpm) / Load (Nm)**	1500/20
Cost Function	Mean Squared Error	**Neurons Number**	15/15	**Training to Validation Ratio**	60:40
Training Goal	1E8	**Delay Number**	240	**Crank Step**	1 Deg
Maximum Epoch	1000	**Transfer Function Layer 1**	Sigmoid	**Number of Iterations**	10
Weights Initialisation	Randomised	**Transfer Function Layer 2**	Linear		

7.4.2 Training Results

This subsection gives the results from training the ANN using data from condition-5 (1500 rpm and 20 Nm). In total, 10 ANNs different initial conditions were trained with the overall ANN's performance ranging from 2.00% to 3.34% RMSE. The best performing ANN was selected which trained in 1691 seconds (0.47 hours) and 38 epochs. Figures 7.9 to 7.11, gives training results for best, average, and worst regions of cylinder pressure reconstruction. Each of these regions have been evaluated and compared against the mean values to rank their degree of success.

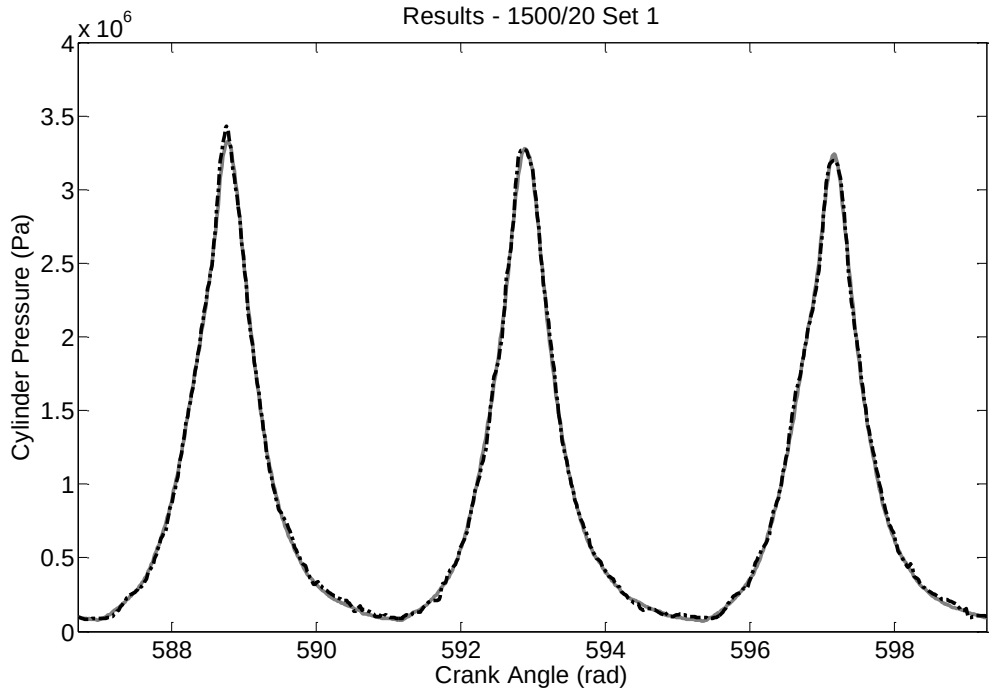

Figure 7.9: Condition-5 Training Results - Best. Measured Cylinder Pressure (Grey Solid Line). Reconstructed Cylinder Pressure (Black Dashed Line). RMSE = 0.71%.

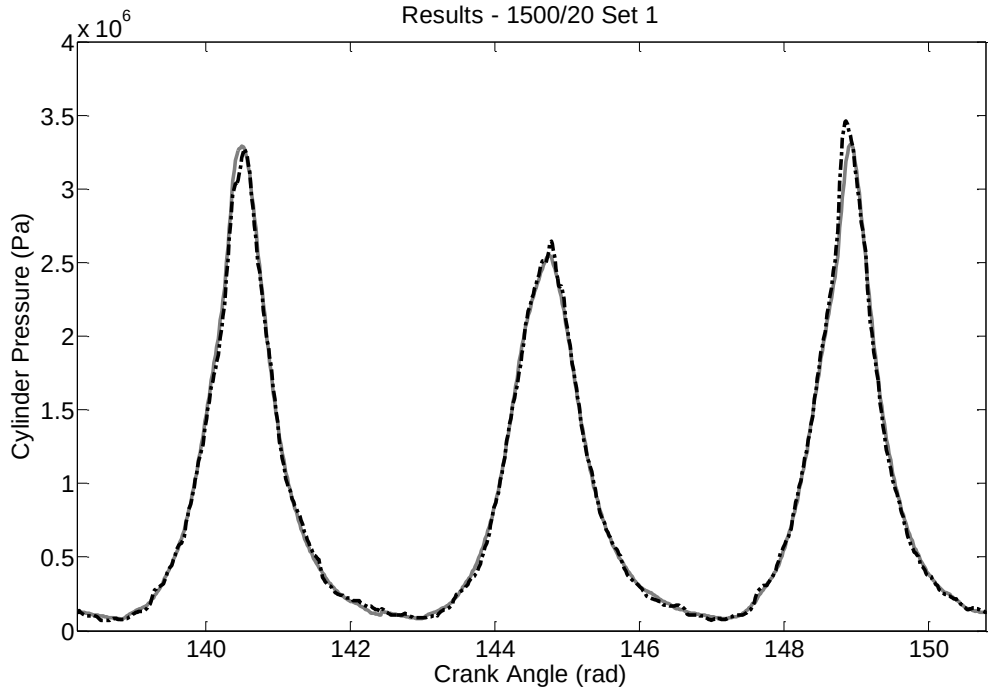

Figure 7.10: Condition-5 Training Results - Average. Measured Cylinder Pressure (Grey Solid Line). Reconstructed Cylinder Pressure (Black Dashed Line). RMSE = 2.16%.

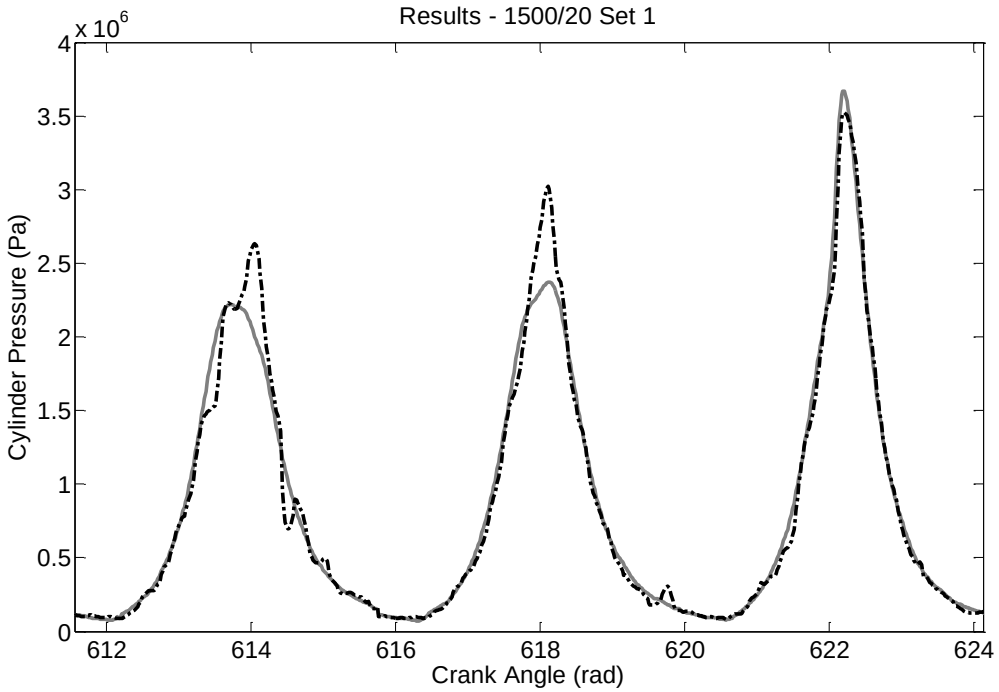

Figure 7.11: Condition-5 Training Results - Worst. Measured Cylinder Pressure (Grey Solid Line). Reconstructed Cylinder Pressure (Black Dashed Line). RMSE = 4.89%.

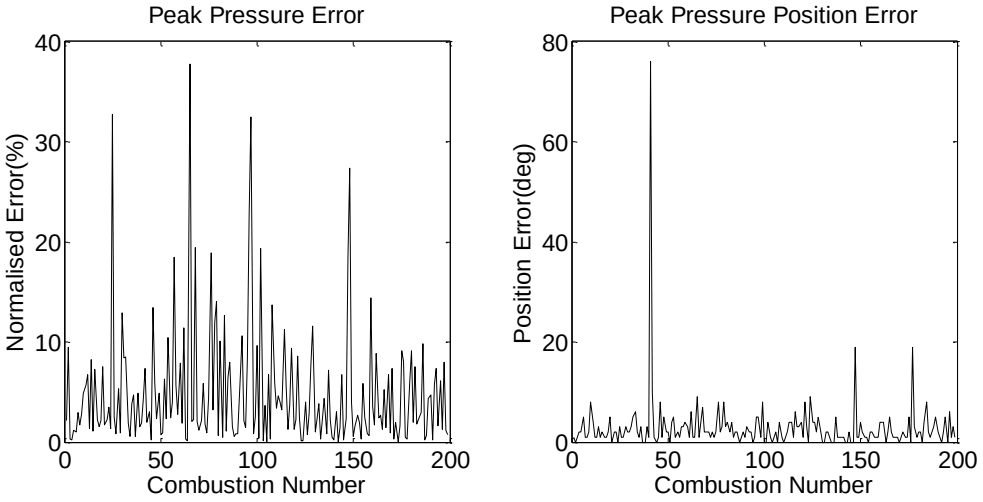

Figure 7.12: Condition-5 Normalised Peak Error Training Results (left). Condition-5 Position of Peak Error Training Results (right)

Figure 7.12 gives the normalised peak error and the peak position error between the measured cylinder pressure and training results for 180 cycles of data. Table 7.6, presents the root-mean-squared error and the standard deviation for 3 key parameters; the overall error, the normalised peak pressure error and the position of peak pressure error.

Table 7.6: Condition-5 Root-Mean-Squared Error (RMSE) and Standard Deviation for the ANN Training

	Training Root-Mean-Squared Error	Training Standard Deviation
Overall Performance	2.01 %	1.99 %
Normalised Peak Error	7.63 %	5.91 %
Peak Pressure Position Error (deg)	4.50	3.86

7.4.3 Generalisation Results

The data used for the generalisation tests was from the same condition (1500 rpm and 20 Nm). However, it was acquired separately from the training data and has not been used by the ANN for training. Figures 7.13 to 7.15, gives generalisation results for best, average, and worst regions of cylinder pressure reconstruction. Each of these regions again, have been evaluated and compared against the mean values to rank their degree of success.

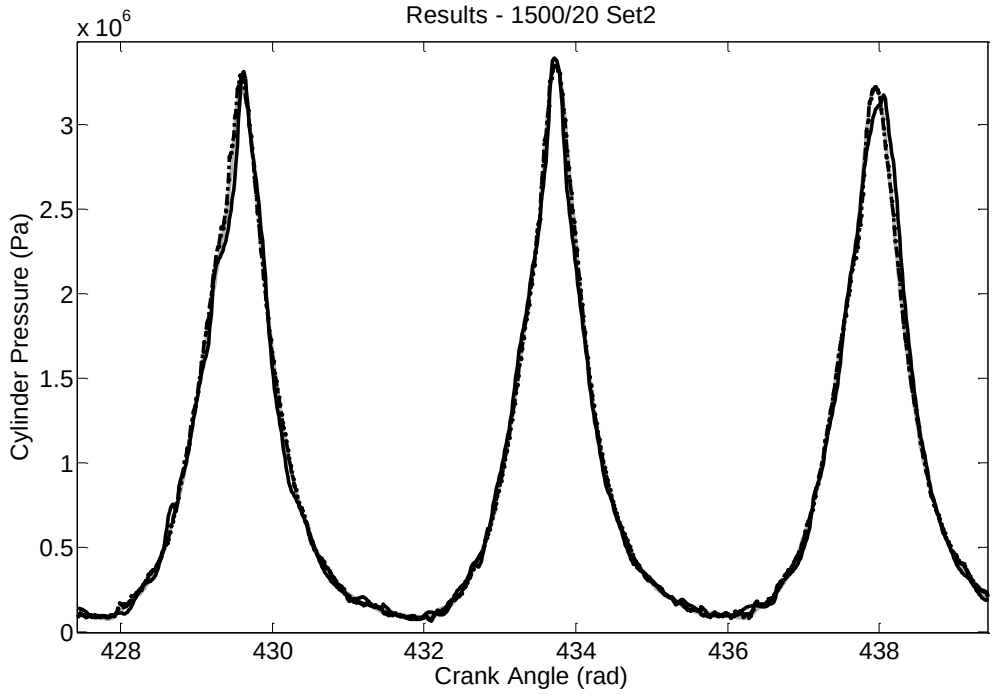

Figure 7.13: Condition-5 Generalisation Results - Best. Measured Pressure (Grey Solid Line). Acceleration Reconstructed Pressure (Black Solid Line). Crank Reconstructed Pressure (Black Dashed Line). RMSE = 1.37%.

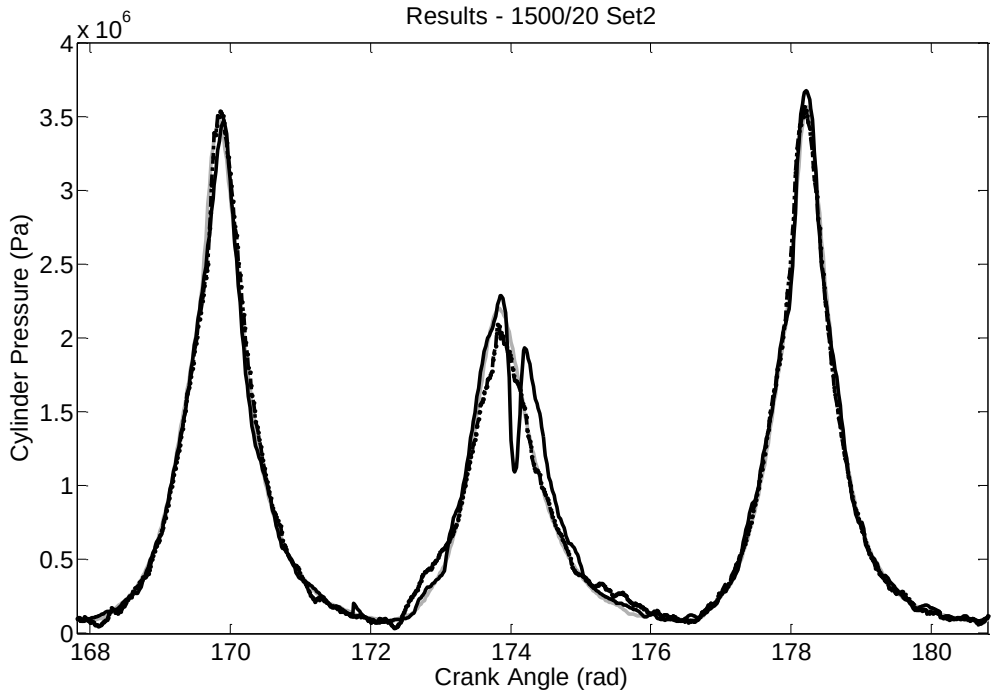

Figure 7.14: Condition-5 Generalisation Results - Average. Measured Pressure (Grey Solid Line). Acceleration Reconstructed Pressure (Black Solid Line). Crank Reconstructed Pressure (Black Dashed Line). RMSE = 2.82%.

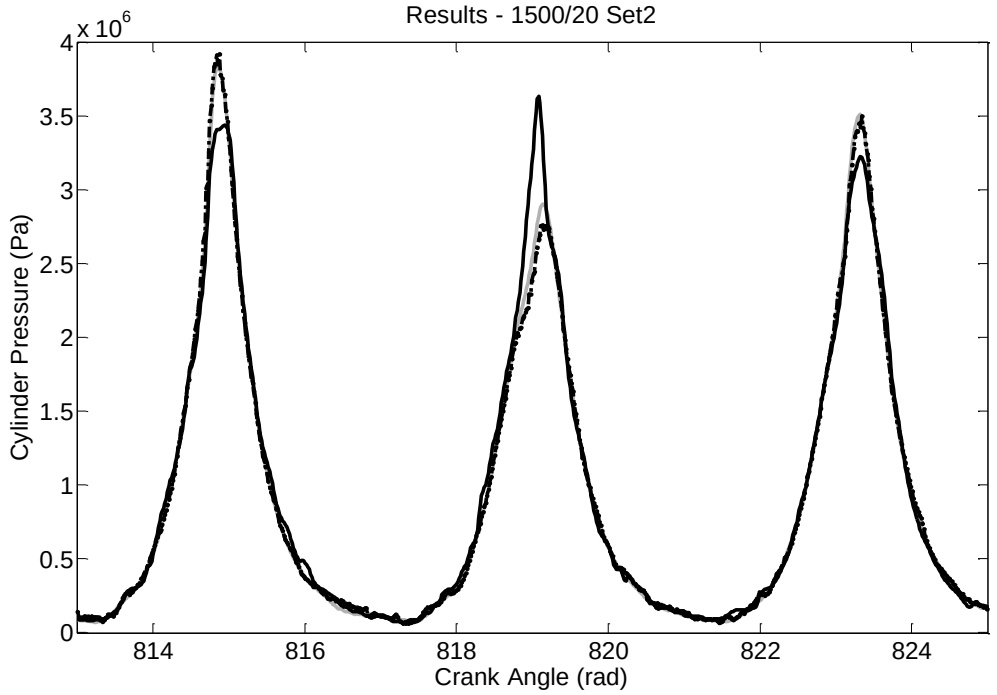

Figure 7.15: Condition-5 Generalisation Results - Worst. Measured Pressure (Grey Solid Line). Acceleration Reconstructed Pressure (Black Solid Line). Crank Reconstructed Pressure (Black Dashed Line). RMSE = 4.47%.

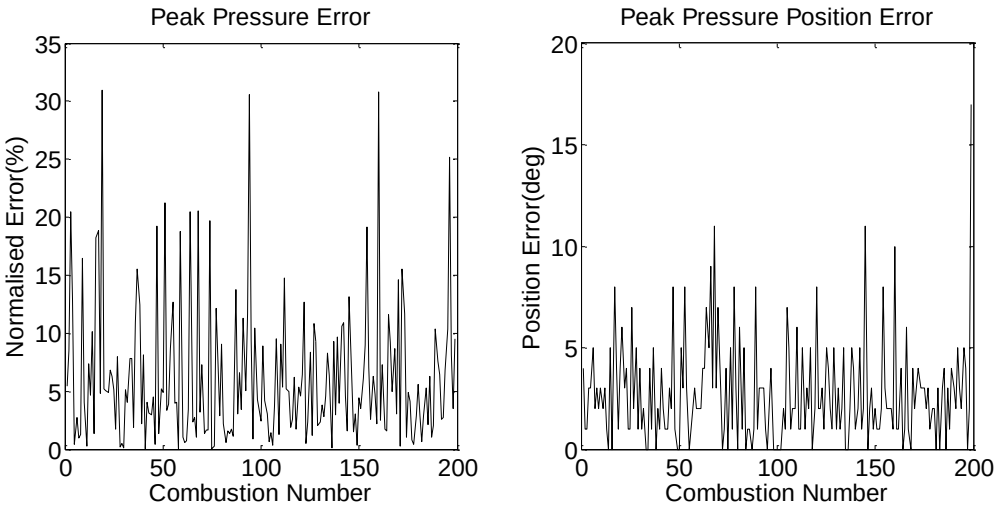

Figure 7.16: Condition-5 Normalised Peak Error Generalisation Results (left). Condition-5 Position of Peak Error Generalisation Results (right)

Figure 7.16 gives the normalised peak error, and the peak position error, between the measured cylinder pressure and generalised results for 180 cycles of data. Table 7.7, gives the root-mean-squared error, and the standard deviation for 3 key parameters; the overall error, the normalised peak pressure error and the position of peak pressure error.

Table 7.7: Condition-5 Root-Mean-Squared Error (RMSE) and Standard Deviation for the ANN Generalisation

	Generalisation Root-Mean-Squared Error	Generalisation Standard Deviation
Overall Performance	2.61 %	2.60 %
Normalised Peak Error	8.60 %	5.97 %
Peak Pressure Position Error (deg)	1.71	1.49

7.4.4 Discussion of Test Condition-5 Results

The training results at condition-5 (1500 rpm and 20 Nm) are not dissimilar to the results at condition-1. The overall error in the training results was again significant, RMSE = 2.01%. Figures 7.9 and 7.10 show examples of best, and average cylinder pressure reconstruction, and these training results are generally very promising. However, Figure 7.11 shows more significant variation and delayed ignition, which results in poorer reconstruction. The generalisation results are also considerably better than previous attempts with an RMSE value equal to 2.61% over 200 cycles. Figure 7.13 and 7.14 demonstrate that this ANN is good at generalisation, even

though the latter shows a significant spike in the reconstructed pressure in the second combustion event. There are significant unexplained errors present in Figure 7.15. With regards to the position of peak pressure error, it is unusually large, 4.50˚, within the training data but is consistent in the generalised results, of 1.71˚. Similar to the previous condition, there seems to be no consistent correlation between the errors generated in the acceleration and crank kinematic based reconstructions. However, when there is a small error in the crank kinematic data the corresponding in the large acceleration base reconstruction error still occurs.

7.5 Results - Test Condition-9

7.5.1 Data and Network Configuration

The last test condition used measured data taken from running the engine at steady-state with a speed of 2000 rpm and a load of 30 Nm. This test condition was selected as it was in the highest power condition acquired and should have more consistent cylinder pressures. Both the training and generalisation data sets underwent the same data process using the steps covered in section 7.2. The ANN used was a time-delay network with one hidden-layer of 15 neurons. The ANN had 240 input delays, where 120 were dedicated to the 'past' inputs and 120 were dedicated to the 'future' inputs. The Levenberg-Marquardt training algorithm was used with a mean squared error cost function and a maximum epoch number of 1000. More information regarding the setup of the training is given in Table 7.8.

Table 7.8: ANN Training Setup for Test Condition-9

Network Name	Net_TD_BA_Test9	**Network Architecture**	Time-Delay	**Test Data**	2000_30_01p_jun2010
Network Training Algorithm	Levenberg–Marquardt	**Hidden Layers Number**	2	**Speed (rpm) / Load (Nm)**	2000/30
Cost Function	Mean Squared Error	**Neurons Number**	15/15	**Training to Validation Ratio**	60:40
Training Goal	1E8	**Delay Number**	240	**Crank Step**	1 Deg
Maximum Epoch	1000	**Transfer Function Layer 1**	Sigmoid	**Number of Iterations**	10
Weights Initialisation	Randomised	**Transfer Function Layer 2**	Linear		

7.5.2 Training Results

This subsection shows the results from training the ANN using data from condition-9 (2000 rpm and 30 Nm). In total, 10 ANNs different initial conditions were trained with the overall performance of the ANNs ranging from 1.48% to 1.61% RMSE. The best performing ANN was selected, which trained in 878 seconds (0.24 hours) and 18 epochs. Figures 7.17 to 7.19, present training results for best, average, and worst regions of cylinder pressure reconstruction. Each of these regions have been evaluated and compared against the mean values to rank their degree of success.

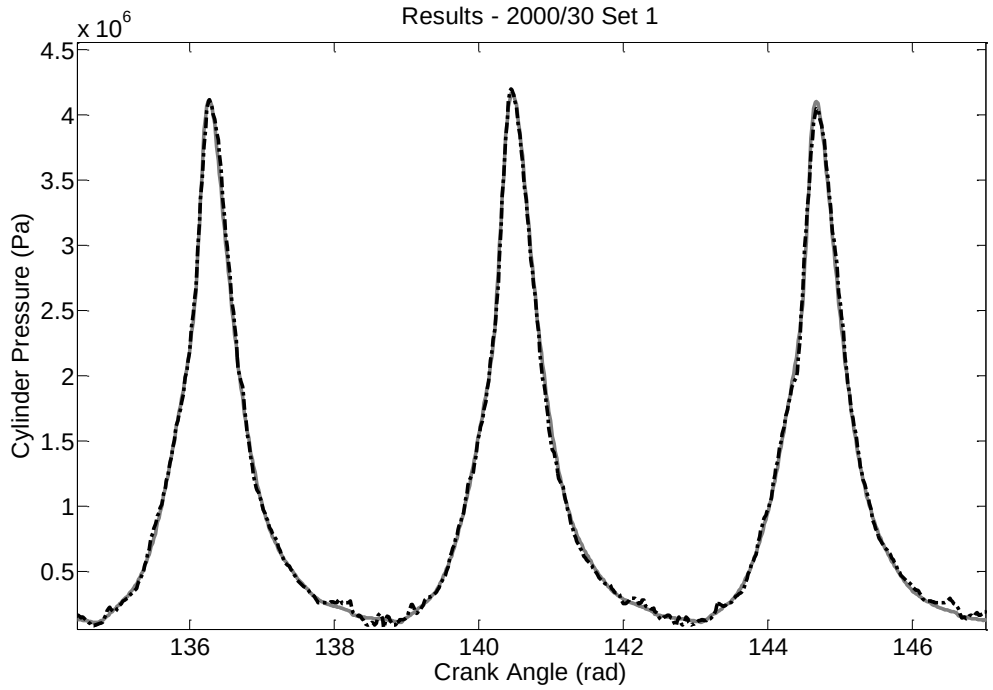

Figure 7.17: Condition-9 Training Results - Best. Measured Cylinder Pressure (Grey Solid Line). Reconstructed Cylinder Pressure (Black Dashed Line). RMSE = 0.95%.

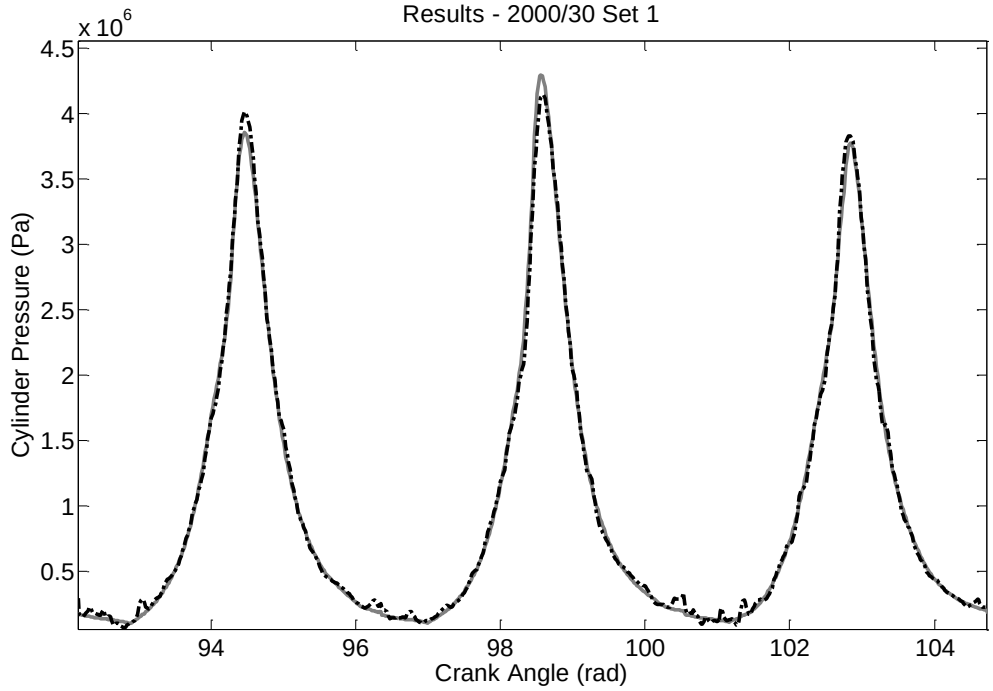

Figure 7.18: Condition-9 Training Results - Average. Measured Cylinder Pressure (Grey Solid Line). Reconstructed Cylinder Pressure (Black Dashed Line). RMSE = 1.25%.

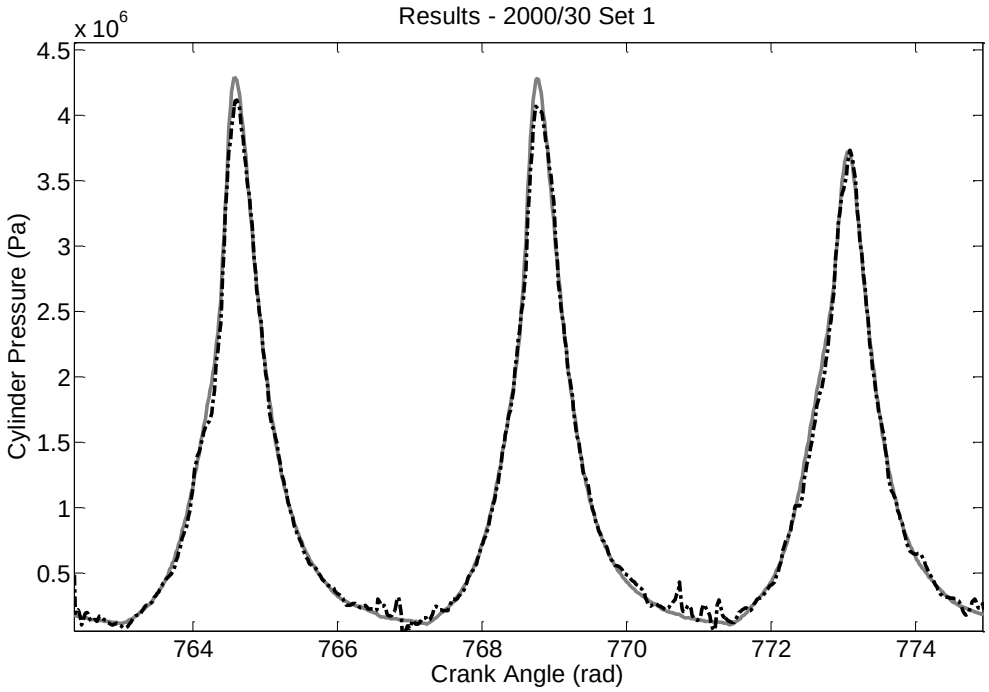

Figure 7.19: Condition-9 Training Results - Worst. Measured Cylinder Pressure (Grey Solid Line). Reconstructed Cylinder Pressure (Black Dashed Line). RMSE = 2.37%.

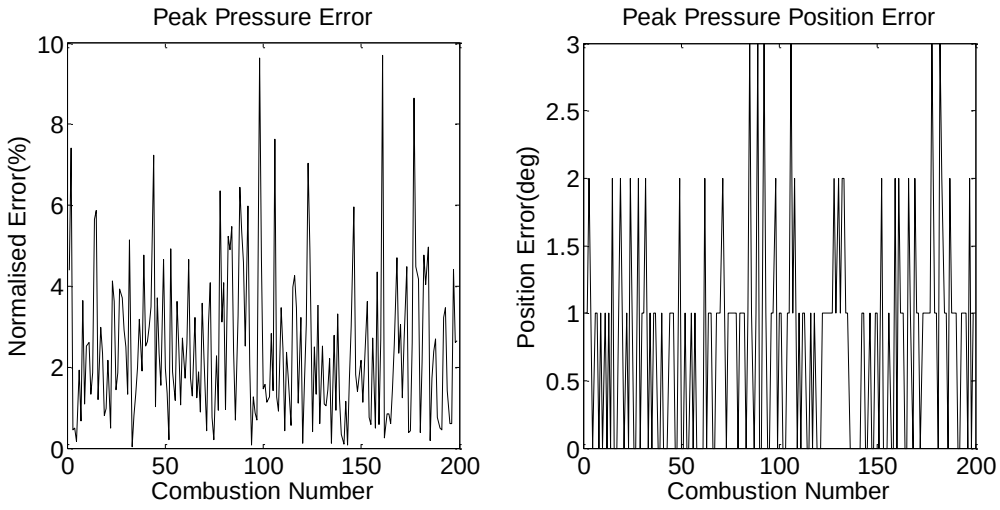

Figure 7.20: Condition-9 Normalised Peak Error Training Results (left). Condition-9 Position of Peak Error Training Results (right)

Figure 7.20 gives the normalised peak error and the peak position error between the measured cylinder pressure and training results for 180 cycles of data. Table 7.9, gives the root-mean-squared error, and the standard deviation for 3 key parameters; the overall error, the normalised peak pressure error, and the position of peak pressure error.

Table 7.9: Condition-9 Root-Mean-Squared Error (RMSE) and Standard Deviation for the ANN Training

	Training Root-Mean-Squared Error	Training Standard Deviation
Overall	1.47 %	1.46 %
Peak Error (%)	3.11 %	1.89 %
Peak Pressure Position Error (deg)	0.59	0.36

7.5.3 Generalisation Results

The data used for the generalisation tests was from the same condition (2000 rpm and 30 Nm). However, it was acquired separately from the training data and has not been used by the ANN for training. Figures 7.21 to 7.23 gives generalisation results for best, average and worst regions of cylinder pressure reconstruction. Each of these regions again, have been evaluated and compared against the mean values to rank their degree of success.

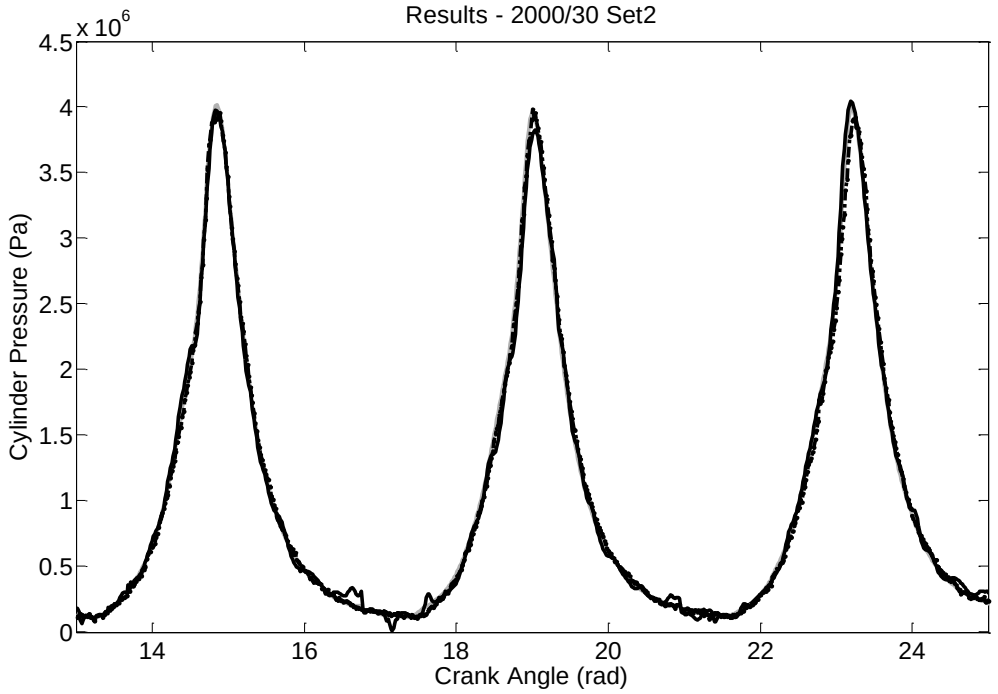

Figure 7.21: Condition-9 Generalisation Results - Best. Measured Pressure (Grey Solid Line). Acceleration Reconstructed Pressure (Black Solid Line). Crank Reconstructed Pressure (Black Dashed Line). RMSE = 1.21%.

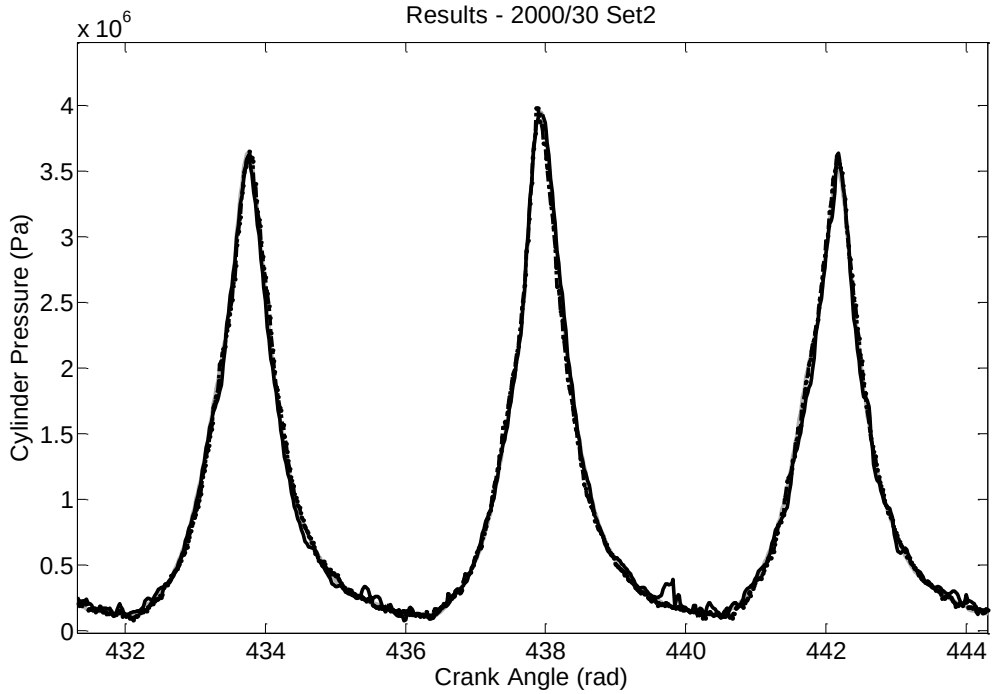

Figure 7.22: Condition-9 Generalisation Results - Average. Measured Pressure (Grey Solid Line). Acceleration Reconstructed Pressure (Black Solid Line). Crank Reconstructed Pressure (Black Dashed Line). RMSE = 1.48%.

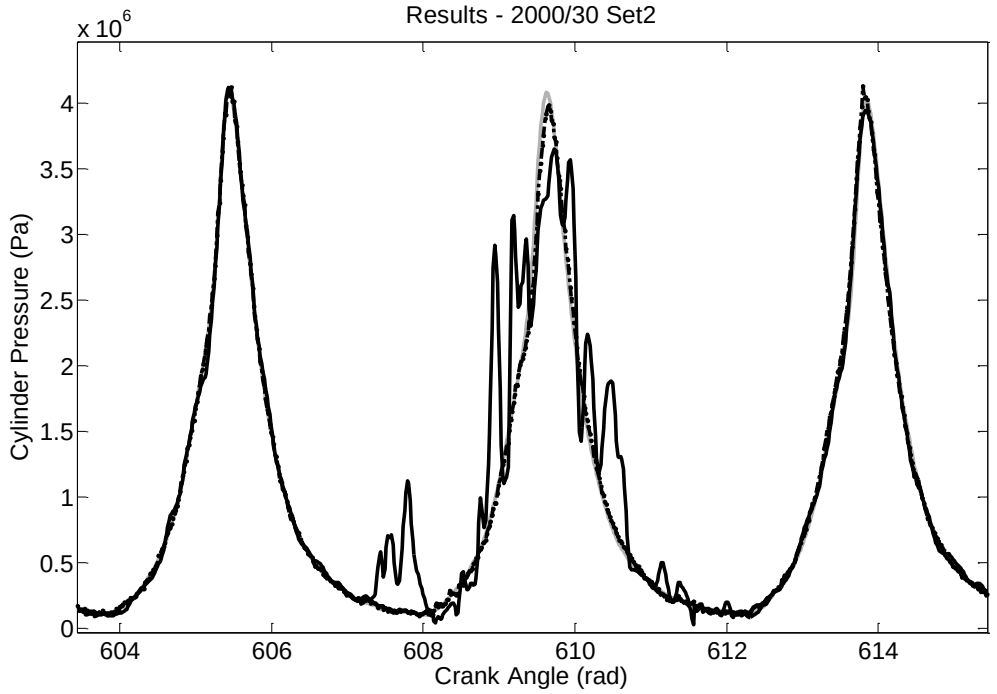

Figure 7.23: Condition-9 Generalisation Results - Worst. Measured Pressure (Grey Solid Line). Acceleration Reconstructed Pressure (Black Solid Line). Crank Reconstructed Pressure (Black Dashed Line). RMSE = 7.06%.

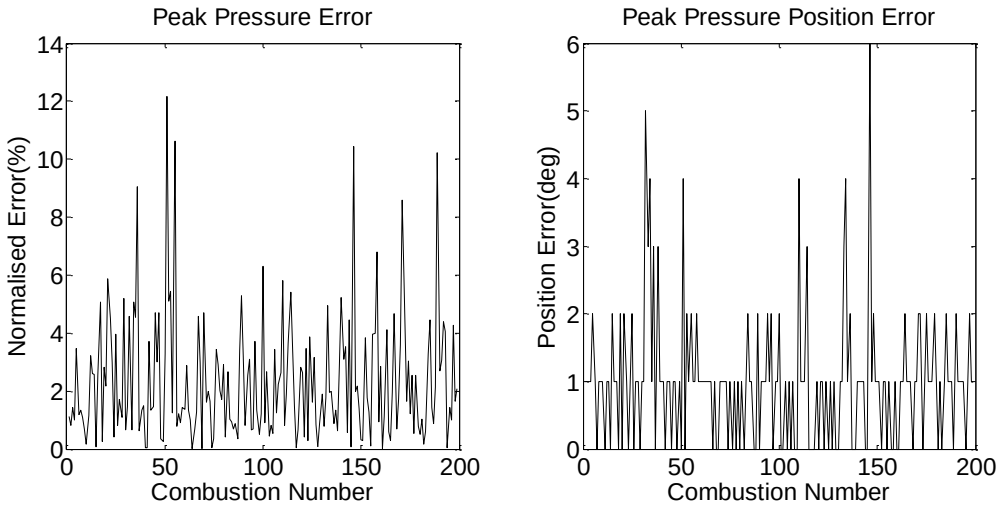

Figure 7.24: Condition-9 Normalised Peak Error Generalisation Results (left). Condition-9 Position of Peak Error Generalisation Results (right)

The reconstruction error in the second combustion event, in Figure 7.23, would appear to be as a result of high frequency noise within the input data. However this is not the case as this would also affect the first and third combustion event. The reason could be that the dynamics of the engine are distinctly different to the training data in this region or the most likely reason is that there is a small abnormality within the data causing the destabilisation of the reconstruction. Figure 7.24 gives the normalised peak error and the peak position error between the measured cylinder pressure and generalised results for 180 cycles of data. The following table, Table 7.10, presents the root-mean-squared error and the standard deviation for 3 key parameters; the overall error, the normalised peak pressure error and the position of peak pressure error.

Table 7.10: Condition-9 Root-Mean-Squared Error (RMSE) and Standard Deviation for the ANN Generalisation

	Generalisation Root-Mean-Squared Error	Generalisation Standard Deviation
Overall	1.98 %	1.97 %
Peak Error (%)	3.14 %	2.11 %
Peak Pressure Position Error (deg)	1.06	0.95

7.5.4 Discussion of Test Condition-9 Results

The training results at condition-9 (2000 rpm and 30 Nm) were much better than seen in the previous test conditions. The key difference between this test condition, and the two previously covered, is that in all three different reconstruction regions (best, average and worst) the training results were extremely good. These can be seen in Figure 7.17, 7.18 and 7.19 with a RMSE = 1.47%, and a normalised peak pressure error of 3.11%. Even the statistically poorest series of reconstructions is a great deal better than previously seen. The generalisation results for both the best, and average regions, are as accurate as the training results; Figure 7.21 and 7.22 respectively. However, the worst results shown in Figure 7.23 contain significant errors, and seem to become unstable within the second combustion event. It can be seen in table 7.9 and 7.10 that the position of peak pressure error is significantly lower than any other condition examined for both engine block vibrations, and crank kinematics in training and generalisation; i.e. 0.59 and 1.06 deg respectively. Similar to the previous condition, there seems to be no consistent correlation between the errors generated in the acceleration and crank kinematic based reconstructions. However, unlike the previous conditions the corresponding large acceleration based errors and small crank base errors do not occur in condition- 9. These errors were also not seen with enough frequency within the other test conditions to prove the link. Therefore, no relationship can be established between the errors and similarities perceived may have just been coincidental.

7.6 A Comparison and Overall Discussion of Results

This section will compare and discuss the generalised results from the trained ANNs for all 9 test conditions. It includes the 3 conditions discussed in detail as well as the other 6. All 9 ANNs were trained and tested using the same methodology and the additional results are provided in Appendix F. Initially, all 9 test conditions were compared with regard to the overall RMSE performance, the normalised peak pressure error and the position of peak pressure error. The range of the cylinder pressure reconstruction results will then be discussed including notable results. Finally, this section will make more general conclusions, regarding the capability of reconstructing cylinder pressure using crankshaft kinematics, the ANN architecture and training methodology, and most significantly, the successfulness of the methodology developed in Chapter 5.

Chapter 6 highlighted and dismissed the idea that the reconstruction potential, when using crank kinematics, is limited to the degree of cylinder pressure variability. Within the results presented in this chapter, there is no significant evidence that the variability impacts on the reconstruction accuracy as successful results are not dependent on the high or low power conditions. This can be shown in Table 7.11. However, it can be seen from these results that the performance of the ANNs seems to be condition dependent. Similar load or speed conditions can give significantly different results. It is believed that this is the result of excessive noise in the input data, which can vary from condition to condition, and not a fundamental flaw in the reconstruction methodology.

Table 7.11: Mean Generalised Performance of 9 Test Conditions

	Test Condition Power	Overall Performance (RMSE)	Normalised Peak Error	Peak Pressure Position Error (deg)
Condition-1	1.05 kW	2.72 %	9.69 %	2.16
Condition-2	1.57 kW	1.32 %	3.14 %	1.31
Condition-3	2.09 kW	1.94 %	3.68 %	1.57
Condition-4	2.09 kW	3.46 %	13.2 %	5.01
Condition-5	3.14 kW	2.61 %	8.60 %	1.71
Condition-6	4.19 kW	2.02 %	2.99 %	0.91
Condition-7	3.14 kW	1.88 %	5.17 %	1.83
Condition-8	4.71 kW	4.33 %	14.1 %	4.79
Condition-9	6.28 kW	1.98 %	3.14 %	1.06

Figures 7.25 to 7.28 show some of the best and worst performing generalised regions of the 9 ANNs trained, giving an overall perspective of the successfulness of using time-delay neural networks, the Levenberg Marquardt algorithm and the methodology developed in Chapter 5. It will also include generalised cylinder pressure reconstruction results that are noteworthy.

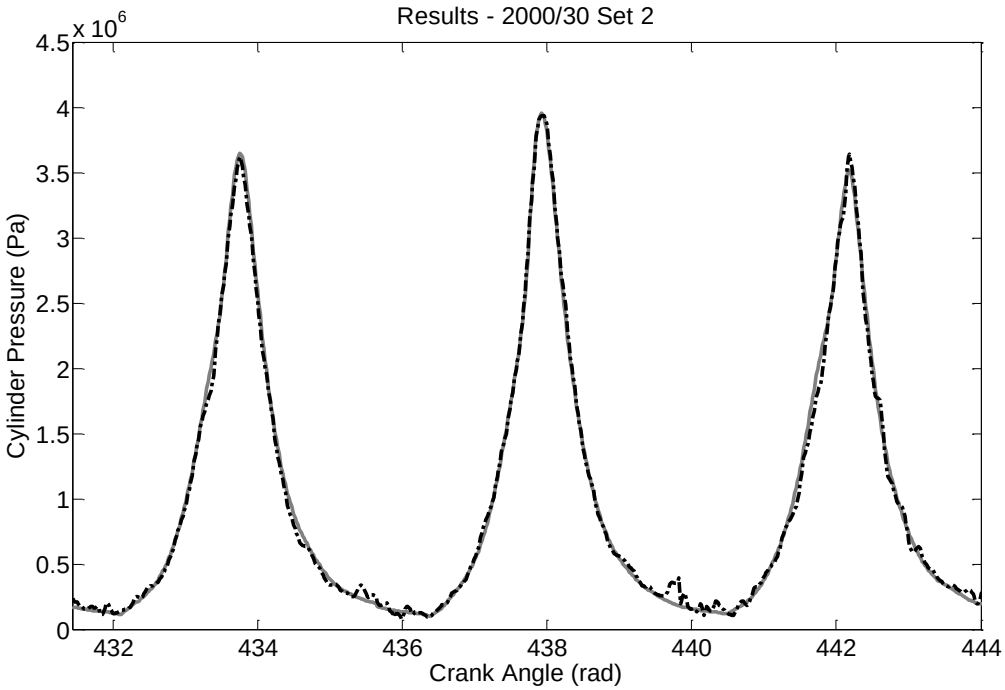

Figure 7.25: Best Performing Generalisation Results - Condition-9. Measured Cylinder Pressure (Grey Solid Line). Reconstructed Cylinder Pressure (Black Dashed Line). RMSE = 1.21%.

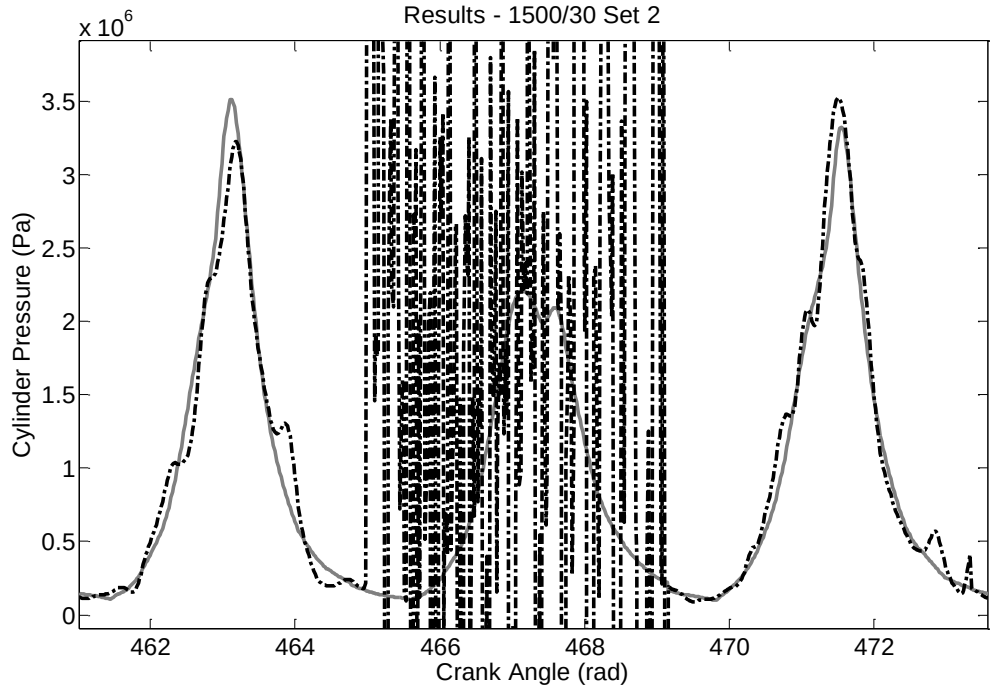

Figure 7.26: Worst Performing Generalisation Results - Condition-8. Measured Cylinder Pressure (Grey Solid Line). Reconstructed Cylinder Pressure (Black Dashed Line). RMSE = 61.7%.

Figure 7.25 and 7.26 show the best region of generalised reconstruction, and the worst region of reconstruction accordingly, across all 9 ANNs and test conditions.

The performance of each is 1.21% and 61.7% RMSE. The reconstruction results produced in Figure 7.26 could cause some concern with the use of block vibration. However, it was found that this instability of the reconstruction was the result of an abnormality within the data. This was included to highlight two points. There is a chance of instability when abnormal data is used with an ANN. But most importantly, the use of a time-delay network has enabled the reconstruction to stabilise where through experience the previously used recurrent ANNs would have great difficulty and often would not. The errors in the results in Figure 7.25 are negligible, and demonstrate that the cylinder pressure can be reconstructed successfully under general conditions, using engine block vibration. It is also evident in Figure 7.26, that the significant errors are not restricted to just the peaks of the cylinder pressure; the errors are also distributed along the whole cylinder pressure profile and not confined to the peak pressure. This confirms that the use of 'future' and 'past' inputs, described in Chapter 5, have the desired effect in accurately reconstructing cylinder pressure, based on the block vibrations

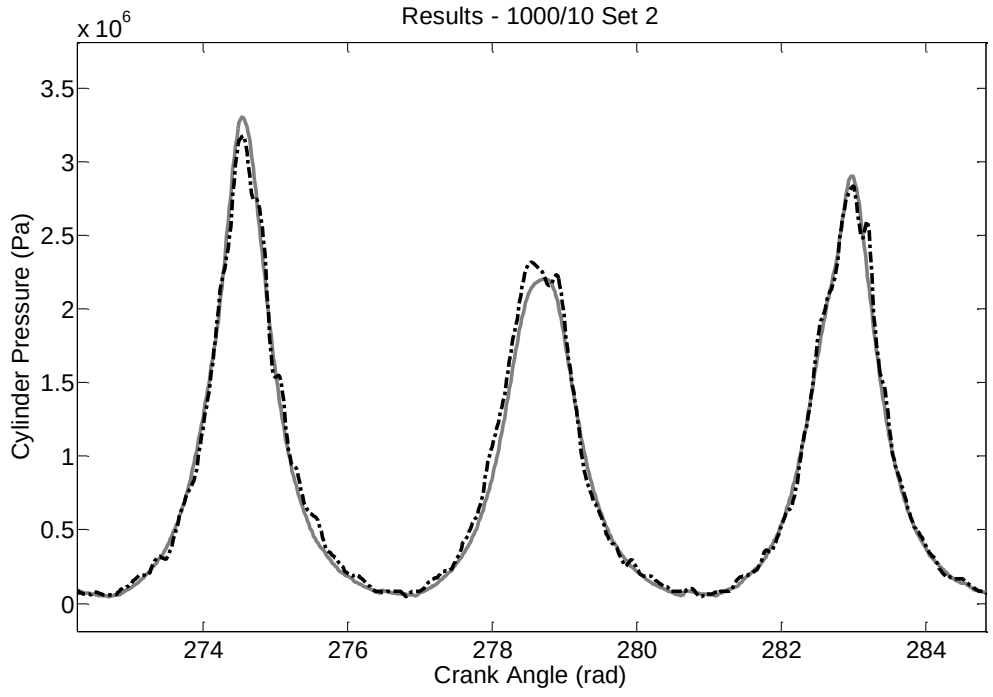

Figure 7.27: Notable Generalisation Results - Condition-8. Measured Cylinder Pressure (Grey Solid Line). Reconstructed Cylinder Pressure (Black Dashed Line). RMSE = 2.07%.

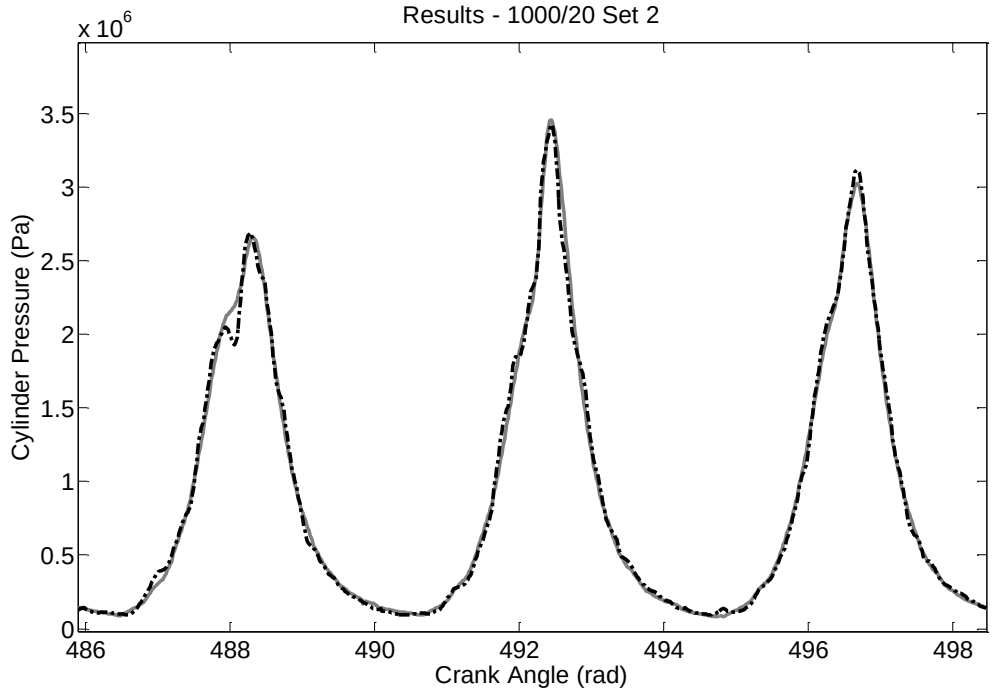

Figure 7.28: Notable Generalisation Results - Condition-5. Measured Cylinder Pressure (Grey Solid Line). Reconstructed Cylinder Pressure (Black Dashed Line). RMSE = 1.54%.

Figure 7.27 and 7.28 give two noteworthy reconstruction results. Each figure shows the ability of the ANN to reconstruct the cylinder pressure from abnormal or uncommon combustion events. In Figure 7.27, the reconstruction of interest is the second combustion event and in Figure 7.28, it is the first. In these cases, the ANNs do not necessarily reconstruct the most accurate cylinder pressure but they do recognise that the combustion event differs from the average, and produces a reasonable reconstruction. Both Figure 7.27 and 7.28 show combustion events with an appreciably late ignition.

Considering the reconstruction of cylinder pressure using engine block vibration generally, the results show good promise. The overall results for generalised reconstruction are much improved on previous published results and give very little evidence of the instability or significant peak pressure errors. This is believed to be a result of the methodology developed in Chapter 5. With respect to the training time and computational efforts required, this performance was unexpected. The resultant training times using on average 240 inputs, 15/15 neurons with 3,631 weights and in excess of 30,000 data points the ANNs, on average, trained within 0.73 hours using a Pc with an Intel i7 quad core processor with 12Gb ram and solid-state drive.

The results given in Chapter 7 validate the use of engine block vibration for reconstructing cylinder pressure, as results are mostly within the target error except for condition-8. The targeted error was 4% consistently for the generalised reconstruction and depending on the test condition, the results ranged between 1.32% and 4.33%. There is still room for improvement and it is believed this is possible, if an even more indiscriminate method of filtering is used.

An observation made when comparing crankshaft kinematics and engine block vibration results; the crankshaft kinematic results reconstructed the magnitude of the peak pressure more accurately, whereas the engine block vibration reconstructed the phase of the maximum pressure more accurately. This can be explained by referring back to the conclusions made in Chapter 5. When reconstructing using crankshaft kinematics, the major problem is the combination of cranktrain inertial dominance and a reduction in the information content surrounding TDC. To accurately reconstruct, it was necessary to use a combination of future and past inputs. This provided information directly pertaining to the energy imparted to the cranktrain, and then allowed accurate reconstruction of the pressure's magnitude. However, due to the lack of information surrounding TDC, pinpointing the position of peak pressure was more difficult. As there is no information loss with engine block vibrations, the opposite is true; the position of peak pressure accuracy is good. However, the engine block vibration peak pressure reconstruction accuracy is poorer because of the increase in noise. To accurately reconstruct both the magnitude and position of peak pressure, a combination of the two approaches may be required. This can be seen when examining tables 6.11 and 7.11.

This chapter demonstrates that reconstructing cylinder pressure can be done successfully on steady-state data. However, again, the ultimate proof of the success of this technology is to test on transient conditions.

Chapter 8

Reconstruction of Cylinder Pressure for Transient Engine Operation

8.1 Introduction and Motivation

So far in the thesis, the primary focus has been on the reconstruction of cylinder pressure from both crankshaft kinematics and engine block vibrations under steady state conditions. The use of steady-state conditions contains simpler dynamics and is ideal for proving the efficacy of this technology. However, the long term use of steady-state conditions is limited and solely testing in this condition provides no guarantee that the approach will be successful under more complex transient conditions. The reason that work on transient reconstruction is important is because the majority of real world automotive IC engine operations are transient. There are some exceptions within the automotive industry, including series hybrid vehicles with range extenders, which are designed to run mainly at fixed steady-state speeds and loads. Outside the automotive industry, steady-state running of IC engines can include stationary power generation and large marine applications. The potential difficulties in reconstructing cylinder pressure under transient conditions are not limited to simple engine load and speed fluctuations. There are certain characteristics of engine dynamics that appear only in transient conditions. These can include heavy fuelling and retardation of the ignition for rapid acceleration, and overrun conditions, when the throttle is closed rapidly.

The majority of work previously undertaken on reconstructing cylinder pressure has been carried out at transient conditions, with little success. One approach attempts to train a single ANN for reconstructing both steady-state and transient conditions. This chapter will examine this approach in addition to two other approaches, which have been developed for this thesis. The chapter will attempt to identify key differences in the training abilities at both steady-state and transient conditions, by testing on a combination of slow and rapid changes in engine conditions.

The chapter is divided into three sections. Section 8.2 will examine the training of a single ANN on a series of steady-state conditions for the transient reconstruction. It will also include effects of training on load of varying conditions and speed varying conditions independently. In section 8.3, multiple ANNs will be trained at different speeds and used to attempt to reconstruct transient cylinder pressure. Section, 8.4, will cover the development of a new ANN structure, which is capable of training on, and reconstructing transient directly, including an adaptation of the Levenberg-Marquardt algorithm for transient operation.

8.2 Transient Reconstruction with a Single ANN

8.2.1 A Load and Speed Varying ANN

This section examines the capability of using a single ANN which is trained across numerous steady-state conditions for the transient reconstruction of cylinder pressure. As mentioned in Chapter 3, the number of different possible transient conditions and engine dynamics that might occur is vast. It has been seen in Chapters 6 and 7, the degree of variability in cylinder pressure under steady-state conditions, where some of the key characteristics of engine dynamics are all constant i.e. engine speed, load, air temperature, and air pressure. Under transient conditions, these additional variables increase the number of possible states the system is in. As a result, the training of an ANN on every possible condition is computationally extremely expensive and not practical. Therefore, the ideal solution is to use a select number of test points for training the ANN which will give the optimum reconstruction for the majority of transient conditions.

The method used to test this approach for reconstructing transient conditions is as follows: crank kinematics was selected as the input to the ANN, motivated by the considerable improvements that have been made, as highlighted in Chapter 6. Owing to inconsistency and higher levels of noise, the use of engine block vibration has been dismissed for transient reconstruction. The same ANN architecture, training algorithm and processing methodology was used as described in Chapter 6. Initially, the number of neurons, layers, and inputs remained the same, with the aim of undertaking a new optimisation once this method had been shown to hold some promise. All 9 test conditions, previously discussed, with speeds ranging from 1000 to 2000 rpm, and torque from 10 to 30 Nm, are used in the training and reconstruction. The data is collected, configured and then ordered randomly to prevent both over-training of the ANN, and biasing of the training, to favour one

condition over another. Previous attempts at reconstructing cylinder pressure using recurrent network architectures do not randomly order the input data. Recurrent networks contain within them a memory and the ability to reconstruct depends heavily on the previous reconstruction attempts. As a result, reordering the data would have a negative effect on the reconstruction. Time delay networks do not have the internal memory; they are not dependant on previous states and treat each reconstruction point independently. Therefore, randomising the data will have no effect on the reconstruction and is a prudent method of ensuring a cross section of data is used for training. The collated data was then used to train the single ANN with the same limits on the reconstruction; namely the same number of epochs and the same performance goal.

Determining the success of this approach is undertaken in two parts. First, the new data is used to test the generalised performance of the reconstruction for each of the steady-state conditions it is trained on. Second, transient data is then tested on the ANN to prove its validity. The selection of the transient conditions to be tested was important. Initially, a relatively slow speed ramp was selected as the transient test condition because it is not too dissimilar (in some regions) to the steady-state data and contains few transient-only engine dynamics but still has varying speeds and loads. The speed ramp selected was from 1000 to 2000 rpm, which occurred within a 30 second period. Owing to the control arrangements fitted in the engine test cell, a true transient, i.e. where full control is exercised over both speed and load is not possible. This means that there is not an accurate value of the load through the transient, as it could not be fixed. However, prior to commencing the speed ramp, the load was initially set at 20 Nm so any fluctuations would be within 10 - 30 Nm data range; the same range as the steady-state data.

The training of the ANN took significantly longer than previously observed because of the increased size of the training set. The ANN trained in 14942 seconds (4.15 hours) in 105 epochs. Figures 8.1 to 8.6 show a select number of generalised results from the steady-state reconstruction using the same ANN.

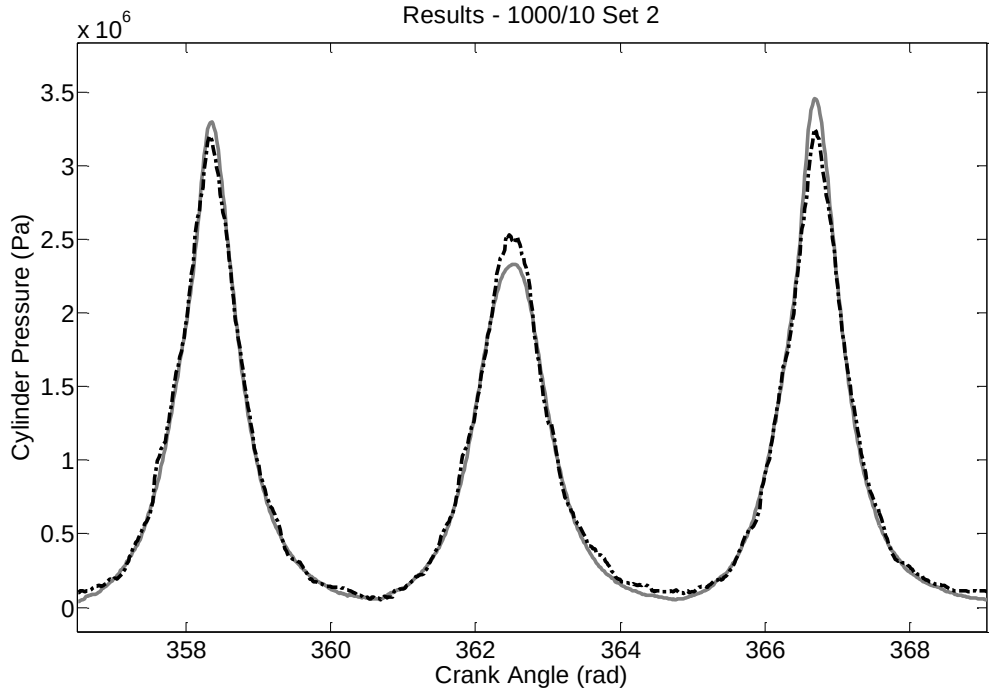

Figure 8.1: Steady-State Condition-1 - 1000 rpm and 10 Nm. Measured Cylinder Pressure (Grey Solid Line). Reconstructed Cylinder Pressure (Black Dashed Line).

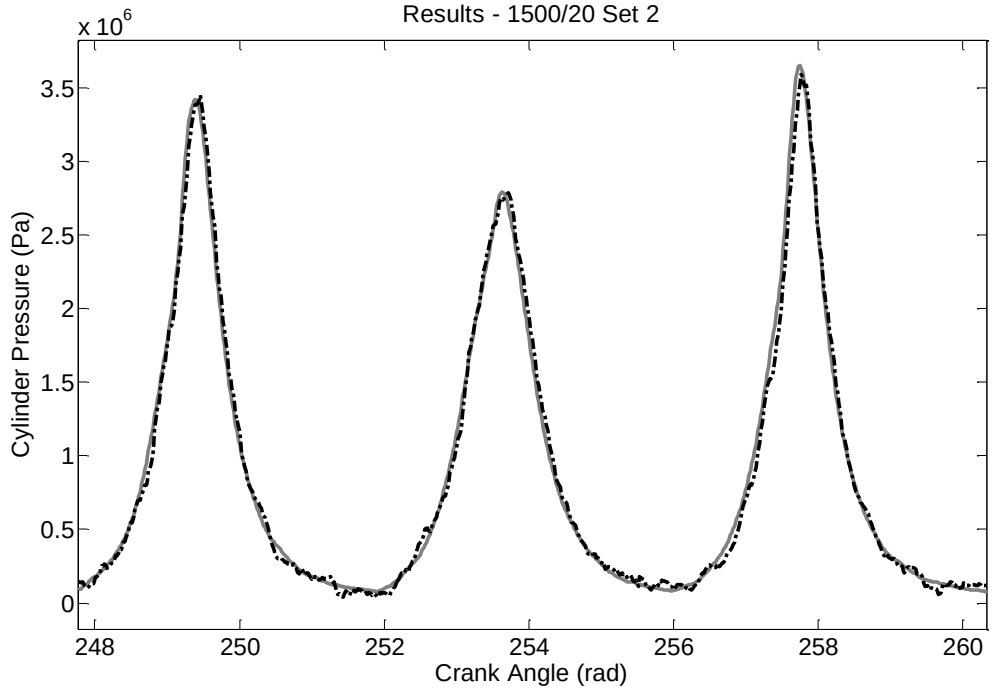

Figure 8.2: Steady-State Condition-5 - 1500 rpm and 20 Nm. Measured Cylinder Pressure (Grey Solid Line). Reconstructed Cylinder Pressure (Black Dashed Line).

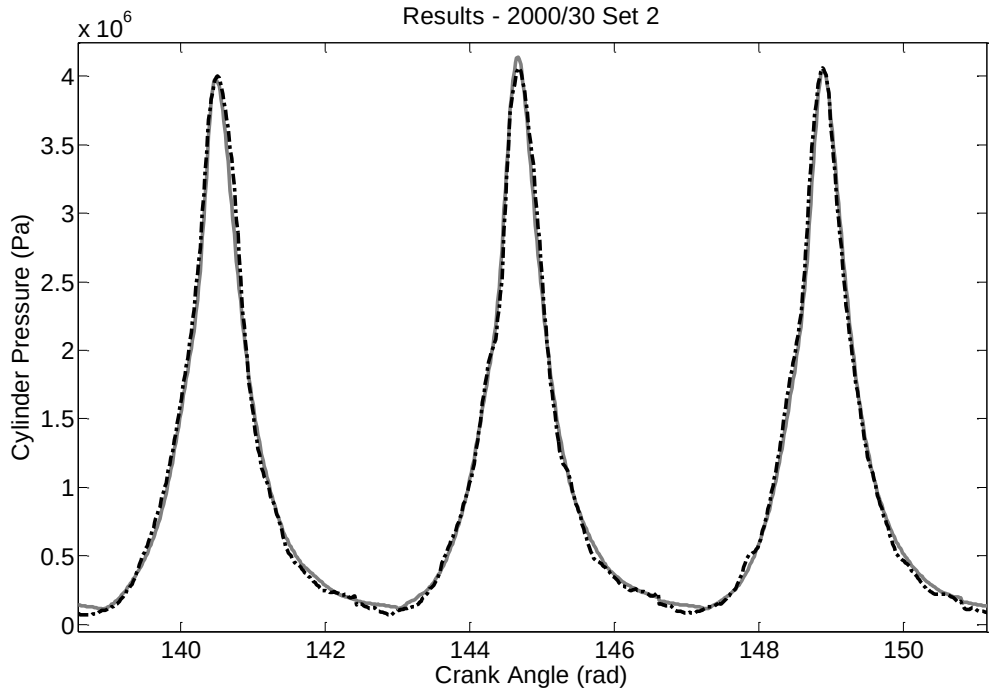

Figure 8.3: Steady-State Condition-9 - 2000 rpm and 30 Nm. Measured Cylinder Pressure (Grey Solid Line). Reconstructed Cylinder Pressure (Black Dashed Line).

Table 8.1: Overall Results for Steady-State Testing on a Single ANN Trained on Multiple Conditions.

	Overall Performance (RMSE)	Normalised Peak Error	Peak Pressure Position Error (deg)
Condition-1	2.18 %	5.45 %	2.69
Condition-2	1.87 %	2.87 %	2.20
Condition-3	1.97 %	4.18 %	2.19
Condition-4	2.45 %	4.15 %	4.48
Condition-5	2.38 %	7.04 %	2.54
Condition-6	1.97 %	4.25 %	1.59
Condition-7	2.93 %	4.05 %	2.55
Condition-8	2.26 %	6.9 %	3.79
Condition-9	2.14 %	4.56 %	1.25

The 3 conditions, given in Figures 8.1 to 8.3, show broadly the results for reconstructing steady-state cylinder pressure from a single ANN trained on multiple conditions. Generally, the results at 1500 and 2000 rpm are accurate, and closely resemble the results presented in Chapter 6. However, the results across all loads at 1000 rpm are poor. Within these results, there is no clear explanation for the errors at low speed; further examination was required. The initial reasoning lays the blame for the poor reconstruction with one of two explanations surrounding the crankshaft kinematics. First, it could be a result of the different degrees of variability between each speed. Even though the variability had been dismissed with regards to training a single ANN with a single condition, the variability may have had an impact when considering multiple conditions. The minimal variability at higher speeds resulted in more consistent crankshaft kinematics which created a significant portion of training data that was similar. Conversely, low speeds contain significant variations which can create training data that can be dissimilar. Even though an attempt was made to distribute the data randomly for all conditions, the inherently similar, higher speed training data, may result in the ANN favouring higher speed conditions. The second possible explanation, and the one that is believed to be most likely, is that as speed increases, the time dependent features, which occur in both the cylinder pressure and crankshaft kinematics, can shift and vary. These inconsistent variations across the transient range could make the ANN, in its current form, incapable of reconstructing all the conditions. Therefore as a result, the ANN trains on data that is easier to reconstruct, i.e. the higher speed conditions.

Even though the results were not ideal, the ANN was tested on the transient results. Figure 8.4 to 8.6, and table 8.2, shows the results for the transient reconstruction from a single ANN.

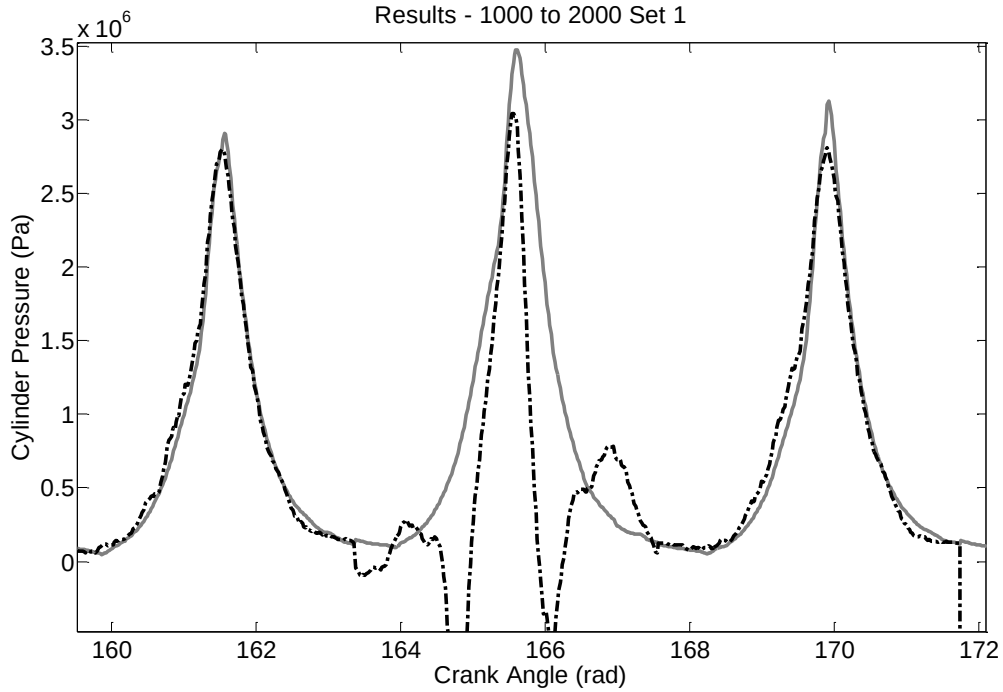

Figure 8.4: Transient Region 1 - 1000 to 2000 rpm. Measured Cylinder Pressure (Grey Solid Line). Reconstructed Cylinder Pressure (Black Dashed Line).

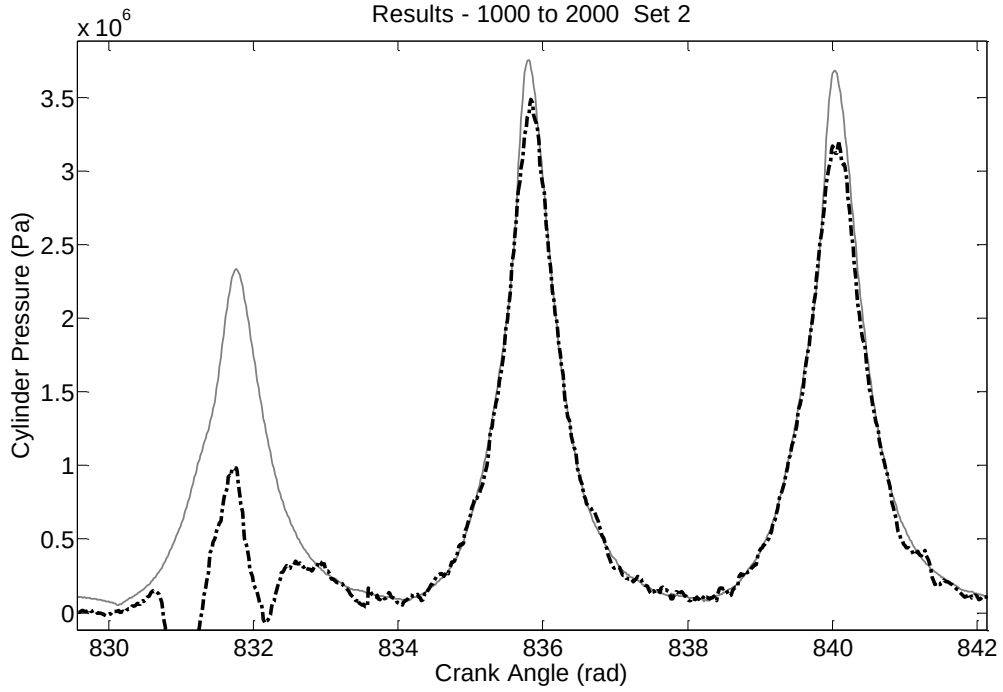

Figure 8.5: Transient Region 2 - 1000 to 2000 rpm. Measured Cylinder Pressure (Grey Solid Line). Reconstructed Cylinder Pressure (Black Dashed Line).

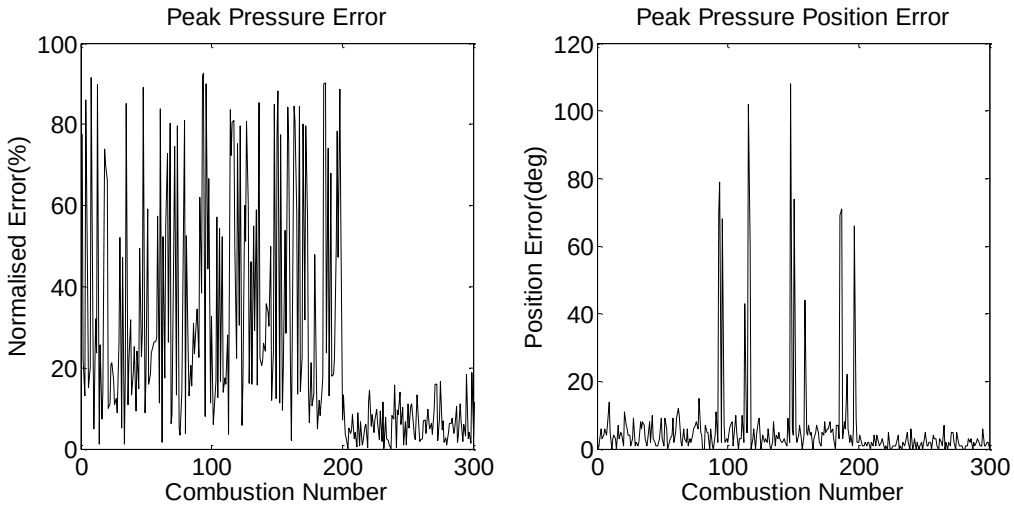

Figure 8.6: Transient Overall Results. Normalised Peak Error Training Results (left) and Position of Peak Error Training Results (right)

Table 8.2: Overall Results for Transient Testing on a Single ANN Trained on Multiple Conditions.

	Generalisation Root-Mean-Squared Error	Generalisation Standard Deviation
Overall Performance	13.71 %	12.63%
Normalised Peak Error	36.5 %	26.4 %
Peak Pressure Position Error (deg)	14.8	13.6

The generalised transient results from a single ANN show three significant trends. The same differences in the reconstruction ability at different speeds, shown earlier with the steady-state generalisation, still occur in the transient results and can be seen clearly in the reduced error later on in the data (at a higher combustion number) in Figure 8.6. Generally, across the whole speed ramp, there was a decrease in the overall reconstruction performance. The final observation seen was that at typically transient events, such as overrun, even though poorer than at other points, the reconstruction results show that the cylinder pressure has varied significantly. The performance of the ANN in reconstructing transient events shows promise, but with the significant difference in the reconstruction at differing speeds, this approach cannot be categorised as being a success. Further work was required to separately examine reconstruction at different loads and speed. This was now undertaken.

8.2.2 A Load Varying ANN

This part of the chapter examines the capability of using a single ANN to train across numerous steady-state load conditions, with constant speed, to find the root cause behind the limitations presented in section 8.2.1. It was expected that the results from the constant-speed varying-load ANN training, would be consistent because there would be no variation in the time dependent features, and the only change would be to the magnitude of combustion. The generalised reconstructed results should have minimal errors, similar to the results in Chapter 6.

The method used to test this approach was the same method used in Section 8.2.1. Crank kinematics was selected owing to the considerable improvements made, as highlighted in Chapter 6. The same ANN architecture, training algorithm, and processing methodology are used. Initially the number of neurons, layers and inputs remains the same. However, only 3 test conditions at 1000 rpm, and torque ranging from 10 to 30 Nm, are used in the training and reconstruction. The data was collected, configured, and then ordered randomly, to train the single ANN with the same limits on the reconstruction.

To determine the success of this approach, new data was used to test the generalised performance of the reconstruction for each of the steady-state conditions it was trained on. However, this section will not present the reconstructed cylinder pressure in transient conditions for two reasons. First, the experimental setup was not designed successfully to run load transients. Second, the aim of this section was not to determine the ability to reconstruct using a load varying ANN, but to determine whether a significantly different approach was needed for reconstructing cylinder pressure with varying loads. Figures 8.7 to 8.8 and Table 8.3 show a select number of generalised results from the steady-state reconstruction, using a single ANN.

.

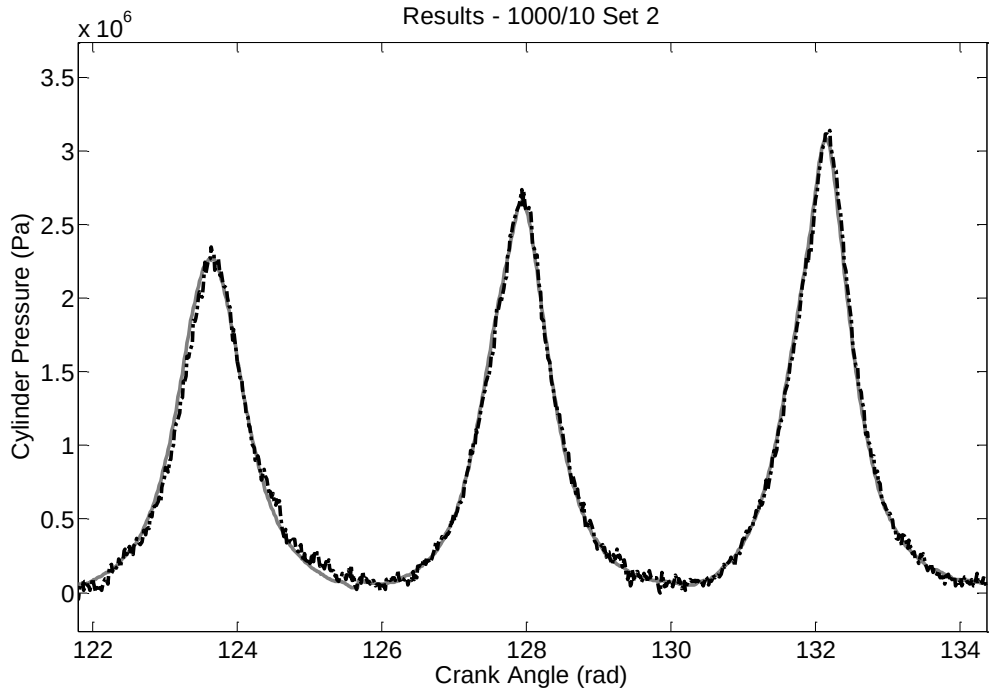

Figure 8.7: Steady-State Condition-1 - 1000 rpm and 10 Nm. Measured Cylinder Pressure (Grey Solid Line). Reconstructed Cylinder Pressure (Black Dashed Line).

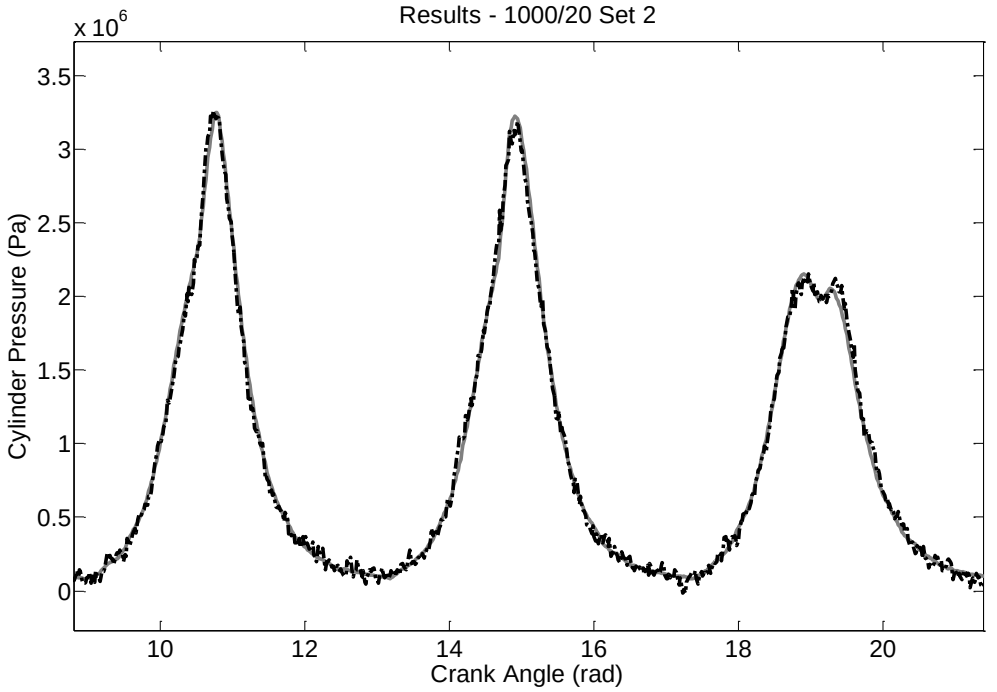

Figure 8.8: Steady-State Condition-2 - 1000 rpm and 20 Nm. Measured Cylinder Pressure (Grey Solid Line). Reconstructed Cylinder Pressure (Black Dashed Line).

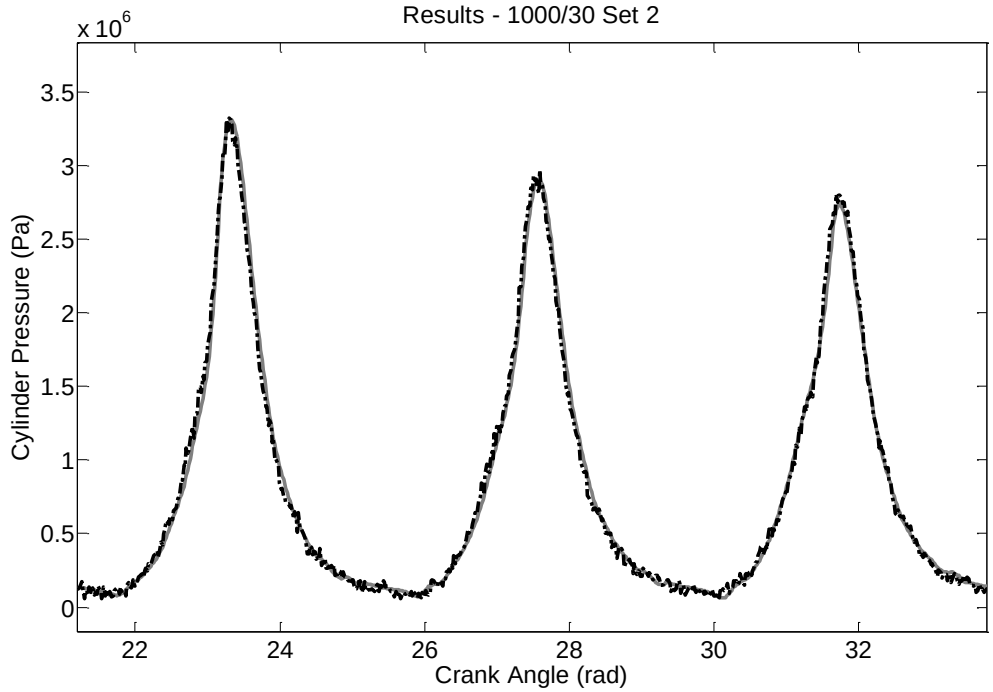

Figure 8.9: Steady-State Condition-3 - 1000 rpm and 30 Nm. Measured Cylinder Pressure (Grey Solid Line). Reconstructed Cylinder Pressure (Black Dashed Line).

Table 8.3: Overall Results for Steady-State Testing on a Single ANN Trained on Constant Speed Varying Load Conditions.

	Overall Performance (RMSE)	Normalised Peak Error	Peak Pressure Position Error (deg)
Condition-1	1.74 %	2.75 %	2.53
Condition-4	1.91 %	3.29 %	2.67
Condition-7	1.65 %	2.63 %	1.90

The 3 conditions shown in Figures 8.7 to 8.9 broadly show the results of reconstructing steady-state cylinder pressure from a single ANN, trained on varying load conditions only. These results were for an engine speed of 1000 rpm, and loads of 10, 20 and 30 Nm. The results for all loads are extremely good, and are comparable to the individual ANNs trained for each condition in Chapter 6. The results from the other speeds (1500 and 2000 rpm) are given in Appendix G, and show the same outcome. Taking into account that the ANN produced cannot categorically be verified to work irrelevant of the load, as a load transient was not possible with the experimental setup, it is believed that this can only be inferred. As

expected, with the load having no relevance to successful transient reconstruction of cylinder pressure, the rest of this section will focus on the source of the problem: i.e. varying speeds.

8.2.3 A Speed Varying ANN

The previous subsection examined the impact on reconstructing using a single ANN with varying load. The next part examines the capability of using a single ANN to train across numerous steady-state speed conditions, with constant load. The results of this examination were expected to be similar to the ones presented in section 8.2.1. Two of the main reasons why significant errors were expected, based on the results in section 8.2.1, were the time dependent aspects of cylinder pressure reconstruction and the variation in the additional loads. One example of an additional load that significantly varies with engine speed is friction. As most of the internal damping can be ideally thought of as hydrodynamic, because of this, the lower the speed of the individual components, the greater the level of damping. One explanation for the different reconstruction accuracies at different speeds was that as speed increases, the time dependent features, which occur in both the cylinder pressure and crank kinematics, can shift and vary, and as a result, make the ANN incapable of reconstructing across various speeds.

The method used to test this approach was the same method used in section 8.2.1. Crank kinematics was selected owing to the considerable improvements that had been made, as highlighted in Chapter 6. The same ANN architecture, training algorithm and processing methodology was used. Initially, the number of neurons, layers and inputs remained the same. However, only 3 test conditions at 10 Nm, and speed ranging from 1000 to 2000 rpm, were used in the training and reconstruction. The data was collected, configured, and then ordered randomly to train the single ANN with the same limits on the reconstruction.

To determine the success of this approach, new data was used to test the generalised performance of the reconstruction for each of the steady-state conditions it was trained on. Again, this section will not present the reconstructed cylinder pressure in transient conditions because the objective was only to determine whether a significantly different approach was needed for reconstructing cylinder pressure with varying speeds. Figures 8.10 to 8.12 and Table 8.4 show a select number of generalised results from the steady-state reconstruction, using a single ANN.

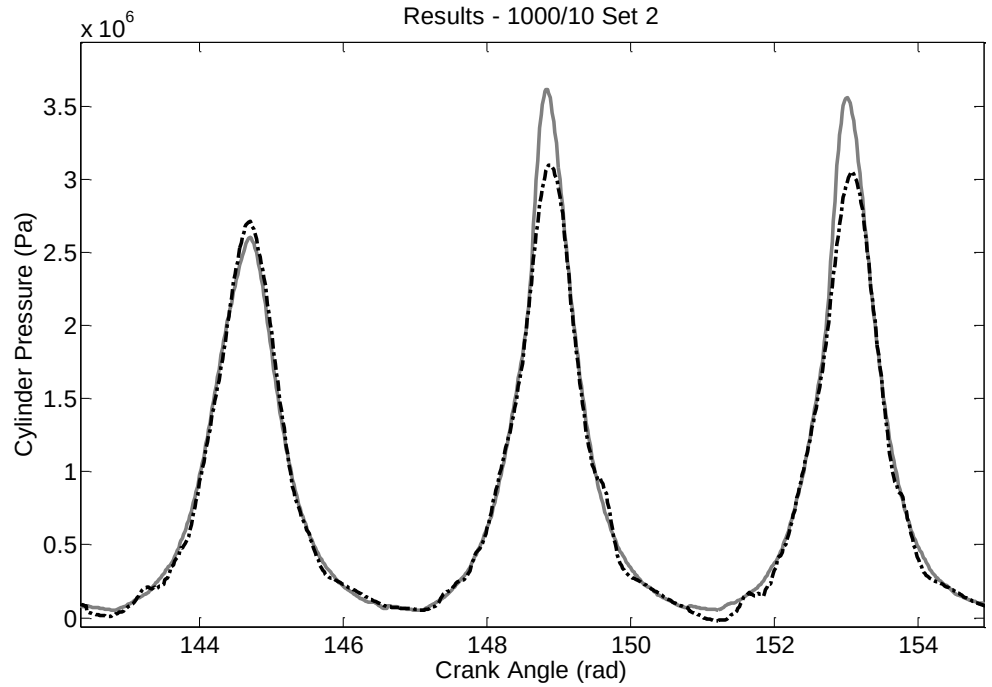

Figure 8.10: Steady-State Condition-1 - 1000 rpm and 10 Nm. Measured Cylinder Pressure (Grey Solid Line). Reconstructed Cylinder Pressure (Black Dashed Line).

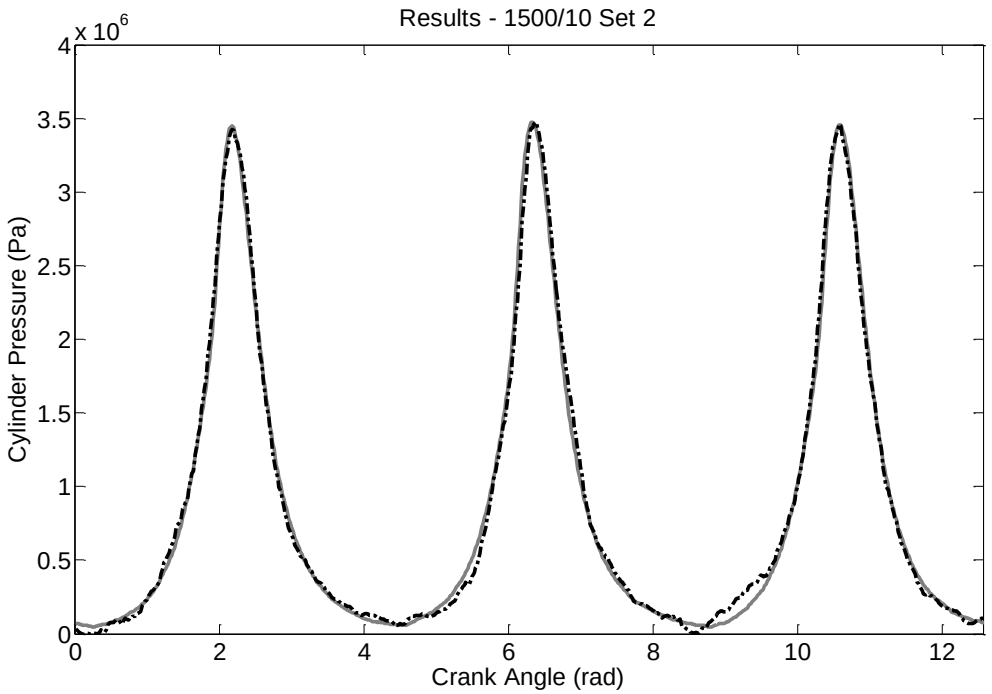

Figure 8.11: Steady-State Condition-5 - 1500 rpm and 10 Nm. Measured Cylinder Pressure (Grey Solid Line). Reconstructed Cylinder Pressure (Black Dashed Line).

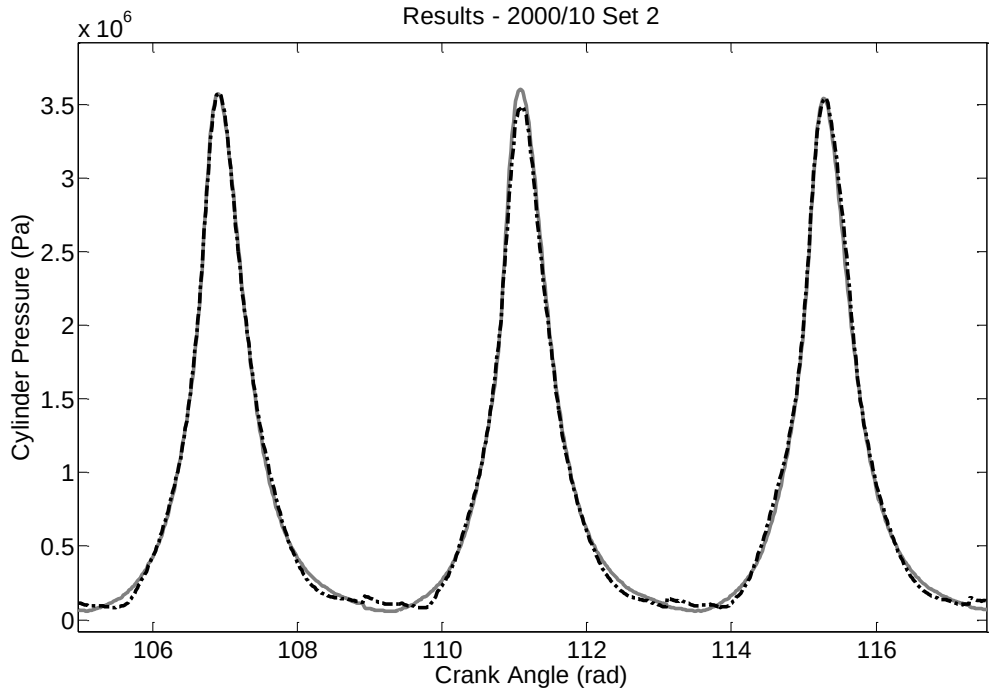

Figure 8.12: Steady-State Condition-9 - 2000 rpm and 10 Nm. Measured Cylinder Pressure (Grey Solid Line). Reconstructed Cylinder Pressure (Black Dashed Line).

Table 8.4: Overall Results for Steady-State Testing on a Single ANN Trained on Constant Load Varying Speed Conditions.

	Overall Performance (RMSE)	Normalised Peak Error	Peak Pressure Position Error (deg)
Condition-1	2.49 %	7.74 %	2.66
Condition-2	1.95 %	2.39 %	1.52
Condition-3	1.78 %	3.12 %	1.53

The 3 conditions given in Figures 8.10 to 8.11 shows broadly, the results of reconstructing steady-state cylinder pressure from a single ANN trained on varying load conditions only. These results were for an engine speed of 1000, 1500 and 2000 rpm with a load of 10 Nm. The results produced for the single ANN show exactly the same type of errors as seen in section 8.2.1; at higher speeds reconstruction is very good, whereas at low speed, there is a significant problem in reconstructing cylinder pressure. These results are evident in the other loads as well. The results from the other loads (20 and 30 Nm) are given in Appendix G, and show the same outcome. As expected, the speed had a significant impact on

successful reconstruction of cylinder pressure in transient conditions. However, the results do not highlight the reasons behind the poor reconstruction. The aim of the remainder of this chapter is to identify the source of the problem and to find a solution for reconstructing within varying speeds.

8.3 Transient Reconstruction with Multiple ANNs

The work presented in Section 8.2 shows a significant issue with reconstructing cylinder pressure at varying speeds, using a single ANN of the size currently used. A new optimisation way undertaken to improve the performance of the ANN by increasing the size. However this failed to have the desired effect. Instead of using a single ANN, the new approach trains multiple ANNs at different conditions to successfully reconstruct cylinder pressure in transient conditions. The results from Section 8.2 show, that because of the changing physics as the engine speed increases, the gulf between the different speed conditions, i.e. 1000 rpm, is too big for a single ANN to train and generalise successfully. The proposed solution was to train multiple ANNs, of the same size and type, across two adjacent speed conditions where there would be minimal differences in time dependent features. This would generate numerous ANNs, each responsible for reconstructing cylinder pressure within separate speed ranges. For transient conditions, reconstruction would require transferring from one ANN to another, as engine speed varies. This would significantly increase the amount of work required to train and to reconstruct, but it is believed that this is the best solution for reconstructing transient conditions.

Again, the basic method used to test this approach and train the ANNs was the same method used throughout Chapter 8. Crankshaft kinematics was selected and the same ANN architecture, training algorithm, and processing methodology was used. The initial number of neurons, layers and inputs remained the same. The only difference was that multiple ANNs were trained with closer speed differences i.e. 100 rpm, which required significantly more engine test data. The current engine test data was acquired at three different speed and load conditions; with a 500 rpm and 10 Nm intervals. The current speed intervals could produce significantly different engine dynamics and would not be sufficiently close to test the proposed approach. However, as found in Section 8.2.2, the load conditions would be adequate as it is believed to be independent of the transient reconstruction issues. Therefore, a considerable amount of the new test data was acquired; i.e. 120 sets of data. These

included 11 different steady-state conditions, where the speeds selected were within the 1000 to 2000 rpm range with 100 rpm intervals. The acquisition for each speed was 30 seconds long, repeated twice and at four different load conditions; motored, 10, 20, and 30 Nm. This produced a total of 88 steady-state data sets. The remaining 32 data sets were additional transient conditions to increase the database of measured engine test data. The data was collected, configured, and then ordered randomly to train each ANN with the same limits on the reconstruction. Each ANN was trained on a pair of adjacent speed conditions; for example 1000 to 1100 rpm, 1100 to 1200 rpm, 1200 to 1300 rpm.

Figures 8.13 to 8.17 show a select number of generalised results from the steady-state reconstruction, using one of the multiple ANNs. The ANN selected was ANN-1 which was trained on data from 1000 and 1100 rpm at 20 Nm.

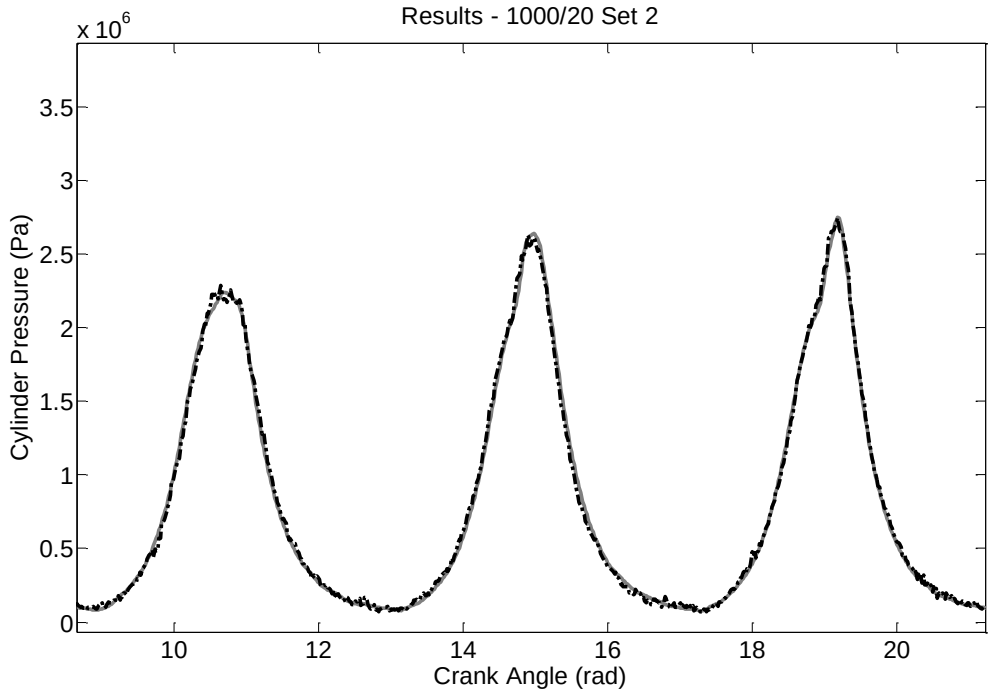

Figure 8.13: Steady-State Condition-1000 rpm and 20 Nm Using ANN-1. Measured Cylinder Pressure (Grey Solid Line). Reconstructed Cylinder Pressure (Black Dashed Line).

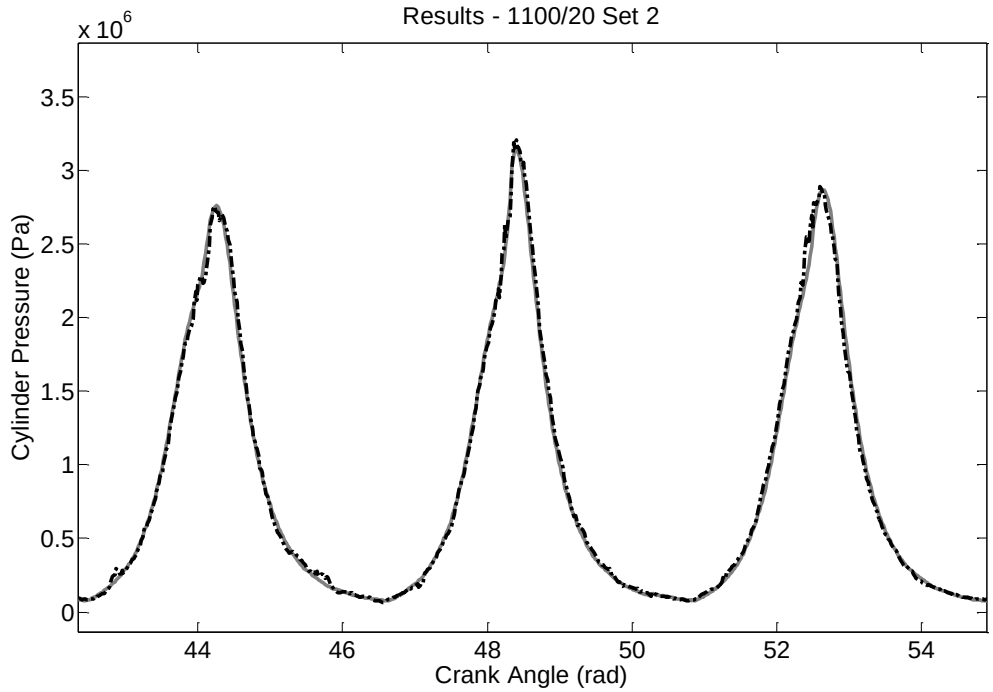

Figure 8.14: Steady-State Condition-1100 rpm and 20 Nm Using ANN-1. Measured Cylinder Pressure (Grey Solid Line). Reconstructed Cylinder Pressure (Black Dashed Line).

Table 8.5: Overall Results for Steady-State Condition Using ANN-1.

	Overall Performance (RMSE)	Normalised Peak Error	Peak Pressure Position Error (deg)
1000 rpm - 20 Nm	1.38 %	2.62 %	2.39
1100 rpm - 20 Nm	1.47 %	2.98 %	2.04

The 2 conditions given in Figures 8.13 to 8.14 show the results from reconstructing steady-state cylinder pressure from one of the ANNs. The ANN was trained on the same engine speed; 1000 and 1100 rpm at 20 Nm. The results for both engine speeds is good and are comparable to the individual ANNs trained for each condition in Chapter 6. The results from the other speed ranges show a similar outcome. These multiple ANNs were then tested on transient conditions. This was carried out by splitting the transient into 10 different regions, with 100 rpm intervals, and presenting each to the trained ANNs. Figures 8.15 to 8.17 and table 8.6 show the results for the reconstruction using the same transient condition examined in section 8.2; 1000 to 2000 rpm speed ramp.

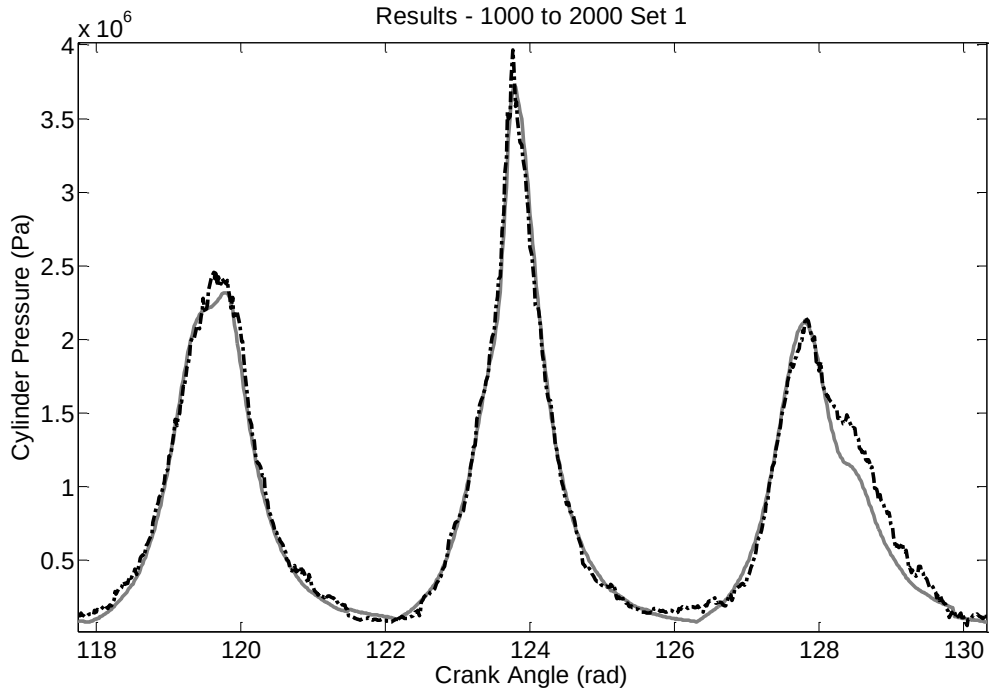

Figure 8.15: Transient Region 1 Using Multiple ANNs. Measured Cylinder Pressure (Grey Solid Line). Reconstructed Cylinder Pressure (Black Dashed Line).

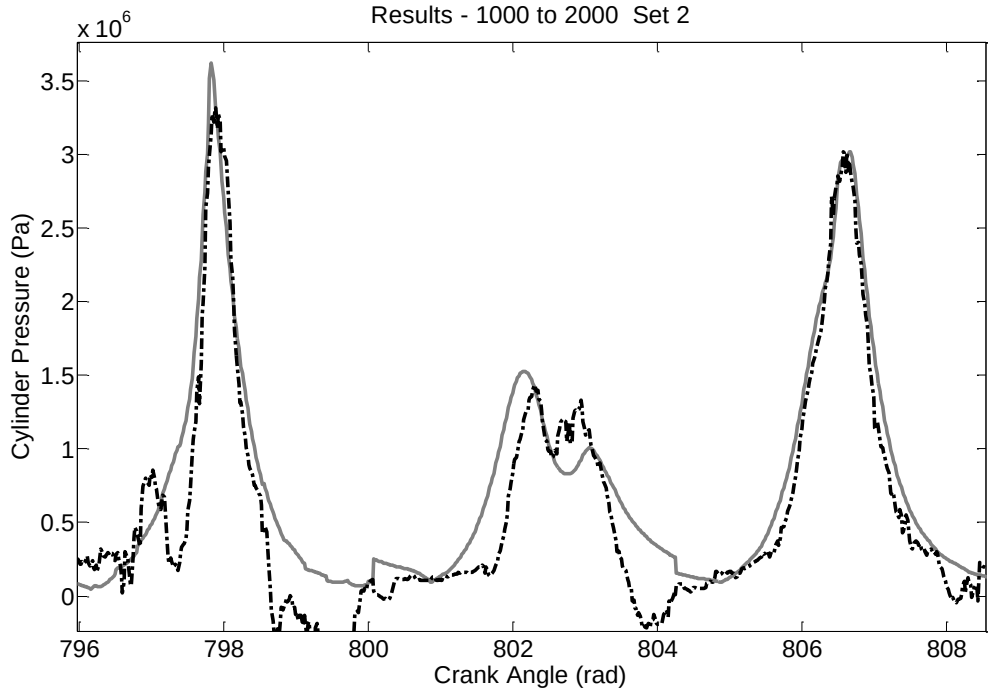

Figure 8.16: Transient Region 2 Using Multiple ANNs. Measured Cylinder Pressure (Grey Solid Line). Reconstructed Cylinder Pressure (Black Dashed Line).

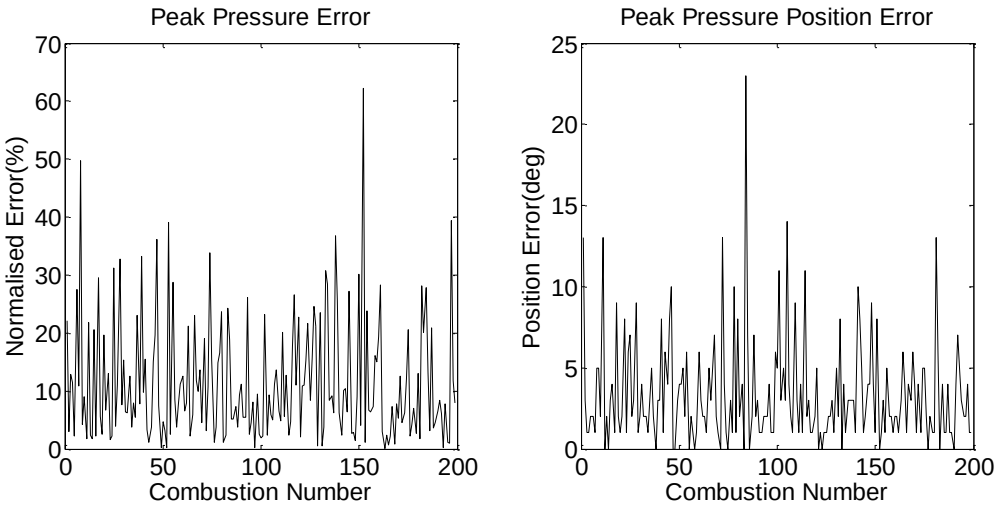

Figure 8.17: Transient Overall Results. Normalised Peak Error Training Results (left) and Position of Peak Error Training Results (right)

Table 8.6: Overall Results for Transient Testing Using Multiple ANNs.

	Generalisation Root-Mean-Squared Error	Generalisation Standard Deviation
Overall Performance	7.70 %	7.63%
Normalised Peak Error	15.4 %	10.4 %
Peak Pressure Position Error (deg)	4.69	3.26

The results generally show an improvement for both the steady-state reconstruction and the transient speed ramp, compared to the results produced using a single ANN for all conditions. Figures 8.15 to 8.17 and Table 8.6 show that even though there is a general improvement, in certain regions, errors are still significant. The most common region for this is where transient dynamics are most apparent i.e. overrun. It can also be stated that generally the transient reconstruction is still poorer than the results seen, when reconstructing steady-state cylinder pressure. The progress made from a single ANN to the use of multiple speed dependent ANNs is notable, and confirms that speed dependent training is necessary for producing an ANN that successfully reconstructs transient cylinder pressure.

8.4 Transient Reconstruction using a Dynamic ANN

The initial approach using a single ANN failed to satisfactorily reconstruct cylinder pressure at varying speeds. However, the results presented in Section 8.3 have

shown significant advances in reconstructing transient conditions by using multiple ANNs; an ANN for each 100 rpm. Using ANNs that vary with speed appears to be the direction showing the most promise. Practically, multiple ANNs have the same architecture and structure. This enables all the weights and biases to be mapped for each specific speed condition, and when reconstructing, the weights and biases would be updated once the engine speed exceeded a predetermined range. However, use of the individual values for each discrete speed, failed to reconstruct the transient-only dynamics with significant speed fluctuations. The idea that each weight and bias, within the ANN structure, could be described by a series of values, leads to a new approach using a novel ANN architecture. Instead of using a string of values to describe a weight or bias, a continuously variable function could be used which would generate a time varying ANN, or more accurately, a Non-Autonomous Neural Network. This NANN architecture was developed during the course of this research; no publication has been found to date putting forward this particular architecture. The NANN would have an additional input, which would be time dependent, or within this application, engine speed. However, this additional input would not be used in the same way as either the crankshaft kinematics or engine block vibrations. It would be used to adapt each weight and bias according to their individual functions. This architecture should enable the training and successful reconstruction of any function where time-dependence is significant. Within this application, it would also allow the direct training of the ANN, using transient data and should enable the successful reconstruction of transient-only dynamics. Figure 8.18 shows the configuration of a Non-Autonomous Neural Network.

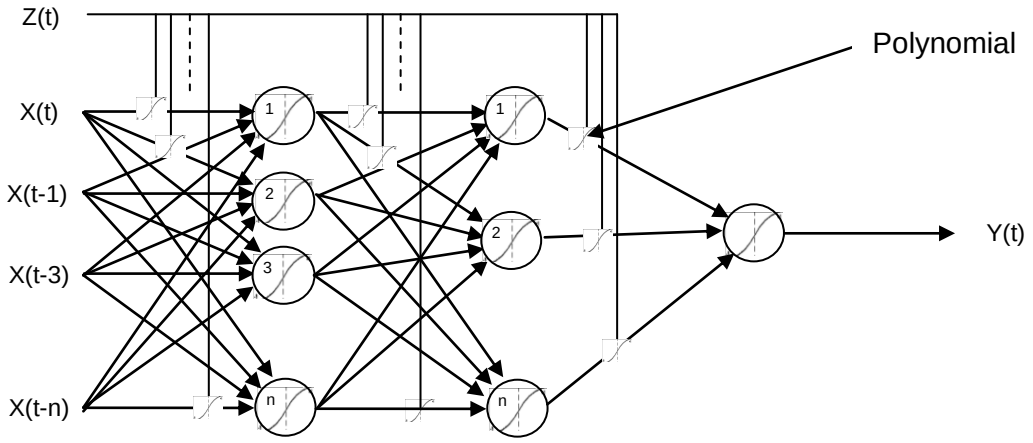

Figure 8.18: Illustration of a Non-Autonomous Neural Network, where Z is the additional input.

The solution is to use a polynomial to describe each speed-dependent function. The use of a polynomial has one distinct advantage; it can be described simply by a series of coefficients. This has two benefits. First, the physical size of the model (number of weights and biases) can be reduced significantly when comparing to the multiple ANN method. Second, the use of coefficients still allows for, with some adaption, the use of numerical optimisation techniques for training the ANN i.e. Levenberg-Marquardt algorithm. The class of polynomial selected for this application was the Chebyshev polynomials. These are used extensively as an approximation to a least-squares-fit, and have proven to be robust. Below is the equation for the definition of the Chebyshev polynomial of the first kind, Z_c, and the first 5 Chebyshev polynomials:

$$F(t) = \sum_{c=0}^{C} C_c \cdot Z_c(t) \tag{8.1}$$

and

$$Z_0(t) = 1, \quad Z_1(t) = t, \quad Z_2(t) = 2t^2 - 1 \tag{8.2}$$
$$Z_3(t) = 4t^3 - 3t, \quad Z_4(t) = 8t^4 - 8t^2 + 1,$$
$$Z_5(t) = 16t^5 - 20t^3 + 5t$$

where $F(t)$ is the result of the function, C_c is the coefficients and $Z_c(t)$ is the Chebyshev polynomials. The Chebyshev polynomial of the first kind to the 5th degree was selected to prevent the NANN becoming too large and taking a significantly long time to train, whilst still retaining the accuracy of the polynomial. As previously stated, it is still possible to train this new ANN architecture using numerical optimisation techniques. The practicality of training the NANN was very much the same as training any of the previous ANNs; it was still trained iteratively using the Levenberg Marquardt algorithm. Previously, the Levenberg-Marquadt algorithm was used to train each weight and bias but this is not possible with the new architecture. Instead, the Levenberg-Marquardt algorithm was used to train the coefficients of the Chebyshev polynomial for each weight and bias and simultaneously trained the NANN. This would significantly increase training time and computational requirements that should guarantee that this new method was fully trained. Sample code for the LMA and a test function for the NANN are given in Appendix B.

Again, the basic method used to test this approach and train the ANNs was the same method used throughout Chapter 8. Crankshaft kinematics was selected and the same processing methodology was used with the new ANN architecture and approach to training. The initial number of neurons, layers and inputs remained the same. The only difference was that instead of each weight and bias being described as single values, they were described by 5 coefficients. The training data selected was transient, and was collected, configured and then ordered randomly to train the NANN in the same way as previously described. With regards to the inputs, the only difference was the additional input used, i.e. the weight and bias functions. This additional input was the mean engine speed, as it was required to be time dependent. Figures 8.18 to 8.25 are selected results for the transient training reconstruction from a NANN.

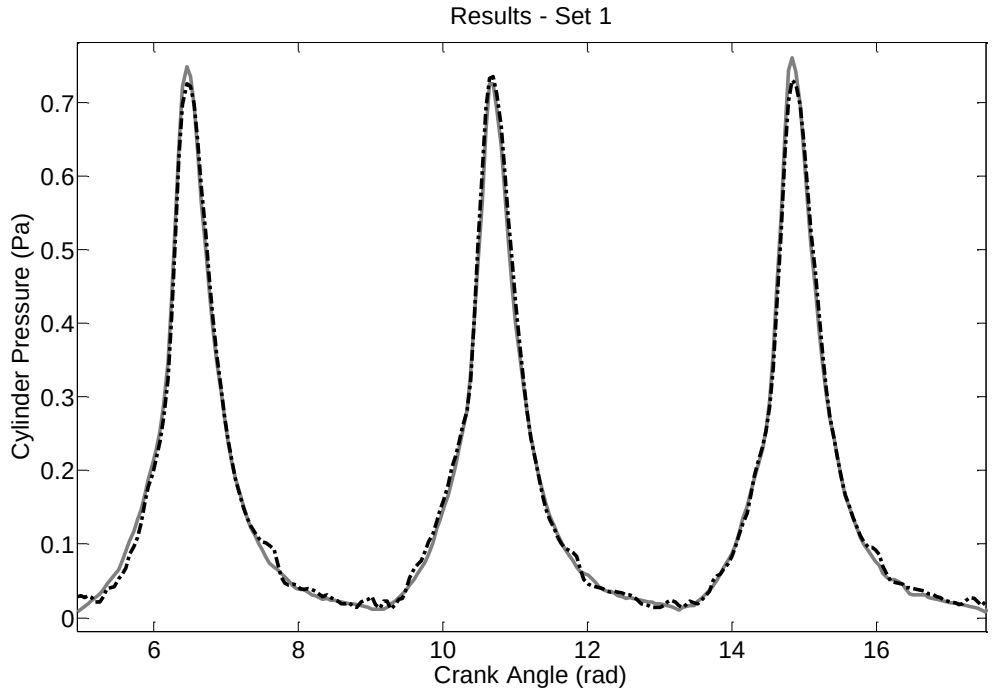

Figure 8.19: Transient Training Results Using NANN. Measured Cylinder Pressure (Grey Solid Line). Reconstructed Cylinder Pressure (Black Dashed Line).

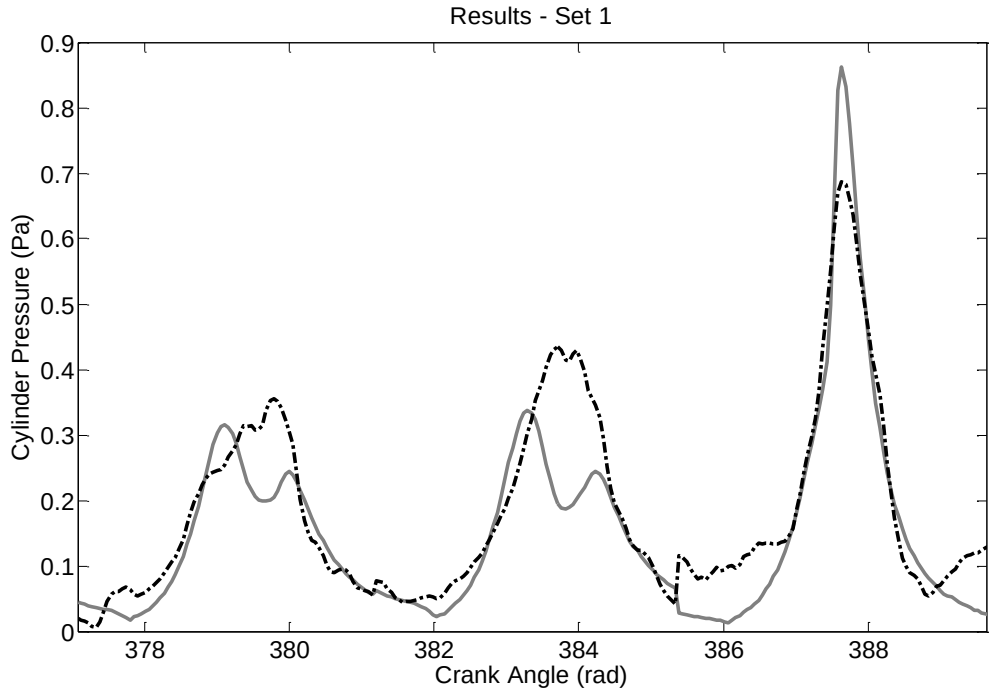

Figure 8.20: Transient Training Results Using NANN. Measured Cylinder Pressure (Grey Solid Line). Reconstructed Cylinder Pressure (Black Dashed Line).

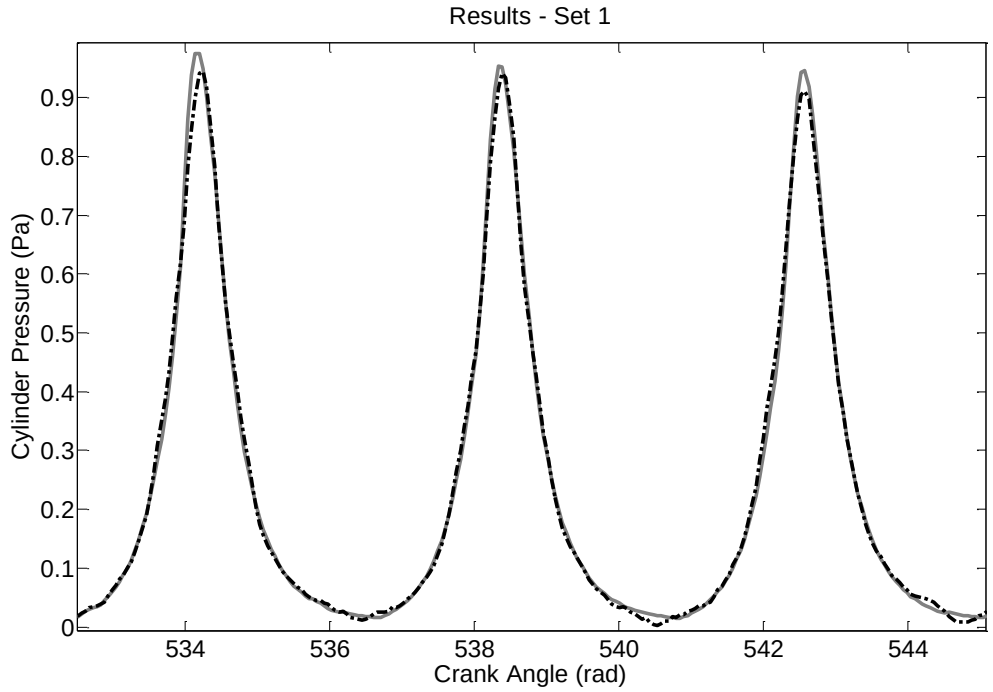

Figure 8.21: Transient Training Results Using NANN. Measured Cylinder Pressure (Grey Solid Line). Reconstructed Cylinder Pressure (Black Dashed Line).

The 3 pressure traces given in Figures 8.19 to 8.21 shows broadly the training results for reconstructing transient cylinder pressure from the NANN. Generally, the results at speeds surrounding 1000 and 2000 rpm are fairly accurate and closely resemble the results presented in Chapter 6. However, the results where the speed variation was significant (overrun) were poorer than the other regions, but the performance was reasonable. Increased training time and training data set size could possibly improve this significantly. This was not undertaken owing to time and computational restrictions.

Even though the results were not ideal, the NANN was still tested on other transient data sets to determine the viability of this approach. Figure 8.22 to 8.25 and table 8.7 show the results for additional transients.

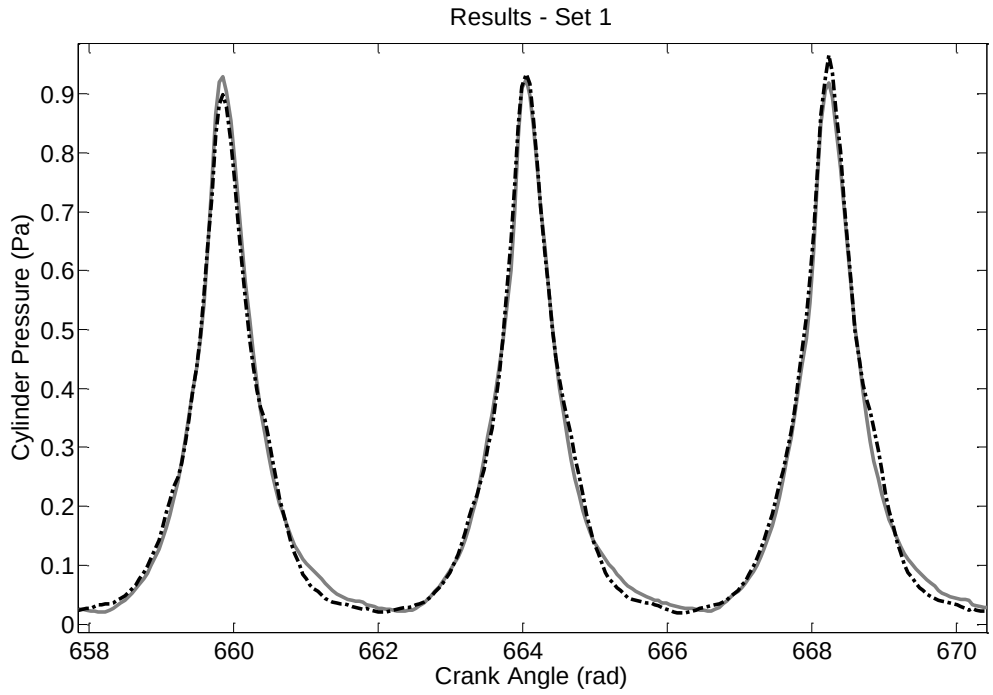

Figure 8.22: Transient Generalisation Results Using NANN. 2000 to 1000 rpm. Measured Cylinder Pressure (Grey Solid Line). Reconstructed Cylinder Pressure (Black Dashed Line).

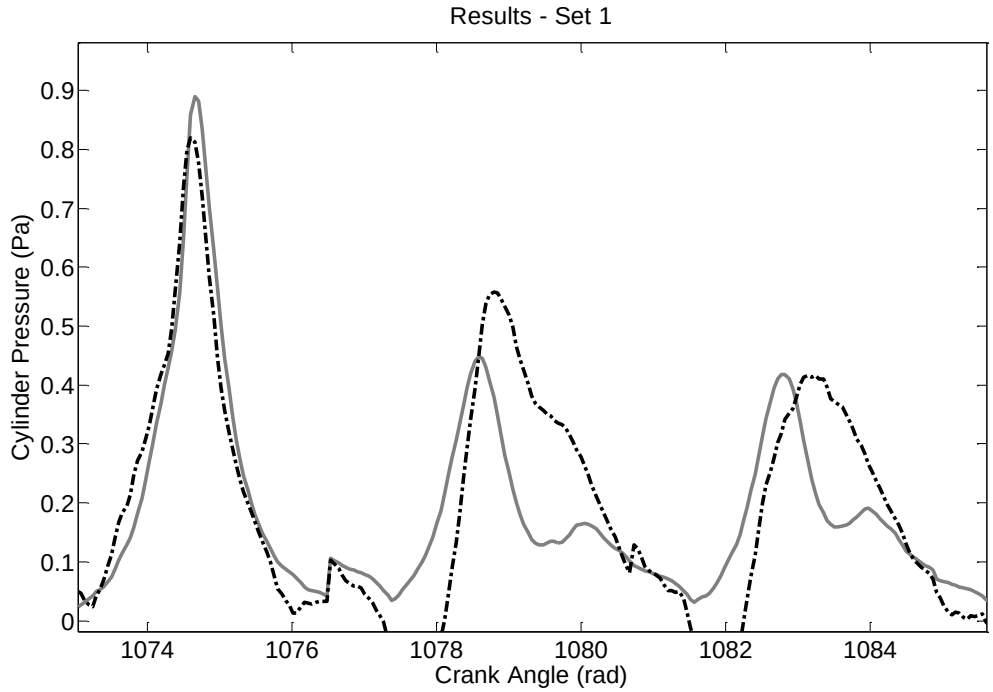

Figure 8.23: Transient Generalisation Results Using NANN. 2000 to 1000 rpm. Measured Cylinder Pressure (Grey Solid Line). Reconstructed Cylinder Pressure (Black Dashed Line).

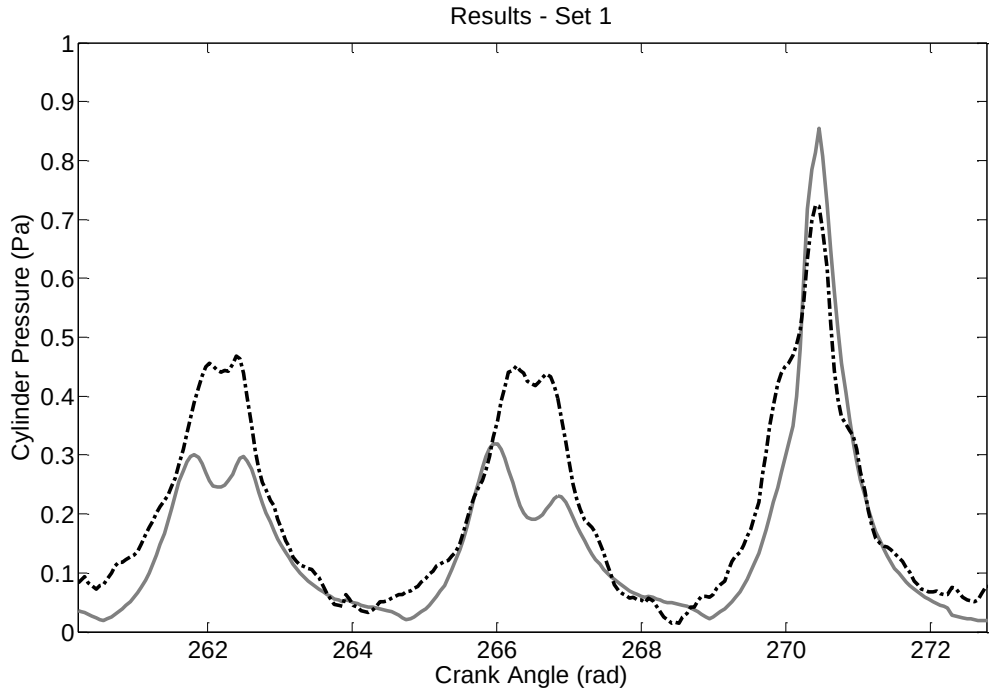

Figure 8.24: Transient Generalisation Results Using NANN. 1000 to 2000 to 1000 rpm. Measured Cylinder Pressure (Grey Solid Line). Reconstructed Cylinder Pressure (Black Dashed Line).

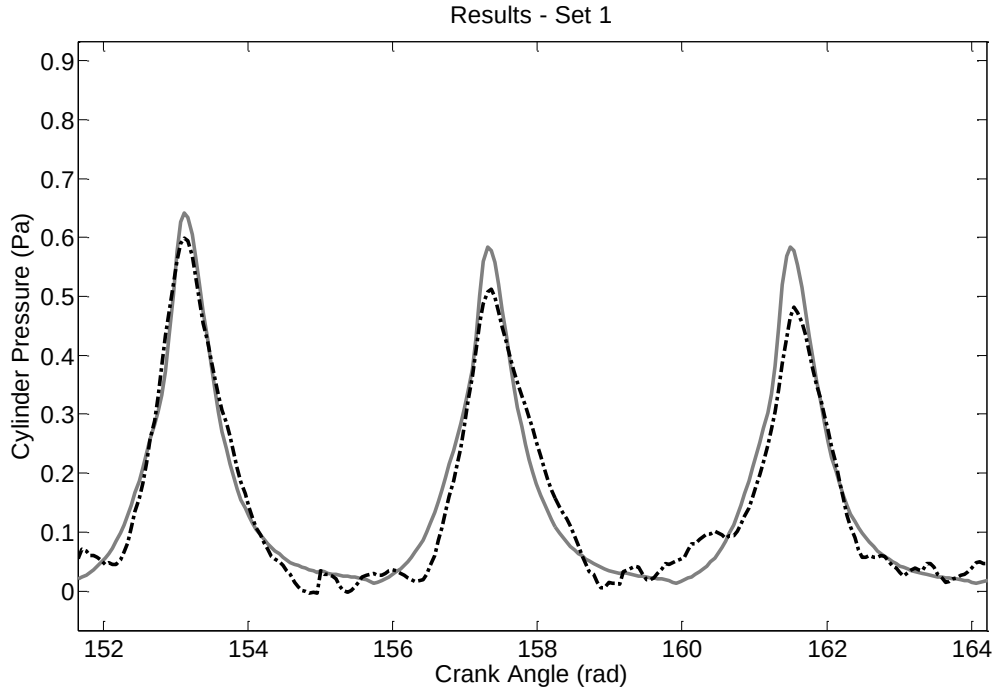

Figure 8.25: Transient Generalisation Results Using NANN. 1000 to 2000 to 1000 rpm. Measured Cylinder Pressure (Grey Solid Line). Reconstructed Cylinder Pressure (Black Dashed Line).

The above results generally show, for both the training and generalised transient reconstruction, more potential than using a single ANN or multiple ANNs in transient specific conditions. Figures 8.22 to 8.25 show that there is reasonable agreement in some regions and better detection of certain combustion characteristics i.e. delayed combustion in Figure 8.24. However, errors are still significant and there are regions where the reconstruction fails, more work is required to improve the accuracy. But most notably, given these types of transient conditions have never been presented to the NANN during training, the network can still identify significantly delayed combustion. in Figure 8.23 The errors most often occurred where transient dynamics were most apparent i.e. overrun. It can also be stated that, generally, the transient reconstruction is still poorer than the results seen when reconstructing steady-state cylinder pressure.

This architecture would allow the weights and biases to vary, as the speed dependent dynamics involved in reconstructing cylinder pressure evolve. From the results gathered, there is reasonable evidence that with more computational power, this approach could prove to be the solution to successfully reconstructing transient cylinder pressure.

Chapter 9

Conclusions

This thesis aimed to develop a robust alternative methodology to reconstruct cylinder pressure through the use of Artificial Neural Networks (ANN) and existing sensors currently fitted to production engines. This methodology reconstructed cylinder pressure from both crank kinematics, via a crank shaft encoder, and cylinder block vibration, via the knock sensor. An aspect that had been overlooked within published literature was the significance the data had in the application. One key idea, reiterated many times in the machine learning literature, is that the successful application is not solely or significantly dependent on the algorithm used, but rather is equally shared in importance between the use of effective algorithms, and the correct use of the data. It is believed that disproportionate weighting had previously been given to the algorithmic approach, over the data, and its use. The underlying theme in this thesis was keeping faithful to the idea that both algorithms and data are equally important for machine learning applications.

Progress was made in the reconstruction of in-cylinder pressure for a 3-cylinder IC production engine under steady-state conditions. This was undertaken primarily with crank kinematics and resulted in the creation of a methodology that overcomes the shortcomings of using recurrent architectures and only past delays. Also, an improvement in the understanding of the cylinder pressure reconstruction, and the limitations in both the previous approaches used.

The initial area examined the quantitative limitations of recurrent neural networks, and alternative, time-delay neural networks, when using crank kinematics. First, this chapter showed by back-to-back comparisons that complex recurrent neural networks were not necessary for the accurate reconstruction of cylinder pressure; a more simple architecture could be used to produce the same level of accuracy. It was also found that through examining both crankshaft kinematics and engine block vibration reconstruction results, key information about the cylinder pressure around

TDC was not present within the training. This missing information was deemed to be a result of several main factors; the variation of the effective radius, the variation in friction at TDC, and more importantly, the dominance of the inertia.

One of the key solutions developed to overcome the problems identified, was a different approach to the ANN input organisation; the use of both future and past delays. This method examined the crankshaft kinematics prior to, and after TDC, which successfully overcame the majority of the issues mentioned. Two additional solutions were found to solve some additional inaccuracies in reconstructing cylinder pressure. These included a less indiscriminate method of filtering crankshaft kinematics in order to ensure that useful information was not eliminated, and creating an ANN for each cylinder to take into account the variability between the different cylinders. The combination of these three solutions into a single methodology, along with the use of a time-delay neural network and Levenberg-Marquardt algorithm, proved to be the solution to overcoming the reconstruction difficulties.

The developed methodology was first tested on the crankshaft kinematics based reconstruction using Time-Delay neural networks and the Levenberg-Marquardt algorithm. The overall results for generalised reconstruction were much improved on previous published results and presented very little evidence of the significant peak pressure errors or the observed instability seen with recurrent networks. These results have also shown that for independent ANNs, trained at different test conditions, the cycle-by-cycle cylinder pressure variability has no effect on the successful cylinder pressure reconstruction. These results validated the use of crank kinematics for reconstructing cylinder pressure, as results were well within target. The targeted cylinder pressure error was 4% consistently for the generalised reconstruction and depending on the test condition, the results ranged between 1.14% and 1.34%. This chapter demonstrated that reconstructing cylinder pressure can be achieved successfully on steady-state data.

The adapted methodology was then tested on the engine block vibration based reconstruction, again using Time-Delay neural networks and the Levenberg-Marquardt algorithm. The results from the reconstruction made similar achievements to the crank kinematics. The overall results for generalised reconstruction were much improved on previous published results using the time-series approach.

However, there was some evidence of the instability and peak pressure errors with the generalised reconstruction results which ranged between 1.32% and 3. 46%. These results have again disproven that for independent ANNs, trained at different test conditions, the cycle-by-cycle cylinder pressure variability has no effect on the successful cylinder pressure reconstruction. The results presented validated the use of engine block vibration for reconstructing cylinder pressure, as the results were within the targeted range for steady-state conditions.

An observation was also made when comparing the crank kinematics and engine block vibration results. The crank kinematic results accurately reconstructed the magnitude of the peak pressure, whereas the engine block vibration accurately reconstructed the position of the maximum pressure. Crankshaft kinematics most significant limitation, when reconstructing, is a combination of cranktrain inertial dominance and a reduction in the information content surrounding TDC. To actually reconstruct cylinder pressure, it was necessary to use a combination of future and past inputs. This provided information directly relating to the energy imparted to the cranktrain and allowed accurate reconstruction of the pressure magnitude. However, owing to the lack of information surrounding TDC, pinpointing the position of peak pressure was more difficult. But there was no information loss with engine block vibrations; in fact the opposite is true; the accuracy in the position of peak pressure is good. However, the engine block vibration peak pressure reconstruction accuracy is poorer because of an increase in noise. To accurately reconstruct both the magnitude and position of peak pressure, a combination of the two approaches may be required.

The final focus was on creating a methodology for reconstructing cylinder pressure during transient engine operation, using crank kinematics. Three different approaches were examined; the first used a single ANN which was trained on multiple steady-state conditions across a given range and then tested on a simple transient: a speed ramp. It was found that, when reconstructing on either the same generalised steady-state conditions or on transient conditions, there was a significant difference in the performance when speed increased. By suitable testing, the load variation was dismissed as the cause of the problem. The performance at mid to high speed (1500 to 2000 rpm) conditions was good, and comparable with the individually-trained ANNs presented. However, at low speed, there were significant issues in reconstructing cylinder pressure accurately. It was reasoned

that there are two possible explanations: that the inherently-similar training data may result in an ANN favouring the higher speed conditions, or the time-dependent features could change significantly with speed. The second approach attempted to resolve the issue of the biasing of the training and time dependence, by using multiple ANNs. Each ANN was trained on a different pair of adjacent conditions with a 100 rpm interval. The results for both the steady-state reconstruction and the transient speed ramp were improved. However, the overall performance of the transient reconstruction was not sufficiently accurate, especially in the transient specific regions. The direction taken from the first approach to the second, in creating ANNs that vary with speed, showed some, but not enough, improvement. Therefore, a new approach was developed, continuing further in this direction including the development of a new ANN architecture. This new architecture was a continuously variable ANN, where the weights and biases are time dependent; called a Non-Autonomous Neural Network (NANN). Each weight and bias would be represented by a Chebyshev polynomial, where it would vary with the speed instead of a constant value. Using a polynomial allows the Levenberg-Marquadt algorithm to be used, with minor alterations. This architecture allows the weights and biases to vary as the speed dependent dynamics involved in reconstructing cylinder pressure vary. From the results gathered, there is reasonable evidence that, with time and significant computational power, this could offer a solution to successfully reconstructing transient cylinder pressure.

To summarise, this thesis has demonstrated that the key to reconstructing cylinder pressure does not lie in the complexity of the ANN architecture or training algorithm, as previously believed. Rather it lies in understanding the importance that the input data and the development of a methodology that is sufficiently robust. It has been verified that by using a combination of future and past inputs, more targeted filtering, and reconstructing for individual cylinders, it is possible to successfully reconstruct cylinder pressure from both crank kinematics and engine block vibrations. The thesis also demonstrates several possible methods for reconstructing cylinder pressure in transient conditions and has developed a new ANN architecture which shows significant promise.

Future Work

There are several key aspects that need to be examined in future work to help advance this technology.

- With respect to crankshaft kinematic based reconstruction, the accuracy seen in this thesis was greater than expected and it is believed that there is little room for improvement in steady-state. However, to make the methodology more desirable, further work will be needed to explore the use of a less accurate and lower resolution crank encoder, similar to production encoders, and achieving comparable reconstruction accuracy.

- With respect to engine block vibration based reconstruction, similar to the use of crankshaft kinematics, the results were better than expected. More work could be put into the use of production specification sensors and a more indiscriminate method of filtering would be required to improve the accuracy of the reconstruction.

- One of the most significant areas for further work is refining the reconstruction under transient conditions. Whether the methodology developed in this thesis is used or another one is created, the key to reconstructing transient conditions is, in significantly increasing the amount of training data used. As a result, the computational needs would be increased and a system would need to be created to manage this with the possible addition of a live demonstrator to prove reconstruction accuracy in real time.

- As two independent methods are now available for steady-state engine conditions, and the prospect looks promising for transient conditions, work can commence with the creation of a fully adaptive methodology to reconstruct and to account for engine wear, significant changes in operating conditions and different fuels.

References

Abu-Nada, EE., Al-Hinti, II., Al-Sarkhi AA., & Akash, BB. 2008. Effect of Piston Friction on the Performance of SI Engine: A New Thermodynamic Approach. ASME.J. Eng. Gas Turbines Power

Bennett, C. 2014. Reconstruction of Gasoline Engine In-Cylinder Pressure using Recurrent Neural Networks. Ph.D. Thesis. University of Sussex: U.K.

Bizon, K., Continillo, G., Mancaruso, E., & Vaglieco, B.M. 2011. Reconstruction of in-cylinder pressure in a diesel engine from vibration signal using ARBF neural network models. SAE International, (2011-24-0161)

Cybenko, G. 1989. Approximation by Superpositions of a Sigmoidal Function. Math. Control Signals Systems 2 . pp.303-314

Eberhart, R. & Kennedy, J. 1995. A new optimizer using particle swarm theory. IEEE Proceedings of the Sixth International Symposium on Micro Machine and Human Science. pp. 39-43

Grasso, A.D., Pennisi, S., Paparo, M. & Patti, D. 2013. Estimation of in-cylinder pressure using spark plug discharge current measurements. European Conference on Circuit Theory and Design (ECCTD) . pp. 1 - 4

Gu, F., Jacob, P.J & Ball, A.D. 1996. A RBF neural network model for cylinder pressure reconstruction in internal combustion engines. IEE Colloquium on Modeling and Signal Processing for Fault Diagnosis No.260 pp.4/1 - 4/11

Gu, F., Jacob, P.J & Ball, A.D. 1999. Non-Parametric models in the monitoring of engine performance and condition. Part 2: Non-intrusive estimation of diesel engine cylinder pressure and its use in fault detection". Proc. Instn Mech. Engrs Part D of Journal of Automotive Engineering Vol. 213, No. D3, pp. 135-143.

Hajderi, A. & Hajdari, V. 2012. Case Study on Determination of Inertia Moments of Details with Complex Shapes. International Journal of Basic & Applied Sciences IJBAS-IJENS Vol:12 No:06.

Hamedovic, H., Raichle, F., Breuninger, J., Ficher, W., Dieterle, W., Klenk, M. & Böhme, J.F. 2005. IMEP-estimation and in-cylinder pressure reconstruction for multicylinder SI-engine by combined processing of engine speed and one cylinder pressure. SAE International, (2005-01-0053)

Haykin, S. 2008. Neural Networks and Learning Machines (Third Edition), Prentice Hall

Heywood, J.B. 2010. Internal Combustion Engine Fundamentals. McGraw-Hill

Huang, G., Huang, G.B., Song, S. & You, K. 2015. Trends in extreme learning machines: A review. Neural Networks 61. pp. 32–48

IC engine energy, 2005. Illustration, viewed 28 May 2015.
<http://www.greencarcongress.com/2005/02/doe_cofunds_12_.html>

Jacob, P.J., Gu, F. & Ball, A.D. 1999. Non-Parametric models in the monitoring of engine performance and condition. Part 1: modelling of non-linear engine processes". Proc. Instn Mech. Engrs Part D of Journal of Automotive Engineering Vol. 213, No. D1, pp. 73-81.

Johnsson, R.. 2006. Culinder pressure reconstruction based on complex radial basis function networks from vibration and speed signals. Mechanical Systems and Signal Processing. Vol. 20 pp. 1923–1940

Kolbeck, A. 2011. Closed loop combustion control - Enabler of future refined engine performance regarding power, efficiency, emissions & NVH under stringent governmental regulation. SAE International, (2011-24-0171)

Kopeliovich, D. [no date]. Engine Bearings and how they work. Viewed 26 May 2015.
<http://kingbearings.com/files/Engine_Bearings_and_How_They_Work.pdf>

Larsson, S. & Schagerberg, S. 2004. SI-Engine Cylinder Pressure Estimation using Torque Sensor, SAE Paper No. 2004-01-1369

Lawrence, S., Back, A.D., Tsoi, A.C, Giles, C.L. 1997. On the Distribution of Performance from Multiple Neural Network Trials, IEEE Transactions on Neural Networks, Volume 8, Number 6, pp. 1507–1517.

Lee, C.E & Taylor, H.F. 1998. A fiber-optic pressure sensor for internal combustion engines. Sensors, Vol. 15, pp.20

Lim, B., Lim, I., Park, J., Son, Y. et al., 1994. Estimation of the Cylinder Pressure in a SI Engine Using the Variation of Crankshaft Speed," SAE Technical Paper 940145.

Mocanu, F & Taraza, D. 2013. Estimation of main combustion parameters from the measured instantaneous crankshaft speed. SAE International, (2013-01-0326)

Nysæther, J.B., Larsen, A. Liverød, B. & Ohlckers, P. 1998. Measurement of package-induced stress and thermal zero shift in transfer molded silicon piezoresistive pressure sensors. J. Micromech. Microeng. Vol. 8, pp. 168

Ideal Otto Cycle, n.d. Illustration, viewed 18 March 2015, <http://ffden-2.phys.uaf.edu/webproj/212_spring_2014/Keanu_Paikai/Keanu_Paikai_2/OttoCycle_2.html >.

Potenza, R. 2006. Engine Cylinder Pressure Reconstruction using Neural Networks and Crank Kinematics. Ph.D. Thesis. University of Sussex: U.K.

Potenza, R., Dunne, J.F., Vulli, S., RIchardson, D & King, P. 2007. Multicylinder engine pressure reconstruction using NARX neural networks and crank kinematics. International Journal of Engine Research, Vol. 8 (6). pp. 499-518.

Rackmil, C & McKay, D. 2010. Sensor-less individual cylinder pressure estimation and closed loop combustion control for cold starts and torque balancing. SAE International, (2010-01-1269)

Rakopoulos, C.D. Giakoumis, E.G. & Dimaratos, A.M. 2007. Evaluation of various dynamic issues during transient operation of turbocharged diesel engine with special reference to friction development, SAE Paper No. 2007-01-0136

Ranjbarkohan, M., Rasekh, M., Hoseini, A., Kheiralipour, K., & Asadi, M. 2011. Kinematics and kinetic analysis of the slider-crank mechanism in otto linear four cylinder Z24 engine. Journal of Mechanical Engineering Research Vol. 3(3), pp. 85-95.

Rivara, N., Dickinson, P.B. & Shenton, A.T. 2009. A transient virtual-AFR sensor using the in-cylinder ion current signal. Mechanical Systems and Signal Processing. Vol. 23 pp. 1672–1682

Rizzoni, G, 1989. Estimate of indicated torque from crankshaft speed fluctuations: a model for the dynamics of the IC engine. IEEE Transactions on Vehicular Technology, Vol. 38

Saraswati, S & Chand, S. 2010. Reconstruction of cylinder pressure for SI engine using recurrent neural network. Neural Comput & Applic

Scott, R. n.d Illustration, viewed 28 May 2015.Shaft Motion during Start-up.
< http://www.machinerylubrication.com/Read/779/journal-bearing-lubrication>

Shadloo, M.S., Poultangari, R., Abdollahzadeh Jamalabadi, M.Y. &. Rashidi, M.M. 2015. A new and efficient mechanism for spark ignition engines. Energy Conversion and Management 96 (2015) 418–429

Shiao, Y. and Moskwa, J., 1994. Misfire Detection and Cylinder Pressure Reconstruction for SI Engines, SAE Technical Paper 940144.

Song, Q., Wu, Y. & Soh, Y. 2008. Robust Adaptive Gradient-Descent Training Algorithm for Recurrent Neural Networks in Discrete Time Domain. IEEE TRANSACTIONS ON NEURAL NETWORKS, VOL. 19, NO. 11

Saraswati, S & Chand, S. 2010. Reconstruction of cylinder pressure for SI engine using recurrent neural network. Neural Comput & Applic

Taglialatela, F. Lavorgna, M. Mancaruso, E.& Vaglieco, B.M. 2013. Determination of combustion parameters using engine crankshaft speed. Mechanical Systems and Signal Processing. Vol. 38 pp. 628–63

The Human Neuron, 2013. Illustration, viewed 18 May 2015, < https://commons.wikimedia.org/wiki/File:Blausen_0657_MultipolarNeuron.png>.

Villarino, R. & Böhme, J.F. 2003. Fast in-cylinder pressure reconstruction from structure-born sound using the EM algorithm. IEEE International Conference on Acoustics, Speech, and Signal Processing. Vol.6. pp. VI-597-600.

Vulli, S. 2006. Engine Cylinder Pressure Reconstruction using Neural Networks and Knock Sensor Measurements. Ph.D. Thesis. University of Sussex: U.K.

Weißenborn, E., Bossmeyer, T. & Bertram, T. 2011. Adaptation of a zero-dimensional cylinder pressure model for diesel engines using the crankshaft rotational speed. Mechanical Systems and Signal Processing 25 (2011) 1887–1910.

Yong, X., Guiyou, H., Chanrong, S., Zhibing, N., and Wu, Z. 2010. Reconstruction of cylinder pressure of I.C. engine based on neural network. IEEE First national conference on persuasive computing, signal processing and applications. pp. 924 - 927

Zhang, J.C., Zhang, J., Lok, T, & Lyu, M. 2007. A hybrid particle swarm optimization–back-propagation algorithm for feedforward neural network training. Applied Mathematics and Computation 185. pp. 1026–1037

Zhao, C., Cheng, Y., and Wang, L. 2014. Pattern recognition method applied to extract in-cylinder pressure excitation a response from measured vibration signals. SAE Technical Paper. 2014-01-2703

Appendix A

Connecting Rod Inertial Torque Calculations

$$d = \mathrm{r}\cos\theta + x\cos\Phi \tag{A.1}$$

$$d_{Piston} = \mathrm{r}\cos\theta + x\sqrt{1-\left(\frac{r\sin\theta}{l}-\frac{\mathrm{os}}{l}\right)^2} \tag{A.2}$$

$$\dot{d}_{Piston} = \omega\left(\frac{r\,x\cos\theta\left(\frac{os}{l}-\frac{r\sin\theta}{l}\right)}{l\sqrt{1-\left(\frac{os}{l}-\frac{r\sin\theta}{l}\right)^2}} - r\,\sin\theta\right) \tag{A.3}$$

$$\ddot{d}_{Piston} = r\omega^2\left(-\cos\theta - \frac{x\,r\cos^2\theta\left(\frac{os}{l}-\frac{r\sin\theta}{l}\right)^2}{l\left(1-\left(\frac{os}{l}-\frac{r\sin\theta}{l}\right)^2\right)^{3/2}} - \frac{x\sin\theta(os-r\sin\theta)-r\cos^2\theta}{l\left(1-\left(\frac{os}{l}-\frac{r\sin\theta}{l}\right)^2\right)^{1/2}}\right) \tag{A.4}$$

$$F_c = m_{Piston}\cdot\ddot{d}_{conrod} - m_{conrod}\cdot g \tag{A.5}$$

$$F_T = F_C\sin(\theta+\Phi) \tag{A.6}$$

$$T_{r-r} = r\left(\frac{\cos\theta\left(\frac{\mathrm{r}\sin\theta}{l}-\frac{os}{l}\right)}{\sqrt{1-\left(\frac{\mathrm{os}}{l}-\frac{r\sin\theta}{l}\right)^2}}+\sin\theta\right)\cdot\left[m_{conrod}r\omega^2\left(-\cos\theta-\frac{x\,\mathrm{r}\cos^2\theta\left(\frac{\mathrm{os}}{l}-\frac{r\sin\theta}{l}\right)^2}{l\left(1-\left(\frac{\mathrm{os}}{l}-\frac{r\sin\theta}{l}\right)^2\right)^{3/2}}-\frac{x\sin\theta(\mathrm{os}-r\sin\theta)-\mathrm{r}\cos^2\theta}{l\left(1-\left(\frac{\mathrm{os}}{l}-\frac{r\sin\theta}{l}\right)^2\right)^{1/2}}\right)-m_{conrod}\cdot g\right] \tag{A.7}$$

Friction model equations - (Kamil et al., 2013)

Crankshaft friction:

$$FMEP_{cr} = c_b \sqrt{\frac{\mu}{\mu_0}} \left(\frac{N D_b^3 L_b n_b}{B^2 L n_c} \right) + c_s \left(\frac{D_b}{B^2 L n_c} \right) + 1.35 \times 10^{-10} \left(\frac{N^2 D_b^2 L_b n_b}{n_c} \right) \quad (A.8)$$

D_b	Bearing diameter	n_b	Number of bearings	B	Cylinder bore
μ	Oil viscosity	n_c	Number of cylinders	c_b	Main journal bearing constant
μ_0	Reference viscosity	L	Engine stroke	c_s	Main journal bearing with seal constant
L_b	bearing length	N	Engine speed		

Reciprocating friction:

$$FMEP_{recip} = c_{ps} \sqrt{\frac{\mu}{\mu_0}} \left(\frac{\bar{S}_p}{B} \right) + c_{pr} \left(1 + \frac{500}{N} \right) \left(\frac{1}{B^2} \right) + 3.03 \times 10^{-4} \sqrt{\frac{\mu}{\mu_0}} \left(\frac{N^2 D_b^3 L_b n_b}{B^2 L n_c} \right) \quad (A.9)$$

$\bar{S}_p$	Mean piston speed	c_{ps}	Piston friction constant	c_{ps}	Piston rings constant

Valvetrain friction:

$$FMEP_{vt} = 244 \sqrt{\frac{\mu}{\mu_0}} \left(\frac{N n_b}{B^2 L n_c} \right) + 4.12 + C_{ff} \left(1 + \frac{500}{N} \right) \left(\frac{n_v}{L n_c} \right) + C_{rf} \left(\frac{N n_v}{L n_c} \right) + C_{oh} \sqrt{\frac{\mu}{\mu_0}} \left(\frac{l_{vmax}^{1.5} N^{0.5} n_b}{B L n_c} \right) + C_{om} \left(1 + \frac{500}{N} \right) \left(\frac{l_{vmax} n_v}{L n_c} \right) \quad (A.10)$$

n_v	Number of valves	c_{ps}	Peak valve lift

The constants C_{ff}, C_{rf}, C_{oh} and C_{om} in the valvetrain term in equation (A.10) are dependent of the valvetrain configuration being considered in the model.

Table A.1: Constants for Valvetrain Friction Terms (Kamil et al., 2013)

Configuration	Type	Flat Follower C_{ff} (KPa-mm)	Roller Follower C_{rf} (KPa-mm-min/rev)	Oscillating Hydrodynamic C_{oh} (KPa-mm-min/rev)$^{1/2}$	Oscillating Mixed C_{om} (KPa)
Single overhead cam (SOHC)	I	200	0.0076	0.5	107
Double overhead cam (DOHC)	I	133	0.0050	0.5	10.7
Single overhead cam (SOHC)	II	600	0.0227	0.2	42.8
Single overhead cam (SOHC)	III	400	0.0151	0.5	21.4
Cam in block (CIB)	IV	400	0.0151	0.5	32.1

Crankshaft moment of inertia calculations

The moment of inertia of the crankshaft, I_g, can found through the summation of the individual inertias:

$$I_g = I_{qk} + I_{qb} + 2I_f + I_{kp} \qquad (A.12)$$

Where I_{qk}represents the moment of inertia of the main journal:

$$I_{qk} = \rho \frac{\pi}{32}(D_1^4 - d_1^4)l_1 \qquad (A.13)$$

I_{qb} represents the moment of inertia of the crankpin to main journal:

$$I_{qb} = \rho\left[\frac{\pi}{32}(D_k^4 - d_k^4)l_k + \frac{\pi}{4}(D_k^2 - d_k^2)l_k R^2 + \frac{\pi}{32}d_k^4(l_k - f)\right] \qquad (A.14)$$

$I_f$represents the moment of inertia of crankshaft web:

$$I_f = \rho\left[\frac{2}{3}bhl\left(\frac{h^2 + l^2}{12} + \frac{R^2}{4}\right) - \frac{\pi}{4}b\left(\frac{d_1^2 + d_k^2}{8} + R^2 d_k^2\right)\right] \qquad (A.15)$$

I_{kp} is the moment of inertia of the counterbalance of the crankshaft.

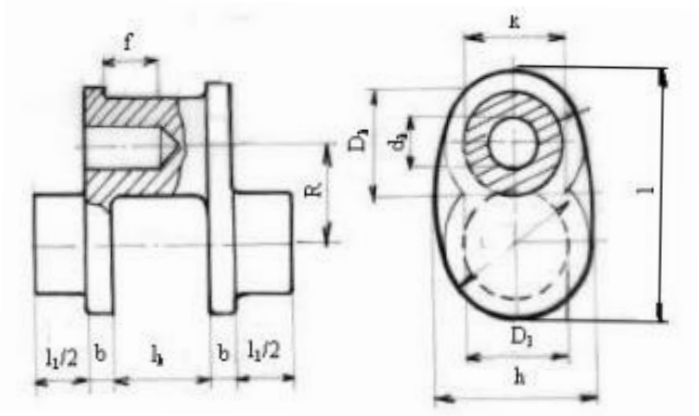

Figure A.2: Illustration of Crankshaft Crank (Hajderi and Hajdari, 2012).

Single cylinder model 1 DOF model - final simplified solution

$$\alpha = \ddot{\theta} = \frac{T_i + T_r + T_L}{J} \tag{A.16}$$

$$\alpha = \left\{ r\left(\frac{-\sigma_1 \cos\theta}{\sigma_2} + \sin\theta\right) \cdot \left[P_G \pi \frac{b^2}{4} - r\omega^2 \left(\frac{x\, l \cos\theta}{x + l} + \frac{\mathrm{r}{\sigma_1}^2 \cos^2\theta}{l^2 \sigma_1\, \sigma_2} + \frac{\mathrm{os}\sin\theta - r}{l^2\, \sigma_2} \right) \cdot (m_{conrod} x + m_{Piston} l) - (m_{Piston} + m_{conrod}) \cdot g \right] - T_L \right\} \cdot J^{-1}$$

$$\sigma_1 = \frac{\mathrm{os}}{l} - \frac{r \sin\theta}{l}\ ,\ \sigma_2 = \sqrt{1 - (\sigma_1)^2} \tag{A.17}$$

Multi-cylinder model (three cylinder) 1 DOF - final simplified solution

$$\alpha = \ddot{\theta} = \frac{\sum_{n=1}^{3} (T_{in} + T_{rn}) + T_L}{J} \tag{A.18}$$

$$\alpha = \left\{ r\left(\frac{-\sigma_1 \cos\theta_1}{\sigma_2} + \sin\theta_1\right) \right.$$
$$\cdot \left[P_{G1}\pi\frac{b^2}{4} - r\omega^2\left(\frac{x\, l\cos\theta_1}{x+l} + \frac{\mathrm{r}{\sigma_1}^2\cos^2\theta_1}{l^2\sigma_1\,\sigma_2} + \frac{\mathrm{os}\sin\theta_1 - r}{l^2\,\sigma_2}\right)\right.$$
$$\left. \cdot (m_{conrod}x + m_{Piston}l) - (m_{Piston} + m_{conrod}) \cdot g \right]$$
$$+ r\left(\frac{-\sigma_1\cos\theta_2}{\sigma_2} + \sin\theta_2\right)$$
$$\cdot \left[P_{G2}\pi\frac{b^2}{4} - r\omega^2\left(\frac{x\, l\cos\theta_2}{x+l} + \frac{\mathrm{r}{\sigma_1}^2\cos^2\theta_2}{l^2\sigma_1\,\sigma_2} + \frac{\mathrm{os}\sin\theta_2 - r}{l^2\,\sigma_2}\right)\right.$$
$$\left. \cdot (m_{conrod}x + m_{Piston}l) - (m_{Piston} + m_{conrod}) \cdot g \right]$$
$$+ r\left(\frac{-\sigma_1\cos\theta_3}{\sigma_2} + \sin\theta_3\right)$$
$$\cdot \left[P_{G3}\pi\frac{b^2}{4} - r\omega^2\left(\frac{x\, l\cos\theta_3}{x+l} + \frac{\mathrm{r}{\sigma_1}^2\cos^2\theta_3}{l^2\sigma_1\,\sigma_2} + \frac{\mathrm{os}\sin\theta_3 - r}{l^2\,\sigma_2}\right)\right.$$
$$\left. \cdot (m_{conrod}x + m_{Piston}l) - (m_{Piston} + m_{conrod}) \cdot g \right] - T_L \Bigg\} \cdot J^{-1}$$

$$\sigma_1 = \frac{\mathrm{os}}{l} - \frac{r\sin\theta_n}{l} \quad \text{where n} = 1,2,3$$
$$\sigma_2 = \sqrt{1 - (\sigma_1)^2}$$

(A.19)

Where n is the cylinder number (1-3)

Appendix B

Sample Levenberg-Marquadt Algorithm (for NANN)

```
clear all, close all, clc

i=240;                                          %Number of Inputs
n=15;                                           %Number of Neurons
k=5;                                            %Chebyshev Degree

siw=n*i*k;                                      %Input Layer Weights
Size
sib=n*k;                                        %Input Layer Bias Size
slw=n*k;                                        %Hidden Layer Weights
                                                    Size
slb=1*k;                                        %Hidden Layer Bias Size

L=siw+sib+slw+slb;                              %Total Weight/Bias Size

I=eye(siw+sib+slw+slb);                         %Identity Matrix
m=0.001;                                        %Mu
d=0.000001;                                     %Constant for Jacbian

l=length(Inputd1);                              %Length/Normalisation
                                                    Constants
l1=min(min(Input1(:,1:l)));
l2=max(max(Input1(:,1:l)-min(min(Input1(:,1:l)))));
l3=min(min(Output1(:,1:l)));
l4=max(max(Output1(:,1:l)-min(min(Output1(:,1:l)))));

x=(Input1(:,l1)-l1)/l2;                         %Input Normalisation
xz=(Input2(:,l1)-l1)/l2;                        %Additional Input
                                                    Normalisation
t=(Output1(:,l1)-l3)/l4;                        %Output Normalisation

x2=xz.^2;                                       %Additional Input
                                                    Constants
x3=xz.^3;
x4=xz.^4;

Wa=randn(L,1);                                  %Weight/Bias
                                                    initialisation
erro=1e10;

for e1=1:100                                    %Epoch Loop

    y11=testnncheb(Wa,x,i,n,xz,k,x2,x3,x4); %Test1 ANN (Chebyshev)
    y1=repmat(y11',1,length(Wa));           %Restructure ANN Results

    parfor b=1:length(Wa)                   %Adjusted Test Using d

        Wa2=Wa;Wa2(b)=Wa2(b)+d;             %Adjusted Weights
        y2(:,b)=testnncheb(Wa2,x,i,n,xz,k,x2,x3,x4); %Tes2t ANN
                                                        (Chebyshev)

    end
```

```
    J=((y1-y2)/d)';                             %Jacobian Matrix
    H=J*J';                                     %Hessian Matrix
    g=J*(y1(:,1)-t');                           %Gradient Vector
    dw=(H + m*I)\g;                             %Weight Adjustments

    Wa=Wa+dw;                                   %Update Weights

    Er=sqrt(mean((y1(:,1)-t').^2));             %RMSE

    if erro>Er                                  %Mu Update
        m=m*5;
    else
        m=m/5;
    end

    erro=Er;

end
```

Sample Test Function (for NANN)

```
function [y ]=testnncheb(wa,x1,i,n,z1,k,x2,x3,x4)

C1=reshape(wa,[k,length(wa)/k])';           %Reshape Weigths
S=size(x1);
for q=1:S(2)                                %Calculation Loop

Wn1(:,1)=C1(:,1)*1 +...                     %Chebyshev degree 1
    C1(:,2)*z1(:,q) +...                    %Chebyshev degree 2
    C1(:,3)*(2*(x2(:,q)) - 1) +...          %Chebyshev degree 3
    C1(:,4)*(4*(x3(:,q)) - 3*z1(:,q)) +...  %Chebyshev degree 4
    C1(:,5)*(8*(x4(:,q)) - 8*(x2(:,q)) + 1);%Chebyshev degree 5

siw=n*i;sib=n;slw=n;slb=1;                  %ANN Weight Organisation
iwn=Wn1(1:siw);
iwn(1:2);
ibn=Wn1(siw+1:siw+sib);
lwn=Wn1(siw+sib+1:siw+sib+slw);
lbn=Wn1(siw+sib+slw+1:siw+sib+slw+slb);
s13n=reshape(iwn,[n,i]);

                                            %ANN Results
y(q)=sum((1./(1+exp(-2*(s13n*x1(:,q) + ibn)))-
1).*lwn(:,1))+lbn(:,1);

end
```

Appendix C

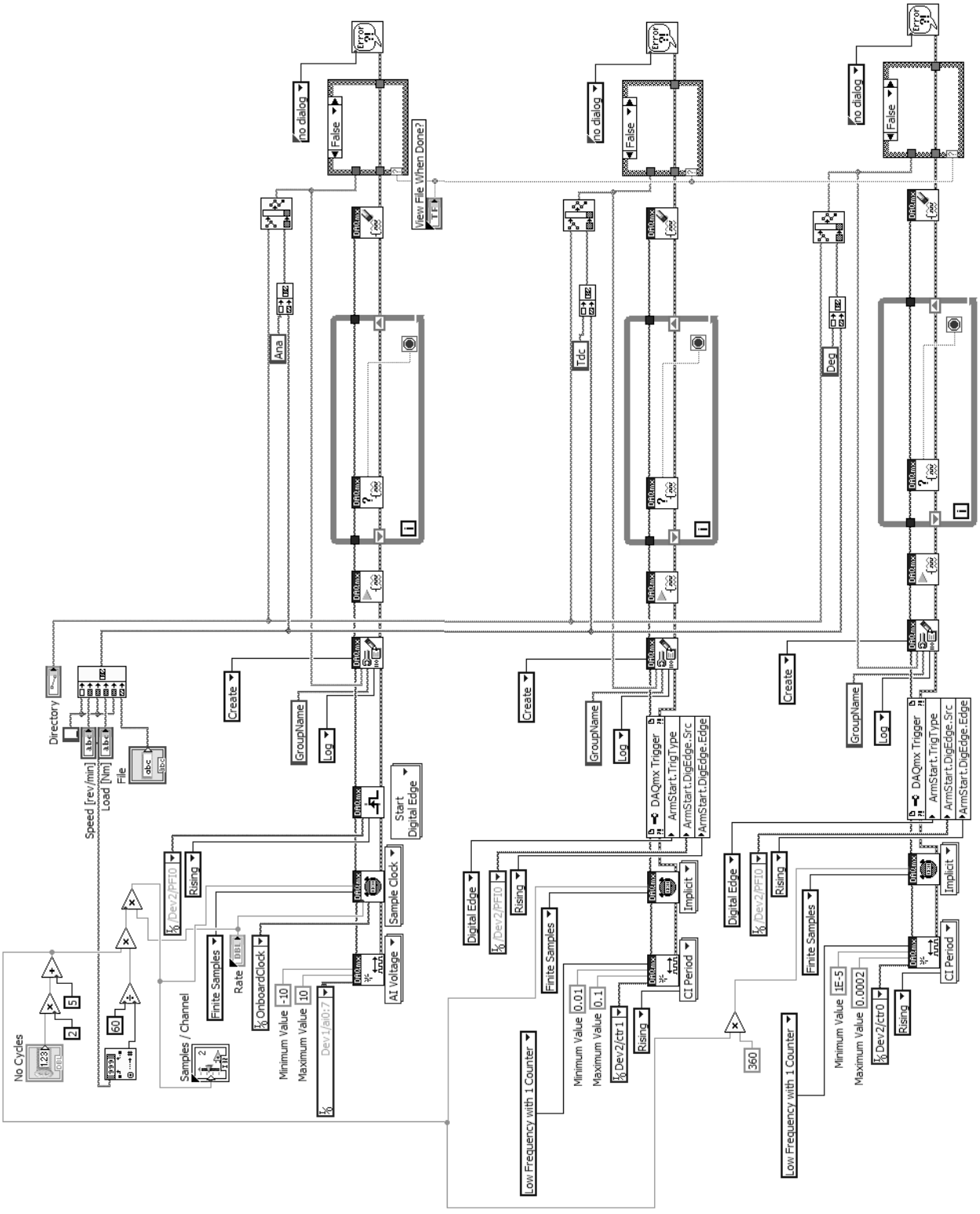

Figure C.1: Large Scale LabVIEW Program for Data Acquisition

Table C.1: Data Acquisitions Analogue Connectivity

Label	Analogue Module	Sensor
1	AI 0	Cylinder-1 Pressure Transducer
2	AI 1	Cylinder-2 Pressure Transducer
3	AI 2	Cylinder-3 Pressure Transducer
4	AI 3	Accelerometer
5	AI 4	Knock Sensor
6	AI 5	Encoder TDC Marker
7	AI 6	Manifold Air Pressure
8	AI 7	Flywheel Inductive Probe

Table C.2: Data Acquisitions Digital Connectivity

Digital Module	Sensor
CTR 0	Encoder 360˚ Position Marker
CTR 1	Encoder TDC Marker

Appendix D

Acceleration Reconstruction Test

The test condition used measured data from running the engine at steady-state with a speed of 1000 rpm and a load of 10 Nm.

Table D1.1: ANN Training Setup for Test Condition-2

Network Name	Net_TD_BA_Test1	**Network Architecture**	Time-Delay	**Test Data**	1000_10_01p_jun2010
Network Training Algorithm	Levenberg–Marquardt	**Hidden Layers Number**	1	**Speed (rpm) / Load (Nm)**	1000/10
Cost Function	Means Squared Error	**Neurons Number**	15	**Training to Validation Ratio**	60:40
Training Goal	1E8	**Delay Number**	60	**Crank Step**	1 Deg
Maximum Epoch	1000	**Transfer Function Layer 1**	Sigmoid	**Number of Iterations**	10
Weights Initialisation	Randomised	**Transfer Function Layer 2**	Linear		

Training Results

In total 10 different ANNs were trained with the overall performance of the ANNs ranging from 2.33% to 2.47% RMSE. The best performing ANN was selected which trained in 1266 seconds (0.35 hours) and 57 epochs.

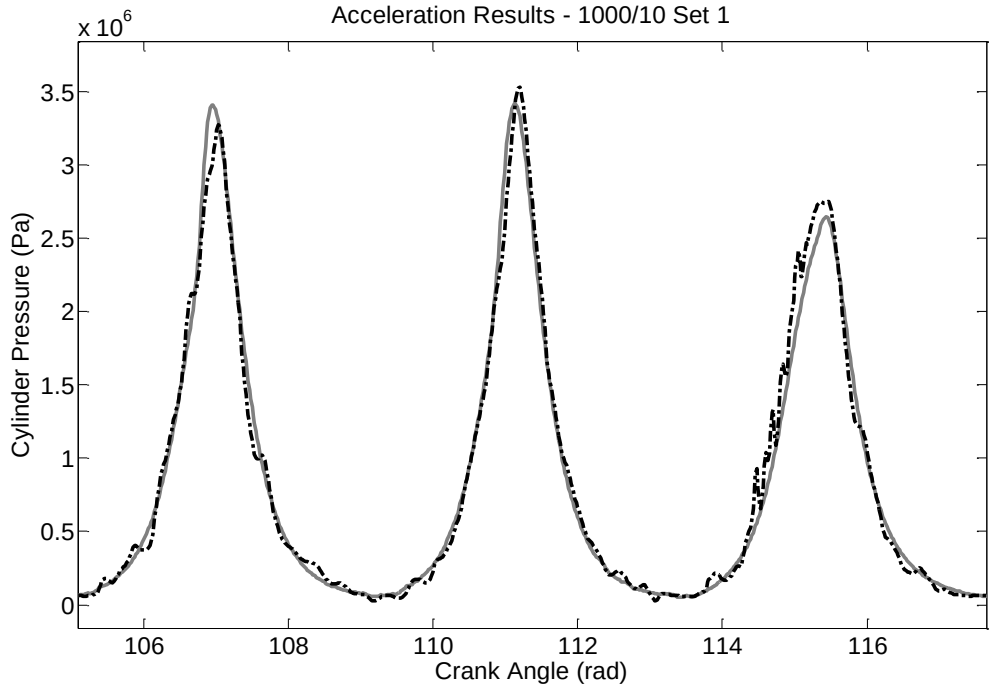

Figure D1.1: Acceleration Training Results. Measured Pressure (Grey Solid Line). Reconstructed Pressure (Black Dashed Line).

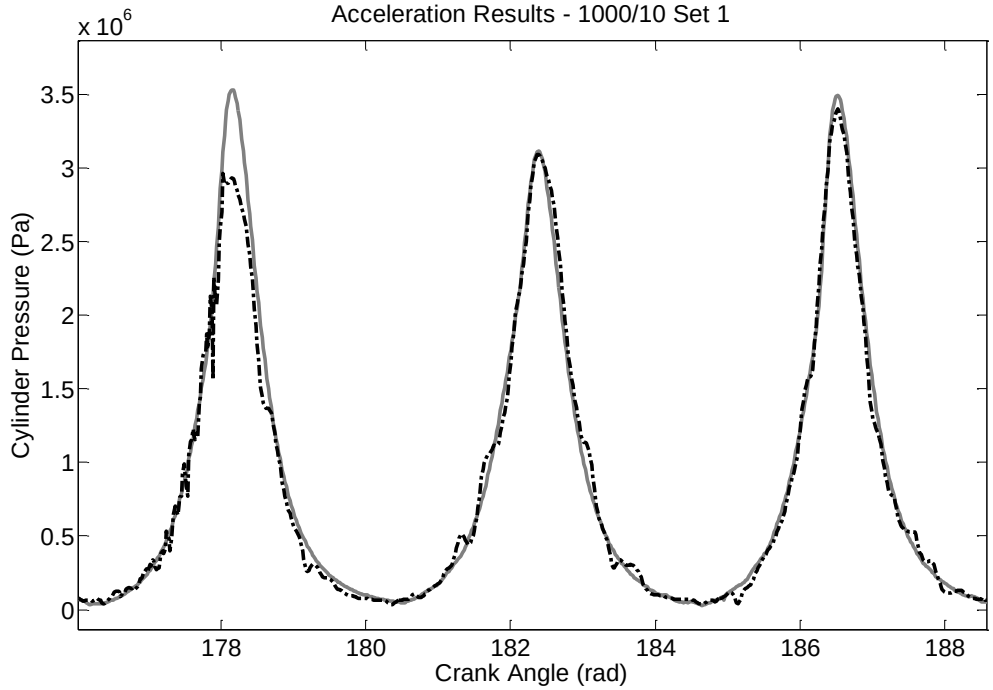

Figure D1.2: Acceleration Training Results. Measured Pressure (Grey Solid Line). Reconstructed Pressure (Black Dashed Line).

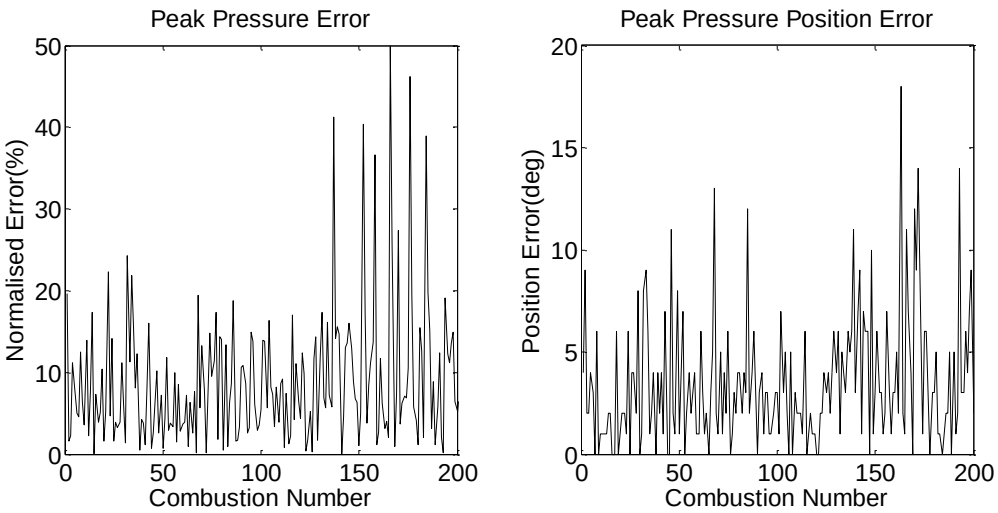

Figure E1.3: Acceleration Normalised Peak Error Training Results (left). Acceleration Position of Peak Error Training Results (right)

Table E1.2: Acceleration Root-Mean-Squared Error (RMSE) and Standard Deviation for the ANN Training

	Training Root-Mean-Squared Error	Training Standard Deviation
Overall Performance	4.58 %	4.58 %
Normalised Peak Error	12.1 %	8.09 %
Peak Pressure Position Error (deg)	5.02	3.37

Generalisation Results

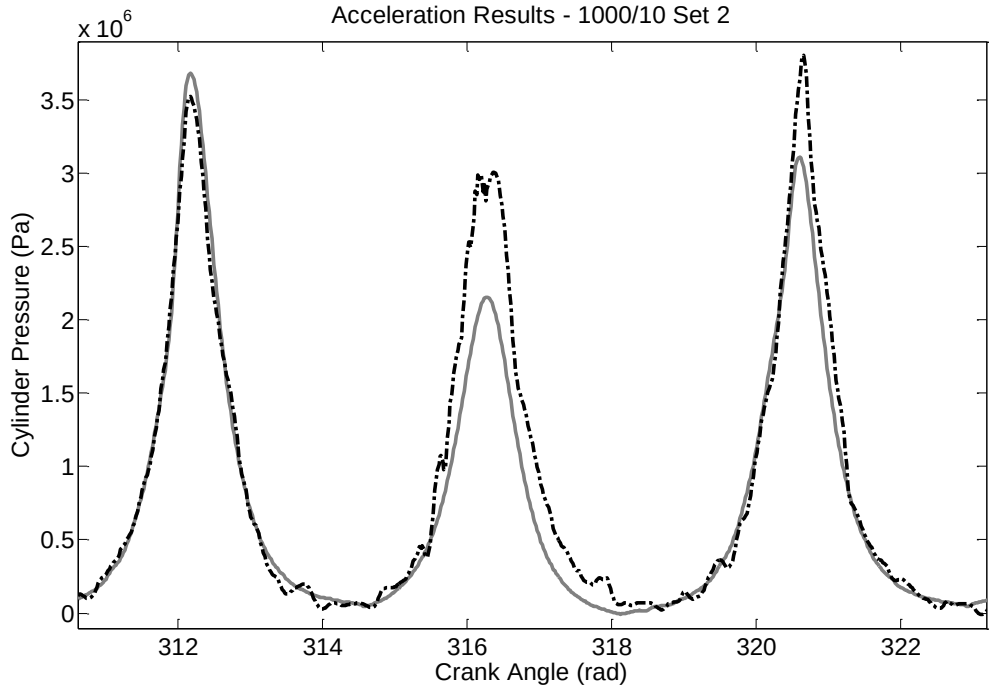

Figure D1.4: Acceleration Generalisation Results. Measured Pressure (Grey Solid Line). Reconstructed Pressure (Black Dashed Line).

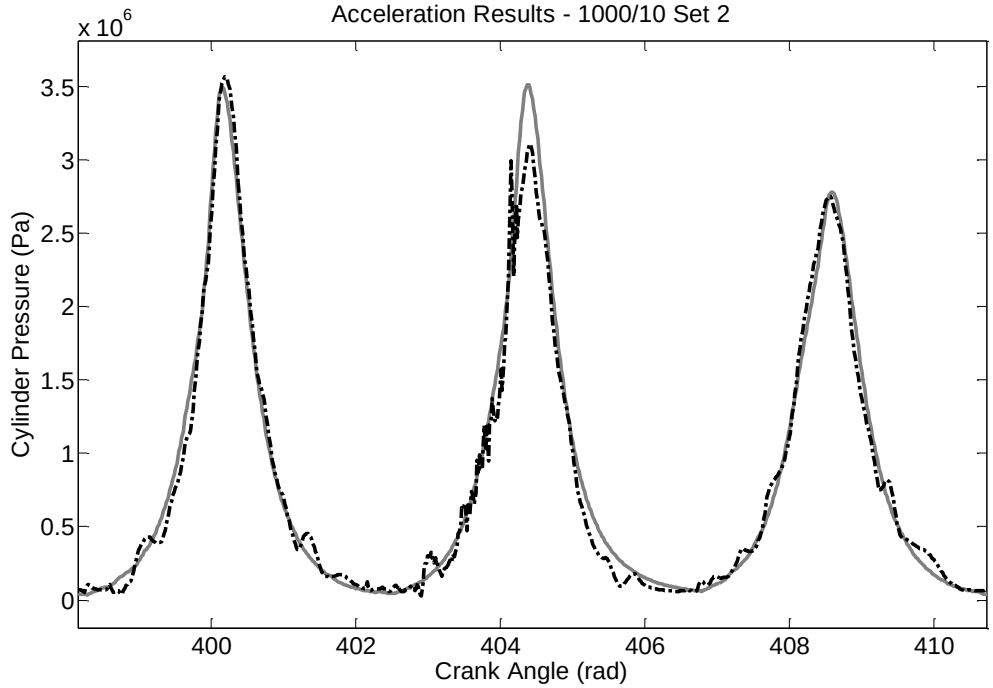

Figure D1.5: Acceleration Generalisation Results. Measured Pressure (Grey Solid Line). Reconstructed Pressure (Black Dashed Line).

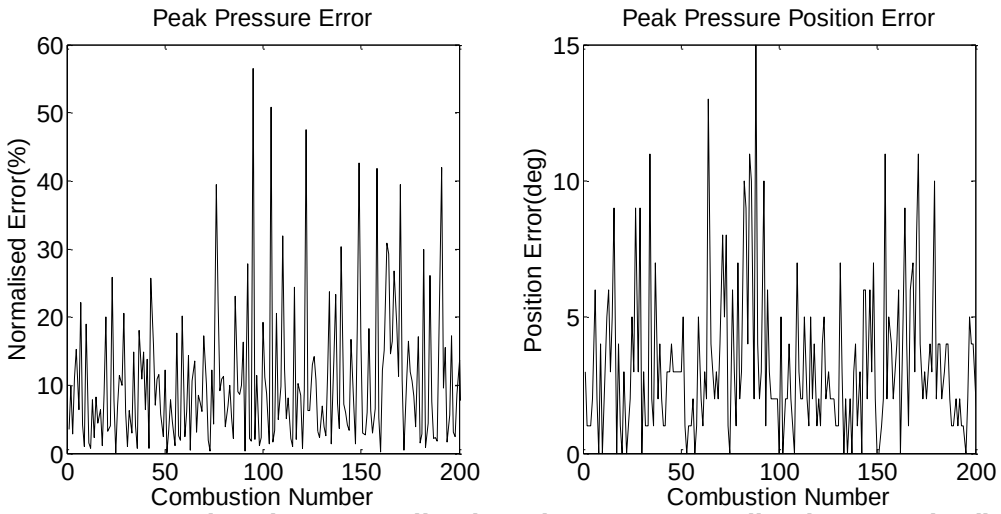

Figure D1.6: Acceleration Normalised Peak Error Generalisation Results (left). Condition-5 Position of Peak Error Generalisation Results (right)

Table E1.3: Acceleration Root-Mean-Squared Error (RMSE) and Standard Deviation for the ANN Generalisation

	Generalisation Root-Mean-Squared Error	Generalisation Standard Deviation
Overall Performance	5.35 %	5.35 %
Normalised Peak Error	14.7 %	10.2 %
Peak Pressure Position Error (deg)	4.42	2.88

Appendix E

Crank Kinematics based Reconstruction Results

Test Condition-2

The first test condition used measured data from running the engine at steady-state with a speed of 1500 rpm and a load of 10 Nm.

Table E1.1: ANN Training Setup for Test Condition-2

Network Name	Net_TD_CK_Test2	**Network Architecture**	Time-Delay	**Test Data**	1500_10_01p_jun2010
Network Training Algorithm	Levenberg–Marquardt	**Hidden Layers Number**	1	**Speed (rpm) / Load (Nm)**	1500/10
Cost Function	Means Squared Error	**Neurons Number**	15	**Training to Validation Ratio**	60:40
Training Goal	1E8	**Delay Number**	240	**Crank Step**	1 Deg
Maximum Epoch	1000	**Transfer Function Layer 1**	Sigmoid	**Number of Iterations**	10
Weights Initialisation	Randomised	**Transfer Function Layer 2**	Linear		

Training Results

In total 10 different ANNs were trained with the overall performance of the ANNs ranging from 1.33% to 1.47% RMSE. The best performing ANN was selected which trained in 1266 seconds (0.35 hours) and 57 epochs.

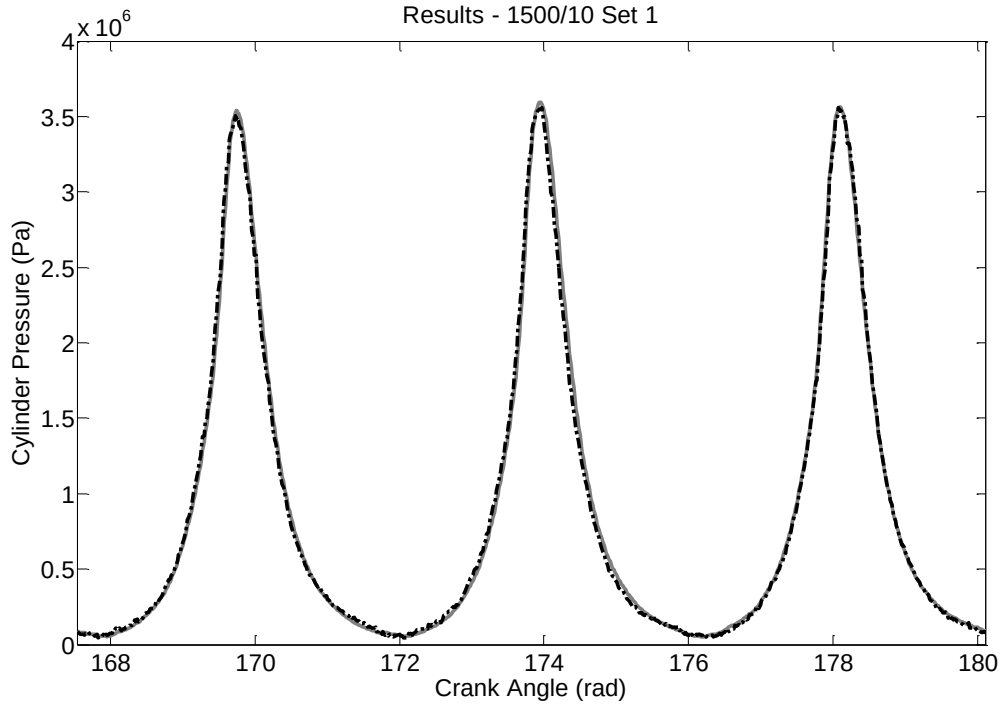

Figure E1.1: Condition-2 Training Results - Best. Measured Cylinder Pressure (Grey Solid Line). Reconstructed Cylinder Pressure (Black Dashed Line). RMSE = 0.82%.

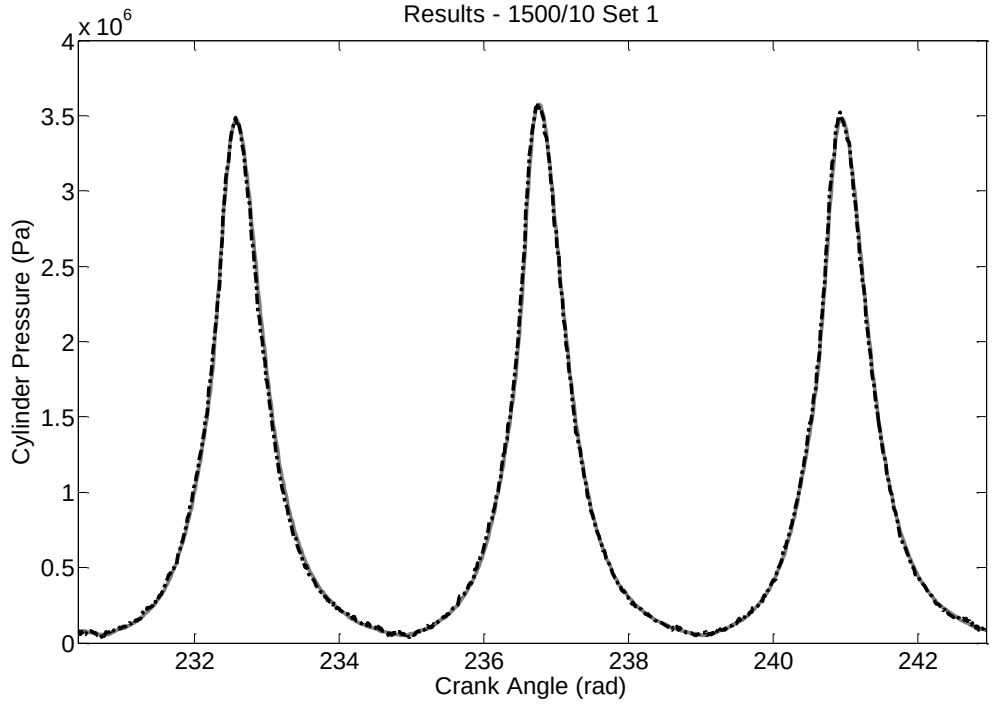

Figure E1.2: Condition-2 Training Results - Average. Measured Cylinder Pressure (Grey Solid Line). Reconstructed Cylinder Pressure (Black Dashed Line). RMSE = 1.02%.

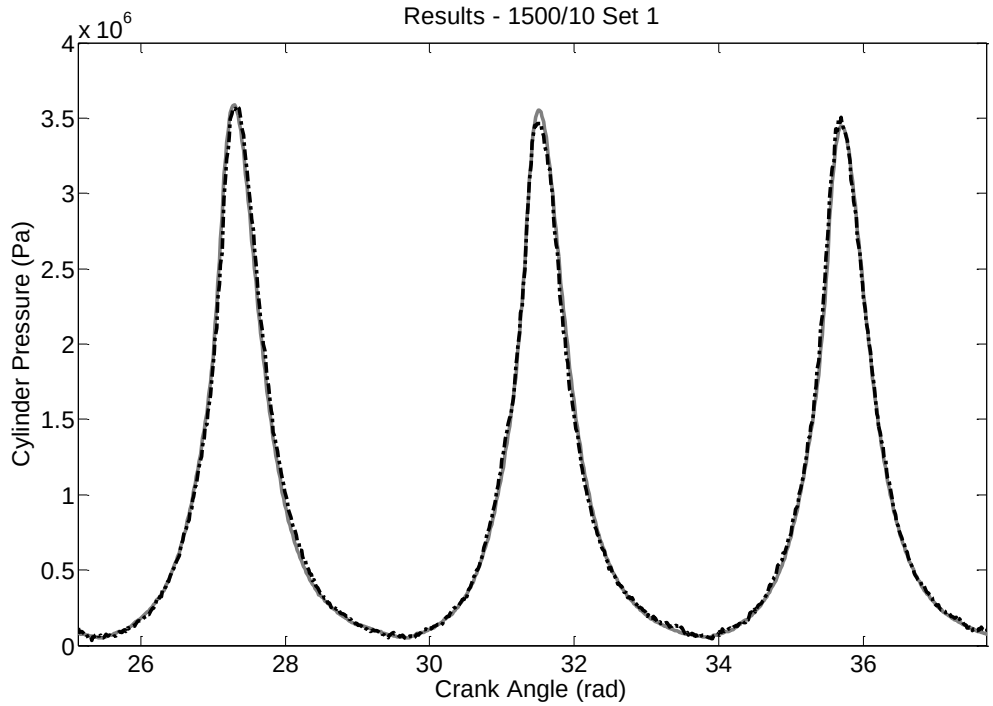

Figure E1.3: Condition-2 Training Results - Worst. Measured Cylinder Pressure (Grey Solid Line). Reconstructed Cylinder Pressure (Black Dashed Line). RMSE = 1.97%.

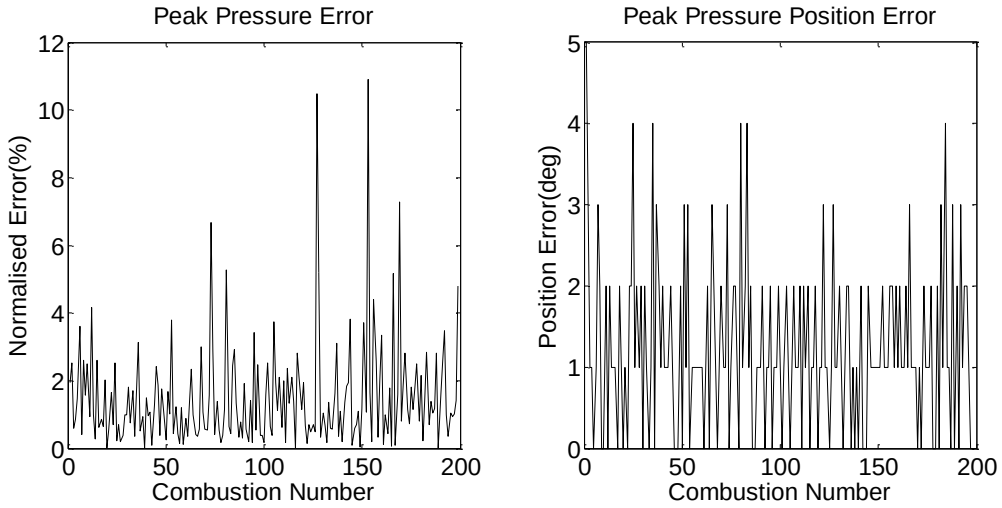

Figure E1.4: Condition-2 Normalised Peak Error Training Results (left). Condition-5 Position of Peak Error Training Results (right)

Table E1.2: Condition-2 Root-Mean-Squared Error (RMSE) and Standard Deviation for the ANN Training

	Training Root-Mean-Squared Error	Training Standard Deviation
Overall Performance	1.38 %	1.38 %
Normalised Peak Error	2.15 %	1.55 %
Peak Pressure Position Error (deg)	1.57	0.99

Generalisation Results

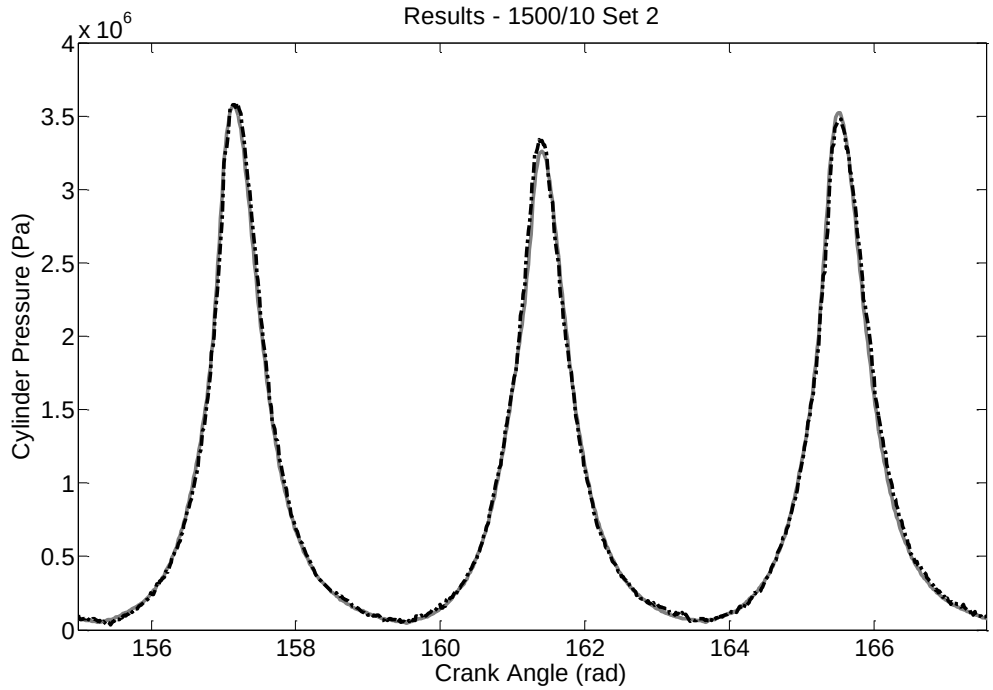

Figure E1.5: Condition-2 Generalisation Results - Best. Measured Cylinder Pressure (Grey Solid Line). Reconstructed Cylinder Pressure (Black Dashed Line). RMSE = 0.79%.

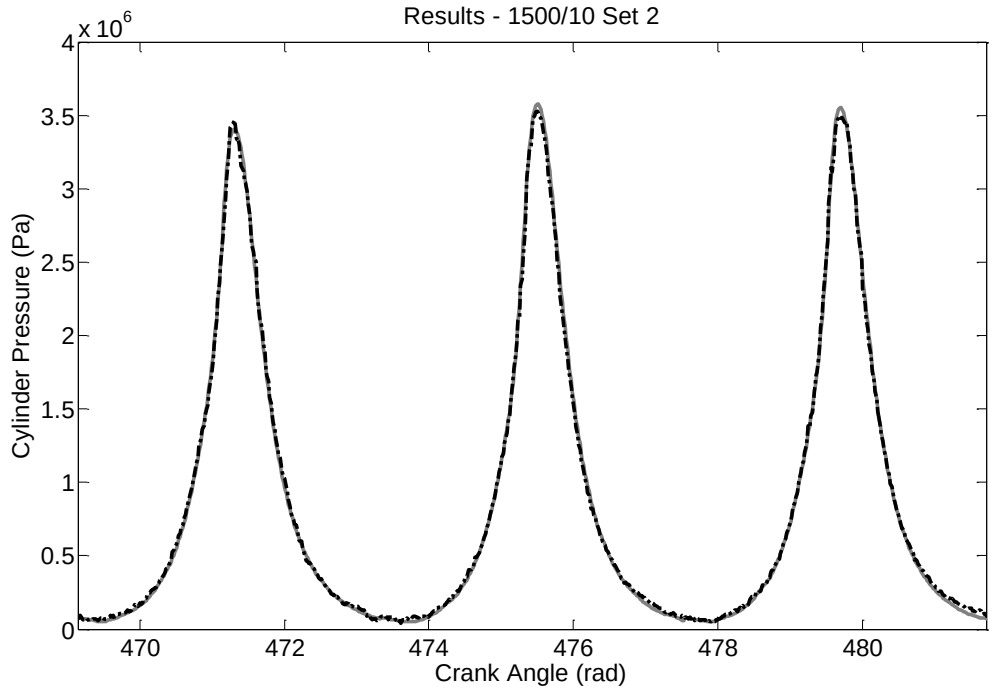

Figure E1.6 Condition-2 Generalisation Results - Average. Measured Cylinder Pressure (Grey Solid Line). Reconstructed Cylinder Pressure (Black Dashed Line). RMSE = 1.43%.

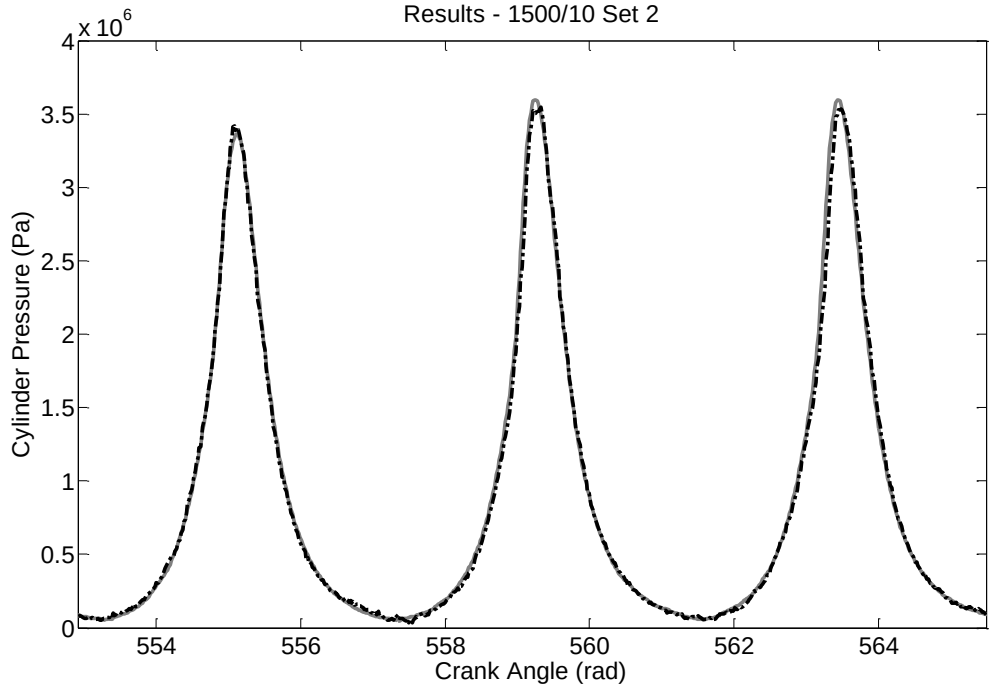

Figure E1.7: Condition-2 Generalisation Results - Worst. Measured Cylinder Pressure (Grey Solid Line). Reconstructed Cylinder Pressure (Black Dashed Line). RMSE = 1.70%.

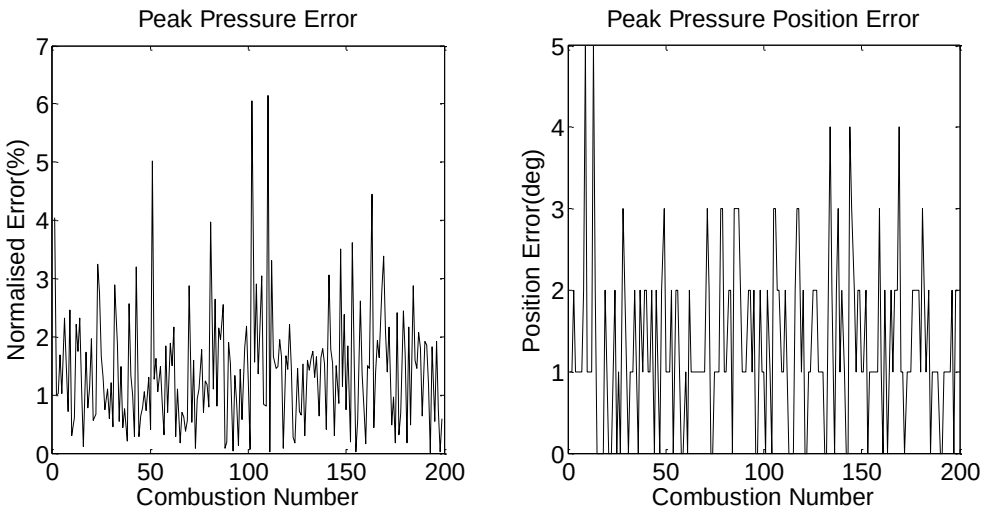

Figure E1.8: Condition-2 Normalised Peak Error Generalisation Results (left). Condition-5 Position of Peak Error Generalisation Results (right)

Table E1.3: Condition-2 Root-Mean-Squared Error (RMSE) and Standard Deviation for the ANN Generalisation

	Generalisation Root-Mean-Squared Error	Generalisation Standard Deviation
Overall Performance	1.32 %	1.32 %
Normalised Peak Error	1.76 %	1.04 %
Peak Pressure Position Error (deg)	1.65	1.00

Test Condition-3

The first test condition used measured data from running the engine at steady-state with a speed of 2000 rpm and a load of 10 Nm.

Table E2.1: ANN Training Setup for Test Condition-3

Network Name	Net_TD_CK_Test3	**Network Architecture**	Time-Delay	**Test Data**	2000_10_01p_jun2010
Network Training Algorithm	Levenberg–Marquardt	**Hidden Layers Number**	1	**Speed (rpm) / Load (Nm)**	2000/10
Cost Function	Means Squared Error	**Neurons Number**	15	**Training to Validation Ratio**	60:40
Training Goal	1E8	**Delay Number**	240	**Crank Step**	1 Deg
Maximum Epoch	1000	**Transfer Function Layer 1**	Sigmoid	**Number of Iterations**	10
Weights Initialisation	Randomised	**Transfer Function Layer 2**	Linear		

Training Results

In total 10 different ANNs were trained with the overall performance of the ANNs ranging from 1.16% to 6.22% RMSE. The best performing ANN was selected which trained in 693 seconds (0.19 hours) and 36 epochs.

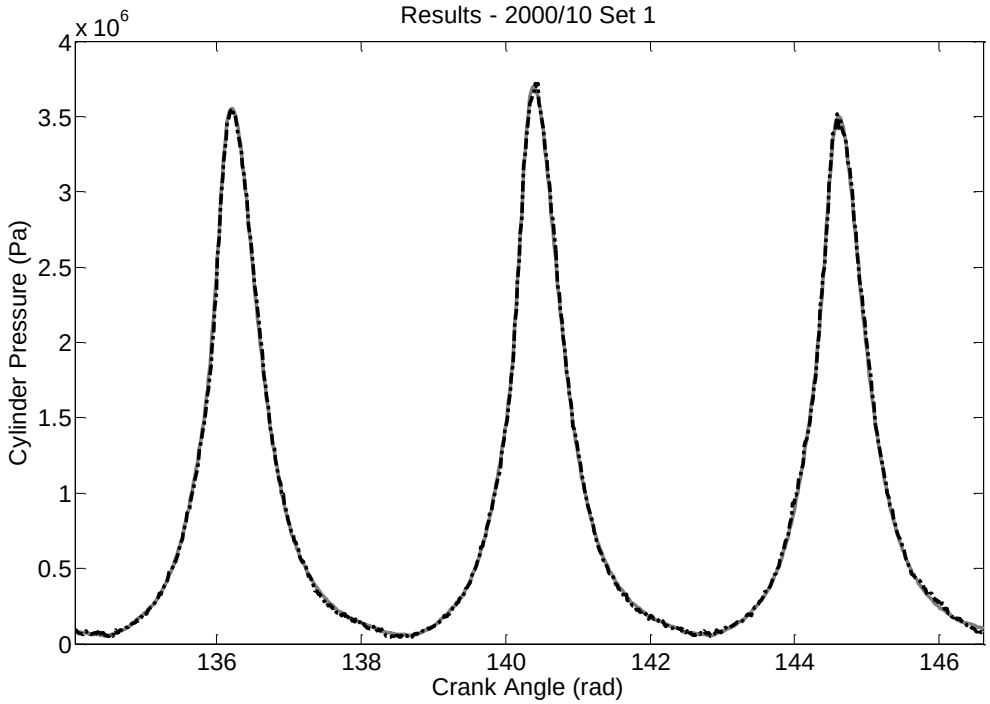

Figure E2.1: Condition-3 Training Results - Best. Measured Cylinder Pressure (Grey Solid Line). Reconstructed Cylinder Pressure (Black Dashed Line). RMSE = 0.58%.

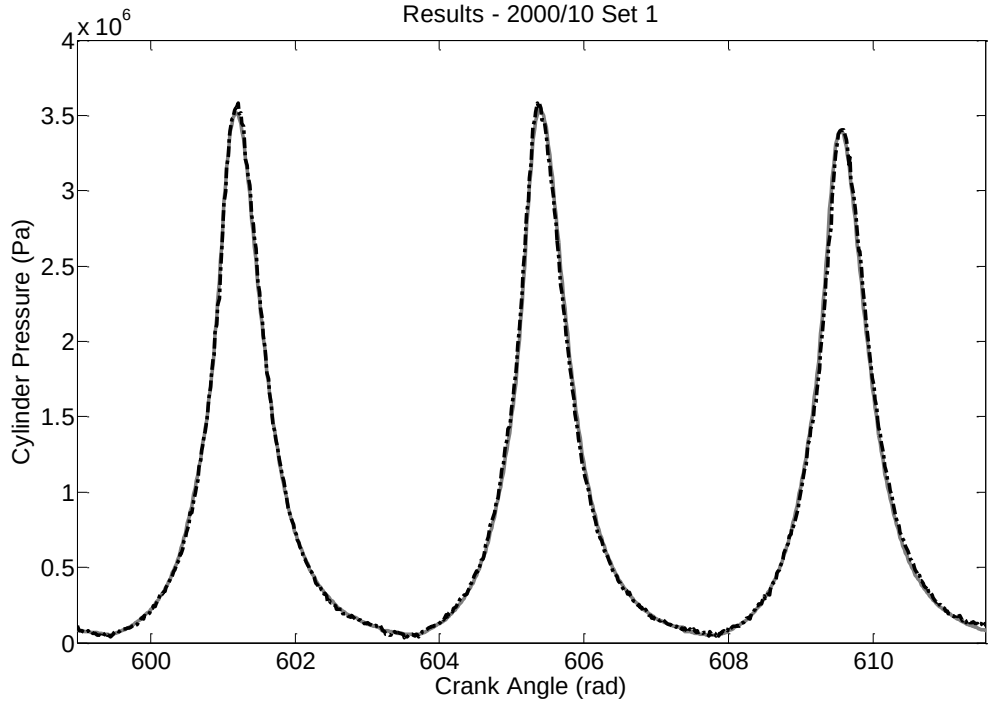

Figure E2.2: Condition-3 Training Results - Average. Measured Cylinder Pressure (Grey Solid Line). Reconstructed Cylinder Pressure (Black Dashed Line). RMSE = 1.04%.

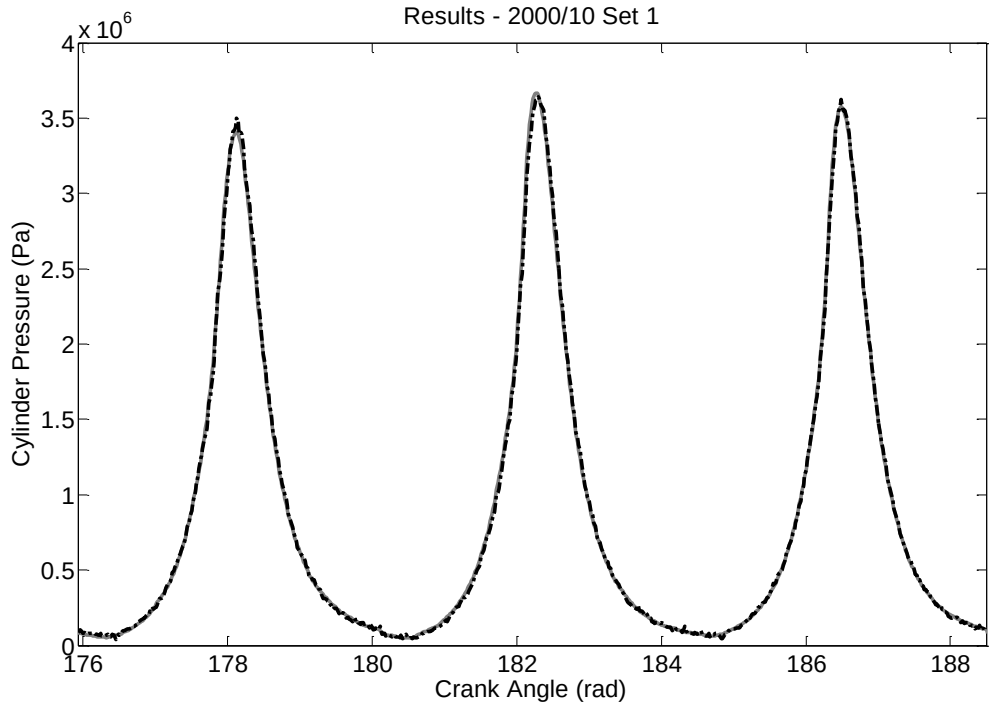

Figure E2.3: Condition-3 Training Results - Worst. Measured Cylinder Pressure (Grey Solid Line). Reconstructed Cylinder Pressure (Black Dashed Line). RMSE = 1.58%.

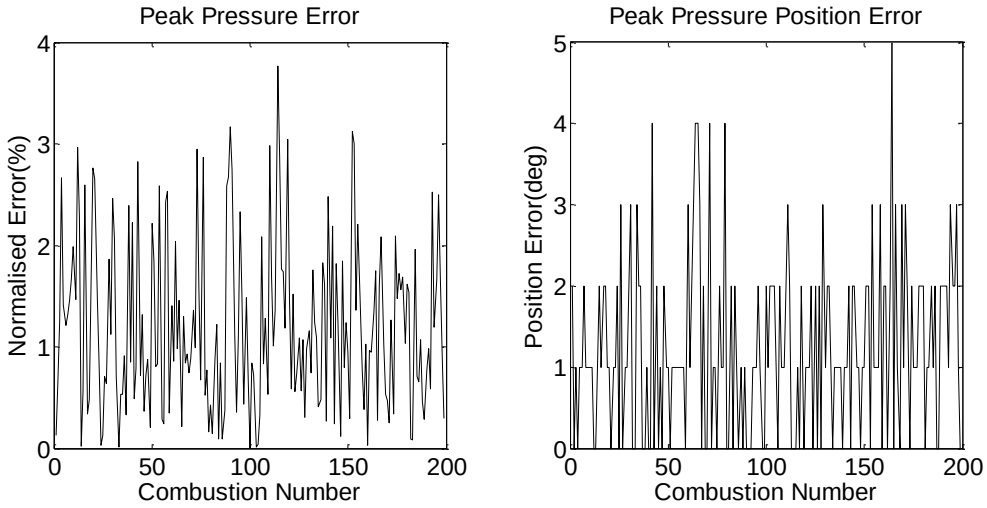

Figure E2.4: Condition-3 Normalised Peak Error Training Results (left). Condition-5 Position of Peak Error Training Results (right)

Table E2.2: Condition-3 Root-Mean-Squared Error (RMSE) and Standard Deviation for the ANN Training

	Training Root-Mean-Squared Error	Training Standard Deviation
Overall Performance	1.15 %	1.15 %
Normalised Peak Error	1.47 %	0.08 %
Peak Pressure Position Error (deg)	1.61	1.05

Generalisation Results

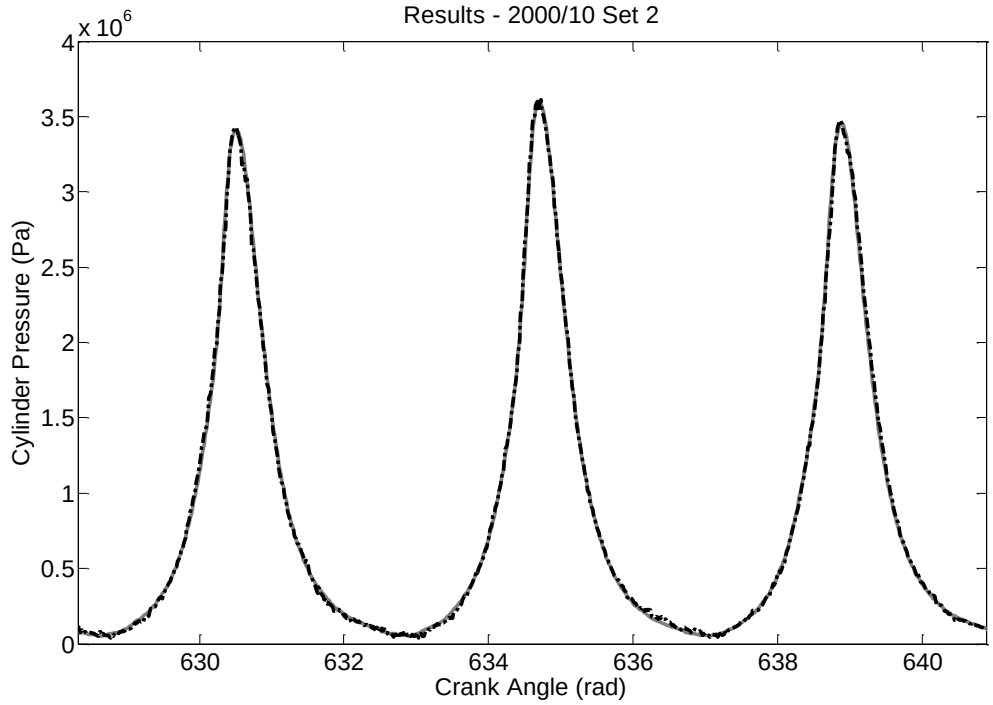

Figure E2.5: Condition-3 Generalisation Results - Best. Measured Cylinder Pressure (Grey Solid Line). Reconstructed Cylinder Pressure (Black Dashed Line). RMSE = 0.75%.

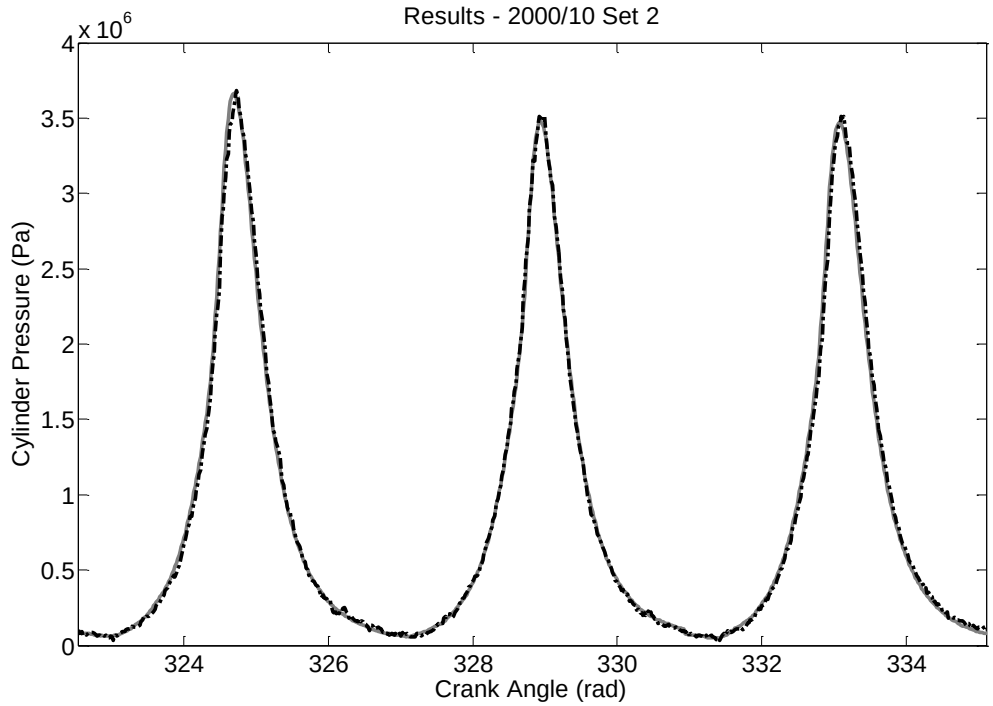

Figure E2.6 Condition-3 Generalisation Results - Average. Measured Cylinder Pressure (Grey Solid Line). Reconstructed Cylinder Pressure (Black Dashed Line). RMSE = 1.12%.

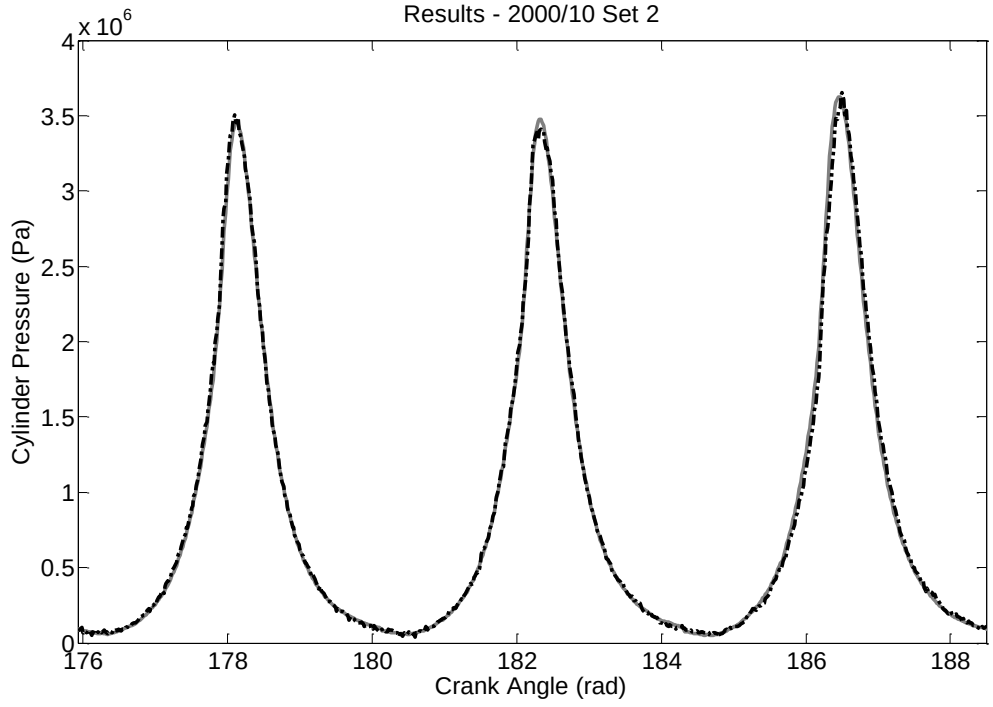

Figure E2.7: Condition-2 Generalisation Results - Worst. Measured Cylinder Pressure (Grey Solid Line). Reconstructed Cylinder Pressure (Black Dashed Line). RMSE = 1.35%.

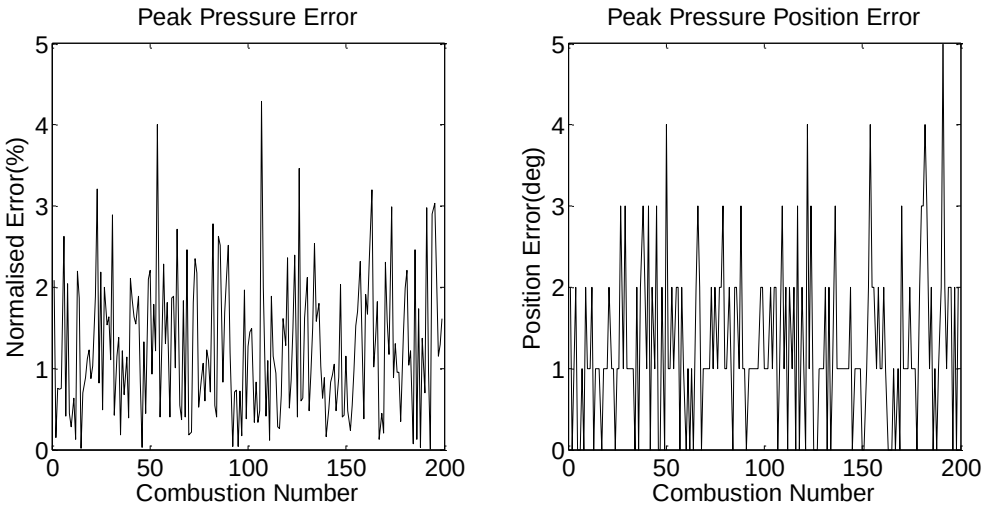

Figure E2.8: Condition-3 Normalised Peak Error Generalisation Results (left). Condition-5 Position of Peak Error Generalisation Results (right)

Table E2.3: Condition-3 Root-Mean-Squared Error (RMSE) and Standard Deviation for the ANN Generalisation

	Generalisation Root-Mean-Squared Error	Generalisation Standard Deviation
Overall Performance	1.24 %	1.24 %
Normalised Peak Error	1.52 %	0.85 %
Peak Pressure Position Error (deg)	1.61	0.98

Test Condition-4

The first test condition used measured data from running the engine at steady-state with a speed of 1000 rpm and a load of 20 Nm.

Table E3.1: ANN Training Setup for Test Condition-4

Network Name	Net_TD_CK_Test4	**Network Architecture**	Time-Delay	**Test Data**	1000_20_01p_jun2010
Network Training Algorithm	Levenberg–Marquardt	**Hidden Layers Number**	1	**Speed (rpm) / Load (Nm)**	1000/20
Cost Function	Means Squared Error	**Neurons Number**	15	**Training to Validation Ratio**	60:40
Training Goal	1E8	**Delay Number**	240	**Crank Step**	1 Deg
Maximum Epoch	1000	**Transfer Function Layer 1**	Sigmoid	**Number of Iterations**	10
Weights Initialisation	Randomised	**Transfer Function Layer 2**	Linear		

Training Results

In total 10 different ANNs were trained with the overall performance of the ANNs ranging from 1.16% to 1.56% RMSE. The best performing ANN was selected which trained in 645 seconds (0.18 hours) and 36 epochs.

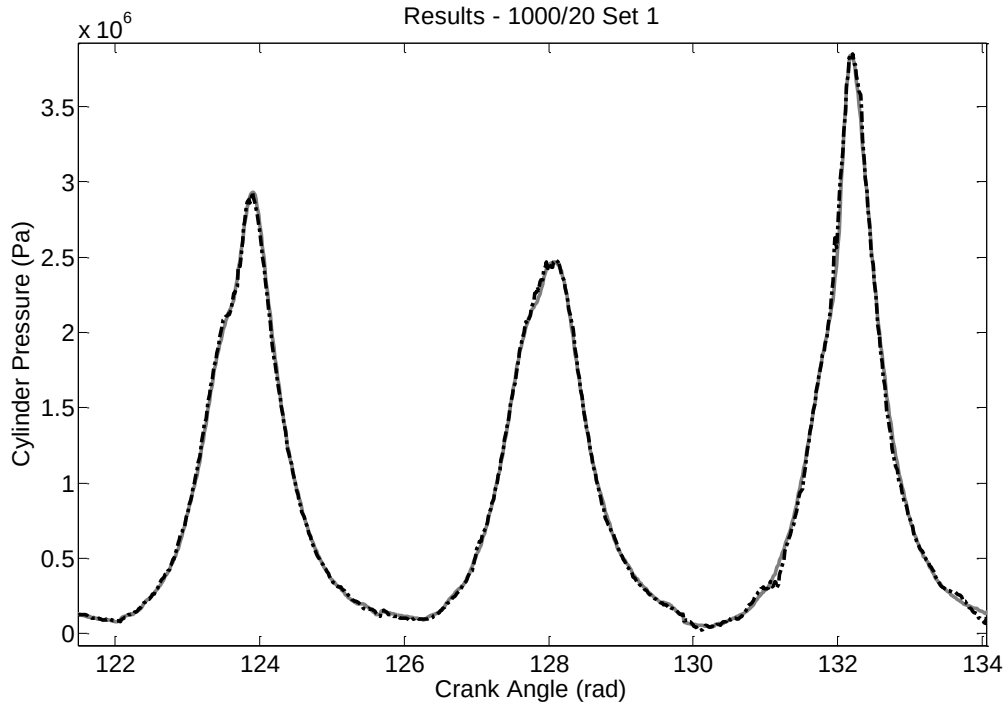

Figure E3.1: Condition-4 Training Results - Best. Measured Cylinder Pressure (Grey Solid Line). Reconstructed Cylinder Pressure (Black Dashed Line). RMSE = 0.79%.

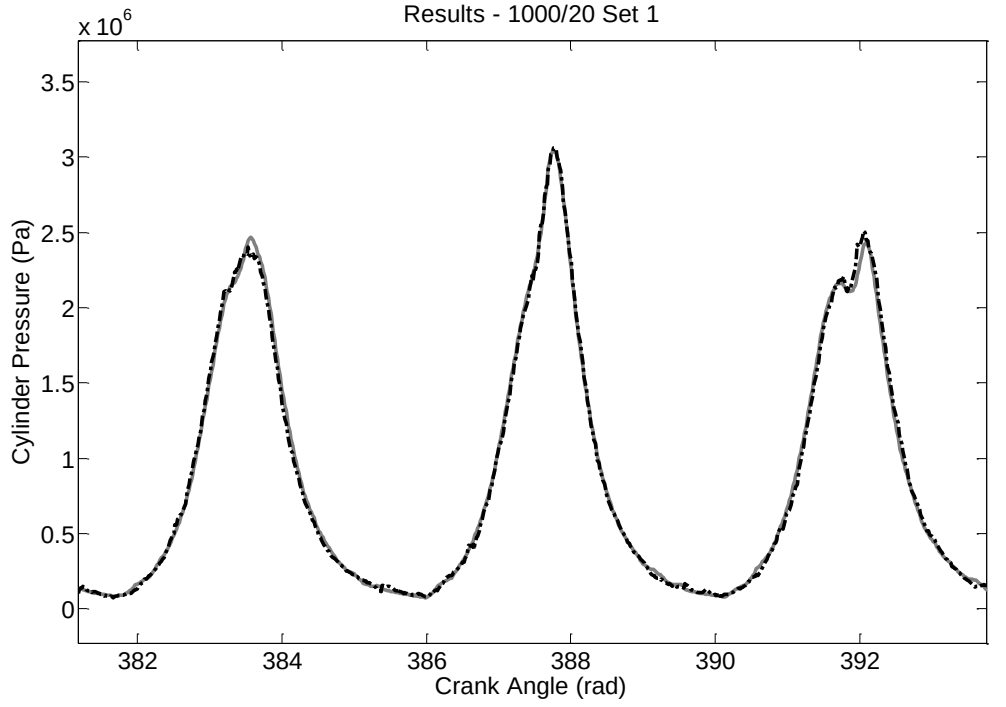

Figure E3.2: Condition-4 Training Results - Average. Measured Cylinder Pressure (Grey Solid Line). Reconstructed Cylinder Pressure (Black Dashed Line). RMSE = 1.19%.

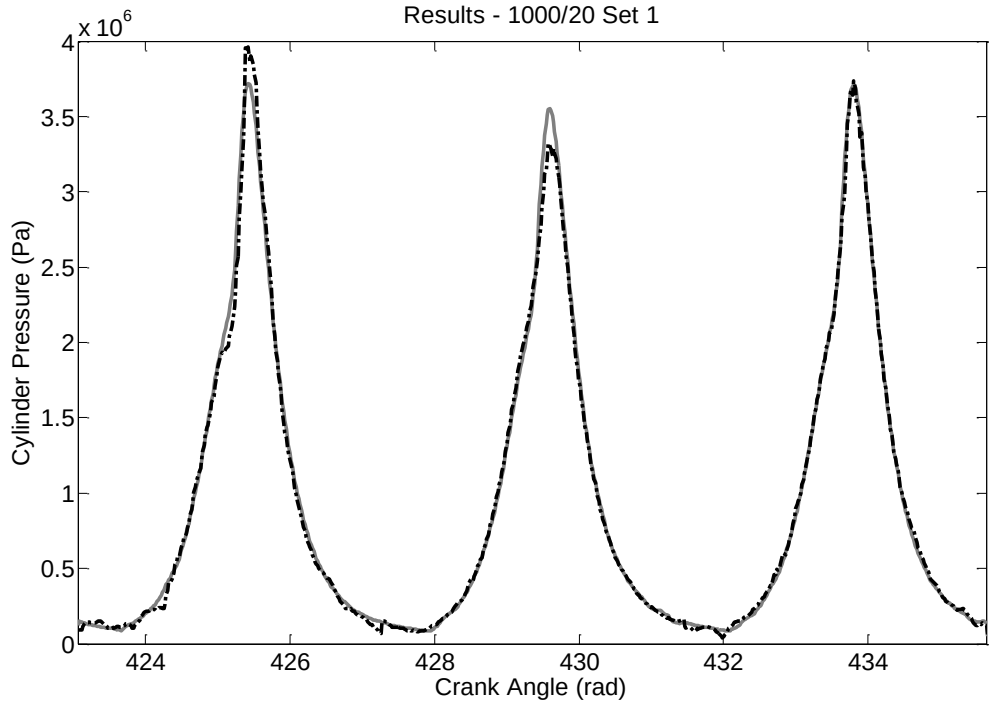

Figure E3.3: Condition-4 Training Results - Worst. Measured Cylinder Pressure (Grey Solid Line). Reconstructed Cylinder Pressure (Black Dashed Line). RMSE = 2.25%.

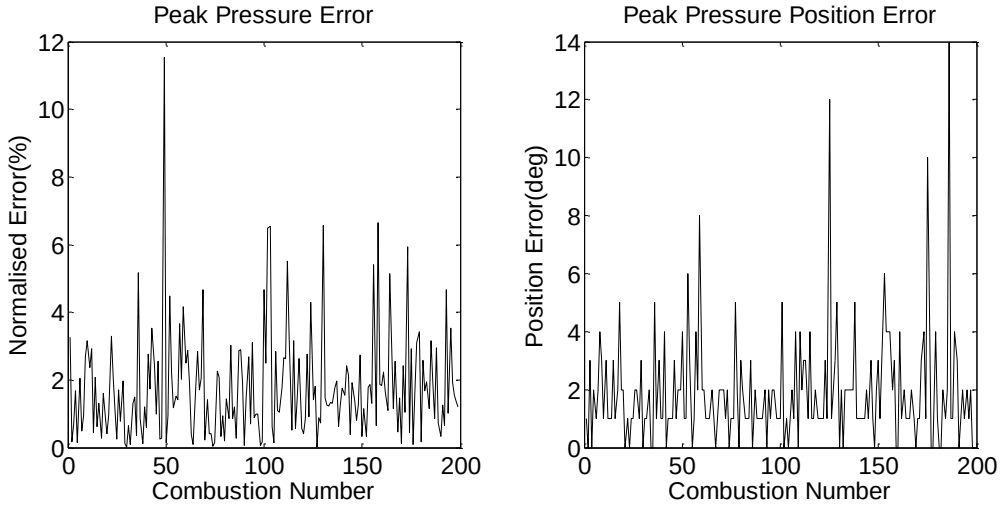

Figure E3.4: Condition-4 Normalised Peak Error Training Results (left). Condition-5 Position of Peak Error Training Results (right)

Table E3.2: Condition-4 Root-Mean-Squared Error (RMSE) and Standard Deviation for the ANN Training

	Training Root-Mean-Squared Error	Training Standard Deviation
Overall Performance	1.09 %	1.09 %
Normalised Peak Error	2.37 %	1.57 %
Peak Pressure Position Error (deg)	2.67	1.89

Generalisation Results

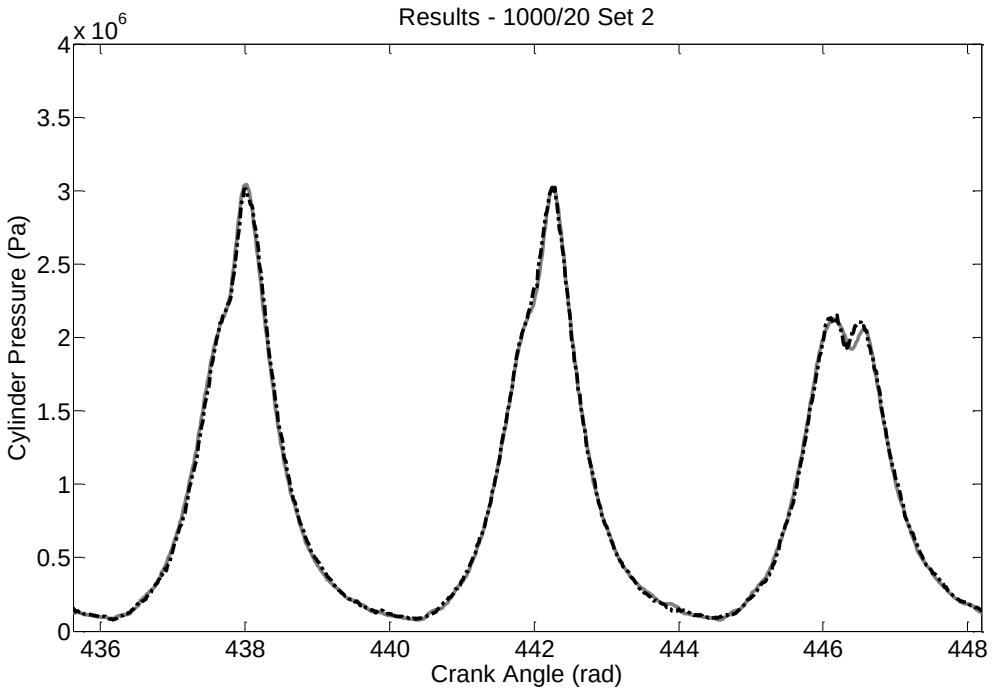

Figure E3.5: Condition-4 Generalisation Results - Best. Measured Cylinder Pressure (Grey Solid Line). Reconstructed Cylinder Pressure (Black Dashed Line). RMSE = 0.81%.

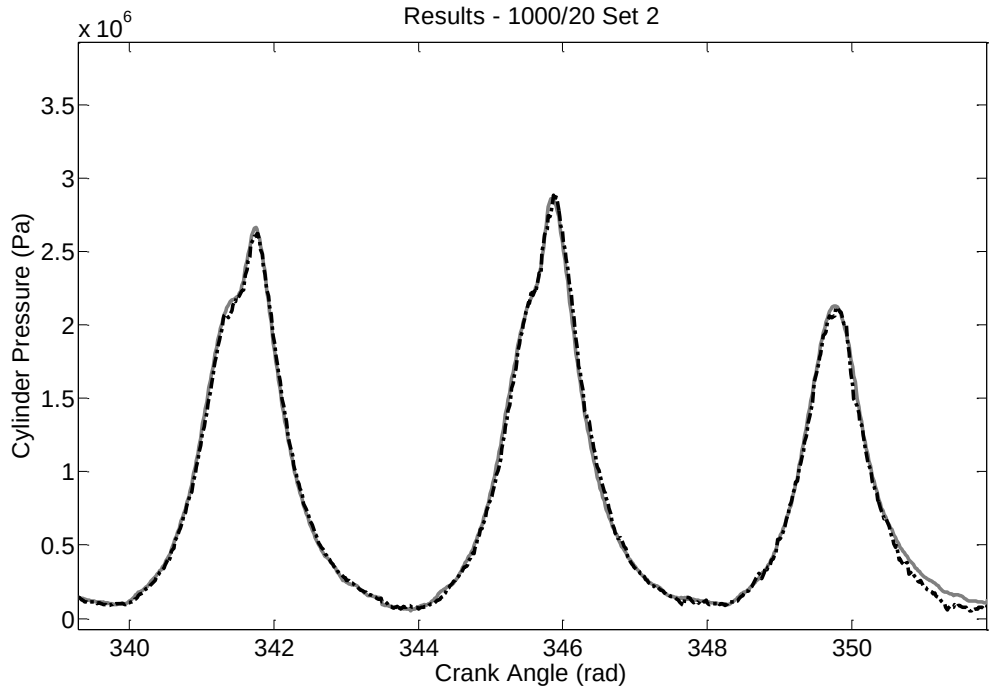

Figure E3.6 Condition-4 Generalisation Results - Average. Measured Cylinder Pressure (Grey Solid Line). Reconstructed Cylinder Pressure (Black Dashed Line). RMSE = 1.09%.

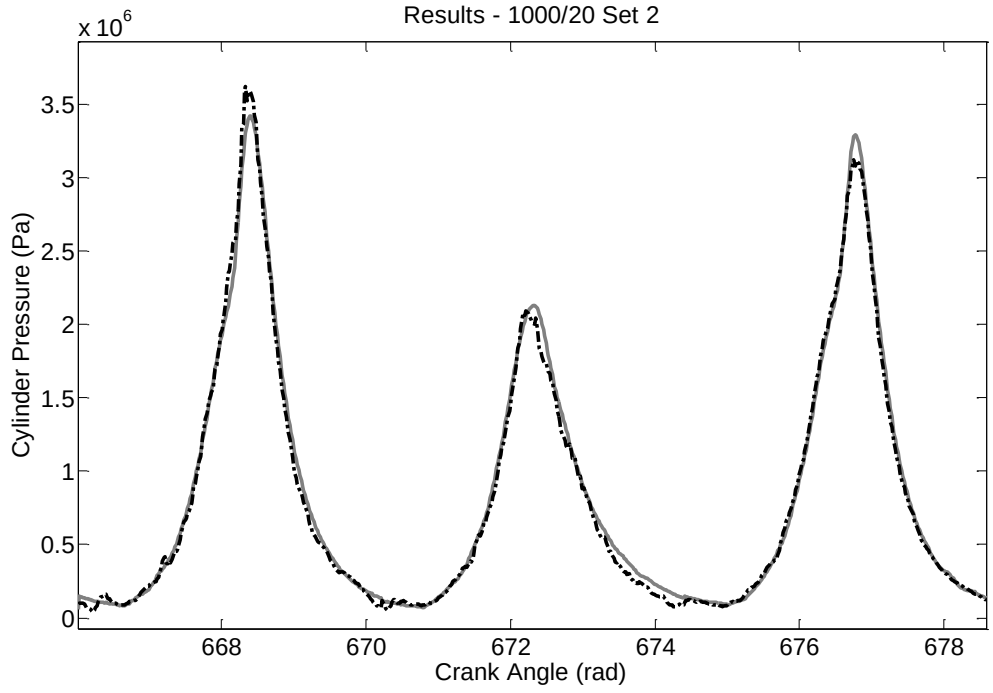

Figure E3.7: Condition-4 Generalisation Results - Worst. Measured Cylinder Pressure (Grey Solid Line). Reconstructed Cylinder Pressure (Black Dashed Line). RMSE = 1.59%.

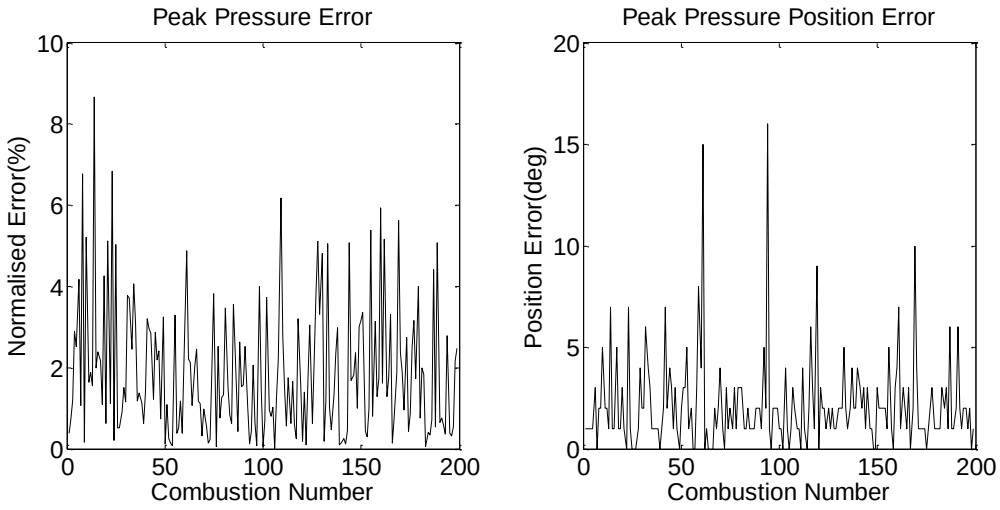

Figure E3.8: Condition-4 Normalised Peak Error Generalisation Results (left). Condition-5 Position of Peak Error Generalisation Results (right)

Table E3.3: Condition-4 Root-Mean-Squared Error (RMSE) and Standard Deviation for the ANN Generalisation

	Generalisation Root-Mean-Squared Error	Generalisation Standard Deviation
Overall Performance	1. 15 %	1.15 %
Normalised Peak Error	2.48 %	1.61 %
Peak Pressure Position Error (deg)	3.08	2.21

Test Condition-6

The first test condition used measured data from running the engine at steady-state with a speed of 2000 rpm and a load of 20 Nm.

Table E2.1: ANN Training Setup for Test Condition-6

Network Name	Net_TD_CK_Test6	**Network Architecture**	Time-Delay	**Test Data**	2000_20_01p_jun2010
Network Training Algorithm	Levenberg–Marquardt	**Hidden Layers Number**	1	**Speed (rpm) / Load (Nm)**	2000/20
Cost Function	Means Squared Error	**Neurons Number**	15	**Training to Validation Ratio**	60:40
Training Goal	1E8	**Delay Number**	240	**Crank Step**	1 Deg
Maximum Epoch	1000	**Transfer Function Layer 1**	Sigmoid	**Number of Iterations**	10
Weights Initialisation	Randomised	**Transfer Function Layer 2**	Linear		

Training Results

In total 10 different ANNs were trained with the overall performance of the ANNs ranging from 1.36% to 1.48% RMSE. The best performing ANN was selected which trained in 498 seconds (0.14 hours) and 27 epochs.

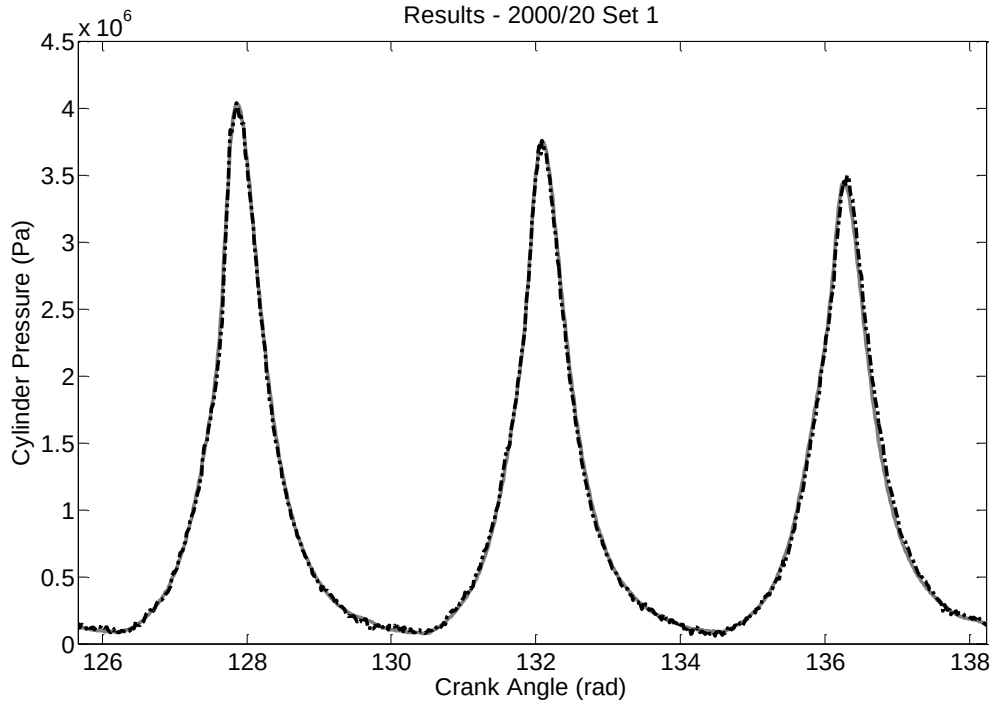

Figure E4.1: Condition-6 Training Results - Best. Measured Cylinder Pressure (Grey Solid Line). Reconstructed Cylinder Pressure (Black Dashed Line). RMSE = 0.77%.

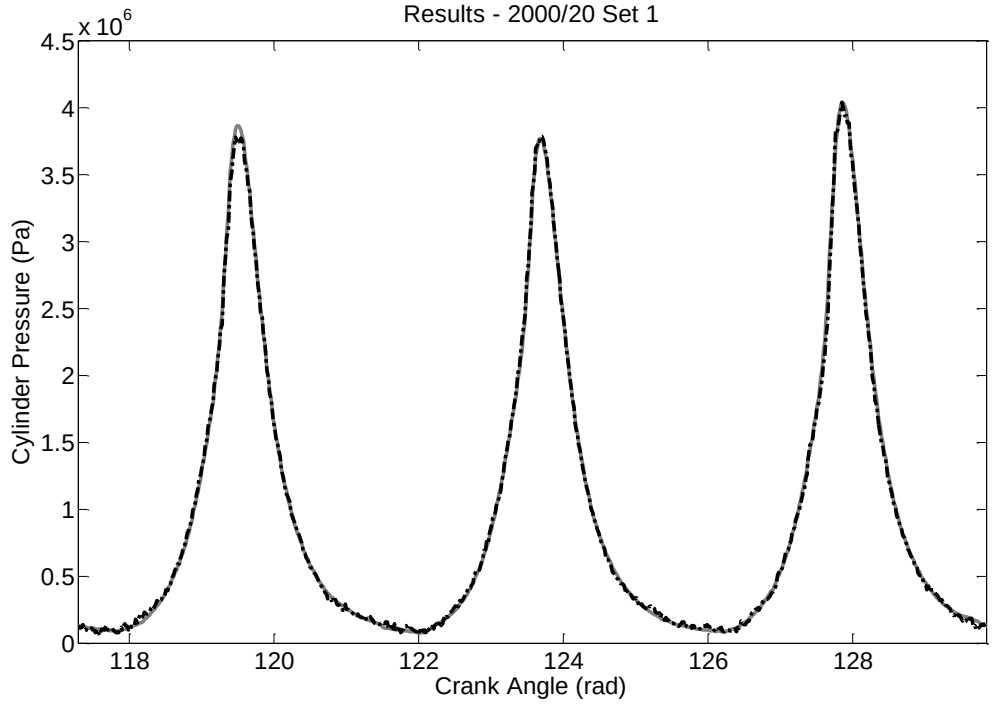

Figure E4.2: Condition-6 Training Results - Average. Measured Cylinder Pressure (Grey Solid Line). Reconstructed Cylinder Pressure (Black Dashed Line). RMSE = 1.03%.

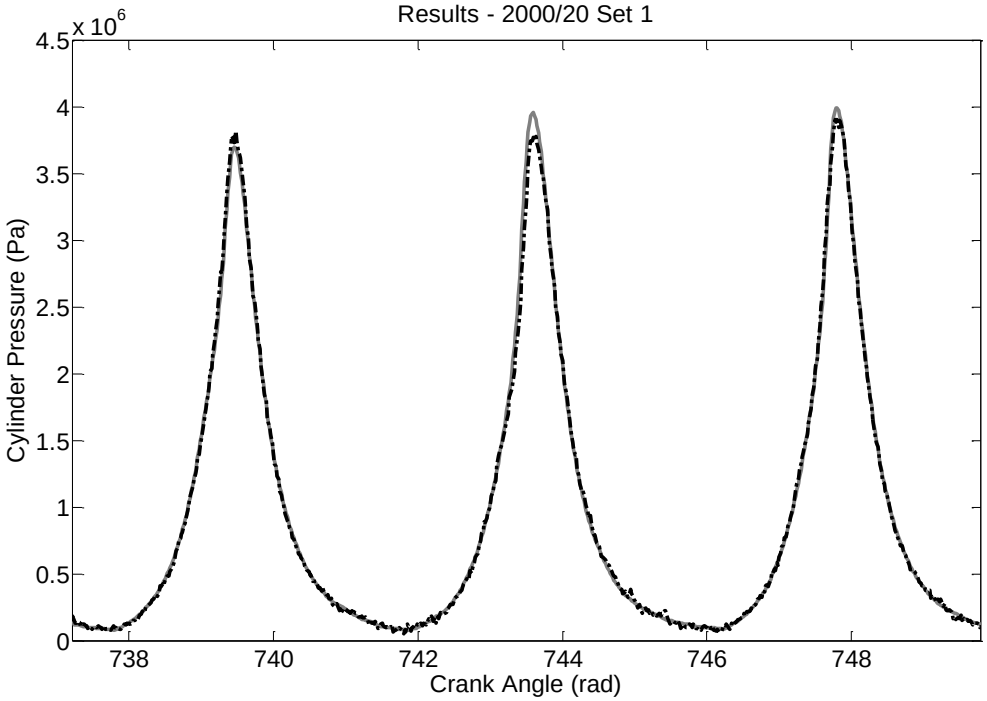

Figure E4.3: Condition-6 Training Results - Worst. Measured Cylinder Pressure (Grey Solid Line). Reconstructed Cylinder Pressure (Black Dashed Line). RMSE = 1.33%.

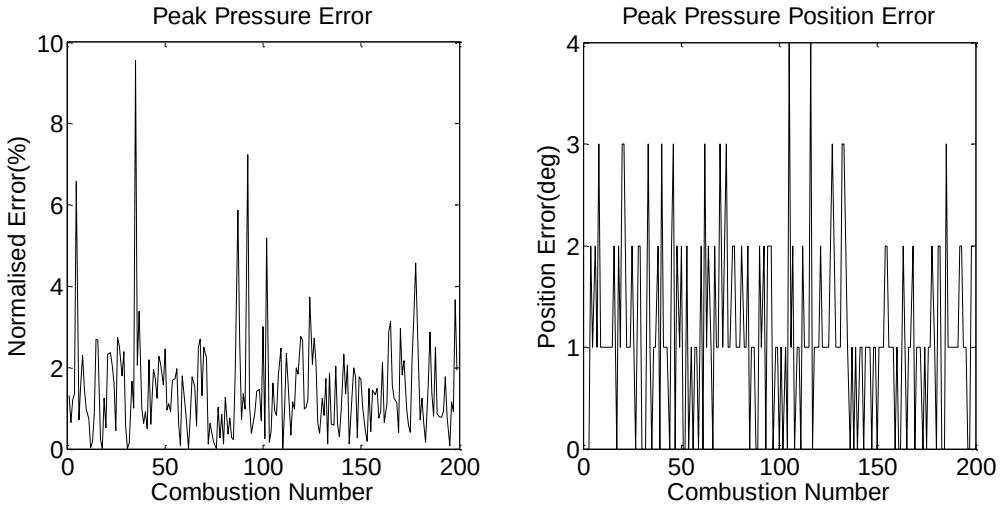

Figure E4.4: Condition-6 Normalised Peak Error Training Results (left). Condition-5 Position of Peak Error Training Results (right)

Table E4.2: Condition-6 Root-Mean-Squared Error (RMSE) and Standard Deviation for the ANN Training

	Training Root-Mean-Squared Error	Training Standard Deviation
Overall Performance	1.29 %	1.28 %
Normalised Peak Error	1.92 %	1.26 %
Peak Pressure Position Error (deg)	1.43	0.89

Generalisation Results

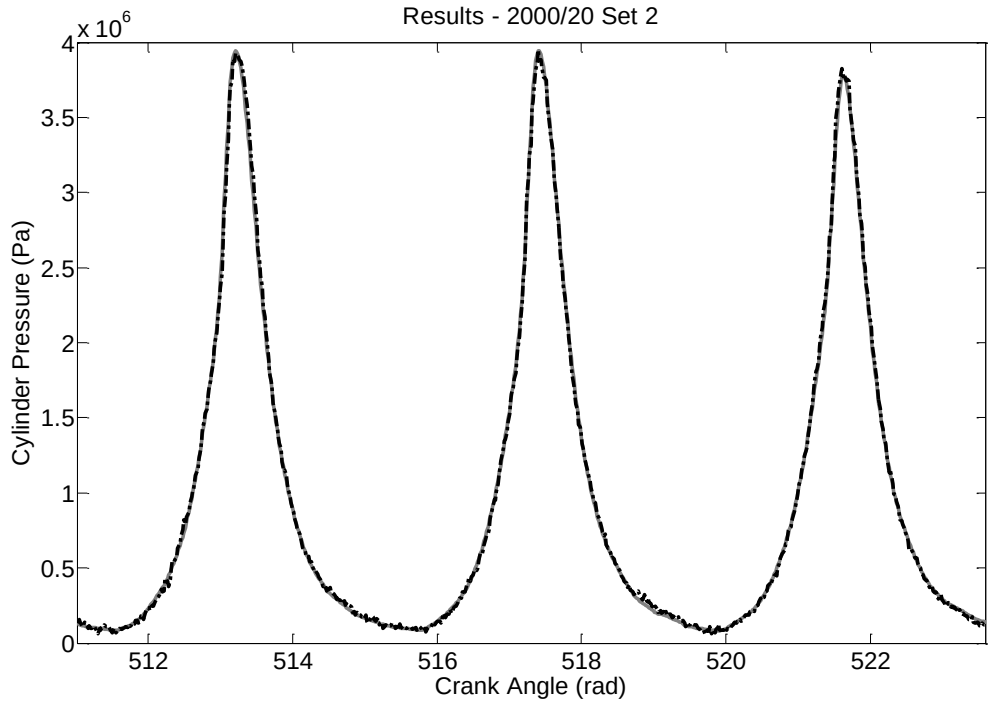

Figure E4.5: Condition-6 Generalisation Results - Best. Measured Cylinder Pressure (Grey Solid Line). Reconstructed Cylinder Pressure (Black Dashed Line). RMSE = 0.84%.

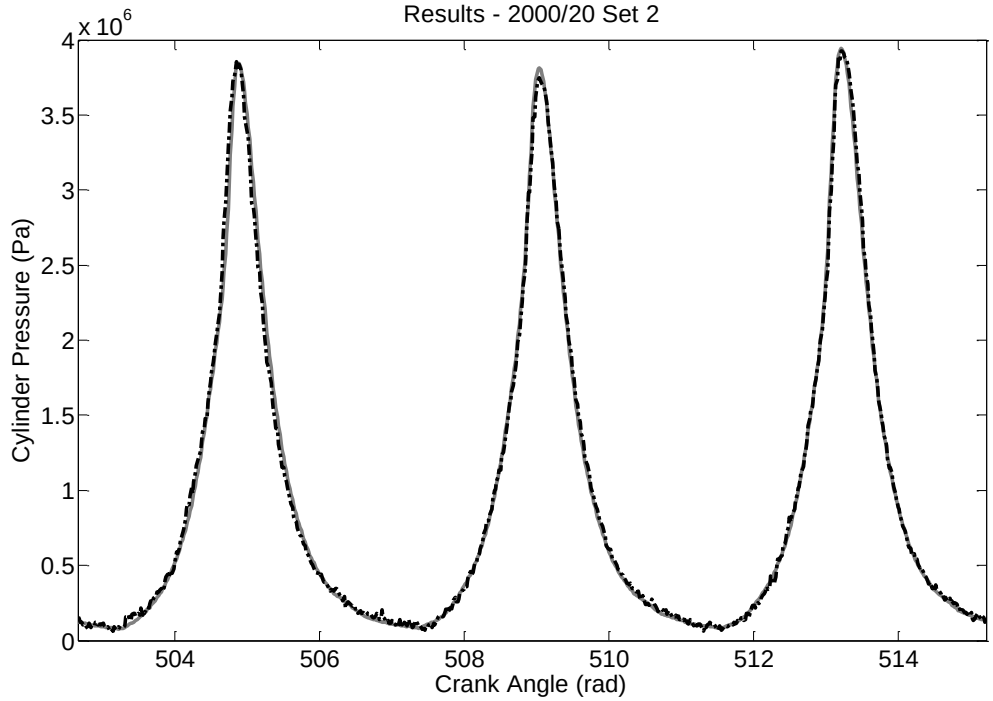

Figure E4.6 Condition-6 Generalisation Results - Average. Measured Cylinder Pressure (Grey Solid Line). Reconstructed Cylinder Pressure (Black Dashed Line). RMSE = 1.13%.

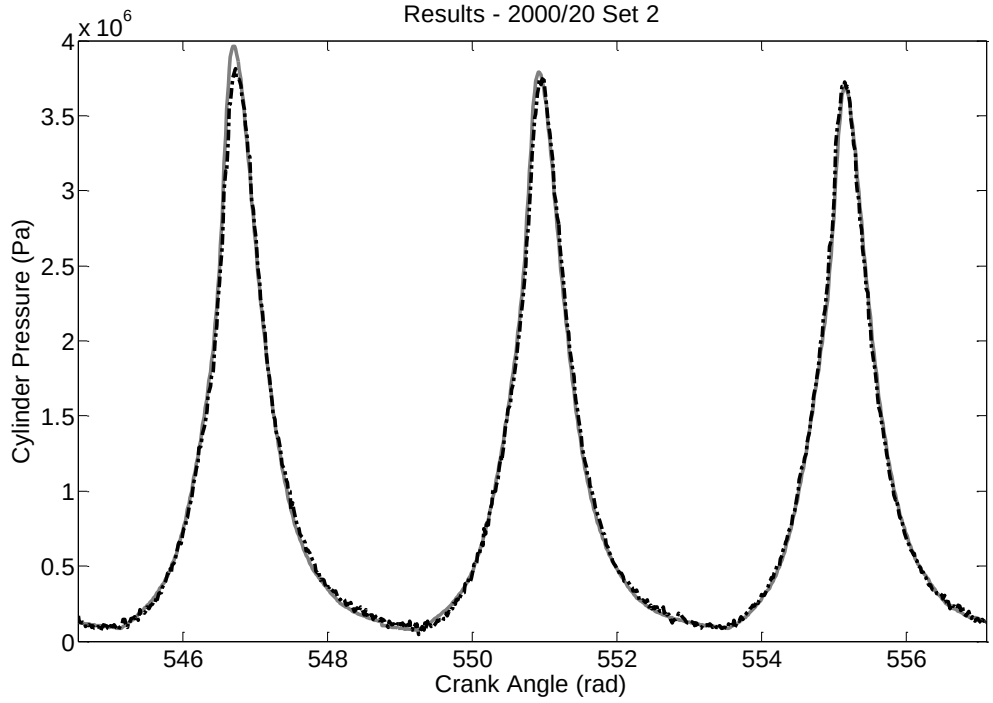

Figure E4.7: Condition-6 Generalisation Results - Worst. Measured Cylinder Pressure (Grey Solid Line). Reconstructed Cylinder Pressure (Black Dashed Line). RMSE = 1.48%.

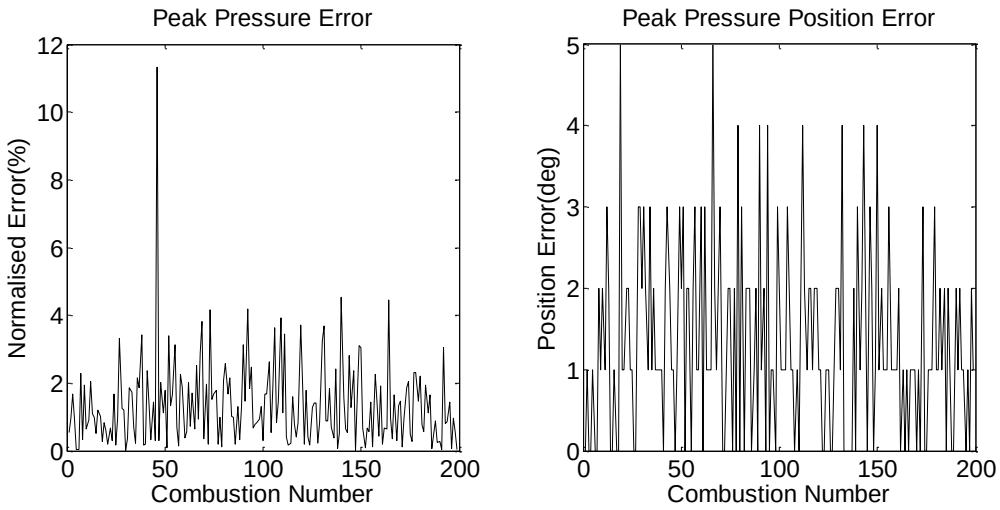

Figure E4.8: Condition-6 Normalised Peak Error Generalisation Results (left). Condition-5 Position of Peak Error Generalisation Results (right)

Table E4.3: Condition-6 Root-Mean-Squared Error (RMSE) and Standard Deviation for the ANN Generalisation

	Generalisation Root-Mean-Squared Error	Generalisation Standard Deviation
Overall Performance	1.34 %	1.33 %
Normalised Peak Error	1.84 %	1.25 %
Peak Pressure Position Error (deg)	1.73	1.13

Test Condition-7

The first test condition used measured data from running the engine at steady-state with a speed of 1000 rpm and a load of 30 Nm.

Table E5.1: ANN Training Setup for Test Condition-7

Network Name	Net_TD_CK_Test7	**Network Architecture**	Time-Delay	**Test Data**	1000_30_01p_jun2010
Network Training Algorithm	Levenberg–Marquardt	**Hidden Layers Number**	1	**Speed (rpm) / Load (Nm)**	1000/30
Cost Function	Means Squared Error	**Neurons Number**	15	**Training to Validation Ratio**	60:40
Training Goal	1E8	**Delay Number**	240	**Crank Step**	1 Deg
Maximum Epoch	1000	**Transfer Function Layer 1**	Sigmoid	**Number of Iterations**	10
Weights Initialisation	Randomised	**Transfer Function Layer 2**	Linear		

Training Results

In total 10 different ANNs were trained with the overall performance of the ANNs ranging from 1.18% to 1.35% RMSE. The best performing ANN was selected which trained in 1747 seconds (0.48 hours) and 114 epochs.

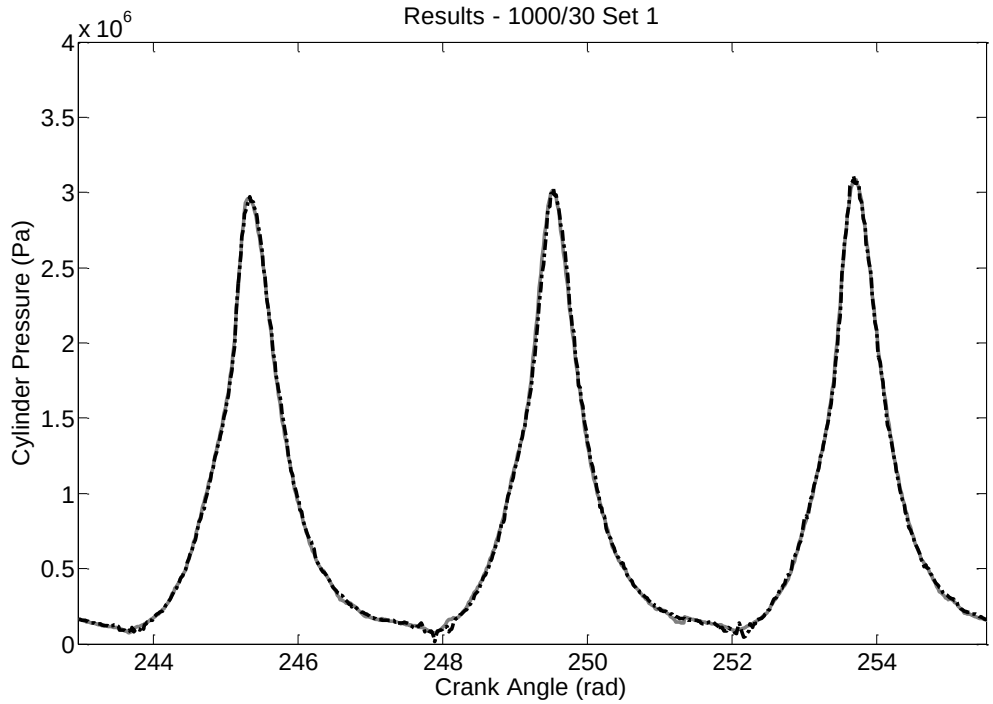

Figure E5.1: Condition-7 Training Results - Best. Measured Cylinder Pressure (Grey Solid Line). Reconstructed Cylinder Pressure (Black Dashed Line). RMSE = 0.75%.

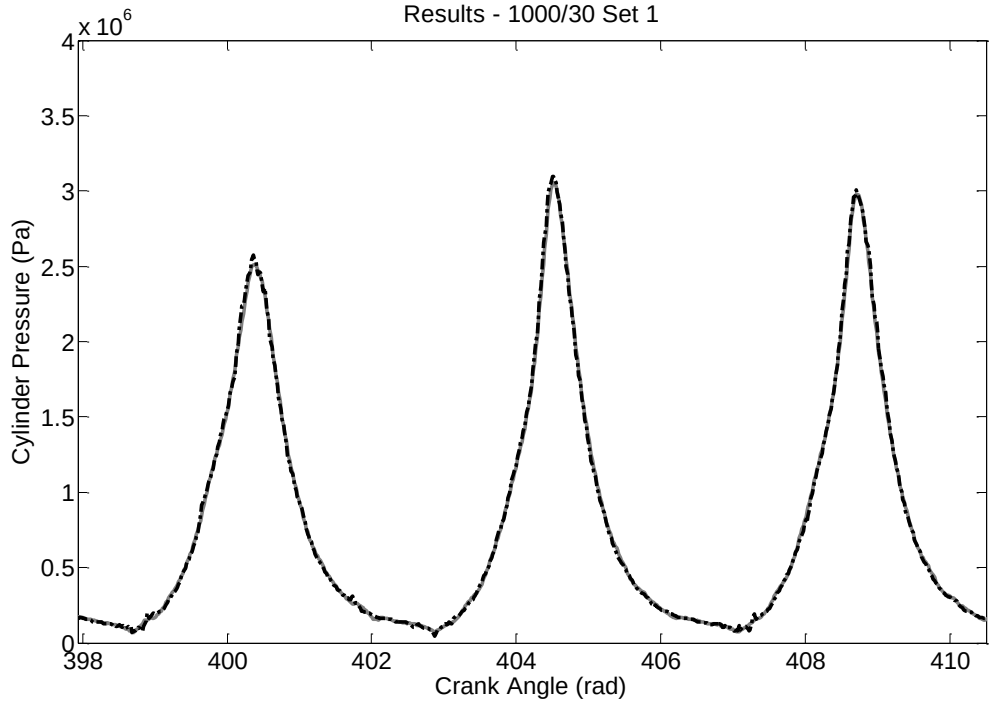

Figure E5.2: Condition-7 Training Results - Average. Measured Cylinder Pressure (Grey Solid Line). Reconstructed Cylinder Pressure (Black Dashed Line). RMSE = 1.16%.

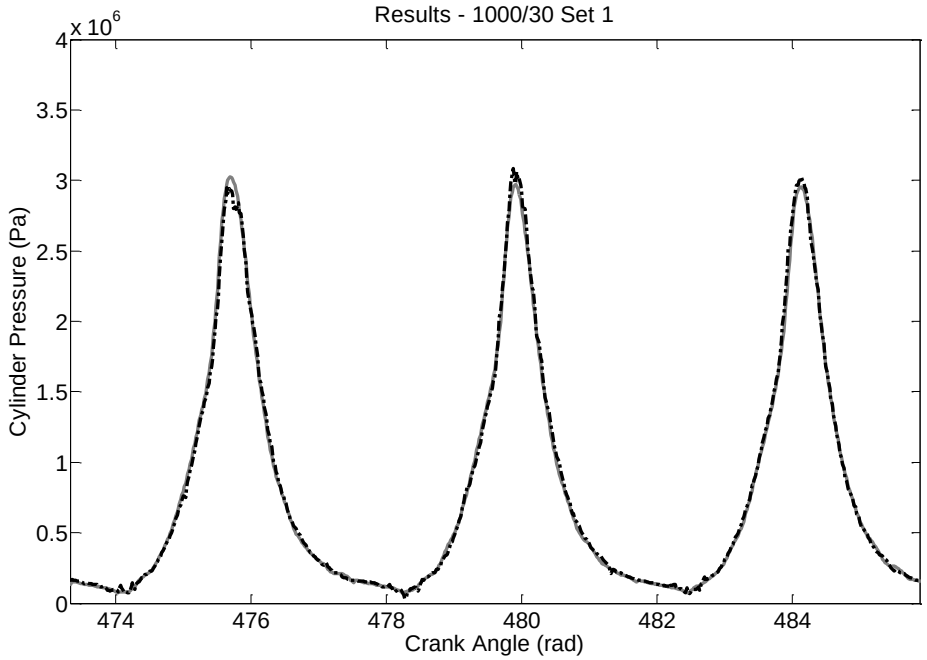

Figure E5.3: Condition-7 Training Results - Worst. Measured Cylinder Pressure (Grey Solid Line). Reconstructed Cylinder Pressure (Black Dashed Line). RMSE = 1.59%.

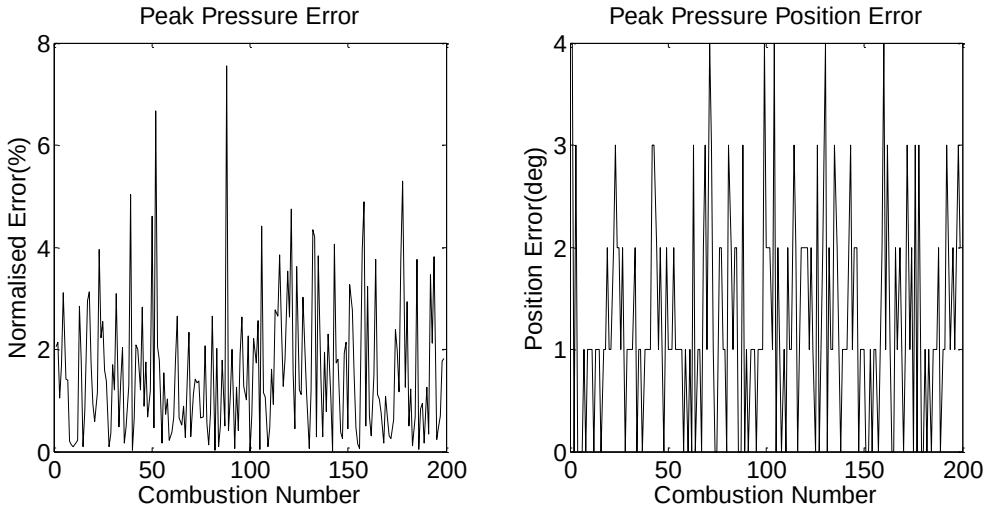

Figure E5.4: Condition-7 Normalised Peak Error Training Results (left). Condition-5 Position of Peak Error Training Results (right)

Table E5.2: Condition-7 Root-Mean-Squared Error (RMSE) and Standard Deviation for the ANN Training

	Training Root-Mean-Squared Error	Training Standard Deviation
Overall Performance	1.17 %	1.17 %
Normalised Peak Error	2.06 %	1.34 %
Peak Pressure Position Error (deg)	1.61	1.02

Generalisation Results

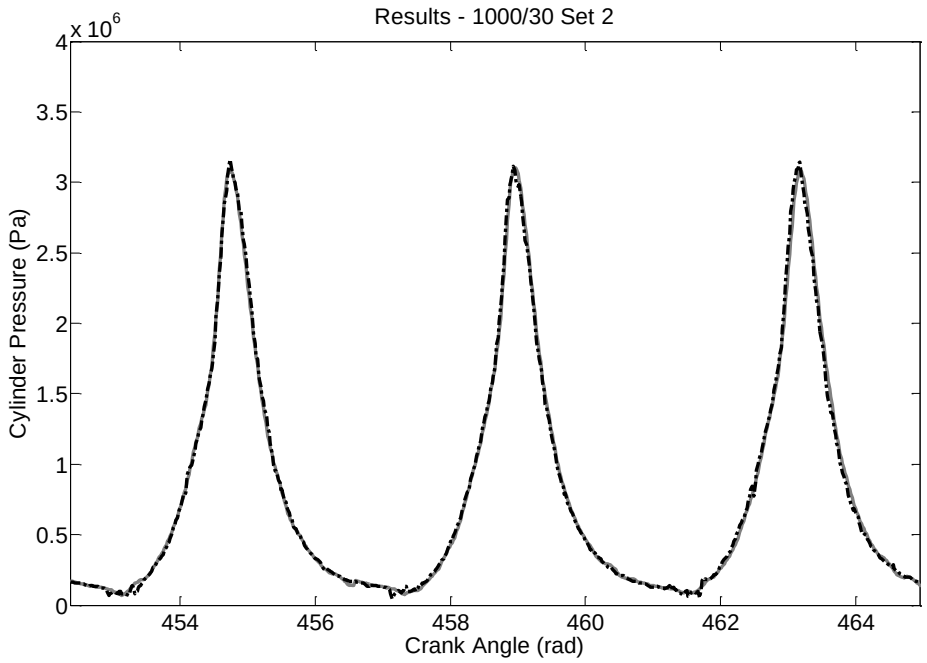

Figure E5.5: Condition-7 Generalisation Results - Best. Measured Cylinder Pressure (Grey Solid Line). Reconstructed Cylinder Pressure (Black Dashed Line). RMSE = 0.83%.

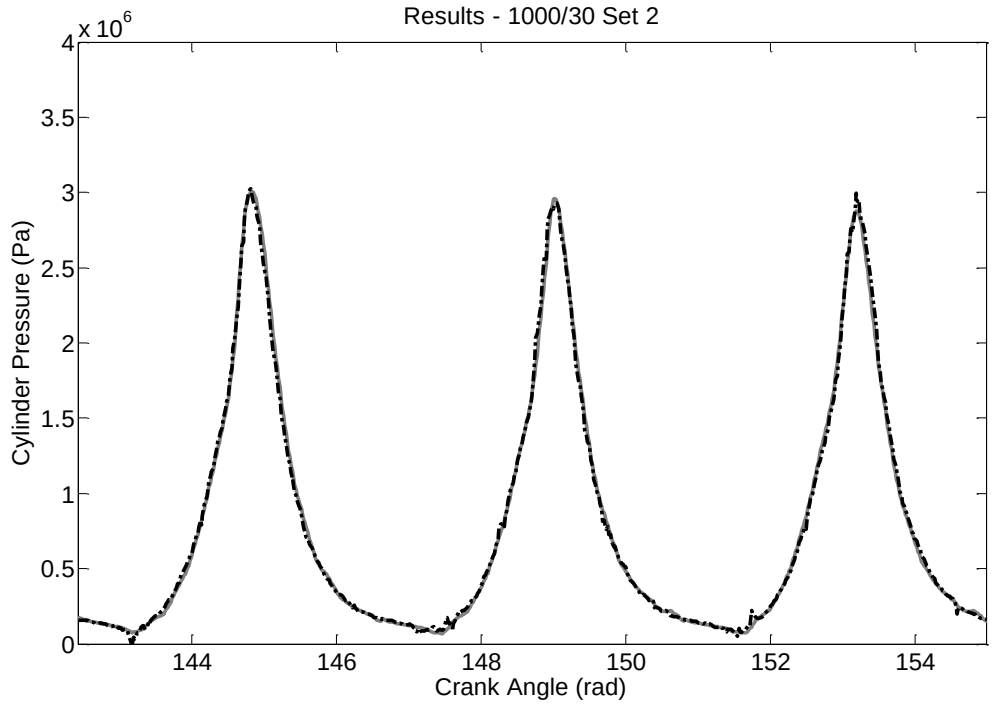

Figure E5.6 Condition-7 Generalisation Results - Average. Measured Cylinder Pressure (Grey Solid Line). Reconstructed Cylinder Pressure (Black Dashed Line). RMSE = 1.30%.

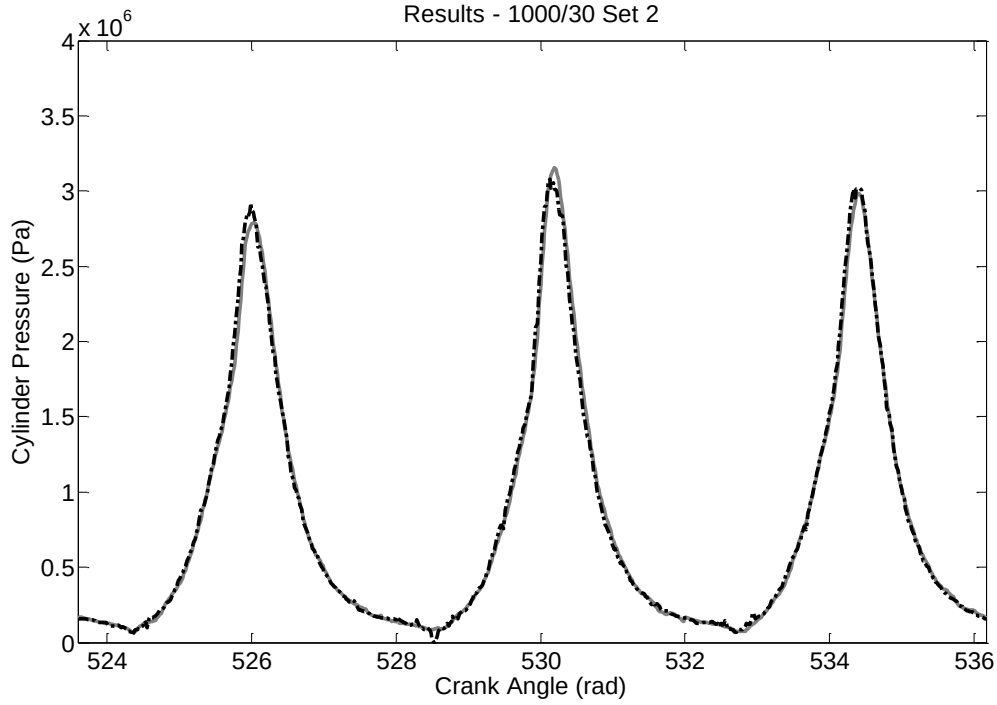

Figure E5.7: Condition-7 Generalisation Results - Worst. Measured Cylinder Pressure (Grey Solid Line). Reconstructed Cylinder Pressure (Black Dashed Line). RMSE = 1.54%.

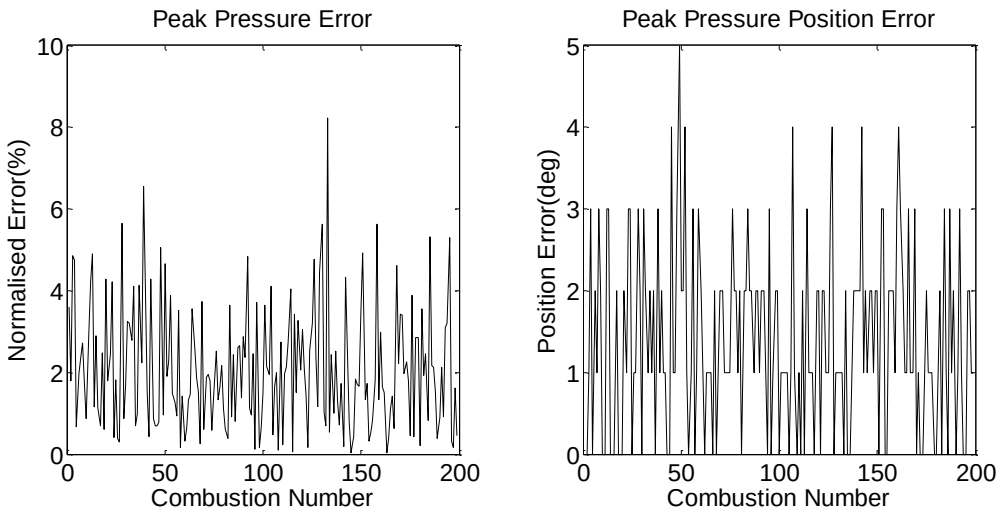

Figure E5.8: Condition-7 Normalised Peak Error Generalisation Results (left). Condition-5 Position of Peak Error Generalisation Results (right)

Table E5.3: Condition-7 Root-Mean-Squared Error (RMSE) and Standard Deviation for the ANN Generalisation

	Generalisation Root-Mean-Squared Error	Generalisation Standard Deviation
Overall Performance	1.32 %	1.31 %
Normalised Peak Error	2.56 %	1.51 %
Peak Pressure Position Error (deg)	1.78	1.10

Test Condition-8

The first test condition used measured data from running the engine at steady-state with a speed of 1500 rpm and a load of 30 Nm.

Table E2.1: ANN Training Setup for Test Condition-8

Network Name	Net_TD_CK_Test8	**Network Architecture**	Time-Delay	**Test Data**	1500_30_01p_jun2010
Network Training Algorithm	Levenberg–Marquardt	**Hidden Layers Number**	1	**Speed (rpm) / Load (Nm)**	1500/30
Cost Function	Means Squared Error	**Neurons Number**	15	**Training to Validation Ratio**	60:40
Training Goal	1E8	**Delay Number**	240	**Crank Step**	1 Deg
Maximum Epoch	1000	**Transfer Function Layer 1**	Sigmoid	**Number of Iterations**	10
Weights Initialisation	Randomised	**Transfer Function Layer 2**	Linear		

Training Results

In total 10 different ANNs were trained with the overall performance of the ANNs ranging from 1.26% to 1.62% RMSE. The best performing ANN was selected which trained in 1649 seconds (0.46 hours) and 95 epochs.

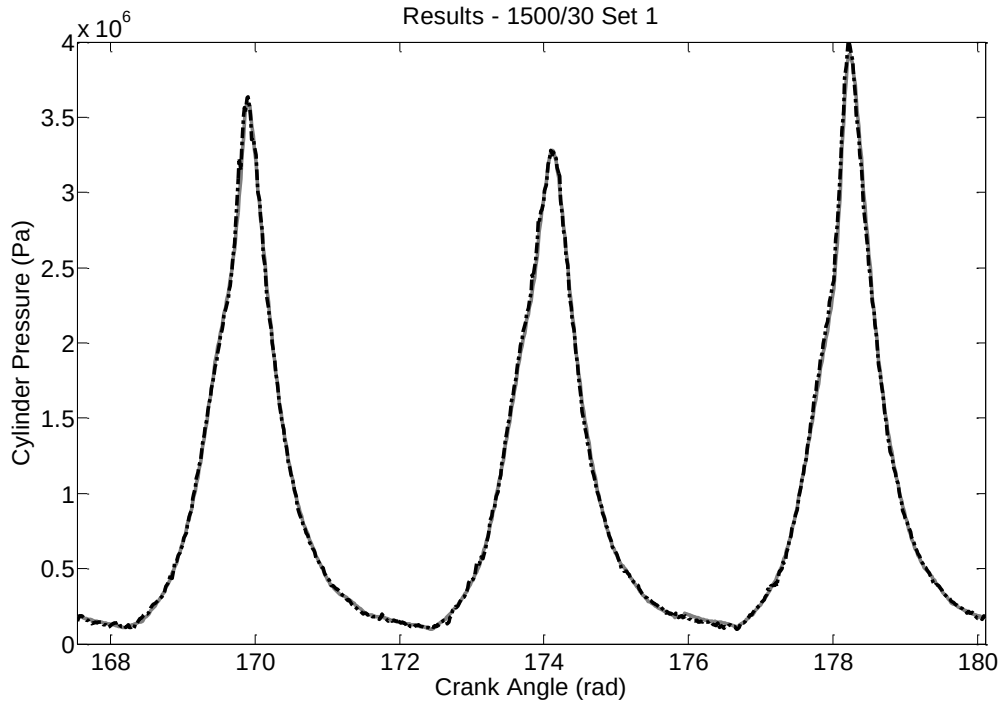

Figure E6.1: Condition-8 Training Results - Best. Measured Cylinder Pressure (Grey Solid Line). Reconstructed Cylinder Pressure (Black Dashed Line). RMSE = 0.74%.

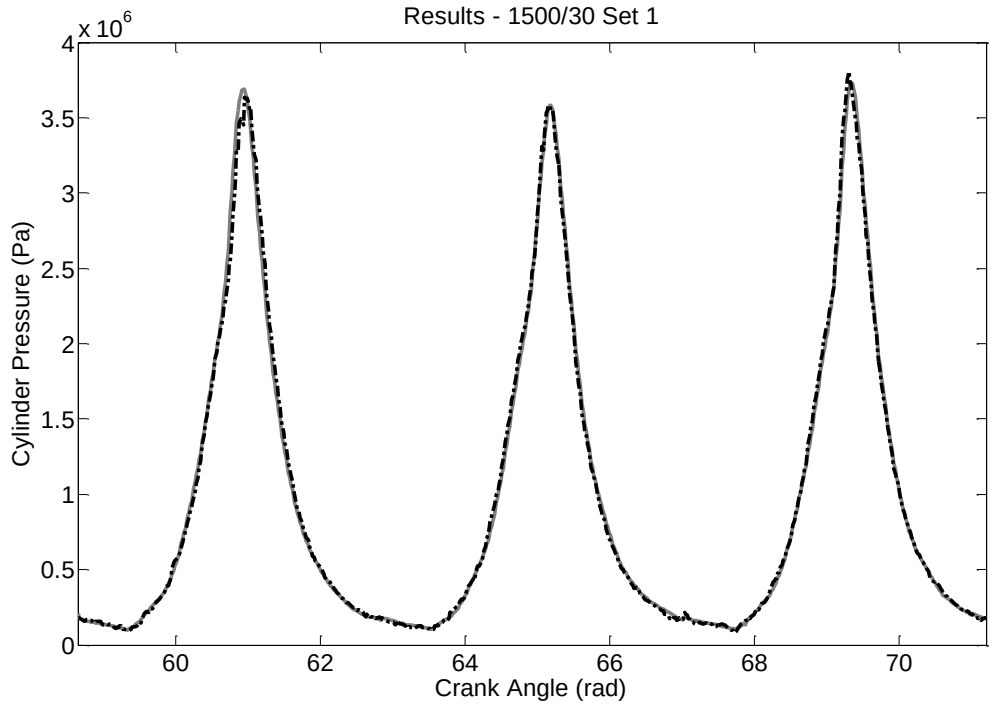

Figure E6.2: Condition-8 Training Results - Average. Measured Cylinder Pressure (Grey Solid Line). Reconstructed Cylinder Pressure (Black Dashed Line). RMSE = 1.21%.

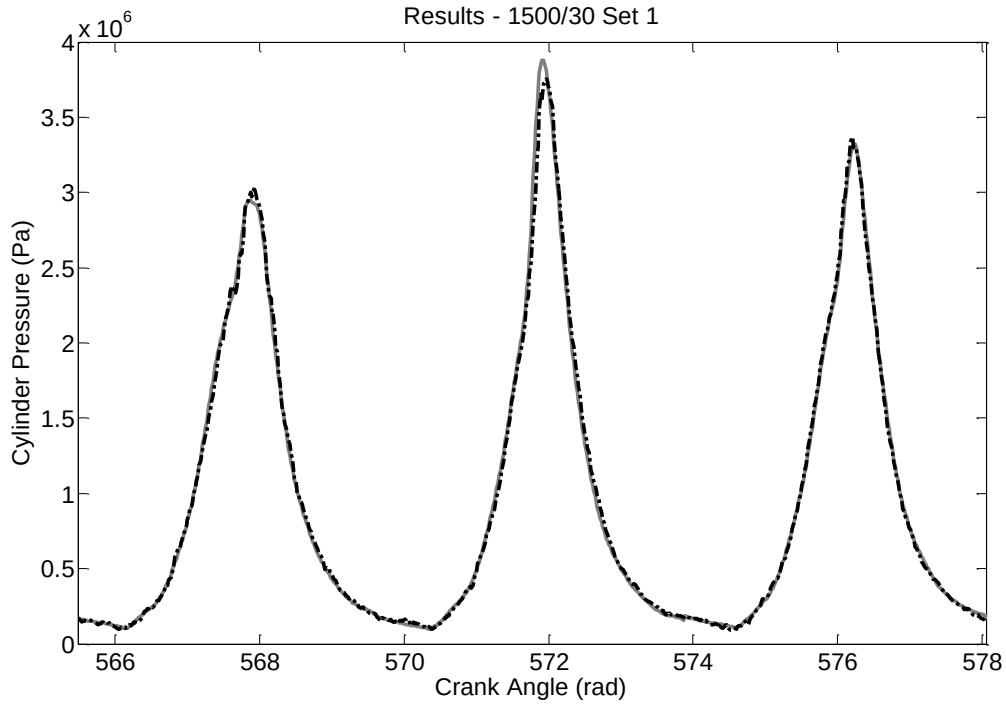

Figure E6.3: Condition-8 Training Results - Worst. Measured Cylinder Pressure (Grey Solid Line). Reconstructed Cylinder Pressure (Black Dashed Line). RMSE = 1.75%.

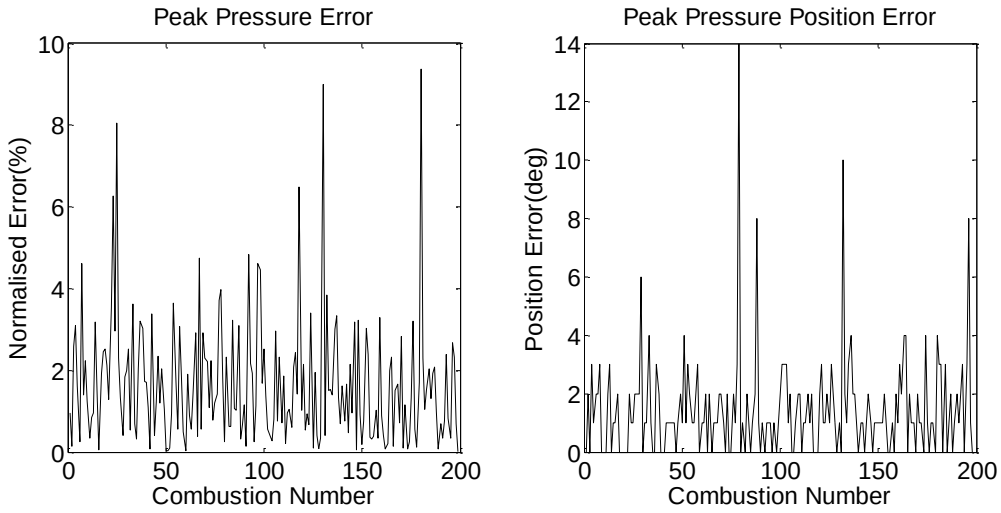

Figure E6.4: Condition-8 Normalised Peak Error Training Results (left). Condition-5 Position of Peak Error Training Results (right)

Table E6.2: Condition-8 Root-Mean-Squared Error (RMSE) and Standard Deviation for the ANN Training

	Training Root-Mean-Squared Error	Training Standard Deviation
Overall Performance	1.19 %	1.19 %
Normalised Peak Error	2.25 %	1.52 %
Peak Pressure Position Error (deg)	2.25	1.70

Generalisation Results

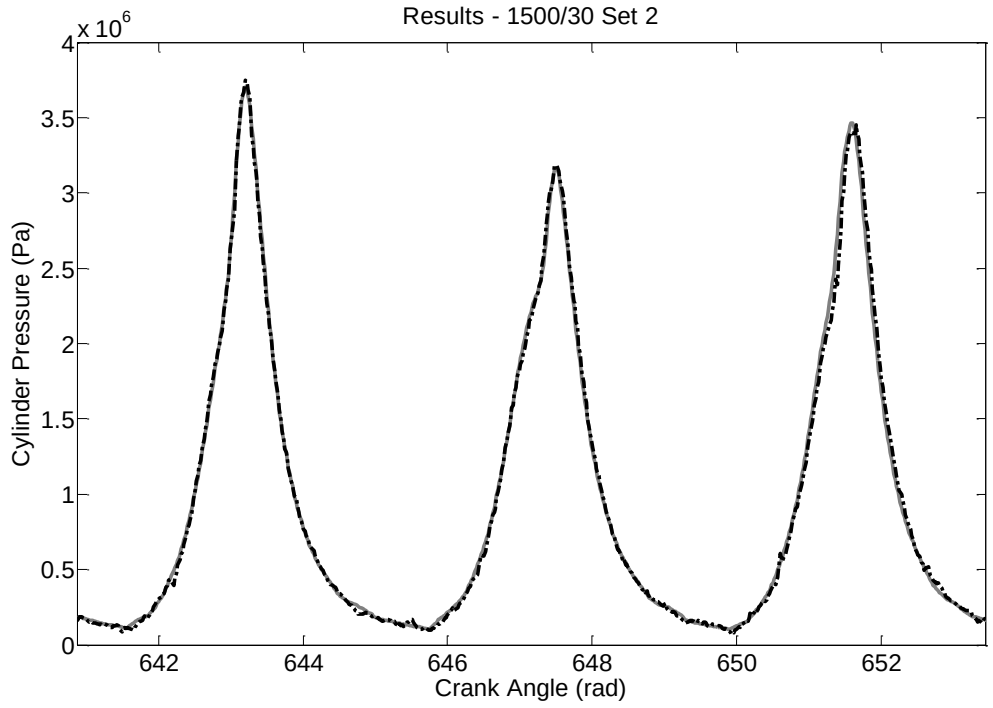

Figure E6.5: Condition-8 Generalisation Results - Best. Measured Cylinder Pressure (Grey Solid Line). Reconstructed Cylinder Pressure (Black Dashed Line). RMSE = 0.72%.

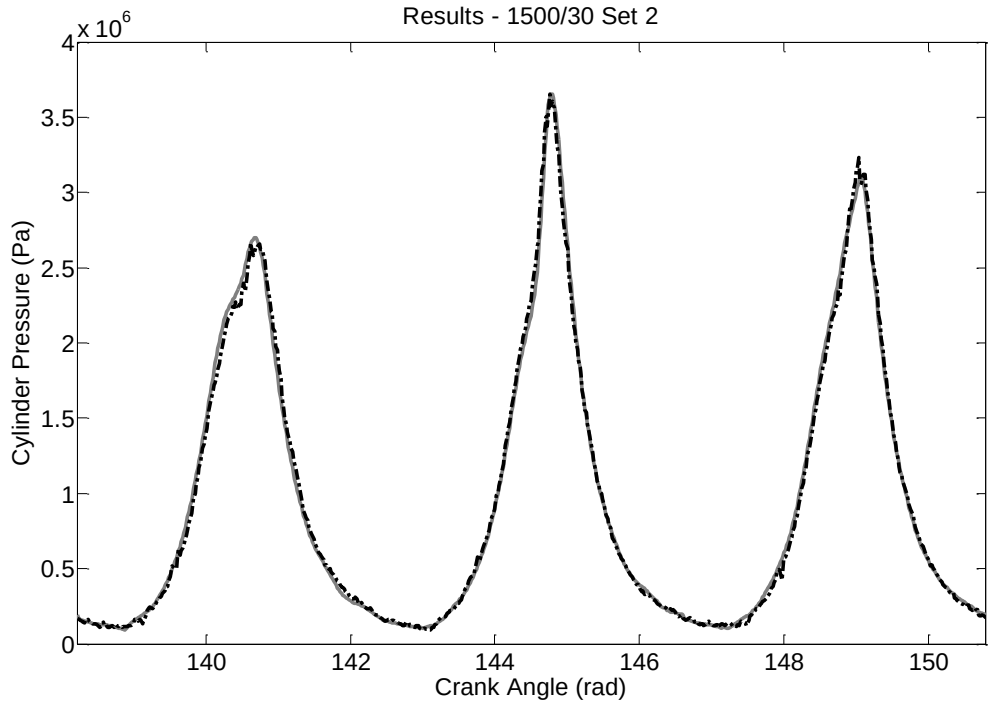

Figure E6.6 Condition-8 Generalisation Results - Average. Measured Cylinder Pressure (Grey Solid Line). Reconstructed Cylinder Pressure (Black Dashed Line). RMSE = 1.21%.

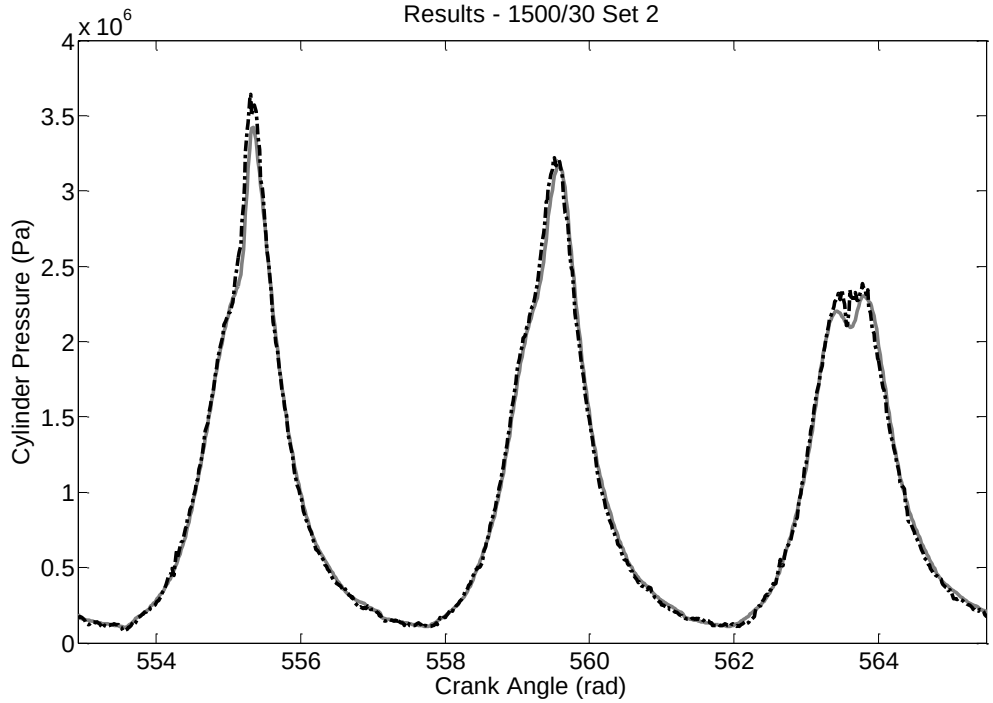

Figure E6.7: Condition-8 Generalisation Results - Worst. Measured Cylinder Pressure (Grey Solid Line). Reconstructed Cylinder Pressure (Black Dashed Line). RMSE = 1.73%.

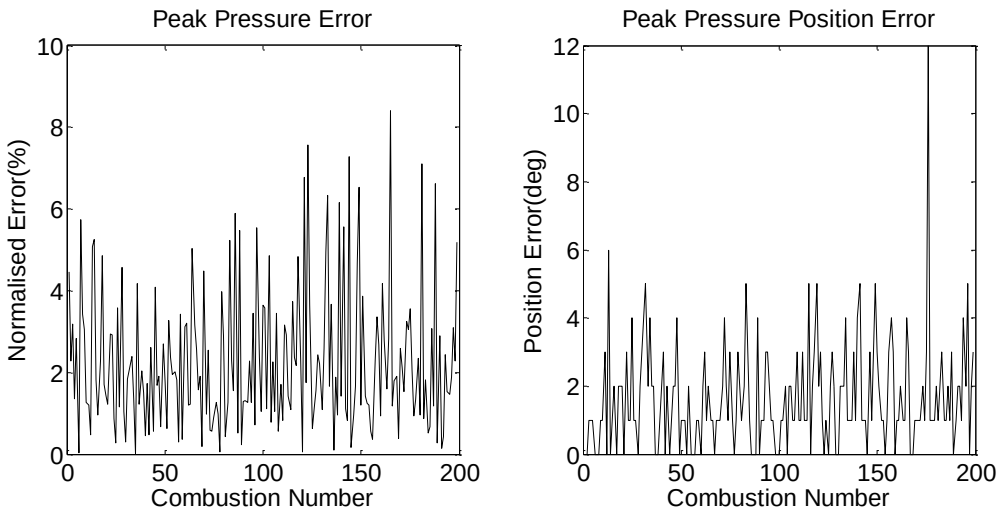

Figure E6.8: Condition-8 Normalised Peak Error Generalisation Results (left). Condition-5 Position of Peak Error Generalisation Results (right)

Table E6.3: Condition-8 Root-Mean-Squared Error (RMSE) and Standard Deviation for the ANN Generalisation

	Generalisation Root-Mean-Squared Error	Generalisation Standard Deviation
Overall Performance	1.30 %	1.29 %
Normalised Peak Error	2.86 %	1.72 %
Peak Pressure Position Error (deg)	2.24	1.53

Appendix F

Engine Block Vibration based Reconstruction Results

Test Condition-2

The first test condition used measured data from running the engine at steady-state with a speed of 1500 rpm and a load of 10 Nm.

Table F1.1: ANN Training Setup for Test Condition-2

Network Name	Net_TD_BA_Test2	**Network Architecture**	Time-Delay	**Test Data**	1500_10_01p_jun2010
Network Training Algorithm	Levenberg–Marquardt	**Hidden Layers Number**	2	**Speed (rpm) / Load (Nm)**	1500/10
Cost Function	Means Squared Error	**Neurons Number**	15/15	**Training to Validation Ratio**	60:40
Training Goal	1E8	**Delay Number**	240	**Crank Step**	1 Deg
Maximum Epoch	1000	**Transfer Function Layer 1**	Sigmoid	**Number of Iterations**	10
Weights Initialisation	Randomised	**Transfer Function Layer 2**	Linear		

Training Results

In total 10 different ANNs were trained with the overall performance of the ANNs ranging from 1.54% to 1.91% RMSE. The best performing ANN was selected which trained in 681 seconds (0.19 hours) in 39 epochs.

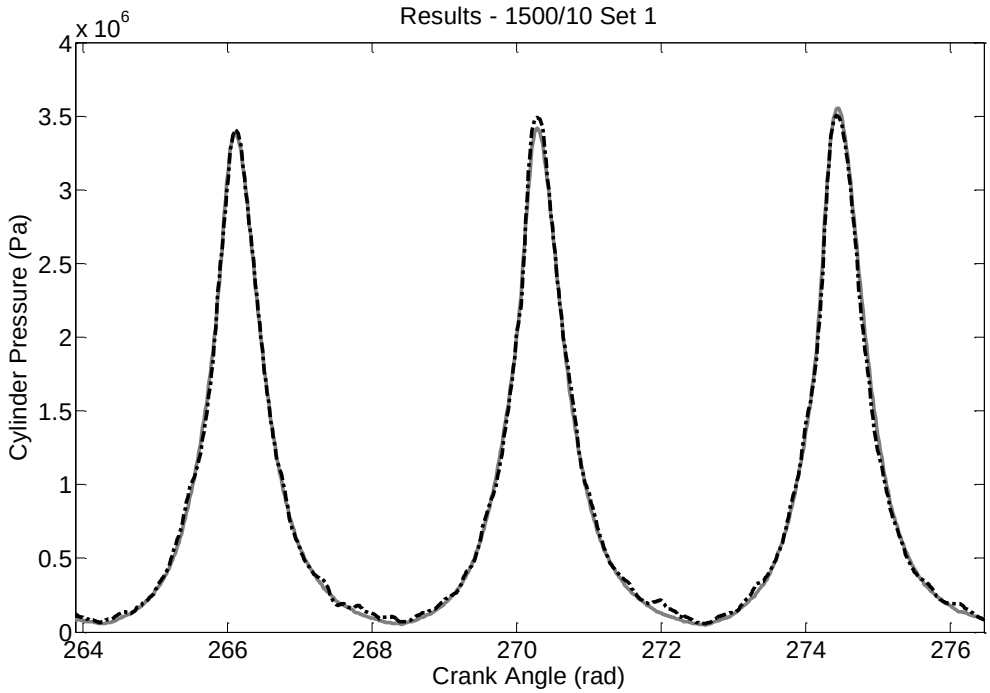

Figure F1.1: Condition-2 Training Results - Best. Measured Cylinder Pressure (Grey Solid Line). Reconstructed Cylinder Pressure (Black Dashed Line). RMSE = 1.16%.

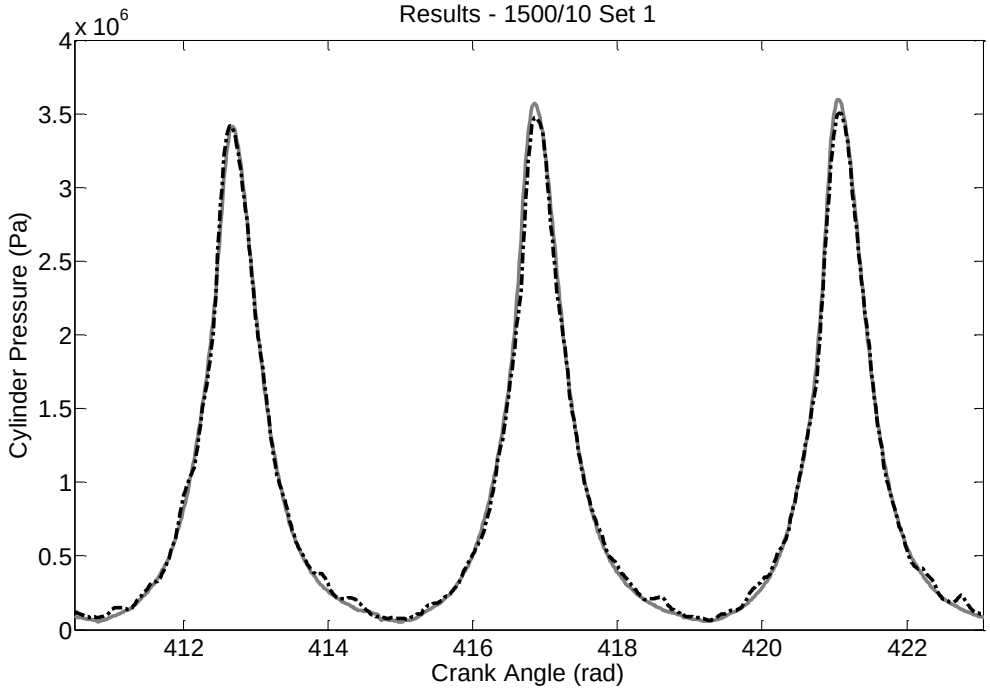

Figure F1.2: Condition-2 Training Results - Average. Measured Cylinder Pressure (Grey Solid Line). Reconstructed Cylinder Pressure (Black Dashed Line). RMSE = 1.56%.

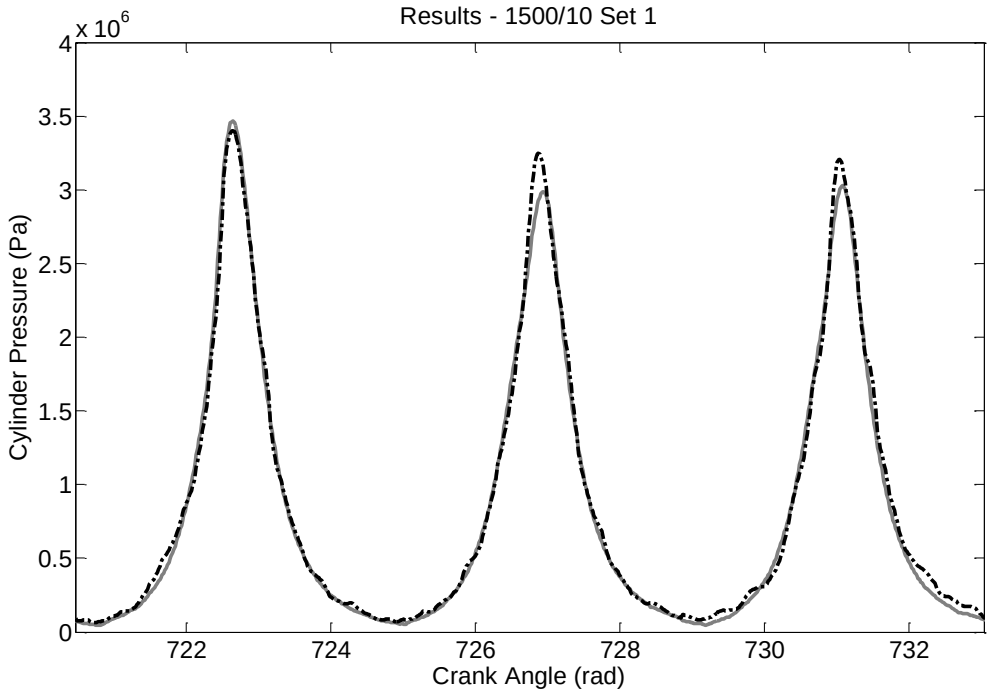

Figure F1.3: Condition-2 Training Results - Worst. Measured Cylinder Pressure (Grey Solid Line). Reconstructed Cylinder Pressure (Black Dashed Line). RMSE = 1.93%.

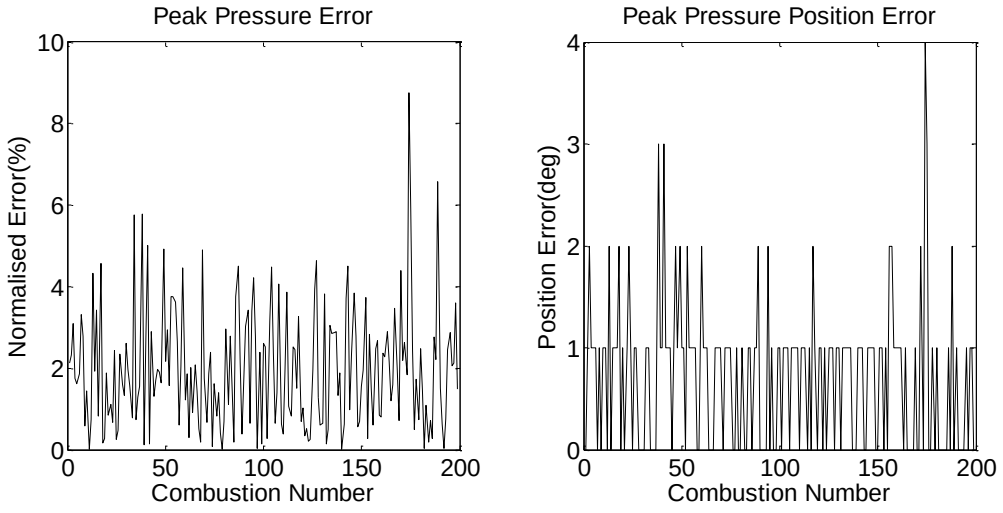

Figure F1.4: Condition-2 Normalised Peak Error Training Results (left). Condition-5 Position of Peak Error Training Results (right)

Table F1.2: Condition-2 Root-Mean-Squared Error (RMSE) and Standard Deviation for the ANN Training

	Training Root-Mean-Squared Error	Training Standard Deviation
Overall Performance	1.55 %	1.54 %
Normalised Peak Error	2.45 %	1.46 %
Peak Pressure Position Error (deg)	1.00	0.71

Generalisation Results

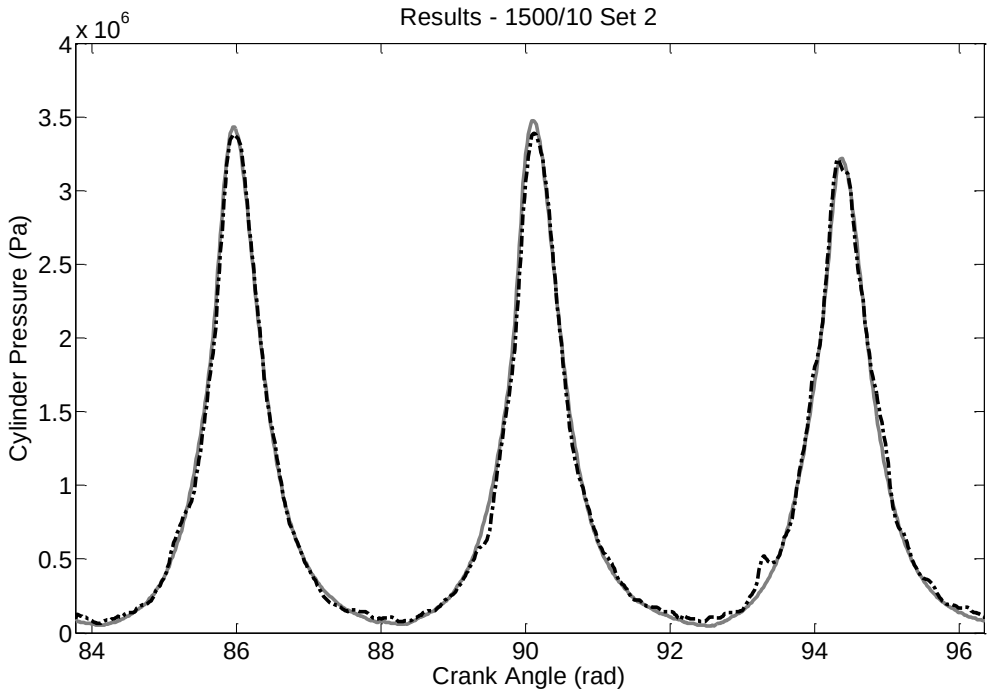

Figure F1.5: Condition-2 Generalisation Results - Best. Measured Cylinder Pressure (Grey Solid Line). Reconstructed Cylinder Pressure (Black Dashed Line). RMSE = 1.47%.

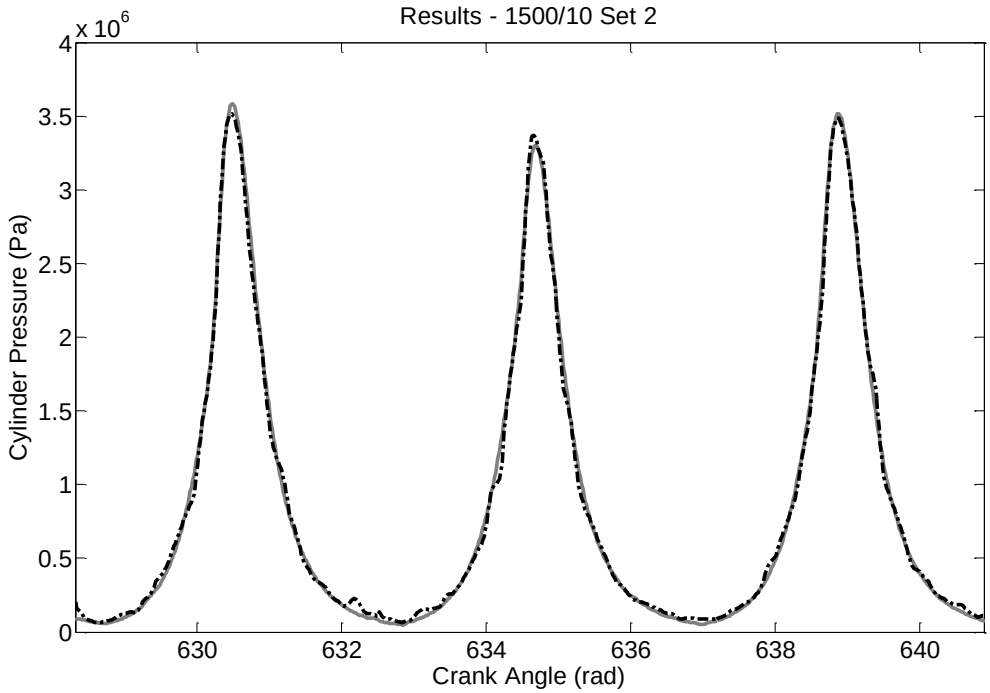

Figure F1.6 Condition-2 Generalisation Results - Average. Measured Cylinder Pressure (Grey Solid Line). Reconstructed Cylinder Pressure (Black Dashed Line). RMSE = 1.92%.

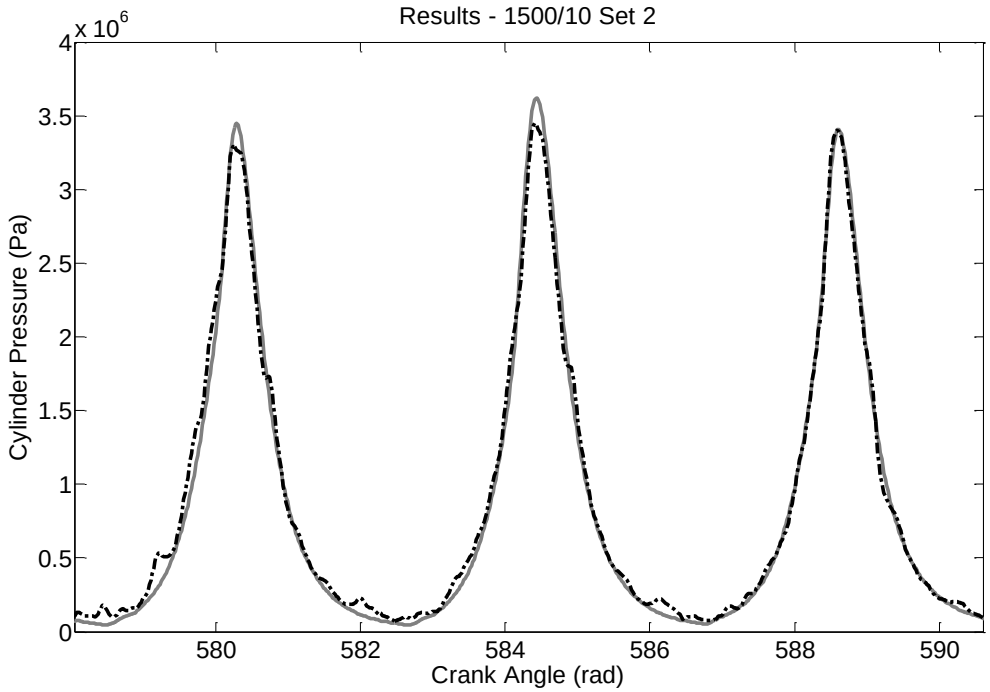

Figure F1.7: Condition-2 Generalisation Results - Worst. Measured Cylinder Pressure (Grey Solid Line). Reconstructed Cylinder Pressure (Black Dashed Line). RMSE = 2.54%.

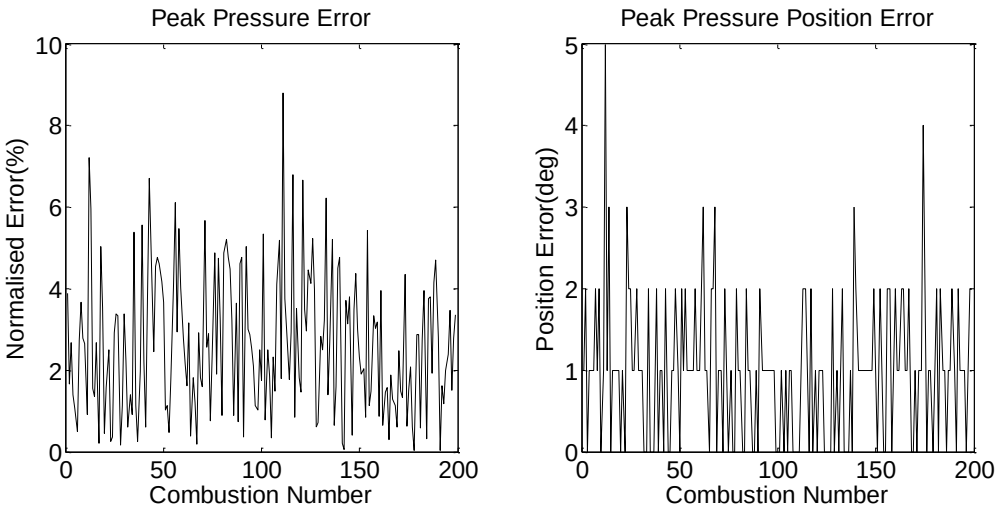

Figure F1.8: Condition-2 Normalised Peak Error Generalisation Results (left). Condition-5 Position of Peak Error Generalisation Results (right)

Table F1.3: Condition-2 Root-Mean-Squared Error (RMSE) and Standard Deviation for the ANN Generalisation

	Generalisation Root-Mean-Squared Error	Generalisation Standard Deviation
Overall Performance	1.32 %	1.32 %
Normalised Peak Error	3.14 %	1.71 %
Peak Pressure Position Error (deg)	1.31	0.86

Test Condition-3

The first test condition used measured data from running the engine at steady-state with a speed of 2000 rpm and a load of 10 Nm.

Table F2.1: ANN Training Setup for Test Condition-3

Network Name	Net_TD_BA_Test3	**Network Architecture**	Time-Delay	**Test Data**	2000_10_01p_jun2010
Network Training Algorithm	Levenberg–Marquardt	**Hidden Layers Number**	2	**Speed (rpm) / Load (Nm)**	2000/10
Cost Function	Means Squared Error	**Neurons Number**	15/15	**Training to Validation Ratio**	60:40
Training Goal	1E8	**Delay Number**	240	**Crank Step**	1 Deg
Maximum Epoch	1000	**Transfer Function Layer 1**	Sigmoid	**Number of Iterations**	10
Weights Initialisation	Randomised	**Transfer Function Layer 2**	Linear		

Training Results

In total 10 different ANNs were trained with the overall performance of the ANNs ranging from 1.61% to 2.67% RMSE. The best performing ANN was selected which trained in 935 seconds (0.26 hours) in 26 epochs.

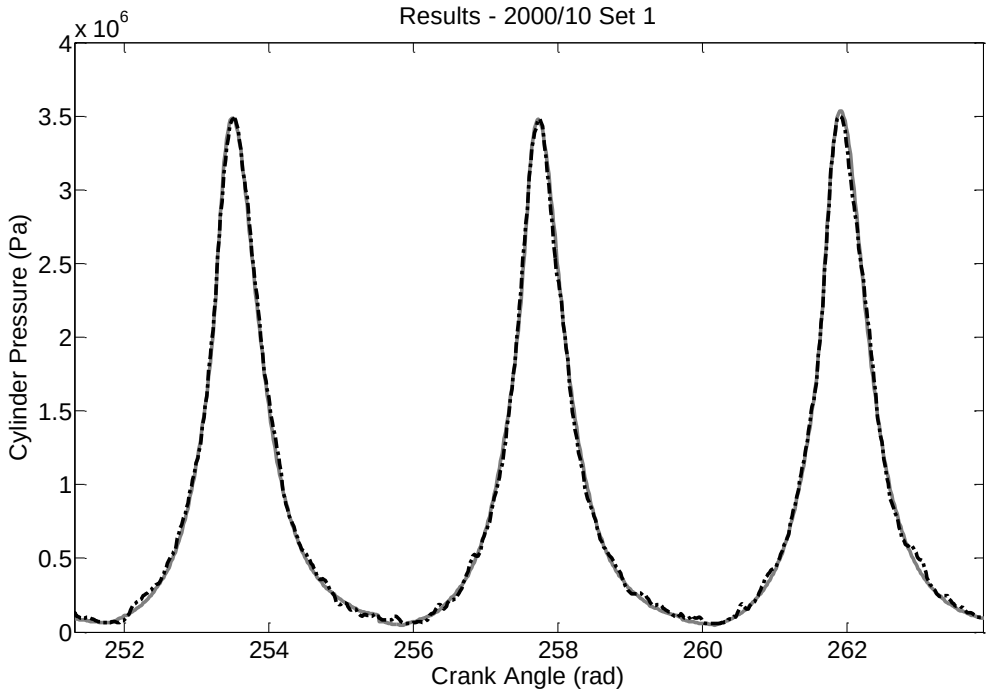

Figure F2.1: Condition-3 Training Results - Best. Measured Cylinder Pressure (Grey Solid Line). Reconstructed Cylinder Pressure (Black Dashed Line). RMSE = 1.03%.

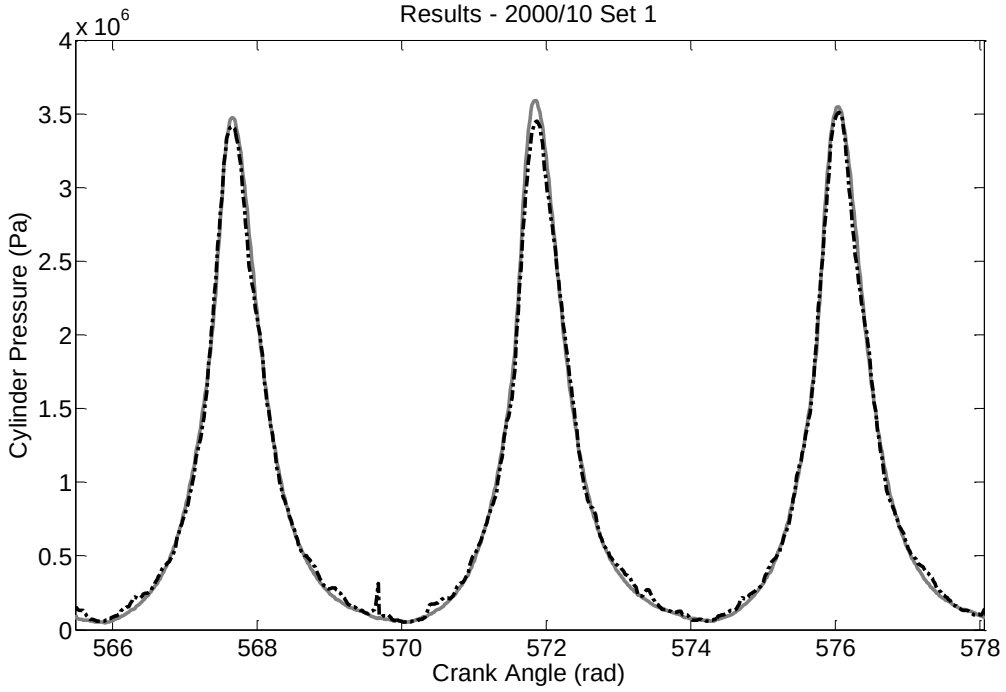

Figure F2.2: Condition-3 Training Results - Average. Measured Cylinder Pressure (Grey Solid Line). Reconstructed Cylinder Pressure (Black Dashed Line). RMSE = 1.54%.

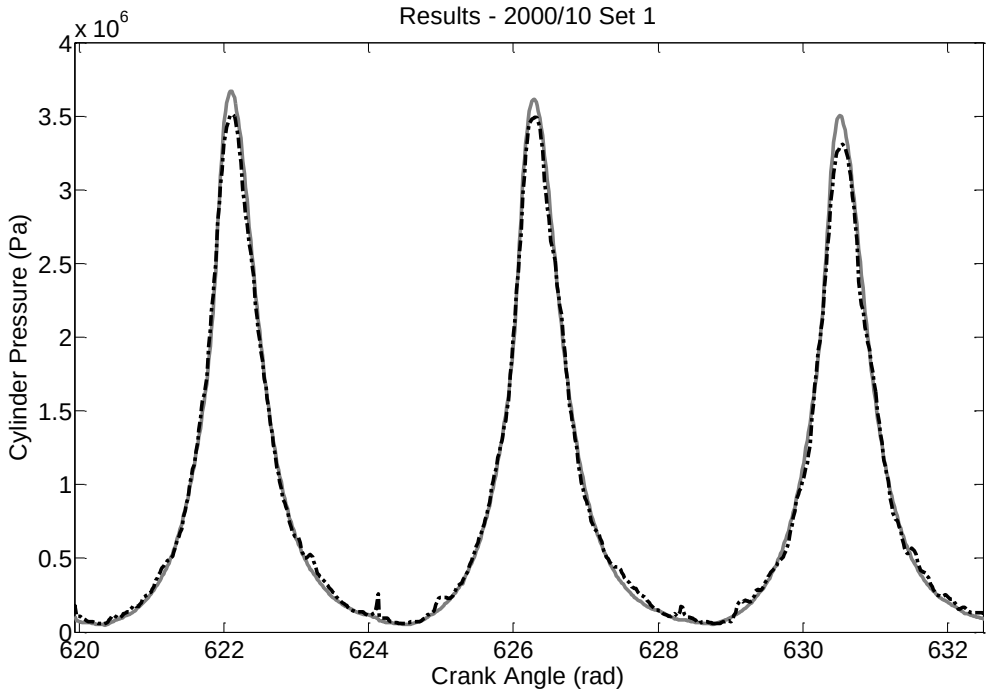

Figure F2.3: Condition-3 Training Results - Worst. Measured Cylinder Pressure (Grey Solid Line). Reconstructed Cylinder Pressure (Black Dashed Line). RMSE = 1.95%.

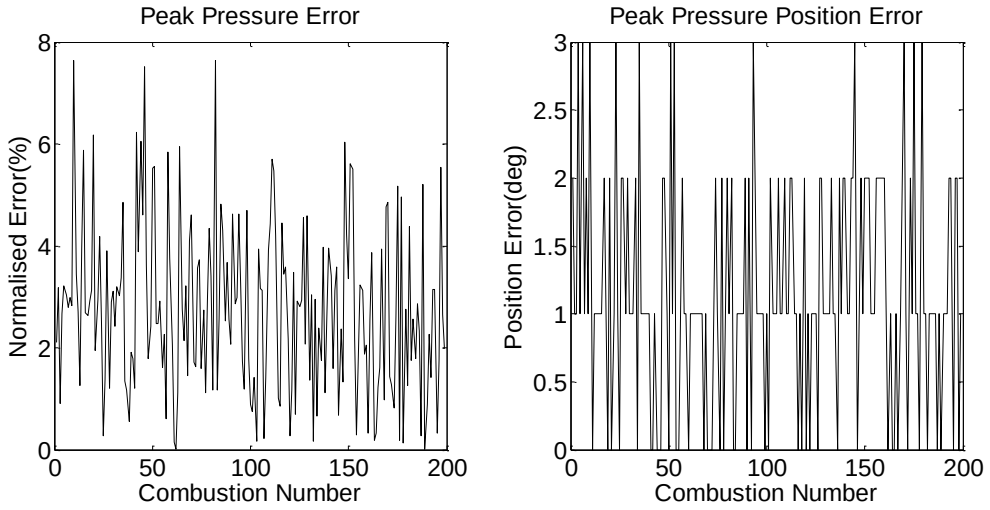

Figure F2.4: Condition-3 Normalised Peak Error Training Results (left). Condition-5 Position of Peak Error Training Results (right)

Table F2.2: Condition-3 Root-Mean-Squared Error (RMSE) and Standard Deviation for the ANN Training

	Training Root-Mean-Squared Error	Training Standard Deviation
Overall Performance	1.61 %	1.60 %
Normalised Peak Error	3.20 %	1.64 %
Peak Pressure Position Error (deg)	1.40	0.83

Generalisation Results

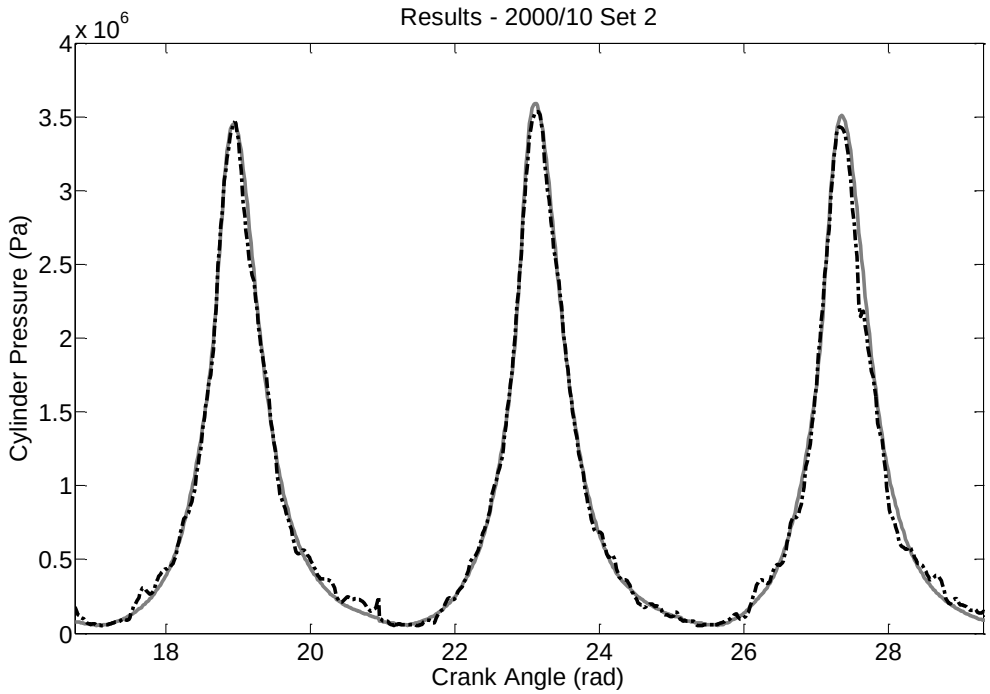

Figure F2.5: Condition-3 Generalisation Results - Best. Measured Cylinder Pressure (Grey Solid Line). Reconstructed Cylinder Pressure (Black Dashed Line). RMSE = 1.30%.

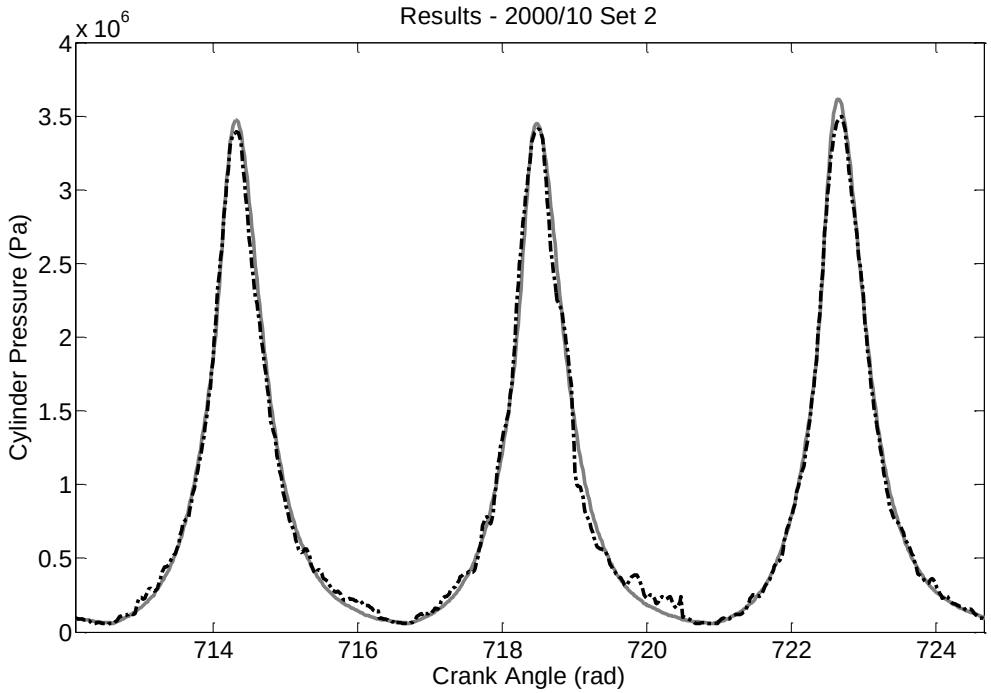

Figure F2.6 Condition-3 Generalisation Results - Average. Measured Cylinder Pressure (Grey Solid Line). Reconstructed Cylinder Pressure (Black Dashed Line). RMSE = 2.04%.

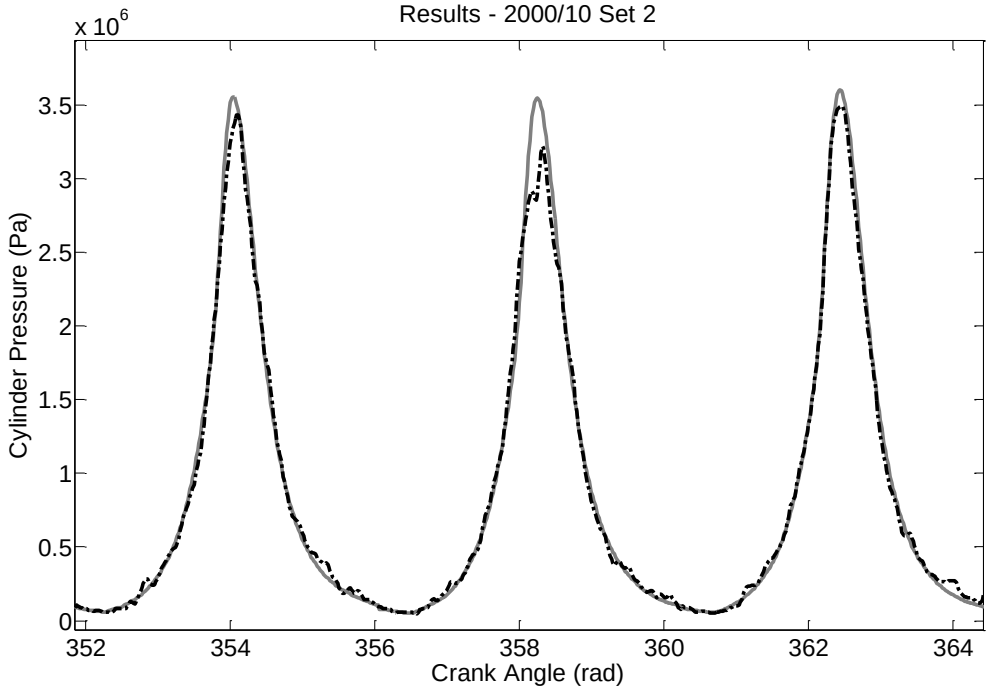

Figure F2.7: Condition-2 Generalisation Results - Worst. Measured Cylinder Pressure (Grey Solid Line). Reconstructed Cylinder Pressure (Black Dashed Line). RMSE = 2.49%.

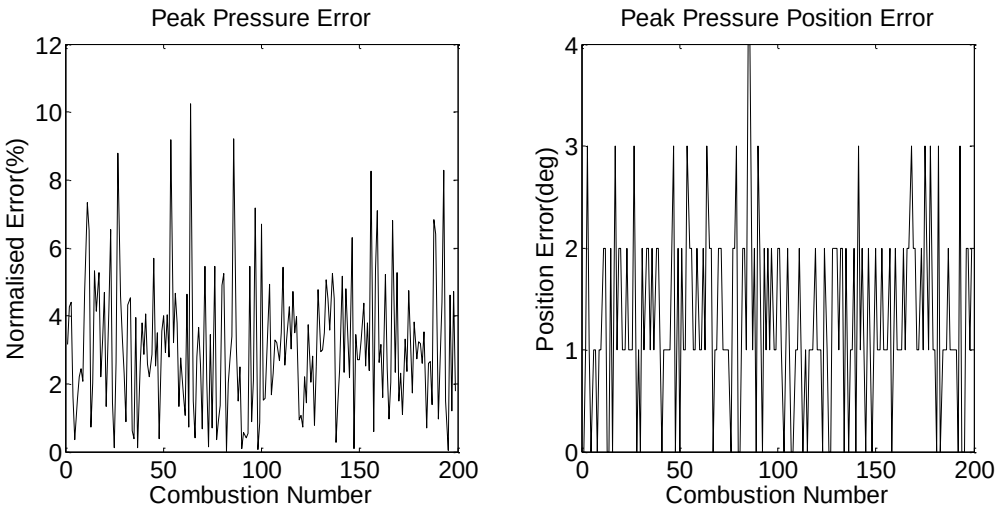

Figure F2.8: Condition-3 Normalised Peak Error Generalisation Results (left). Condition-5 Position of Peak Error Generalisation Results (right)

Table F2.3: Condition-3 Root-Mean-Squared Error (RMSE) and Standard Deviation for the ANN Generalisation

	Generalisation Root-Mean-Squared Error	Generalisation Standard Deviation
Overall Performance	1.94 %	1.93 %
Normalised Peak Error	3.68 %	1.99 %
Peak Pressure Position Error (deg)	1.57	0.88

Test Condition-4

The first test condition used measured data from running the engine at steady-state with a speed of 1000 rpm and a load of 20 Nm.

Table F3.1: ANN Training Setup for Test Condition-4

Network Name	Net_TD_BA_Test4	**Network Architecture**	Time-Delay	**Test Data**	1000_20_01p_jun2010
Network Training Algorithm	Levenberg–Marquardt	**Hidden Layers Number**	2	**Speed (rpm) / Load (Nm)**	1000/20
Cost Function	Means Squared Error	**Neurons Number**	15/15	**Training to Validation Ratio**	60:40
Training Goal	1E8	**Delay Number**	240	**Crank Step**	1 Deg
Maximum Epoch	1000	**Transfer Function Layer 1**	Sigmoid	**Number of Iterations**	10
Weights Initialisation	Randomised	**Transfer Function Layer 2**	Linear		

Training Results

In total 10 different ANNs were trained with the overall performance of the ANNs ranging from 2.68% to 4.25% RMSE. The best performing ANN was selected which trained in 2177 seconds (0.60 hours) in 33 epochs.

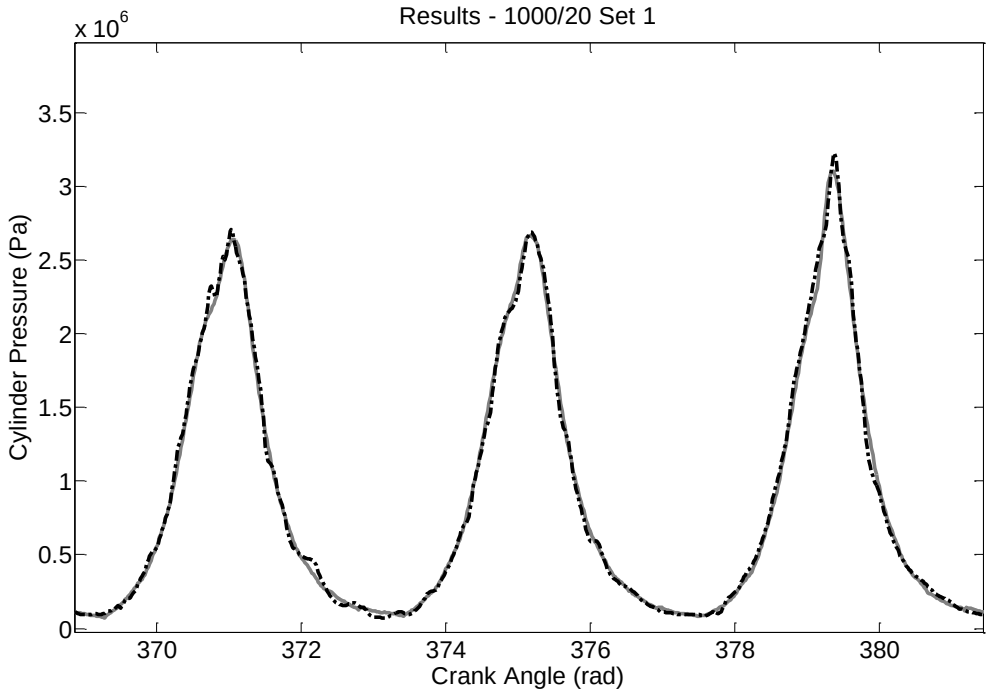

Figure F3.1: Condition-4 Training Results - Best. Measured Cylinder Pressure (Grey Solid Line). Reconstructed Cylinder Pressure (Black Dashed Line). RMSE = 1.23%.

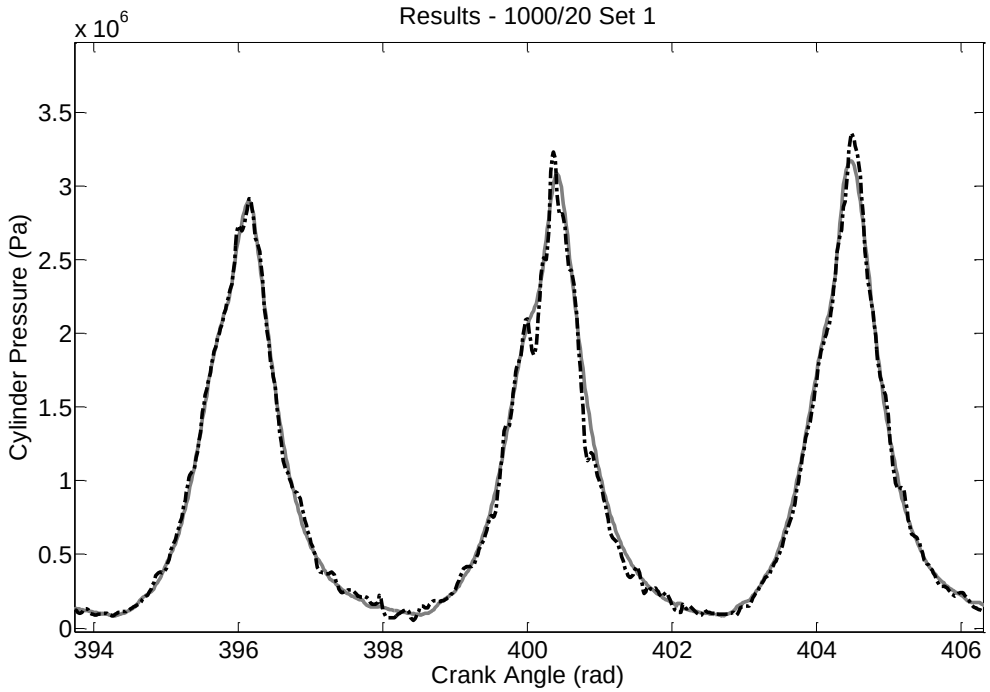

Figure F3.2: Condition-4 Training Results - Average. Measured Cylinder Pressure (Grey Solid Line). Reconstructed Cylinder Pressure (Black Dashed Line). RMSE = 2.71%.

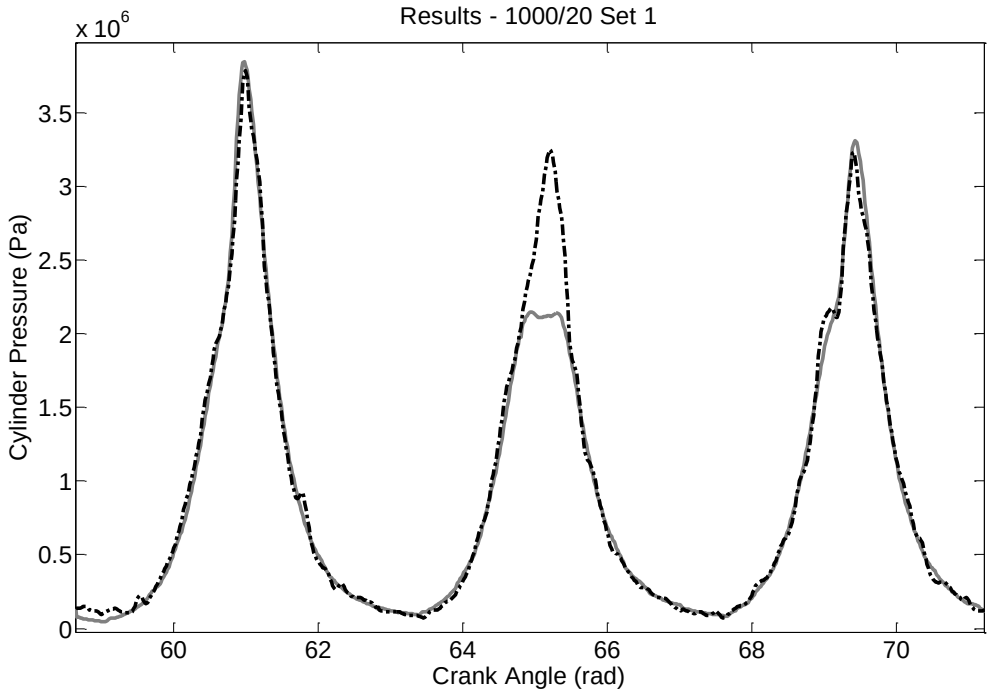

Figure F3.3: Condition-4 Training Results - Worst. Measured Cylinder Pressure (Grey Solid Line). Reconstructed Cylinder Pressure (Black Dashed Line). RMSE = 4.53%.

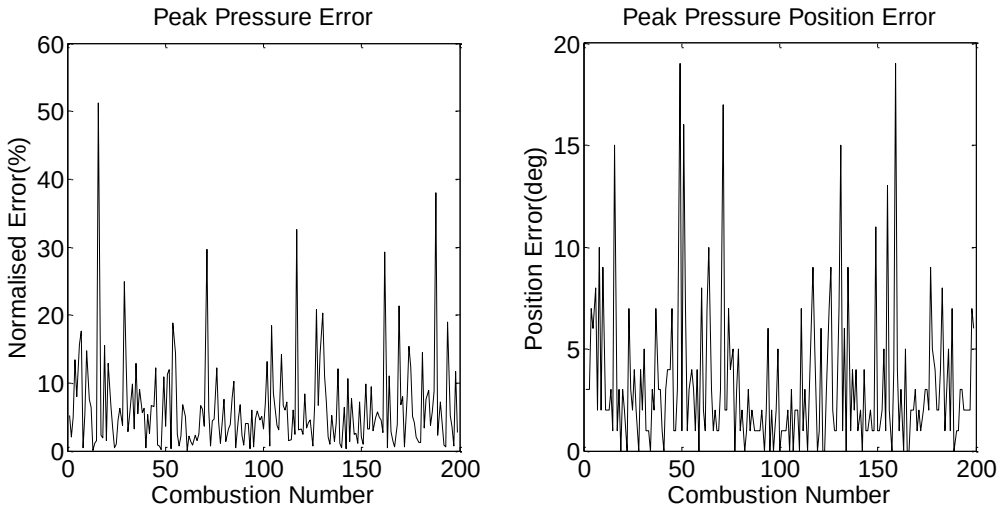

Figure F3.4: Condition-4 Normalised Peak Error Training Results (left). Condition-5 Position of Peak Error Training Results (right)

Table F3.2: Condition-4 Root-Mean-Squared Error (RMSE) and Standard Deviation for the ANN Training

	Training Root-Mean-Squared Error	Training Standard Deviation
Overall Performance	2.71 %	2.71 %
Normalised Peak Error	4.76 %	3.49 %
Peak Pressure Position Error (deg)	2.77	1.49

Generalisation Results

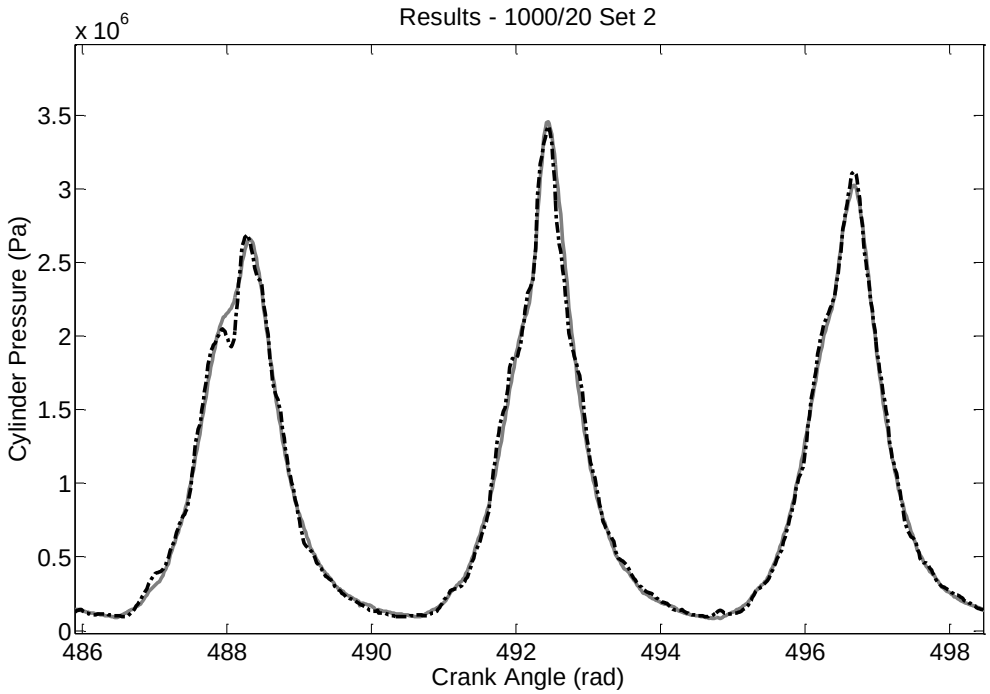

Figure F3.5: Condition-4 Generalisation Results - Best. Measured Cylinder Pressure (Grey Solid Line). Reconstructed Cylinder Pressure (Black Dashed Line). RMSE = 1.54%.

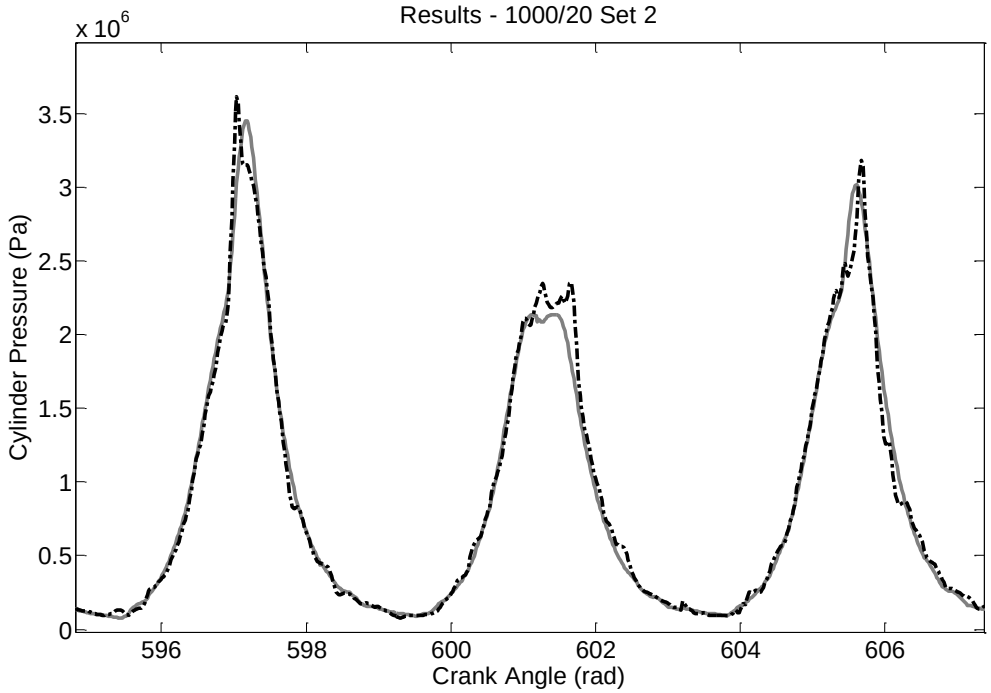

Figure F3.6 Condition-4 Generalisation Results - Average. Measured Cylinder Pressure (Grey Solid Line). Reconstructed Cylinder Pressure (Black Dashed Line). RMSE = 2.66%.

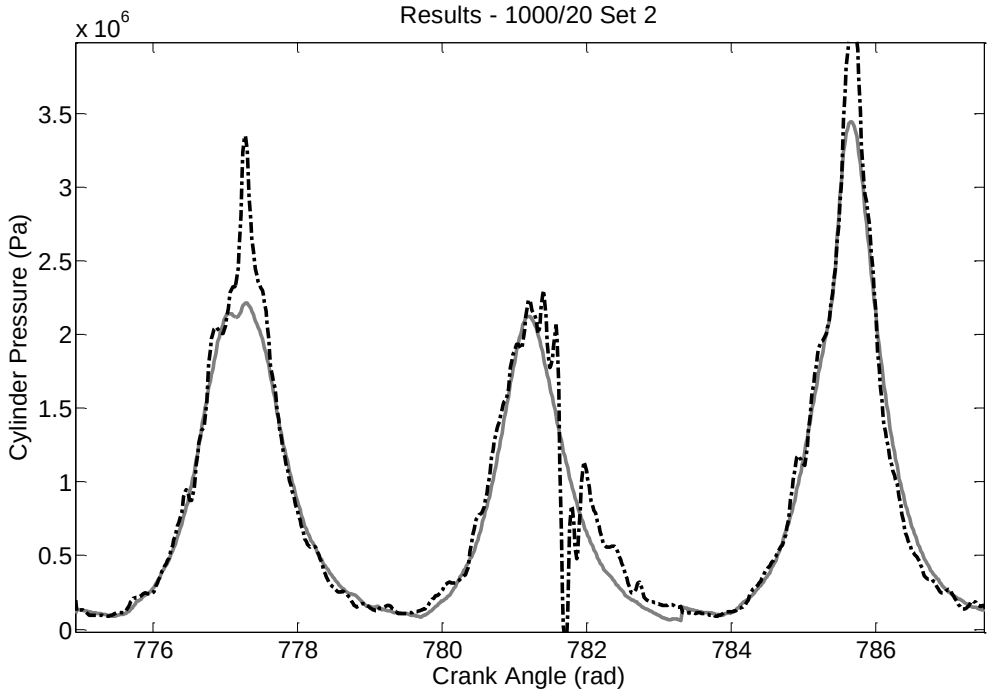

Figure F3.7: Condition-4 Generalisation Results - Worst. Measured Cylinder Pressure (Grey Solid Line). Reconstructed Cylinder Pressure (Black Dashed Line). RMSE = 5.49%.

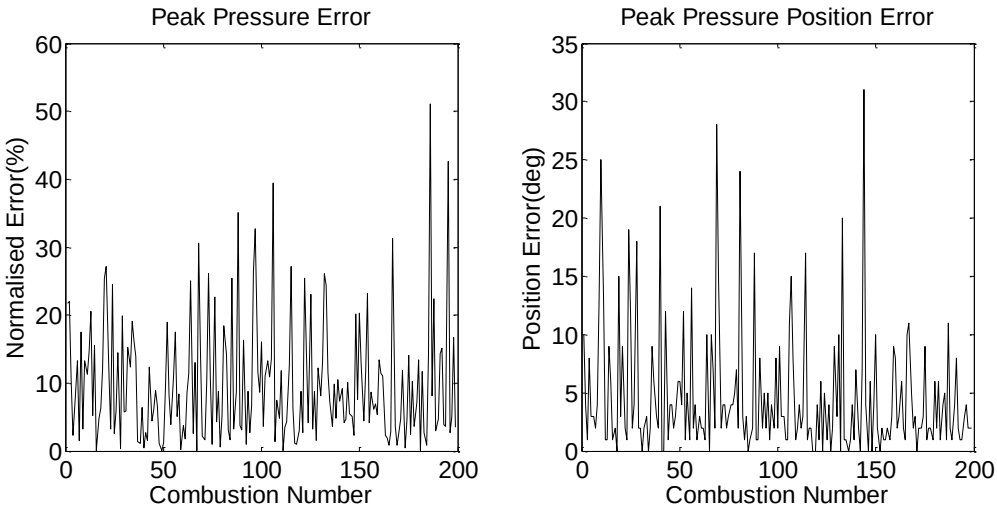

Figure F3.8: Condition-4 Normalised Peak Error Generalisation Results (left). Condition-5 Position of Peak Error Generalisation Results (right)

Table F3.3: Condition-4 Root-Mean-Squared Error (RMSE) and Standard Deviation for the ANN Generalisation

	Generalisation Root-Mean-Squared Error	Generalisation Standard Deviation
Overall Performance	3.46 %	3.44 %
Normalised Peak Error	13.2 %	8.84 %
Peak Pressure Position Error (deg)	5.01	3.36

Test Condition-6

The first test condition used measured data from running the engine at steady-state with a speed of 2000 rpm and a load of 20 Nm.

Table F4.1: ANN Training Setup for Test Condition-6

Network Name	Net_TD_BA_Test6	**Network Architecture**	Time-Delay	**Test Data**	2000_20_01p_jun2010
Network Training Algorithm	Levenberg–Marquardt	**Hidden Layers Number**	2	**Speed (rpm) / Load (Nm)**	2000/20
Cost Function	Means Squared Error	**Neurons Number**	15/15	**Training to Validation Ratio**	60:40
Training Goal	1E8	**Delay Number**	240	**Crank Step**	1 Deg
Maximum Epoch	1000	**Transfer Function Layer 1**	Sigmoid	**Number of Iterations**	10
Weights Initialisation	Randomised	**Transfer Function Layer 2**	Linear		

Training Results

In total 10 different ANNs were trained with the overall performance of the ANNs ranging from 1.69% to 1.86% RMSE. The best performing ANN was selected which trained in 1057 seconds (0.29 hours) in 15 epochs.

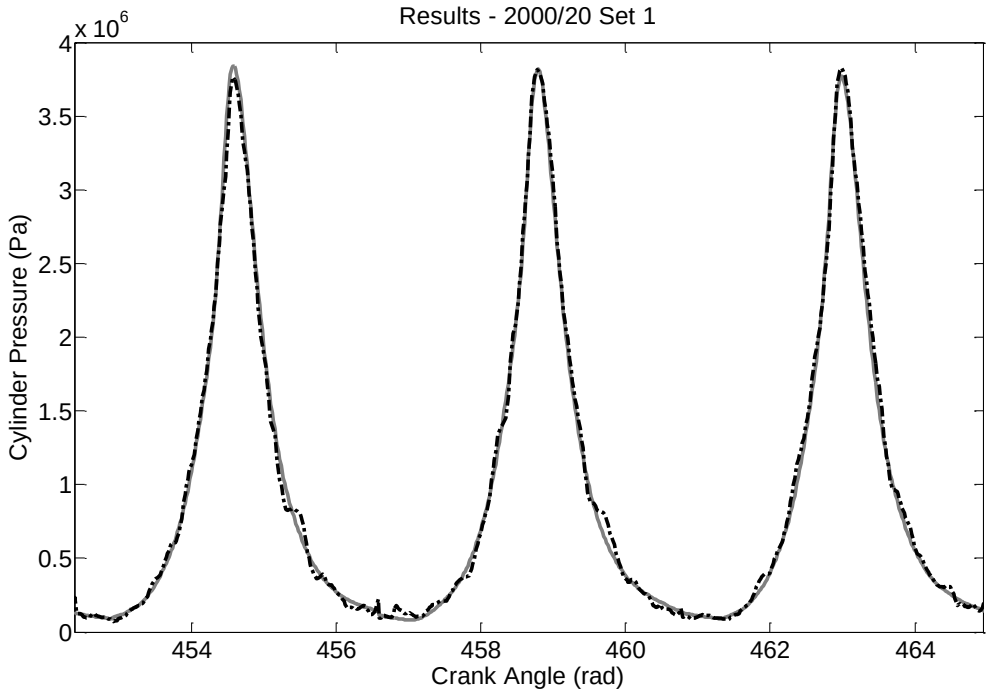

Figure F4.1: Condition-6 Training Results - Best. Measured Cylinder Pressure (Grey Solid Line). Reconstructed Cylinder Pressure (Black Dashed Line). RMSE = 1.31%.

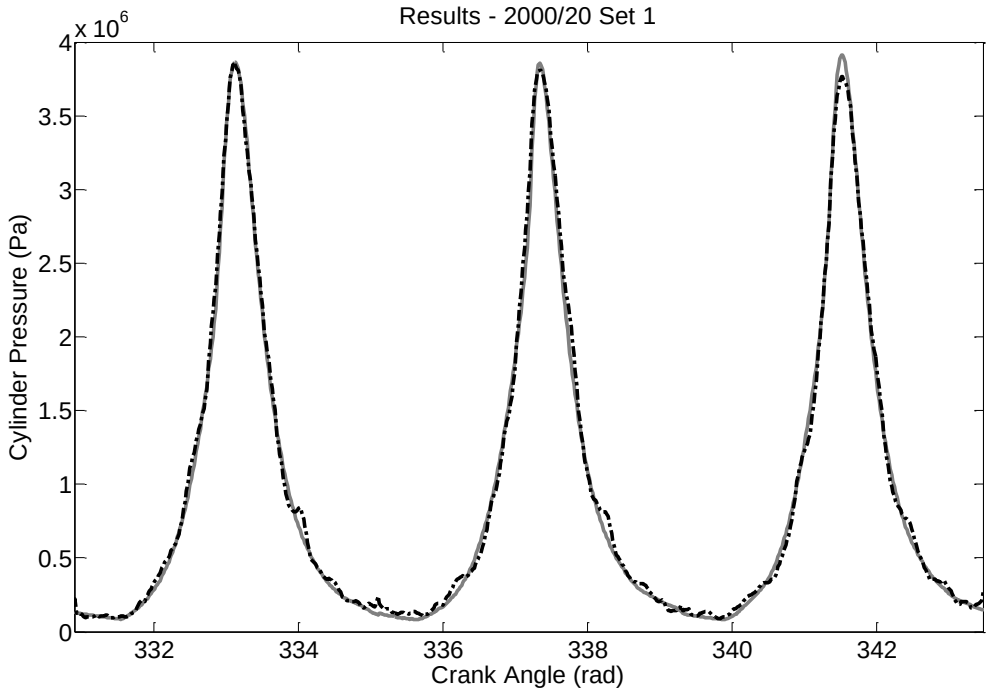

Figure F4.2: Condition-6 Training Results - Average. Measured Cylinder Pressure (Grey Solid Line). Reconstructed Cylinder Pressure (Black Dashed Line). RMSE = 1.69%.

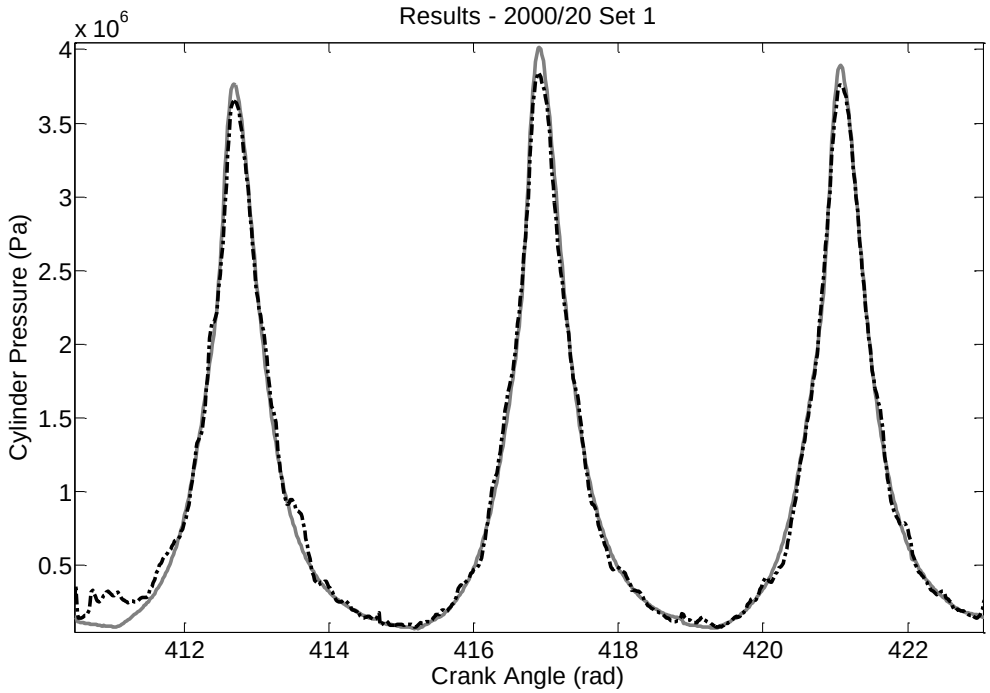

Figure F4.3: Condition-6 Training Results - Worst. Measured Cylinder Pressure (Grey Solid Line). Reconstructed Cylinder Pressure (Black Dashed Line). RMSE = 2.39%.

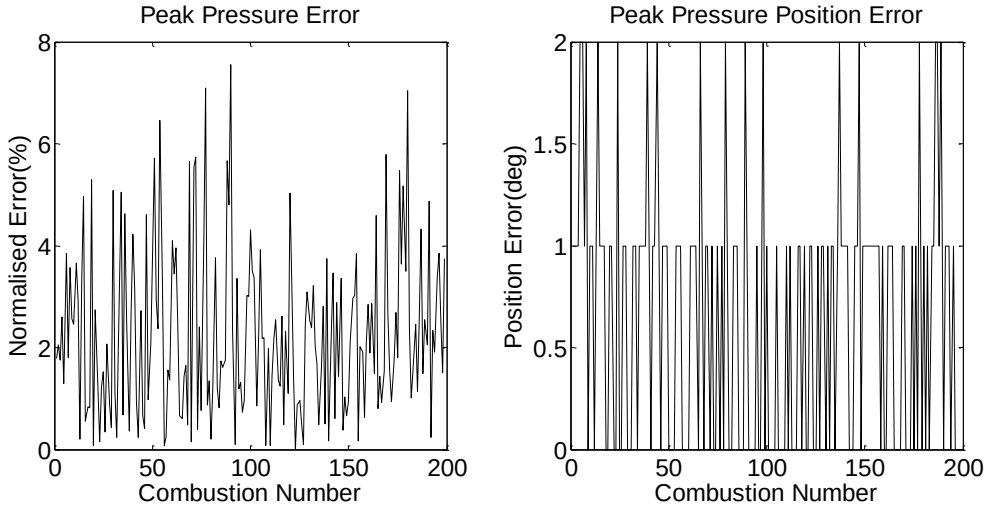

Figure F4.4: Condition-6 Normalised Peak Error Training Results (left). Condition-5 Position of Peak Error Training Results (right)

Table F4.2: Condition-6 Root-Mean-Squared Error (RMSE) and Standard Deviation for the ANN Training

	Training Root-Mean-Squared Error	Training Standard Deviation
Overall Performance	1.69 %	1.66 %
Normalised Peak Error	2.77 %	1.61 %
Peak Pressure Position Error (deg)	0.91	0.63

Generalisation Results

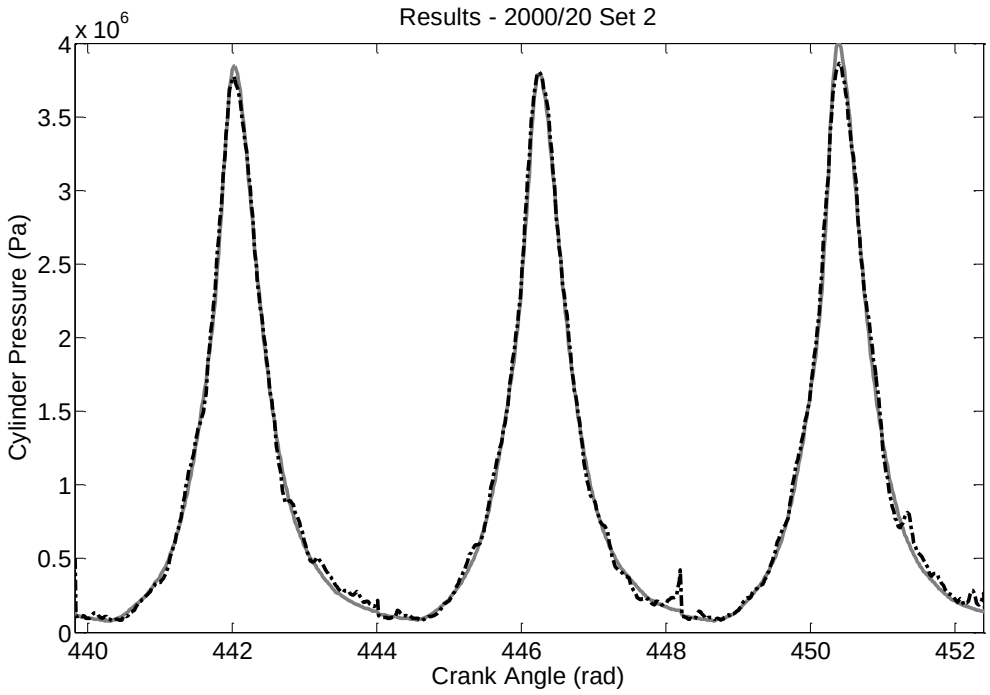

Figure F4.5: Condition-6 Generalisation Results - Best. Measured Cylinder Pressure (Grey Solid Line). Reconstructed Cylinder Pressure (Black Dashed Line). RMSE = 1.59%.

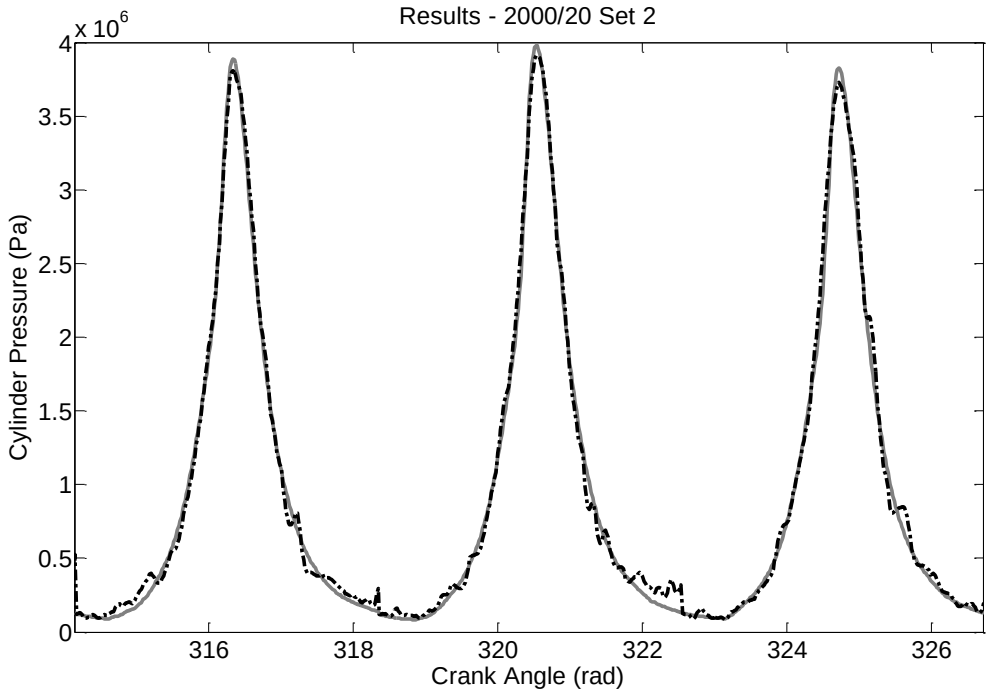

Figure F4.6 Condition-6 Generalisation Results - Average. Measured Cylinder Pressure (Grey Solid Line). Reconstructed Cylinder Pressure (Black Dashed Line). RMSE = 2.03%.

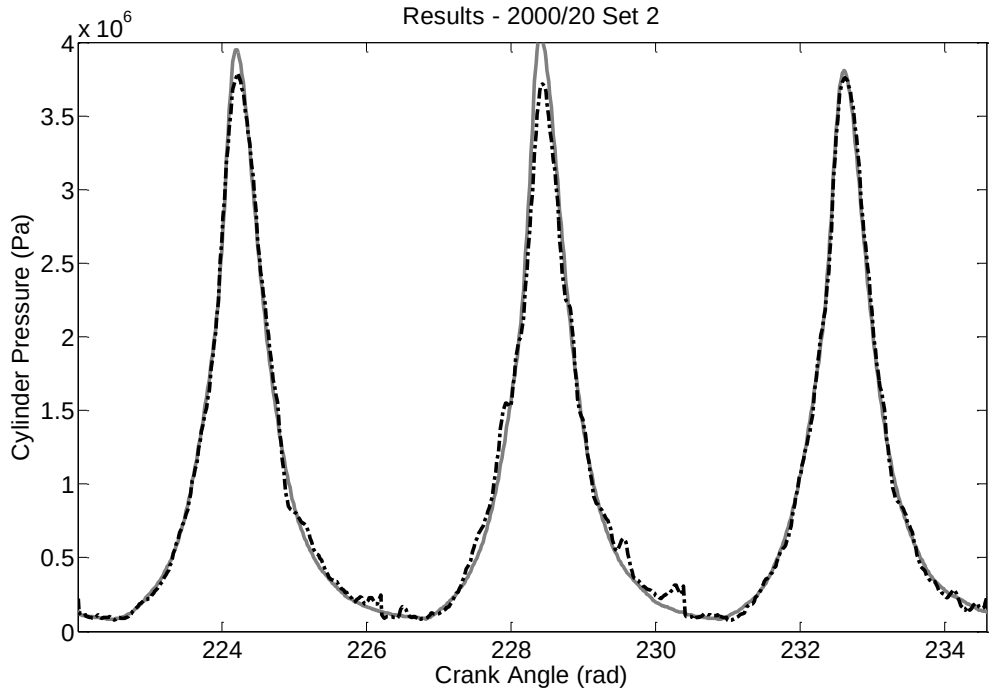

Figure F4.7: Condition-6 Generalisation Results - Worst. Measured Cylinder Pressure (Grey Solid Line). Reconstructed Cylinder Pressure (Black Dashed Line). RMSE = 2.48%.

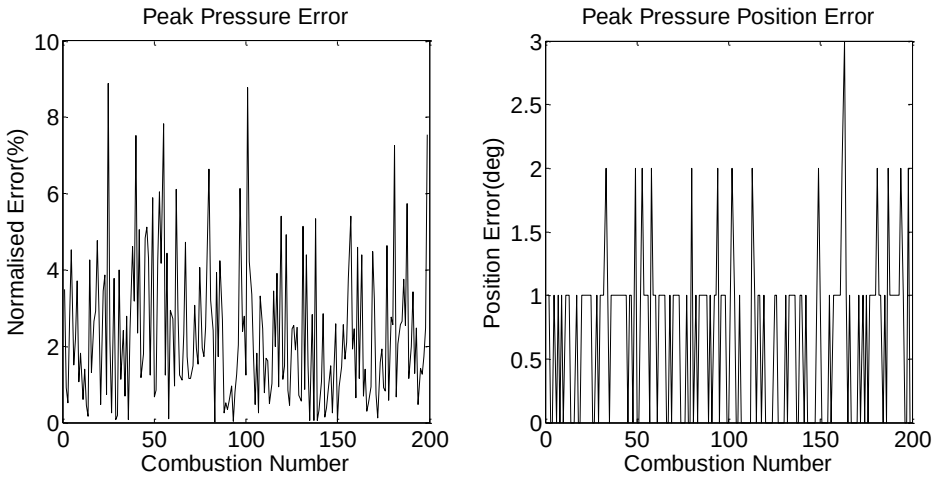

Figure F4.8: Condition-6 Normalised Peak Error Generalisation Results (left). Condition-5 Position of Peak Error Generalisation Results (right)

Table F4.3: Condition-6 Root-Mean-Squared Error (RMSE) and Standard Deviation for the ANN Generalisation

	Generalisation Root-Mean-Squared Error	Generalisation Standard Deviation
Overall Performance	2.02 %	1.96 %
Normalised Peak Error	2.99 %	1.86 %
Peak Pressure Position Error (deg)	0.91	0.62

Test Condition-7

The first test condition used measured data from running the engine at steady-state with a speed of 1000 rpm and a load of 30 Nm.

Table F5.1: ANN Training Setup for Test Condition-7

Network Name	Net_TD_BA_Test7	**Network Architecture**	Time-Delay	**Test Data**	1000_30_01p_jun2010
Network Training Algorithm	Levenberg–Marquardt	**Hidden Layers Number**	2	**Speed (rpm) / Load (Nm)**	1000/30
Cost Function	Means Squared Error	**Neurons Number**	15/15	**Training to Validation Ratio**	60:40
Training Goal	1E8	**Delay Number**	240	**Crank Step**	1 Deg
Maximum Epoch	1000	**Transfer Function Layer 1**	Sigmoid	**Number of Iterations**	10
Weights Initialisation	Randomised	**Transfer Function Layer 2**	Linear		

Training Results

In total 10 different ANNs were trained with the overall performance of the ANNs ranging from 1.88% to 1.97% RMSE. The best performing ANN was selected which trained in 859 seconds (0.24 hours) in 32 epochs.

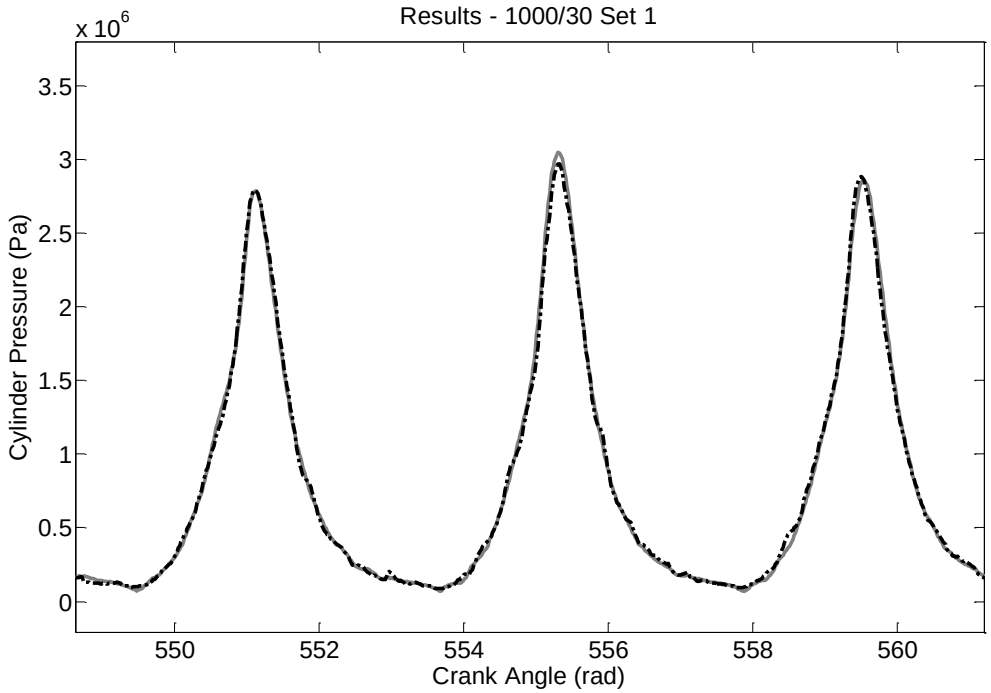

Figure F5.1: Condition-7 Training Results - Best. Measured Cylinder Pressure (Grey Solid Line). Reconstructed Cylinder Pressure (Black Dashed Line). RMSE = 1.07%.

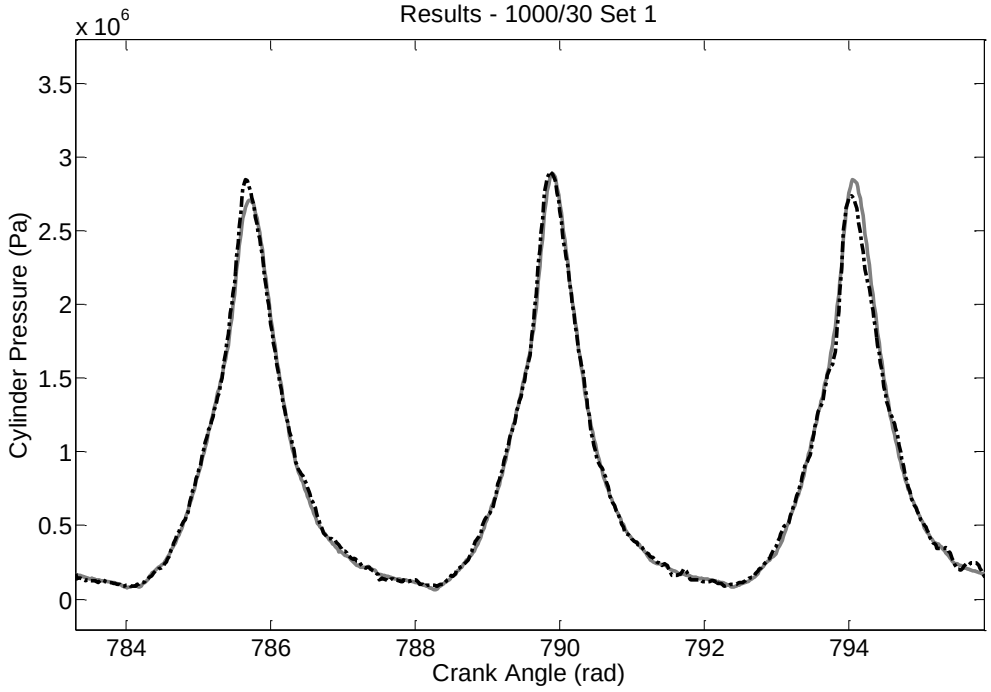

Figure F5.2: Condition-7 Training Results - Average. Measured Cylinder Pressure (Grey Solid Line). Reconstructed Cylinder Pressure (Black Dashed Line). RMSE = 1.74%.

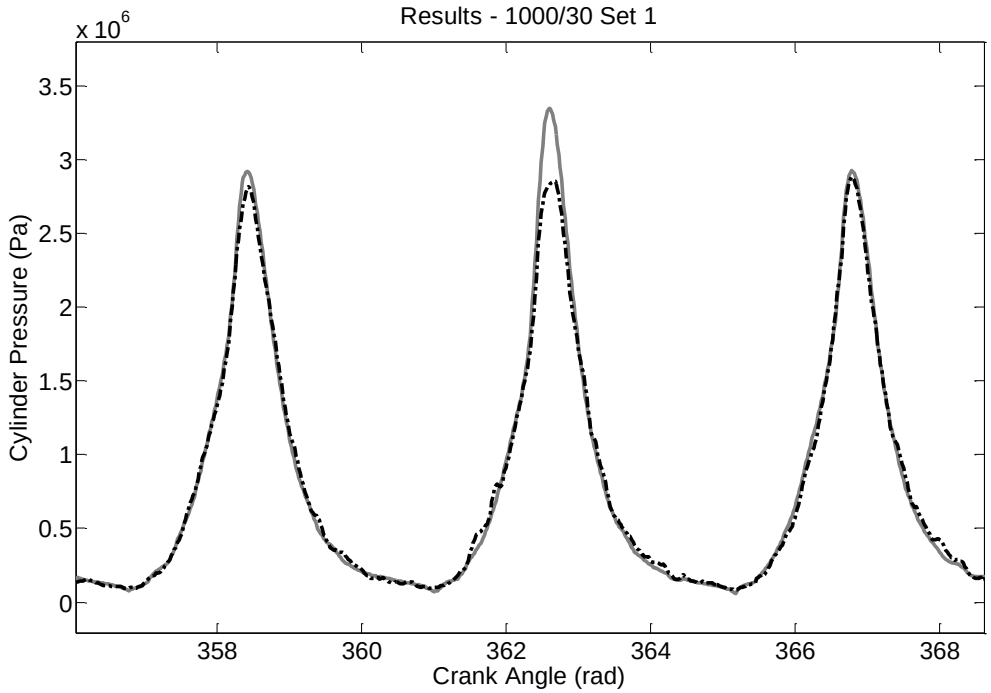

Figure F5.3: Condition-7 Training Results - Worst. Measured Cylinder Pressure (Grey Solid Line). Reconstructed Cylinder Pressure (Black Dashed Line). RMSE = 2.56%.

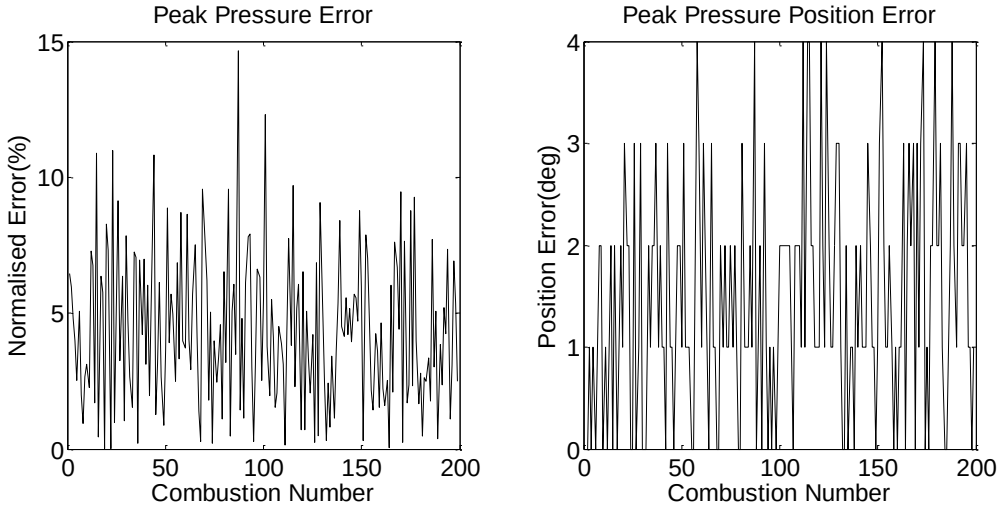

Figure F5.4: Condition-7 Normalised Peak Error Training Results (left). Condition-5 Position of Peak Error Training Results (right)

Table F5.2: Condition-7 Root-Mean-Squared Error (RMSE) and Standard Deviation for the ANN Training

	Training Root-Mean-Squared Error	Training Standard Deviation
Overall Performance	1.88 %	1.87 %
Normalised Peak Error	5.17 %	2.79 %
Peak Pressure Position Error (deg)	1.83	1.12

Generalisation Results

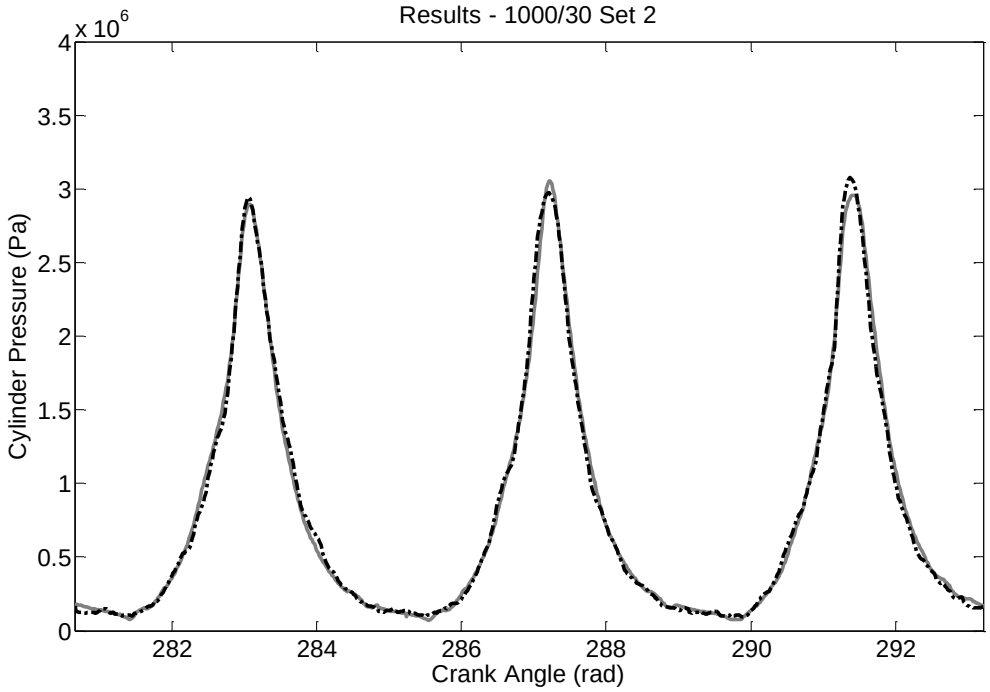

Figure F5.5: Condition-7 Generalisation Results - Best. Measured Cylinder Pressure (Grey Solid Line). Reconstructed Cylinder Pressure (Black Dashed Line). RMSE = 1.33%.

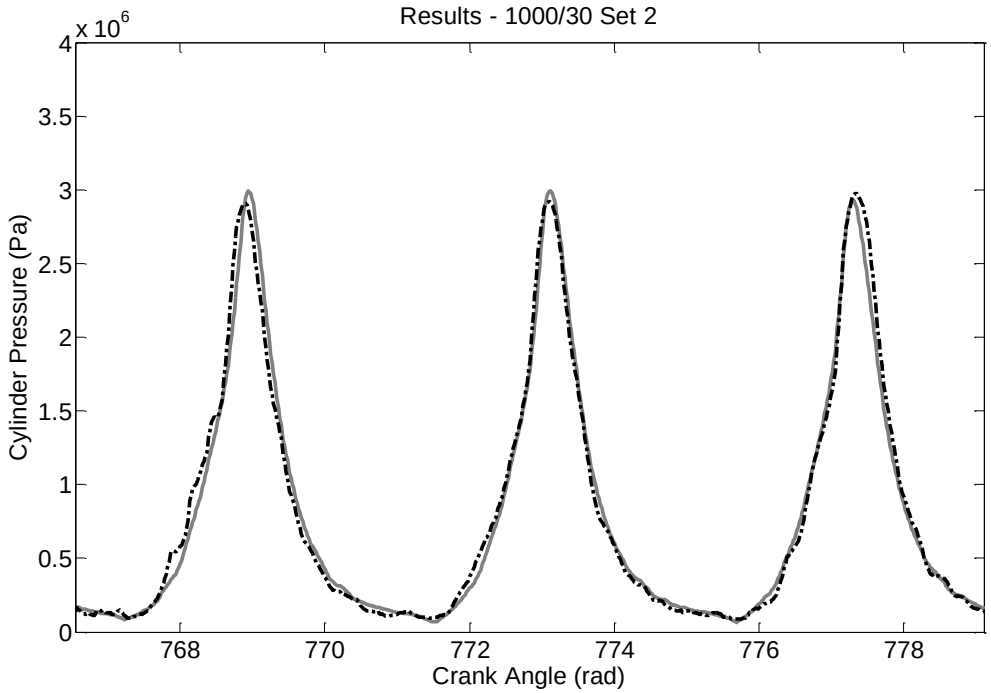

Figure F5.6 Condition-7 Generalisation Results - Average. Measured Cylinder Pressure (Grey Solid Line). Reconstructed Cylinder Pressure (Black Dashed Line). RMSE = 2.15%.

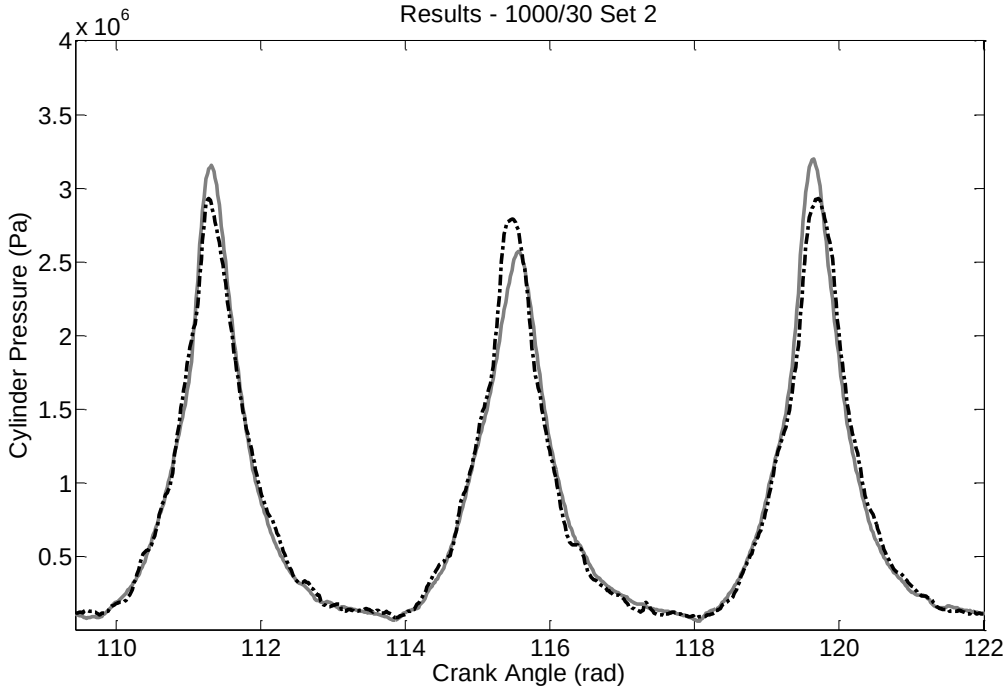

Figure F5.7: Condition-7 Generalisation Results - Worst. Measured Cylinder Pressure (Grey Solid Line). Reconstructed Cylinder Pressure (Black Dashed Line). RMSE = 3.25%.

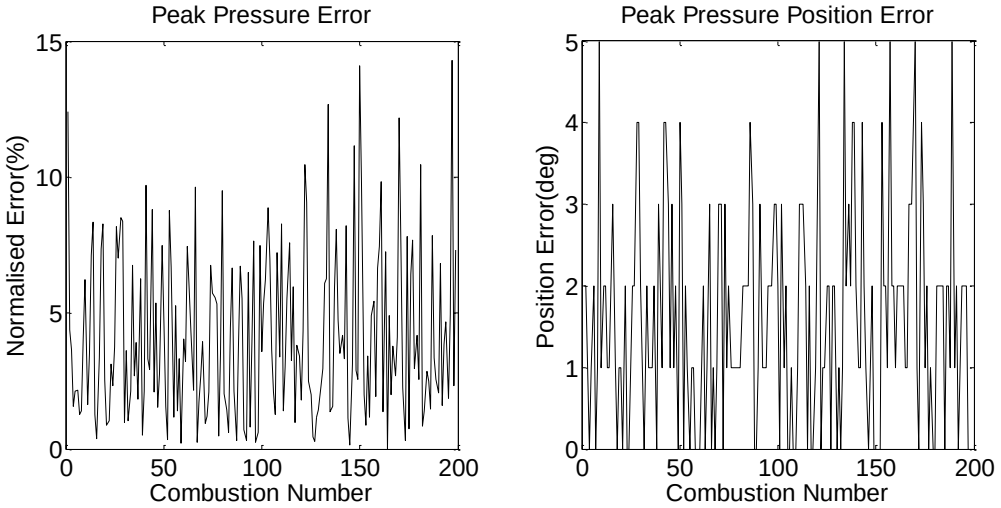

Figure F5.8: Condition-7 Normalised Peak Error Generalisation Results (left). Condition-5 Position of Peak Error Generalisation Results (right)

Table F5.3: Condition-7 Root-Mean-Squared Error (RMSE) and Standard Deviation for the ANN Generalisation

	Generalisation Root-Mean-Squared Error	Generalisation Standard Deviation
Overall Performance	2.27 %	2.26 %
Normalised Peak Error	5.19 %	3.07 %
Peak Pressure Position Error (deg)	2.03	1.28

Test Condition-8

The first test condition used measured data from running the engine at steady-state with a speed of 1500 rpm and a load of 30 Nm.

Table F6.1: ANN Training Setup for Test Condition-8

Network Name	Net_TD_BA_Test8	**Network Architecture**	Time-Delay	**Test Data**	1500_30_01p_jun2010
Network Training Algorithm	Levenberg–Marquardt	**Hidden Layers Number**	2	**Speed (rpm) / Load (Nm)**	1500/30
Cost Function	Means Squared Error	**Neurons Number**	15/15	**Training to Validation Ratio**	60:40
Training Goal	1E8	**Delay Number**	240	**Crank Step**	1 Deg
Maximum Epoch	1000	**Transfer Function Layer 1**	Sigmoid	**Number of Iterations**	10
Weights Initialisation	Randomised	**Transfer Function Layer 2**	Linear		

Training Results

In total 10 different ANNs were trained with the overall performance of the ANNs ranging from 3.48% to 3.72% RMSE. The best performing ANN was selected which trained in 2577 seconds (0.72 hours) in 112 epochs.

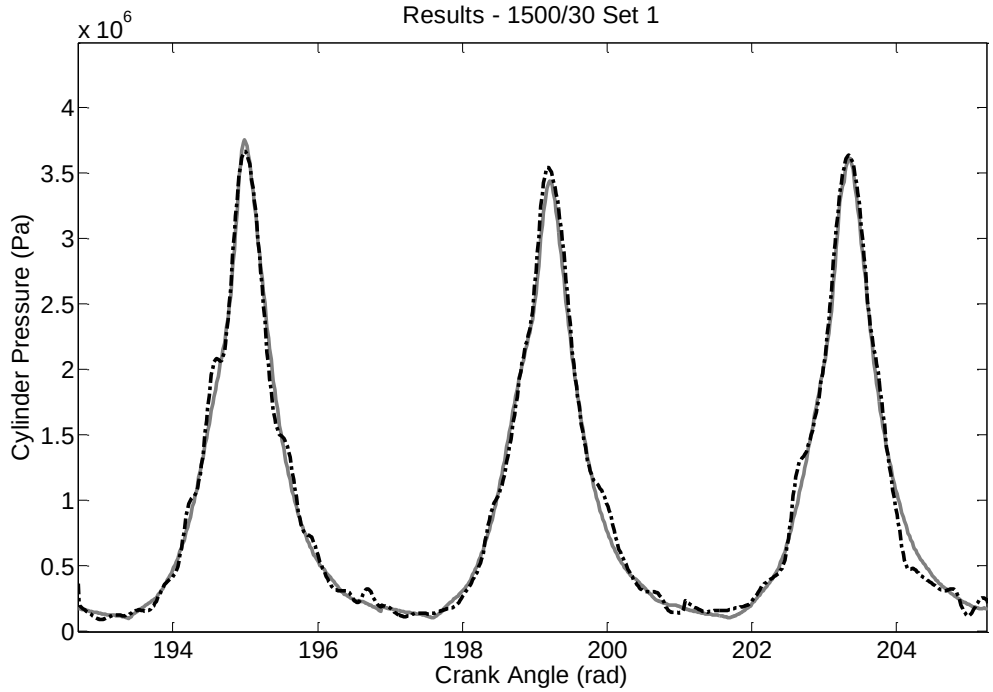

Figure F6.1: Condition-8 Training Results - Best. Measured Cylinder Pressure (Grey Solid Line). Reconstructed Cylinder Pressure (Black Dashed Line). RMSE = 2.16%.

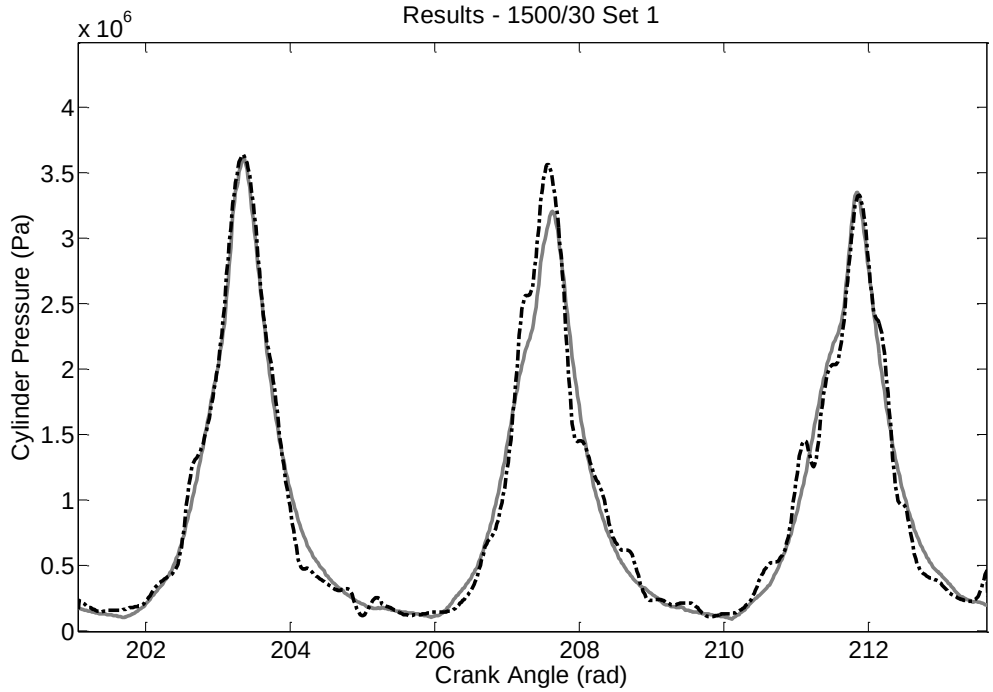

Figure F6.2: Condition-8 Training Results - Average. Measured Cylinder Pressure (Grey Solid Line). Reconstructed Cylinder Pressure (Black Dashed Line). RMSE = 3.16%.

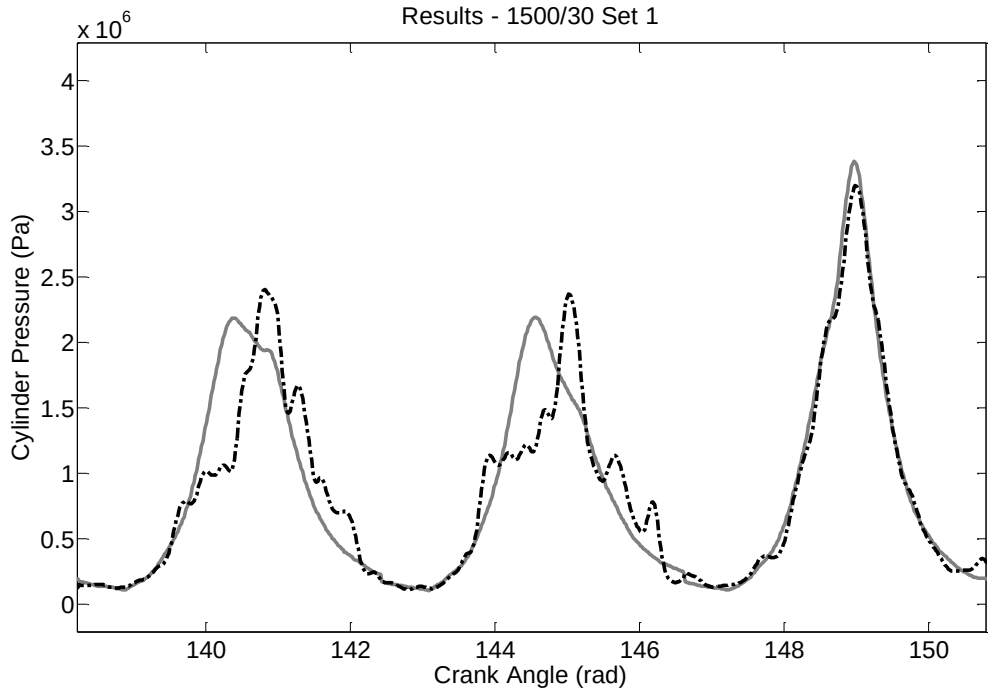

Figure F6.3: Condition-8 Training Results - Worst. Measured Cylinder Pressure (Grey Solid Line). Reconstructed Cylinder Pressure (Black Dashed Line). RMSE = 7.40%.

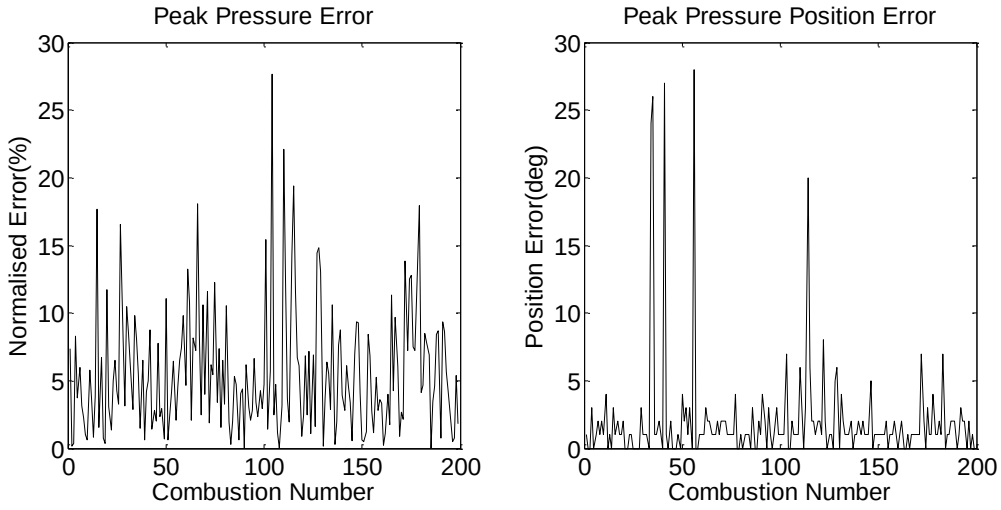

Figure F6.4: Condition-8 Normalised Peak Error Training Results (left). Condition-5 Position of Peak Error Training Results (right)

Table F6.2: Condition-8 Root-Mean-Squared Error (RMSE) and Standard Deviation for the ANN Training

	Training Root-Mean-Squared Error	Training Standard Deviation
Overall Performance	3.18 %	2.91 %
Normalised Peak Error	7.21 %	4.58 %
Peak Pressure Position Error (deg)	2.46	2.00

Generalisation Results

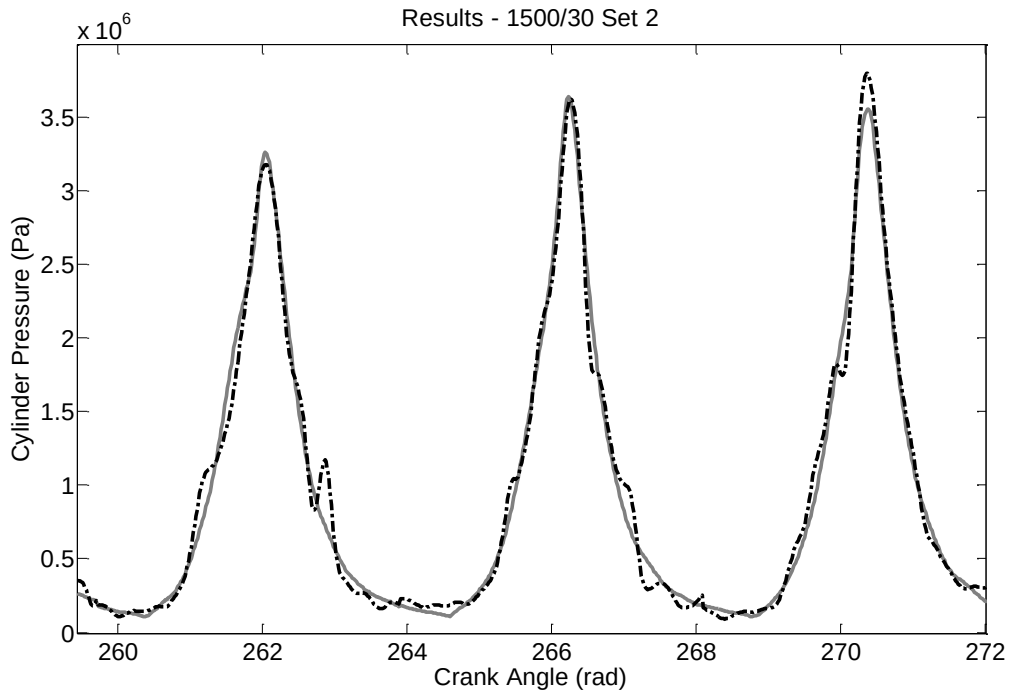

Figure F6.5: Condition-8 Generalisation Results - Best. Measured Cylinder Pressure (Grey Solid Line). Reconstructed Cylinder Pressure (Black Dashed Line). RMSE = 2.79%.

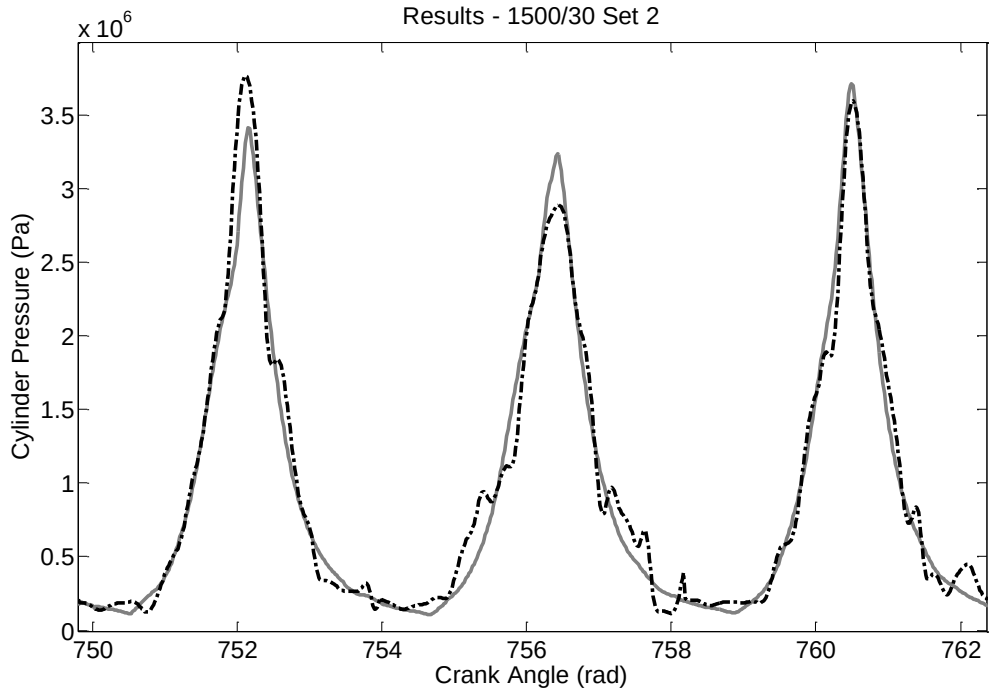

Figure E6.6 Condition-8 Generalisation Results - Average. Measured Cylinder Pressure (Grey Solid Line). Reconstructed Cylinder Pressure (Black Dashed Line). RMSE = 3.59%.

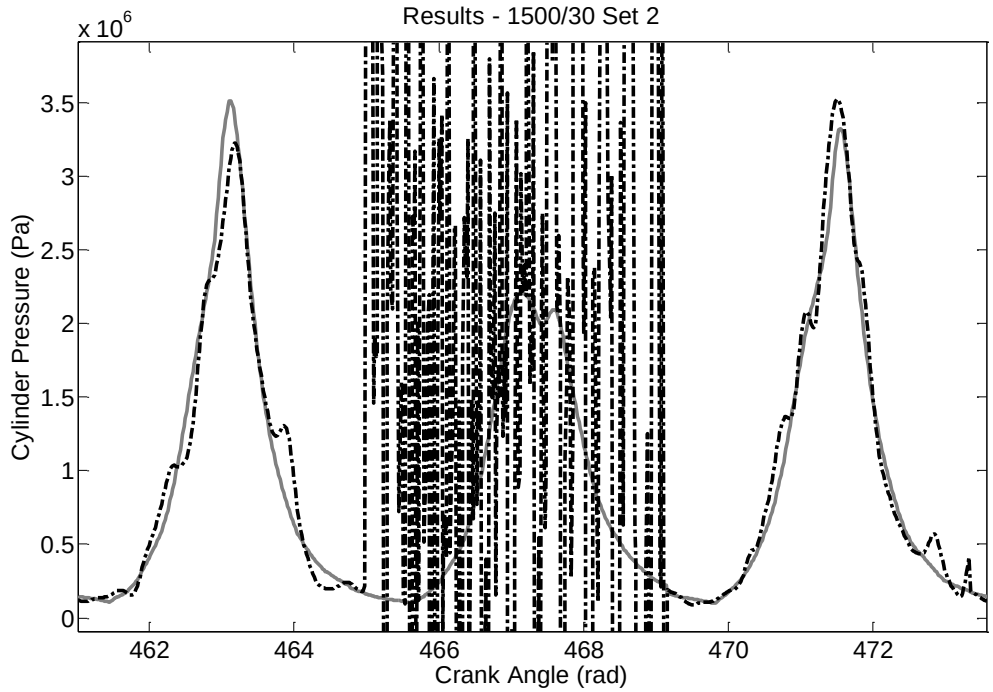

Figure E6.7: Condition-8 Generalisation Results - Worst. Measured Cylinder Pressure (Grey Solid Line). Reconstructed Cylinder Pressure (Black Dashed Line). RMSE = 61.7%.

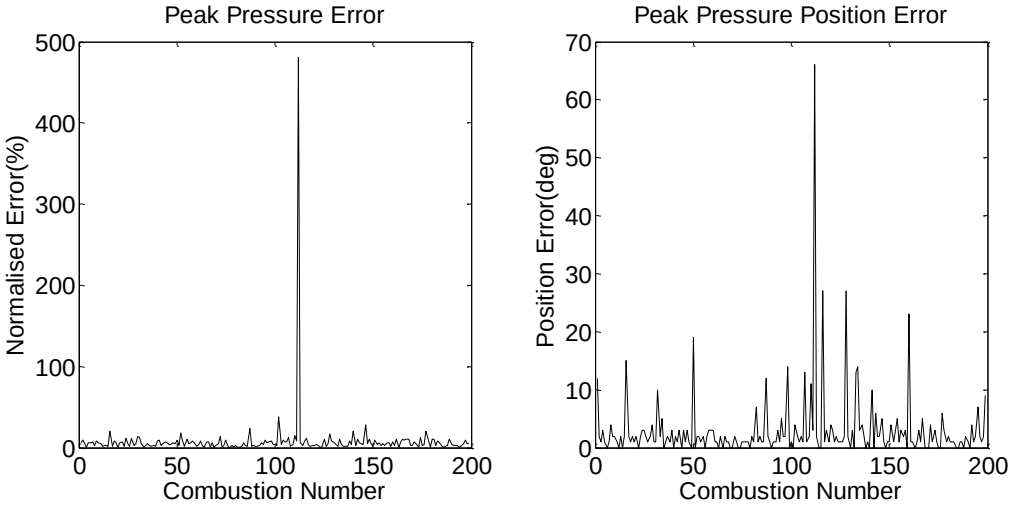

Figure E6.8: Condition-8 Normalised Peak Error Generalisation Results (left). Condition-5 Position of Peak Error Generalisation Results (right)

Table F6.3: Condition-8 Root-Mean-Squared Error (RMSE) and Standard Deviation for the ANN Generalisation

	Generalisation Root-Mean-Squared Error	Generalisation Standard Deviation
Overall Performance	4.33 %	4.19 %
Normalised Peak Error	14.1 %	13.72 %
Peak Pressure Position Error (deg)	4.79	4.13

Appendix G

Additional Load Varying Results

Test Condition-2, 5 and 8 - 1500 rpm

Table G1.1: Overall Results for Steady-State Testing on a Single ANN Trained on Constant Speed Varying Load Conditions

	Overall Performance (RMSE)	Normalised Peak Error	Peak Pressure Position Error (deg)
Condition-2	1.47 %	2.12 %	1.98
Condition-5	1.44 %	3.43 %	2.62
Condition-8	1.48 %	2.94 %	2.90

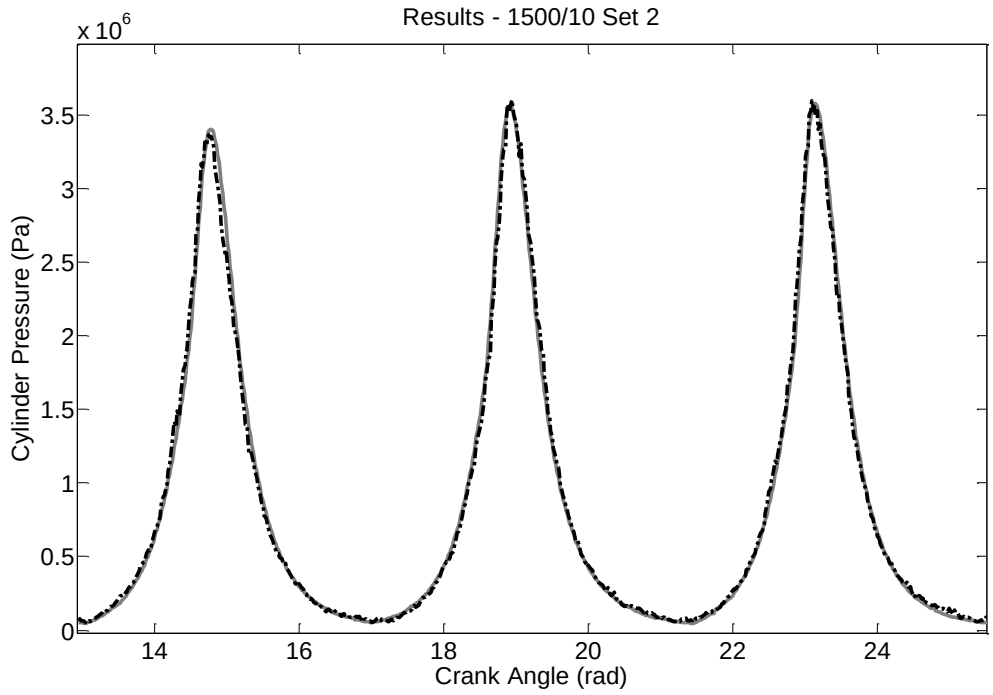

. Figure G1.1: Steady-State Condition-2 - 1500 rpm and 10 Nm. Measured Cylinder Pressure (Grey Solid Line). Reconstructed Cylinder Pressure (Black Dashed Line).

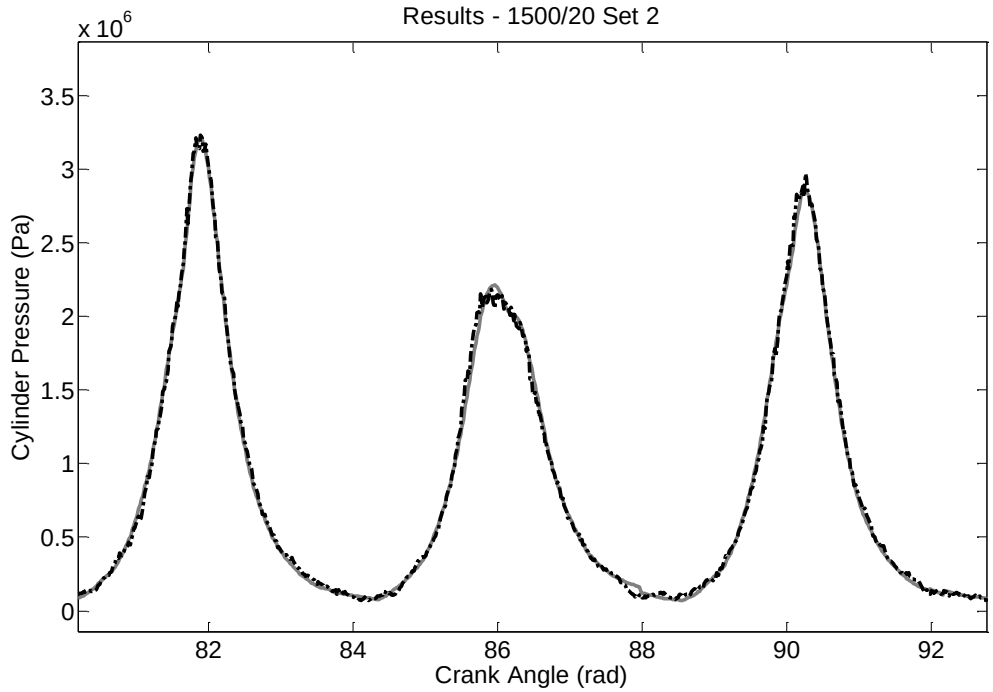

Figure G1.2: Steady-State Condition-5 - 1500 rpm and 20 Nm. Measured Cylinder Pressure (Grey Solid Line). Reconstructed Cylinder Pressure (Black Dashed Line).

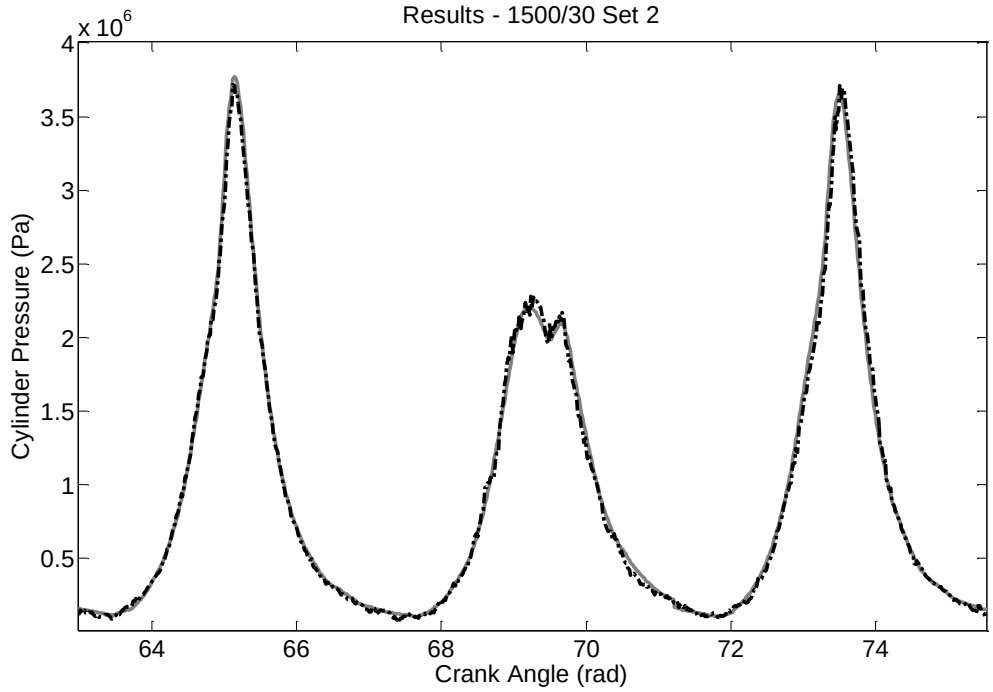

Figure G1.3: Steady-State Condition-8 - 1500 rpm and 30 Nm. Measured Cylinder Pressure (Grey Solid Line). Reconstructed Cylinder Pressure (Black Dashed Line).

Test Condition-3, 6 and 9 - 2000 rpm

Table G1.2: Overall Results for Steady-State Testing on a Single ANN Trained on Constant Speed Varying Load Conditions.

	Overall Performance (RMSE)	Normalised Peak Error	Peak Pressure Position Error (deg)
Condition-3	1.33 %	2.08 %	1.63
Condition-6	1.30 %	1.16 %	1.48
Condition-9	1.36 %	2.29 %	1.51

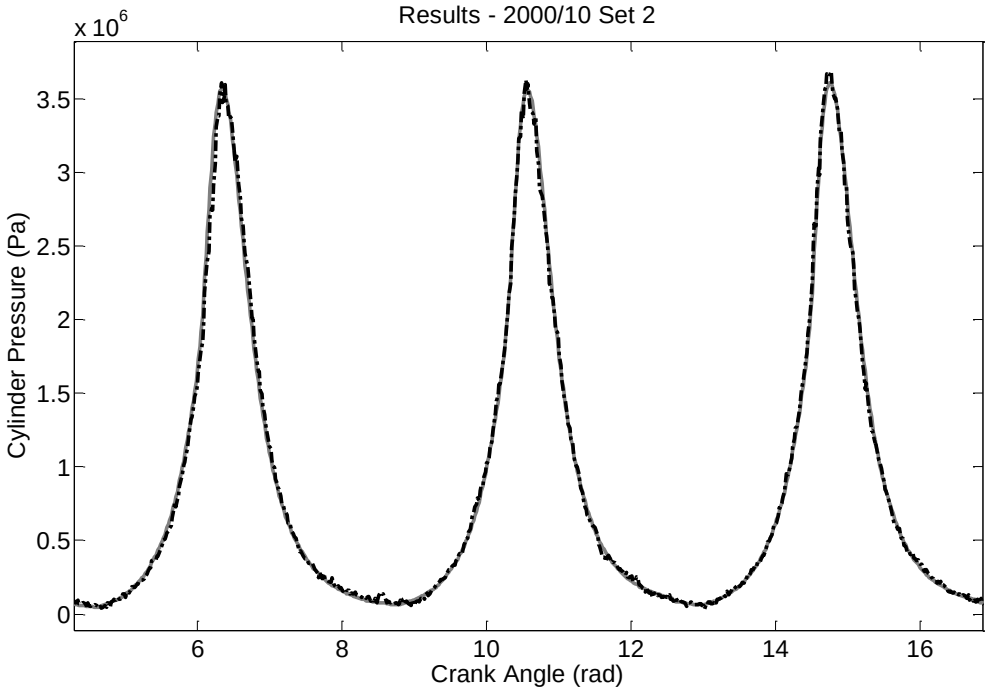

Figure G1.4: Steady-State Condition-3 - 2000 rpm and 10 Nm. Measured Cylinder Pressure (Grey Solid Line). Reconstructed Cylinder Pressure (Black Dashed Line).

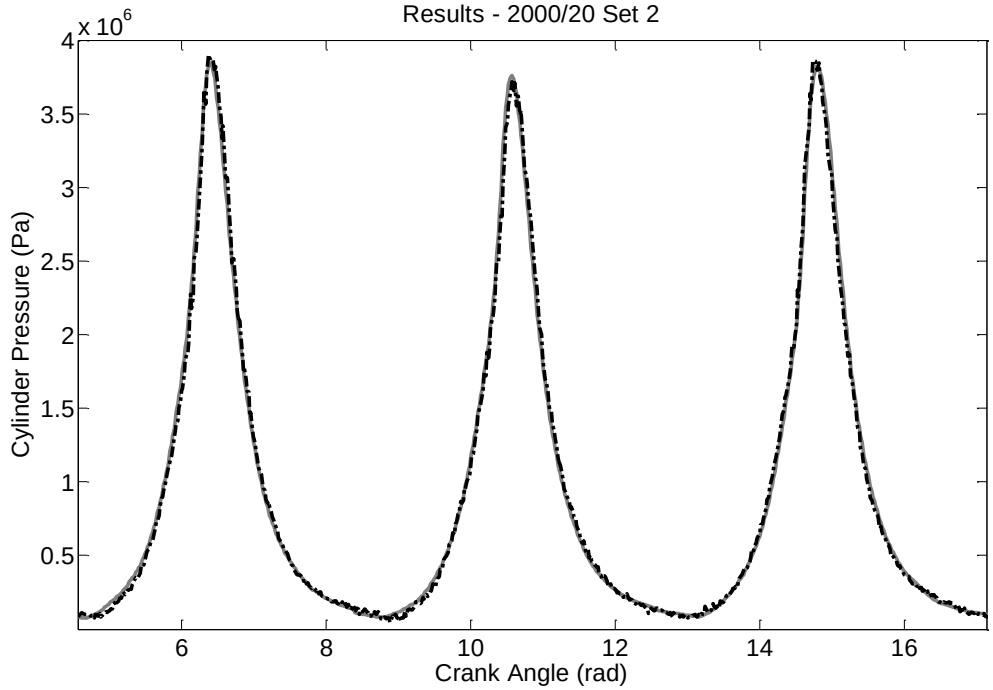

Figure G1.5: Steady-State Condition-6 - 2000 rpm and 20 Nm. Measured Cylinder Pressure (Grey Solid Line). Reconstructed Cylinder Pressure (Black Dashed Line).

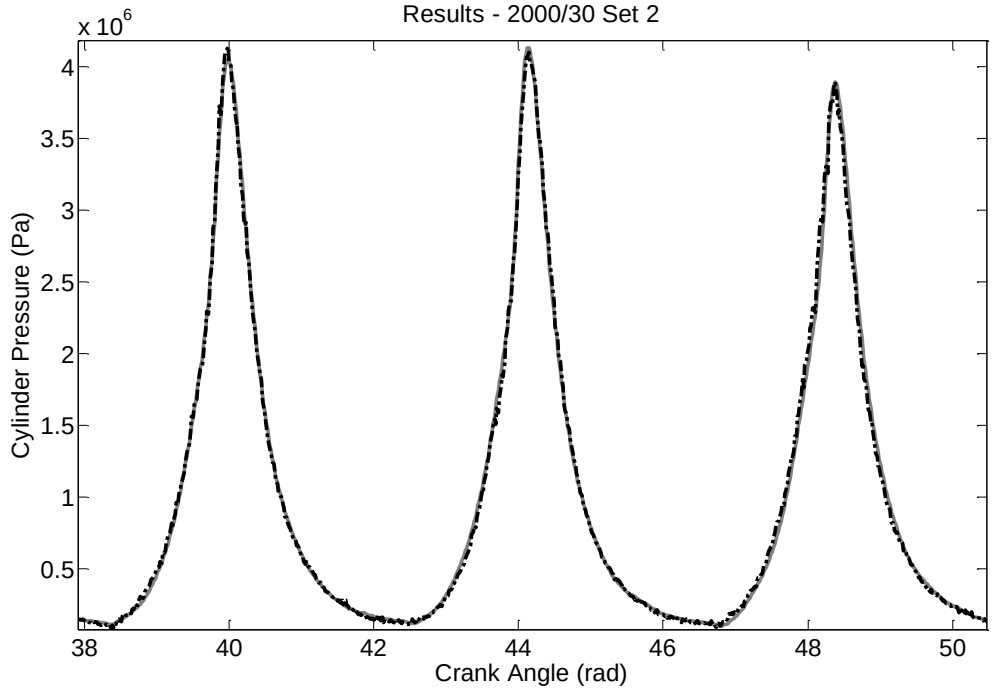

Figure G1.6: Steady-State Condition-9 - 2000 rpm and 30 Nm. Measured Cylinder Pressure (Grey Solid Line). Reconstructed Cylinder Pressure (Black Dashed Line).

Additional Speed Varying Results

Test Condition-2, 5 and 8 - 20 Nm

Table G2.1: Overall Results for Steady-State Testing on a Single ANN Trained on Constant Speed Varying Load Conditions.

	Overall Performance (RMSE)	Normalised Peak Error	Peak Pressure Position Error (deg)
Condition-4	2.89 %	9.45 %	6.93
Condition-5	2.13 %	9.09 %	3.07
Condition-6	1.60 %	3.24 %	1.49

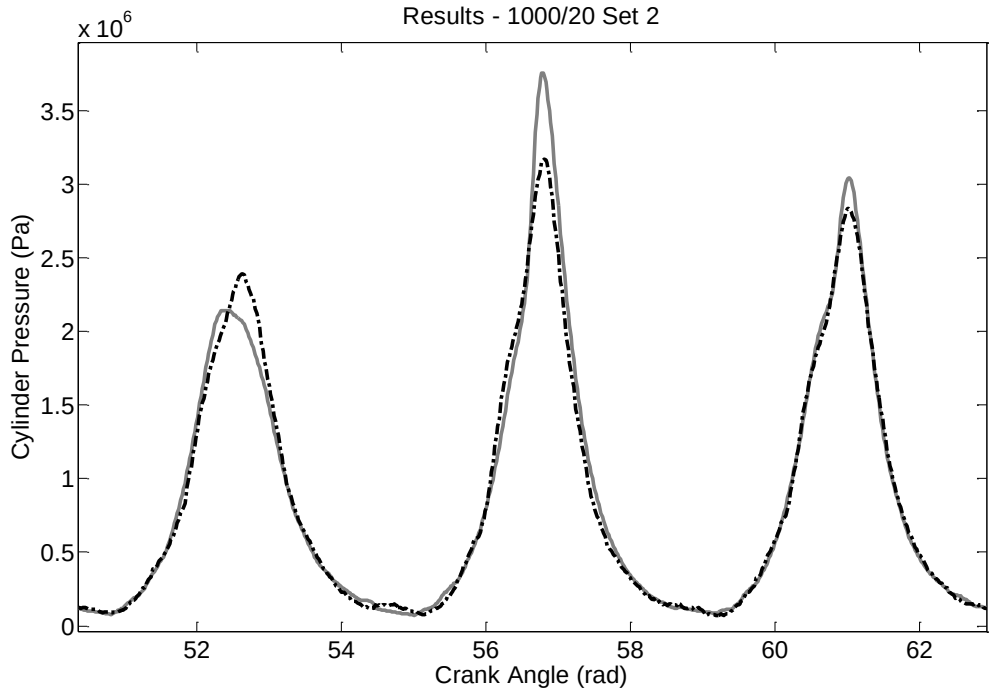

Figure G2.1: Steady-State Condition-4 - 1000 rpm and 20 Nm. Measured Cylinder Pressure (Grey Solid Line). Reconstructed Cylinder Pressure (Black Dashed Line).

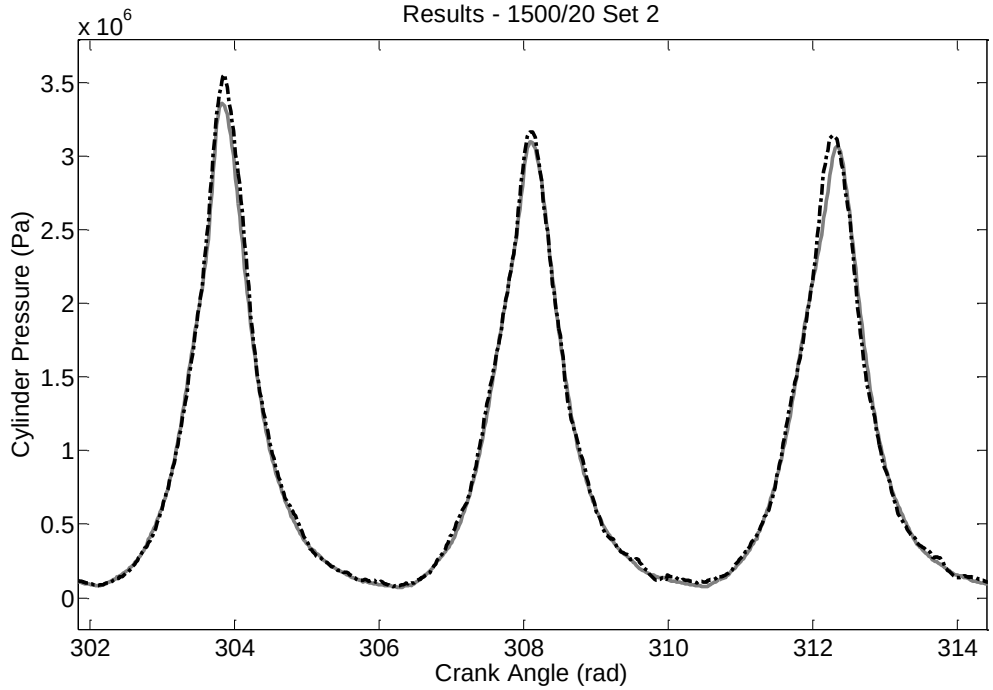

Figure G2.2: Steady-State Condition-5 - 1500 rpm and 20 Nm. Measured Cylinder Pressure (Grey Solid Line). Reconstructed Cylinder Pressure (Black Dashed Line).

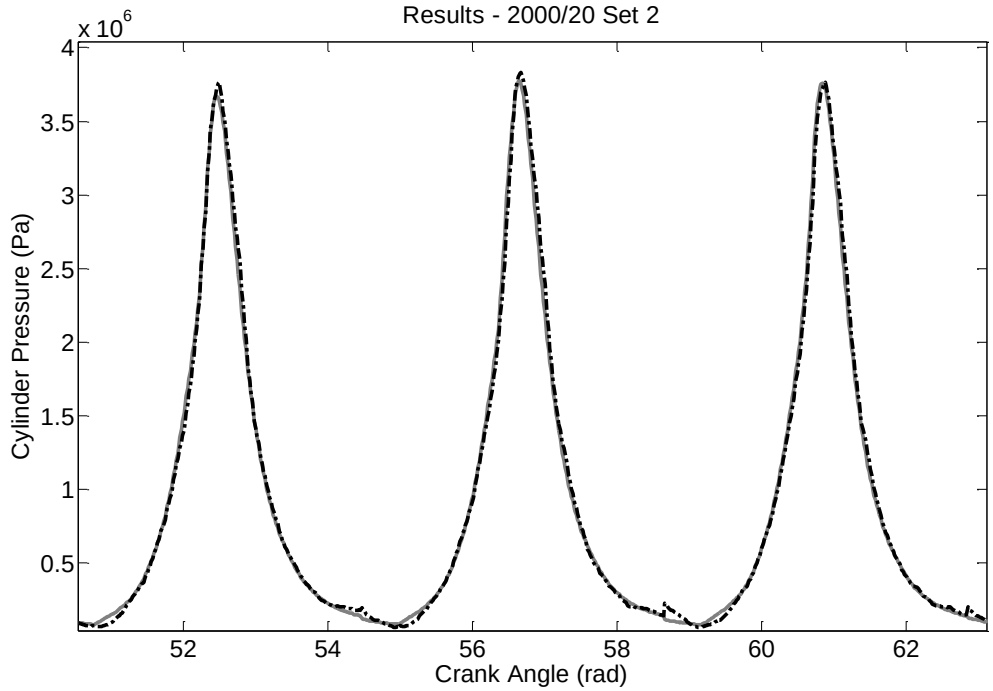

Figure G2.3: Steady-State Condition-6 - 2000 rpm and 20 Nm. Measured Cylinder Pressure (Grey Solid Line). Reconstructed Cylinder Pressure (Black Dashed Line).

Test Condition-7, 8 and 9 - 2000 rpm

Table G2.2: Overall Results for Steady-State Testing on a Single ANN Trained on Constant Speed Varying Load Conditions.

	Overall Performance (RMSE)	Normalised Peak Error	Peak Pressure Position Error (deg)
Condition-7	2.50 %	4.41 %	2.25
Condition-8	1.82 %	4.39 %	2.06
Condition-9	1.52 %	3.55 %	1.46

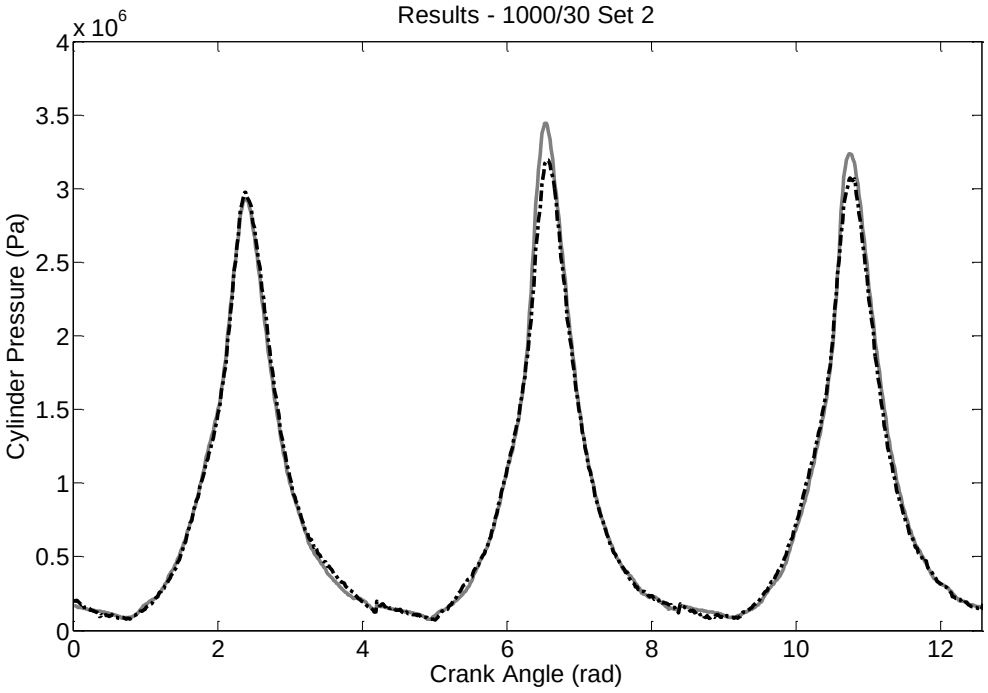

Figure G2.4: Steady-State Condition-7 - 1000 rpm and 30 Nm. Measured Cylinder Pressure (Grey Solid Line). Reconstructed Cylinder Pressure (Black Dashed Line).

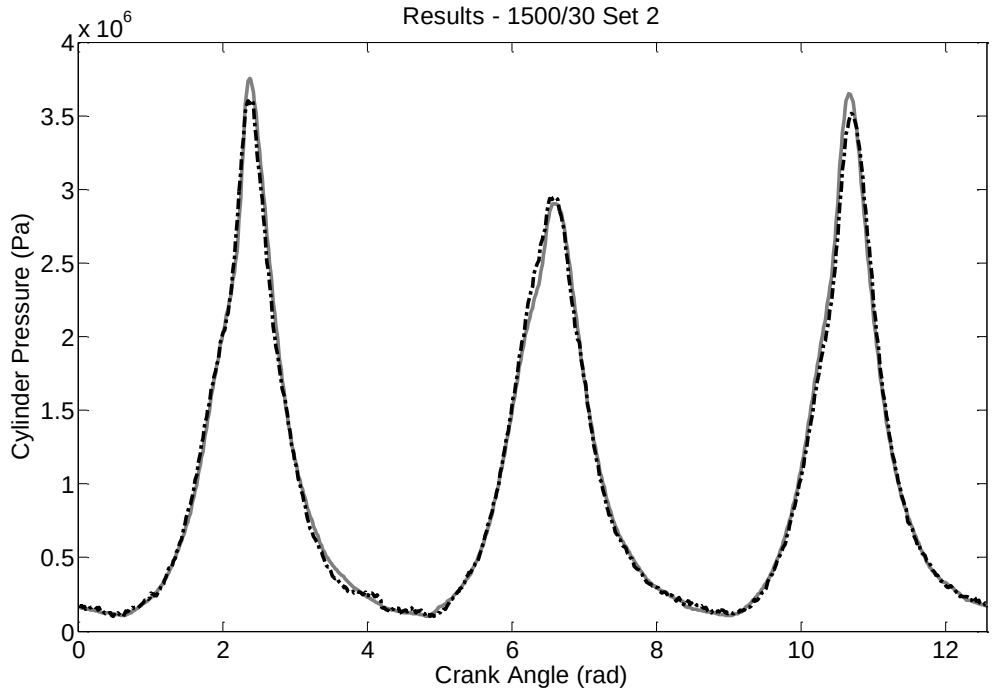

Figure G2.5: Steady-State Condition-8 - 1500 rpm and 30 Nm. Measured Cylinder Pressure (Grey Solid Line). Reconstructed Cylinder Pressure (Black Dashed Line).

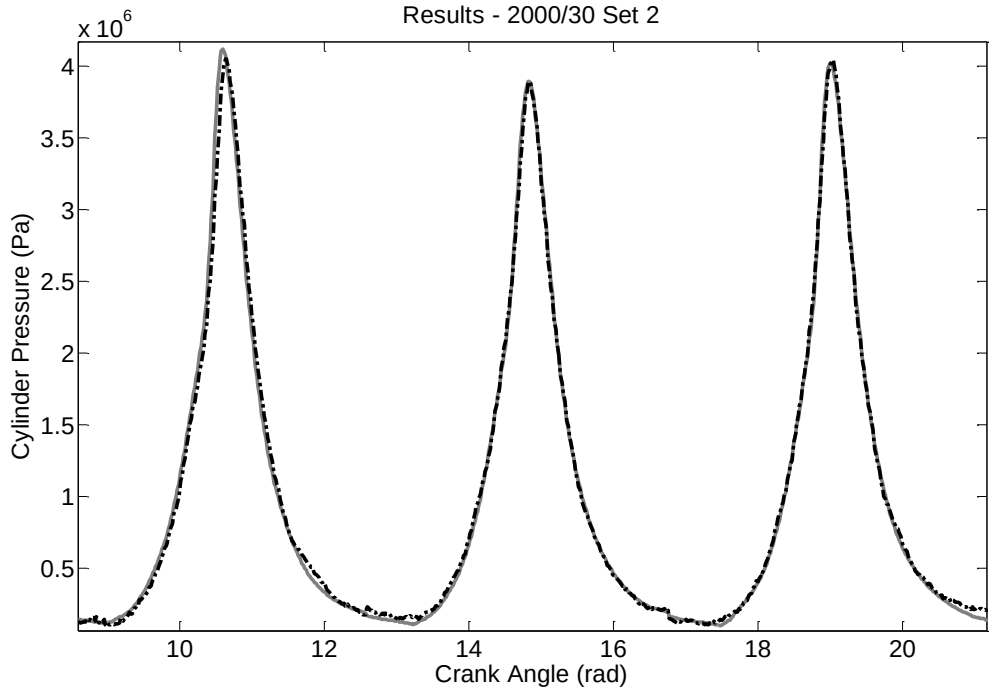

Figure G2.6: Steady-State Condition-9 - 2000 rpm and 30 Nm. Measured Cylinder Pressure (Grey Solid Line). Reconstructed Cylinder Pressure (Black Dashed Line).